INTERNATIONAL REVIEW OF CYTOLOGY
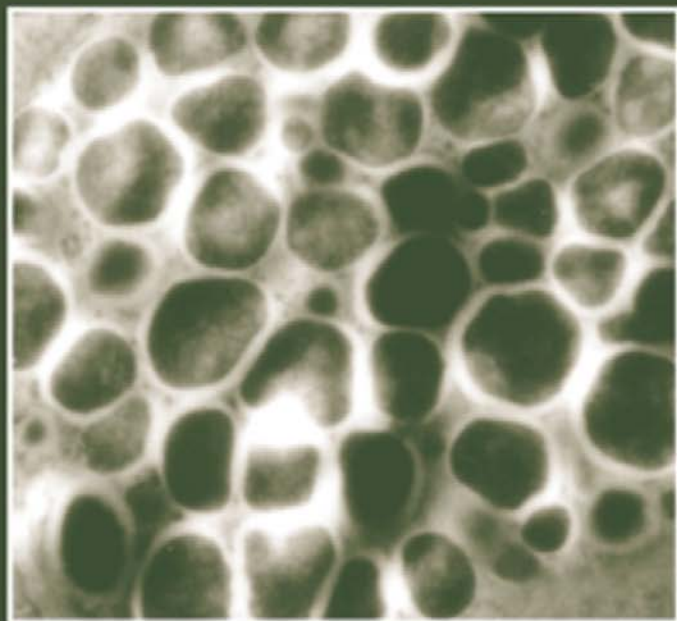
A SURVEY OF CELL BIOLOGY

Edited by
Kwang W. Jeon

Volume 211

International Review of Cytology

A Survey of Cell Biology

Edited by

Kwang W. Jeon
Department of Biochemistry
University of Tennessee
Knoxville, Tennessee

VOLUME 211

CONTENTS

Cytoskeleton-Dependent Transport and Localization of mRNA

Howard Stebbings

Special Cytochemistry in Cell Biology

Tetsuji Nagata

Plasticity and Stabilization of Neuromuscular and CNS Synapses: Interactions between Thrombin Protease Signaling Pathways and Tissue Transglutaminase

Barry W. Festoff, Zhiming Suo, and Bruce A. Citron

Adipokinetic Hormones of Insect: Release, Signal Transduction, and Responses

Dick J. Van der Horst, Wil J. A. Van Marrewijk, and Jacques H. B. Diederen

Iron Metabolism in Mammalian Cells

Brandie L. Walker, Jacqueline W. C. Tiong, and Wilfred A. Jefferies

CONTRIBUTORS

Numbers in parentheses indicate the pages on which the authors' contributions begin.

Bruce A. Citron (153), *Neurobiology Research Laboratory, University of Kansas Medical Center, Kansas City Veterans Affairs Medical Center, Kansas City, Missouri 64128*

Jacques H. B. Diederen (179), *Department of Biochemical Physiology, Faculty of Biology and Institute of Biomembranes, Utrecht University, 3584 CH Utrecht, The Netherlands*

Barry W. Festoff (153), *Neurobiology Research Laboratory, University of Kansas Medical Center, Kansas City Veterans Affairs Medical Center, Kansas City, Missouri 64128*

Wilfred A. Jefferies (241), *Biotechnology Lab and Biomedical Research Centre, and Departments of Medical Genetics, Microbiology and Immunology, and Zoology, University of British Columbia, Vancouver, BC, Canada V6T 1Z3*

Tetsuji Nagata (33), *Department of Anatomy and Cell Biology, Shinshu University School of Medicine, Matsumoto 390-8621, Japan; and Department of Anatomy and Physiology, Nagano Women's Junior College, Nagano 380-0803, Japan*

Howard Stebbings (1), *School of Biological Sciences, Washington Singer Laboratories, University of Exeter, Exeter EX4 4QG, United Kingdom*

Zhiming Suo (153), *Neurobiology Research Laboratory, University of Kansas Medical Center, Kansas City Veterans Affairs Medical Center, Kansas City, Missouri 64128*

Jacqueline W. C. Tiong (241), *Biotechnology Lab and Biomedical Research Centre, and Departments of Medical Genetics, Microbiology and Immunology, and Zoology, University of British Columbia, Vancouver, BC, Canada V6T 1Z3*

Dick J. Van der Horst (179), *Department of Biochemical Physiology, Faculty of Biology and Institute of Biomembranes, Utrecht University, 3584 CH Utrecht, The Netherlands*

Wil J. A. Van Marrewijk (179), *Department of Biochemical Physiology, Faculty of Biology and Institute of Biomembranes, Utrecht University, 3584 CH Utrecht, The Netherlands*

Brandie L. Walker (241), *Biotechnology Laboratory and Biomedical Research Centre, and Departments of Medical Genetics, Microbiology and Immunology, and Zoology, University of British Columbia, Vancouver, BC, Canada V6T 1Z3*

Cytoskeleton-Dependent Transport and Localization of mRNA

Howard Stebbings

School of Biological Sciences, Washington Singer Laboratories, University of Exeter, Exeter EX4 4QG, United Kingdom

Messenger RNAs are localized in both somatic and germ cells as a means of focusing the translation of proteins at specific cellular sites. The signals for this lie within the mRNA, and these are recognized by proteins in the cell. The latter appear to be attached via linker proteins to the transport machinery for localization. In some instances it is a myosin motor which translocates along actin microfilaments, and in others kinesin or dynein motors appear to be responsible for driving the movement of mRNA along microtubule substrates. The way that cytoskeleton-based mRNA translocation is regulated is speculated upon.

KEY WORDS: mRNA, RNA-binding proteins, Motor proteins, Cytoskeleton, Microtubules, Microfilaments. © 2001 Academic Press.

I. Introduction

In contrast to mRNAs for membrane and secreted proteins, which are directed to the endoplasmic reticulum, mRNAs encoding a range of spatial determinants, regulatory proteins and cytoskeletal proteins may be localized to different specified regions of a cell. This is clearly an efficient means of localizing a protein within the cytoplasm, and over the past 15 years an increasing number of mRNAs has been shown to be localized in many different cell types and a wide range of eukaryotic organisms. These include yeast, ameba, insects, vertebrates including mammals, and also plants. Most studies have been of large cells, often eggs and embryos, but investigations have not been confined to germ cells since asymmetric somatic cells have also been valuable experimental material, and in these instances mRNA localization has been linked with the establishment and maintenance of cell polarity.

It has been appreciated that cellular localization of mRNA could be achieved in a variety of ways (St. Johnston, 1995), including selective and local RNA protection, diffusion with some kind of anchoring process or, the subject of this article, active transport involving the cytoskeleton.

The signal for the localization is the *cis*-acting sequence, usually in the 3′UTR of the localized messages and this is recognized by, and localization has been shown to be dependent upon, *trans*-acting RNA-binding proteins in the cytoplasm.

Active localization of RNA also depends on an intact cytoskeleton, and indeed associations between RNAs and the cytoskeleton were identified even before the phenomenon of mRNA localization was discovered. In many cases including oocytes (Pokrywka and Stephenson, 1991; Elisha *et al.,* 1995), neurons (Bassell *et al.,* 1994b), and oligodendrocytes (Ainger *et al.,* 1993), microtubule (MT) components of the cytoskeleton are essential for mRNA localization, while in others such as yeast (Long *et al.,* 1997; Takizawa *et al.,* 1997), ameba (Han *et al.,* 1997), and fibroblasts (Sundell and Singer, 1991), microfilaments are the key element. This dependency is not specified by the transcript, however, since there are instances where an mRNA is localized in a MT-dependent fashion in one system while the same mRNA is localized by a microfilament-dependent mechanism in another.

A large amount of evidence from many systems has suggested that localized mRNAs are packaged into particles for transport. Active transport of these particles in one or another direction along MTs clearly requires an anterograde or retrograde MT motor, while transport along microfilaments necessitates a myosin motor. Some progress has recently been made in identifying the motors involved in different instances and in unraveling the macromolecular RNA transport complexes in order to discover the way their components interact with each other for transport. Finally, once at the specified cellular site the localized mRNA must be anchored and translated, and evidence suggests that the cytoskeleton is intimately involved in this also.

II. Localization of mRNAs

A. Model Systems for Studying mRNA Localization

mRNAs are localized to specific cytoplasmic sites in many eukaryotic cells, but the phenomenon has been most easily and extensively studied in large cells—often gametes—and also somatic cells which show high degrees of asymmetry. Attention has been focused on examples from model experimental organisms, including yeast, *Drosophila,* and *Xenopus,* as well as *Caenorhabditis* and zebrafish, all of which are amenable to genetic and molecular approaches and these have enabled advances to be made through the identification and molecular cloning of

genes involved in RNA localization and analysis of their gene products. Neurons have also been the subject of study because of their physiological importance and their extreme asymmetry that relies on the transport of large numbers of components including mRNAs between the cell body and the extending dendritic and axonal processes. This section briefly introduces the occurrence of mRNA localization in a range of cells and organisms, the identity of localized mRNAs where known, and the particular significance of their localization in each instance.

1. ASH1 mRNA in Budding Yeast

During diploidization in homothallic strains of budding yeast, *Saccharomyces cerevisiae,* haploid spores germinate and grow to a certain size when they bud and mitosis occurs. *ASH1* mRNA is localized to the budded daughter at the end of anaphase (Long *et al.,* 1997; Takizawa *et al.,* 1997) and codes for a transcriptional repressor required to repress the *HO* gene. This is an example of the asymmetric segregation of a cell-fate determinant at cell division. Its localization results in Ash 1 protein accumulation in the daughter and depletion in the mother, where HO is expressed. HO is an endonuclease that causes mating type switching in the mother cell (Bobola *et al.,* 1996; Sil and Herkowitz, 1996).

2. mRNA during Differentiation of *Naegleria gruberi* Amebae into Flagellates

Naegleria gruberi amebae differentiate into flagellated cells, each possessing two flagella. In doing so they form two basal bodies from which the two flagella grow. A MT cytoskeleton also forms from the region of their two basal bodies—the ameboid form not having possessed MT arrangements. Formation of these organelles requires tubulins, among other building blocks, and Han and coworkers (1997) have shown that mRNAs encoding α- and β-tubulins, as well as mRNAs for other differentiation-specific components such as flagellar calmodulin, are localized to the region of the forming basal bodies. The mRNAs are localized independently, and transcripts not involved in the differentiation were not localized. This, it appears, is a highly efficient means of localizing tubulin subunits for localized assembly into different microtubule aggregates.

3. β-Actin in Fibroblasts and Neuronal Growth Cones

β-Actin mRNA has been shown to be localized at the leading edge, the lamella, of several types of asymmetric cells including fibroblasts and in the growth cones of extending neurons. These regions of the cell show extensive polymerization of actin filaments which function in both the development of polarity and the motility of these migrating cells (Ross *et al.,* 1997). Growth factors which induce

cell proliferation and chemotaxis also stimulate the active transport and localization of the β-actin mRNA to the leading edges of fibroblasts and in doing so have a bearing on cytoskeletal organization (Latham *et al.,* 1994).

Similarly, the protrusion of filopodia from growth cones also depends on actin polymerization and plays a large part in the motility and pathfinding of these neuronal extremities. Localized polymerization of actin during process outgrowth has been equated with the localization of β-actin mRNA into growth cones and has been shown to be regulated by neurotrophins—well known chemoattractants (Zhang *et al.,* 1999).

4. mRNAs Encoding Cytoskeletal Proteins in Neurons

Many mRNAs have been localized to cell processes of neurons, including those encoding MT-associated proteins (MAPs), proteins important in the spacing and dynamics of MTs in the different compartments of these polarized cells. MAP2 mRNA is found in dendrites and its localization would appear to be the mechanism by which MAP2 is restricted to dendritic MTs (Kuhl and Skehel, 1998), while tau mRNA which encodes the axonal MAP, tau, is targeted to axons (Litman *et al.,* 1997).

5. *Prospero* mRNA in *Drosophila* Neuroblasts

During differentiation of the neuroblast lineage of the *Drosophila* embryonic central nervous system (CNS), stem cells divide asymmetrically and bud off a succession of small ganglion mother cells. Prospero protein, a cell fate determinant homeodomain transcription factor and, independently and possibly as a backup mechanism, *prospero* mRNA are localized to the ganglion mother cells (Broadus *et al.,* 1998). Here the protein has been shown to enter the nucleus and influence gene expression.

6. mRNAs during Insect Oogenesis

The localization of mRNAs has been extensively studied during insect oogenesis. In most, but not all, insects the oocyte nuclei are transcriptionally inactive and during oogenesis rely on the contribution of many components including RNA from highly synthetic nurse cells to which they are connected. The transfer of components from nurse cells to the oocytes takes place most dramatically in ovaries of hemipteran insects, largely because in this order the nurse cells are retained at the anterior while the developing oocytes are displaced in a chain down the ovariole. The result is that the oocytes and nurse cells are connected by extended intercellular channels known as nutritive tubes, often over several millimeters—a considerable distance on a cellular scale. Large quantities of RNA have been shown to travel down the nutritive tubes at a rate of $\sim$30 μm/h, probably passively and

as monomeric ribosomes (Macgregor and Stebbings, 1970). However, a smaller faster fraction translocating at ~200 μm/h has also been resolved (Mays, 1972). This is believed to be actively transported mRNA, and poly(A) mRNA has been detected in the nutritive tubes and subsequently the oocytes by means of *in situ* hybridization (Capco and Jeffery, 1979).

In almost all other insect orders the nurse cells, if present, are closely connected to each other and an oocyte by short ring canals, and the two cell types form an egg chamber and travel down the ovariole together. The sibling origin of the nurse cells and oocyte, following a specified number of rounds of division and incomplete cytokinesis, is more obvious in these instances and in *Drosophila* this results in an oocyte being connected to 15 nurse cells. Large numbers of maternal messages (Dubowy and Macdonald, 1998) transcribed in nurse cells pass intercellularly to very precise locations in the oocyte. *bicoid* and *oskar* mRNAs, for example, are localized to the anterior and posterior ends, respectively, of the oocyte, where they are involved in axis specification of the fly (St. Johnston and Nüsslein-Volhard, 1992). This has proved an important and popular model for studying mRNA localization.

7. Localization of *Vg1* mRNA during Oogenesis in *Xenopus*

Some 20 mRNAs have been found to localize to either the animal or the vegetal pole during *Xenopus* oogenesis (King *et al.,* 1999). Most studied is the stepwise localization of *Vg1* mRNA that starts off being homogeneously distributed within the oocyte but becomes localized to the vegetal pole. *Vg1* mRNA injected into oocytes is also localized to the vegetal cortex (Yisraeli and Melton, 1988). *Vg1* encodes a growth factor believed to be involved in diverse developmental events including right/left asymmetry, the induction of mesoderm, and endoderm specification.

8. Localization of Myelin Basic Protein mRNA in Oligodendrocytes

Myelin basic protein (MBP) mRNA has been shown to be localized to the peripheral processes of oligodendrocytes, cells which are involved in the myelination of neurons (Carson *et al.,* 1998). MBP is a major structural component of myelin membranes. Its RNA localization occurs both within the nervous system and, conveniently, *in vitro*. In cultured oligodendrocytes the processes extend into large membrane sheets which are equivalent to the unwrapped myelin sheaths surrounding axons and, as in other systems, RNA trafficking occurs in a stepwise fashion—in this case from the nucleus, to the perikaryon, into the cell processes and ultimately to the myelin compartment.

B. Visualization of mRNA Localization and Transport

The spatial distribution of polyribosomes in cells has been assessed by studying the fluorescence of the nucleic acid stain acridine orange and has been shown to be nonuniform in a variety of cell types including fibroblasts and neurons (Fulton *et al.,* 1980). Cellular distribution of RNA has also been investigated by means of autoradiography, and with suitably chosen time-course experiments not only the site of synthesis, and the transport, but also the destination of RNA can be readily monitored. Ovaries of hemipterans provide an example where autoradiography has been used effectively to plot the synthesis of RNA in polyploid nurse cells, followed by its passage along intercellular nutritive tubes into the previtellogenic oocytes (Macgregor and Stebbings, 1970). The technique has also allowed the rates of movement of RNA to be estimated.

Autoradiography, however, does not allow distinction between the different species of RNA, and studies with hemipteran ovaries have been extended by the use of *in situ* hybridization using a poly(U) probe to detect poly(A)-containing RNA. A large proportion of eukaryotic mRNAs are polyadenylated so that most of the mRNAs in the cell can be detected in this way. This technique showed an accumulation of poly(A) mRNA in the nurse cells, its presence within the nutritive tubes, and a further accumulation within the transcriptionally inactive oocytes (Capco and Jeffery, 1979). The distribution in the latter was described as homogeneous for most, but not all, of the duration of oogenesis. The same sort of probes have been used to detect the pattern of polyadenylated mRNAs over time in a number of other examples including nerve axons (Olink-Coux and Hollenbeck, 1996). However, while the detection of heterogeneous populations of mRNAs is adequate for addressing certain questions, specific probes for particular mRNAs have been widely used in *in situ* hybridization experiments (see section II) to study their distribution in an ever-increasing range of cells from a wide variety of organisms, and this clearly permits more specific questions to be addressed. Similar *in situ* hybridizations have also been carried out to detect RNAs tagged with reporter sequences using antisense reporter RNA probes. *In situ* hybridization has been carried out at the electron, as well as the light-microscopical, level, and ultrastructural *in situ* hybridization has allowed the position of mRNAs to be determined more precisely, and indeed at nanometer resolution (Bassell *et al.,* 1994a,b).

In situ hybridization provides no direct information regarding the dynamics of mRNA localization and the dye SYTO 14, which is membrane permeable and fluoresces when bound to nucleic acids, has been used to monitor and estimate the rates of movement of endogenous RNA in neuritic processes of living neuronal cells in culture (Knowles *et al.,* 1996). This dye stained migrating particles which were distinguishable from mitochondria and which were shown to contain poly(A) RNA, and more specifically β-actin mRNA, by means of *in situ* hybridization.

Using more focused labeling of mRNA, fluorescein-conjugated MBP mRNA was microinjected into oligodendrocytes and, once incorporated into particles, their movement was observed in real time (Ainger *et al.,* 1993). Similarly, fluorescently-labeled *oskar* mRNA has been injected into *Drosophila* oocytes and its movement studied (Glotzer *et al.,* 1997).

Significant advances have recently come from observing mRNA movements *in vivo* using GFP technology, and this has been based either on labeling the mRNA itself or alternatively the appropriate RNA-binding protein (see section V). In yeast, methods have been developed for indirectly tagging *ASH1* mRNA (Bertrand *et al.,* 1998; Beach *et al.,*1999), and this enabled characteristics of the movement to be monitored. GFP-labeled *ASH1* mRNA was seen, for example, by this method to be localized to the sites of polarized growth in budded cells, migrating back to the neck before cell division. Alternatively, in *Drosophila,* GFP labeling was of a protein product of the gene, *exuperantia,* known to be essential for the localization of *bicoid* mRNA to the anterior of the oocyte. In this case a GFP–Exuperantia fusion protein was expressed in the ovary, and formed particles in the nurse cells which were observed as they passed into the adjacent oocyte (Theurkauf and Hazelrigg, 1998). The movements were observed using digitally enhanced fluorescence microscopy in real time or in time-lapse sequences.

III. Factors Involved in mRNA Recognition

A. *Cis*-Acting Factors (Zipcodes)

Cis-acting sequence elements, which function in the localization of mRNAs specifying their pathways and patterns usually, but not invariably, reside in the mRNA 3′UTR. These *cis*-acting signals, which have been called "zipcodes," have been identified and analyzed in a variety of systems with experiments involving the introduction into cells of mRNA tagged with a reporter sequence, and with a range of deletions or mutations in the region of the RNA conferring localization (Bashirullah *et al.,* 1998). This has suggested that their complexity may vary with the complexity of the localization events in a particular instance.

In yeast, although the 3′UTR of *ASH1* proved sufficient to localize a reporter mRNA, three further *cis*-acting elements were found within the *ASH1* coding region, each of which when fused to a *lacZ* reporter gene, was sufficient to localize the reporter mRNA to the bud. Localization specificity, in the 3′UTR and also the coding region, depended not on sequence but on the secondary and tertiary structure of a 118-nt stem loop (Chartrand *et al.,* 1999; Gonzalez *et al.,* 1999).

In *Drosophila* oogenesis localization signals have been identified for a number of mRNAs particularly *bicoid* and *oskar*. In the case of *bicoid* mRNA a large 625nt segment of the 3′UTR was initially shown to contain the localization signal

(Macdonald and Struhl, 1988) and sequences involved were later narrowed down to a number of smaller regions including a 50-nt *bicoid* localization element (BLE1) which is involved in the early stages (Macdonald *et al.,* 1993). However, further studies showed that many deletions interfered with *bicoid* localization, indicating that localization signals consisted of a number of elements probably acting at different steps in the process. Similarly, in the case of *oskar* mRNA, multiple signals have been identified in a 1.1-kb segment of the 3′UTR which mediate distinct steps as the transcript passes from the nurse cells to the anterior of the oocyte and ultimately to its posterior (Ephrussi and Lehmann, 1992; Kim-Ha *et al.,* 1993).

The significance of the 3′UTR in mRNA localization has been illustrated in a novel way following the alternative processing of RNA derived from the *hu-li tai shao* (*hts*) gene in *Drosophila* (Whittaker *et al.,* 1999). This produces a number of transcripts within the ovary with different classes of 3′UTRs which localize differently. Three *hts* transcripts are found in the nurse cells but only one translocates to, and is localized within, the oocyte. Its localization signal was identified to the 3′UTR since when this was replaced by the 3′UTR of α-tubulin, an mRNA which is not localized at any stage of oogenesis, the transcript was not transported into the oocyte. The *cis*-acting signal for transport was identified as a 150-nt region within the 345-nt 3′UTR, although other elements proved to be necessary for anchorage of the transcript.

In fibroblasts, a fragment of the 3′UTR of *c-myc* mRNA, the localization signal, was sufficient to localize reporter sequences to the perinuclear region of transfected cells (Veyrune *et al.,* 1996). Using a transfection assay in which coding sequences for β-galactosidase were fused to sequences derived from chicken β-actin cDNA it was shown that localization of β-actin mRNA to the leading edge of fibroblasts required conserved elements in the 3′UTR including a 54-nt zipcode and a less active 43-nt segment (Kislauskis *et al.,* 1994). This was then confirmed using antisense oligonucleotides complementary to this region. Mutations or deletions of the zipcode reduced but did not totally eliminate the localization activity, suggesting, as seen with *Drosophila bicoid* mRNA, that different motifs contribute to this. Sequence analysis of the zipcode showed several regions that are conserved among β-actin mRNAs of a number of species—regions that are not present in other mRNAs (Ross *et al.,* 1997).

The same is true of *Vg-1* mRNA localization in *Xenopus* oocytes. Here the minimal requirement for localization has been studied using deletion mutants injected into oocytes showing that a 340-nt localization element was both required and sufficient for localization to the vegetal cortex (Mowry and Melton, 1992; Deshler *et al.,* 1998). More specifically, two subelements have been identified (Gautreau *et al.,* 1997). One is at its 5′ end (1–135), and another at the 3′ end (210–340) and each contains an RNA-binding protein binding site. Both are required for vegetal localization to occur, although some localization takes place solely with a duplicated 5′ subelement.

Deletion analysis and microinjection assays into oligodendrocytes have identified the *cis*-acting elements in MBP mRNA (Ainger *et al.,* 1997). This found two separate *cis*-acting signals, one of which, the RNA transport signal (RTS) comprised of 21 nucleotides is necessary and sufficient for transporting MBP mRNA along oligodendrocyte processes and another, the RNA localization signal (RLS), which is required for its localization to the myelin compartment. Both are found in the 3′UTR of the mRNA. Sequences homologous to the RTS occur in RNAs that are transported in other cells, suggesting that it may be a general transport signal. These findings were confirmed when either the RTS or the RLS were inserted into nonlocalized RNAs—a procedure that leads to transport or localization in the host cell.

Fascinatingly, in neurons the sequences located in the 3′UTR of tau mRNA, which target the transcript to axonal processes, target neuronal tau mRNA, injected into *Xenopus* oocytes, to the vegetal cortex along with *Vg1* mRNA, suggesting that similar localization mechanisms exist in the two cell types (Litman *et al.,* 1996).

Genetic and molecular dissection of these localized mRNAs including yeast *ASH1* (Chartrand *et al.,* 1999; Gonzalez *et al.,* 1999), *Drosophila bicoid* (Ferrandon *et al.,* 1997; Macdonald and Kerr, 1998), and *K10* (Serano and Cohen, 1998) and chicken fibroblast β-actin (Ross *et al.,* 1997) has pointed to the fact that no single sequence is responsible, but that a number of dispersed elements result in secondary and tertiary stem–loop structures which provide localization specificity. It is these that appear to be recognized by *trans*-acting RNA-binding proteins.

B. *Trans*-Acting Factors: RNA-Binding Proteins

Trans-acting factors that function in RNA localization include RNA-binding proteins that recognise *cis*-acting stem–loop signals of localized mRNAs, and transport them, anchor them, and control their translation. Such proteins have been identified in a number of systems and some have revealed high homology, leading to the view that the same mechanism may exist to localize different mRNAs in a range of cell types. Included is the protein which binds to the zipcode sequence in the 3′UTR of β-actin mRNA, which is localized to the leading edge of migrating fibroblasts. Band shift mobility assays, UV cross-linking, and affinity purification studies identified a protein of 68 kDa (ZBP-1) which binds to a portion of the zipcode (Ross *et al.,* 1997). Furthermore, antibodies to ZBP-1 coimmunoprecipitated other proteins of 120, and 25 kDa, suggesting that they function as part of a complex.

Xenopus Vg1 mRNA requires Vg1 RNA-binding protein (Vera) for localization to the vegetal cortex of oocytes. Vg1 RBP is a 69-kDa protein that binds to specific regions in the 3′UTR of the mRNA (Schwartz *et al.,* 1992). There has been shown to be ~78% homology between Vg1 RBP and chicken fibroblast ZBP1 and both have five RNA-binding motifs (four K homology [KH] and one RNA recognition motif [RRM]) (Deshler *et al.,* 1998; Havin *et al.,* 1998).

Further *trans*-acting RNA-binding proteins have been identified from mammalian brain which bind in assays to the MBP mRNA RTS. Most prominent of these is a 36-kDa protein, hnRNP A2, a heterologous nuclear RNA-binding protein, which immunocytochemistry has shown to be both nuclear and cytoplasmic. hnRNPs pass between the nucleus and cytoplasm, raising the possibility that the cytoplasmic localization event is initiated in the nucleus. In oligodendrocytes it was particularly seen in the processes and myelin compartments, which is in agreement with its role in cytoplasmic mRNA localization in these regions of the cell (Hoek *et al.,* 1998).

A similar hnRNP has also been found to play a prominent role in *Drosophila* oocytes. At the oocyte stage the dorsoventral axis specification of the fly involves the localization of *gurken* mRNA to the dorsal anterior region of the oocyte. This has been shown to depend on one isoform of the hnRNP homolog, Squid (Norvell *et al.,* 1999).

Drosophila has also provided the most fully studied RNA-binding protein involved in mRNA localization—Staufen. Originally identified by genetic analysis, it participates in the anterior localization of *bicoid* and the posterior localization of *oskar* mRNAs in oocytes during oogenesis, and these events determine the primary anteroposterior axis. Staufen is not, however, confined to germ cells and is also involved with the cell-cycle-specific localization of *prospero* mRNA to the ganglion mother cell during neurogenesis (Broadus *et al.,* 1998). This shows that the zipcodes of different transcripts can be recognized by the same protein.

Since its initial identification in *Drosophila,* Staufen has been shown to be a member of a family of RNA-binding proteins. Homologs from a range of invertebrates and vertebrates (including humans) have been sequenced, and the former have been shown to include five double-stranded RNA-binding domains (dsRBDs), and the latter four of these domains. These functional domains are the only regions of the proteins to be conserved (Ramos *et al.,* 2000). In humans, Staufen has been shown to be expressed in many tissues and in mammalian neurons; for example, where different mRNAs are localized to different cell processes, Staufen is compartmentalized to the cell body and the dendrites, but is absent from the axons (Kiebler *et al.,* 1999; Wickham *et al.,* 1999). Although no specific neuronal mRNA has been shown to interact with Staufen, their general occurrence has suggested that Staufen may be widely involved in mRNA localization. In elucidating the role of Staufen, one domain has been shown to be required for *bicoid* and *oskar* mRNA localization and, although it has not been demonstrated, probably binds to these directly. Another domain is involved in directing the localization of *prospero* in neuroblasts and appears to also be involved in the regulation of translation of *oskar* mRNA. A further domain, which differs from the other five in that it is split into two halves and contains an inserted loop which is also conserved, is required for the localization of *oskar* mRNA, suggesting that it links the transcript to the transport machinery (Micklem *et al.,* 2000). Interestingly, mammalian Staufen contains a MT-binding domain similar to that of MAP1

that is not found in *Drosophila* Staufen, deletion of which abolishes its interaction with microtubules (Wickham *et al.,* 1999).

Genetic analysis of *ASH1* mRNA localization in yeast has shown it to require a number of genes (*She1–She5*), one of which, *She2,* encodes an RNA-binding protein specific for *ASH1* mRNA. She2p is capable of binding independently to any one of the three zipcode localization elements and, since these show different sequences, is thought to recognize the zipcode stem–loop structure (Böhl *et al.,* 2000). It shows no sequence homology to any other RNA-binding protein.

C. Ribonucleoprotein Transport Complexes

Evidence from a number of cells and organisms including yeast, oligodendrocytes, fibroblasts, neurons, and also *Drosophila* embryos has shown that localized mRNAs, on binding to *trans*-acting proteins, may be organized into particles for transport (Bertrand *et al.,* 1998; Ainger *et al.,* 1993; Taneja *et al.,* 1992; Knowles *et al.,* 1996; Ferrandon *et al.,* 1994). This suggested that macromolecular ribonucleoprotein transport complexes form and these are likely to include a variety of *trans*-acting factors including linker and adapter proteins and components of the translational and translocational machinery (Fig. 1).

One of the first examples of the formation of mRNA granules was seen with the microinjection of labeled MBP mRNA into cultured mouse oligodendrocytes (Ainger *et al.,* 1993). Within a few minutes many hundreds of granules per cell, all approximately 0.3 μm in diameter, formed in the perikaryon of the cell. These granules traveled down the many cell processes to the cell periphery at approximately 0.2 μm/s, and this was also the first visualization of the movement of mRNA in living cells.

A similar approach was also found to produce comparable granules in *Drosophila* embryos. When *bicoid* mRNA, or its 3′UTR, was introduced into early embryos it recruited the RNA-binding protein Staufen into particles, in this case, of up to 1 μm (Ferrandon *et al.,* 1994). Particles did not form on introduction of nonlocalized mRNAs. Genetic studies have implicated a number of other genes in the localization of both *bicoid* and *oskar* mRNA, which has been shown to depend on the sequential action of Exuperantia, Swallow, and Staufen at successive stages of oogenesis. This suggests that mRNAs are complexed, perhaps transiently, with a number of proteins for transport including, of course, those that drive motility and are discussed fully in Section V. Likewise, Staufen does not function alone in the localization of *prospero* mRNA in *Drosophila* neuroblasts, but interacts with at least two of the proteins, Miranda (Shen *et al.,* 1998; Schuldt *et al.,* 1998) and Inscuteable (Li *et al.,* 1997). Functionally Miranda localizes *prospero* mRNA through its interaction with Staufen, and both have the same cellular distribution.

A Staufen appears to perform the same function in rat neurones where GFP-labeled Staufen has been shown to form into fluorescent granules for transport
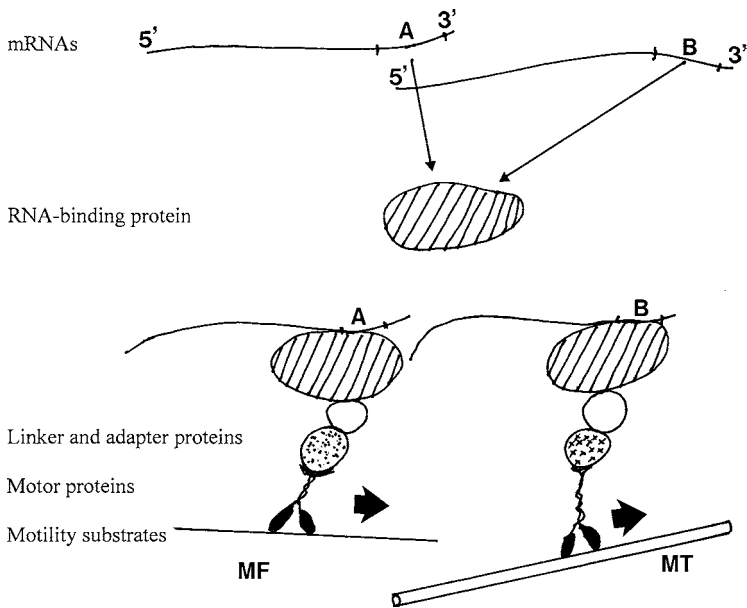
FIG. 1 Diagram showing the interaction of components within ribonucleoprotein transport complexes. Here an RNA-binding protein recognizes an mRNA, or indeed different mRNAs, and then is linked via an adaptor protein(s) to an appropriate motor protein (myosin, kinesin, or dynein) which drives movement of the complex along either microfilaments (MF) or microtubules (MT). Components of mRNA transport complexes have been identified and characterized to varying degrees in different systems (see text).

along dendrites (Köhrmann *et al.,* 1999). Importantly, too, experiments with anti-MT agents have indicated that MTs are required for the actual assembly of the Staufen-containing particles, as well as their transport—the subject of section IV.

Although considerable progress has therefore been made in identifying candidate components within transport complexes from a number of systems the discovery of their full spectrum of proteins clearly requires biochemical analysis. In the first of such studies Wilhelm and coworkers (2000a) isolated mRNA transport complexes from *Drosophila* ovaries for biochemical analysis. Following differential centrifugation of extracts from *Drosophila* ovaries they sought to identify the fraction containing the Exuperantia protein, already discussed, and found it to be in a much heavier fraction than would be expected for the monomeric protein. This suggested that the increased size of the particles could be due to Exuperantia being complexed with other proteins as well as with RNA. Analysis of the Exuperantia-containing fraction showed that it contained at least seven proteins as well as *oskar* mRNA, although surprisingly *bicoid* mRNA was not detected. RNase treatment reduced its size considerably, to Exuperantia and one other

protein—Yps, an RNA-binding protein believed to have a role in the repression of translation. This approach showed that at least one other protein interacted directly with Exuperantia. The role of the remaining proteins is still to be determined. From these studies a model was formulated in which Exuperantia, although probably not binding directly to the mRNA, is a core component of the RNA translocation complex, and since it is known that Exuperantia has a role in the localization of different transcripts to different regions of the oocyte, the model suggests that a sorting process must occur once the complex arrives in the oocyte from the nurse cells.

In the most completely characterized example yeast *ASH1* RNP particles move from mother to daughter cells. Their formation has been shown to be dependent upon stem–loop structures in the mRNA (Deshler *et al.,* 1998) and they have been found to contain a family of proteins including She2p, She3p, and She1p— a myosin motor (Takizawa and Vale, 2000). The interaction of these proteins, and regions of these proteins, has been investigated in two-hybrid interaction assays, and coprecipitation experiments revealed that She2p associates with *ASH1* mRNA independently of the other components of the particles. This association, however, is reinforced by She3p, and She3 is believed to be a bridge between the *ASH1* mRNA–She2 complex and She1, a myosin motor (Böhl *et al.,* 2000). However, as pointed out, these may not be the only components of the particle complex.

IV. Microtubules and Microfilaments: Substrates for mRNA Transport

A. mRNA-Cytoskeletal Associations

Appreciation of an affiliation between the cytoskeleton and mRNA predates comprehension that the cytoskeleton is involved in mRNA localization. It was based on the fact that when cytoskeletons are extracted from cells by treatment with nonionic detergents such as Triton X-100 a large proportion of the cell's RNA is found in the cytoskeletal fraction (Hesketh and Pryme, 1991). More specifically, hybridization studies have shown localized mRNAs to be enriched in cytoskeletal extracts from many systems, including *Xenopus* (Yisraeli *et al.,* 1990) and *Drosophila* oocytes (Pokrywka and Stephenson, 1994). In some cases attempts were made to differentiate between the cytoskeletal elements involved by applying anti-microfilament or anti-MT agents such as cytochalasin or colchicine, prior to assessing the release of mRNA from the cytoplasmic matrix depleted of either microfilaments or MTs. In other cases, taxol-isolated MTs have been prepared from homogenates of, for example, *Xenopus* oocytes and these have been shown to be enriched in the localized mRNA, *Vg1* (Elisha *et al.,* 1995). It has also been possible in at least one instance, the ovarian nutritive tubes of *Notonecta* (Stephen *et al.,* 1999),

to demonstrate mRNA attached to native MTs dissected from the ovaries. These findings of localized mRNA attached to isolated cytoskeletal organelles have been supported by ultrastructural *in situ* hybridization, which has shown labeled RNA colocalized with MTs in some cells and microfilaments in others (Bassell *et al.,* 1994a,b).

Regarding the nature of the association between mRNA and the cytoskeleton, as has been discussed there is considerable evidence that this involves RNA-binding proteins since there are many instances reported of the latter being linked either directly or indirectly to the cytoskeleton. *Xenopus* Vg1 RNA-binding protein, for example, has been shown to mediate the association of *Vg1* mRNA with MTs in oocytes (Elisha *et al.,* 1995). Similarly, mammalian Staufen, which possesses a MT-associated protein (MAP)-binding site, attaches to microtubules *in vitro* (Wickham *et al.,* 1999). A Staufen-like protein also attaches to native ovarian nutritive tube microtubules from *Notonecta* and does so in a nucleotide-dependent fashion, suggestive of a motor protein-mediated mechanism (Hurst *et al.,* 1999).

B. Evidence of a Role for Microtubules and Microfilaments in mRNA Transport

While the demonstration of an association between mRNA, RNA-binding proteins, and the cytoskeleton pointed to a role for the different cytoskeletal elements in mRNA transport and localization, pharmacological experiments involving the application of anti-MT and anti-microfilament agents to living systems confirmed this. These experiments are not always possible as in some cases the cytoskeletal elements are stable and unaffected by the drugs. However, where they have been carried out successfully they have been very telling. The feeding of the antimitotic agent, colchicine, to *Drosophila* resulted in the depolymerization of the MT system within the egg chambers with the result that maternal mRNAs were not correctly localized within the oocytes (Pokrywka and Stephenson, 1991). Similarly in *Xenopus,* the application of anti-MT agents resulted in the failure of mRNAs to localize correctly within the oocytes (Elisha *et al.,* 1995). RNA translocation was also shown to be inhibited when oligodendrocytes are treated with anti-MT agents, but was unaffected by anti-microfilament treatments (Carson *et al.,* 1997).

Intriguingly, in neurons the anti-MT agent colchicine prevented the localization of β-actin mRNA to the growth cones, whereas treatment of fibroblasts with cytochalasins—agents that prevent the polymerization of actin filaments—resulted in β-actin mRNA being incorrectly localized, showing that two different mechanisms can localize the same RNA in different cell types.

Genetic studies have also been useful. Mutations in actin, profilin, and tropomyosin all prevented *ASH1* RNA localization in yeast, pointing to a role for a microfilament system (Long *et al.,* 1997). Microtubules were found not to be involved in this instance because tubulin mutations had no effect.

By contrast, perturbation of the MT system in certain *Drosophila* mutants results in an abnormal localization of mRNAs in the oocyte. In *gurken* mutants, for example, the microtubule arrangements have aberrant polarity (Gonzalez-Reyes *et al.,* 1995), and this correlates with the atypical localization of transcripts.

Direct observations following the introduction of mRNAs into cells has more closely implicated the cytoskeleton with mRNA transport and localization. The particles which formed when MBP mRNA was introduced into cultured oligodendrocytes were nonextractable with nonionic detergents, aligned themselves into tracks along MTs and moved toward the cell periphery at 0.2 μm/s. Similarly, those that form on recruitment of Staufen when *bicoid* mRNA was introduced into *Drosophila* embryos chambers did so in a MT-dependent fashion and then moved along MTs at rates equivalent to active transport recorded by membrane-bound vesicles in other systems (Ferrandon *et al.,* 1994). In a comparable study, the dynamics of Staufen behavior was investigated in mammalian neurons transfected with a Staufen–GFP fusion protein. Here Staufen recruitment into granules and translocation into dendrites was observed directly and shown to be dependent on MTs (Kohrmann *et al.,* 1999). By contrast, the Staufen-dependent movement of *prospero* mRNA in *Drosophila* neuroblasts depends on actin filaments, showing that the same RNA-binding protein can be translocated by different mechanisms in different tissues. In each case the movements were suggestive of motor-driven transport, the subject of the following section.

C. The Organization of the Cytoskeleton as Substrates for mRNA Transport

Since cytoskeletal elements are capable of acting as substrates for mRNA transport and localization it is important to appreciate the way they are organized within the cell. Fortuitously, the organization of the cytoskeleton in many of the model systems discussed in section II (see Fig. 2 in the color insert) had been elucidated well before its equation with mRNA transport and localization. This was because of investigations into the role of the cytoskeleton in the development and maintenance of cell asymmetry as well as in different forms of cell motility, and particularly the transport of membrane-bound organelles and vesicles. Since the discovery of MTs and microfilaments in cells their arrangements had been investigated by electron microscopy where this was possible, but most successfully by immunocytochemistry, where the different cytoskeletal elements could be portrayed and their interrelationships deduced in a single preparation.

The heteropolymeric substructure of MTs leading to their defined polarity is well known, as is the way that in most instances they derive from a MT organizing center (MTOC) (Tucker, 1984). Similarly with actin microfilaments, the bundles and networks that these polar polymers form in the cytoplasm and their positioning relative to general cell morphology particularly during cell migration have become

clearer (Mitchison and Cramer, 1996). In addition, the interrelationships between the different cytoskeletal elements and the proteins which mediate interactions between them are increasingly well appreciated (Langford, 1995).

As is well known, MTs and microfilaments are both capable of dynamic behavior, so that while in certain systems the MTs and microfilaments are long-lived and stable, in others they are dynamically unstable (Mitchison and Kirschner, 1984; Pollard and Cooper, 1986; and see Cassimeris *et al.,* 1987), showing constant depolymerization and repolymerization, resulting in continual rearrangements.

In most animal cells the MT complement of the cell derives from an MTOC close to the nucleus, and MTs radiate outward with their plus ends toward the cell periphery and their minus ends embedded in the MTOC. Anterograde movement along the MTs is therefore toward the cell membrane with retrograde movement toward the nucleus. The same arrangement holds essentially for highly asymmetric cells such as neurons, where the MTOC is close to the nucleus in the cell body, and MTs run the length of the greatly extended axons as well as the dendritic processes. In axons lengths of MTs derived from the MTOC are believed to overlap, and all show the regular polarity, with their plus ends toward the synapse and their minus ends toward the cell body, whereas in dendrites there is an anomaly, since MTs showing both polarities are found in these processes (Baas *et al.,* 1988). The axonal cytoskeleton is not exclusively MTs as actin microfilaments and intermediate neurofilaments are also found, and there is considerable debate as to how slow axonal transport delivers these cytoskeletal structures into the axon (see Brown, 2000). In neuronal growth cones there is a complex array of actin filament networks, the dynamic behavior of which is fundamental to growth cone extension. A similar array of filaments is found in lamellipodia of fibroblasts, and these flattened portions of migrating cells appear to function in the same way as the extending growth cone.

Perhaps because oocytes are so large the arrangements of the cytoskeleton within them has been particularly difficult to determine. In *Drosophila* oogenesis a number of studies have shown that a single MTOC is seen located at the posterior of an oocyte in early egg chambers. In these instances MTs run forward from the MTOC toward the anterior of the oocyte, and then intercellularly through the ring canals into the adjacent nurse cells. As oogenesis progresses, however, the MTOC itself migrates forward to the anterior of the oocyte with the result that the intercellular MTs are retained as previously, but further MTs form to extend backward toward the posterior of older oocytes (Theurkauf *et al.,* 1992, 1993; Cooley *et al.,* 1994).

This intercellular MT system is very greatly exaggerated in the ovaries of hemipteran insects. In insects such as *Notonecta,* the back-swimmer, the nurse cells within an ovariole are retained anteriorly while the developing oocytes progress backward to form a chain. While doing so, at least for a period during oogenesis, the oocytes remain connected to the anterior synthetic nurse cells by way of an extending nutritive tube. Nutritive tubes contain many thousands of MTs (Macgregor and Stebbings, 1970), all of the same polarity (Stebbings and Hunt, 1983), and

these are believed to support the nutritive tube from collapse, to function as a sieve against entry and nonspecific transport of large cellular components into the oocyte from the nurse cells, but most importantly to act as substrates for directed motor protein-driven transport (Anastasi *et al.,* 1990).

In *Xenopus* oocytes the microtubules initially appear to emerge radially from around the germinal vesicle. However, as development proceeds MTs concentrate and form a complex web on the vegetal side of the germinal vesicle (Robb *et al.,* 1996). This network of MTs has been described as having no obvious organization, and therefore it is difficult to assess how these provide polarized tracks for translocation toward the vegetal pole.

Cytoskeletal arrangements in budding yeast, *S. cerevisiae,* have been investigated using anti-actin antibodies and fluorescent phalloidin to detect microfilaments and anti-tubulin to observe MTs (Kilmartin and Adams, 1984). The former highlighted fibers of varying thickness, believed to be bundles of microfilaments, extending from the mother cells into newly formed buds, with actin-staining dots at the tips of the buds. The authors suggested that the dots might play a role in determining the orientation of the actin filaments in the mother cell and, significantly as far as the present discussion is concerned, that the filament bundles might be involved in the translocation of material into the bud. Bundles of cytoplasmic MTs were also seen at both ends of the intranuclear spindle at appropriate stages of the cell cycle.

V. Molecular Motors and RNA Transport

A. The Active Transport of mRNA and Colocalization of Transported mRNA and Motor Proteins

Since RNA has been seen to be actively transported along MTs in some cells and microfilaments in others the assumption has been that it is driven by the molecular motors, kinesin, dynein, or myosin, depending on the direction of transport and the substrate involved, as has been shown for a range of membrane-bound organelles in a variety of cell types (Goodson *et al.,* 1997; Lane and Allan, 1998). Extensive studies have shown that kinesin comprises a superfamily of motor proteins, kinesin, and a large number of kinesin-like proteins (KLPs) which share a highly conserved motor domain, but show variability in the remainder of the molecule (see Moore and Endow, 1996; Hirokawa, 1998). All but one subfamily are MT plus-end-directed motors. There are at least two subclasses of cytoplasmic dyneins, both MT minus-end-directed motors (see Vaisberg *et al.,* 1996). Multiple classes of myosins also exist (see Mooseker and Cheney, 1995). Many of these different groups of motors drive the movements of membrane-bound organelles and compartments in cells, while others are involved in the functioning of the mitotic spindle. With this

sizeable number of motors the question of whether different members of the motor families transport specific organelles and, if so, which ones has proved difficult to address (see Goodson *et al,* 1997). There is some evidence, for example, of individual members of a motor family being tissue-specific (Okada *et al.,* 1995) and also organelle-specific (Nangaku *et al.,* 1994), and one class of kinesins, MT minus-end-directed motors, appears to be limited to the spindle.

Regarding mRNA translocation, the concept of one member of a motor family being specific for the transport of a particular transcript seems unlikely and, with one exception, an appreciation of which motor is involved in the transport of a message in a particular system would appear to be some way off. Indeed, evidence for motors transporting mRNA in cells at all has been difficult to obtain.

The original indication of a role for motor proteins in mRNA transport came from their accumulation at sites of mRNA localization. Dynein, for example, was shown to accumulate in *Drosophila* oocytes, rather than the nurse cells with which they are connected, at sites of, and coincident with, the localization of mRNAs (Li *et al.,* 1994). Interpretation of this result was difficult, however, since the mRNA localization still occurred in flies with mutations in the cytoplasmic dynein heavy chain gene (McGrail and Hays, 1997). In a further example a kinesin–β-galactosidase fusion protein was seen to colocalize with *oskar* mRNA at the posterior of late *Drosophila* oocytes (Clark *et al.,* 1997).

Further indications of motor-driven mRNA translocation also came from studies of *in vivo* movement of mRNA-containing particles. In oligodendrocytes these were seen to occur with the characteristics and rates suggestive of kinesin-driven transport (Ainger *et al.,* 1993). Investigations into the movement in *Drosophila* ovarioles of a GFP–Exuperantia fusion protein, which could be a component of *bicoid*-containing ribonucleoprotein particles, showed it to take place in a stepwise fashion. This pointed to the possible action of a number of different microtubule motors during transport of mRNA from the nurse cells to the oocyte (Theurkauf and Hazelrigg, 1998).

B. Microtubule Motors and mRNA Transport

The importance of not only MTs, but also a kinesin motor for the translocation of MBP mRNA in oligodendrocytes was shown following the suppression of kinesin expression using anti-sense oligonucleotides (Carson *et al.,* 1997). In addressing a role for motor proteins data showing a physical association between a motor and mRNA appeared crucial. To this end indirect evidence for the association role of a motor protein with mRNA has come from studies investigating the binding of poly(A) RNA to MT bundles isolated from the ovarian nutritive tubes of *Notonecta* (see section II). These showed that the attachment of the RNA to the MTs is nucleotide-sensitive, a property consistent with a motor protein-mediated interaction between the RNA and the MTs. Moreover the pattern of nucleotide

sensitivity was more consistent with a kinesin-mediated interaction in this case, and immunocytochemistry showed that a kinesin was indeed present in this system (Stephen *et al.,* 1999). This was not to suggest that the poly(A) RNA is attached directly to the motor protein, and significantly a Staufen-like RNA-binding protein has been shown to be associated with the same MT bundle and with the same profile of nucleotide-sensitivity as the RNA (Hurst *et al.,* 1999). These findings are consistent with a hypothesis in which RNA is bound to Staufen, which in turn is attached directly or indirectly to a MT motor protein (probably a kinesin), which drives the complex along the MT substrate.

Recent work has supported this hypothesis in which, for transport, transcripts associate indirectly with a motor protein, and evidence for this has come from binding studies to the putative RNA-binding protein, Swallow, one of the proteins essential for the localization of *bicoid* mRNA at the anterior of a *Drosophila* oocyte (Schnorrer *et al.,* 2000). Swallow functions as soon as *bicoid* mRNA reaches the oocyte from the nurse cells and Swallow mutants show a phenotype similar to ovaries treated with anti-MT agents (see section VII). In these *bicoid* mRNA is spread throughout the oocyte. Schnorrer and coworkers (2000) showed that the anterior localization of *bicoid* mRNA in the oocyte depended on the anterior localization of Swallow, particularly its C-terminus, but that the dependency was not reciprocal. Experiments with colchicine illustrated that the anterior localization of Swallow depended on MTs, and even more importantly that the correct localization depended on the polarity of the MTs, since mislocalization occurred in mutants in which normal polarity was disturbed. Using yeast two-hybrid screens to investigate binding partners of Swallow, screening *Drosophila* ovarian cDNA with Swallow, they were able to identify clones that encode the light chain of dynein, the retrograde MT motor. The same binding was observed in reciprocal assays, and taking this further, with random fragments of *swallow* cDNA the coiled coil domain in the center of the molecule was found to be the region responsible for the interaction. These studies appeared to be the first to implicate dynein in the localization of *bicoid* mRNA to the anterior of the *Drosophila* oocyte, and this is certainly consistent with the fact that the MTOC and hence the minus ends of the MTs are positioned similarly.

Conversely, the plus ends of the MTs are toward the posterior of the oocyte in *Drosophila,* so that a plus-end-directed motor would be required to transport *oskar* mRNA to the posterior pole. A candidate for this has come from studies of *Drosophila* mutant females lacking the kinesin heavy chain (KHC). These progress through oogenesis but fail in embryogenesis (Brendza *et al.,* 2000) and while in *Khc*-null oocytes the anterior localization of *bicoid* mRNA was found to be normal the localization of *oskar* to the posterior of the oocyte did not take place and, having passed from the nurse cells to the oocyte this transcript traveled no further. In confirmatory experiments the normal localization of *oskar* mRNA to the oocyte posterior could be rescued by a wild-type *Khc* transgene, indicating again that kinesin could transport *oskar* mRNA along MTs toward their plus ends at

the posterior pole. Interestingly, complementary experiments showed that kinesin was also needed for the transport of Staufen as well as *oskar* mRNA and this is consistent with the Staufen and *oskar* mRNA forming complexes for transport (Brendza *et al.,* 2000). The same study, however, has indicated that Staufen and kinesin may not be linked directly (see also section VI).

In *Xenopus* there is an aggregation toward the vegetal half of the egg of specialized cytoplasm, the germ plasm, which among other components contains several mRNAs including *Vg1* (Forristall *et al.,* 1995). Studies with inhibitors have shown that this aggregation requires MTs (Ressom and Dixon, 1988). A group four of KRPs have been identified in *Xenopus* oocytes, two of which are required for mitosis, but one (Xklp1) being required for the localization of germ plasm (Robb *et al.,* 1996). Whether this kinesin directly or indirectly transports mRNA remains to be determined.

C. Myosin Motors and mRNA Transport

As mentioned previously, there is good evidence for the involvement of one specific motor protein in mRNA localization—that of *ASH1* mRNA in budding yeast. This transcript has been shown to translocate along actin filaments, driven by a myosin motor. More specifically, genetic analysis involving the deletion of one of the two Class V unconventional myosin genes in the cell, Myo4p, results in defects in the transport component of *ASH1* mRNA localization. In investigating evidence for an association between Myo4p and *ASH1* mRNA, Münchow and coworkers (1999) found that these colocalize in the cell and also coimmunoprecipitate. Moreover the colocalization and *in vivo* association depended on additional proteins, two of a group of She proteins, also shown to be necessary for proper localization of *ASH1* mRNA (Long *et al.,* 1997). As previously discussed, it has recently been shown that She2p binds to the mRNA, and that She3p then links She2p to the myosin motor for translocation (Böhl *et al.,* 2000). Other She proteins may be involved in assembling mRNA into particles for transport (Section III) and in regulating RNA translation (Section VI).

In further cases of RNA translocation along actin filaments, such as the Staufen-dependent localization of *prospero* mRNA in *Drosophila* neuroblasts, it is presumed that the transport is driven by myosin, although this has not yet been shown.

VI. Anchorage and Translation of mRNA

mRNA localization and translation are often closely linked, with translation being repressed during translocation and activation on reaching its destination. This

serves to localize gene expression to focused regions of the cytoplasm. Elements within the 3′UTR are involved in the repression of translation and, for example, in *Xenopus* oocytes the translation of *Vg1* mRNA is repressed during its translocation to the vegetal pole by the binding of a 38-kDa protein to a 350-nt sequence within the 3′UTR. The latter is distinct from the localization element. On reaching the vegetal pole the mRNA translation is derepressed, and the protein is expressed (Wilhelm *et al.,* 2000b).

Similar site-specific derepression of translation has been investigated in the case of localized myelin basic protein mRNA in oligodendrocytes. In this case the *cis*-acting RNA transport signal positioned in the 3′UTR together with *trans*-acting hnRNP A2, which are essential for localization, were found to also enhance translation of the message on reaching its destination. Here they did so via their interactions with proteins bound to the 5′ cap of the mRNA (Kwon *et al.,* 1999).

The 5′ end of the transcript has also been found to be involved with the regulation of translation of certain messages during *Drosophila* oogenesis. In the case of *bicoid* mRNA translation is repressed in passage between the nurse cells and the anterior of the oocyte, and this has been shown to be linked to the length of the poly(A) tail (Sallés *et al.,* 1994). This contrasts with other transcripts, such as *oskar* mRNA, which are translationally repressed until localized to the posterior of the oocyte, the repression of translation depending on sequences in the 3′UTR and involving RNA-binding proteins (Kim-Ha *et al.,* 1993). These include Bruno (Kim-Ha *et al.,* 1995) and a 50-kDa protein (p50) (Gunkel *et al.,* 1998). Derepression of translation is actively mediated by elements in the 5′ region of the mRNA once it reaches the posterior of the oocyte.

It has been postulated that, following translocation in cells, mRNAs might be anchored by attachment to the cytoskeleton (Wilhelm and Vale, 1993). Experiments with cytoskeletal inhibitors have shown that in *Xenopus* oocytes, for example, while the translocation of mRNA requires MTs, the anchoring of the message depends on microfilaments (Yisraeli *et al.,* 1990), and more direct evidence is now emerging for this. p50 is a universal protein in pro- and eukaryotes and is abundant in messenger ribonucleoprotein particles (mRNPs), where it is thought to contribute to the mRNA packaging while at the highest concentrations, and as already mentioned, it acts as a translational repressor. Yeast two-hybrid screens have shown actin to be a binding partner for p50, and *in vitro* binding assays have shown a high affinity between p50 and actin. Further, the strength of the interaction is mRNA-dependent and strongest at low p50/mRNA ratios when translation was not repressed (Ruzanov *et al.,* 1999). As the authors point out, this is consistent with p50 providing a molecular bridge between mRNA and the actin cytoskeleton at the destination and site of translation of the localized mRNA.

The anchorage or docking function in the case of yeast *ASH1* mRNA to cortical sites in the tip of the daughter bud would appear to be via the association of She5 protein with the actin cytoskeleton. In *She5* mutants the mRNA translocates from the mother cell into the bud but fails to anchor (Beach *et al.,* 1999).

As well as being attached to microfilaments the possibility also exists that in some cases mRNA might be anchored to MTs. In support of this, protein complexes from PC12 cells that bind RNA have been found to contain a MAP, MAP1A. In addition therefore to being involved in the regulation of translation, the MAP component of the complex would imply an attachment to MTs (DeFranco *et al.,* 1998). The MAP1-like binding domain on mammalian Staufen (Wickham *et al.,* 1999) may serve the same function.

VII. Concluding Remarks and Perspectives

As will have been seen, the transport and localization of mRNAs in cells depends on different cytoskeletal elements in different cell types. In some instances, such as in yeast, actin microfilaments and myosin are clearly the key machinery while in others, such as *Drosophila* oogenesis, MTs and MT motors play this role. Neither is there always likely to be a distinct dichotomy of function, since a similar situation may exist to that of membrane transport in nerve axons, which takes advantage of both MT and microfilament systems, relying on MTs for long-range transport, and microfilaments for shorter distances (Langford, 1995). Indeed, there is good evidence in some examples of cooperation between cytoskeletal elements in mRNA localization, with translocation of mRNA being sensitive to MT inhibitors and anchorage of that same mRNA being disrupted by inhibitors of microfilaments (Yisraeli *et al.,* 1990). It is also possible that mRNA could translocate along MTs driven by a MT motor and ultimately be anchored to MTs via a MAP.

Consideration of cytoskeletal-based translocation has necessarily to take account of the arrangements of MTs and microfilaments in cells, which is often well known, and the fact that both polymers have intrinsic polarity, which is recognized by the motor proteins that use them as substrates for transport. The directionality of motor movements is well understood so that, for example, knowing the arrangement and polarity of MTs in a particular system allows the prediction of the involvement of a plus- or minus-end-directed MT motor.

Identification of the motors responsible for the translocation of membranous organelles has not proved trivial, and similar but even greater difficulties are being experienced in determining which motor transports an mRNA. Inhibitor treatments for motor driven transport are sometimes telling but may not be sufficiently specific, and experiments with function-blocking antibodies have proved difficult to interpret (Lane and Allan, 1998). Observations of colocalization have given some indication of the involvement of a motor in the translocation of a message, but such observations have limited value and may certainly be incomplete since it has been found that even single motor molecules are sufficient to drive movement (Wang *et al.,* 1995).

In determining which motor is involved in RNA translocation, genetic approaches involving gene deletion and the expression of mutated proteins have started to be extremely valuable and focused, and indeed have allowed the indentification of the myosin motor involved in translocation of an mRNA in yeast (Bloom and Beach, 1999). However, results from these methods are sometimes difficult to interpret unambiguously, as has been found with mutated dynein heavy chains in *Drosophila* oogenesis (McGrail and Hays, 1997). *In vitro* reconstruction and reactivation, as a means of probing and understanding underlying mechanisms, has been the aim for many motile systems, but clearly necessitates a full appreciation of all the interacting components, as well as the regulatory mechanisms that function *in vivo*. This will be the ultimate aim of those studying mRNA translocation in different systems.

Aside from the identification of the motor involved in the translocation of a particular RNA, the mechanism of targeting a motor to a particular cargo is also an important question. The specificity of motor proteins for different membranous cargoes has been addressed and different organelles have been shown to possess unique members of the kinesin family (Hirokawa, 1996), and possibly unique dyneins (Vaisberg *et al.,* 1996). The basis of this, however, has yet to be resolved. There is evidence that the membrane protein kinectin may act as a receptor for kinesin and the multiprotein complex dynactin, which is an activator of cytoplasmic dynein-driven membrane movement, may also act as a dynein receptor (see Vallee and Sheetz, 1996). By contrast, during spindle function the chomosomal DNA appears to bind direcly to the kinesin, chromokinesin (Afshar *et al.,* 1995), although a direct attachment of motor to nucleic acid is unlikely in the case of mRNA translocation. Indeed, as discussed, there are well-documented examples of transcripts being bound to proteins which attach directly, or more usually indirectly, to both microfilament and MT motors for translocation. In the most fully investigated example yeast *ASH1* mRNA bound to She2p has been shown to associate via other proteins with a myosin for transport along microfilaments (Böhl *et al.,* 2000). A parallel can also be drawn with the RNA-binding protein Staufen, which is involved in the localization of *bicoid* and *oskar* mRNA in *Drosophila* ovaries. Staufen has been shown to be recruited by the transcript for translocation along and has been shown to attach to MTs in a nucleotide-dependent fashion typical of a motor-mediated interaction. This attachment may be indirect via a number of protein linkers. This is certainly supported by analysis of mRNA transport particles which have been shown to contain a complex of proteins (Wilhelm *et al.,* 2000a). A further aspect that is clear is that an RNA-binding protein has the ability to identify different mRNA cargoes, as seen in the case of Staufen and *bicoid* and *oskar* mRNAs.

With membrane transport, especially in instances where bidirectional movements occur, some studies have suggested the temporary recruitment of a motor for translocation, although increasing evidence has pointed to organelles possessing different directional motors simultaneously with regulation being achieved

by phosphorylation which differentially influences opposing motors (Reese and Haimo, 2000). The situation appears to be complicated, however, since in nerve axons for example antibody blocking experiments and mutational approaches have shown that interference with one motor disrupts both anterograde and retrograde movements, suggesting that although the different motors do not interact they appear to be interdependent (Martin *et al.,* 1999).

With mRNA movements, it is most unlikely that a particular transcript would be required to move in opposing directions along the cytoskeleton, simultaneously or otherwise. However, RNA-binding proteins such as Staufen and ZBP-1 are capable of mediating RNA localization by microtubule or microfilament-dependent mechanisms in different systems (Oleynikov and Singer, 1998; Havin *et al.,* 1998). This shows that they are able to interact with two different localization mechanisms and must either have binding motifs for microtubule and microfilament motors or, more probably, form macromolecular particles containing different motor subunits.

With this complexity of interactions it will not be easy to unravel the regulatory mechanisms involved in precise and coordinated translocation of the many different transcripts to their varied cellular destinations. Regarding regulation, there is a wealth of evidence for phosphorylatory control of motor activity of both kinesin (McIlvain *et al.,* 1994; Lindesmith *et al.,* 1997) and dynein (Allan, 1995; Runnegar *et al.,* 1999). It is possible, too, that changes in phosphorylation might affect the association of motors with *trans* acting proteins in the same way that such changes influence motor associations with membranes (Sato-Yoshitake *et al.,* 1992; Niclas *et al.,* 1996). Still further, the discovery that the level of phosphorylation modulates the association between localized mRNAs and RNA-binding proteins (Chen *et al.,* 1997) suggests that phophorylation/dephosphorylation mechanisms may regulate mRNA translocation at a number of levels, and deciphering these will provide significant challenges for the future.

Acknowledgment

References

Afshar, K., Barton, N. R., Hawley, R. S., and Goldstein, S. L. B. (1995). DNA binding and meiotic chromosomal localization of the *Drosophila* Nod kinesin-like protein. *Cell* **81,** 129–138.

Ainger, K., Avossa, D., Diana, A. S., Barry, C., Barberese, E., and Carson, J. H. (1997). Transport and localization elements in myelin basic protein mRNA. *J. Cell Biol.* **138,** 1077–1087.

Ainger, K., Avossa, D., Morgan, F., Hill, S. J., Barry, C., Barberese, E., and Carson, J. H. (1993). Transport and localization of exogenous myelin basic protein mRNA injected into oligodendrocytes. *J. Cell Biol,* **123,** 431–441.

Allan, V. (1995). Protein phosphatase 1 regulates the cytoplasmic dynein-driven formation of endo-plasmic reticulum networks *in vitro*. *J. Cell Biol.* **128,** 879–891.

Anastasi, A., Hunt, C., and Stebbings, H. (1990). Isolation of microtubule motors from an insect ovarian system: Characterization using a novel motility substratum. *J. Cell Sci.* **96,** 63–69.

Bass, P. W., Deitch, J. S., Black, M. M., and Banker, G. A. (1988). Polarity organization of microtubules in hippocampal neurons: Uniformity in the axon and nonuniformity in the dendrite. *Proc. Natl. Acad. Sci. USA* **85,** 8335–8339.

Bashirullah, A., Cooperstock, R. L., and Lipshitz, H. D. (1998). RNA localization in development. *Annu. Rev. Biochem.* **67,** 335–394.

Bassell, G. J., Powers, C. M., Taneja, K. L., and Singer, R. H. (1994a). Single mRNAs visualized by ultrastructural *in situ* hybridization are principally localized at actin filament intersections in fibroblasts. *J. Cell Biol.* **126,** 863–876.

Bassell, G. J., Singer, R. H., and Kosik, K. S. (1994b). Association of poly(A) mRNA with microtubules in cultured neurons. *Neuron* **12,** 571–582.

Beach, D. L., Salmon, E. D., and Bloom, K. (1999). Localization and anchoring of mRNA in budding yeast. *Curr. Biol.* **9,** 569–578.

Bertrand, E., Chartrand. P., Schaefer, M., Shenoy, S. M., Singer, R. H., and Long, R. M. (1998). Localization of *ASH1* mRNA particles in living yeast. *Mol. Cell* **2,** 437–445.

Bloom, K., and Beach, D. L. (1999). mRNA localization: motile RNA, asymmetric anchors. *Curr. Opin. Microbiol.* **2,** 604–609.

Bobola, N., Jansen, R.-P., Shin, T. H., and Naysmyth, K. (1996). Asymmetric accumulation of Ash1p in postanaphase nuclei depends on a myosin and restricts yeast mating-type switching to mother cells. *Cell* **84,** 699–709.

Böhl, F., Kruse, C., Frank, A., Ferring, D., and Jansen, R.-P. (2000). She2p, a novel RNA-binding protein tethers *ASH1* mRNA to the Myo4p myosin motor via She3p. *EMBO J.* **19,** 5514–5524.

Brendza, R. P., Serbus, L. R., Duffy, J. B., and Saxton, W. M. (2000). A function for kinesin 1 in the posterior transport of *oskar* mRNA and Staufen protein. *Science* **266,** 590–596.

Broadus, J., Fuerstenberg, S., and Doe, C. Q. (1998). Staufen-dependent localization of *prospero* mRNA contributes to neuroblast daughter-cell fate. *Nature* **391,** 792–795.

Brown, A. (2000). Slow axonal transport: Stop and go traffic in the axon. *Nat. Rev. Mol. Cell Biol.* **1,** 153–156.

Capco, D. G., and Jeffery, W. R. (1979). Origin and spatial distribution of maternal RNA during oogenesis of an insect, *Oncopeltus fasciatus. J. Cell Sci.* **39,** 63–76.

Carson, J. H., Kwon, S. J., and Barbarese, E. (1998). RNA trafficking in myelinating cells. *Curr. Opin. Neurobiol.* **8,** 607–612.

Carson, J. H., Worboys, K., Ainger, K., and Barbarese, E. (1997). Translocation of myelin basic protein mRNA in oligodendrocytes requires microtubules and kinesin. *Cell Motil. Cytoskel.* **38,** 318–328.

Cassimeris, L. U., Walker, R. A., Pryer, N. K., and Salmon, E. D. (1987). Dynamic instability of microtubules. *BioEssays* **7,** 149–154.

Chartrand, P., Meng, X. H., Singer, R. H., and Long, R. M. (1999). Structural elements required for localization of *ASH1* mRNA and a GFP reporter particle *in vivo*. *Curr. Biol.* **9,** 333–336.

Chen, S-M., Su, C., and Yang, U-C. (1997). Phosphorylation can modulate the association of different sets of RNA binding proteins with the *Vg1* localization signal RNA. *Biochem. Biophys. Res. Commun.* **234,** 419–423.

Clark, I., Ruohola-Baker, H., Jan, L. Y., and Jan, Y. N. (1995). Transient posterior localization of a kinesin fusion protein reflects anterior-posterior polarity of the *Drosophila* oocyte. *Curr. Biol.* **4,** 289–300.

Cooley, L., and Theurkauf, W. E. (1994). Cytoskeletal functions during *Drosophila* oogenesis. *Science* **266,** 590–596.

DeFranco, C., Chicurel, M. E., and Potter, H. (1998). A general RNA-binding complex that includes the cytoskeleton-associated protein MAP1A. *Mol. Biol. Cell* **9,** 1695–1708.

Deshler, J. O., Highett, M. I., and Schnapp, B. J. (1998). A highly conserved RNA-binding protein for cytoplasmic RNA localization in vertebrates. *Curr. Biol.* **8,** 489–496.

Dubowy, J., and Macdonald, P. M. (1998). Localization of mRNAs to the oocyte is common in *Drosophila* ovaries. *Mech. Dev.* **70,** 193–195.

Elisha, Z., Havin, L., Ringel, I., and Yisraeli, J. K. (1995). Vg1 RNA binding protein mediates the association of Vg1 RNA with microtubules in *Xenopus* oocytes. *EMBO J.* **14,** 5109–5114.

Ephrussi, A., and Lehmann, R. (1992). Induction of germ cell formation by oskar. *Nature* **358,** 387–392.

Ferrandon, D., Elphick, L., Nüsslein-Volhard, C., and St Johnston, D. (1994). Staufen protein associates with the 3′UTR of *bicoid* mRNA to form particles that move in a microtubule-dependent manner. *Cell* **79,** 1221–1232.

Ferrandon, D., Koch, L., Westhof, E., and Nüsslein-Volhard, C. (1997). RNA–RNA interaction is required for the formation of specific *bicoid* mRNA 3′UTR-Staufen ribonucleoprotein particles. *EMBO J.* **16,** 1751–1758.

Forristall, C., Pondel, M., and King, M. L. (1995). Patterns of localization and cytoskeletal association of two vegetally localized RNAs, Vg1 and Xcat-2. *Development* **121,** 201–208.

Fulton, A. B., Wan, K. M., and Penman, S. (1980). The spatial distribution of polyribosomes in 3T3 cells and the associated assembly of proteins into the skeletal framework. *Cell* **20,** 849–857.

Gautreau, D., Cote, C. A., and Mowry, K. L. (1997). Two copies of a subelement from the Vg1 RNA localization sequence are sufficient to direct vegetal localization in *Xenopus* oocytes. *Development* **124,** 5013–5020.

Glotzer, J. B., and Ephrussi, A. (1996). mRNA localization and the cytoskeleton. *Semin. Cell Dev. Biol.* **7,** 357–365.

Glotzer, J. B., Saffrich, R., Glotzer, M., and Ephrussi, A. (1997). Cytoplasmic flows localize injected *oskar* RNA in *Drosophila* oocytes. *Curr. Biol.* **7,** 326–337.

Gonzalez, I., Buonomo, S. B. C., Naysmyth, K., and von Ahsen, U. (1999). ASH1 mRNA localization in yeast involves multiple secondary structural elements and ASH1 protein translation. *Curr. Biol.* **9,** 337–340.

Gonzalez-Reyes, A., Elliot, H., and St. Johnston, D. (1995). Polarization of both major body axes in *Drosophila* by gurken-torpedo signalling. *Nature* **375,** 654–658.

Goodson, H. V., Valetti, C., and Kreis, T. E. (1997). Motors and membrane traffic. *Curr. Opin. Cell Biol.* **9,** 18–28.

Gunkel, N., Yano, T., Markussen, F.-H., Olsen, L. C., and Ephrussi, A. (1998). Localization-dependent translation requires a functional interaction between the 5′ and 3′ ends of *oskar* mRNA. *Genes Dev.* **12,** 1652–1664.

Hamill, D., Davis, J., Drawbridge, J., and Suprenant, K. A. (1994). Polyribosome targeting to microtubules: Enrichment of specific mRNAs in a reconstituted microtubule preparation from sea urchin embryos. *J. Cell Biol.* **127,** 973–984.

Han, J. W., Park, J. H., Kim, M., and Lee, J. (1997). mRNAs for microtubule proteins are specifically colocalized during the sequential formation of basal body, flagella, and cytoskeletal microtubules in the differentiation of *Naegleria gruberi. J. Cell Biol.* **137,** 871–879.

Havin, L., Git, A., Elisha, Z., Oberman, F., Yaniv, K., Schwartz, S. P., Standart, N., and Yisraeli, J. K. (1998). RNA-binding protein conserved in both microtubule- and microfilament-based RNA localization. *Genes Dev.* **12,** 1593–1598.

Hazelrigg, T. (1998). The destinies and destinations of RNAs. *Cell* **95,** 451–460.

Hesketh, J. E., and Pryme, I. F. (1991). Interaction between mRNA, ribosomes and the cytoskeleton. *Biochem J.* **277,** 1–10.

Hirokawa, N. (1996). Organelle transport along microtubules—The role of KIFs. *Trends Cell Biol.* **6,** 135–141.

Hirokawa, N. (1998). Kinesin and dynein superfamily proteins and the mechanism of organelle transport. *Science* **279,** 519–526.

Hoek, K. S., Kidd, G. J., Carson, J. H., and Smith, R. (1998). hnRNP A2 selectively binds the cytoplasmic transport sequence on myelin basic protein mRNA. *Biochemistry* **37,** 7021–7029.

Hurst, S., Talbot, N. J., and Stebbings, H. (1999). A staufen-like protein in translocation channels linking nurse cells to oocytes in *Notonecta* shows nucleotide-dependent attachment to microtubules. *J. Cell Sci.* **112,** 2947–2955.

Jeffery, W. R. (1982). Messenger RNA in the cytoskeletal framework: Analysis by *in situ* hybridization. *J. Cell Biol.* **95,** 1–7.

Kiebler, M. A., Hemraj, I., Verdake, P., Köhrmann, M., Fortes, P., Marión, R. M., Ortin, J., and Dotti, C. G. (1999). The mammalian staufen protein localizes to the somatodendritic domain of cultured hippocampal neurons: Implications for its involvement in mRNA transport. *J. Neurosci.* **19,** 288–297.

Kilmartin, J. V., and Adams, E. M. (1984). Structural rearrangements of tubulin and actin during the cell cycle of yeast *Saccharomyces. J. Cell Biol.* **98,** 922–933.

Kim-Ha, J., Kerr, K., and Macdonald, P. M. (1995). Translational regulation of *oskar* mRNA by bruno, an ovarian RNA-binding protein, is essential. *Cell* **81,** 403–412.

Kim-Ha, J., Webster, P. J., Smith, J. L., and Macdonald, P. M. (1993). Multiple RNA regulatory elements mediate distinct steps in localization of oskar mRNA. *Development* **119,** 169–178.

King, M. L., Zhou, Y., and Bubunenko, M. (1999). Polarizing genetic information in the egg: RNA localization in the frog oocyte. *BioEssays* **21,** 546–557.

Kislauskis, E., Zhu, X., and Singer, R. H. (1994). Sequences responsible for intracellular localization of β-actin messenger RNA also affect phenotype. *J. Cell Biol.* **127,** 441–451.

Knowles, R. B., and Kosik, K. S. (1997). Neurotrophin-3 signals redistribute RNA in neurons. *Proc. Natl. Acad. Sci. USA* **94,** 14,804–14,808.

Knowles, R. B., Sabry, J. H., Martone, M. E., Deerinck, T. J., Ellisman, M. H., Bassell, G. J., and Kosik, K. S. (1996). Translocation of RNA granules in living neurons. *J. Neurosci.* **16,** 7812–7820.

Kohrmann, M., Luo, M., Kaether, C., DesGroseillers, L., Dotti, C. G., and Kiebler, M. A. (1999). Microtubule-dependent recruitment of Staufen-green fluorescent protein into large RNA containing granules and subsequent dendritic transport in living hippocampal neurons. *Mol. Biol. Cell* **19,** 2945–2953.

Kuhl, D., and Skehel, P. (1998). Dendritic localization of mRNAs. *Curr. Opin. Neurobiol.* **8,** 600–806.

Kwon, S., Barbarese, E., and Carson, J. E. (1999). The *cis*-acting RNA trafficking signal from myelin basic protein mRNA and its cognate trans-acting ligand hn RNP A2 enhance cap-dependent translation. *J. Cell Biol.* **147,** 247–256.

Lane, J., and Allan, V. (1998). Microtubule-based membrane movement. *Biochim. Biophys. Acta.* **1376,** 27–55.

Langford, G. M. (1995). Actin- and microtubule-dependent organelle motors: Interrelationships between the two motility systems. *Curr. Biol.* **7,** 82–88.

Latham, V. M., Kislauskis, E. H., Singer, R. H., and Ross, A. F. (1994). Beta-actin mRNA localization is regulated by signal transduction mechanisms. *J. Cell Biol.* **126,** 1211–1219.

Li, M-g., McGrail, M., Serr, M., and Hays, T. S. (1994). *Drosophila* cytoplasmic dynein, a microtubule motor that is asymmetrically localized in the oocyte. *J. Cell Biol.* **126,** 1475–1494.

Li, P., Yang, X., Wasser, M., Cai, Y., and Chia, W. (1997). Inscuteable and Staufen mediate assymetric localization and segregation of *prospero* RNA during *Drosophila* neuroblast cell divisions. *Cell* **90,** 437–447.

Lindesmith, L., McIlvain, J. M., Jr., Argon, Y., and Sheetz, M. P. (1997). Phosphotransferases associated with the regulation of kinesin motor activity. *J. Biol. Chem.* **272,** 22,929–22,933.

Litman, P., Barg, J., Rindzoonski, L., and Ginzburg, I. (1997). Subcellular localization of tau mRNA in differentiating neuronal cell culture: Implications for neuronal polarity. *Neuron* **10,** 627–638.

Litman, P., Behar, L., Elisha, Z., Yisraeli, J. K., and Ginzburg, I. (1996). Exogenous tau RNA is localized in oocytes: Possible evidence for evolutionary conservation of localization mechanisms. *Dev. Biol.* **176,** 86–94.

Long, R. M., Singer, R. H., Meng, X., Gonzalez, L., Naysmyth, K., and Jansen, R.-P. (1997). Mating type switching in yeast controlled by asymmetric localization of *ASH1* mRNA. *Science* **277,** 383–387.

Macdonald, P. M., and Kerr, K. (1998). Mutational analysis of an RNA recognition element that mediates localization of *bicoid* mRNA. *Mol. Cell Biol.* **18,** 3788–3795.

Macdonald, P. M., Kerr, K., Smith, J. L., and Leask, A. (1993). RNA regulatory element BLE1 directs the early steps of *bicoid* mRNA localization. *Development* **118,** 1233–1243.

Macdonald, P. M., and Struhl, G. (1988). *Cis*-acting sequences responsible for anterior localization of *bicoid* mRNA in *Drosophila* embryos. *Nature* **336,** 595–598.

Macgregor, H. C., and Stebbings, H. (1970). A massive system of microtubules associated with cytoplasmic movement in telotrophic ovarioles. *J. Cell Sci.* **6,** 431–449.

McIlvain, J. M., Jr., Burkhardt, J. K., Hamm-Alvarez, S., Argon, Y., and Sheetz, M. P. (1994). Regulation of kinesin activity by phosphorylation of kinesin-associated proteins. *J. Biol. Chem.* **269,** 19,175–19,182.

Martin, M. A., Iyadurai, S. J., Gassman, A., Gindhart, J. G., Jr., Hays, T. S., and Saxton, W. M. (1999). Cytoplasmic dynein, the dynactin complex, and kinesin are interdependent and essential for fast axonal transport. *Mol. Biol. Cell* **10,** 3717–3728.

Mays, U. (1972). Stofftransport in ovar von *Pyrrhocoris apterus. Z. Zellforsch. Mikrosk. Anat.* **123,** 395–410.

McGrail, M., and Hays, T. S. (1997). The microtubule motor cytoplasmic dynein is required for spindle orientation during germline cell divisions and oocyte differentiation in *Drosophila. Development* **124,** 2409–2419.

Micklem, D. R., Adams, J., Grunert, S., and St Johnston, D. (2000). Distinct roles of two conserved Staufen domains in *oskar* mRNA localization and translation. *EMBO J.* **19,** 1366–1377.

Mitchison, T. J., and Cramer, L. P. (1996). Actin-based cell motility and cell locomotion. *Cell* **84,** 371–379.

Mitchison, T. J., and Kirschner, M. (1984). Dynamic instability of microtubule growth. *Nature* **312,** 237–242.

Moore, J. D., and Endow, S. A. (1996). Kinesin proteins: A phylum of motors for microtubule-based motility. *Bioessays* **18,** 207–219.

Mooseker, M. S., and Cheney, R. E. (1995). Unconventional myosins. *Annu. Rev. Cell Dev. Biol.* **11,** 633–675.

Mowry, K. L., and Melton, D. A. (1992). Vegetal messenger RNA localization directed by a 340-nt RNA sequence element in *Xenopus* oocytes. *Science* **255,** 991–994.

Münchow, S., Sauter, C., and Jansen, R.-P. (1999). Association of the class V myosin Myo4p with a localised messenger RNA in budding yeast depends on She proteins. *J. Cell Sci.* **223,** 1511–1518.

Nangaku, M., Sato Yoshitake, R., Okada, Y., Noda, Y., Takemura, R., Yamazaki, H., and Hirokawa, N. (1994). KIF1B, a novel microtubule plus end-directed monomeric motor protein for transport of mitochondria. *Cell* **79,** 1209–1220.

Nasmyth, K., and Jansen, R. P. (1997). The cytoskeleton in mRNA localization and cell differentiation. *Curr Opin. Cell Biol.* **9,** 396–400.

Niclas, J., Allan, V. J., and Vale, R. D. (1996). Cell cycle regulation of dynein association with membranes modulates microtubule-based organelle transport. *J. Cell Biol.* **133,** 585–593.

Norvell, A., Kelley, R. L., Wehr, K., and Schübach, T. (1999). Specific isoforms of Squid, a *Drosophila* hnRNP, performs distinct roles in Gurken localization during oogenesis. *Genes Dev.* **13,** 864–876.

Okada, Y., Yamazaki, H., Sekine Aizawa, Y., and Hirokawa, N. (1995). The neuron-specific kinesin superfamily protein KIF1A is a unique monomeric motor for anterograde axonal transport of synaptic vesicle precursors. *Cell* **81,** 769–780.

Oleynikov, Y., and Singer, R. H. (1998). RNA localization: Different zipcodes, same postman? *Trends Cell Biol.* **8,** 381–383.

Olink-Coux, M., and Hollenbeck, P. J. (1996). Localization and active transport of mRNA in axons of sympathetic neurons in culture. *J. Neurosci.* **16,** 1346–1358.

Pokrywka, N. J., and Stephenson, E. C. (1991). Microtubules mediate the localization of *bicoid* RNA during *Drosophila* oogenesis. *Development* **113,** 55–66.

Pokrywka, N. J., and Stephenson, E. C. (1994). Localized RNAs are enriched in cytoskeletal extracts of *Drosophila* oocytes. *Dev. Biol.* **166,** 210–219.

Pollard, T. D., and Cooper, J. A. (1986). Actin and actin-binding proteins. A critical evaluation of mechanisms and functions. *Ann. Rev. Biochem.* **55,** 987–1035.

Ramos, A., Grünert, S., Adams, J., Micklem, D. R., Proctor, M. R., Freund, S., Bycroft, M., St. Johnston, D., and Varani, G. (2000). RNA recognition by a Staufen double-stranded RNA binding domain. *EMBO J.* **19,** 997–1009.

Reese, E. L., and Haimo, L. T. (2000). Dynein, dynactin, and kinesin II's interaction with microtubules is regulated during bidirectional organelle transport. *J. Cell Biol.* **151,** 155–165.

Ressom, R. E., and Dixon, K. E. (1988). Relocation and reorganization of germ plasm in *Xenopus* embryos after fertilization. *Development* **103,** 507–518.

Robb, D. L., Heasman, J., Raats, J., and Wylie, C. (1996). A kinesin-like protein is required for germ plasm aggregation in *Xenopus. Cell* **87,** 823–831.

Ross, A. F., Oleynikov, Y., Kislauskis, E. H., and Taneja, K. L. (1997). Characterization of a β-actin mRNA zipcode-binding protein. *Mol. Cell Biol.* **17,** 2158–2165.

Runnegar, M. T., Wei, X. H., and Hamm-Alvarez, S. (1999). Increased protein phosphorylation of cytoplasmic dynein results in impaired motor function. *Biochem. J.* **342,** 1–6.

Ruzanov, P. V., Evdokimova, V. M., Korneeva, N. L., and Hershley, J. W. B. (1999). Interaction of the universal mRNA-binding protein p50, with actin: A possible link between mRNA and microfilaments. *J. Cell Sci.* **112,** 3487–3496.

Sallés, F. J., Lieberfarb, M. E., Wreden, C., Gergen, J. P., and Strickland, S. (1994). Coordinate initiation of *Drosophila* development by regulated polyadenylation of maternal messenger RNAs. *Science* **266,** 1996–1999.

Sato-Yoshitake, R., Yorifuji, H., Inagaki, M., and Hirokawa, N. (1992). The phosphorylation of kinesin regulates its binding to synaptic vesicles. *J. Biol. Chem.* **267,** 23,930–23,936.

Schnapp, B. J. (1999). RNA localization: A glimpse of the machinery. *Curr. Biol.* **9,** R725–R727.

Schnorrer, F., Bohmann, K., and Nusslein-Volhard, C. (2000). The molecular motor dynein is involved in targeting Swallow and *bicoid* RNA to the anterior pole of *Drosophila* oocytes. *Nat. Cell Biol.* **2,** 185–190.

Schuldt, A. J., Adams, J. H. J., Davidson, C. M., Micklem, D. R., Haseloff, J., St. Johnston, D., and Brand, A. H. (1998). Miranda mediates asymmetric protein and RNA localization in the developing nervous system. *Genes Dev.* **12,** 1847–1857.

Schwartz, S. P., Aisenthal, L., Elisha, Z., Oberman, F., and Yisraeli, J. K. (1992). A 69 kDa RNA binding protein from *Xenopus* oocytes recognizes a common motif in two vegetally localized maternal mRNAs. *Proc. Natl. Acad. Sci. USA* **89,** 11895–11899.

Serano, T. L., and Cohen, R. S. (1998). A small predicted stem loop structure mediates oocyte localization of *Drosophila K10* mRNA. *Development* **121,** 3809–3818.

Severt, W. L., Biber, T. U. L., Wu, X.-Q., Hecht, N. B., DeLorenzo, R. J., and Jakoi, E. R. (1999). The suppression of testis–brain RNA binding protein and kinesin heavy chain disrupts mRNA sorting in dendrites. *J. Cell Sci.* **112,** 3691–3702.

Shen, C-P., Knoblich, J. A., Chan, Y-M., Jiang, M-M., and Jan, L. Y. (1998). Miranda as a multidomain adapter linking apically localized Inscuteable and basally localized Staufen and Prospero during asymmetric cell division in *Drosophila. Genes Dev.* **12,** 1837–1846.

Sil, A., and Herskowitz, I. (1996). Identification of an asymmetrically localized determinant, ASH1p, required for lineage-specific transcription of the yeast *HO* gene. *Cell* **84,** 710–719.

Stebbings, H., and Hunt, C. (1983). Microtubule polarity in the nutritive tubes of insect ovarioles. *Cell Tiss. Res.* **233,** 133–141.

Stephen, S., Talbot, N. J., and Stebbings, H. (1999). Poly(A) mRNA is attached to insect ovarian microtubules *in vivo* in a nucleotide-sensitive manner. *Cell Motil. Cytoskel.* **43,** 159–166.

Stephenson, E. C., Chao, Y. G., and Fackenthal, J. D. (1988). Molecular analysis of the swallow gene of *Drosophila melanogaster. Genes Dev.* **2,** 1655–1665.

St. Johnston, D. (1995). The intracellular localization of messenger RNAs. *Cell* **81,** 161–170.

St. Johnston, D., Beuchle, D., and Nüsslein-Volhard, C. (1991). *Staufen,* a gene required to localize maternal RNAs in the *Drosophila* egg. *Cell* **66,** 51–63.

St. Johnston, D., and Nüsslein-Volhard, C. (1992). The origin of pattern and polarity in the *Drosophila* embryo. *Cell* **68,** 201–219.

Sundell, C. L., and Singer, R. H. (1991). Requirement of microfilaments in sorting of actin messenger RNA. *Science* **252,** 1275–1277.

Takizawa, P. A., Sil, A., Swedlow, J. R., Hershkowitz, I., and Vale, R. D. (1997). Actin-dependent localization of an RNA encoding a cell-fate determinant in yeast. *Nature* **389,** 90–93.

Takizawa, P. A., and Vale, R. D. (2000). The myosin motor, Myo4p, binds ASH1 mRNA via the adapter protein, She3p. *Proc. Natl. Acad. Sci. USA* **97,** 5273–5278.

Taneja, K. L., Lifshitz, L. M., Fay, F. S., and Singer, R. H. (1992). Poly(A) RNA codistribution with microfilaments: Evaluation by *in situ* hybridization and quantitative digital imaging microscopy. *J. Cell Biol.* **119,** 1245–1260.

Theurkauf, W. E., Alberts, B. M., Jan, Y. N., and Jongens, T. A. (1993). A central role for microtubules in the differentiation of *Drosophila* oocytes. *Development* **118,** 169–1180.

Theurkauf, W. E., and Hazelrigg, T. I. (1998). *In vivo* analysis of cytoplasmic transport and cytoskeletal organization during *Drosophila* oogenesis: Characterization of a multi-step anterior localization pathway. *Development* **125,** 3655–3666.

Theurkauf, W. E., Smiley, S., Wong, M. L., and Alberts, B. M. (1992). Reorganization of the cytoskeleton during *Drosophila* oogenesis: Implications for axis specification and intercellular transport. *Development* **115,** 923–936.

Tucker, J. B. (1984). Spatial organization of microtubule-organizing centers and microtubules. *J. Cell Biol.* **99,** 555–625.

Vaisberg, E. A., Grissom, P. M., and McIntosh, J. R. (1996). Mammalian cells express three distinct dynein heavy chains that are localized to different cytoplasmic organelles. *J. Cell Biol.* **133,** 831–842.

Vallee, R. B., and Sheetz, M. P. (1996). Targeting of motor proteins. *Science* **271,** 1539–1544.

Veyrune, J.-L., Campbell, G. P., Wiseman, J., Blanchard, J.-M., and Hesketh, J. E. (1996). A localization signal in the 3′ untranslated region of c-*myc* mRNA targets c-*myc* mRNA and β-globin reporter sequences to the perinuclear cytoplasm and cytoskeletal-bound polysomes. *J. Cell Sci.* **109,** 1185–1194.

Wang, S., and Hazelrigg, T. (1994). Implications for *bcd* mRNA localization from spatial distribution of *exu* protein in *Drosophila* oogenesis. *Nature* **369,** 400–403.

Wang, S-Z., and Adler, R. (1995). Chromokinesin: A DNA-binding, kinesin-like nuclear protein. *J. Cell Biol.* **128,** 761–768.

Wang, Z., Khan, S., and Sheetz, M. P. (1995). Single cytoplasmic dynein molecule movement: Characterization and comparison with kinesin. *Biophys. J.* **69,** 2011–2023.

Wickham, L., Duchaîne, T., Luo, M., Nabi, I. R., and DesGroseillers, L. (1999). Mammalian Staufen is a double-stranded RNA- and tubulin-binding protein which localizes to the rough endoplasmic reticulum. *Mol. Cell. Biol.* **19,** 2220–2230.

Whittaker, K. L., Ding, D., Fisher, W. W., and Lipshitz, H. D. (1999). Different 3′ untranslated regions target alternatively processed *hu-li-tai shao* (*hts*) transcripts to distinct cytoplasmic locations in *Drosophila. J. Cell Sci.* **112,** 3385–3398.

Wilhelm, J. E., Mansfield, J., Hom-Booher, N., Wang, S., Turck, C. W., Hazelrigg, T., and Vale, R. D. (2000a). Isolation of a ribonucleoprotein complex involved in mRNA localization in *Drosophila* oocytes. *J. Cell Biol.* **148,** 427–439.

Wilhelm, J. E., and Vale, R. D. (1993). RNA on the move: The mRNA localization pathway. *J. Cell Biol.* **123,** 269–274.

Wilhelm, J. E., Vale, R. D., and Hegde, R. S. (2000b). Coordinate control of translation and localization of Vg1 mRNA in *Xenopus* oocytes. *Proc. Natl. Acad. Sci. USA* **97,** 13,132–13,137.

Wu, X. Q., and Hecht, N. B. (2000). Mouse testis brain ribonucleic acid-binding protein/translin colocalizes with microtubules and is immunoprecipitated with messenger ribonucleic acids encoding myelin basic protein, alpha calmodulin kinase II and protamines 1 and 2. *Biol. Reprod.* **62,** 720–725.

Yisraeli, J. K., and Melton, D. A. (1988). The maternal mRNA Vg1 is correctly localized following injection into oocytes. *Nature* **336,** 592–595.

Yisraeli, J. K., Sokol, S., and Melton, D. A. (1990). A two-step model for the localization of a maternal mRNA in *Xenopus* oocytes: Involvement of microtubules and microfilaments in translocation and anchoring of Vg1 mRNA. *Development* **108,** 289–298.

Zhang, H. L., Singer, R. H., and Bassell, G. J. (1999). Neurotrophin regulation of β-actin mRNA and protein localization within growth cones. *J. Cell Biol.* **147,** 59–70.

This Page Intentionally Left Blank

Special Cytochemistry in Cell Biology

Tetsuji Nagata

Department of Anatomy and Cell Biology, Shinshu University School of Medicine,
Matsumoto 390-8621, Japan; and Department of Anatomy and Physiology, Nagano
Women's Junior College, Nagano 380-0803, Japan

Cytochemistry is a science of localizing chemical components of cells and
organelles on histological sections by using various techniques. We first aimed at
studying cytochemistry by developing new techniques using various principles
such as enzyme cytochemistry, microincineration, microspectrophotometry,
radioautography, cryo-techniques, X-ray microanalysis and
immunocytochemistry. We first concentrated on developing methodologies in the
1960s to 1970s. We then applied these special techniques to various kinds of cells
in men and animals. Earlier, I proposed to classify these methods into three
categories, i.e., chemical, physical, and biological techniques. The methodology
has been well developed to form a new science which should be designated as
"general cytochemistry" similarly to the general histology. On the other hand,
these techniques should be applied to various cells in various organ systems, such
as the skeletal, muscular, digestive, respiratory, urinary, reproductive, endocrine,
circulatory, nervous and sensory systems similarly to the special histology or the
histology of organs. I summarize the results of cytochemical studies on cells of
various organs carried out in our laboratory during these 44 years since 1955. The
results obtained from cytochemical studies applied to various cells in respective
organ systems should be designated as "special cytochemistry."

KEY WORDS: Cytochemistry, Microscopy, Enzymes, Radioautography,
Immunocytochemistry, X-ray microanalysis. © 2001 Academic Press.

I. Introduction

The science named *histochemistry and cytochemistry* was first established by the
development of techniques for demonstrating alkaline phosphatase activity by

Gomori (1939) and Takamatsu (1938, 1939) independently in the 1930s. Histo- and cytochemistry is a science for localizing chemical components of cells and tissues on histological sections by using various techniques. Since I started my career as an anatomist and histologist in 1955, I first aimed at studying histo-and cytochemistry by developing new techniques using various principles such as enzyme cytochemistry, microincineration, microspectrophotometry, radioautography, cryotechniques, X-ray microanalysis, and immunocytochemistry. We first concentrated on developing methodologies in 1960s to 1970s. We then applied these special techniques to various kinds of cells and tissues in men and animals. The special histo- and cytochemical techniques are now well developed and systematized.

At the present time many textbooks of histo- and cytochemistry are available throughout the world which deal with only the methodology, consisting of techniques for tissue processing and demonstrating chemical components in tissue sections (Danielli, 1953; Glick, 1949; Gomori, 1952; Graumann and Neumann, 1958–1974; Lillie and Fullmer, 1976; Pearse, 1953, 1980–1991). Earlier, I proposed to classify these methods into three categories, i.e., chemical, physical, and biological techniques (Nagata, 1995b, 1999b). Recently, the methodology has been so well developed to form a new science which should be designated as "general histo- and cytochemistry," similar to "general histology." On the other hand, these techniques should be applied to all the organ systems, such as the skeletal, muscular, digestive, respiratory, urinary, reproductive, endocrine, circulatory, nervous, and sensory. The results of these applications to all the organ systems should be collected and designated as a new science, i.e., "histochemistry of the organs," like the histology of the organs (Nagata, 1995b, 1999b). These results should form a new field in biomedical sciences that can be designated as "special histochemistry," forming part of "microscopic anatomy" together with "special histology."

We made efforts to apply these techniques to various organ systems since 1970s (Nagata, 1999b) and collected data from all the organs, including data on the aging process from prenatal and postnatal development to adult and senescent stages. The data include not only three-dimensional structure of organs but also the four-dimensional structure taking the time dimension into account, by labeling cells and tissues in connection with the individual aging. These data were compiled to form a new field of medical science, which should be designated as "histochemistry of organs" or "special histo- and cytochemistry," similar to the histology of organs. We summarize the results of cytochemical studies on cells of various organs carried out in our laboratory from 1955 to 2000.

II. Cytochemistry in Cell Biology

A. Historical Review on Cytochemical Methods

The history of histo- and cytochemistry is believed to be as old as histology itself (Lison, 1936; Pearse, 1953). In the early 19th century, histo- and cytochemical

research, to study chemical components of biological structure in combination with chemistry and biology, started first in botany in France (Raspail, 1825). Raspail stained starch in plant tissues blue with potassium iodide solution under a light microscope and demonstrated the localization microscopically. He then published his first essay on microscopic chemistry (Raspail, 1830). In Germany in the 1840s to 1870s, histochemistry in zoology and medicine was developed mainly as biological chemistry, together with histology, introducing methods involving tiissue destruction for analyzing chemical components (Lehmann, 1842). Among these zoologists, anatomists, and pathologists, who were at that time interested in analyzing chemical constituents in animal tissues including men, Miescher (1874) was the first to introduce cell fractionation for analyzing nucleic acids in the nuclei of leukocytes. During these times, the new science was called "microchemie" in French or "Mikrochemie" in German, which means "microchemistry" in English. Microchemistry was, in other words, microscopic chemistry or chemical microscopy and meant to observe chemical reactions *in situ* under microscopy.

In the early 20th century, aniline dyes were frequently used to stain tissues in anatomy and pathology. Normal histology was studied not only in anatomy but also in physiology. Histologists and pathologists were much interested in new dyes and less interested in histochemistry at that time. When Lison (1936) published his famous work "Histochemie Animale," many histologists were again interested in histochemistry. Lison classified histochemical techniques into two categories, "méthodes extra situm" or "méthodes extractives" and "méthodes histochimiques in situ" or "méthodes topochimique." The former included cell fractionation and microchemistry, while the latter included *in situ* histochemistry, which he proclaimed to be a new science studying chemical components of tissues without tissue destruction. Then many histologists, anatomists, pathologists, and physiologists started to study this new science and published many papers and books dealing with histochemistry and cytochemistry. Innumerable literature as well as textbooks are available from 1950s to 1990s. Representative books in the mid 20th century are Glick (1949), Gomori (1952), Danielli (1953), Lillie (1954), Mellor (1955), Eränko (1955), and Pearse (1980–1991). These books refer only to the histochemical techniques, classifying these methods into several categories such as tissue processing, staining procedures for nucleic acids, proteins, carbohydrates, lipids, enzymes, fluorescence microscopy, and immunostaining. In the 1960s to 1970s, many histochemists tried to develop new methodologies employing various principles and published innumerable original papers in various journals.

B. Classification of Cytochemical Methods

1. Chemical Methods

The chemical methods in cytochemistry consist of various chemical reactions such as staining of DNA with Feulgen reaction (Feulgen and Rossenbeck, 1924),

staining of proteins with Millon reactions (Bensley and Gersh, 1933), glucides with the periodic acid–Schiff (PAS) reaction (MacManus, 1948) and high-iron diamine–alcian blue (HID-AB) sequence (Fig. 1A; see color insert), and lipids with Sudan (Lillie, 1944), enzymes (Gomori, 1939), and inorganic substances. The bases for these chemical reactions are well understood (Nagata, 1974; Nagata and Iwadare, 1984).

2. Physical Methods

The physical methods in cytochemistry consist of various reactions such as microincineration (Raspail, 1830), cryo-techniques (Altmann, 1889), microspectrophotometry (Caspersson, 1950), fluorescence microscopy, confocal laser scanning microscopy, radioautography, and X-ray microanalysis (Nagata, 1991). The bases of these methods depend on physical phenomena such as very low or high temperature, various sources of lights, and radiations from radioisotopes (Nagata, 1994d) or X-rays (Nagata, 2000d). We developed several methods for radioautography (Fig. 1B) and X-ray microanalysis.

3. Biological Methods

The biological methods in cytochemistry employ biological reactions which can be observed in living plants and animals. They were developed later than chemical and physical methods and only immunocytochemistry (Coons *et al.,* 1941) and lectin staining (Sharon and Lis, 1972) are now available. We developed some modified techniques for immunocytochemistry (Fig. 1C) and lectin staining (Fig. 1D).

C. Special Cytochemistry in Cell Biology

When methods of demonstrating various chemical components in cells and tissues were well developed, applications of these technologies gradually increased. The applications of the general histochemistry to anatomy of men and animals are called "special histochemistry or histochemistry of organs" (Nagata, 1999b). On the other hand, applications of general cytochemistry to cell biology should be designated as "special cytochemistry," where emphasis is placed on cell organelles in respective cell types in various organ systems.

III. General Cytochemistry

A. Chemical Methods in Cytochemistry

The chemical reactions can be divided into two categories, color reactions for light microscopy and electron-dense deposits for electron microscopy.

1. Color Reactions for Light Microscopy

Color reactions for demonstrating various substances have been developed. Among them, we mainly used reactions whose intensities and absorbances parallel concentrations of substances for applying them to microspectrophotometry (Nagata, 1972a). The methods that we used in cytochemistry will be briefly described below.

a. Nucleic Acids   The most specific chemical reaction for nucleic acids in cytochemistry is the reaction of Feulgen (Feulgen and Rossenbeck, 1924). This reaction depends on hydrolysis by hydrochloric acid of the purine–desoxypentose linkage of DNA in nuclear chromatin, resulting in aldehyde, which is colored purple by Schiff's reagent (Schiff, 1865). Since the color density and the absorption of this reaction was first shown by Widström (1928) to parallel DNA contents of respective cells, it was used for microspectrophotometry by Pollister and Ris (1947). They also reported the use of methyl green-pyronin staining for both DNA and RNA in microspectrophotometry. RNA can be stained by several methods such as Azure B (Flax and Himes, 1952) or cresyl violet (Ritter *et al.,* 1961). We used a modified Feulgen reaction for quantitation of DNA in various cell nuclei (Nagata, 1966a, 1972a).

b. Proteins   Total proteins consisting of various amino acids can be stained with such color reactions as mercuric bromphenol blue (Mazia *et al.,* 1953) or naphthol yellow S (Deitch, 1955). Some basic proteins are stained with Fast Green (Alfert and Geschwind, 1953) and gallocyanine chrome alum (Jobst and Sandritter, 1965), and only some amino acids in proteins can be stained with specific dyes, e.g., tryptophane and tyrosin with Millon reactions (Rasch and Swift, 1960), tyrosin with diazotization-coupling (Ritter and Berman, 1963), tryptophane with *p*-dimethylaminobenzaldehyde-nitrite (Augusten *et al.,* 1969), arginin with Sakaguchi reaction (Deitch, 1961), and SH groups with DDD reaction (Cafrany *et al.,* 1955). We used some of modified staining procedure for total and basic proteins (Nagata, 1972a).

c. Glucides   Glucides are classified into several categories: monosaccharides, disaccharides, oligosaccharides, and polysaccharides. Several procedures for demonstrating glucids with color reactions based on the PAS reaction are available. The theory of the reaction is based on the fact that aqueous periodic acid oxidizes 1,2 glycol groups in cells which consist of carbohydrates to produce aldehydes which are colored by Schiff's reagent, basic fuchsin. Among of the modified procedures, we used PAS reaction after Fand and Thorell (1962) and Gahrton (1966) for microspectrophotometry. We also used PAS-AB or HID-AB sequence (Fig. 1A) to differentiate mucosubstances in goblet cells in the intestine (Nagata and Kawahara, 1999). The HID-AB sequence (Scott, 1972) is considered to differentiate black-stained sulfated complex carbohydrate from blue-stained carboxylated mucosubstance lacking sulfate esters (Nagata and Kawahara, 1999).
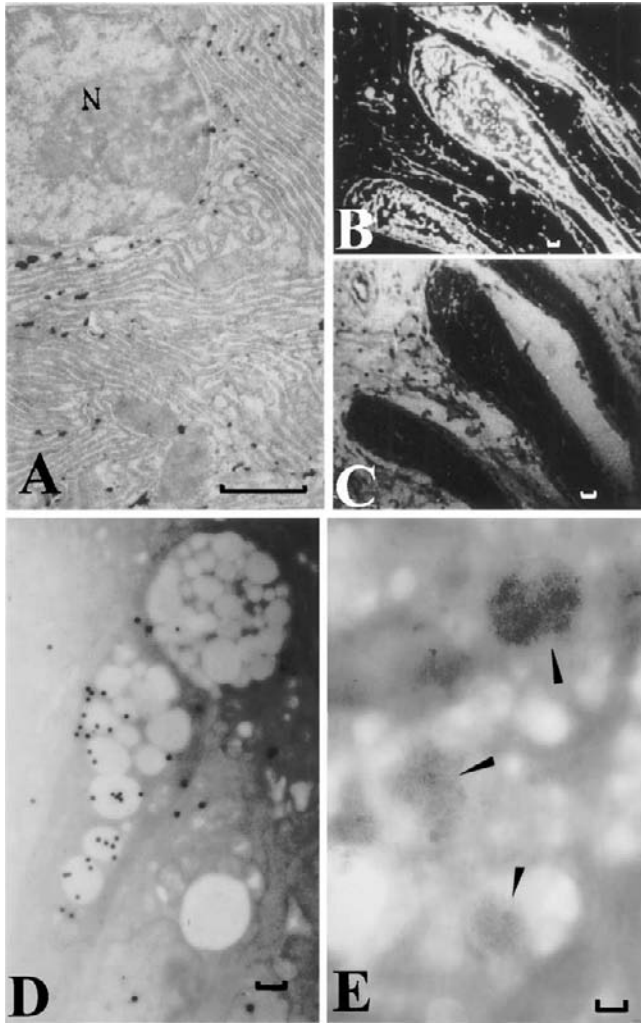
FIG. 2   General cytochemistry 2: Electron-dense deposits for electron microscopy and spodogram for light microscopy. (A) Electron micrograph showing lipase activity in pancreatic acinar cells of an adult mouse. The pancreatic tissue was prefixed in buffered glutaraldehyde, incubated in a medium for lipase, postfixed in buffered osmium tetroxide, embedded, sectioned, and observed by electron microscopy. Electron-dense deposits which demonstrate lipase activity are localized in endoplasmic reticulum ($\times 11{,}250$; bar $= 1\ \mu$m). (B) Dark field light micrograph of a dog skin tissue, fixed in ethanol formalin, dehydrated, embedded in paraffin, sectioned, heated to $600°$C in an oven, and observed by dark field microscopy. The white figures demonstrate spodogram of inorganic substances, mainly calcium, in the hair follicles ($\times 150$; bar $= 10\ \mu$m). (C) A control serial section of the same tissue as in B but stained with H&E. Compare with B ($\times 150$; bar $= 10\ \mu$m). (D) Electron radioautogram of a goblet cell in the deeper crypt of the colonic epithelium of an adult mouse after injection with ^{35}SO$_4$, fixed at 30 min, sectioned,

d. Lipids Lipids consist of fatty acids and alcohols and can be classified into simple lipid esters and compounds lipids. The old and common procedures for demonstrating simple lipid droplets in cells are fat-soluble Sudan dyes, which were discovered by Daddi (1896). Later Lillie (1944) developed this method in pathology. We used either Sudan III or Sudan black in 70% alcohol in cytochemistry.

e. Enzymes Recent development of histo- and cytochemistry began from enzyme histochemistry when Gomori (1939) and Takamatsu (1938, 1939) found the principle for demonstrating alkaline phosphatase activity independently by hydrolyzing the substrate with the enzyme and producing lead precipitate colored black with sulfide. Then, varieties of techniques for demonstrating various enzymes were developed in the 1950s to 1960s so extensively that Pearse described in his textbook (Pearse, 1953), "Although a few years ago only 2 or 3 enzymes could be demonstrated in the tissues by histochemical means, there are now techniques for at least 18," but after 5 years he amended the description to "for at least 45." Now this sentence must be amended to read "for at least 200," employing several principles resulting in color reactions such as, metal precipitation, azo-dyes, tetrazolium salts, and 3,3′-diaminobenzidine (DAB) osmium. Since around 2100 enzymes were registered biochemically in the enzyme committee of the International Union of Biochemistry (1979), the number of enzymes demonstrable cytochemically is too small. Among them, we developed and studied several enzymes such as cytochrome oxidase (Nagata, 1956), urate oxidase (Yokota and Nagata, 1973), catalase (Yokota and Nagata, 1974), acid and alkaline phosphatase, nonspecific esterase (Nagata and Murata, 1980), arylsulfatase (Murata *et al.,* 1975), lipase (Fig. 2A) (Nagata, 1974), and phospholipase (Nagata and Iwadare, 1984). We also used some other enzymes to localize specific cell organelles such as glucose-6-phosphatase (Wachstein and Meissel, 1956; Tice and Barnett, 1962) for demonstration of endoplasmic reticulum, thiamine pyrophosphatase (Novikoff and Goldfisher, 1961) for Golgi apparatus, cytochrome oxidase (Seligman *et al.,* 1968) for mitochondria, and acid phosphatase (Mayahara and Chang, 1978) for lysosomes and used them to observe the three-dimensional ultrstructure of cell organelles (Nagata, 1995c, 1997b, 2000a,c).

---

and radioautographed and observed by electron microscopy. Many electron-dense silver grains are localized over the Golgi zone and mucous droplets in the goblet, demonstrating incorporation of radiosulfate into sulfomucins ($\times$4800, original magnification; bar $= 1~\mu$m). (E) Electron micrograph of a mouse liver, prefixed in glutaraldehyde, rapidly frozen, cryosectioned with a cryo-ultramicrotome, immunostained with ferritin–anti-urate oxidase conjugate, and stained negatively with phosphotungstic. acid. Electron-dense ferritin particles are seen in peroxisomes in the hepatocyte ($\times$52,000, original magnification; bar $= 0.1~\mu$m).

f. Pigments   Several pigments can be found in various cells and tissues, such as melanin, lipofuscin, ceroids, hemoglobin, hemosiderin, and bilirubin. Among them, we studied the localization of melanin and its precursors in the skin by argentaffine reaction (Nagata *et al.,* 1957a).

g. Inorganic Substances   Varieties of methods for demonstrating inorganic elements, especially metals, by color reactions have been developed. The color reaction produced by union of a dye with a metal or metal salt is called lake-formation (Venkataraman, 1952). Numerous techniques exist for the demonstration of metals such as iron, copper, gold, silver, mercury, lead, nickel, aluminum, and zinc. Among them, color reactions for inorganic iron were frequently used such as Prussian blue or Turnbull blue. However, the specificities of these techniques were mostly unsatisfactory. We employed only two physical techniques, microincineration (Fujiwara *et al.,* 1957) and radioautography (Nagata *et al.,* 1977b) for demonstration of inorganic substances.

2. Electron-Dense Deposits for Cytochemical Staining by Electron Microscopy

When electron microscopes were developed and applied to biology in the 1950s, histologists and pathologists observed thin sections obtained from tissues and cells after electron staining with uranium and lead. Later, histochemists started to use electron microscopy for localizing *in situ* chemical reactions in the 1960s by producing electron-dense deposits at cell organelle levels (Barka and Anderson, 1963). Such a field of study on subcellular localization of chemical components of cells was designated as electron microscopic cytochemistry or ultracytochemistry (Ogawa and Barka, 1993). Various enzyme activities were first demonstrated by means of similar techniques used for light microscopy, resulting in metal precipitation such as lead deposits for acid phosphatase (Sheldon *et al.,* 1955). Other metal deposits, such as copper, gold, barium, cerium, cadmium, and strontium were also used for demonstration of various enzyme activities. Then, electron-dense macromolecules produced by azo dyes and tetrazolium salts were used for enzyme cytochemistry (Hayat, 1972–1976). Likewise, varieties of macromolecules, i.e., DNA, RNA, proteins, glucides, lipids, and amines were lately demonstrated by labeling with electron-dense deposits, for example using enzyme–gold complex localizing DNA and RNA (Bendayan, 1981). Among these techniques we developed and applied several methods for both macromolecules, polyethyleneimine (PEI) for glycoproteins (Duan and Nagata, 1993) and periodic acid–thiocarbohydroazide–silver proteinate (PA-TCH-SP) for glucides (Murata *et al.,* 1977b), as well as enzymes, such as lipase (Fig. 2A) (Nagata, 1974), phospholipase (Nagata and Iwadare, 1984), catalase (Yokota and Nagata, 1974), and urate oxidase (Yokota and Nagata, 1977).

a. PA-TCH-SP for Glucides Typical glucides such as glycogen particles contained in various cells can be demonstrated by PAS color reaction at light microscopic level as well as several techniques resulting some electron dense deposits at electron microscopic level. The typical demonstration techniques of vicinal hydroxyl groups in glycogen by electron microscopy available are the periodic acid–thiocarbohydroazide–silver proteinate method (Thiéry, 1967), the periodic acid–pentafluorophenylhydrazine method (Bradbury and Stoward, 1967), the periodic acid–methenamine silver method (Rambourg, 1967), the periodic acid–Schiff reagent–metallic salt method, and, in particular, the phosphotungstic acid method (Thiéry, 1967). Among them, we improved the PA-TCH-SP method and found it to be the most suitable from the viewpoints or reaction specificity, reproducibility, and sufficiency of electron density (Murata *et al.,* 1977b). We oxidized epoxy resin sections in 1% periodic acid solution for 20 min, immersed in 0.2% thiocarbohydrazide solution dissolved in 20% acetic acid for 40 min, rinsed in 10 and 5% acetic acid, stained in 1% aqueous silver proteinate solution for 30 min, rinsed, and dried. After staining, fine electron-dense reaction products were observed in the cytoplasm of the megakaryocytes and blood platelets of albino rabbits (Murata *et al.,* 1977a,b) as well as in the mucous granules in the goblet cells in mouse colonic epithelium (Fig. 9AB) (Nagata, 2000c).

b. PEI for Glycoproteins Polyethyleneimine stains anionic sites of proteoglycans in various tissues (Sauren *et al.,* 1991). We improved the staining methods by immersing tissues in 0.5% PEI solution containing 8% sucrose for 30 min, fixed doubly in 0.1% glutaraldehyde and 2% osmium tetroxide, dehydrated, embedded in epoxy resin, and sectioned. Thus, the PEI binding sites in the glomerular extracellular matrices of mouse kidney (Duan and Nagata, 1993) and the hyaline cartilage of mouse trachea (Li *et al.,* 1994) were demonstrated.

3. Enzyme Cytochemistry

Techniques for demonstrating enzyme activity at the light microscopic level were extensively developed in the 1950s to 1970s. Then, techniques for demonstrating enzyme activity at the electron microscopic level, producing electron-dense deposits, followed the light microscopic color reaction over time. When Pearse (1953) described electron histochemistry, only two or three enzymes could be demonstrated in the tissues by histochemical means at electron microscopic level by applying the existing techniques to electron microscopy. However, now this sentence must be amended to read "at least 80." The principle for demonstrating enzyme activity employs several procedures to produce electron-dense deposits such as metal precipitation, azo-dyes, tetrazolium salts, and DAB osmium. Since around 2100 enzymes were registered biochemically in the enzyme committee (1979), the number of enzymes demonstrable cytochemically by electron

microscopy is too small, less than attributable to light microscopy. It is hoped that many more techniques for demonstrating other enzyme activities, especially by electron microscopy, will be further developed.

We developed and studied only several enzymes, such as cytochrome oxidase (Nagata, 1956), urate oxidase (Yokota and Nagata, 1974), catalase (Yokota and Nagata, 1974), acid and alkaline phosphatase, nonspecific esterase (Nagata and Murata, 1980), arylsulfatase (Murata *et al.,* 1975), lipase (Nagata, 1974), and phospholipase (Nagata and Iwadare, 1984). Other enzyme activities such as DAB (Angermüller and Fahimi, 1981) reaction for peroxisomes, glucose-6-phosphatase (G-6-Pase) activity (Tice and Barrnett, 1962) for endoplasmic reticulum, thiamine pyrophosphatase (TPPase) activity (Novikoff and Goldfischer, 1961), acid phosphatase activity (AcPase) for lysosomes (Mayahara and Chang, 1978), cytochrome oxidase activity (Seligman *et al.,* 1968) for mitochondria, and ZIO reaction (Vrensen and de Groot, 1974) for Golgi apparatus were also employed to demonstrate these marker enzymes in respective cell organelles for three-dimensional observation of cell organelles in thick specimens by high-voltage electron microscopy (Nagata, 1995c, 1997b, 1999a,e, 2000b).

B. Physical Methods in Cytochemistry

Physical methods applied to cytochemistry are the changes of temperature of specimens such as microincineration (Raspail, 1830) at high temperatures and cryo-techniques (Altmann, 1889) at low temperatures and effects of wavelength on absorption such as microspectrophotometry (Caspersson, 1950), fluorescence microscopy, and confocal laser scanning microscopy, or utilization of radiation such as radioautography and X-ray microanalysis (Nagata, 1991). The bases of these methods are physically well known. Among these techniques we employed microinicineration, cryo-techniques, microspectrophotometry, fluorescence microscopy, radioautography, and X-ray microanalysis.

1. Methods Using High or Low Temperatures

a. Microincineration   Since most cells and tissues, except the bones and the teeth, consist mostly of organic compounds the technique of microincineration was first developed to study the inorganic components, mainly the metals, in various cells many years ago (Raspail, 1830). Later the routine technique was established by Scott and Horning (1953). We studied inorganic elements in the skin using microincineration modifying Scott technique, by fixing tissues in a mixture of 9 vol of absolute ethanol and 1 vol of neutral formalin, dehydrating, embedding in paraffin, sectioning, heating the slides carrying sections to 600°C in an oven, and observing by dark field microscopy (Nagata *et al.,* 1957b) (Figs. 2B and 2C).

b. Cryotechniques The cryo-techniques applied to cytochemistry consist of three techniques, cryo-fixation followed by cryo-sectioning, freeze–drying, and freeze–substitution. Varieties of combinations of these procedures were successfully utilized in cytochemistry to prevent loss of soluble compounds in cells, displacement of cell constituents by diffusion, and denaturation of chemical components, especially enzymes. Historically, the cryo-technique to fix and freeze–dry tissues was first introduced to cytochemistry by Altmann (1889, 1894). The procedure was later improved by Gersh (1932) for light microscopy and then for electron microscopy (Gersh, 1956). Frozen sectioning was first used by Schultz-Brauns (1931) for light microscopy, cooling the tissues with a CO_2 jet, and the techniques were later improved by designing a cold knife cooled with dry ice (Adamston and Tayler, 1948), which led to the development of commercially available cryo-stats. Finally the cryo-sectioning was applied to electron microscopy (Fernandez-Moran, 1952). We used these techniques by designing freeze–drying apparatuses (Nawa *et al.,* 1965, 1969) and applied them to both radioautography, demonstrating soluble radiolabeled compounds (Nagata *et al.,* 1969; Nagata, 1972b, 1994a,b; Nagata and Murata, 1977), and enzyme cytochemistry (Yokota and Nagata, 1973, 1974) by electron microscopy (Fig. 2E).

2. Methods Using Lights with Different Wave Lengths

In cytochemistry both visible and invisible lights with various wavelengths from ultraviolet rays to infrared rays were employed by light microscopy. Ultraviolet rays were used to observe the absorption bands of both DNA and RNA, while visible rays at definite wavelengths were used for microspectrophotometry of different color reactions. We used microspectrophotometry using both invisible ultraviolet rays and the visible spectrum (Nagata, 1966a, 1972a).

a. Ultraviolet Rays Using UV rays, we could measure the nucleic acid contents in various cells (Nagata, 1966a, 1972a). The DNA and RNA which contain purin and pyrimidine have the absorption band in the wavelength of 260 nm (Caspersson, 1936, 1950). Since the absorption was proportional to the concentration of the nucleic acids when measured by using this wavelength, the content of each cell could be determined by subjecting the cell, which was sandwiched between a quartz slide and a quartz coverslip, to the ultraviolet rays of the wavelength of 260 nm. In this case, however, only the total sum of both DNA and RNA was obtained. The advantage of this method is that living cells in tissue culture could be measured, so that the total quantity of both nucleic acids could be determined. However, errors in the measurement increased due to the difference between the refractive indices of the medium and the coverslips or the surface of the cells. Therefore, it was preferred to fix the cells and to enclose them in glycerol. By using fixed cells, DNA and RNA could be measured separately by removing either

DNA or RNA with DNase or RNase. However, this method is not used at present because errors could be caused during the extraction of DNA or RNA.

b. Microspectrophotometry   Microspectrophotometry was originally developed by Caspersson (1936) and widely used to measure the contents of nucleic acids of various cells (Wied, 1966). We used an Olympus single-beam microspectropho-tometer Model MSP-A-IV (Nagata, 1966a), which was designed according to the instrument developed as Koana-Naora type (Naora, 1951). The procedure for mea-suring the contents of various cytochemical compounds in the cells is based on the same principle as ordinary spectrophotometry using different wavelengths, both visible and invisible UV rays, depending upon the chemical components we mea-sured. As visible rays we used 560 nm for DNA stained with Feulgen reaction, 650 nm for RNA stained with Azur B, 585 nm for RNA stained with cresyl violet, 435 nm for total proteins stained with Naphthol yellow S, 610 nm for total pro-teins stained with mercuric bromphenol blue, 635 nm for basic proteins stained with fast green, 500 nm for basic proteins stained with gallocynine chromalum, 500 nm for tyrosin and tryptophane stained with Millon reaction, 520 nm for ty-rosin stained with diazotization-coupling, 625 nm for tryptophane stained with *p*-dimethyl-aminobenzaldheyde-nitrite reaction, 520 nm for arginine stained with Sakaguchi reaction, 530 nm for SH-groups stained with DDD reaction, 560 nm for NH_2 and COOH stained with Ninhydrin–Schiff reaction, and 560 nm for glucides stained with PAS reaction. Some of the enzyme reactions such as succinate dehy-drogenase (580 nm), isocitrate dehydrogenase (580 nm), alkaline phosphatase (575 and 501 nm), acid phosphatase (517 nm), glucose-6-phosphatase (550 nm), and aminopeptidase (520 nm) could also be measured using absorptions at different wavelengths (Nagata, 1972a).

c. Flow Cytometry   Recently automatic analysis on DNA ploidy pattern of cell populations was developed using flow cytometers, which are rather expensive apparatuses. Tissues were fixed in 70% ethanol at 4°C, mechanically minced with scissors in a sodium citrate buffer at pH 7.6, and then trypsinized to produce cell suspensions, digested with RNase, and finally stained with propidium iodide for DNA (Alanen, 1989). Cell suspensions were filtered through nylon mesh and the DNA contents of around 10,000 nuclei were measured with a flow cytometer and the S-phase fraction of cells (SPF) was calculated (Dean, 1985). We recently used this procedure for estimating the proliferative activity of parathyroid gland cells surgically obtained from human patients and compared with other immunostaining labeling indices (Xiao-Lin *et al.,* 1996).

3. Methods Using Radiations

The radiations due to electromagnetic waves can physically be divided into four types, alpha-rays, beta-rays, gamma-rays, and X-rays, according to wavelength,

from short to long. Three methods were employed using radiations in cytochemistry, i.e., microradiography, microradioautography, and X-ray microanalysis.

Microradiography is a technique to observe the picture of small tissue specimens penetrated by radiation from soft X-rays resulting in negative images such as chest X-ray films. The small X-ray films are observed by light microscopy. Radioautography is the autograph produced by radiation. It is a technique for demonstrating the patterns of localization of radioactive substances in various specimens incorporating radioactive compounds. The radioautograms can be observed by both light and electron microscopy. X-ray microanalysis is carried out by means of analytical electron microscopes which consist of scanning or transmission electron microscopes equipped with X-ray analyzers. To analyze trace elements in small biological specimens, tissue blocks or thin sections are irradiated with electron beams at a small spot and the emitted X-rays are analyzed with either energy-dispersive or wave-dispersive X-ray analyzers.

a. Microradiography   In cytochemistry, microradiography is used to observe hard tissues such as bone and tooth, penetrated by soft X-rays, resulting in negative images. We used microradioautography to observe the sliced bone tissues (Nagata, 1995b). By this procedure differences of mineralization in tissue sections can be observed by light microscopy.

b. Radioautography   Radioautography is a technique for demonstrating the patterns of localization of radioactive substances in various specimens (Fig. 1B). The specimen, which consists of tissues and cells in contact with the photographic emulsion containing developed silver grains, is called a *radioautograph,* while the pattern of silver grains on the radioautograph is called a *radioautogram,* and the procedure for producing radioautographs is designated as *radioautography*. A radioautograph is an autograph produced by radiation. An *autograph* is a positive picture made by itself. Therefore, the term *radioautogram* means, etymologically, the positive picture produced by radiation that is emitted from the object itself, resulting in an autogram. To the contrary, autoradiogram consists of an autogram and a radiogram. The prefix *auto* means automatic, while the term *radiogram* means the picture of the object which is penetrated by rays resulting in negative images such as microradiogram or chest X-ray films. Thus, autoradiogram etymologically means a negative picture of the specimen produced automatically with radiation emitted from another radiation source away from the specimens (Nagata, 1992). It is now accepted that the both terms, *radioautography* and *autoradiography,* are considered to be synonyms. On the other hand, the term *radioautography* or *autoradiography* means only the techniques for demonstrating the patterns of silver grains in specimens. The radioautography is only the techniques for producing the specimens (radioautographs) for demonstrating the pictures (radioautograms). On the contrary, the present author advocated a new concept, named *radioautographology*. This new term is the coinage synthesized from *radioautography* and

-ology, expressing a new science derived from radioautography. The concept of radioautographology is a science for localizing the radioactive substances in the structure of the objects and to analyze and to study the significance of these substances in the structure (Nagata, 1998b). The science, radioautographoloy, can be divided into two parts, general radioautographology and special radioautographology. The former deals with the principle and techniques of radioautography, while the latter deals with the application of radiography to various materials (Nagata, 1998b). General radioautographology is the technology including all the natural sciences for producing the specimens, which contain radioactive compounds, procedure for tissue preparations, and the methods for getting tissues to make contact with the photographic emulsions and giving exposure for a certain period of time to produce the latent images of the radioactive substances in the specimens and then developing the emulsion to produce the silver metal grains, thus enabling comparisons of both the specimens and the radioautograms in order to learn the localization of radioactive substances in the specimens. We developed the technologies for light and electron microscopic radioautography (Nagata, 1998a) and applied them to cell biology and cytochemistry (Nagata, 1996ab, 1997a, 1998b).

In order to carry out general radioautographologic procedures, three fields of knowledge—physics, concerning the radioactivity; histology and histochemistry, dealing with the fixation, embedding, sectioning, and staining of tissues and cells; and photographic chemistry, requirring photographic emulsions—are necessary. Physics of radioactive substances includes knowledge dealing with radioactive isotopes and radioisotope (RI)-labeled compounds. The radioactive compounds used in radioautography are mainly composed of inorganic or organic compounds that are artifically labeled with RIs, and can be incorporated into human or animal bodies by experiment. The radioactivity emitted from the radioactive isotopes are divided into three kinds of rays, i.e., alpha, beta, and gamma. Among these, the beta ray is the best for radioautography because of its shorter range and the strongest ionization. For radioautography, various kinds of RIs are used, which are listed in Table I. Among them, ^{3}H, ^{14}C, ^{35}S, and ^{125}I are very often utilized for both macro- and microradioautography because they can label various inorganic compounds usually used in biological and medical research.

The RI-labeled compounds used for radioautography in cytochemistry can be classified into two categories, i.e., the precursors, which are incorporated into macromolecules such as nucleic acids (DNA and RNA), proteins, glucides, and lipids, and the other target tracers, which are small molecular compounds such as hormones, neurotransmitters, vitamins, inorganic substances, drugs, and others (Table I). DNA is the main component of nucleoproteins and consists of deoxyribose, phosphate, and bases which contain adenine (A), guanine (G), and cytosine (C). [^{3}H]Thymidine is incorporated into the bases. RNA is composed of ribose, phosphate, and the bases, A, U, G, and C. In order to demonstrate RNA synthesis, ^{3}H-labeled cytidine was formerly used (Nagata, 1967a). However, [^{3}H]cytidine

TABLE I

Radiolabeled Compounds Used in Microscopic Radioautography

Research purpose	Radiolabeled compounds
Macromolecular precursors	
Nucleic acids	
DNA	^{3}H-thymidine
RNA	^{3}H-uridine
Proteins	
Secretory granules	^{3}H-glycine, ^{3}H-leucine, etc.
Collagen	^{3}H-proline, ^{3}H-hydroxyproline
Glucides	
Simple polysaccharides	^{3}H-glucose, ^{3}H-glucosamine, etc.
Mucosubstances	^{35}SO$_4$
Lipids	^{3}H-glycerol, ^{3}H-fatty acids, etc.
Target tracers (small molecular compounds)	
Hormones	^{3}H-steroids, ^{3}H-insulin, etc.
Neurotransmitters	^{3}H-GABA, ^{3}H-dopamine, etc.
Vitamins	^{3}H-vitamin A, B, C, D, etc.
Inorganic substances	^{22}NaCl, ^{45}CaCl$_2$, ^{205}HgCl$_2$, etc.
Drugs	^{3}H-antibiotics, ^{3}H-anti-allergics, etc.
Toxins and others	^{3}H-ouabain, ^{3}H-strychnine, etc.

From T. Nagata. Radiolabelling of soluble and insoluble compounds as demonstrated by light and electron microscopy. In *Recent Advances in Cellular and Molecular Biology.* Vol. 6 (R. J. Wegmann and M. A. Wegmann, Eds.), Leuven; Peeters; pp. 9–21.

could also be incorporated into DNA, although very little, so that demonstration of DNase digestion was necessary to verify RNA synthesis. On the contrary, [^{3}H]5-uridine was shown to be specifically incorporated into only RNA (Nagata, 1991; Nagata *et al.,* 1967a). The proteins consist of polypeptides and the protein synthesis of cells and tissues can be demonstrated by light and electron microscopic radioautography after administration of RI-labeled amino acids such as [^{3}H]glycine, [^{3}H]leucine, [^{3}H]phenylalanine, or tryptophane, which are incorporated into endoplasmic reticulum, Golgi apparatus, and then secretory granules or cytoplasmic ground substance and finally discharged from the cells (Nagata, 1967b, 1991). On the other hand, [^{3}H]proline or [^{3}H]hydroxiproline are incorporated into endoplasmic reticulum and Golgi apparatus of fibroblasts and discharged to the extracellular matrix, forming collagen bundles (Oliveira *et al.,* 1991, 1995; Ma and Nagata, 2000). Glucides are classified biochemically into monosaccharide, disaccharide, and polysaccharide. Monosaccharide and disaccharide are small, water-soluble molecules that cannot be fixed by chemical fixation, but only by cryofixation for soluble compounds. Therefore, only polysaccharide synthesis as well as mucosubstances which can be labeled with ^{35}S-labeled mucosubstances are

usually demonstrated by light and electron microscopic radioautography (Figs. 1B and 2D). The lipids are esters of high fatty acids and can be classified into simple lipids and compound lipids. The former is composed of glycerol and fatty acids, while the latter is composed of both lipids and other components such as phosphates, glucides, or proteins. In order to demonstrate lipid synthesis by light and electron microscopic radioautography, incorporation of either [^{3}H]glycerol or ^{3}H-labeled fatty acids was examined.

In order to study the localization of radioactive compounds in animal bodies, the compounds labeled with specific RIs are usually administered orally to the small animals such as rats and mice or by injections given subcutaneously, intramuscularly, intravenously, or intraperitoneally. All the small animals such as mice and rats were anesthetized after administration of radioactive compounds by either oral administration or injections, and are sacrificed at a given time, usually 1 h after the RI administration, either by decapitation or by perfusing via the left ventricle of the heart with 2.5% glutaraldehyde in 0.1 M cacodylate buffer, pH 7.2, depending on whether insoluble or soluble radioautography will be carried out. For conventional insoluble radioautography the perfusion fixation can be used and the tissues from various organs were taken out, cut into small pieces, soaked in the same glutaraldehyde fixative at 4°C for 1 h, postfixed in 1% osmium tetroxide in the same buffer for 1 h, dehydrated with graded ethanol, and embedded in epoxy resin. On the other hand, *in vitro* labeling of cultured cells and tissue blocks obtained from either animals or human biopsy materials were incubated in media containing radioactive compounds, using CO_2 incubator under normal conditions at 37°C for a given time, usually 1 h or up to a few hours. They were then rinsed in Hanks' solution, fixed in the same buffered glutaraldehyde and osmium tetroxide solutions, dehydrated, and embedded in epoxy resin as above. For the soluble radioautography, however, perfusion fixation cannot be used. The whole bodies of the small animals or organs and tissues taken out after decapitation without using any solution, should be immediately cryo-fixed by either a metal contact method or an immersion method cooled with liquid nitrogen and processed by cryosectioning or freeze–drying or freeze–substitution (Nagata, 1994b). Macroscopic radioautography (RAG) of whole bodies of small animals usually employs cryofixation by immersion into dry ice and acetone mixture and cryo-sectioned in a large cryostat microtome (Ullberg, 1954, 1977; Shimada and Watanabe, 1994). Embedded tissues in epoxy resin can be used for either light microscopic RAG (LMRAG) or electron microscopic RAG (EMRAG). For LMRAG, thick sections at 2 μm are cut on an ultramicrotome and placed on clean glass slides and warmed for extension and drying. For electron microscopy, ultrathin sections of 100 nm thickness are cut, generally using a conventional transmission electron microscope with accelerating voltage at 100 kV. It is generally accepted that the thinner the section is, the better the resolution, but also the less radioactivity it contains and the longer the exposure time needed for radioautography. If any intermediate high-voltage electron microscope is available at such accelerating voltages as 200, 300, or 400 kV, thicker sections at 200 or 300 nm thick can be used. We prefer

to use semithin sections at 200 nm thickness at 400 kV in order to shorten the exposure time (Nagata, 1998a). Ultramicrotomes of mechanical feeding type are preferable to thermal feeding type because of the accuracy of the section thickness, which affects the number of silver grains by radioautography. Ultrathin or semithin sections are picked up onto either platinum or gold meshes in order to prevent the copper meshes from rusting through the histologic and radioautographic treatment, especially the development. Alternatively, collodion-coated copper grid meshes can be used.

We developed simple standard techniques for demonstrating insoluble compounds in various cells and tissues of experimental animals and quantifying the contents of synthesized macromolecules in each cell and cell organelle by both light and electron microscopy. The localization of silver grains developed by means of ordinary radioautography, however, demonstrates only the insoluble radioactive substances bound to the macromolecules fixed in the cell with the chemical fixatives used (Nagata, 1992). On the other hand, radioisotopes bound to the small molecules which are not fixed with ordinary chemical fixatives are washed away through conventional routine procedures such as fixation, dehydration, embedding, sectioning, and radioautographic procedures, so that these compounds cannot be illustrated. Ordinary radioautographic procedures can be designated as "wet-mounting radioautography," since the tissues are processed through both conventional wet treatments and the application of wet radioautographic emulsions to the specimens. In order to demonstrate any soluble radioactive compound, special techniques are required in accordance with the characteristics of the radioisotopes used for radioautography. The techniques for microscopic radioautography developed in our laboratory can be divided into two categories, i.e., wet-mounting radioautography for insoluble compounds such as macromolecular synthesis and dry-mounting radioautography for soluble compounds such as small molecular compounds, each can be subdivided into two methods: light microscopy and electron microscopy. For wet-mounting radioautography by chemical fixation, small animals such as mice and rats are anesthetized and sacrificed either by decapitation or by perfusing via the left ventricles of the hearts with 2.5% glutaraldehyde in 0.1 M cacodylate buffer, pH 7.2, and the tissues from various organs are taken out, cut into small pieces, soaked in the same glutaraldehyde fixative at 4°C for 1 h and postfixed in 1% osmium tetroxide in the same buffer for 1 h, dehydrated with graded ethanol, and embedded in epoxy resin. On the other hand, cultured cells and tissue blocks, incubated in media containing radioactive compounds *in vitro,* using CO_2 incubator under normal conditions at 37°C for given times, are rinsed in Hanks' solution, fixed in the same buffered glutaraldehyde and osmium tetroxide solutions, dehydrated, and embedded in epoxy resin as above. The tissue blocks are cut on an ultratome for either light microscopy (LM) (2 μm thick) or electron microscopy (EM) (0.1–2 μm) and placed onto either glass slides or grid meshes using water. In some cases, the whole mount cells on either glass coverslips or coated meshes in vitro are fixed, dried and used for wet-mounting radioautography to observe the whole cells without sectioning (Nagata, 1997b). In order to observe

isolated cells obtained from the tissues in vivo, small tissue blocks are oscillated in Ranvier's alcohol and isolated, smeared on glass slides, fixed in Carnoy's fluid, and wet-mounted for LMRAG (Nagata *et al.,* 1961). *In situ* hybridization using RI-labeled probes for specific proteins can be carried out to detect their mRNAs, followed by the technique of LMRAG with chemical fixation (Nagata and Kong, 1998; Nagata *et al.,* 1999b).

The techniques of radioautography of soluble compounds can be theoretically classified into two categories from the viewpoint of fixation used (Nagata *et al.,* 1969, Nagata and Murata, 1977). In the precipitation method, the labeled soluble compound is fixed in a mixture containing a substance which reacts with the soluble radioactive compounds, forming a precipitation, so that the fixed tissues can be processed through routine histological procedures followed by a routine wet-mounting radioautography to demonstrate the labeled precipitation. This principle was first used in detecting soluble ^{45}Ca by Nagata and Shimamura (1958, 1959a,b) in light microscopic radioautography of several tissues fixed in a formaldehyde solution containing ammonium oxalate to form calcium oxalate precipitation. At the electron microscopic level, Mizuhira *et al.* (1968) later used this method by fixing the tissues labeled with [^{3}H]thiamine with a glutaraldehyde solution containing platinum chloride to form thiamine–PtC16 precipitation, or fixing labeled [^{3}H]cholesterol with a mixture containing digitonin. This procedure, however, is limited to the radioactive compounds that can be precipitated with any other specific compounds. Moreover, there are many possibilities of diffusion of the labeled compounds when they are precipitated with the fixatives.

By the freezing method, on the other hand, the labeled tissues are quickly frozen in a cooled liquid such as isopentane or propane cooled to its melting point with liquid nitrogen. Then the tissues can be cut by cryo-microtomy. At the light microscopic level, the frozen tissues can be cut in a cryostat and the frozen sections are placed in contact with radioautographic emulsions by various methods. At the light microscopic level, the frozen tissues can be cut in a cryostat at a thickness of around 20–30 μm and the frozen sections are placed in contact with radioautographic emulsions by various techniques. Many papers have been published on this problem. We first used a large-wire loop to produce dry films which were air-dried and applied to cryostat sections placed on glass slides (Nagata and Nawa, 1966a). This procedure is very convenient and will be described in detail. At the electron microscopic level, however, only a few papers have been published on this principle, cryo-ultramicrotomy. Appleton (1964) and Christensen (1971) discussed the possibility of this method but they did not show any results, while we (Nagata and Murata, 1977) reported results for the first time. To the contrary, Mizuhira *et al.* (1981) and Futaesaku and Mizuhira (1986) reported a new technique for ultramicrotomy utilizing interposed films, which is, however, not an ideal procedure because it employs cryosectioning after tissues are immersed into sucrose solution and picking up cryosections with sucrose droplets and applying wet radioautographic emulsion.

On the other hand, freeze–dried or freeze–substituted tissues can be embedded in paraffin or resin for light microscopy and dry sections mounted on precoated slides. Edwards and Udupa (1957) and Smitherman *et al.* (1963) used freeze–dried and paraffin-embedded sections. Miller *et al.* (1964) applied the wire-loop method as part of the dry mounting procedure at the light microscopic level. We improved this technique first at the light microscopic level (Nagata and Nawa, 1966a) and then applied it at the electron microscopic level (Nagata *et al.,* 1977a). Stirling and Kinter (1967) embedded freeze–dried tissues in silicon-araldite and the plastic sections were wet-mounted with a dropping procedure but not dry-mounting.

To demonstrate soluble small molecular compounds, cryo-fixation and dry-mounting radioautography should be routinely employed for both LMRAG and EMRAG (Nagata, 1992, 1994b, 1996b, 1978b).

To fix the tissues quickly by cryo-fixation, we soak the tissues into a quenching fluid which is cooled with a cooling agent. The quenching fluids we usually use are propane (melting point, $-169°C$), isopentane ($-161°C$), or hexane ($-94°C$). These reagents are liquids at low temperatures and conduct heat very well. They also bubble when they contact tissues. Among them, propane is explosive, while hexane has a rather higher melting point. Therefore, isopentane is very often used (Nagata, 1994a,b). Instead of quenching fluids, a pure copper block is sometimes used in direct contact with the tissues. As cooling agents, the following substances or mixtures of two substances are generally used: liquid helium (boiling point, $-269°C$), liquid nitrogen ($-196°C$), liquid air ($-190°C$), dry ice and ether ($-60°C$), dry ice and nonane ($53°C$). Among these, liquid nitrogen is the most frequently used. We usually use the combination of isopentane or propane as the quenching fluid and liquid nitrogen as the cooling agent or a copper block as metal contact and liquid nitrogen as the cooling agent. Recently, cryo-instruments such as RF-2 (Eiko, Tokyo, Japan), JFD-RFA (JEOL, Tokyo, Japan), cryoblock, or cryovacublock (Reichert-Jung, Germany) are commercially available. Liquid nitrogen (200–300 ml) is carefully poured into a Dewer flask. A 50-ml beaker is placed in the liquid nitrogen, and 20–30 ml of isopentane or propane is poured into the beaker. We prefer isopentane to propane. Within a few minutes the liquid isopentane begins to solidify at its melting point of $-160°C$ as it is cooled by the liquid nitrogen at $-196°C$. The tissue blocks or free cells adhering to a small piece of aluminum foil are plunged quickly into the isopentane with a pair of forceps. The frozen tissues are then removed from the isopentane, using a small cup, which is made with a piece of aluminum foil 3×3 cm in size, molded with a No. 00 gelatin capsule in order to prevent ice crystal formation, and transferred into liquid nitrogen in a Dewer flask and stored under the liquid nitrogen until processing. In this process, if the tissues are exposed to the air, ice crystals will grow larger, and the fine structure will be damaged. The frozen tissues are then processed through freeze–drying or freeze–substitution. Both cryo-sectioned and freeze–dried specimens and freeze–dried or freeze–substituted and embedded specimens should be coated with dry radioautographic emulsions without using any water. This

procedure is designated as dry-mounting radioautography (Nagata, 1994b). The procedures for dry-mounting radioautography can be divided into two–light microscopic and electron microscopic—procedures. Historically, various procedures were employed in the literature for light microscopic dry-mounting radioautography as described previously.

Since the first application of cryostat sections on precoated slides at very low temperature by Appleton (1964), many authors recommended this technique at the light microscopic level. However, those procedures are very complicated if treating both specimens and emulsions. We first used dry-films produced with a large wire-loop which were air-dried and applied to cryostat sections placed on glass slides (Nagata and Nawa, 1966a). We believe that this method is the most convenient one. The procedure is briefly as follows. Cryostat sections are placed onto glass slides and dried. Dry epoxy resin sections are expanded over the slids with a drop of ethylene glycol without using any water. Radioautographic emulsion is diluted with an equal part of distilled water at 45°C. We use Konica NR-M2 emulsion from Konica (formerly Sakura) Ltd. (Tokyo, Japan). Any other emulsion, such as available from Kodak, can be used. Ten milliliters of diluted emulsion is added with 0.2 ml at 2% aqueous solution of dioctyl sodium sulfosuccinate (a surfactant) in order to prevent the emulsion film from bursting. A thin film of emulsion is obtained by dipping a wire loop, 2.5 cm in diameter, which is made of platinum wire or vinyl-coated iron wire and set with a piece of Scotch tape on a glass slide as a handle. The handle is set horizontally on a flat desk for air-drying. After air-drying for 1–2 min, when the center of emulsion film is gelled and dried, appearing transparent, but the peripheral zone is still wet, appearing opaque, the film is applied to the slide horizontally. The glass slide is kept in a Petri dish and warmed at 28°C in an incubator for 1 h for drying the emulsion. Several glass slides are placed in a black light-tight plastic slide box that contains desiccant (silica gel), and the top is sealed with black tape. The slide box is kept in a refrigerator at 4°C for exposure. After an appropriate exposure time, the glass slides are processed for development and then stopped in stop bath, fixed in a fixer, and stained with toluidine blue solution for staining. Control tissues should be fixed with chemical fixative, dehydrated, embedded, wet-sectioned, and wet-mounted by conventional dipping procedure.

For electron microscopic dry-mounting procedure, tissues are fixed by rapid freezing and freeze–dried or freeze–substituted; they are dry-sectioned and have to be radioautographed by the dry-mounting procedure (Nagata *et al.,* 1969; Nagata and Murata, 1977). The grids carrying dry sections (either freeze–dried or freeze–substituted Epon embedded sections or freeze–sectioned and freeze–dried) are coated with carbon at 5–10 nm thick before emulsion application. They are then put on a grid holder made of a glass slide (25×75 mm) and three glass rods (3 mm in diameter and 10 mm in length). The routine procedures for dry-mounting are briefly as follows. Radioautographic emulsion is diluted 1 part in 10 with distilled water at 45°C in the dark room. Ten milliliters of the diluted emulsion is added to 0.2 ml of 2% aqueous solution of dioctyl sodium sulfosuccinate and

is maintained at 45°C in a thermobath for several minutes to complete mixing. Dioctyl sodium sulfosuccinate, a surface-activating agent is used to prevent the emulsion films from bursting while they are being dried in the air. We use Konica NR–H2 emulsion, produced by Konica Co., Ltd. (Tokyo, Japan). Other emulsions for electron microscopic radioautography such as Kodak NTB or Ilford L4 can be used in a similar way. All the procedures are as follows. A thin film of the emulsion thus prepared is obtained by dipping a platinum wire loop, about 1cm in diameter, into the emulsion (Nagata *et al.,* 1969). Instead of a small platinum wire loop, a large vinyl-coated iron wire loop, 2.5 cm in diameter, can also be used (Nagata, 1998a). The handle of the wire loop is set on a flat surface for air-drying (for 1–2 min). The best condition for applying the film to the grid is in such a way that the peripheral zone of the film appears gelled but wet (opaque) while the central zone is gelled and almost dry, appearing transparent. The films are almost 100% air-dried without breaking by use of dioctyl sodium sulfosuccinate solution. Without this agent, the films will burst most of the time. The dried films are then applied to the grids on the holders like quoits. The grids are then transferred into Petri dishes and are warmed at 37°C for 1 h to help the films adhere to the grids. The grids are kept in a light-tight container with desiccant and sealed with black vinyl tape and kept in a refrigerator at 4°C for exposure.

On the other hand, when several grids are attached to a square glass block, 12.5 mm in length, a large wire loop, 2.5 cm in diameter, can be used similarly to the wet-mounting procedure, and several blocks are placed on a slide. They are exposed, developed, fixed, and stained simultaneously. Further details in special radioautographology will be described in respective sections in special cytochemistry.

c. Electron Microscopy and X-ray Microanalysis   Electron microscopes are one of the physical tools used in cytochemistry which were developed since the first construction of transmission electron microscope by Knoll and Ruska (1932), later developed to be both transmission and to scanning microscopy. We have used mainly conventional transmission electron microscopes at accelerating voltages from 50 to 100 kV to observe cytochemical reactions. However, since the recent development of high-voltage electron microscopes at accelerating voltages from 400 to 1000 kV, we have made use of the excellent transmission ability to observe thicker biological specimens such as whole mount cultured cells or thick sections stained with histochemical reactions in order to observe the three-dimensional ultrastructure of cell organelles (Nagata, 1995c, 1997b, 1999a,e, 2000).

On the other hand, X-ray microanalysis is carried out by means of analytical electron microscopes which consist of scanning or transmission electron microscopes and X-ray analyzers (Chandler, 1976). To analyze trace elements in small biological specimens, tissue blocks or thin sections, electron beams (with diameters 5–100 nm) are irradiated at a small spot (with diameters 5–100 nm) and the emitted X-rays are analyzed with either an energy-dispersive X-ray analyzer

(EDX) or a wave-dispersive X-ray analyzer (WDX). To analyze the elements in biological specimens, EDX is usually preferred to WDX because all the elements can be detected by EDX. We used transmission analytical electron microscopes equipped with X-ray microanalyzers, i.e., Hitachi H-700 with EMAX-1800E (Horiba, Kyoto, Japan), JEOL JEM 200CX with Kevex 7000-77 (Kevex, UK), and JEOL JEM-4000EX with TN-5400 (Tracor-Northern, Middleton, USA), at accelerating voltages from 100 to 400 kV. X-ray microanalysis is an excellent method for qualifying and quantifying basic elements in biological specimens. We quantified the end products of cytochemical reactions such as Ag in radioautograms or Ce in phosphatase activity or endogeneous trace elements such as Zn, Ca, and S, which originally exist in karyoplasm, cytoplasm, or cell organelles of various cells and intracellular matrix after conventional chemical fixation or cryo-fixation. From our results, it was shown that X-ray microanalysis using intermediate high-voltage transmission electron microscopy at 300 or 400 kV was very useful, resulting in high P/B ratios for quantifying these trace elements in biological specimens (Nagata, 1991, 1993, 2000c). We first started to use X-ray microanalysis in order to quantify the silver grains in electron microscopic radioautograms (Nagata, 1991; Nagata and Usuda, 1985, 1986). Then we studied other elements such as Zn, Ce, S, and Ca observed in various cell types under normal and experimental conditions. X-ray microanalysis on silver grains in radioautograms will be described here in general cytochemistry, while the other elements will be described in respective sections on special cytochemistry.

In order to quantify the concentrations of radiolabeled compounds incorporated into cells and tissues, the number of silver grains was counted with the unaided eye (grain counting). However, it was very troublesome to count the number of silver grains on many photographs one by one. We tried to quantify the silver contents on EMRAG using X-ray microanalysis. Initially, we used the energy dispersive X-ray microanalyzers in the STEM mode, a Hitachi H-700 electron microscope equipped with Horiba EMAX-1800E or a JEOL JEM 200CX equipped with Kevex 7000-77, where the specimens were observed in the STEM mode (Nagata and Usuda, 1985, 1986). The peak counts of Ag–K lines were counted with a probe current of 500 pamp and a small probe diameter (2 μm) in the nucleolus for 100 s with a dead time of 30% as was shown previously (Nagata, 1993).

However, we recently changed to a JEOL JEM-4000EX high-voltage electron microscope equipped with Tracor-Northern TN-5400 EDX in the TEM mode, which is better than the STEM mode because we can observe the structure directly when measuring (Nagata, 1991). In order to quantify the silver content in silver grains in radioautograms, we first used the radioautograms prepared from mouse hepatocytes or pancreatic acinar cells labeled with either [3H]thymidine or [3H]uridine as the models. The diameter of microprobe ranged from 0.2 to 1 μm. The integrated detecting time was 100 s and the dead time was 30%. The beam currents were from 2 to 8 namp and the accelerating voltages from 100, 200, 300, 350, and 400 kV. Figure 2D shows an example of electron microscopic

radioautogram of mouse colon labeled with $^{35}SO_4$, demonstrating mucosubstance synthesis. Figure 3A shows four spectra obtained from a single silver grain observed at accelerating voltages of 100, 200, 300, and 400 kV, demonstrating Ag–Kα, respectively. The results showed the mean peak counts and background counts of silver grains measured at different accelerating voltages, 100, 200, 300, 350, and 400 kV. The peak to background ratios (P/B) at the different accelerating voltages were determined. The curve of the P/B ratios of silver grains calculated, as a function of the accelerating voltage from 100 to 400 kV is shown in Fig. 3B. A maximum was found at 350 kV. We further tested to quantify several elements in biological specimens by 400-kV high-voltage analytical electron microscopy and found it useful to increase the P/B ratio. It was also shown by Bando *et al.* (1985) and Bando (1995) that the P/B ratios of Ag, Al, and Ge in inorganic materials such as ceramics increased with increasing accelerating voltage from 100 to 400 kV, similar to biological specimens.

C. Biological Methods in Cytochemistry

The biological reaction was first introduced into cytochemistry by Coons *et al.* (1941), when they demonstrated the localization of proteins by the fluorescent antibody method. Later, the lectins obtained from plants were also introduced into cytochemistry as another biological reaction to demonstrate sugar residues of glycoproteins (Sharon and Lis, 1972). We used both techniques to demonstrate proteins and glycoproteins.

1. Immunocytochemistry

Coons and his collaborators (Coons *et al.,* 1941) first demonstrated the localization of proteins by the fluorescent antibody method, making use of the very high specificity of immune reactions of animals producing antibody in the localization of antigenic proteins. Then, various techniques were developed by many scientists to label and visualize the localization of antigenic proteins at both light and electron microscopic levels using such markers as fluorochrome (FITC, RITC) and enzymes (horseradish peroxidase, HRP) for light microscopy and metals (ferritin or colloidal gold particles) for electron microscopy. Among of these techniques, we made use of immunofluorescence and peroxidase–anti-peroxidase (PAP) techniques (Usuda and Nagata, 1991) for light microscopy (Fig. 1C) and developed immunoferritin (Fig. 2E) and immunogold techniques (Figs. 13G and 13H) for localizing some enzymes for electron microscopy (Yokota and Nagata, 1974, 1977; Usuda and Nagata, 1991; Usuda *et al.,* 1990, 1991a,b,c, 1994, 1995, 1996).

a. Antibody Localization with Fluorescence and Color Reactions for Light Microscopy   We first used to label the antibodies with fluorochromes such as

A

B
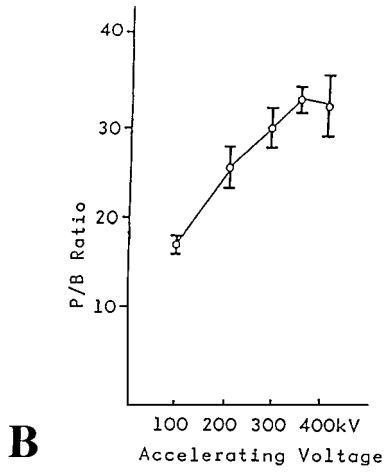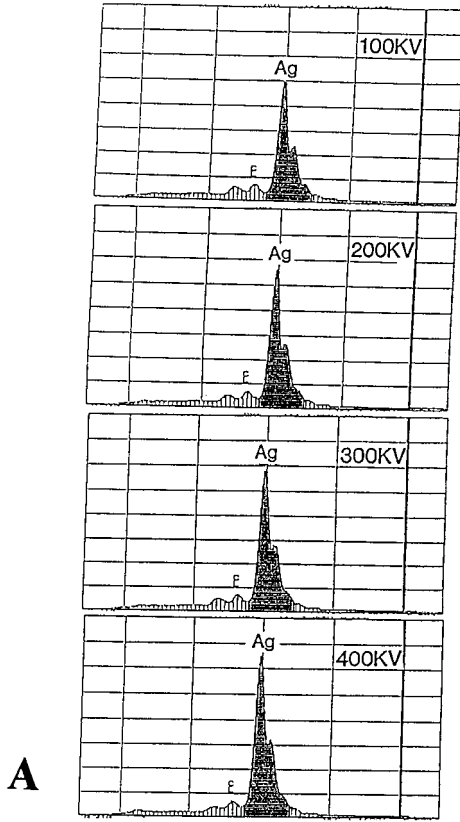
FITC (fluorescein iso-thiocyanate) to localize the antigens in cultured cells. Some cell strains cultured on coverslips from experimental animals such as hepatocytes from Wistar rats or primary cultures of human biopsy materials such as thyroid cancer tissues were rinsed in Hanks' solution, fixed in absolute acetone, and stained with FITC-labeled antibodies such as anti-catalase (Fig. 1C), a peroxisomal enzyme, or anti-keratin and vimentin with anti-rabbit IgG (Murayama *et al.,* 1986). The antibody localization was observed by fluorescence microscopy (Fig. 1C). Since the fluorescence would soon fade away within a few weeks, photography should be carried out immediately after the specimens are prepared. Then, we used a PAP technique modified by Sternberger (1979) to demonstrate the localization of several enzymes such as protein kinase C in the retina and the cerebellum (Usuda *et al.,* 1991a), and the thyroid (Shimizu *et al.,* 1991). Protein kinase C is a diacylglycerol-, phospholipid-, and calcium ion-independent protein kinase and it is generally accepted as playing important roles in cell immunity, mitosis, and cytoskeletal movement (Usuda *et al.,* 1991a). We first purified protein kinase C from rabbit retina and studied immunohistochemical localization of protein kinase C isozymes (types I, II, and III) in the retina and cerebellum using monoclonal antibodies. The rabbits tissues were fixed in 4% paraformaldehyde/0.1 M phosphate buffer, pH 7.4, immersed in graded sucrose solutions (10, 15, and 20%), and frozen in a mixture of dry ice and acetone. Frozen sections were cut on a cryostat microtome at 6 μm thickness and collected on gelatin-coated glass slides. The sections were stained in the sequence of 2% normal rabbit serum for 30 min; primary antibodies (10 μg/ml of protein concentration of IgG fraction or 100 times diluted mouse ascitic fluid) for 2 h; rabbit anti-mouse IgG (DAKO, Copenhagen, Denmark), diluted 1:50, for 1 h; and mouse peroxidase–anti-peroxidase complex (DAKO), diluted 1:250, for 1 h. All three antibody solutions were made with 50 mM Tris–HCl, pH 7.5/150 mM NaCl containing 1% normal rabbit serum. All the treated sections were finally incubated in the medium for peroxidase which contained 0.05% DAB (3,3′-diaminobenzidine tetrachloride) and 0.01% H_2O_2 in Tris–HCl, pH 7.2, for 15 min and counterstained with 1% methyl green solution (Usuda *et al.,* 1991a). Some other immunostaining such as PCNA/cyclin (Hanai *et al.,* 1993), BrdU (Xiao-Lin *et al.,* 1996), and Ki-67 (Xiao-Lin *et al.,* 1996) were

---

FIG. 3   X-ray microanalysis of silver grains in radioautograms. (A) Spectra obtained from a specimen prepared from mouse hepatocytes labeled with [³H]thymidine and observed in a JEOL JEM-4000EX high-voltage electron microscope equipped with Tracor-Northern TN-5400 EDX in the TEM system. The diameter of microprobe ranged from 0.2 to 1 μm. The integrated detecting time was 100 s and the dead time was 30%. The beam currents were from 2 to 8 nA and the accelerating voltages from 100, 200, 300, and 400 kV, demonstrating Ag$K\alpha$, respectively. Copyright permission from T. Nagata (2000d, Fig. 11, p. 23). (B) Relation between P/B ratios and accelerating voltages. The peak to background (P/B) ratios at the different accelerating voltages from the spectra in A were calculated. The curve of the P/B ratios of silver grains determined and plotted as a function of the accelerating voltage from 100 to 400 kV. A maximum was found at 350 kV. Copyright permission from T. Nagata (2000d, Fig. 12, p. 23).

also employed using ABC (avidin–biotin–peroxidase complex) followed by DAB reaction.

b. Antibody Localization with Metal-Conjugate Staining for Electron Microscopy We used two kinds of metal-conjugates, ferritin first and then colloidal gold later. Ferritin, one of the metaloproteins, containing 23% iron, with a molecular weight of around 600,000 to 700,000 Da, can be observed as electron-opaque particles by electron microscopy. The approach to label the antibody with ferritin was first introduced by Singer (1959). In order to demonstrate the localization of urate oxidase and catalase in peroxisomes by electron microscopy, we first used immuno-ferritin staining in combination with cryo-sectioning (Fig. 2E), since the immuno-ferritin conjugate could not penetrate into the intact cells because of its large molecular weight (Yokota and Nagata, 1974, 1977). The tissues were prefixed with 2% glutaraldehyde or 4% formaldehyde in 0.1 M phosphate buffer, pH 7.4, for 60 min and cut into small blocks with a razor blade, washed in the same buffer, and immersed in 50% sucrose or 30% glycerin in 0.05 M phosphate buffer for 1–4 h at 4°C. The tissue blocks were frozen in liquid nitrogen and cryosections were cut with an LKB ultrotome equipped with a cryokit (LKB, Bromma, Sweden). The temperatures of the specimens and the glass knives were controlled at −160 to −120°C and −140 to −100°C, respectively. The cryosections were cut on dry glass knives and were placed onto grid meshes by means of small droplets of saturated sucrose, which were formed on the tip of a fine plastic cannula combined with a needle of a 1-ml syringe (Nagata *et al.,* 1978). The grids carrying cryosections with sucrose droplets were floated consecutively on a large droplet of 0.05 M phosphate buffer, pH 7.4, on 0.15 M NaCl, and on 0.01 M glycine–phosphate-buffered saline (PBS) on a parafilm sheet for 5 min in order to resolve sucrose. The grids were placed on the surface of large droplets of ferritin–antibody conjugate and allowed to incubate for 5–10 min. The excess conjugate was removed by floating the grids on the surface of five large droplets of Gly–phosphate-buffered saline (PBS). For control, a few grids were treated with 1.5% antibody solution, and then incubated with the conjugate. All the grids were refixed with 2% glutaraldehyde in 0.1 M phosphate buffer, pH 7.4, by floating on the surface of the fixative for 10 min, washed with running distilled water, and finally negatively stained with 0.2% phosphotungustic acid (Yokota and Nagata, 1973, 1974, 1977).

Recently, colloidal gold particles conjugated with protein A to antibodies, frequently used instead of ferritin particles because of the better contrast of gold particles than ferritin by electron microscopy. Protein A is the protein produced by *Staphylocuccus aureus* and specifically binds to IgG of various animals. The protein A–colloidal gold method was introduced by Roth *et al.* (1978) for immuno-electron staining. Since the homogeneous sizes of gold particles can be used, two or three antibodies can be stained and observed simultaneously (Bendayan 1982; Usuda *et al.,* 1991c). Moreover, the density of colloidal gold particles are

in proportion to the concentration of the bound antibody, the quantification of immuno-staining can be carried out. We developed the protein A–gold immuno-staining by postembedding technique in combination with the cryotechnique by rapid freezing and freeze–substitution without chemical fixatives for demonstrating peroxisomal enzymes such as urate oxidase, catalase, D-amino acid oxidase, L-α-hydroxyacid oxidase, glycolate oxidase, and acyl-CoA oxidase in rat liver, kidney, and intestine (Usuda *et al.,* 1990, 1996; Usuda and Nagata, 1991). Tissue blocks were rapidly frozen by metal contact freezing in liquid nitrogen ($-196°$C) and were freeze–substituted with absolute acetone without any chemical fixatives at $-80°$C in a deep freezer for 48 h and then the temperature of the freezer was gradually raised to $-20°$C and kept at $-20°$C for 3 h. The tissues were then transferred to Lowicryl K4M solution and polymerized at $-20°$C with a UV polymerizer. They were kept in the deep freezer at $-20°$C overnight and ultrathin sections were cut on a Porter-Blum MT2B ultramicrotome for immunostaining. Thin sections were collected on formvar-coated nickel grids. They were stained first with catalase or any other antibody, then with protein A–colloidal gold particles, and finally with uranyl acetate and lead citrate. To observe two antibodies on the same section, for example, one side of the section was stained with the antibody for D-amino acid oxidase antibody and 15-nm protein A–colloidal gold particles, and the other side of each section was stained with the antibody for catalase and 5-nm protein A–colloidal gold particles (Usuda *et al.,* 1991c). For control staining, the sections were stained only with protein A–gold solution or IgG fraction of nonimmune rabbit serum instead of antibodies.

2. Lectin Cytochemistry

Lectins were found as carbohydrate-binding proteins obtained from various plants such as *Ricinnus communis* agglutinin from castor beans, concanavalin A from Jack beans, peanut agglutinin from peanut *Arachis hypogaea* or animals such as *Helix pomatin* agglutinin from snails which specifically bind to sugar residues in glycoproteins such as lactose, mannose, *N*-acetyl-galactosamine, or *N*-acetyl-glucosamine, respectively (Goldstein and Hayes, 1978). These specificities were applied to demonstrate the localization of these sugar residues by labeling the lectins with such markers as FITC, HRP, avidin–biotin, ferritin, or gold particles as lectin-conjugates for visualizing the lectin-binding sites by both light and electron microscopy (Roth and Binder, 1978). We used some lectin conjugates to demonstrate several sugar residues in various specific cells by light and electron microscopy (Hanai *et al.,* 1994a,b,c,d).

a. Lectin Binding Sites of Sugar Residues with Avidin–Biotin Staining for Light Microscopy We studied the compositional changes in glycoconjugates in mouse kidney (Fig. 1D) and retina using 16 kinds of biotinylated lectin, followed by the ABC (avidin–biotin complex) and DAB methods for light microscopy (Hanai

et al., 1994a,b,c,d). For the ABC method, tissues were fixed in 4% paraformalde-
hyde/0.1 M sodium phosphate, pH 7.4, for 24 h, immersed in graded sucrose
solutions, 10, 15, and 20%, for 12 h each, frozen at $-80°C$ in a mixture of dry ice
and *n*-hexane, and frozen sections cut on a cryostat microtome. The frozen sec-
tions were placed onto glass slides and stained with biotinylated lectins followed
by ABC according to Hsu *et al.* (1981). Briefly, sections were stained with biotiny-
lated lectin (2 μg/ml) for 1 h and with avidin–biotin–peroxidase complex (Vector
Laboratories, Burlington, CA) for 1 h. The reaction products were visualized by
the DAB reaction, 0.05% DAB (Wako, Tokyo, Japan), and 0.01% hydrogen perox-
ide in 0.05 M Tris–HCl buffer, pH 7.2, for 10 min (Hanai *et al.,* 1994a,b,c,d). The
controls were stained with only with ABC without biotinylated lectins and staining
with mixtures of biotinylated lectins and their respective inhibitory sugars. The
biotinylated lectins and inhibitory sugars used are listed in Table II. As the results,
lectin binding sites for specific sugar residues with brown positive reaction can be
localized, while control reactions should be negative.

TABLE II
Biotinylated Lectins and Inhibitory Sugars Used for Staining

Lectin	Abbreviation	Inhibitory sugars
Canvalia ensiformis	ConA	Man, MM, MG
Dolichos biflorus	DBA	GalNAc
Lens culinaris	LCA	Man, MM, MG
Phaseolus vulgaris E4	PHA-E4	GalNAc
Arahis huposaea (peanut)	PNA	Gal, Lactose
Ricinus communis 120	RCA 120	Gal, Lactose
Ulex europaerus I	UEA-I	Fucose
Triticum vulgaris	WGA	GlcNAc, chito-oligosaccharide
Agaricus bisporis	ABA	Gal, GalNAc
Datura stramonium	DSA	Chito-oligosaccharide
Lotus tetragonolobus	Lotus	Fucose
Maackia amurensis	MAM	Lactose
Phaseolus vulgaris L4	PHA-L4	GalNAc
Ricinum communis 60	RCA60	Gal, Lactose
Glycine max (soybean)	SBA	GalNAc
Sambucus sieboldiana	SSA	Lactose

Abbreviations for inhibitory sugars: GalNAc = N-acetyl-D-galactosamine,
GlcNAc = N-acetyl-D-glucosamine, Gal = D-galactose, Man = mannose, MM =
methyl-α-D-mannoside, MG = methyl-α-D-glucoside
From T. Nagata and Y. Kong (2000).

b. Lectin Binding Sites of Sugar Residues with Protein A–Gold Staining for Electron Microscopy For electron microscopy, we studied the compositional changes in glycoconjugates in mouse kidney and retina using 16 kinds of biotinylated lectin, followed by protein A–gold technique instead of ABC and DAB methods for light microscopy (Hanai *et al.,* 1994d), slightly modified from Roth (1983). For the protein A–gold method, tissues were fixed in buffered 0.1% glutaraldehyde and 4% paraformaldehyde/0.1 M sodium phosphate, pH 7.4, for 24 h, embedded in Lowicry K4M at a low temperature (−20°C). Ultrathin sections were cut and stained by biotinylated lectin conjugates followed by streptavidin–colloidal gold (10 nm) complex. After routine electron staining with uranyl acetate and lead citrate, the positive sites can be demonstrated with gold particle localization (Hanai *et al.,* 1994d). The controls should be stained with only colloidal gold–protein A complex without biotinylated lectins and staining with mixtures of biotinylated lectins and their respective inhibitory sugars similar to the ABC method. The biotinylated lectins and inhibitory sugars used are the same as in Table II.

IV. Special Cytochemistry

A. Locomotive Cells

The locomotive cells consist of bone and cartilage cells, synovial cells, joint and ligament cells in the skeletal system, and the skeletal muscle cells in the muscular system. Among the special cells in locomotive organs, we studied the cartilage and bone cells in salamanders, synovial cells in men, ligaments in men and skeletal muscle cells in mice.

1. Bone and Cartilage Cells

With regards the bone and cartilage cells, we studied the skeletons of aging salamanders from hatching to senescence (Nagata, 1998c). The forelimbs and hind limbs of salamanders are composed of bones and cartilage which are covered with skeletal muscles, connective tissues, and epidermis consisting of stratified squamous epithelial cells in the outermost layer. The bones of juvenile salamanders at 4 weeks consisted of the hyaline cartilage. The hyaline cartilage consisted of spherical or polygonal cartilage cells or chondrocytes at the center. They were surrounded by rich interstitial ground substance which stained deep blue with toluidine blue staining. The spherical cartilage cells at the center of the bone changed their shape to a flattened shape under the perichondrium or free joint surfaces. Some of the nuclei of the chondrocytes were labeled with silver grains. Mitotic figures were frequently seen in spherical cartilage cells in young animals. Examination of radioautograms at the young stages such as 4 weeks after hatching showed that
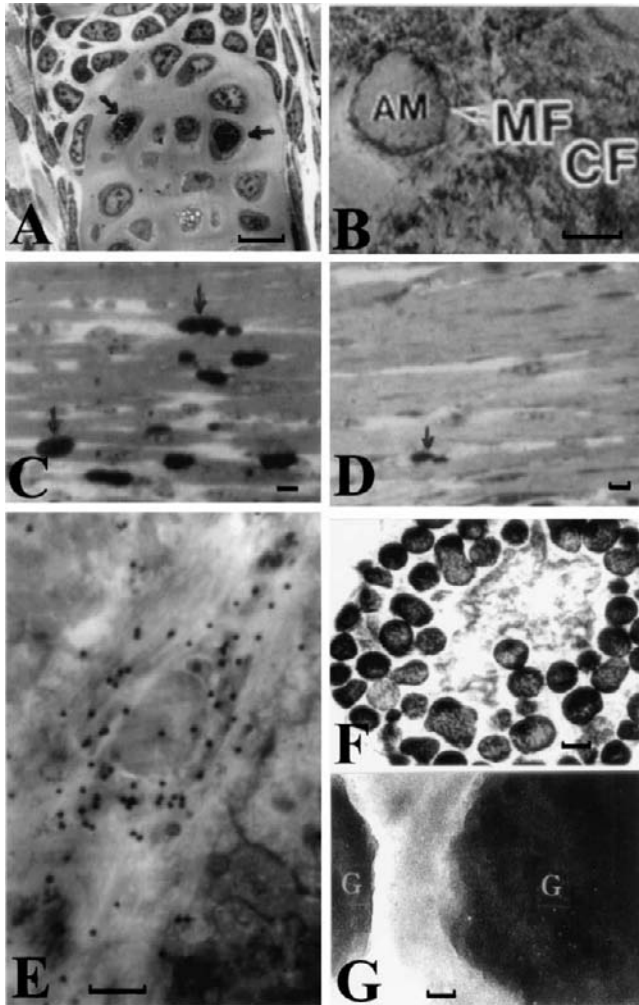
FIG. 4 Special cytochemistry 1: The locomotive cells and mast cells. (A) Light microscopic radio-autogram (LMRAG) of the bone of a forelimb of a salamander at 4 weeks after hatching, labeled with [^{3}H]thymidine. Many nuclei of cartilage cells are labeled with silver grains showing DNA synthesis (×1200; bar = 10 μm). Permission from T. Nagata (1998c, Fig. 1, p. 4). (B) Electron microgram of an Epon-embedded section of the interlaminar portion of the human yellow ligament. Each elastic fiber contains a central amorphous material (AM) which is surrounded by myofilaments (MF) and many collagen fibers (CF) (×7500; bar = 1 μm). (C) LMRAG of the intercostal muscle fibers of a mouse embryo at day 17. Many labeled nuclei are found between the myotubes (×260; bar = 10 μm). Permission from K. Hayashi et al. (1993, Fig. 6, p. 557). (D) LMRAG of the inter-costal muscle fibers of a newborn mouse at day 1. Only a few labeled nuclei are found between the striated myofibers (×260; bar = 10 μm). Permission from K. Hayashi et al. (1993, Fig. 9, p. 557). (E) Electron microscopic radioautogram (EMRAG) of the quadriceps femoris muscle of a normal

many spherical cartilage cells and flattened cartilage cells were predominantly labeled (Fig. 4A). At 6 weeks after hatching, the bones enlarged and the number of cartilage cells increased. At this stage, however, the number of labeled cells in the cartilage cells decreased as compared with the previous stage. The bones in juvenile animals at 8, 9, 10, and 11 weeks enlarged gradually. Radioautograms at these stages showed that the number of the labeled cells remarkably reduced as compared with those at 4 and 6 weeks. In the adult salamanders at 8–12 months, the bones showed complete mature structure and examination of radioautograms revealed that the number of labeled cells reached almost zero. No difference was found in the morphology and labeling between the forelimbs and the hind limbs at any stage.

The labeling indices of respective cell types changed with aging as expressed by mean in each group. The labeling index of the cartilage cells was lower than the epithelial cells. The peak of the labeling index of the cartilage cells in both forelimbs and hind limbs was found to be about 15–18% at 4 weeks after hatching. The labeling index of the cartilage cells in both limbs at 6 weeks rapidly decreased to about 4–6%, increased at 8 weeks to about 7–8%, and finally decreased to 2–3% gradually from 8 weeks to 9 weeks with aging and fell down to 0–1% at 10 weeks. The labeling index of cartilage cells from 10 weeks to 12 months stayed very low, around 0–1%.

2. Synovial Cells

The joints of animals consisted of two or three or more bones and the synovial membranes covering the bones. The synovial membranes are composed of the collagenous fibers interspersed with the synovial cells which are fibroblasts and lining cells. We studied macromolecular synthesis of the synovial cells of the joints surgically obtained from 15 elderly patients suffering from rheumatoid arthritis. Both the normal and rheumatoid cells were cultured and labeled *in vitro* with [^{3}H]thymidine, [^{3}H]uridine, and [^{3}H]leucine and radioautographed. DNA, RNA, and protein syntheses were observed by light microscopic radioautography in both normal and rheumatoid cells. As the results, no significant difference was observed between the labeling indices of normal and rheumatoid cells labeled with [^{3}H]thymidine. Many silver grains were observed in both the rheumatoid synovial lining cells and sublining cells labeled with [^{3}H]uridine. However, a small

adult mouse labeled with [^{3}H]taurine, processed for freeze–substitution, followed by dry-mounting radioautography. Many silver grains appeared on sarcoplasmic reticulum, myofilaments, mitochondria, and sarcoplasmic membrane ($\times$7500; bar = 1 μm). (F) Low-power electron micrograph of a mast cell, obtained from rat peritoneal exudate which was quickly frozen, freeze–substituted, embedded in Epon, and dry-sectioned ($\times$3750; bar = 1 μm). Permission from T. Nagata (2000d, Fig. 26a, p. 30). (G) High-power magnification photograph of two specific granules (G) from the same specimen as shown in Fig. 4F. ($\times$1500; bar = 0.2 μm). Permission from T. Nagata (2000d, Fig. 26b, p. 30).

number of silver grains were observed in these cells labeled with [³H]leucine. From the results, it was concluded that the synovial cells synthesized DNA, RNA, and proteins in both normal and rheumatoid conditions. However, the quantities of these macromolecules synthesized in these synovial cells varied in respective individuals and no significant difference was found between the normal and rheumatoid cells (Kobayashi and Nagata, 1994).

3. Ligament Cells

The ligaments which bind 2 or more bones are composed of dense regular connective tissues consisting of collagenous bundles and interspersing fibroblasts or fibrocytes. We studied the human yellow ligaments in younger and elderly patients suffering from the ossification of the ligaments which were surgically obtained (Ono, 1991; Ono and Nagata, 1988, 1992; Ono *et al.,* 1994). We first studied the calcium content in biopsies of the lumbar yellow ligament (ligamentum flavum) obtained from human patients suffering from the ossification of the ligaments and lumbar canal stenosis (Ono, 1991; Ono and Nagata, 1988, 1992; Ono *et al.,* 1994). The specimens were cut into three portions, i.e., the interlaminar portion (Fig. 4B), the ligament inserted portion in the upper part of the lamina and the upper part of the laminar portion (the ossified tissue). Each was divided into two and one part was quickly frozen by the metal contact method at $-192°$C, followed by cryosectioning (0.5 μm) with an LKB cryo-NOVA ultramicrotome and freeze–dried at $-80°$C while another part was double-fixed in buffered 2.5% glutaraldehyde and 1% osmium tetroxide followed by dehydration and embedding in Epon, respectively. Semithin Epon sections (0.2 μm) and cryo-sections were analyzed with a JOEL JEM 4000EX TEM system equipped with a Tracor-Northern energy–dispersive X-ray microanalyzer (TN-5400) at an accelerating voltage of 300 kV. From the results, it was shown that much more soluble Ca and P was present in freeze–dried cryosections of the ligament-inserted portion than in chemically fixed specimens of the same patients (Fig. 8). It is concluded that a sizable fraction of soluble calcium in the unmineralized fibrocartilage zone was detected, which was considered to be the characteristic of the mineralization process in the human lumbar yellow ligaments.

4. Skeletal Muscle Cells

The muscle cells are contractile cells responsible for the movements of various parts of animals and can be classified into three kinds, skeletal, smooth, and cardiac. The cardiac muscle cells are the component of the heart and the smooth muscle cells are the parts of the walls of the visceral organs. They will be described in respective sections. The skeletal muscle cells are the essential component of the locomotive organs and will be treated here.

As chemical reactions, skeletal muscle fibers from chickens and frogs were stained with a modified Golgi silver impregnation method and the reaction products

in the sarcoplasmic reticulum (SR) were observed three dimensionally by high-voltage electron microscopy at 400 kV (Hayashi and Nagata, 1991). The results revealed that the networks of SR in both twitch and slow muscle fibers of chickens and frogs were classified into two categories, intermyofibrillar SR and subsarcolemmal SR. The intermyofibrillar SR in twitch fibers was basically similar, consisting of three or four typical structural regions. The configuration of the intermyofibrillar SR in twitch fibers is divided into two main groups which represented the SR in the fast twitch and slow twitch fibers. The structure of subsarcolemmal SR in slow tonic fibers was almost the same as in twitch fibers, forming polygonal mesh at the center of A-band and a loose tubular network including distended cisternae (Hayashi and Nagata, 1991).

The DNA synthesis of ddY mouse intercostal muscles from prenatal day 13 through postnatal 24 months was studied by [^{3}H]thymidine radioautography (Hayashi and Nagata, 1993). Many nuclei were labeled in myotubes at embryonic days 13–19 (Fig. 4C), while the number of labeled nuclei decreased after birth (Fig. 4D). The labeling indices revealed chronological changes, reaching a peak at embryo day 13, and decreasing gradually after birth to 0% at 3 months. We also studied the DNA synthesis of rat thigh muscles when injured and labeled with [^{3}H]thymidine, demonstrating satellite cell regeneration, as well as the DNA synthesis of satellite cells in the muscles of dystrophy chickens. When Wistar rat thigh muscles were injured and labeled with [^{3}H]thymidine, satellite cells were labeled, showing that the regenerating muscle fibers originated from satellite cells (Sakai *et al.,* 1977). In the thigh muscles of dystrophy chickens, [^{3}H]thymidine was incorporated into the satellite cells by LMRAG (Oguchi and Nagata, 1980) and EMRAG (Oguchi and Nagata, 1981), demonstrating the regeneration in these cells, which cannot be observed in normal muscles. As for the incorporation of [^{3}H]taurine, however, no difference was found between normal and dystrophy mice by chemical fixation and wet-mounting radioautography (Terauchi *et al.,* 1988). When [^{3}H]taurine was administered to normal or dystrophy mice (518 kBq/g body weight) and their skeletal muscles were observed by freeze–substituted or freeze–dried specimens followed by dry-mounting radioautography, silver grains appeared on sarcoplasmic reticulum, myofilaments, mitochondria, and sarcoplasmic membranes (Terauchi and Nagata, 1993), showing soluble compounds (Fig. 5E). By this method, more silver grains were observed in normal mice than dystrophy mice. To the contrary, only few silver grains were observed in the specimens which were fixed with conventional glutaraldehyde and osmium tetroxide fixation followed by wet-mounting radioautography (Terauchi and Nagata, 1993).

B. Cardiovascular Cells

The cardiovascular cells composing the cardiovascular system of animals are consisted of the cardiac muscle cells of the heart, the vascular cells of the blood and lymph vessels, the blood cells including erythrocytes, leukocytes, lymphocytes,
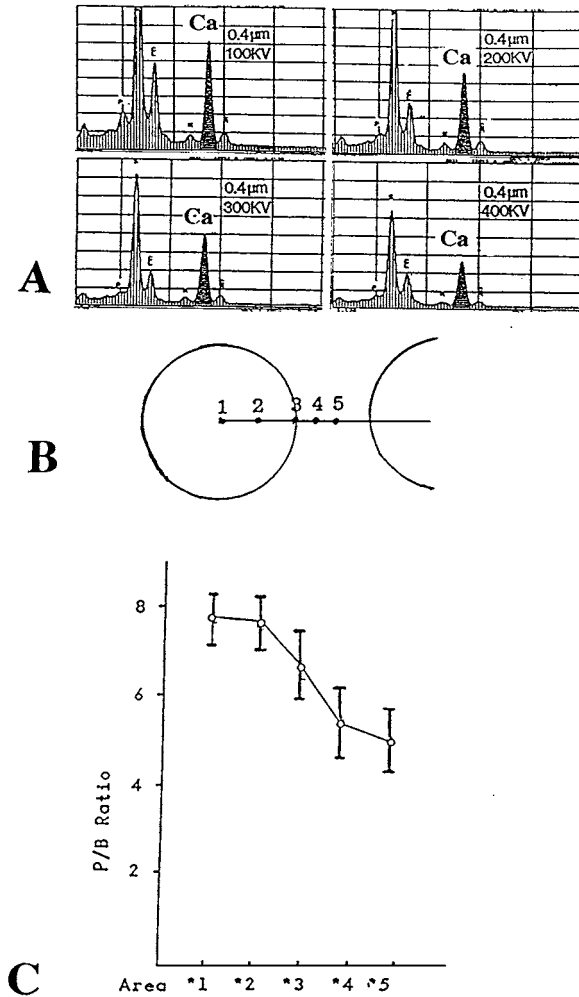
FIG. 5   X-ray micronalysis of Ca in mast cell granules. (A) X-ray spectra obtained from mast cell granules, sectioned either at 0.4 μm thickness and observed with JEM 4000EX TEM system with a Tracor-Northern TN-5400 analyzer at accelerating voltages of 100, 200, 300, and 400 kV. Two peaks of CaK_α and K_β can be seen. Permission from T. Nagata (2000d, Fig. 27, p. 31). (B) Diagram showing five areas between the granule and surrounding cytoplasm of a mast cell as seen in Figs. 4F and 4G. Area 1, center of the granule, area 2, the midpoint between the center and the membrane of the granule, area 3, the point on the limiting membrane of the granule, area 4, the midpoint between the limiting membrane of the granule and the cytoplasmic ground substance, area 5, the midpoint in the cytoplasm between the two granules. Permission from T. Nagata (2000d, Fig. 29, p. 32). (C) Transitional curve of P/B ratios in relation to the intracellular localization between the granules and surrounding cytoplasm as shown in Fig. 12. Permission from T. Nagata (2000d, Fig. 30, p. 32).

thrombocytes and their immature cells, as well as other free cells such as mast cells and the splenic and lymphatic cells.

1. Cardiac Muscle Cells

Ultrastructural and histochemical changes of cardiac muscle cells of rats during global ischemia and reperfused rat heart were observed by electron microscopy (Yanagiya, 1994; Yanagiya *et al.,*1994). Ultrastructural changes of mitochondria were evaluated by scoring the mitochondiral changes and densitometry of the matrix as a marker of the density of the granules of the mitochondrial matrix. For demonstrating cytochrome oxidase activity in mitochondria, 3,3′-diamino-benzidine (DAB) reaction was used. Histochemical modification of the cytochrome oxidase activities were evaluated by using a scoring system of localization of cytochrome oxidase and by densitometry of the mitochondria. In the ischemic groups, ultrastructural changes, such as a decrease of mitochondrial matrix granules and disruption of cristae, were observed from 60 min ischemia. However, no particular ultrastructural changes were observed from 60 to 240 min ischemia (Yanagiya *et al.,* 1994). In perfusion after 60 min ischemia, the ultrastructural changes were recovered. However, the changes caused by 120 min ischemia did not recover. The cytochrome oxidase activity in mitochondria did not change until 240 min ischemia. However, the activity was sparsely observed in the 240-min ischemia group. The enzyme histochemical changes of cytochrome oxidase activity may lag behind the ultrastructural changes of mitochondria (Yanagiya, 1994).

On the other hand, nucleic acid synthesis in cultured fibroblasts from the hearts of chick embryos was studied by light microscopic radioautography (Nagata and Nawa, 1966b). The incorporation of [3H]thymidine into each nucleus of a binucleate cell was a little less than that of a mononucleate cell, but the total of the two nuclei of a binucleate cell was almost twice that of a mononucleate cell. The incorporation of [3H]uridine in the two nuclei of a binucleate cell was twice that of a mononucleate cell, while the incorporation of [3H]uridine in the cytoplasm of a binucleate cell was less than twice that of a mononucleate cell. It was concluded that the nucleic acid synthesis of both DNA and RNA increased in binucleate cells compared to that seen in mononucleate cells of chick embryo heart fibroblasts (Nagata and Nawa, 1966).

2. Vascular Cells

The blood vessels, both arteries and veins, consist of three layers: from inside to outside, the tunica intima, the media, and the adventitia. Those layers are formed with connective tissues and the smooth muscles. We studied the localization of antihypertensive drugs in the supramesenteric arteries of the spontaneous hypertensive rats (Suzuki *et al.,* 1994). Two kinds of antihypertensive drugs, labeled with RI, [3H]benidipine hydrochloride (Kyowa Hakko Kogyo Co., Shizuoka, Japan),

and [^{3}H]nitrendipine (New England Nuclear, Boston, MA) were used. Both intra-venous administration into rats and *in vitro* incubation for 10 to 30 min were employed. For light and electron microscopic radioautography, both wet-mounting radioautograms after chemical fixation and dry-mounting radioautograms after cryo-fixation and freeze–substitution were prepared. The silver grains due to the antihypertensive drugs were localized over the plasma membrances and the cytoplasm of the fibrocytes in the intima and the smooth muscle cells in the media, suggesting the pharmacological active sites (Suzuki *et al.,* 1994).

3. Blood Cells

The mature blood cells circulating in the blood vessels of various animals are classified into 3 types, the erythrocytes, the leukocytes, and the blood platelets. Those mature cells are formed either in the lymphatic tissues in the lymphatic organs or the myeloid tissues in the bone marrow, where various immature cells, lymphoblasts, erythroblasts, myeloblasts and meyocytes, and megakaryocytes can be observed. Among these blood cells, we studied macromolecular synthesis and their cytochemical localization in leukocytes, megakaryocytes, and blood platelets. As enzyme cytochemistry, arylsulfatase B activity in the rabbit blood platelets was observed by electron microscopy (Murata *et al.,* 1975). The results showed that the reaction products were exclusively localized in the alpha granules of the platelets. The localization of the activity in each platelet showed different staining patterns, which suggested variable functional heterogeneity in the granules (Murata and Nagata, 1976). The ultrastructural localization of acid mucosubstances in the human basophilic leukocytes was studied with dialyzed iron (DI) and observed by light and electron microscopy (Murata and Nagata, 1976). It was demonstrated that DI-positive mucosubstances were localized on the cell membranes and specific granules of normal human basophilic leukocytes (Murata and Nagata, 1976). In the lymphocytes obtained from genetic mucosaccharidosis patients (Hurler's, Hunter's, and Morquio's syndromes) numerous vacuoles were found in the cytoplasm which showed DI-positive mucosubstances as well as acid phosphatase activity revealing the participation of endocytosis in the formation of these vacuoles (Murata *et al.,* 1977a,c).

4. Mast Cells

Mast cells are widely found distributed in the loose connective tissues of most mammals, as well as in the serous exudate in the peritoneal cavity as one of the free cells. We studied the fine structure and nucleic acid and mucosubstance syntheses of normal mast cells and Dunn and Potter's mastcytoma cells in mice and rats by electron microscopic radioautography (Murata *et al.,* 1977d, 1978b). The results showed that the labeling index of [^{3}H]thymidine incorporation in normal mast cells was very low (0.37%) while that of mastcytomas cells was

high (Murata *et al.,* 1977b). Some of the normal mast cells and mastcytoma cells incorporated [^{3}H]thymidine, [^{3}H]uridine, and $^{35}SO_4$, demonstrating DNA, RNA, and mucosubstance syntheses. The incorporation of [^{3}H]thymidine was observed in the nuclei and mitochondria, that of [^{3}H]uridine in nuclei, nucleoli, mitochondria, and ribosomes, and that of $^{35}SO_4$ in the Golgi apparatus and the granules (Murata *et al.,*1978b).

On the other hand, we demonstrated intracellular localization of a synthetic anti-allergic drug, tranilast, by radioautography (Nagata *et al.,* 1986; Nishigaki *et al.,* 1987). As was demonstrated by light and electron microscopic radioautography, accumulation of silver grains over mast cell granules suggested the inhibition of degranulation of mast cells for anti-allergic reaction (Nagata *et al.,* 1986; Nishigaki *et al.,* 1990). From these results, it was presumed that this agent might interfere with the Ca influx resulting in the histamine release in allergic reaction. Therefore, we examined quantitatively Ca concentration in mast cells. Mast cells were collected from the peritoneal exudate of Wistar strain rats, centrifuged, cryo-fixed in isopentane cooled with liquid nitrogen, freeze–substituted, embedded in Epon, and dry-sectioned. Figure 4F shows an electron micrograph of a rat mast cell, cryo-fixed, freeze–substituted, embedded in Epon, and dry-sectioned (Nagata, 2000d). Specific granules appear electron dense. Figure 4G is a high-power magnification of two specific granules from the same specimen as shown in Fig. 4F. For X-ray microanalysis a JEM 4000EX TEM system with a Tracor-Northern TN-5400 analyzer was used with a fixed beam current at 3.2 nA and 2 μm in diameter for 100 s with a dead time of 30%, changing the accelerating voltages from 100 to 400 kV. Figure 5A shows the four spectra obtained from a mast cell granule, sectioned at 0.4 μm and observed at 100 to 400 kV. There are two peaks of Ca$K\alpha$ and -$K\beta$. The peak counts of Ca$K\alpha$ and background counts of mast cell cytoplasm cut at either 0.2 or 0.4 μm and observed at 100, 200, 300, 350, and 400 kV are calculated. Comparing the two curves of the P/B ratios obtained from thinner (0.2 μm) and thicker sections (0.4 μm), it was shown that the results from the thicker sections were higher than those from thinner sections. We initially tried to verify the relationship between the section thickness and Ca concentrations as was well known under the name of Lambert's law by microspectrophotometry (Nagata, 1972a). However, this relation was not proved to be a clear linearity but only approximate correlation. In any case, the maximum was found at 300 kV in both curves. Therefore, we used 300 kV for further quantification. In order to detect the intracellular distribution of Ca ions in mast cells in relation to granules, we set up five areas around a granule in mast cell cytoplasm. They are designated as areas 1, 2, 3, 4, and 5, as shown in Fig. 5B. Area 1 is the center of a granule, while area 2 is the midpoint between the center of the granule and the limiting membrane of the granule, area 3 is the limiting membrane of the granule, area 4 is the midpoint between the limiting membrane of the granule and the cytoplasmic ground substance surrounding the granule, and area 5 is the midpoint in the ground substance between the two granules. We calculated the mean peak counts
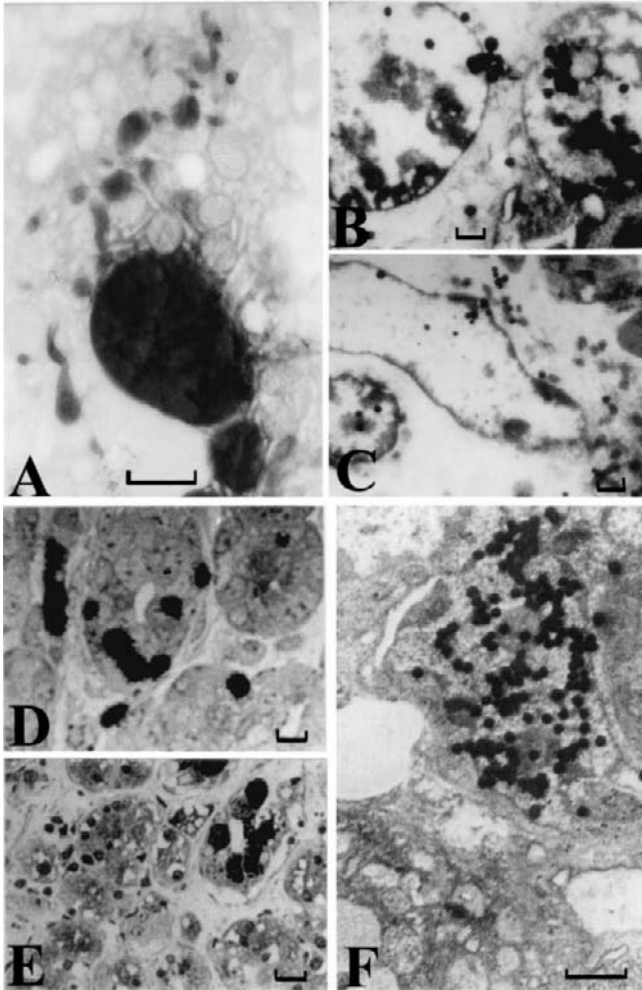
FIG. 6   Special cytochemistry 2: The spleen cells and the submandibular gland cells. (A) Electron micrograph of a reticular cell in the spleen of a newborn mouse at postnatal day 1, showing AcPase activity by cerium substrate method. Electron-dense deposits are localized in lysosomes ($\times$9,000; bar = 1 μm). Permission from T. Nagata (2000d, Fig. 14, p. 25). (B) EMRAG of labeled lymphoblasts in a newborn mouse spleen, at postnatal day 1, labeled with [^{3}H]leucine, demonstrating protein synthesis ($\times$3750; bar = 1 μm). Permission from T. Nagata and M. T. Olea (1999, Fig. 1, p. 4). (C) EMRAG of a labeled littoral cell in a newborn mouse spleen, at postnatal day 14, labeled with [^{3}H]leucine, demonstrating protein synthesis ($\times$3750; bar = 1 μm). Permission from T. Nagata and M. T. Olea (1999, Fig. 4, p. 4). (D) LMRAG of the submandibular gland obtained from a 1 day old newborn mouse labeled with [^{3}H]thymidine *in vitro* and radioautographed. Many nuclei of acinar cells and ductal cells are labeled with silver grains demonstrating DNA synthesis ($\times$375; bar = 10 μm). Original picture. (E) LMRAG of the submandibular gland obtained from a 1-year-old senescent mouse labeled

of $CaK\alpha$ and background counts at the five points in 10 mast cells sectioned at 0.4 μm at accelerating voltage of 300 kV. The results are shown in Fig. 13 as a transitional curve of the P/B ratios obtained from five points of mast cell granules. The maximum was found at the point 1, which is the center of the granule. From these results, it was demonstrated that highest concentration of calcium ions was found at the center of the granule and it was speculated that high concentrations of calcium ions inhibited the discharge of granules (Nagata, 2000d).

5. Splenic Cells

The spleen is one of the blood cell forming organs and is composed of the lymphatic tissues. We studied [^{3}H]thymidine incorporation into the splenic cells of aging mice from newborn to adult and senescence in connection with the lysosomal acid phosphatase activity (Olea, 1991; Olea and Nagata, 1991). The acid phosphatase activity as demonstrated by means of the cerium substrate method was observed in the splenic tissues at various ages from postnatal day 1, to 1 and 2 weeks, to 1 and 2 months, and to 10 months (Olea, 1991; Olea and Nagata, 1991). Electron-dense deposits were localized in the lysosomes of macrophages, reticular cells, and littoral cells in all the aging groups. The intensity of the reaction products as visually observed (Fig. 6A) to increase from 1 day to 1 week, reaching the peak at 1 week, and then decreased from 2 weeks to 10 months by X-ray microanlysis in the TEM mode, with beam currents from 2 to 8 namp and an accelerating voltage from 100, 200, 300, 350, and 400 kV using a microprobe from 1 to 2 μm in diameter and the integrating detecting time for 100 s with the detecting dead time of 30%. The presence of cerium was confirmed with two peaks at 4.84 and 5.26 keV, respectively (Fig. 7A). These spectra did not interfere with the osmium line at 1.914 keV. When the cerium spectra were observed by changing the accelerating voltage from 100 to 400 kV, the intensities of the peaks decreased with increasing accelerating voltages. On the other hand, the background also decreased with the changing of accelerating voltage. However, the average P/B ratio increased from 100 to 400 kV (Fig. 7B), similar to that of Ag. Thus, the X-ray microanalysis was carried out on all lysosomes demonstrating AcPase activity using accelerating voltage at 300 kV (Olea and Nagata, 1991). The P/B ratio increased from postnatal day 1 to 1 week and decreased from 2 weeks to 10 months (Fig. 7C). The results obtained from X-ray microanalysis accorded well with the results of visual observations (Olea and Nagata, 1992a).

---

with [^{3}H]thymidine *in vitro* and radioautographed. Only a few nuclei of ductal cells are labeled with silver grains ($\times$375; bar $=$ 10 μm). (F) EMRAG of the submandibular gland obtained from a 1-day-old newborn mouse labeled with [^{3}H]thymidine *in vitro* and radioautographed. Many silver grains are localized over the nucleus of an intercalated ductal cell ($\times$7500; bar $=$ 1 μm).
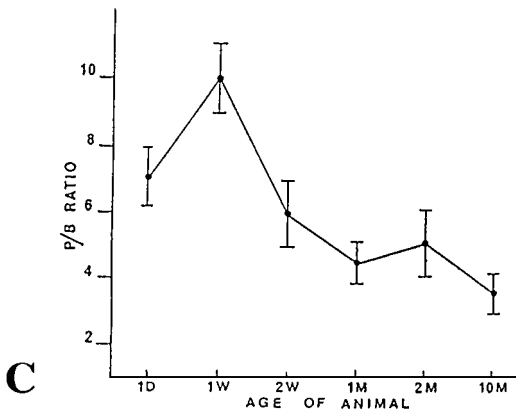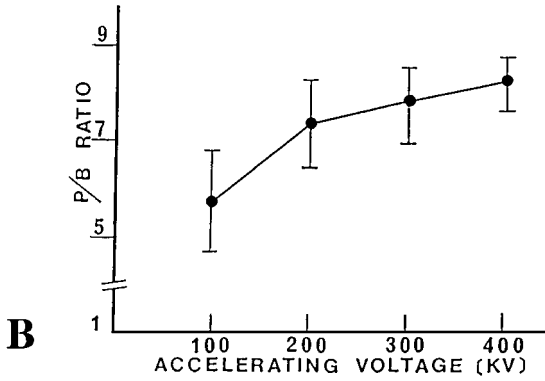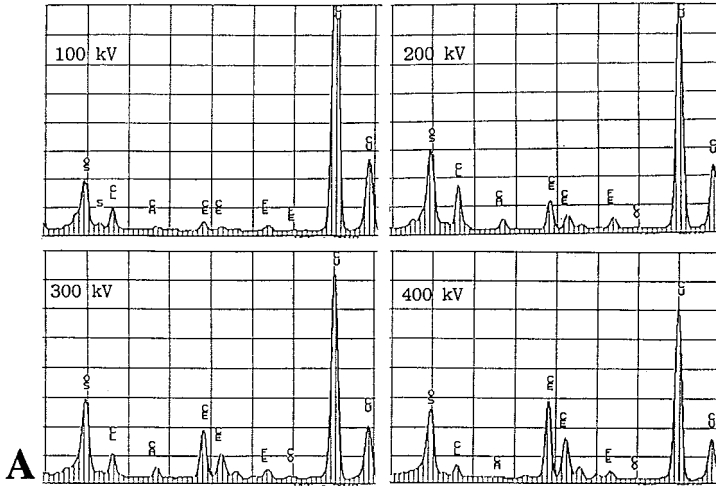
The incorporation of [^{3}H]thymidine, demonstrating DNA synthesis, was mainly observed in hematopoietic cells in the spleens of animals from postnatal day 1 to 10 months (Olea and Nagata, 1992a). The labeling index was the maximum (25%) at day 1 and decreased through 1, 2, 4, 8, and 40 weeks (a few percent). A correlation between DNA synthesis and AcPase activity was examined by comparing two cell populations in the cell cycle, the S-phase cells which were labeled with [^{3}H]thymidine and the non-S-phase cells or the interphase cells which were not labeled. It was demonstrated that the former showed an increase and decrease of much more AcPase activity with the aging (from 700 at postnatal week 1 to 200 at 10 months as expressed with the number of AcPase positive lysosomes per cell), while the latter showed less activity and no change (constantly around 200). On the other hand, the number of labeled cells and the grain counts in the hematopoietic cells in the spleens labeled with [^{3}H]uridine, demonstrating RNA synthesis, from postnatal day 1 increased through 1 and 2 weeks, reaching the maximum, and decreased through 4, 8, and 40 weeks, different from DNA synthesis (Olea and Nagata, 1992b). The protein synthesis, as demonstrated by [^{3}H]leucine incorporation in aging mouse spleen, showed the labeling in hematopoietic cells and littoral cells (Figs. 6B and 6C). The labeling index and the grain counts with [^{3}H]leucine increased from embryonic stage through postnatal day 1 to 2 weeks, reaching the maximum, then decreased through 1, 6, and 12 months (Nagata and Olea, 1999), similar to the changes observed in RNA synthesis.

6. Bone Marrow Cells

The bone marrow consists of meyloid tissues, one of the blood-forming organs, distributed in the bones of animals. We studied the localization of mucosubstances by chemical staining and macromolecular synthesis by radioautography in the rabbit bone marrow. By means of PA-TCH-SP staining intracytoplasmic glycogen granules were illustrated (Murata *et al.,* 1977b, 1978a). The glycogen particles in the cytoplasm of mature megakaryocytes had a mean diameter of 21.1 nm, while those in the blood platelets had a mean diameter of 26.2 nm. The staining pattern of the particles in the platelets was classified into three types according to the staining intensity (Murata *et al.,* 1977b). Moreover, a very weak reaction was also observed in the granules of three kinds of granulocytes (Murata *et al.,*

FIG. 7   X-ray microanalysis of Ce on spleen sections stained with acid phosphatase activity. (A) X-ray spectra of CeK_α obtained from sections stained with acid phosphatase reaction by cerium substrate method shown in Fig. 6A, as observed by X-ray microanalysis at different accelerating voltages of 100, 200, 300, and 400 kV, respectively. Permission from M. T. Olea and T. Nagata (1991, Fig. 2, 3, p. 159). (B) Relationship between accelerating voltages and P/B ratios of Ce from acid phosphatase activity in mouse splenic reticulocyte, calculated from the spectra in Fig. 15. Permission from M. T. Olea and T. Nagata (1991, Fig. 6, p. 160). (C) Quantitative distribution of Ce measured in terms of P/B ratio in different age groups of mice from 1 day to 10 months after birth. Permission from M. T. Olea and T. Nagata (1992a, Fig. 5, p. 120).

1978a). On the other hand, the bone marrow cells were studied by means of light and electron microscopic radioautography after labeling with carrier-free sulfuric acid $^{35}SO_4$ for 10, 30, and 60 min *in vitro* as well as by detecting S in the granules of granulocytes with X-ray microanalysis (Murata *et al.,* 1979). From the results by radioautography, silver grains were observed in the Golgi apparatus at 10 min and then migrated to granules in three kinds of granulocytes, heterophil, acidophil, and basophil granulocytes at 30 and 60 min. Immature granulocytes showed more active incorporation than mature ones. By X-ray microanalysis, S was detected in the granules of all three kinds of granulocytes. It was concluded that incorporated inorganic S was utilized for the synthesis of acid glucosaminoglycans (Murata *et al.,* 1979).

C. Digestive Cells

The digestive cells consist of the salivary gland cells and epithelial cells in the oral cavity, esophageal cells, gastric cells, intestinal cells, the liver cells, and the pancreatic cells composing the digestive organs. We studied all these cells by means of various cytochemical reactions.

1. Salivary Gland Cells

We studied the DNA synthesis of mouse submandibular gland at various ages from embryo to postnatal 2 years (Chen *et al.,* 1995, Nagata *et al.,* 2000). The submandibular gland of male mouse embryonic day 19 consisted with the glandular acini and duct system. The duct system was composed of juxtaacinar (JA) cells, intercalated duct (ICD) cells, and striated duct (SD) cells. Many labeled developing acinar cells (AC), JA, and ICD cells were observed. At postnatal days 1 (Fig. 6D) to 3, there were more JA cells and secretary granules than those of former stage. JA cells were cuboidal cells, characterized by small darkly stained granules in the supranuclear cytoplasm and by basophilic mitochondria, mostly at the basal half of the cells. JA cells were present at the acinar-intercalated duct junction of the mouse submandibular gland. Many labeled AC, JA, ICD, and SD cells were also observed by electron microscopy (Fig. 6F). At postnatal week 2 to 3 months, developing immature acinar cells gradually matured to acinar cells, and JA cells increased and granular convoluted tubule (GCT) cells appeared. At postnatal month 6 to 2 years, the GCT cells were very well developed and were composed of the taller cells packed with many granules and became highly convoluted, and only a few labeled cells were found (Fig. 6E).

The aging changes of frequency of five main individual cell types in submandibular glands of male mouse from embryonic day 19 to postnatal 2 years of age are shown in Fig. 8A. At embryonic day 19, the gland consisted of developing acinar cells (49%), ICD cells (37%), JA cells (3%), and SD cells (11%). At birth, JA
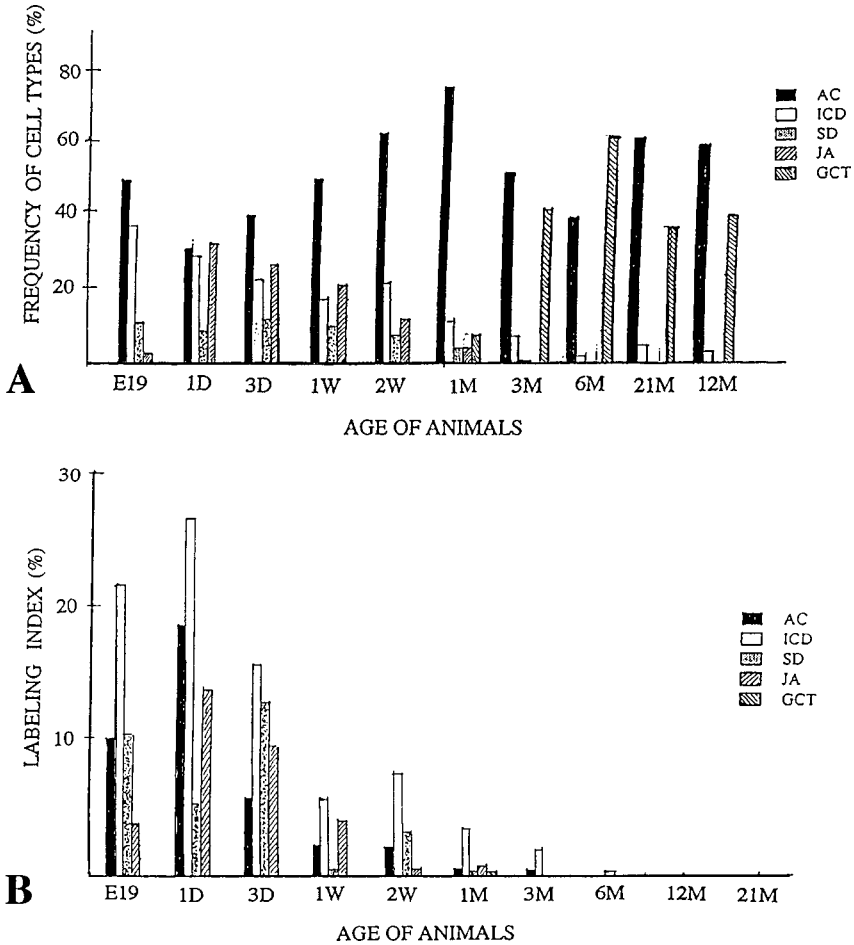
FIG. 8   Histogram showing the frequencies of appearance of the five individual cell types and their labeling indices in the submandibular glands of male ddY mice at respective ages. (A) Histogram showing the frequencies of appearance of the five individual cell types at respective ages. AC, acinar cells; ICD; intercalated duct cells; SD; striated duct cells; JA, juxtaacinar cells; GCT, granular convoluted cells. Permission from T. Nagata *et al.* (2000b, Fig. 11, p. 12). (B) Histogram showing the labeling indices of the five individual cell types in the submandibular glands of male ddY mice at respective ages. Abbreviations are the same as in (A) Permission from T. Nagata *et al.* (2000b, Fig. 12, p. 12).

cells increased rapidly to 32% and thereafter decreased gradually. At 1 month of age, JA cells disappeared and GCT cells appeared and increased rapidly in number with age. They reached a maximum at 6 months. Then they decreased gradually from 6 to 21 months. The quantity proportion of acini was relatively stable during these periods. The frequency of ICD cells was the highest (37%) at 1 day after

birth. Thereafter, it gradually decreased month by month and reached 2.6% at 21 months, while the ratio of SD cells persisted at 7–12% from embryonic day 19 to postnatal week 2 and it disappeared at 3 months after birth. The proliferative activity of the cell population is expressed by the labeling index which is defined as the percentage of labeled nuclei with [3H]thymidine in a given cell population. The labeling index of the entire gland cells increased from 13.6% at embryonic day 19 to 18.3% at neonate, when it reached the first peak (Fig. 8B). Then it declined to 2.2% at 1 week of age. A second small peak (2.9%) occurred at 2 weeks. Thereafter, the labeling index decreased progressively to less than 1% at 4 weeks of age and then remained low. The analysis of the labeling indices of respective cell types revealed that the first peak at neonate was due to the increased labeling indices of AC, ICD, and JA cells, and the second peak at 2 weeks was due to the increase of ICD and SD cells (Fig. 8B). Thereafter, the labeling index of ICD cells decreased steadily but remained higher than those of any other cell type (Chen *et al.,* 1995; Nagata *et al.,* 2000b). Since the labeling index of ICD cells was more than the other cell types and persisted for a long time, it was suggested that ICD cells concerned with the generation of other cell types (Nagata *et al.,* 2000b).

The sulfate uptake and accumulation in several mouse digestive organs were also studied by light microscopic radioautography (Nagata *et al.,* 1999a). Two litters of normal ddY mice 30 days after birth, each consisting of three animals, were studied. One litter of animals was sacrificed at 30 min after the intraperitoneal injections with phosphate-buffered $Na_2^{35}SO_4$, and the other litter animals were sacrificed at 12 h after the injections. Then the submandibular glands and the sublingual glands were taken out. The tissues were fixed, dehydrated, embedded in epoxy resin, sectioned, coated with radioautographic emulsion, exposed, developed, stained with toluidine blue, and analyzed by light microscopy. As a result, many silver grains were observed on serous cells of the salivary glands at 30 min and 12 h after the injection. The numbers of silver grains at 30 min were less than those at 12 h. From the results, it was concluded that glycoprotein synthesis was demonstrated in both the submandibular and sublingual glands by radiosulfate incorporation. In the salivary glands the silver grains were more observed in serous cells than in mucous cells at 30 min, while in mucous cells were more observed at 12 h than at 30 min after the injection. These results show the time difference of glycoprotein synthesis in the two glands (Nagata *et al.,* 1999a).

2. Esophageal Cells

The esophagus of mammals consists of epithelial cells, connective tissue cells, and skeletal or smooth muscle cells. The DNA synthesis of the esophagus of aging mice labeled with [3H]thymidine was studied by light and electron microscopy. The labeled cells were mainly found in the basal layer of the esophageal epithelium. The nuclei and nucleoli of labeled cells were larger than those of unlabeled cells, but contained fewer cell organelles. The labeling indices in respective aging groups

showed a peak at 1 day (12%) after birth and decreased with aging to a few percent at 2 years (Duan *et al.,* 1992, 1993, 1994).

3. Gastric Cells

The gastric cells consist of mucosal epithelial cells, mucosal connective tissue cells, smooth muscle cells in the muscular layer, and serosal epithelial cells. We studied the cytochemical reactions and radioautography mainly in the gastric mucosal epithelial cells of both human and animal tissues. Cytochemical staining for mucosubstances in the gastric mucosae of 50 human patients undergoing surgery was studied (Iida *et al.,* 1978). Normal gastric surface and foveolar epithelial cells stained intensively with PAS, indicating the presence of intracellular mucins by light microscopy. By electron microscopy, the free surface of the normal gastric epithelial cells was covered by a small amount of glycocalyx stained with PA-TCH-SP and they contained many PA-TCH-SP-positive secretory granules at the apical portions (Iida *et al.,* 1978). In the area where well-developed intestinal metaplasia were present, the surface cells were completely replaced by absorptive cells which did not contain PAS-positive mucosubstances nor PA-TCH-SP-positive granules. These results suggested that the metaplastic epithelial cells transformed from the normal foveolar epithelial cells (Iida *et al.,* 1978).

With regards the experimental animals, the pyrolic and cardiac regions of the stomachs of 4-week-old adult ddY strain mice were stained with HID-AB sequence. The cells of surface epithelium and the glands of the body of the stomach were not stained with HID or AB. However, the pyrolic glands showed HID affinity and were colored black demonstrating sulfated complex carbohydrate (Nagata and Kawahara, 1999).

On the other hand, the turnover of fundic glandular cells by [^{3}H]thymidine radioautography was extensively investigated by Leblond and coworkers (Leblond, 1981). We studied the secretion process in G-cells by electron microscopic [^{3}H]amino acid radioautography. When rat stomach tissues were labeled with [^{3}H]glutamic acid and [^{3}H]glycine *in vitro* at varying time intervals, silver grains in the radioautograms appeared first over the Golgi zones and then migrated to secretory granules and were stored in the cytoplasm, suggesting the secretory kinetics (Sato, 1978; Sato *et al.,* 1977). We also studied the mechanism of serum albumin passing through the gastric epithelial cells by electron microscopic radioautography. When rat stomach tissues were labeled with [^{132}I]albumin *in vitro* at varying time intervals, silver grains in the radioautograms appeared over rough endoplasmic reticulum within 3 min and then moved to the Golgi apparatus in 10 min, and onto secretory granules and into the lumen in 30 min, suggesting the pathway of serum albumin from the blood vessels through the gastric mucous epithelial cells into the gastric lumen (Komiyama *et al.,* 1978).

When incorporation of radiosulfate into sulfated complex carbohydrate in rat stomach was studied by labeling with ^{35}SO$_4$ *in vivo,* silver grains appeared over

the glandular epithelial cells of the pyloric gland but not those of the fundic gland cells, demonstrating the mucous synthesis in the former glands (Nagata *et al.,* 1988; Nagata and Kawahara, 1999).

The radiosulfate uptake and accumulation in mouse stomach were also studied by light microscopic radioautography (Nagata *et al.,* 1999a). Two litters of normal ddY mice 30 days after birth, each consisting of three animals, were studied. One litter of animals was sacrificed at 30 min after the intraperitoneal injections with phosphate-buffered $Na_2{}^{35}SO_4$, and the other litter animals were sacrificed 12 h after the injections. Then the antrum and the fundus of the stomach were taken out. The tissues were fixed, dehydrated, embedded in epoxy resin, sectioned, coated with radioautographic emulsion, exposed, enveloped, stained with toluidine blue, and analyzed by light microscopy. As a result, many silver grains were observed on the mucosa and submucosa of the stomach at 30 min after the injection. Then at 12 h after the injection silver grains were observed on some of the stomach glands. The numbers of silver grains observed in the stomach at 30 min were less than those at 12 h. The results showed the time difference of glycoprotein synthesis in the stomach (Nagata *et al.,* 1999a).

4. Intestinal Cells

The intestines of mammals are divided into two portions, small and large intestines, which can be further divided into several portions, the duodenum, jejunum, ileum, cecum, colon, and rectum. The intestinal cells in any portions consist of columnar epithelial cells including absorptive and secretory cells, mucosal connective tissue cells, smooth muscle cells, and serosal epithelial cells. We studied the chemical reactions and macromolecular synthesis by radioautography, mainly in the epithelial cells.

The portions of the small and large intestines, the duodenum, the jejunum, and the proximal and the distal colon, were stained with HID-AB sequence (Nagata and Kawahara, 1999). The surface absorptive cells in the small and large intestines did not show any staining with HID-AB sequence. However, goblet cells in small and large intestines stained either HID or AB, showing variations in respective regions. Goblet cells deeper in the colonic crypt differed from those higher in the crypts in showing weaker staining for carbohydrate, lesser accumulation of secretion in the apical cytoplasm and distinct staining of a surpranuclear focus interpreted as being Golgi zone (Fig. 1A). Goblet cells deeper in the colonic crypts differed from those higher in the crypts in showing weaker staining for carbohydrate, a lesser accumulation of secretion in the apical cytoplasm and distinct staining of a supranuclear focus interpreted as the Golgi zone. In general, the goblet cells in the upper region of the crypts stained black with HID, while the goblet cells in the deeper regions stained blue with AB (Fig. 1A). The HID staining, which is considered to be specific for demonstration of sulfated complex carbohydrate, correlated well with radioautographic evidence of radiosulfate incorporation

(Fig. 1B) (Nagata and Kawahara, 1999). When the colonic goblet cells of normal mice were stained with the PA-TCH-SP reactions for mucopolysacharides, the positive reaction with electron-dense deposits appeared in the mucous granules in the Golgi area as well as the goblets in the apical cytoplasm of the goblet cells (Figs. 9A and 9B). The mucous granules in the Golgi area and the goblets can be observed three-dimensionally as superimposed particles in stereo-pair pictures (Figs. 9A and 9B).

As for the physical reactions, nucleic acid synthesis, especially [^{3}H]thymidine radioautography, was carried out in the small and large intestines (Fig. 9C). The cells labeled with [^{3}H]thymidine were localized in the crypts of both small and large intestines, a region defined as the proliferative zone. In the colon of aging mice from fetal to postnatal 2 years, the labeled cells in the columnar epithelia were frequently found in the perinatal groups from embryo to postnatal day 1. However, the labeling indices became constant from the suckling period until senescence (Morita *et al.,* 1994a). Jin (1996) examined the labeling indices of respective cell types in each layer of mouse colon such as columnar epithelial cells, lamina propria, lamina muscularis mucosae, tunica submucosa, inner circular muscle layer, outer longitudinal muscle layer, outer connective tissue, and serous membrane of the colon and found that most labeling indices decreased after birth (10%) to 2 months (a few percent), except the epithelial cells, which kept constant value to senescence (10–15%). Similar results were also obtained from the cecal tissues of mouse (Jin and Nagata, 1995a,b).

On the other hand, the synthesis of mucosubstances in goblet cells as well as in absorptive epithelial cells was studied using $^{35}SO_4$ in the duodenum, jejunum, and colon at varying time intervals 30, 60, and 180 min after the administration (Nagata *et al.,* 1988a). The results showed that silver grains over goblet cells in the lower region of the colonic crypt transferred rapidly from 30 to 180 min, while they transferred slowly in goblet cells in the upper region of the colonic crypt (Fig. 1B), leading to the conclusion that the rates of transport and secretion of mucous products of the goblet cells at these two levels in the crypts were different. By electron microscopy silver grains first appeared over the Golgi zone at 30 min (Fig. 2D) and then moved to the secretory granules at 60 and 180 min. By light and electron microscopic radioautography, the incorporation of $Na_2{}^{35}SO_4$ into sulfated complex carbohydrate has been investigated in the mouse small and large intestines (Nagata and Kawahara, 1999). Quantitative differences have been observed in the relative uptake of radiosulfate in the various labeled cells of each organ. Incorporation by the colon in goblet cells exceeded that elsewhere in the deep goblet cells of the colonic crypts. Migration of label progressed during the time tested from the supranuclear Golgi region to the deep position of the goblet and then extended throughout the mucosubstance in the goblet in the superficial goblet cells of the colon. The radioautographic and cytochemical staining differences between secretory cells in the deeper region compared with the upper region of the colonic crypts are considered to reflect differences in the rate of transport
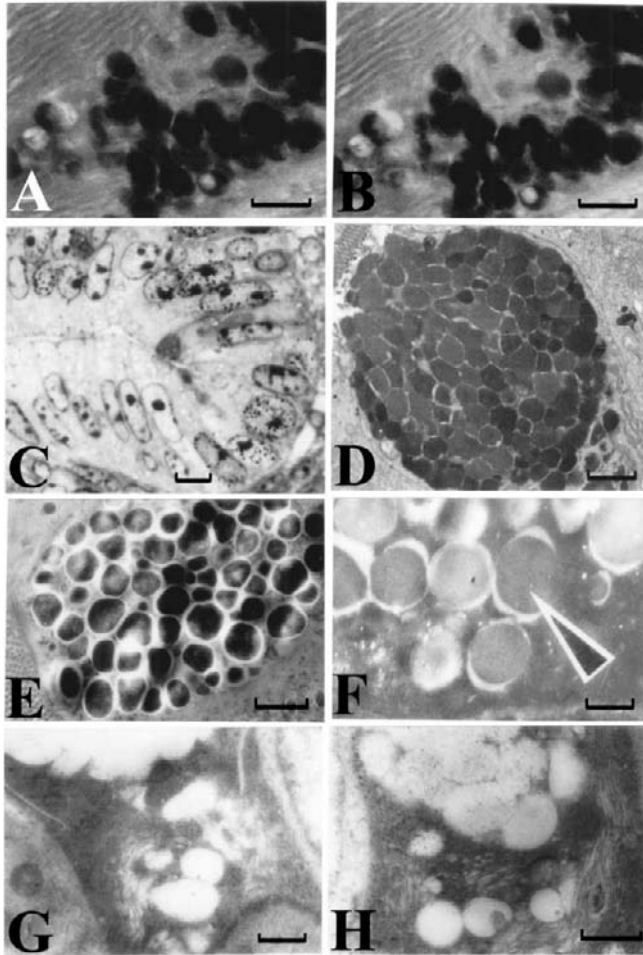
FIG. 9   Special cytochemistry 3: The intestinal cells. (A and B) Stereo-pair high-voltage electron micrographs of a colonic goblet cell of a mouse colon, fixed, thick sectioned, and stained with PA-TCH-SP, tilting +8 (A) and −8 (B), observed by high-voltage electron microscopy at 1000 kV. The two pictures can be seen with a stereoscope or by stereoscopic imaging. Electron-dense mucous granules piling up in the cytoplasm at center (× bar = 1 μm). Permission from T. Nagata (2000c, Fig. 12, p. 398). (C) LMRAG of mouse colonic epithelium at fetal day 19, labeled with [³H]thymidine and radioautographed. Several labeled epithelial cells are localized in the lower half of the crypt (right) (×675; bar = 5 μm). Permission from C. Jin (1996, Fig. 1, p. 257). (D) Electron micrograph of a mouse proximal colon, fixed chemically with 2.5% glutaraldehyde in phosphate buffer, pH 7.4, dehydrated, embedded in Epon, sectioned using water according to the conventional technique, and stained with uranyl acetate and lead citrate. Electron-dense mucigen granules can be seen in the apical cytoplasm of the cell fusing together (×6000; bar = 1 μm). Permission from T. Nagata *et al.* (2000c, Fig. 1, p. 4). (E) Electron micrograph of a goblet cell of mouse proximal colon, cryofixed by metal contact method using a JFD-RFA

of secretory products in the theca and the rate of secretion at the low levels in the crypt. These results show the time differences of glycoprotein synthesis in respective organs. The sulfate uptake and accumulation in several mouse digestive organs were also studied by light microscopic radioautography (Nagata *et al.,* 1999a). Two litters of normal ddY mice 30 days after birth, each consisting of three animals, were studied. One litter of animals was sacrificed 30 min after the intraperitoneal injections with phosphate-buffered $Na_2{}^{35}SO_4$, and the other litter animals were sacrificed 12 h after the injections. Then several digestive organs, the parotid gland, the submandibular gland, the sublingual gland, the antrum and fundus of the stomach, the duodenum, the jejunum, the ileum, the cecum, the ascending colon, and the descending colon were taken out and radioautographed. As a result, many silver grains were observed on villous cells and crypt cells of the small intestines and whole mucosa of the large intestines at 30 min after the injection. Then at 12 h after the injection silver grains were observed on mucigen granules of goblet cells in the small intestines and the large intestines. The numbers of silver grains observed in respective organs at 30 min were less than those at 12 h. From the results, it is concluded that glycoprotein synthesis was demonstrated in several digestive organs by radiosulfate incorporation.

We also studied the aging changes of [³H]glucosamine uptake in the mouse ileum, and found that the silver grains in the columnar epithelial cells were mainly localized over brush broders and the Golgi region, whereas in the goblet cells they were over the Golgi region and mucous granules. The number of silver grains increased from 6 months up to 2 years (Morita 1993). In order to quantify the elemental constituents of glycoproteins in mucigen granules of colonic goblet cells in mice under different fixations, mouse colonic tissues were treated either cryo-fixed, cryo-sectioned and freeze–dried (Fig. 9E), or freeze–substituted, embedded, and dry-sectioned (Nagata *et al.,* 2000c). The other tissues were also chemically fixed (Fig. 9D), embedded, and wet-sectioned. All the specimens were analyzed with a JEOL JEM-4000EX TEM system equipped with a Tracor-Northern energy-dispersive X-ray analyzer TN5400 at accelerating voltages of $300-400\,kV$. The results showed that S and some other elements were better demonstrated in

---

freezing apparatus cooled with liquid nitrogen, freeze-substituted in absolute acetone containing osmium tetroxide, embedded in Epon, and dry-sectioned. The apical cytoplasm of these goblet cells containing mucigen granules appears to be amorphous and dense, surrounded with amorphous cytoplasm with cell organelles ($\times 6750$; bar $= 1\ \mu$m). Permission from T. Nagata *et al.* (2000c, Fig. 3, p. 5). (F) Electron micrograph of a Paneth cell in the duodenum of a 1-month-old mouse, fixed in buffered glutaraldehyde, embedded in Epon, sectioned, and stained with uranyl acetate and lead citrate. The granule indicated with an arrow was studied by X-ray microanalysis ($\times 6000$; bar $= 1\ \mu$m). Permission from T. Nagata (2000d, Fig. 23, p. 29). (G and H) Electron micrographs of the goblet cells in the lower crypts of proximal colons of mice at different ages, showing Golgi regions ($\times 6000$; bar $= 1\ \mu$m). (G) A goblet cell of a prenatal day 19 fetus. (H) A goblet cell of an adult mouse at postnatal 1 month. Permission from T. Nagata (2000d, Fig. 31, p. 33).

cryo-fixed sections than chemically fixed ones. Among the cryo-techniques tested, cryo-sections followed by freeze–drying was the best to preserve various elements in the granules. Then freeze–substituted plastic embedded absolute dry sections without any trough liquid followed. The freeze–substituted plastic-embedded dry-sectioning on ethylene glycol induced some loss of K. A higher concentration of S in the mucigen granules of the goblet cells than in the cytoplasmic matrix suggests that S is the constituent of the glycoproteins in the granules in colonic goblet cells (Nagata *et al.,* 2000c).

We previously demonstrated the presence of zinc (Zn) in the specific granules of Paneth cells of mouse duodenum and goblet cells of mouse colon (Fig. 9F) by X-ray microanalysis (Fig. 10A) (Ichikawa *et al.,* 1994). In order to quantify the zinc content in these granules, we first studied the zinc concentrations in a model system. As a model experiment, we prepared Epon sections containing zinc sulfate at concentrations of either 0.05 and 0.1%. The two spectra (not shown) obtained from two Epon sections containing 0.05 and 0.1% zinc sulfate cut at 0.2 μm and observed at 100 kV by a JEOL JEM-4000EX TEM with a TN-5400 EDX system, with beam currents from 2 to 8 namp and the microprobe at 1 μm in diameter and a detection time of 100 s appeared similar to that in Fig. 10A. Comparing the two peaks of Zn obtained from 0.05 and 0.1% concentrations, the latter was higher than the former (Nagata, 2000d). The average peak counts and backgrounds in two kinds of sections containing 0.05 and 0.1% concentrations, were calculated. From the results, P/B ratios at different concentrations were plotted. In such a figure the linear relationship between the Zn concentration and the P/B ratio can be observed approximately like Beer's law in case of microspectrophotometry (Nagata, 1972a).

When the sections containing 0.1% zinc sulfate were analyzed with the JEM-4000EX NT-5400 TEM system, with beam currents from 2 to 8 namp and a microprobe at 1 μm in diameter and a detection time of 100 s, with a dead time of 30%, changing the accelerating voltage from 100 to 400 kV, spectra showing Zn peaks were obtained (not shown). The peak counts as well as the background changed from 100 to 400 kV. The results were plotted as the changes of P/B ratio related to accelerating voltage (Fig. 10B). The maximum of these curves was observed at 200 kV, different from the results obtained with Ag and Ce. Therefore, we used 200 kV for further quantification in the case of Zn. Analyzing many individual mice at various ages from newborn to adults and further to senescence, all the data expressing P/B ratio are plotted (Fig. 10C). These data show that the aging changes of zinc contents in the granules of mouse duodenum Paneth cells as expressed by P/B ratios increased from postnatal days 2 and 7 to 2 and 2 months, reaching a peak at 1 month, and then decreased to 2 years.

On the other hand, quick-frozen and freeze-dried cryosections prepared from the three portions of the intestines, the duodenum, the proximal, and distal colons, obtained from five groups of aging mice from postnatal day 14 and months, 1, 3, 6, and 18, were studied (Kametani *et al.,* 1998). By quantitative X-ray microanalysis, the peaks of 5 elements decreased in the order of S, K, Cl, P, and Ca in the duodenum
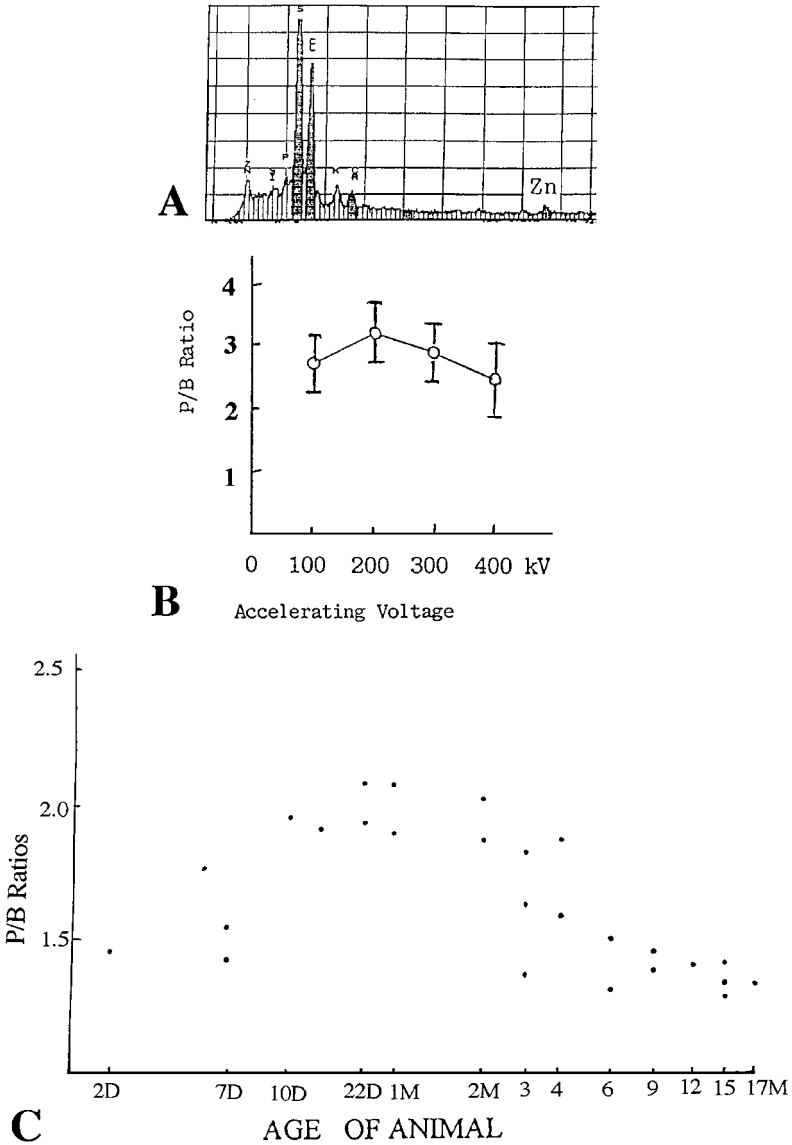
FIG. 10   X-ray microanalysis of Zn in the intestine. (A) X-ray spectrum obtained from the granule of the Paneth cell of a mouse at postnatal month 15, indicated with an arrow in Fig. 9F, showing ZnK_α without Os peak. The Cl peak is due to epoxy resin. Permission from T. Nagata (2000d, Fig. 23, p. 29). (B) Transitional curve showing the relationship between the accelerating voltages and the P/B ratios of Zn calculated from the X-ray spectra obtained from model experiments. T. Nagata (2000d, Fig. 21, p. 28). (C) Relationship between the aging of mice and P/B ratios of Zn in the granules in Paneth cells of the duodenum at respective ages. Permission from T. Nagata (2000d, Fig. 24, p. 29).

at 5 months, the peaks declined in the order of K, S, Cl, Ca, and P at 3 months in the proximal colon, and the peaks declined as S, K, Ca, Cl, and P at 3 months in the distal colon. The highest average ratio of S was obtained in the duodenum at 1 month and this value declined with age. In the proximal colon, the average ratio of K was highest at 1 month and then declined with aging. In the distal colon, the highest average ratio of S was at 3 months and the highest average ratio of K was at 1 month. Significant differences were found between these peaks (Kametani *et al.,* 1998).

As was shown by light and electron microscopic radioautography, goblet cells of mouse colon labeled with $^{35}SO_4$ for 30, 60, and 180 min demonstrated mucosubstances synthesis incorporating radiosulfate (Figs. 1B and 2D). In order to determine the total content of sulfur in the Golgi regions of the goblet cells in different regions of the colon at different ages of animals, X-ray microanalysis was carried out (Maruyama and Nagata, 1987). Nine groups of aging ddY mice, aged from fetal day 19, postnatal days 1, 3, 8, 14, and months 1, 2, 6, and 12, each consisting of three litter mates, were used. The proximal colon was fixed in phosphate-buffered 2.5% glutaraldehyde and 1% osmium tetroxide, embedded in Epon, and sectioned at 0.2 or 0.4 μm thick. For X-ray microanalysis a high-voltage JEOL JEM 4000EX TEM system equipped with a Tracor-Northern energy dispersive X-ray microanalyzer TN-5400 was used with a fixed beam current at 3.2 nA and 2 μm in diameter for 100 s with a dead time of 30%, changing the accelerating voltages at 100, 200, 300, and 400 kV for preliminary experiments. Figures 9G and 9H are electron micrographs showing Golgi regions of colonic goblet cells in the lower crypts of aging mice from postnatal week 1 (Fig. 9G) to 1 month (Fig. 9H). The peak counts of S and background counts of goblet cell cytoplasm of the upper and lower crypt goblet cells at 0.2 or 0.4 μm thickness are observed at 100, 200, 300, 350, and 400 kV. Figure 11A shows the curve of the P/B ratios of goblet cell granules observed at varying accelerating voltages from 100 to 400 kV. The maximum was found at 300 kV (Nagata, 2000d). Therefore, we used 300 kV for further quantification. The P/B ratios of sulfur in mucigen granules in the goblet cells in the lower crypts of mice aged from fetal day 19 to postnatal day 3 were higher than in the upper crypts of the same ages. The spectrum at 30 days was the highest in both the upper and lower crypts. However, the P/B ratios at 14 days were the highest in both the upper and the lower crypts. The curves obtained from P/B ratios in both upper and lower crypt cells in relation to aging are shown in Fig. 11B. These results demonstrated that the P/B ratios of sulfur in the goblet cells of aging mice increased from perinatal stages to postnatal 2 weeks and decreased to senescence at 1 year and they were higher in the upper crypts than in the lower (Nagata, 2000d).

The changes of elements in the goblet cell secretory granules in the three portions of the jejunum, proximal and distal colons aging from 14 days to 18 months after birth were studied by quantitative electron probe X-ray microanalysis on quick-frozen and freeze–dried cryosections calculating P/B ratios of each element (Ichikawa *et al.,* 1994). As the results of the analysis of five elements, the peaks declined in turn S–K$_\alpha$ (sulfur), K–K$_\alpha$ (potassium), Cl–K$_\alpha$ (chlorine), P–K$_\alpha$
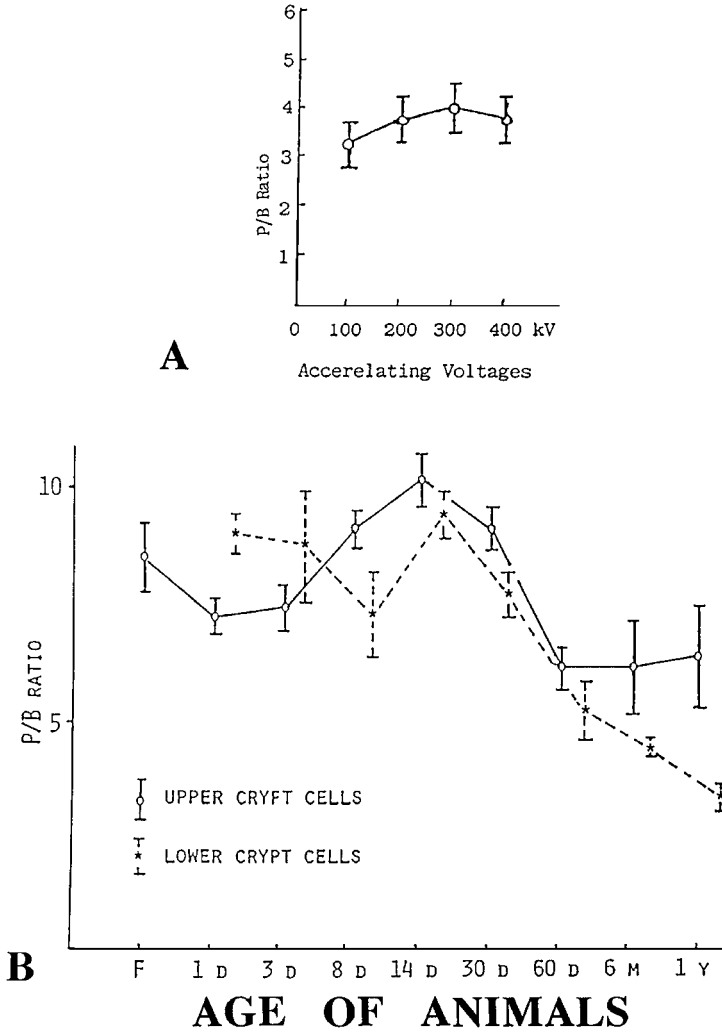
FIG. 11 X-ray microanalysis of S in mucigen granules in the goblet cells in the colons of mice. (A) Transitional curve of P/B ratio of S in mucigen granules in goblet cells of mice observed at different accelerating voltages from 100 to 400 kV. (B) Relationship between the aging of mice and P/B ratios of S in mucigen granules in the goblet cells in upper and lower crypts of the colons. Permission from T. Nagata (2000d, Figs. 33 and 34, p. 34).

(phosphorus), and Ca–Kα (calcium) in the jejunum at 1 month. In the proximal colon, the peaks declined in turn K–Kα, S–Kα, Cl–Kα, Ca–Kα and P–Kα at 3 months. On the other hand, in the distal colon, the peaks declined in turn S–Kα, K–Kα, Ca–Kα, Cl–Kα, and P–Kα at 3 months. The highest average P/B ratio of S was obtained in the jejunum at 1 month, and declined afterward with aging. In

the proximal colon, the average P/B ratio of K was the highest at 3 months and then declined with aging. The highest average P/B ratio of S was at 3 months. The highest average P/B ratio of K was at 1 month in the distal colon. The ratio of peak counts to the background was calculated on each granule. Significant differences in the P/B ratios of S and K between the proximal and distal colons were found out. As for S, the jejunum and the distal colon had the highest ratios and the proximal colon had the second. Concerning K, the proximal colon had the highest ratio and the jejunum and the distal colon had the second. The secretory granules of goblet cells in the three portions of intestinal tracts were shown to contain a different amount of each element. Especially, the amount of S appeared the most different from the proximal to the distal colon.

We studied immunostaining for PCNA/cyclin (Morita *et al.,* 1994a) and peroxisomal enzymes (Usuda and Nagata, 1984; Usuda *et al.,* 1991b, 1995) and lectin staining in the intestines (Morita *et al.,* 1994b). We fixed the colonic tissues of litter mice of six aging groups from embryonic day 19, to newborn postnatal days 1, 5, 21, adult 2 months, and senescent 11 months in methacarn and immunostained the colonic epithelium for cyclin proliferating nuclear antigen (PCNA/cyclin), which appear from G1 to S phase of the cell cycle, with the monoclonal antibody and the avidin–biotin peroxidase complex technique (Morita *et al.,* 1994a). The immunostaining positive cells were localized in the crypts of colons similarly to the labeled cells with [^{3}H]thymidine by radioautography, a region defined as the proliferative zone. The positive cells in the columnar epithelia were frequently found in the perinatal groups from embryo to postnatal day 1 and became constant from postnatal day 5 until senescence (Morita *et al.,* 1994a). Comparing the results by immunostaining with the labeling index by radioautography, it was found that the former was higher in each aging group than the latter. The reason for the difference should be due to the fact that PCNA/cyclin-positive cells included not only S-phase cells but also the late G1 cells (Morita *et al.,* 1994a). We also studied immunostaining of peroxisomal enzymes (Usuda and Nagata, 1984; Usuda *et al.,* 1995) and peroxisome-specific membrane polypeptide (PMP) in the jejunal epithelial cells of rats (Usuda *et al.,* 1991b). The jejunal tissues of Wistar rats were fixed in 4% paraformaldehyde/0.1% glutaraldehyde/0.1 M phosphate buffer, pH 7.4, embedded in Lowicryl K4M at $-20°$C, and immunostained with antibodies for catalase, acyl-CoA oxidase, bifunctional proteins, ketoacyl-CoA thiolase, urate oxidase, HMG CoA reductase, serine:pyruvate aminotransferase, sterol carrier protein 2,2,4-dienoyl-CoA reductase, apolipoprotein E, L-α-hydroxy acid oxidase, glycolate oxidase, D-amino acid oxidase for peroxisomal matrix and 70-, 40-, 26-, and 22-kDa PMPs for peroxisomal membrane by protein A–gold technique. The results demonstrated that the jenual peroxisomes contained only catalase, acyl-CoA oxidase, bifunctional protein, and ketoacyl-CoA thiolase in the peroxisomal matrix and 70- and 40-kDa PMPs in the membrane.

On the other hand, colonic tissues of mice from several aging groups were fixed in paraformaldehyde/glutaraldehyde and stained with two lectins, WGA and DSA,

to demonstrate the sugar residues of the glycoproteins in the goblet cells. From the results, it was shown that the staining pattern of the goblet cell granules in the colonic epithelia in various aging groups changed from the perinatal to postnatal development to the senescence (Morita *et al.,* 1994b).

5. Liver Cells

The liver of the mammals is a very large gland and consists of several types of cells. The hepatocyte is the main component of the liver, composing the liver parenchyma which form the hepatic lobules, surrounded by the connective tissue cells, sinusoidal endothelial cells, satellite cells of Kupffer, fat-storing cells, and bile epithelial cells. In the livers of perinatal animals, the liver cells includes hematopoietic cells such as erythroblasts, myeloblasts, and magakaryocytes. We studied cytochemical reactions mainly in hepatocytes of rats and mice. As enzyme cytochemical reaction, we studied DAB reaction demonstrating catalase (EC 1.11.1.6 hydrogen peroxidase) activity in the livers of rats and mice. We first observed the morphological changes of cell organelles in mouse hepatocytes administered with sodium dehydrocholate and found an increase in peroxisomes, dilatation of endoplasmic reticulum, development of Golgi complex, and mitochondrial swelling (Yokota and Nagata, 1968). Then, the peroxisomes in mouse hepatocytes were stained with DAB reaction to demonstrate catalase (EC 1.11.1.6 hydrogen peroxide oxidoreductase) activity in combination with the immunostaining (Yokota and Nagata, 1977). The peroxisomes in rat hepatocytes were also demonstrated by DAB reaction (Fig. 12A; see color insert) and the increase of the number of peroxisomes by the administration of peroxisome proliferators such as DEHP (Ohno *et al.,* 1981, 1982), clofibrate (Takebe, 1992; Takebe and Nagata, 1985), and bezafibrate (Momose *et al.,* 1993) were observed (Fig. 12B). The three-dimensional ultrastructure of cell organelles in whole-mount cultured hepatocytes, such as the Golgi apparatus stained with ZIO reaction (Vrensen and de Groot, 1974) or TPPase activity (Novikoff and Goldfisher, 1961), endoplasmic reticulum (Figs. 12C and 12D) stained with G-6-Pase activity (Tice and Barrnett, 1962), mitochondria stained with cytochrome oxidase activity (Seligman *et al.,* 1968), peroxisomes (Figs. 12E–12I) stained with DAB reaction (Angermüller and Fahimi, 1981) after administration of clofibrate (Figs. 12E and 12F), fixed in glutaraldehyde, dehydrated, and dried with a critical point dryer were observed by high-voltage electron microscopy at 400–1000 kV (Nagata, 1995c, 1997b, 1999a, 2000a, 2001). The time course of peroxisome proliferation in cultured hepatocytes under experimental conditions such as in culture media containing clofibrate or bezafibrate was observed three-dimensionally, revealing the proliferation of DAB-positive particles piling up between endoplasmic reticulum at 24 h which were encapsulated into large vacuoles (Figs. 12E and 12F), suggesting degenerative changes, at 48 h (Nagata, 1999a, 2000a, 2001). Thus, it was possible to analyze these changes four-dimensionally, taking the time dimension into account

(Nagata, 1995b). Thick sections of rat liver tissues, fixed and stained with DAB reaction, embedded in epoxy resin, cut as thick as 5 μm were also observed with high-voltage electron microscopy at 1000 kV. These thick specimens, both whole mount cultured cells and thick Epon sections, were observed by high-voltage electron microscopy taking stereo-pair pictures, tiling the specimens at both $+8$ and -8 and the stereo-pair pictures were observed with a stereoscope or alternatively anaglyph-type color pictures were composed of red pictures from right side and green pictures from left side and observed with a pair of anaglyph (red and green) glasses (Figs. 12G–12I). Using these techniques, proliferation of peroxisomes in rat hepatocytes cultured in a medium containing such a peroxisome proliferator as clofibrate was observed three-dimensionally with a set of stereo-pairs (Figs. 12E and 12F) or with an anaglyph-type color picture (Figs. 12G–12I). Using a JEOL JIM-5000 image analyzer (JEOL, Tokyo, Japan), two contour lines plotted from the two stereo-pair pictures at a thickness or depths of 0.2 μm were composed into one and were observed with the anaglyph-type glasses (JEOL, Tokyo, Japan), demonstrating the depth or height of respective cell organelles similarly to the geographical maps of mountains (Figs. 12H and 12I).

On the other hand, the phospholipase B (EC 3.1.1.5 lysolecithin acyl hydrolase) activity in the liver of mouse was also studied by the enzyme cytochemical method at electron microscopic level which was developed in our laboratory (Nagata and Iwadare, 1984). The reaction products were localized on the end of the smooth endoplasmic reticulum, the lysosomes and lipid droplets in mouse hepatocytes.

As for the physical reactions, we studied DNA contents of nuclei in mononucleate hepatocytes and binucleate hepatocytes by means of microspectrophotometry in young and aged rats (Nagata, 1961a,b,c). We first prepared isolated hepatocytes from the liver tissues of rats and stain with the Feulgen reaction suitable to microspectrophotometry differentiating mononucleate and binucleate cells (Nagata, 1961a,b). Then the DNA contents of the nuclei in both mononucleate and binucleate hepatocytes in young and aged rats separately. It was found that more tetraploid nuclei were found in the nuclei of mononucleate hepatocytes than the nuclei in binucleate hepatocytes in young rats, while there were more tetraploid nuclei in both mononucleate and binucleate hepatocytes in aged rats (Nagata, 1961c).

On the other hand, studies on macromolecular synthesis in the livers of aging mice were extensively carried out (Nagata, 1994c, 1995a, 1999c). As for the nucleic acid synthesis, we first studied the difference between the mononucleate and binucleate hepatocytes of adult rats, injected with [^{3}H]thymidine, and radioautographed (Nagata, 1962; Nagata *et al.,* 1961). The results showed that the frequency of labeled cells was greater in the mononucleate cells than in the binucleate cells. The labeled binucleate cells are categorized into two types, i.e., cells with one of the two nuclei labeled and cells with two nuclei labeled. The former was more frequently observed than the latter. Grain counts revealed that the amount of DNA synthesized in the binucleate cell with one nucleus labeled was the same as that in

the monoucleate cell, while the total amount of DNA synthesized in the binucleate cell with two labeled nuclei was almost twice as that of the mononucleate cell (Nagata *et al.,* 1966).

Light and electron microscopic radioautography of prenatal and postnatal normal mice at various ages labeled with [^{3}H]thymidine revealed that many silver grains were localized over the nuclei of various cell types composing the liver, i.e., hepatocytes (Fig. 13A), sinusoidal endothelial cells (Fig. 13B), Kupffer's cells, Ito's fat-storing cells, bile ductal epithelia cells, fibroblasts, and hematopoietic cells (Ma, 1988; Ma and Nagata, 1990a,b). In hematopoietic cells, silver grains were observed over the nuclei of erythroblasts (Fig. 13C), myeloblasts, lymphoblasts, and megakaryocytes. However, most hematopoietic cells disappeared on postnatal day 14. At fetal day 19, the liver tissues chiefly consisted of hepatocytes and haematopoietic cells and no lobular orientation was observed (Fig. 13C). At day 1 and 3 days after birth, lobular formation started and finally the hepatic lobules were formed at day 9 after birth. During the perinatal period, almost all kinds of cells were labeled with [^{3}H]thymidine. Percentage of labeled hepatocytes was the highest at fetal day 19, and rapidly decreased after birth to day 3. From days 9 to 14, the percentage of labeled hepatocytes (labeling index) decreased gradually and finally reached the lowest at 24 months (Fig. 14A). When the labeling indices of hepatocytes in 3 hepatic acinar zones were analyzed, the indices decreased in zone 2 (intermediate zone) and zone 3 (peripheral zone) on days 3 end 9 after birth, whereas they increased in zone 1 (central) on day 9, and then they altogether decreased from day 14 to 24 months (Fig. 14B). When the size and number of cell organelles in both labeled and unlabeled hepatocytes were estimated quantitatively by image analysis with an image analyzer, Digigramer G/A (Mutoh Kogyo Co. Ltd., Tokyo, Japan), the area size of the cytoplasm (150–200 μm^2), nucleus (40–50 μm^2), mitochondria (40–50 μm^2), endoplasmic reticulum (40–60 μm^2), and the number of mitochondria in the unlabeled hepatocytes were greater than those of the labeled cells (Ma and Nagata, 1990a; Nagata 1995a). These data demonstrate that the cell organelles of the hepatocytes that synthesized DNA were not as well developed as those not synthesizing DNA during the postnatal development. In some of unlabeled hepatocytes, several silver grains were occasionally observed localizing over mitochondria and peroxisomes, as was formerly reported (Nagata *et al.,* 1967, 1982). The mitochondrial DNA synthesis was first observed in cultured hepatocytes of chickens and mice *in vitro* (Nagata *et al.,* 1967). The percentages of other cell types such as sinusoidal endothelial cells showed also decrease from perinatal period to 24 months.

When [^{3}H]uridine was administered to animals or cultured cells are incubated in a medium containing [^{3}H]uridine *in vitro* and radioautograms were prepared, silver grains first appeared over the chromatin of the nucleus and nucleolus of all the cells within several minutes, then silver grains spread over the cytoplasm within 30 min, showing messenger RNA and ribosomal RNA (Nagata, 1966b; Nagata and Nawa, 1966b). We studied quantitative changes of RNA synthesis in the livers of adult
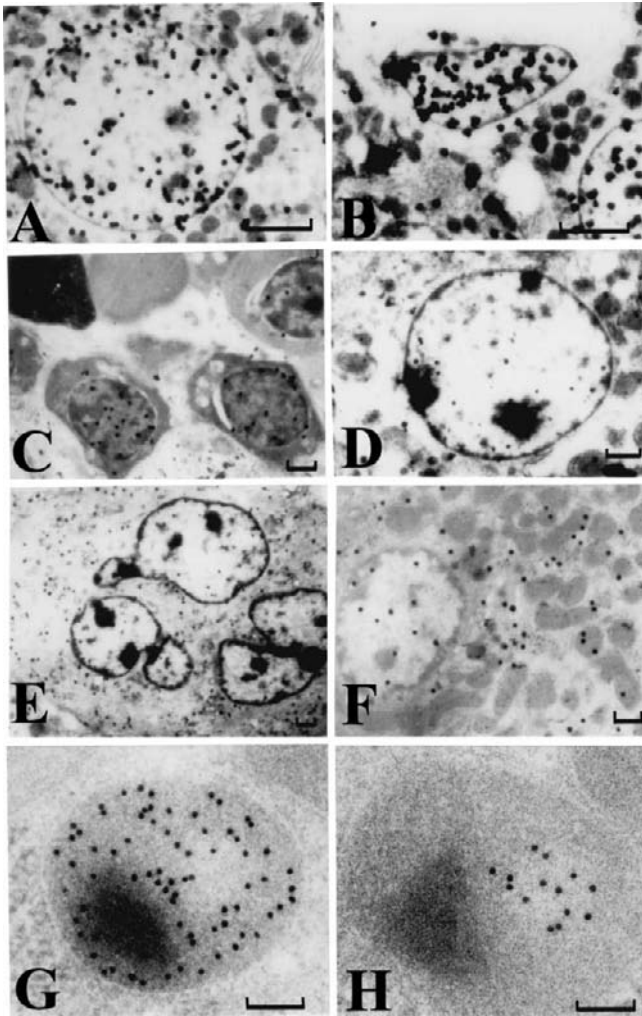
FIG. 13 Special cytochemistry 5: The liver cells II. (A) EMRAG of a hepatocyte of a 14-day-old mouse, injected with [³H]thymidine and radioautographed. Many silver grains are localized over the chromatin in the nucleus, showing DNA synthesis (×9000; bar = 1 μm). Permission from T. Nagata (1995c, Fig. 3, p. 25). (B) EMRAG of a sinusoidal endothelial cell in the liver of a 14-day-old mouse, injected with [³H]thymidine and radioautographed. Many silver grains are localized over the chromatin in the nucleus, showing DNA synthesis (×9000; bar = 1 μm). Permission from T. Nagata (1995c, Fig. 3, p. 25). (C) EMRAG of hematopoietic cells in the liver of a prenatal day 19 mouse fetus, injected with [³H]thymidine and radioautographed. Many silver grains are localized over the chromatin in three nuclei of erythroblasts, showing DNA synthesis (×3750; bar = 1 μm). Permission from T. Nagata (1995c, Fig. 3, p. 25). (D) EMRAG of a hepatocyte of a 1-month-old mouse, injected with [³H]uridine and radioautographed. Many silver grains are localized over the nucleolus and the chromatin in the nucleus, showing RNA synthesis (×4500; bar = 1 μm). Permission from T. Nagata (1995c, Fig. 7, p. 29).

mice before and after feeding by incoroporations of [³H]uridine (Nagata, 1966b). The results showed that the incorporation of [³H]uridine was greater in binucleate hepatocytes than mononucleate (Nagata, 1967b). Then we studied aging changes of [³H]uridine incorporation in the livers and pancreases of aging mice at various ages from prenatal embryos to postnatal aged mice by LM and EMRAG. When aged mice were injected with [³H]uridine, LM and EM radioautograms showed that silver grains were localized over the nucleoli, nuclear chromatin (both euchromatin and heterochromatin), mitochondria, and rough surfaced endoplasmic reticulum of hepatocytes (Fig. 13D) and other types of cells such as sinusoidal endothelial cells, Kupffer's cells, Ito's fat-strong cells, ductal epithelial cells, fibroblasts and hematopoietic cells in the livers at various ages (Nagata, 1995a; Ma and Nagata, 1990b). By quantitative analysis, the total number of silver grains in nucleus, nucleolus, and cytoplasm of each hepatocyte increased gradually from fetal day 19 to postnatal days, reached the maximum postnatal day 14, and then decreased to 24 months. The number of silver grains in nucleolus, when classified into two compartments, grains over granular components and those over fibrillar components, both increased in parallel after birth, reached the maximum on day 14, and then decreased through 24 months with aging. However, when the ratio (%) of silver grains over euchromatin, heterochromatin of the nuclei, and granular components and fibrillar components of the nucleoli are calculated, the ratio remained constant at each aging point.

We first studied protein synthesis of mouse hepatocytes by incorporation of [³H]leucine and [³H]tryptophane before and after feeding (Nagata, 1967b). The results showed that the incorporations of both amino acids were greater in binucleate hepatocytes than mononucleate (Nagata, 1967b). When [³H]leucine was injected into several groups of mice at various ages and light and electron microscopic

---

(E) EMRAG of a megakaryocyte in the hematopoietic cells in the liver of a prenatal day 19 mouse fetus, injected with [³H]leucine and radioautographed. Many silver grains are localized over the chromatin in six nuclei as well as in cytoplasm, showing protein synthesis (×2250; bar = 1 μm). Permission from T. Nagata (1995c, Fig. 10, p. 32). (F) EMRAG of a hepatocyte in the liver of a postnatal 2-month-old mouse, injected with [³H]proline and radioautographed. Many silver grains are observed over the nucleus and cell organelles in cytoplasm such as Golgi apparatus, endoplasmic reticulum, mitochondria, and peroxisomes, showing collagen and protein synthesis (×3750; bar = 1 μm). Permission from H. Ma and T. Nagata (2000, Fig. 7, p. 21). (G) Electron micrograph of a hepatocyte of a normal adult male Wistar rat liver, fixed in paraformaldehyde and glutaraldehyde mixture, embedded in Lowicryl K4M, sectioned, and stained with anti-catalase antibody by the protein A–gold technique. Gold particles for catalase can be seen over the peroxisomal matrix (×75,000; bar = 0.1 μm). (H) Electron micrograph of a hepatocyte of a normal adult male Wistar rat liver, fixed in paraformaldehyde and glutaraldehyde mixture, embedded in Lowicryl K4M, sectioned, and stained with anti-D amino acid oxidase antibody by the protein A–gold technique. Gold particles for catalase can be seen over the peroxisomal matrix. Note the localization of gold particles over an electron lucent area in the peroxisomes (×75,000; bar = 0.1 μm).
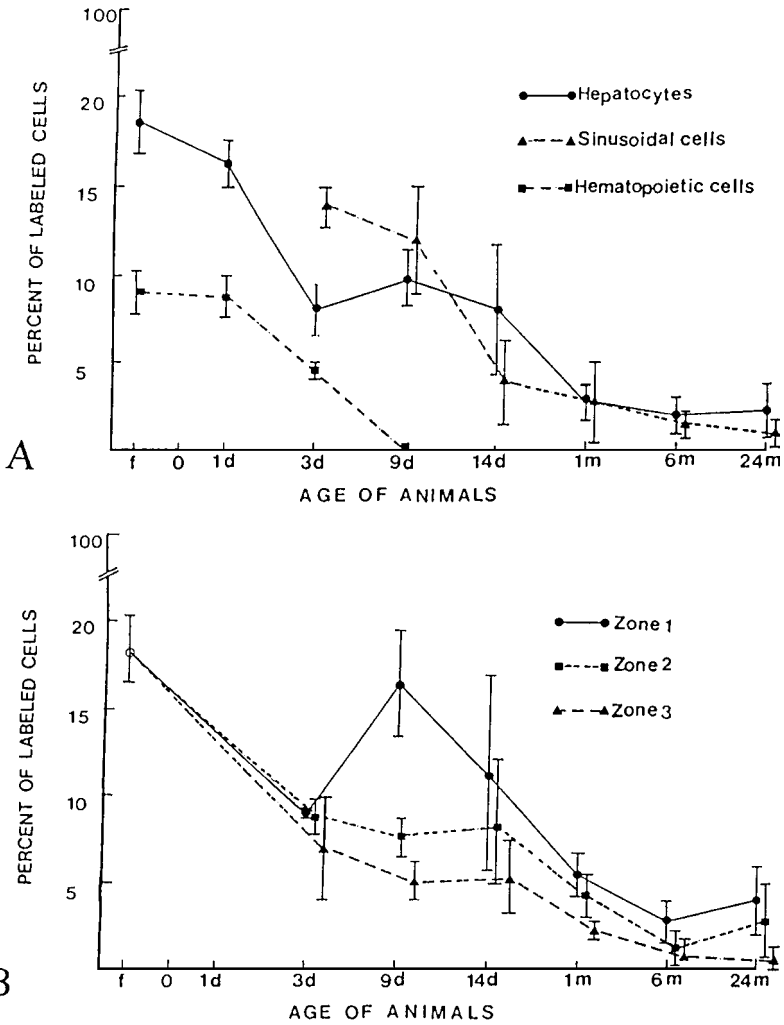
FIG. 14 Transitional curves of labeling indices in the livers of aging mice after injection of [³H]thymidine. (A) Labeling indices of hepatocytes, sinusoidal endothelial cells, and hematopoietic cells in respective aging groups as expressed by means ± standard deviations. (B) Labeling indices of hepatocytes in the three zones of hepatic lobules in respective aging groups as expressed by means ± standard deviations. Permission from T. Nagata (1995c, Fig. 4, p. 26).

radioautograms were prepared, silver grains were observed over all cell types of the liver (Ma *et al.,* 1991), i.e., hepatocytes, sinusoidal endothelial cells, ductal epithelial cells, Kupffer's cells, Ito's fat storing cells, fibroblasts, and hematopoietic (Fig. 13E) cells (Ma *et al.,* 1991). In hepatocytes, number of silver grains in cytoplasm and karyoplasm increased from perinatal animals to 1-month postnatal

animals and decreased with aging to 24 months. The number of silver grains observed over respective cell organelles—Golgi apparatus, mitochondria, endoplasmic reticulum—changed with age, reaching the maximum at 1 month but the ratio remained constant at each point. When [^{3}H]proline was injected into mice at various ages from prenatal embryos to postnatal senescence and quantitative changes of collagen and protein synthesis in the livers were studied by electron microscopic radioautography, silver grains were localized over the nuclei, cytoplasmic matrix, endoplasmic reticulum, Golgi apparatus, mitochondria, and peroxisomes of almost all the cells at various ages (Fig. 13F). The number of silver grains in the nuclei, cytoplasmic matrix, endoplasmic reticulum, mitochondria, Golgi apparatus, and peroxisomes of hepatocytes gradually increased from embryo, reached the maximum at 1 and 6 months after birth, and decreased with age until 24 months. The number of silver grains localized over the extracellular collagen fibrils and matrices was not so many in respective aging groups and did not show any remarkable changes with aging. From the results, it was concluded that [^{3}H]proline was incorporated not only into collagen but also into the structural proteins of hepatocytes under normal aging conditions (Ma and Nagata, 2000).

Polysaccharides can be classified into simple polysaccharide and complex polysaccharide. We studied [^{3}H]glucose incorporation into glycogen in the liver, in connection to soluble compounds (Nagata and Murata, 1977; Nagata *et al.,* 1997a). Soluble [^{3}H]glucose, which was demonstrated by cryo-fixation and dry-mounting radioautography, was localized over the nucleus, cell organelles and cytoplasmic ground substance of hepatocyte diffusely. By conventional chemical fixation and wet-mounting radioautography, silver grains were localized only over glycogen granules, endoplasmic reticulum, and Golgi apparatus. The relation of glycogen synthesis to aging has not yet been clarified.

We observed lipid synthesis in the liver using [^{3}H]glycerol in connection to soluble compounds (Nagata *et al.,* 1977a). When adult mice were injected with [^{3}H]glycerol and the livers were cryo-fixed at $-196°$C, freeze–substituted, embedded in epoxy resin, dry-sectioned, and prepared for dry-mounting radioautography, many silver grains appeared over the nuclei and cytoplasm diffusely. However, when the same liver tissues were fixed chemically in buffered glutaraldehyde and osmium tetroxide and radioautographed by conventional wet-mounting procedures, very few silver grains were observed only over the endoplasmic reticulum and lipid droplets, which demonstrated macromolecular lipid synthesis. The relation between macromolecular lipid synthesis and aging has not yet been clarified.

When the livers of Wistar rats administered orally with [^{3}H]tranilast, one of the synthetic anti-allergic agents, synthesized by Kissei Pharmaceutical Co. (Matsumoto, Japan), *N*-(3, 4-dimethoxycinnamoyl) anthranilic acid, which was labeled with ^{3}H by NEN (Boston, MA) and observed by LMRAG, many silver grains were seen over the hepatocyte nuclei and cytoplasm. The grain counts reached the maximum at 3 h after the administration, which suggested the metabolic process in

the liver (Momose *et al.,* 1989). Intracellular localization of a peroxisome prolifer-ator, ^{14}C-labeled bezafibrate, was also demonstrated in cultured rat hepatocytes by LM and EMRAG (Momose and Nagata, 1993, Momose *et al.,* 1995). About 90% of all the silver grains were localized over the cytoplasm. On EMRAG of whole mount cultured cells, silver grains were localized on cytoplasmic matrix especially over the endoplasmic reticulum. The results showed that the receptor of peroxisome proliferator was associated with the endoplasmic reticulum (Momose *et al.,* 1995).

We studied immunostaining for peroxisomal enzymes (Usuda *et al.,* 1991b,c, 1995, 1996) and lectin staining in the liver (Morita *et al.,* 1991). We first studied immunostaining of peroxisomal enzymes in mouse liver, urate oxidase (Yokota and Nagata, 1973, 1977), and catalase (Yokota and Nagata, 1974), using cryosections and ferritin-antibody oxidase conjugates (Fig. 2E), together with the conventional enzyme cytochemical methods. The two enzymes were localized on the perox-isomes of mouse hepatocytes and it was found that the number of peroxisomes in mouse hepatocytes decreased after birth but sometimes increased after admin-istration of several peroxisome proliferators such as clofibrate, bezafibrate, and DEHP. We recently developed immunostaining of peroxisomal enzymes by protein A–colloidal gold complex technique using freeze–substitution embedding for electron microscopy (Usuada *et al.,* 1990; Usuda and Nagata, 1991). The hep-atic tissues of Wistar rats were fixed in 4% paraformaldehyde/0.1% glutaralde-hyde/0.1 M phosphate buffer, pH 7.4, embedded in Lowicryl K4M at $-20°$C, and immunostained with antibodies for catalase, acyl-CoA oxidase, bifunctional proteins, 3-ketoacyl-CoA thiolase, urate oxidase, HMG CoA reductase, serine: pyruvate aminotransferase, sterol carrier protein 2,2,4-dienoyl-CoA reductase, apolipoprotein E, L-α-hydroxy acid oxidase, glycolate oxidase, acy-CoA oxidase, D-amino acid oxidase for peroxisomal matrix, and 70-, 40-, 26-, and 22-kDa PMPs for peroxisomal membrane by the protein A–gold technique. The results demon-strated that a peroxisome of rat hepatocyte is a spherical ornagelle with a single limiting membrane, containing a homogeneous matrix and a high electron dense core. The peroxisomal matrix of rat hepatocytes can be divided into two subcom-partments, the electron-lucent subcompartment and the electron-dense subcom-partment (Usuda *et al.,* 1995). The peroxisomal membrane contains 70-, 41-, 26-, and 22-kDa PMPs (Usuda *et al.,* 1991b, 1994, 1996). The matrix of hepatic perox-isomes contains catalase (Fig. 13G), D-amino acid oxidase (Fig. 13H), acyl-CoA oxidase, L-α-hydroxy acid oxidase, glycolate oxidase, acy-CoA oxidase, bifunc-tional protein, and 3-ketoacyl-CoA thiolase in the peroxisomal matrix and urate oxidase in the core (Usuda *et al.,* 1994, 1995, 1996). The electron-lucent subcom-partment of the matrix contains only D-amino acid oxidase (Fig. 13H), while the electron-dense subcompartment contains all other enzymes (Usuda *et al.,* 1996). The immunogold techniques were also applied to the livers of different species. It was demonstrated that species-specific differences were observed in the size and shape of the peroxisomes and the ultrastructure of the core in man, monkey, cow, cat, dog, rat, mouse, frog, and so on (Usuda *et al.,* 1995, 1996).

We stained livers of Wistar rats with WGA (wheat germ agglutinin) and DSA (Datura stramonium agglutinin) and observed by light and electron microscopy (Morita *et al.,* 1992). For light microscopy, the liver tissues were fixed in para-formaldehyde, immersed in sucrose solution, frozen with dry ice and hexan, cryo-stat sections were stained with biotinylated lectins and avidin–biotin–peroxidase complex, and visualized by DAB reaction. For electron microscopy, tissues were fixed in paraformaldehyde/glutaraldehyde, frozen and freeze–substituted, embedded in Lowicryl K4M at a low temperature, and ultrathin sections were stained with biotinylated lectins and streptavidin–colloidal gold complex. The reaction products were mainly localized along the sinusoids with both WGA and DSA by light microscopy. The gold particles for both WGA and DSA by electron microscopy were observed over the cell surface of microvilli, in the space of Disse, and canaliculi, as well as over the lysosomes and Golgi apparatus of hepatocytes (Morita *et al.,* 1992).

6. Pancreatic Cells

The mammalian pancreas is an exocrine and endocrine organ and it consists of both exocrine portion and endocrine portion. The exocrine portion is composed of ductal epithelial cells, centro-acinar cells, acinar cells, and connective tissue cells, while the endocrine portion, the islet of Langerhans, is composed of three types of endocrine cells, A, B, and C cells, and connective tissue cells. As for the chemical reactions, enzyme cytochemistry on lipase and phospholipase by electron microscopy which were developed in our laboratory was studied. The reaction products by lipase (EC 3.1.1.3 glycerol ester hydrolase) activity using Tween 80 as substrate and substituted with lead nitrate were observed in cisternae of the endoplasmic reticulum (Fig. 15A), Golgi apparatus, and the peripheral zones of the secretory granules (Fig. 15B) of normal and pancreatic mice and rats (Nagata, 1974; Murata *et al.,* 1968; Nagata *et al.,* 1968; Nagata and Murata, 1972, 1980). The enzymes produced in the pancreatic acinar cells such as amylase, trypsin and chymotrypsin were formerly localized in the secretory granules in the pancreatic acinar cells homogeneously (Beaudoin *et al.,* 1985).

With regards the physical reactions, DNA and RNA synthesis in mouse pancreas by radioautography were studied. Light and electron microscopic radioautograms of the pancreas revealed that the nuclei of pancreatic acinar cells (Fig. 15C), centro-acinar cells (Fig. 15D), ductal epithelial cells, and endocrine cells were labeled with [3H]thymidine. The labeling indices of these cells reached the maxima at day 1 after birth and decreased gradually to 24 months (Fig. 16). The maximum in the acinar cells proceeded to the ductal and centro-acinar cells (Nagata *et al.,* 1984; Nagata and Usuda, 1986). On the other hand, light and electron microscopic radioautograms of pancreas of mouse injected with [3H]uridine showed incorporations into exocrine and then in endocrine cells, and more in pancreatic acinar cells (Fig. 15EF) than in ductal or centro-acinar cells. Among the acinar cells,
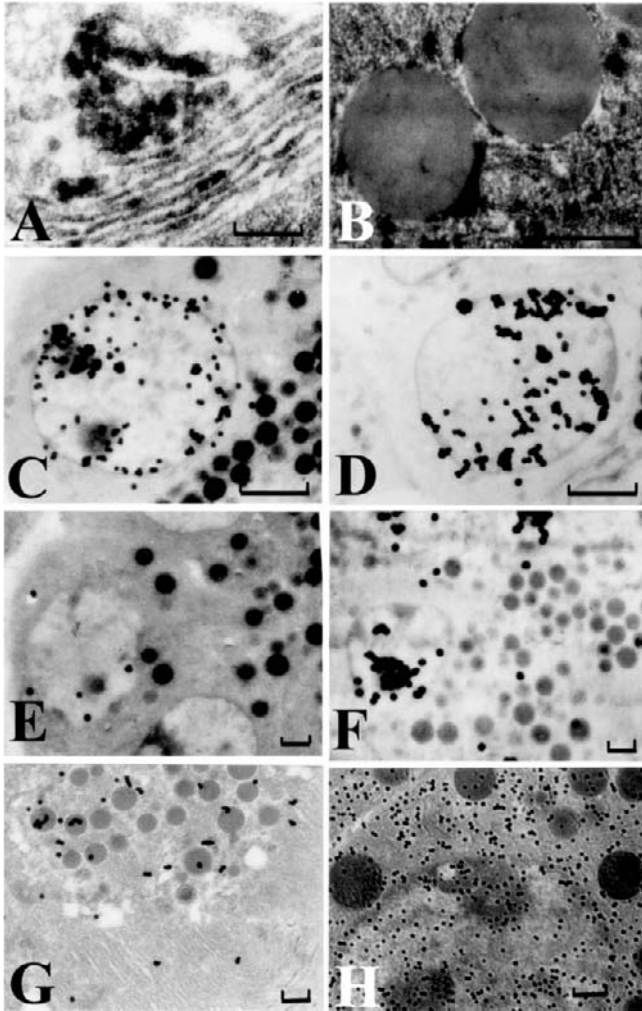
FIG. 15   Special cytochemistry 6: The pancreatic cells. (A) Electron micrograph of mouse pancreatic acinar cell showing lipase activity with Tween 80 medium. The reaction products are observed in cisternae of the endoplasmic reticulum (×7000; bar = 1 μm). (B) Electron micrograph of mouse pancreatic acinar cell, showing lipase activity at the peripheral zones of the two secretory granules (×14,000; bar = 1 μm). (C) EMRAG of a pancreatic acinar cell of a 14-day-old mouse, injected with [^{3}H]thymidine and radioautographed. Many silver grains are localized over the chromatin in the nucleus, showing DNA synthesis (×9000; bar = 1 μm). Permission from T. Nagata (1995c, Fig. 6, p. 28). (D) EMRAG of a centro-acinar cell in the pancreas of a 14-day-old mouse, injected with [^{3}H]thymidine and radioautographed. Many silver grains are localized over the chromatin in the nucleus, showing DNA synthesis (×9000; bar = 1 μm). Permission from T. Nagata (1995c, Fig. 6, p. 28). (E) EMRAG of two pancreatic acinar cells of a newborn mouse at postnatal day 1, injected with [^{3}H]uridine and
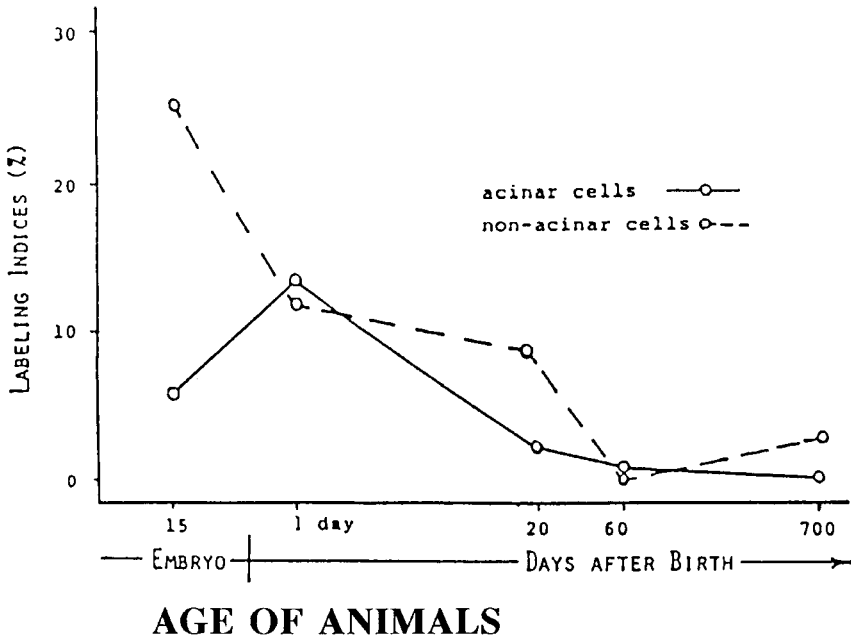
FIG. 16 Transitional curves of the labeling indices of respective cells in the pancreas of aging mice labeled with [³H]thymidine at various ages. Permission from T. Nagata (1999c, Fig. 15, p. 693).

the number of silver grains increased after birth (Fig. 15E) to day 14 (Fig. 15F) and then decreased with age (Nagata *et al.,* 1986). Quantitation of silver grains in the nucleoli, chromatin, and cell body were carried out by X-ray microanalysis (Nagata *et al.,* 1986), which verified the results obtained by visual grain counting (Nagata, 2000d).

As for the protein synthesis in the pancreas, [³H]leucine incorporation into endoplasmic reticulum, Golgi apparatus and to secretory granules of pancreatic

radioautographed. Only a few silver grains are localized over the chromatin in the nucleus, showing RNA synthesis (×3750; bar = 1 μm). Permission from T. Nagata (1995c, Fig. 9, p. 31). (F) EMRAG of two pancreatic acinar cells of a 14-day-old mouse, injected with [³H]uridine and radioautographed. Many silver grains are localized over the nucleolus and the chromatin in the nucleus, showing RNA synthesis (×3750; bar = 1 μm). Permission from T. Nagata (1995c, Fig. 9, p. 31). (G) EMRAG of a pancreatic acinar cell of a 14-day-old mouse, injected with [³H]leucine and radioautographed. Many silver grains are localized over the secretory granules, Golgi apparatus and endoplasmic reticulum, showing protein synthesis (×3750; bar = 1 μm). Permission from T. Nagata (2000e, Fig. 9, p. 12). (H) EMRAG of a pancreatic acinar cell of a 14-day-old mouse, injected with [³H]glucosamine and radioautographed. Many silver grains are observed over the nucleus, nucleous, and cell organelles in cytoplasm such as Golgi apparatus, endoplasmic reticulum, and cytoplasmic ground substance, showing glucide synthesis (×4500; bar = 1 μm). Permission from T. Nagata (1995c, Fig. 12, p. 34).

acinar cells was first demonstrated by Jamieson and Palade (1967). We have studied [³H]glycine incorporation into these cell organelles of mouse pancreatic acinar cells in connection with soluble compounds (Nagata *et al.,* 1977a). Then, the quantitative aspects of protein synthesis with regards the aging from prenatal to postnatal stages fetal day 19, to postnatal days 1, 3, 7, 14, and 1, 2, 5 and 12 months have also been clarified, showing an increase of silver grain counts labeled with [³H]leucine after birth, reaching a peak from postnatal week 2 to 1 month (Fig. 15G), and decreasing from 2 months to 1 year (Nagata, 2000e; Nagata and Usuda, 1993).

As for the glucides, we have studied incorporation of [³H]glucosamine into the pancreas of aging mice at various ages by light and electron microscopic radioautography (Nagata *et al.,* 1992). When perinatal baby mice received [³H]glucosamine injection and the pancreatic tissues were radioautographed, silver grains were observed over exocrine and endocrine pancreatic cells. However, the number of silver grains was not so many. When juvenile mice at the age of 14 days after birth were examined, many silver grains appeared over the exocrine pancreatic acinar cells (Fig. 15H). Fewer silver grains were observed over endocrine pancreatic cells and ductal epithelial cells. The grains in the exocrine pancreatic acinar cells were localized over the nucleus, endoplasmic reticulum, Golgi apparatus, and secretory granules, demonstrating glycoprotein synthesis. Adult mice at the ages of 1 or 6 months or senile mice at the ages of 12 or 24 months showed very few silver grains on radioautograms. Thus, the glucide synthesis in the pancreas of mice revealed quantitative changes, an increase and then a decrease of [³H]glucosamine incorporation with aging (Nagata *et al.,* 1992).

The lipids are esters of high fatty acids and can be demonstrated by light and electron microscopic radioautography with the incorporations of either [³H]glycerol or ³H-labeled fatty acids. When litters of ddY mice on fetal day 19, postnatal days 1, 3, 7, 14, and 1, 2, 6, and up to 12 months were injected with [³H]glycerol and the pancreases were prepared for light and electron microscopic radioautography, silver grains were observed in both exocrine and endocrine cells of respective ages (Nagata *et al.,* 1988b, 1990). In perinatal animals from fetal day 19 to postnatal days 1, 3, and 7, cell organelles were not well developed in exocrine and endocrine cells and the number of silver grains was very small (Nagata *et al.,* 1988b). In 14-day-old juvenile animals, cell organelles such as endoplasmic reticulum, Golgi apparatus, mitochondria, and secretory granules were well developed and many silver grains were observed over these organelles and nuclei in both exocrine and endocrine cells. The number of silver grains was more in exocrine cells than endocrine cells. In 1-, 2-, and 6-month-old adult animals, numbers of silver grains remained constant. In 12-month-old senescent animals, silver grains were fewer than in younger animals. The number of silver grains expressed the quantity of lipids synthesis, which increased from perinatal period to adult and decreased to senescence (Nagata *et al.,* 1990).

Experimental studies to clarify the pathogenesis of experimental pancreatitis were carried out by means of LM and EMRAG. Several male Wistar rats were

treated with daily DL-ethionine injections for 2 days or for 1 month to cause the acute and chronic experimental ethionine pancreatitis. Then, both normal and experimental pancreatitis animals were injected with [^{3}H]ethionine and the pancreatic tissues after 5 and 10 min were fixed and processed for LM and EMRAG (Yoshizawa *et al.,* 1974). As a result, many more silver grains were observed over the secretory granules and the lumen of the exocrine pancreatic tissues of pancreatitis animals than the normal animals, suggesting the pathogenesis of the ethionine-induced pancreatitis to have rapid intracellular transport of ethionine (Yoshizawa *et al.,* 1974).

On the other hand, another group of several male Wistar rats was fed with 20% ethanol for 3 months to cause alcoholic pancreatitis. Both the normal and the experimental pancreatitis animals were then injected with [^{3}H]leucine and the pancreatic tissues after 5 to 60 min of injection were fixed and processed for LM and EMRAG (Yoshizawa *et al.,* 1977). As a result, fewer silver grains were observed over the secretory granules and the lumen of the exocrine pancreatic tissues of pancreatitis animals than the normal animals, suggesting lower protein synthetic activity in the alcohol-induced pancreatitis animals (Yoshizawa *et al.,* 1977). We analyzed silver grains by X-ray microanalysis. In EMRAG obtained from the pancreas of fetal day 19 embroys and newborn day 1 and newborn day 14 mice (Figs. 15E and 15F) labeled with [^{3}H]uridine, demonstrating RNA synthesis, the number of silver grains in the nuclear chromatin, and cytoplasm increased (Nagata and Usuda, 1985; Nagata, 1991, 1993). In order to quantify the silver contents of grains observed over the nucleoli, nuclei, and cytoplasm, X-ray spectra were recorded by energy dispersive X-ray microanalysis (JEM-4000EX TN5400), demonstrating Ag–K$_\alpha$ peaks at higher energies (not shown). Thus, P/B ratios expressing relative silver contents were determined and compared between the two age groups. Table III shows the results obtained by X-ray microanalysis in different cell compartments in 1- and 14-day-old animal groups. The results obtained by visual grain counting in different cell compartments in 1- and 14-day-old animals are also listed. The number of silver grains was calculated to express the counts per unit area to be compared with the XMA counts. These two results, the silver content analyzed by X-ray microanalysis and the results obtaining from visual grain counting were in good accordance with each other (Table III). In the literature, Hodges and Muir (1975) were the first to quantify silver contents on EMRAG obtained from cultured cells labeled with [^{3}H]thymidine by observation with a scanning electron microscope (SEM). Our report (Nagata and Usuda, 1985; Nagata 1991, 1993) was the first to quantify the silver grains in the TEM mode. This procedure should be useful in calculating and recording the data with an on-line computer.

D. Respiratory Cells

The respiratory organ of mammals can be divided into two portions, the air conducting passages and the respiratory portion. The former consists of the nose,

TABLE III

Comparison between Visual Grain Counts and X-ray Microanalysis
on Electron Microscopic Radioautograms

Cell compartment	Age of animals	
	1 day	14 days
Corrected grain counts (CNT/cm$^2 \times 10^{-8}$)		
Nucleolus	2.60	5.35
Nucleus	0.29	0.88
Cytoplasm	0.15	0.21
Corrected XMA counts (CNT/cm$^2 \times 10^{-8}$)		
Nucleolus	4130.1	21068.1
Nucleus	61.6	176.8
Cytoplasm	15.5	51.7

From T. Nagata (1993).

the pharynx, the larynx, the trachea, and the bronchus, while the latter consists of the lung. We studied cytochemical reactions in both the tracheal cells and the pulmonary cells.

1. Tracheal Cells

The tracheas of mammals are composed of ciliated pseudostratified columnar epithelial cells, connective tissue cells, smooth muscle cells, and hyalin cartilage cells. As for the chemical reactions in tracheal cells, age-related alterations of the proteoglycans were observed in the tracheal cartilage matrix of ddY strain mice at various ages, from postnatal days 1, 3, 7, and 14 and 1, 3, 6, 12, and 15 months, with the cationic dye polyethyleneimine (PEI) and observed by electron microscopy (Li *et al.,* 1994). In newborn and jevenile animals (from 1 day to 1 month), the intensity and size of PEI reaction products increased, resulting in the formation of territorial matrix and the decrease of the space between the PEI aggregates and the collagen fibers. In adult mice, from 1 month to 6 months, the intensity (Fig. 17A) and size (Fig. 17B) of PEI aggregates kept stable. However, in the senile stage from 6 to 15 months the PEI reaction decreased in the interterritorial matrix. These results demonstrated the age-related changes of proteoglycans in the tracheal cartilage matrix (Li *et al.,* 1994).

The changes of DNA synthesis of tracheal cells in aging mice were studied by LM and EMRAG (Sun *et al.,* 1997a). The tracheae of eight groups of mice from fetal day 18 to 2 years after birth were examined (Figs. 18A and 18B). The results demonstrated that the DNA syntheses and morphology of tracheal cells
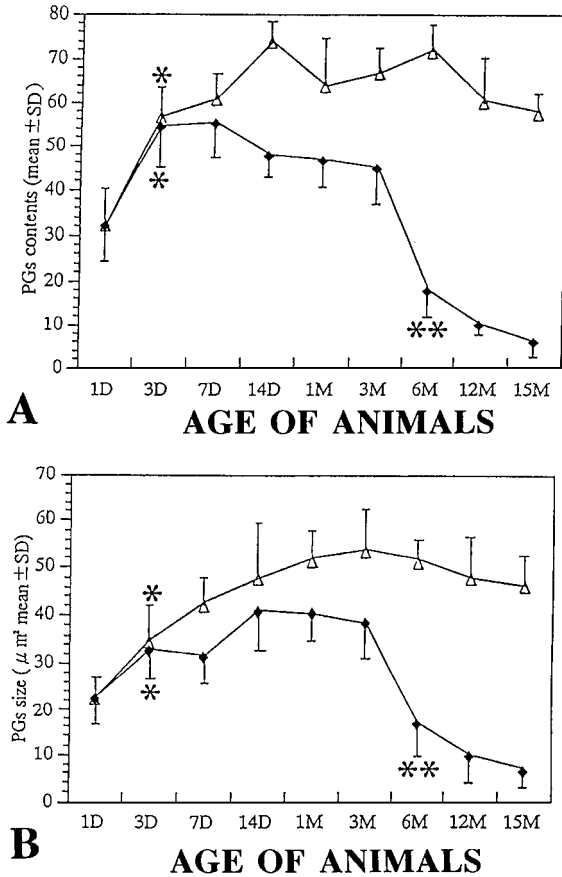
FIG. 17 Transitional curves of proteoglycan contents in the hyaline cartilage of mouse trachea at various ages. (A) Transitional curves of proteoglycan contents as expressed by the mean areas of PEI aggregates/total area (mean ± standard deviation). *Significantly higher than day 1; **significantly lower than day 1. (B) Area size of PEI aggregates (μm^2). Open triangles, territorial matrix, closed rectangles, interterritorial matrix. Permission from S. Li *et al.* (1994, Fig. 11, p. 133).

in the mouse tracheae changed due to aging. The radioautograms revealed that the DNA synthesis in the nuclei of ciliated cells was observed only in the fetal animals (Fig. 18A). However, the DNA synthesis in nonciliated cells and basal cells was observed in both prenatal and postnatal animals (Fig. 18B). The labeling indices of these cells reached their maximum on fetal day 18 (8–11%) and then declined from postnatal day 3 to 2 years (a few percent). The ciliated cell could not synthesize DNA and proliferate in the postnatal stage. They are supposed to be derived by the division and transformation of basal cell. On the other hand, the DNA synthesis of chondrocytes was the highest on embryonic day 18 (9%)
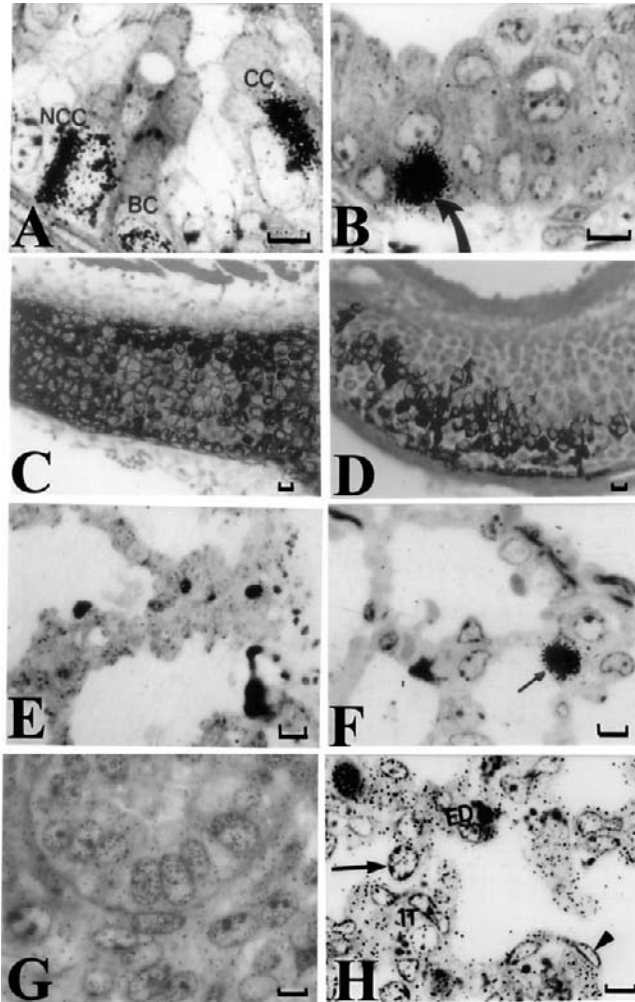
FIG. 18   Special cytochemistry 7: The respiratory cells. (A) LMRAG of the trachea of an embryonic day 18 mouse fetus injected with [³H]thymidine and radioautographed. Many silver grains are localized over the three nuclei of nonciliated cells (NCC) at left, a basal cell (BC) at bottom, and a ciliated cell (CC) at right, showing DNA synthesis (×1125; bar = 50 μm). Permission from L. Sun *et al.* (1997a, Fig. 1, p. 214). (B) LMRAG of a the trachea of a mouse at postnatal 1 month, injected with [³H]thymidine and radioautographed. Many silver grains are localized over the nucleus of a basal cell (arrow) at right, showing DNA synthesis (×1125; bar = 50 μm). Permission from L. Sun *et al.* (1997a, Fig. 9, p. 215). (C) LMRAG of the trachea of an embryonic day 19 mouse fetus, injected with ³⁵SO₄ and radioautographed. Note that the numerous silver grains showing the incorporations of the radiosulfate accumulate over the interterritorial and territorial matrices but not so much over the chondrocytes (×400; bar = 50 μm). Permission from T. Nagata (2000f, Fig. 1, p. 379). (D) LMRAG of the hyaline cartilage of the trachea of a newborn mouse at postnatal day 3, injected with ³⁵SO₄ and radioautographed. Note that the number of silver grains accumulating over the

and rapidly declined on postnatal day 3 (2%). The chondrocytes lost the ability to synthesize DNA at 2 months after birth (0%). The DNA syntheses of other cells (including fibroblasts, smooth muscle and glandular cells) were highest on fetal day 18 (8%) and fell markedly on the day 3 after birth (2%) and decreased progressively due to aging to zero at 2 years (Sun *et al.,* 1997a). The incorporation of $^{35}SO_4$ of the trachea in aging mice was also studied (Nagata, 1999d). As a result, silver grains indicating the incorporation of radiosulfate were found over the cartilage matrices and the cartilage capsules in the hyaline cartilages of the tracheae of fetal (Fig. 18C) and postnatal newborn mice (Fig. 18D). The grain density as analyzed by grain densitometry was the maximum on fetal day 19 (1100 per μm^2). The grain density then decreased from fetal day 19 to the postnatal days 1, 3, 9, and 14 (100 per μm^2) reaching almost zero at day 30 and no silver grain was found in the animals aged from 2 to 12 months. The silver grains in the perinatal animals at postnatal days 1 and 3, disappeared from the internal layer to the external layer of the cartilage and from the interterritorial matrix to the territorial matrix and the cartilage capsule. In the juvenile animals at postnatal days 9 and 14, intense incorporations were observed disseminatedly over several groups of cartilage capsules in the external layer. The results indicated that the glycoproteins constituting the cartilage matrix were synthesized from prenatal to postnatal day 30 (Nagata, 1999d). No incorporation was observed in the aging animals from postnatal day 1 to 12 months (Nagata, 2000f).

2. Pulmonary Cells

The lungs of mammals are composed of the alveolar epithelial cells and the interstitial cells of the alveoli and the endothelial cells of the blood capillaries. DNA

---

interterritorial and territorial matrices decreased from the internal layer of the cartilage to the external layer. Intense incorporations of the radiosulfate are observed disseminatedly over several groups of cartilage capsules ($\times 400$; bar $= 10$ μm). Permission from T. Nagata (2000f, Fig. 2, p. 379). (E) LMRAG of the lung of a newborn mouse at postnatal day 1, injected with [^{3}H]thymidine and radioautographed. Many silver grains are localized to the nuclei of type 1 epithelial cells and interstitial cells, showing DNA synthesis ($\times 750$; bar $= 50$ μm). Permission from L. Sun *et al.* (1995, Fig. 3, p. 853). (F) LMRAG of the lung of an adult mouse at postnatal 1 month, injected with [^{3}H]thymidine and radioautographed. Many silver grains are localized over the nucleus of a type 2 epithelial cell (arrow), showing DNA synthesis ($\times 750$; bar $= 50$ μm). Permission from L. Sun *et al.* (1995, Fig. 7, p. 855). (G) LMRAG of the lung of an embryonic day 16 mouse fetus, incubated *in vitro* with [^{3}H]uridine and radioautographed. Only several silver grains are localized over the chromatin of several nuclei of type 2 epithelial cells, showing RNA synthesis ($\times 750$; bar $= 50$ μm). Permission from L. Sun (1995, Fig. 1, p. 1063). (H) EMRAG of the lung of a juvenile mouse at postnatal 1 week, incubated *in vitro* with [^{3}H]leucine and radioautographed. Many silver grains are localized over the nuclei and cytoplasm of type 1 epithelial cell (arrowhead), type 2 epithelial cell (arrow), interstitial cell (IT), and endothelial cell (ED), showing protein synthesis ($\times 750$; bar $= 50$ μm). Permission from L. Sun *et al.* (1997b, Fig. 5, p. 466).

synthesis of aging mouse lung was studied by LM (Sun *et al.,* 1994, 1995a) and EMRAG (Sun *et al.,* 1995b). DNA synthesis and morphological changes of the pulmonary cells of 11 groups of mice from fetal day 16 to 22 months after birth were studied by light microscopic radioautography after [³H]thymidine incorporation (Sun *et al.,* 1994). A detailed investigation was then carried out to determine the localization and the frequency of [³H]thymidine incorporation with the age-related change of pulmonary cells in the mouse lung from embryos (Fig. 18E) to postnatal newborns (Fig. 18F) and adults by both LM and EMRAG (Sun *et al.,* 1995a,b). The results showed that the labeling indices of DNA synthesis of pulmonary cells changed with aging (Fig. 19). The examination of radioautograms demonstrated that the activity of DNA synthesis of type 1 epithelial cells was very low, which reached the peak on day 3 after birth, decreased gradually with aging, and lost the ability from postnatal month 6 onward. On the other hand, the labeling indices of type 2 epithelial, interstitial, and endothelial cells were the highest on the fetal day 16 and then declined the lung developed, but increased again on the postnatal day 3 and decreased gradually with age. These data provided the evidence that the DNA syntheses of type 2 epithelial, interstitial, and endothelial cells were the largest on fetal day 16 and then decreased with the developing of the lung due to aging.

The aging changes of DNA synthesis in the lungs of salamanders, on the other hand, from larval (2 months after fertilization), juvenile (1 month), adult (10 and 12 months after metamorphosis), and senescent (5 years) were also studied by
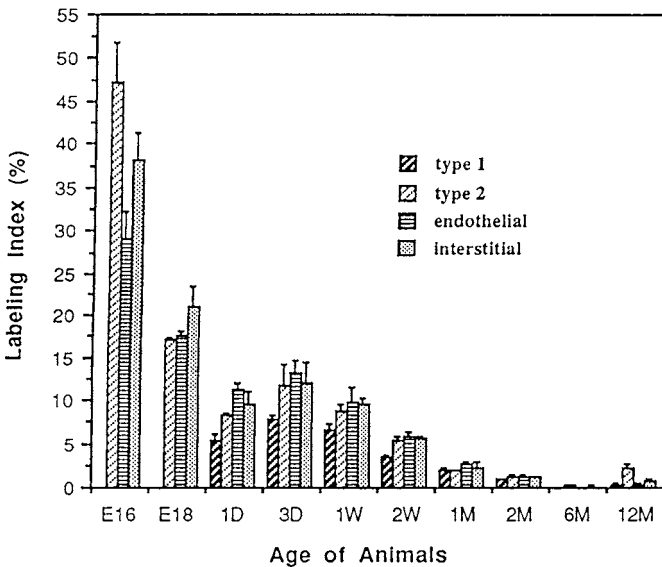
FIG. 19   Histograms showing the aging changes in labeling indices of respective cell types in the lungs of mice at various ages, labeled with [³H]thymidine (mean ± standard deviation). Permission from T. Nagata (1999c, Fig. 19, p. 695).

LMRAG after [³H]thymidine incorporation (Matsumura *et al.,* 1994). The result showed that the labeling indices in the ciliated cells and mucous cells in the superficial layer of young animals were higher than those of the basal cells and they decreased in adults, demonstrating aging changes in salamanders. On the other hand, an inhalation experiment of [³H]thymidine by means of a nebulizer into the lungs of 1-week-old mice was carried out (Duan *et al.,* 1994). After 45 min inhalation, the lung tissues were taken out and processed by either rapid-freezing and freeze–substitution for dry-mounting radioautography or conventional chemical fixation for wet-mounting radioautography. By wet-mounting RAG silver grains were observed in the nuclei of a few alveolar type 2 cells and interstitial cells, demonstrating DNA synthesis. By dry-mounting RAG numerous silver grains were located diffusely over all the epithelial cells and interstitial cells, demonstrating soluble compounds (Duan *et al.,* 1994).

When the lung tissues of mice were labeled with [³H]uridine, RNA synthesis was observed in all cells of the lung at various ages (Fig. 18G) (Sun, 1995). The number of silver grains changed with aging. The grain counts in type 1 epithelial cells increased from day 1 after birth and reached a peak at 1 week, while the counts in type 2 epithelial cells and interstitial cells increased from embryo day 16 and reached peaks at 1 week after birth. They diminished with the developing of the lung with aging.

The aging changes in protein synthesis of respective cell types of mouse lungs were investigated in ddY strain mice from fetal day 16 to senility (22 months postnatal) by using [³H]leucine light microscopic radioautography (Fig. 18H) (Sun *et al.,* 1997b). The results revealed that the protein syntheses of types I and II epithelial cells, interstitial and endothelial cells in the mouse lung changed due to aging. The protein synthesis of type I epithelial cells was the highest on the first day after birth, increased again at 1 week after birth, and then decreased gradually to 22 months after birth with aging. The protein syntheses of type II epithelial, interstitial, and endothelial cells reached the highest level on fetal day 16, declined progressively with age, and increased again at the first week after birth and then decreased gradually from 2 weeks to senility. Our results suggest that the decrease in protein synthesis is correlated with the decremental changes in DNA and RNA synthesis in the lung with aging.

E. Urinary Cells

The urinary cells can be divided into kidney cells and urinary tracts cells.

1. Kidney Cells

The mammalian kidney consists of the nephrons, which can be divided into two components: renal corpuscles and uriniferous tubules. The renal corpuscles are

composed of glomeruli which are covered with Bowman's capsules. They are localized in the outer zone of the kidney, the renal cortex, while the uriniferous tubules are composed of two portions, the proximal and distal portions, which can further be divided into several portions and run from the outer zone of the kidney, the renal cortex, to the inner zone, the medulla.

We studied the glomerular extracellular matrices and anionic sites stained with PEI in aging ddY mice at various ages (Duan and Nagata, 1993). Morphometric data revealed that thickening of the glomerular basement membranes, formation of nodules in the basement membranes, and the mesangial matrix increase were found to be the primary age-related changes in aging mice. There were also electron-dense PEI-positive deposits in mesangial and subepithelial regions. Quantitative analysis showed that glomerular basement membrane thickness, number and size of nodules, and the area of the mesangial matrix were significantly correlated to the age of animals (Duan and Nagata, 1993).

We also studied enzyme–cytochemical reactions in kidney cells. Catalase (EC 1.11.1.6 hydrogen peroxidase), as demonstrated by DAB reaction can be demonstrated in peroxisomes of the uriniferous tubule cells in the kidney of rat (Ohno, 1985; Ohno *et al.,* 1978). The number of DAB-positive peroxisomes increased in rat kidney when the animals were fed on DEHP, a peroxisome proliferator, similar to the hepatocytes or rats as was described in the section of the liver cells. Phospholipase B (EC 3.1.1.5 lysolecithin acyl hydrolase) activity was first observed by electron microscopy (Nagata and Iwadare, 1984). The results showed that the reaction products were localized over the terminal portions of smooth surfaced endoplasmic reticulum in the uriniferous tubules of mouse kidney. Acid phosphatase (EC 3.1.3.2) activity in the proximal convoluted tubules of aging mice at various ages was also studied (Olea *et al.,* 1991). On the other hand, X-ray microanalysis was carried out to qualify and quantify cerium content in the end products of acid phosphatase activity in the kidneys of aging ddY mice in several groups from newborn day 1 to 10 months (Olea and Nagata, 1991). Eighteen groups of ddY mice, from postnatal day 1, 1 and 2 weeks, and 1, 2, and 10 months, were used. The kidney tissues were prefixed in buffered glutaraldehyde, incubated in lanthanade-based glycerophosphate medium containing cerium as the capture reagent for 60 min, postfixed in buffered osmium tetroxide, dehydrated, embedded in Epoxy resin, ultrathin sectioned, and observed by electron microscopy. On the electron micrographs, image analysis was carried out to count the number and size of acid phosphatase-positive lysosomes and the intensity of the reaction products was quantified by X-ray microanalysis. The specimens were observed with a JEOL JEM-4000EX electron microscope attached to a Tracor-Northern TN-5400 EDX microanalyzer loaded with routine software. The reaction products (precipitate) in 200 lysosomes in the proximal tubule cells of the kidney at TEM mode for 100 seconds live time at varying accelerating voltages from 100, 200, 300, to 400 kV. The results showed that the peak-to-background ratios (P/B) at different accelerating voltages was highest at 300 kV. Therefore, X-ray microanalysis in

quantifying cerium content showing acid phosphatase activity in lysosomes was carried out at 300 kV. It was found that the intensity decreased from day 1 to 10 months. The results demonstrated that the number and size of acid phosphatase positive granules (lysosomes) increased significantly from postnatal day 1 to 1 week, reaching a peak at 1 week, and then gradually declined until 10 months. By X-ray microanalysis, the presence of cerium which was the end products of the acid phosphatase activity, was confirmed qualitatively in the electron-dense reaction products of lysosomes (figure not shown). The intensity of the reaction, however, decreased from 1 day to 10 months. These results demonstrated that the acid phosphatase activity in the kidney was related to the growth, development, and aging of the animals.

A radioautographic study on DNA synthesis using [3H]thymidine was carried out in three groups of ddY mouse embryos from prenatal day 13 (Fig. 20A), day 15 (Fig. 20B), to day 19 *in vitro,* as well as perinatal mice from prenatal day 19 to postnatal day 1, 8, 30, 60, and 365 (1 year) *in vivo* (Hanai, 1993; Hanai and Nagata, 1994a,b). The labeling indices by LMRAG (Hanai, 1993) in glomeruli (28 to 32%) and uriniferous tubules (31 to 33%) in the superficial layer were higher than those (10 to 12% and 8 to 16%) in the deeper layer from the late fetal to the suckling period and then decreased with aging from weaning to senescence. Electron microscopic radioautography revealed the same results (Hanai and Nagata, 1994a). On the other hand, the incorporation of [3H]thymidine was observed in the mitochondrial matrix of cultured kidney cells from chickens and mice *in vitro,* demonstrating mitochondrial DNA synthesis by EMRAG (Nagata *et al.,* 1967). When the kidneys of several groups of aging mice from embryo to postnatal year 1 were radioautographed with [3H]uridine both *in vitro* and *in vivo,* RNA synthesis was observed in all the cells of the kidneys at various ages. The numbers of silver grains demonstrating the incorporation of [3H]uridine in glomeruli (34.6 per cell) and uriniferous tubules (56.4 per cell) were higher in the superficial layer than those (15.6 and 18.6 per cell) in the deeper layer at embryonic day 15 and decreased gradually with aging (Hanai and Nagata, 1994b). The incorporations of [3H]glucosamine in the kidney of aging mice demonstrated by light and electron microscopic RAG revealed that the numbers of silver grains in both the glomeruli and the uriniferous tubules were less in the embryonic stage, but increased postnatally and reached peaks at 1 to 2 weeks and then decreased to senescence. The results showed that glucide synthesis in the kidney cells also changed with age in animals (Joukura, 1996; Joukura and Nagata, 1995; Joukura *et al.,* 1996).

Immunocytochemical localization of retinal binding protein by the PAP method was observed in the lysosomes of the proximal tubules of the human kidney (Usuda *et al.,* 1983). The localization of D-amino acid oxidase stained by the PAP method was found in the fine cytoplasmic granules of the proximal tubules of rat kidney by LM, while protein A–gold particles were exclusively confined in peroxisomes in the proximal tubules. The fine localization of gold particles was found only in the central core matrix of the peroxisomes, which suggested a specific intraorganellar
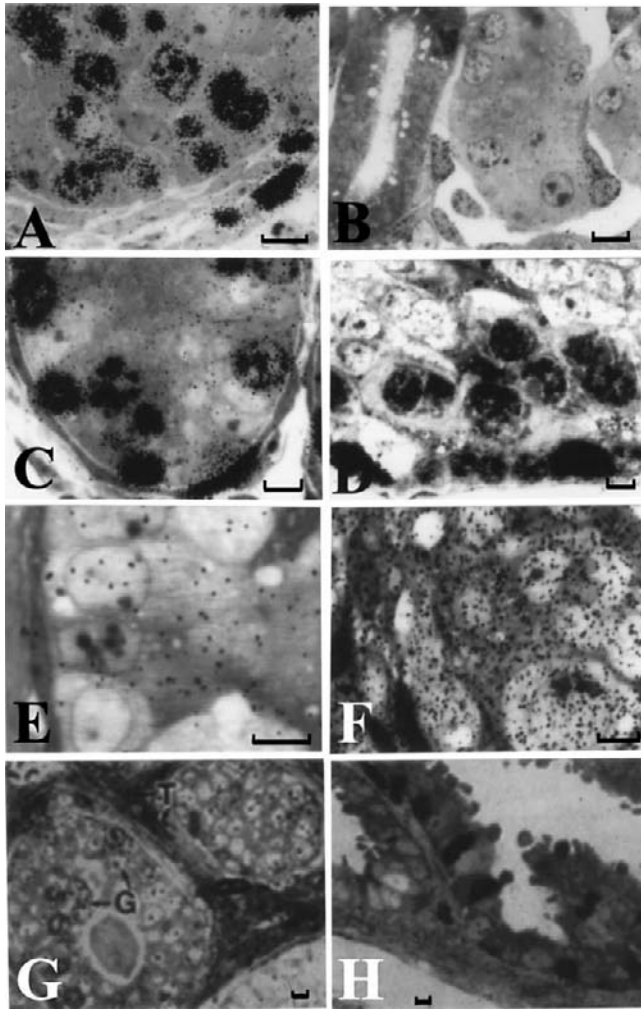
FIG. 20 Special cytochemistry 8: The uro-genital cells. (A) LMRAG of the metanephros of a mouse embryo at day 13.5 of the gestational stage, labeled with [^{3}H]thymidine *in vitro*. Many labeled nuclei can be seen ($\times 1200$; bar $= 50$ μm). Permission from T. Hanai (1993, Fig. 1, p. 83). (B) LMRAG of the metanephric cortex of a mouse embryo at day 15.5 of the gestational stage, labeled with [^{3}H]thymidine *in vitro*. Less nuclei are labeled ($\times 800$; bar $= 50$ μm). Permission from T. Hanai (1993, Fig. 2, p. 84). (C) LMRAG of the testis of a male mouse at postnatal day 7, labeled with [^{3}H]thymidine *in vitro* ($\times 800$; bar $= 50$ μm). Permission from F. Gao (1993, Fig. 3, p. 662). (D) LMRAG of the testis of a male mouse at postnatal year 1, labeled with [^{3}H]thymidine *in vitro* ($\times 750$; bar $= 50$ μm). Permission from F. Gao (1993, Fig. 10, p. 663). (E) LMRAG of the testis of a male mouse at postnatal day 3, labeled with [^{3}H]uridine *in vitro* ($\times 1500$; bar $= 50$ μm). Permission from F. Gao (1993, Fig. 13, p. 664). (F) LMRAG of the testis of a male mouse at postnatal day 1, labeled with [^{3}H]leucine *in vitro* ($\times 1125$; bar $= 50$ μm). Permission from F. Gao (1993, Fig. 18, p. 665). (G) LMRAG of the
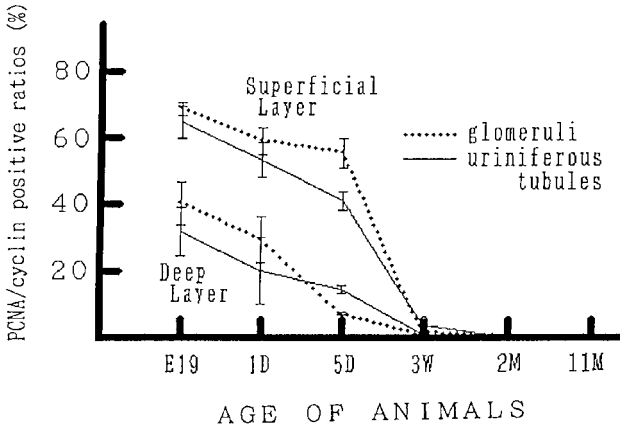
FIG. 21 Aging changes of PCNA/cyclin positive ratios in mouse kidney cells immunostained with PCNA/cyclin antibody from prenatal day 19 to postnatal month 11 (mean ± standard deviation). Permission from T. Hanai *et al.* (1993, Fig. 6, p. 188).

localization of this enzyme (Usuda *et al.,* 1986). On the other hand, immuno-cytochemical localization of PCNA/cyclin was carried out in the same animals in several aging groups as radioautography using [³H]thymidine (Hanai *et al.,* 1993). The results from the PCNA/cyclin positive indices in the respective aging groups (Fig. 21) were almost the same as the labeling indices with [³H]thymidine radioautography (Hanai, 1993; Hanai and Nagata, 1994a,b). On the other hand, lectin histochemistry was applied to demonstrate compositional changes in gly-coconjugate mouse kidney cortex due to aging (Hanai *et al.,* 1994a,b,c,d). Mouse kidney tissues of prenatal and postnatal aging groups from fetal day 19 to postnatal month 10 were fixed in paraformaldehyde, cryosectioned, and stained with 16 kinds of biotinylated lectins, followed by ABC. The reaction products with WGA were localized in the glomerular podocytes and tubule basement membranes of adult cortex. The localizations of other lectins (ConA, DSA, SSA, ABA, LCA, PHA-E4, RCA60, and RCA20) were different. The main localization of reaction products for ConA in adult cortex was in the cytoplasm and brush borders of prox-imal tubules and the blood capillaries of glomeruli. The localization for SSA in the blood capillaries of glomeruli and tubule basement membrane. Reaction products for DSA, ABA, LCA, PHA-E4, RCA60, and RCA20 were localized in the brush

ovary of a female mouse at postnatal day, labeled with [³H]thymidine *in vitro.* The nuclei of the granulosa (G) and theca (T) cells are labeled with silver grains (×400; bar = 50 μm). Permission from S. Li and T. Nagata (1995, Fig. 1, p. 187). (H) LMRAG of the oviduct of a female mouse at postnatal day 30, labeled with [³H]thymidine *in vitro.* Several nuclei in the epithelial cells are labeled (×400; bar = 50 μm). Permission from S. Li and T. Nagata (1995, Fig. 1, p. 187).

borders of proximal tubules and the blood capillaries of glomeruli. The reaction products for Lotus were localized in the cytoplasm and the brush borders of proximal tubules of adult cortex (Fig. 1D). The deep layer of the cortex was consistently positive for Lotus during development and aging. Four other lectins (MAM, PNA, SBA, PHA-L4) showed similar changes in the localization of reaction products, blood capillaries of glomeruli, and brush borders of proximal tubules. The localization for UEA-I was consistently negative in developing and aging kidney cortex but positive only in the erythrocytes in adult cortex. These results demonstrated aging changes in glycoconjugates in the kidney cells.

2. The Urinary Tract Cells

The urinary tract cells are composed of the ureteric cells, bladder cells, and urethral cells. We studied the bladder cells of rats by LMRAG after oral administration of [^{3}H]tranilast, an anti-allergic agent produced by Kissei Pharmaceutical Co. (Momose *et al.,* 1989; Nishigaki *et al.,* 1990). It was found that this agent specifically localized over the transitional epithelial cells and endothelial cells of the veins in the mucosa for a long time, which suggested the relationship between the histopathology of the cystitis observed clinically after the administration of the drug in human patients (Nishigaki *et al.,* 1990).

F. Genital Cells

The genital cells are the components of the genital or reproductive organs of animals. The genital cells of mammals can be grouped into two types: the male and the female genital cells.

1. Male Genital Cells

The male genital organ consists of the testis and its excretory ducts such as ductuli efferentes, ductus epididymidis, ductus deferens, ejaculatory ducts, auxiliary glands, and penis. Among these organs, the testis was the main target of the scientific interests. Formerly, Clermont (1963) demonstrated using [^{3}H]thymidine radioautography that several stages of development of the spermatogonia were found at different levels in the germinal epithelium of mature man and rodents, with the most primitive germ cells found at the base and the more differentiated cells located at higher levels. We studied the DNA, RNA, and protein syntheses in aging mouse testis by radioautography, demonstrating the incorporations of [^{3}H]thymidine, [^{3}H]uridine, and [^{3}H]leucine into various cells of the seminiferous tubules (Gao, 1993; Gao *et al.,* 1994). At embryonic and neonatal stages DNA synthesis of gonocytes was weak and only a few labeled spermatogonia could be observed during the perinatal stages. The labeled spermatogonia were recognized

at 4 days after birth (Fig. 20C) and the number of labeled gonocytes increased from 2 weeks, keeping high levels to 1 and 2 years (Fig. 20D). The labeling index of spermatogonia first peaked at 3 weeks and stayed constant until senescence (Fig. 22A). However, the myoid cells and Sertoli's cells labeled with [^{3}H]thymidine were frequently observed at perinatal stages from embryo to postnatal day 7 (Fig. 22B), while the labeling indices of both cells decreased from young adulthood (postnatal week 2) to senescence (Gao, 1993). On the other hand, the RNA synthesis and protein synthesis of various cells in the seminiferous tubules were studied using [^{3}H]uridine and [^{3}H]leucine incorporations (Gao *et al.,* 1994). The synthetic activities as shown by grain counting with [^{3}H]uridine and [^{3}H]leucine were weak at the embryonic and neonatal stages but increased at adult stages and maintained high levels until senescence (Gao *et al.,* 1994). These results show that DNA synthesis in myoid cells and Sertoli's cells increase at the perinatal stages and decrease from postnatal week 2, while DNA synthesis in spermatogonia increases from postnatal week 2 together with RNA and protein syntheses to senescence.

2. Female Genital Cells

The female genital organ consists of the ovary, oviduct, uterus, vagina and external genitals. We studied chemical reactions as well as macromolecular synthesis in the ovary, oviduct and uterus of aging mice by radioautography. We used an established cell line, CHO-K1 cells, obtained from the Chinese hamster ovary for *in vitro* experiments (Nagata, 1995c, 1997b, 1999a, 2000a,c). The CHO-K1 cells were trypsinized, suspended in Ham's F12 medium (Nissui, Tokyo, Japan) supplemented with 10% newborn bovine serum (Flow Laboratories, Stanmore, NSW, Australia), seeded on formval-coated gold mesh in plastic petri dishes (Falcon Plastic, USA), and incubated in a CO_2 incubator at 37°C for several days. For the experimental pinocysis, the cells were cultured in a medium containing HRP, 1 mg/ml medium, for 24 and 48 h to induce pinocytosis. The cells were fixed in 2.5% glutaraldehyde solution in 0.1 M cacodylate buffer for 1 h, stained with DAB reaction (Angermüller and Fahimi, 1981), dehydrated in a critical point dryer (Hitachi HCP-1), and observed by high-voltage electron microscopy using either JEOL JEM-4000EX at 400 kV or Hitachi H-1250M at 1000 kV, taking stereo-pair pictures by tilting the specimens both at +8 and −8, and then the stereo-pair pictures were observed with stereoscopes or anaglyph-type color pictures were composed from red and green pictures from both sides. When these CHO-K1 cells were observed after culture with a medium containing HRP for 24 and 48 h, the cells incorporated HRP particles into their cytoplasm by pinocytosis and many DAB-positive vesicles throughout their cytoplasm from 24 to 48 h. The relative relationship between the dense DAB-positive pinocytotic vesicles and the other less dense cell organelles such as mitochondria and endoplasmic reticulum were observed three-dimensionally (Nagata, 1999a, 2000a,c).
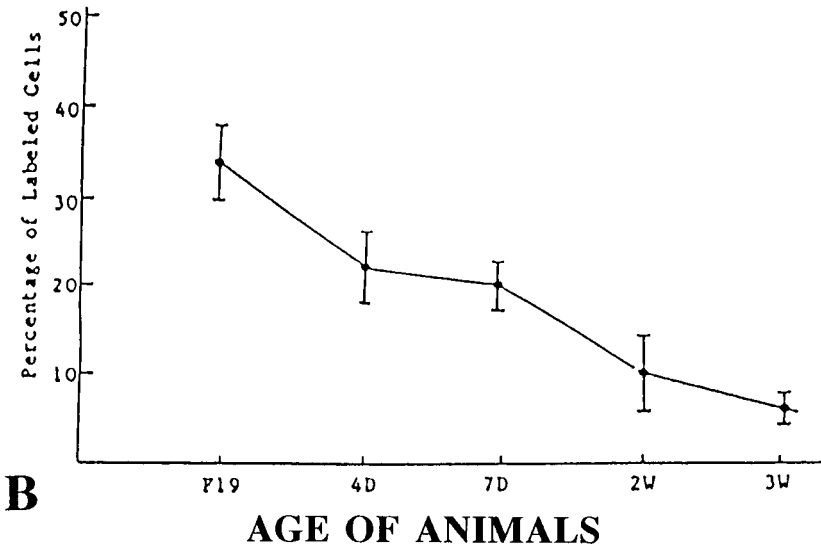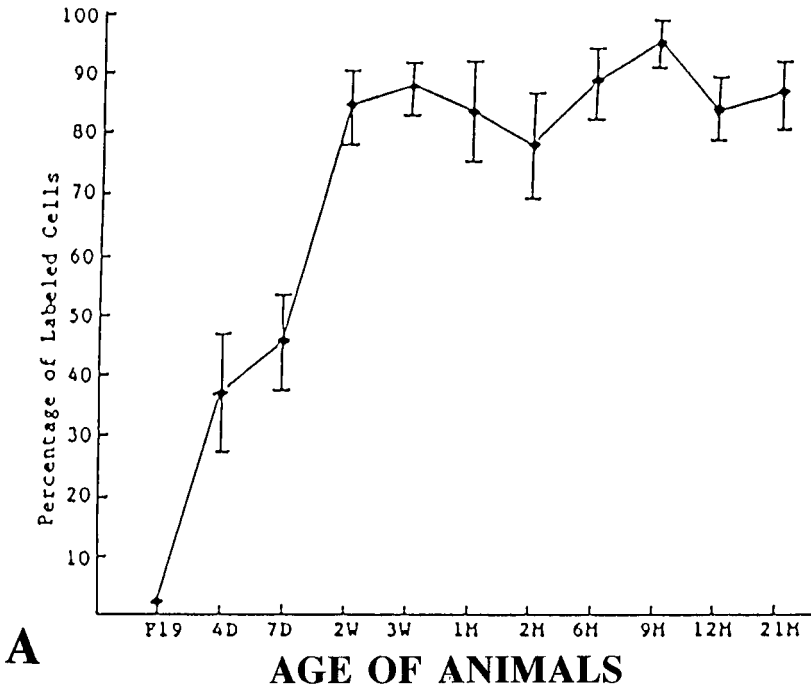
FIG. 22   Aging changes of labeling indices of mouse male genital cells at various ages, labeled with [^{3}H]thymidine *in vitro*. (A) Labeling indices of spermatogonia. (B) Labeling indices of Sertoli cells. Permission from F. Gao (1993, Figs. 28 and 29, p. 670).

With regards to the physical methods, we studied DNA and RNA syntheses in the developing virgin mice, six litters of 36 female mice at various ages, by [^{3}H]thymidine and [^{3}H]uridine radioautography. The [^{3}H]thymidine incorporations were active in all surface epithelial cells and stromal and follicular cells of the ovary (Fig. 20G) between postnatal days 1 and 7 (80–90%) and decreased from day 14 (20–30%) and maintained a lower level (a few percent) to day 60 (Li, 1994; Li and Nagata, 1995), while [^{3}H]uridine incorporations were active in all surface epithelial cells and stromal and follicular cells of the ovary between postnatal days 1 and 7 and maintained medium levels from day 14 on. On the other hand, the mucosubstance synthesis with radiosulfate, $^{35}SO_4$, was studied in the ovaries of mice during the estrus cycle (Li *et al.,* 1992). Four groups of female ddY mice, ages 8–10 weeks, were divided into four groups, diestrus, proestrus, estrus, and metestrus, according to the vaginal smears. The ovaries were taken out, labeled with $^{35}SO_4$ *in vitro* and radioautographed. In all the animals, silver grains were localized over the granulosa and theca cells. Almost all compartments of the ovary were labeled. The grain counts per cell changed according to cell cycle. From the results, it is concluded that all the cells of the ovary incorporated mucosubstances throughout the estrus cycle (Li *et al.,* 1992).

The DNA and RNA syntheses in the oviducts of developing virgin mice at various ages were studied by [^{3}H]thymidine and [^{3}H]uridine radioautography (Li, 1994; Li and Nagata, 1995). The DNA synthesis was active in all surface epithelial cells and stromal and smooth muscle cells (Fig. 20H) between postnatal days 1 and 3 and decreased from day 7 to day 60, while the RNA synthesis was observed in the epithelial and stromal cells at postnatal day 1 and increased to days 7 and 14 and then decreased to day 60 (Li and Nagata, 1995). The DNA synthesis of the uterus epithelium and stroma and smooth muscle cells was active at days 1 and 3 and decreased from day 7 to day 60, while RNA synthesis of the uterus increased from day 3 to day 14 and decreased from day 30 to day 60 (Li, 1994; Li and Nagata, 1995). These results showed that both DNA and RNA syntheses, as expressed by labeling indices and grain counting, were active in all kinds of cells, such as surface epithelial cells, stromal cells, and follicular cells of the ovaries between postnatal days 1 and 7, then they decreased from day 14 to day 60. However, the DNA synthesis in the epithelial cells and the stromal cells of both the uteri and the oviducts was active at postnatal days 1 and 3 and decreased from day 7 to day 60. The RNA synthesis in the uteri and oviducts was active at postnatal day 1, increased from day 1 to day 14, and decreased from day 30 to day 60. The unparalleled alteration of the DNA and RNA syntheses was shown between the ovary and the uterus or oviduct (Li and Nagata, 1995).

It was well known that the uterus of the rodent becomes receptive to blastcyst implantation only for a limited period. This is called the implantation window which is intercalated between refractory states of the endometrium whose cycling is regulated by ovarian hormones (Yoshinaga, 1988). We studied the changes of DNA, RNA, and protein synthesis by [^{3}H]thymidine, [^{3}H]uridine, and [^{3}H]leucine

incorporations in the endometrial cells of pregnant–ovariectomized mice after time-lapse effect of nidatory estradiol (Yamada and Nagata, 1992a,b, 1993, Yamada, 1993). From the results, it was concluded that the endometrial cells showed topographical and chronological differences in the nucleic acid and protein synthesis. The time-coincident peak of RNA and protein synthesis detected in the endometrial cells at the anti-mesometrial side of the implantation site probably reflected the activation moment of the implantation window. The protein synthesis in the decidual cells of pregnant mice uteri was compared to the endometrial cells of virgin mice uteri using [³H]proline and [³H]tryptophane incorporation (Oliveira *et al.,* 1991, 1995). The results demonstrated that silver grains were localized over the endoplasmic reticulum and the Golgi apparatus of fibroblasts and accumulated over collagen fibrils in the extracellular matrix, suggesting that the decidual cells produced collagen in the matrix. The quantitative analysis showed that both incorporations in the decidual cells increased in the pregnant mice more than that seen in the endometrial cells in virgin mice. With regards the biological reaction, we studied PCNA/cyclin immunostaining in the ovary, oviduct and uterus (Li, 1994). It was demonstrated that PCNA/cyclin-positive cells were observed in the ovarial follicular epithelium, ovarial interstitial cells, tubal epithelial cells, tubal interstitial cells, uterine epithelial cells, and uterine interstitial cells (Li, 1994). The positive cells increased from postnatal day 1 to 3 and 7 days and then decreased from 14 days to senescence. These results accorded well with the results obtained from the [³H]thymidine radioautography (Li, 1994; Li and Nagata, 1995).

G. Endocrine Cells

The endocrine organs of mammals consist of the hypophysis, pineal body, thyroid, parathyroid, thymus, adrenal, pancreatic islet and genital glands. Among those organs, we studied mercury chloride incorporation in the thyroid cells in the human patients as well as enzyme cytochemistry and macromolecular synthesis in the thyroid, parathyroid, adrenal, and steroid-secreting cells of both sexes, the Leydig cells of the testis, and the ovarian follicular cells in mice.

1. Thyroid Cells

Human normal thyroid tissues and thyroid cancer tissues obtained from struma patients by surgery were labeled *in vitro* with $^{205}HgCl_2$ and processed through both conventional chemically fixed wet-mounting radioautography and freeze–dried dry-mounting radioautography (Nagata, 1994b; Nagata *et al.,* 1977b). The results revealed that numerous silver grains showing the soluble component of mercury were found diffusely in thyroid cancer cells (Fig. 23A) but fewer silver grains showing insoluble component were observed in cancer and (Fig. 23B) normal
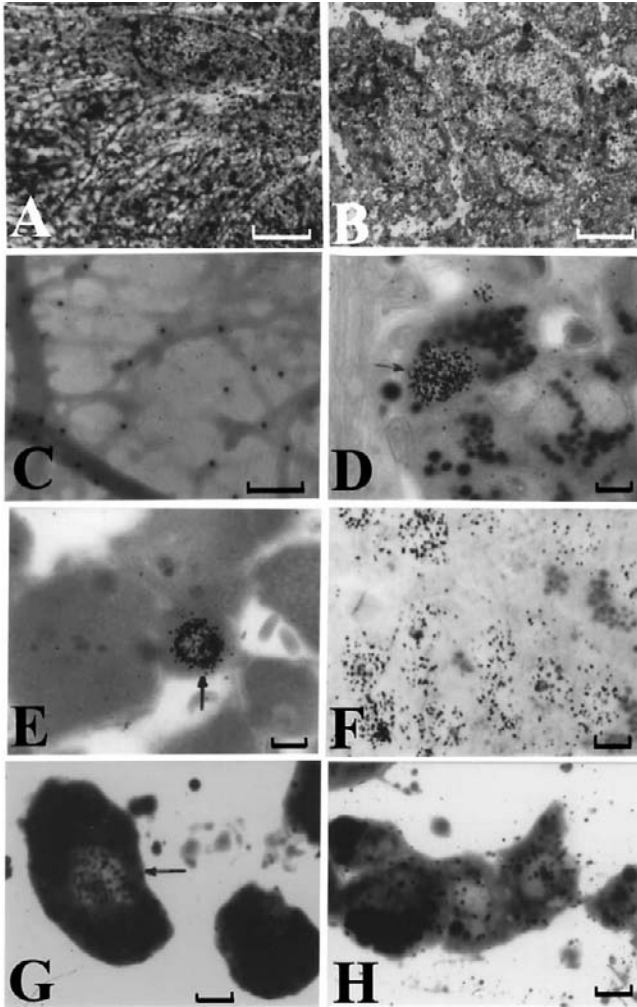
FIG. 23 Special cytochemistry 9: The endocrine cells. (A) EMRAG of human thyroid cancer cells labeled with ^{205}HgCl$_2$ *in vitro,* rapidly frozen, freeze–dried, embedded in Epoxy resin, dry-sectioned, and radioautographed by dry-mounting procedure. Many silver grains can be seen over the nuclei and cytoplasm, indicating both soluble and insoluble mercury. ($\times$15,000; bar = 0.1 μm). Copyright permission from T. Nagata (1994b, Fig. 13, p. 487). (B) EMRAG of human thyroid cancer cells labeled with ^{205}HgCl$_2$ *in vitro* the same as in A, but fixed chemically in cacodylate-buffered glutaraldehyde and osmium tetroxide, dehydrated, embedded in Epoxy resin, wet-sectioned and radioautographed by wet-mounting procedure. Only very few silver grains can be seen over the nuclei and cytoplasm, indicating only insoluble mercury ($\times$15,000; bar = 0.1 μm). Copyright permission from T. Nagata (1994b, Fig. 13, p. 487). (C) Electron micrograph of a human thyroid cancer cell cultured *in vitro,* fixed in paraformaldehyde and glutaraldehyde mixture, embedded in Lowicryl K4M, sectioned, and stained with anti-keratin antibody by the protein A–gold technique. Note the localization of gold particles around the electron lucent keratin filaments ($\times$75,000; bar = 0.1 μm).

thyroid cells (Nagata *et al.,* 1977b). The results supported the concentration of hot mercury in the thyroid cancer cells in the human struma patients as clinically observed.

We first studied intracellular localization of anti-keratin and anti-vimentin antibodies labeled with FITC in the normal thyroid cells and thyroid cancer cells obtained from 10 human patients who were clinically diagnosed as having thyroid cancer (Murayama *et al.,* 1986). After 6 weeks in culture, almost all cells from both normal thyroid and thyroid cancer cells showed fluorescence localization in their cytoplasm surrounding the nuclei. On the other hand, when they were stained with anti-vimentin antibody, only weak fluorescences were observed in the cytoplasm of normal and cancer cells. The results showed that those cells contained keratin filaments (Maruyama *et al.,* 1986). The intracellular localization of both keratin and vimentin were also demonstrated by protein A–gold staining at the electron microscopic level. The colloidal gold particles were observed to bind to either keratin (Fig. 23C) or vimentin filaments. We also studied the protein kinase C activity in normal thyroid cells and cancer cells obtained from the human patients by the immunocytochemical method (Shimizu *et al.,* 1991). The thyroid tissues surgically removed from 49 human patients suffering from thyroid diseases, consisting of 5 adenomatous goiter, 5 Grave's disease, 17 follicular adenoma, 11 papillary carcinoma, and 11 follicular carcinoma, were examined and the normal tissues surrounding the tumors were used as normal materials. Small tissue pieces were fixed in 10% phosphate-buffered formalin solution, dehydrated, embedded in paraffin, cut, and picked up on glass slides. Protein kinase C isozymes were purified from rabbit cerebellum and injected into 4-week-old BALB/c mice, and spleen cells were harvested and fused with SP2/0 myeloma cells. Hybrid clones were tested, positive clones were subcloned, and three types of monoclonal antibodies were purified, which were designated as MC-1a, MC-2a, and MC-3a; these recognized the protein kinase C isozymes types I, II, and III, respectively (Shimizu *et al.,* 1991). The sections were stained with the PAP method according to

FIG. 23 (*continued*) (D) LMRAG of the zona glomerulosa of the adrenal cortex of a postnatal day 14 mouse, injected with [^{3}H]thymidine, demonstrating DNA synthesis in the nucleus ($\times$900; bar $= 50\,\mu$m). Copyright permission from M. Ito (1996, Fig. 10, p. 283). (E) LMRAG of the zona fasciculata of the adrenal cortex of a postnatal month 6 mouse, injected with [^{3}H]thymidine, demonstrating DNA synthesis in the nucleus ($\times$900; bar $= 50\,\mu$m). Copyright permission from M. Ito (1996, Fig. 22, p. 285). (F) LMRAG of the zona glomerulosa of the adrenal cortex of a prenatal day 19 mouse, injected with [^{3}H]uridine, demonstrating RNA synthesis in the nuclei, nucleoli, and cytoplasm ($\times$1000; bar $= 50\,\mu$m). (G) LMRAG of the interstitial tissue of the testis of a mouse at postnatal month 12, labeled with [^{3}H]thymidine *in vitro,* demonstrating DNA synthesis in the nucleus of a Leydig cell (arrow) ($\times$1000; bar $= 50\,\mu$m). Copyright permission from T. Nagata (2000b, Fig. 7, p. 10). (H) LMRAG of the interstitial tissue of the testis of a mouse at postnatal day 3, labeled with [^{3}H]uridine *in vitro,* demonstrating RNA synthesis in several Leydig cells ($\times$1000; bar $= 50\,\mu$m). Copyright permission from T. Nagata (2000b, Fig. 9, p. 11).

Sternberger (1979). Briefly, the sections were stained in the following sequence: 2% normal rabbit serum, 30 min; primary antibody (100 μg/ml protein concentration of IgG fraction), 2 h; rabbit mouse IgG diluted $\times$ 50, 1 h; mouse peroxidase–anti-peroxidase complex diluted $\times$250, 1 h. All three antibody solutions were made with 50 mM Tris–HCl, pH 7.5/150 mM NaCl containing 1% normal rabbit serum. All the sections were incubated in the DAB medium for perixodase containing 0.05% 3,3$'$–diaminobenzidine tetrachloride and 0.012% H_2O_2 in Tris–HCl buffer, pH 7.2, for 15 min. As a result, normal thyroid cells showed negative reaction for type I, while weakly positive reactions were observed for types II and III (Shimizu *et al.,* 1991). Different reactions were observed in cancer cells, which will be described under Cancer Cells (Section I). PCNA/cyclin activity stained with immnonocytochemistry in normal human thyroid cells surgically obtained from thyroid cancer patients was compared with the thyroid cancer cells (Shimizu *et al.,* 1993). The results revealed that the labeling index by PCNA/cyclin activity was lower in normal thyroid cells than the thyroid cancer cells.

2. Parathyroid Cells

The parathyroid cells are the components of the parathyroid glands that lie in the capsule of the thyroid gland in man. The parathyroid cells consist of two types of epithelial cells: principal cells and oxyphilic cells. We studied the proliferative activity of the parathyroid epithelial cells surgically obtained from 1 normal and 29 (19 hyperplasia, 10 adenoma) hyperfunctioning human parathyroid glands. For flow cytometry, tissues were fixed in 70% ethanol at 4°C, mechanically minced with scissors in a sodium citrate buffer at pH 7.6, and incubated with a sequence of solutions of cycle test DNA reagent kit (Becton Dickinson, San Jose, CA). The samples were first incubated with 0.003% trypsin, then with 0.01% RNase to digest RNA, and finally with 0.04% propidium iodide for staining the nuclear DNA. The DNA contents of 10,000 nuclei were measured with a FACScan flow cytometer (Becton Dickinson) and %SPF was calculated via the rectangle fitting model program (Dean, 1985). On the other hand, tissues were labeled with BrdU (Sigma, London, UK) in RPMI 1640 culture medium (GIBCO, Gaithersburg, MD) at 37°C for 60 min *in vitro,* embedded in paraffin, sectioned, and stained for BrdU with anti-BrdU monoclonal antibody solution (Dakopatts, Glostrup, Denmark) and then with peroxidase-conjugated anti-mouse IgG (MBL, Nagoya, Japan) and finally with DAB. Some other paraffin sections were incubated with a Ki-67 monoclonal antibody solution (MIB-1, Immunotech, SA, Marseille, France), incubated with biotinylated anti-mouse IgG and the ABC reagent (Vectastain kit), and finally with DAB. As the results, Both BrdU and Ki-67 labeling indices were low, ranging from 0% (normal) to 0.06% (adenoma) and 0.17% (hyperplasia) or from 0.25 (normal) to 0.71% (adenoma) and 0.97% (hyperplasia), respectively. The BrdU indices were lower than the Ki-67 indices. However, the %SPF determined by flow cytometry was consistently higher than both the BrdU and Ki-67 indices. The

discrepancy could not be explained. These results suggested that the hypofunctioning parathyroid gland cells were characterized by low proliferative activity (Xiao-Lin *et al.,* 1996).

3. Adrenal Cells

The adrenal cells are the components of the adrenal glands, which can be divided into two types, i.e., the cortical cells and the medullary cells. We studied chemical reactions in mouse adrenal cells demonstrating the phospholipase activity, which showed intense reactions localizing over the lysosomes and limiting membranes of lipid droplets in the cortical cells (Nagata and Iwadare, 1984).

Incorporation of [^{3}H]thymidine in the adrenal glands was observed in several groups of aging mice from embryo to postnatal newborn, young, and adult senescent 2 years by LM and EMRAG (Ito, 1996; Ito and Nagata, 1996). The DNA synthesis was found in all zones of the adrenal cortex, i.e., the zona glomerulosa (Fig. 23D), zona fasciculata (Fig. 23E), and zona reticularis of the cortex, as well as the medulla from immature prenatal stage to mature postnatal senescent ages. The labeling indices in the respective zones showed the maximum at perinatal stage and then gradually decreased to senescent stages in both the cortex (Fig. 24A) and the medulla (Fig. 24B). (Ito, 1996; Ito and Nagata, 1996). On EMRAG the cell organelles in the labeled cells were less developed than the unlabeled cells in the same zone at the same aging stage (Ito and Nagata, 1996; Nagata *et al.,* 2000a). These results demonstrate that the adrenal cells in each zone proliferate independently throughout the animal's life, not migrating from one zone to another as was formerly proposed (Nussdorfer, 1986).

On the other hand, the incorporation of [^{3}H]uridine was found in all layers of both cortex and medulla in the adrenal glands of ddY mice from fetal day 19 (Fig. 23F) to postnatal 12 months by LMRAG (Liang, 1998) and EMRAG (Liang *et al.,* 1999). On LMRAG, it was revealed that the numbers of silver grains were higher in perinatal young animals than in older animals and higher in the glomerulosa than in the fasciculata, reticularis, and medulla. On EMRAG, the cell organelles such as endoplasmic reticulum, ribosomes, Golgi apparatus, mitochondria with tubular or vesicular cristae, and lipid droplets were more frequently observed in the cytoplasm of the cells in the three zones of the cortex and the medulla at later postnatal and senescent stages. The result from grain counting per unit area as well as per cell, was the highest in the cortex and the medulla at fetal day 19 and then gradually decreased with aging. The silver grains on EMRAG were localized over the nucleoli, euchromatin, endoplasmic reticulum, ribosomes, and mitochondria of the cells in the three zones of the cortex and the medulla. The number of mitochondria per cell, the number of labeled mitochondria per cell, and the mitochondrial labeling indices increased along with aging (Liang *et al.,* 1999; Nagata *et al.,* 2000a). The results demonstrated the correlation between mitochondrial nucleic acid synthesis and the aging of animals.
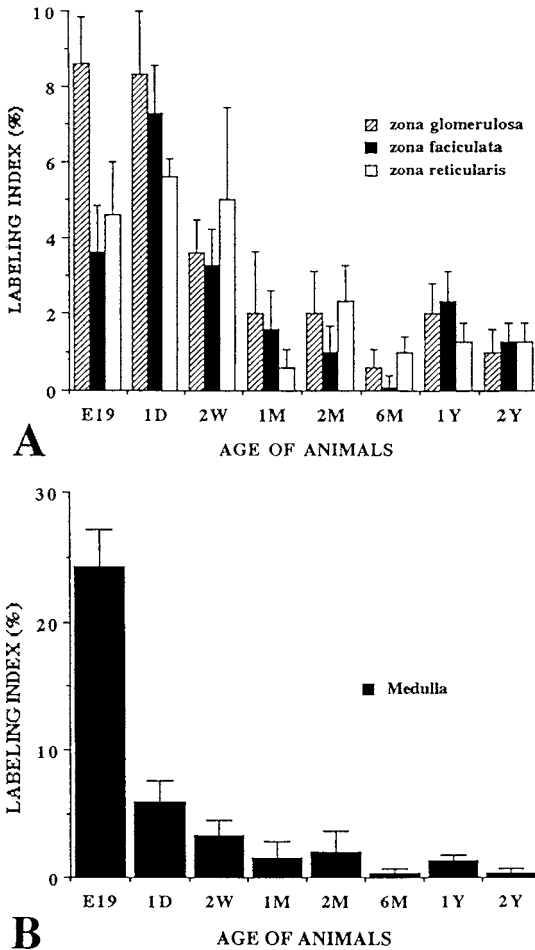
FIG. 24 Histograms showing transitional changes of the labeling indices indicating DNA synthesis in respective zones of the adrenal cortex (A) and the adrenal medulla (B) of mice at various ages. Copyright permission from T. Nagata (2000b, Fig. 12, p. 12).

4. Langerhans Islet Cells

We studied macromolecular synthesis in the islet cells of Langerhans of mouse pancreas by LM and EMRAG together with the exocrine pancreatic cells, using RI labeled precursors such as [^{3}H]thymidine (Nagata *et al.,* 1984; Nagata and Usuda, 1986), [^{3}H]uridine (Nagata and Usuda, 1985; Nagata, 1991, 1993), [^{3}H]leucine (Nagata and Usuda, 1993; Nagata 2000e), and [^{3}H]glucosamine (Nagata *et al.,* 1992). The results showed that the islets cells, A, B, and C cells, incorporated

those precursors to synthesize DNA, RNA, proteins, and glucides. The labeling index of DNA synthesis and the densities of silver grains showing RNA, protein, and glucide syntheses were high at prenatal and earlier postnatal stages from day 1 to day 14 and then decreased from 1 month to 1 year due to aging. However, the labeling indices by [3H]thymidine and the grain counts by [3H]uridine and [3H]leucine in the endocrine cells were less than those in the exocrine cells at the same ages.

5. Leydig Cells

The cells of Leydig can be found in the interstitial tissues between the seminiferous tubules of the testis of mammals. They are identified as spherical, oval, or irregular in shape and their cytoplasm contained lipid droplets. We studied the macromolecular synthesis of the cells in the testis of several groups of litter ddY mice at various ages from fetal day 19 to postnatal aging stages up to 2 years senescence by LM and EMRAG using [3H]thymidine, [3H]uridine, and [3H]leucine incorporations (Gao *et al.,* 1995a,b; Nagata *et al.,* 2000b).

The Leydig cells from embryonic stage to senescent stages were labeled with [3H]thymidine as observed by LMRAG (Fig. 23G). The changes of the numbers of labeled Leydig cells with the DNA synthesis were found after the [3H]thymidine incorporation into the nuclei of these cells in different aging groups. Only a few cells were labeled after [3H]thymidine at embryonic day 19. At early postnatal stages, there was a slight increase of the number of labeled cells. The number of labeled cells from perinatal stage to postnatal day 14 and 1, 2, and 6 months were similar to the values found at prenatal and early postnatal stages. The notable increases in the number of labeled Leydig cells were found from 9 months to 2 years in senescence. The labeling indices with [3H]thymidine in perinatal stages to postnatal 6 months were low (5–10%) but increased at 9 months and maintained high level (50–60%) to 2 years (Gao *et al.,* 1995b). The labeling indices at senescent stages still maintained a relatively high level and they were obviously higher than those of young animals. By electron microscopy, typical Leydig cells contained abundant cell organelles such as smooth-surfaced endoplasmic reticulum, Golgi apparatus, and mitochondria with tubular cristae. The silver grains were mainly localized over the euchromatin of labeled nucleus. Some of the grains were also localized over some of the mitochondria in both the nuclei labeled and unlabeled cells.

The incorporation of [3H]uridine into RNA was observed in almost all the Leydig cells in the interstitial tissues of the testis from embryonic day 19 to 2 years after birth (Gao *et al.,* 1995a; Nagata *et al.,* 2000b). A few silver grains over the nuclei and cytoplasm of the Leydig cells labeled with [3H]uridine were observed at embryonic day 19. The silver grains over those cells slightly decreased at postnatal days 1, 3 (Fig. 23H), and 7. The number of the silver grains over the nuclei increased from postnatal month 1 onward. The average number of silver grains over the cytoplasm increased gradually and reached the maximum at 12 months after birth.

At each stage, the activity of RNA synthesis was specifically localized over the euchromatin in the nucleus and nucleolus as observed by EMRAG. From adult to senescent stages, the activity of RNA synthesis maintained a higher level in their nuclei than in their cytoplasm. In the cytoplasm of Leydig cells in respective aging groups some of the mitochondria and endoplasmic reticulum were also labeled with silver grains. It is noteworthy that the average grain counts increased prominently in the senescent aging groups at 1 and 2 years after birth.

The incorporation of [^{3}H]leucine into proteins was observed in almost all the Leydig cells in the interstitial tissues of the testis. The silver grains were located over the nuclei and cytoplasm of respective Leydig cells. The aging change of protein synthesis of Leydig cells among different aging groups was also found (Gao *et al.,* 1995a; Nagata *et al.,* 2000a). At embryonic day 19, the silver grains of Leydig cells labeled with [^{3}H]leucine was observed in both nucleus and cytoplasm and there was no obvious difference between the number of silver grains on the cytoplasm and the nucleus. The number of silver grains decreased at postnatal day 1 and then increased at days 3 and 7. However, the number of silver grains on the nucleus and in the cytoplasm decreased from 1 month to 3 months and increased again from 6 months onward, maintaining a high level from adult to senescent stages. Some of the silver grains were also localized over some of the mitochondria in respective age groups as observed by EMRAG. These results indicate that the DNA, RNA, and protein syntheses in Leydig cells are maintained at rather high level even at senescent stages at postnatal 1 and 2 years.

6. Ovarian Follicular Cells

DNA and RNA synthesis of ovarian follicular cells were studied in the developing ddY mice ovaries in several aging groups at postnatal days 1, 3, 7, 14, 30, and 60 by LM and EMRAG using [^{3}H]thymidine (Fig. 20G) and [^{3}H]uridine (Li and Nagata, 1995). From the results it was shown that both DNA and RNA synthesis in the ovarial follicular cells, as expressed with labeling indices and grain counts, increased significantly from postnatal day 1 to 7 postnatal day and then decreased from day 14 to day 60 (Li and Nagata, 1995). Comparing the results to those from other female genital cells, a paralleled alteration of both DNA and RNA synthesis was revealed between the ovarian follicular cells and other uterine or oviductal cells (Li and Nagata, 1995).

H. Neurosensory Cells

The neurosensory cells are the components of the nervous system and the sensory system of mammals. Among the various neurosensory cells, we mainly studied the nerve cells in the cerebrum, the cerebellum, the spinal cord, and the peripheral nerve cells, as well as the sensory cells in the ocular tissues and the cutaneous tissues.
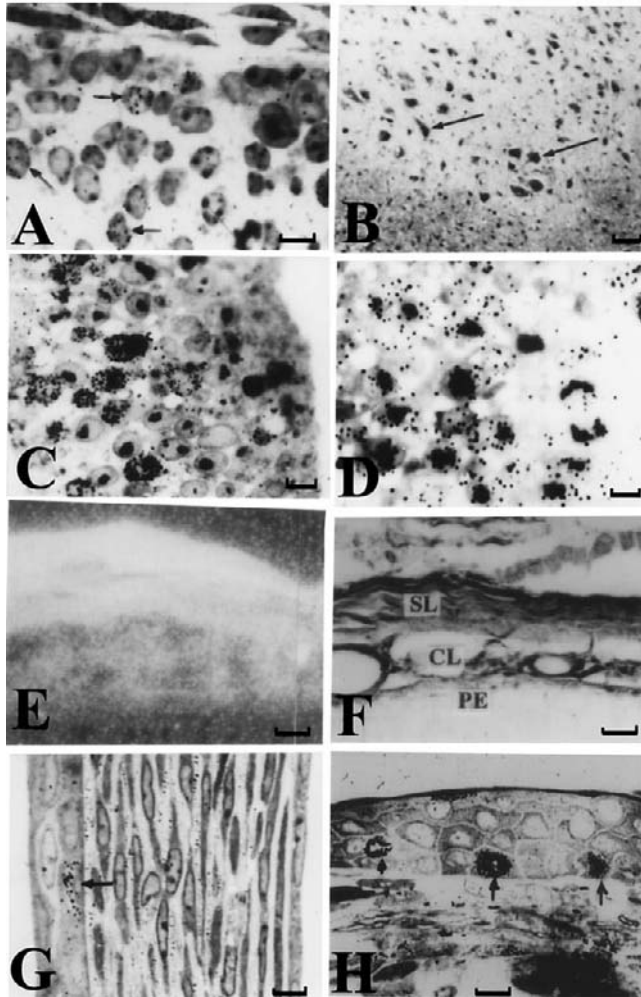
FIG. 25   Special cytochemistry 10: The neurosensory cells. (A) LMRAG of a fetal mouse cerebellum, labeled with [^{3}H]thymidine, demonstrating DNA synthesis of a few neuroblasts (arrows) ($\times$900; bar = 50 μm). Permission from H. Cui (1995, Fig. 2, p. 1141). (B) LM photograph of the spinal cord of a mouse at postnatal day 14 immunostained with rabbit anti-TGF-β1 polyclonal IgG and biotinylated goat anti-rabbit IgG followed by the ABC method. Note that the ventral horn motoneurons (arrows) are strongly positive, while the white matter (bottom) shows weak immunoreactivity ($\times$70; bar = 500 μm). Permission from T. Nagata *et al.* (1999b, Fig. 4, p. 80). (C) LMRAG of the optic vesicle of a chick embryo at day 2, labeled with [^{3}H]thymidine, demonstrating DNA synthesis in the nuclei of the outer portion of the optic vesicle layer ($\times$750; bar = 50 μm). Permission from W. Gunarso *et al.* (1997, Fig. 2, p. 191). (D) LMRAG of the optic vesicle of a chick embryo at day 2, labeled with [^{3}H]uridine, demonstrating RNA synthesis in the nuclei and cytoplasm of the outer portion of the optic vesicle layer ($\times$750; bar = 50 μm). (E) Dark-field photograph of the skleral layer (top), choroid layer (middle), and pigment

1. Nerve Cells

The nerve cells or neurons can be grouped into two types: the central nerve cells and the peripheral nerve cells. With regards the central nerve cells, radioautographic studies on DNA synthesis, glucose incorporation, and mRNA in both brains and spinal cords were carried out. The DNA synthesis was studied in the cerebella of nine groups of aging mice from embryo to postnatal 1 year using [³H]thymidine radioautography (Cui, 1995). The labeled nuclei, both the precursors of neurons and glioblasts, were observed in the external granular layer of the cerebella (Fig. 25A) by LMRAG and EMRAG from embryonic day 19 to postnatal day 14 and disappeared in 1 month. The peak of labeling index was at postnatal day 3 in both neuroblasts (Fig. 26A) and glioblasts (Fig. 26B). The endothelial cells of the cerebellar vessels were progressively labeled, reaching the peak at 1 week after birth. Changes of glucose uptake in the gerbil hippocampus were studied using [³H]deoxyglucose by cryo-fixation, freeze–substitution, and dry-mounting radioautography under postischemic conditions (Izumiyama *et al.,* 1987). The results demonstrated that the neurons in the hippocampus subjected to ischemia revealed higher uptake of soluble glucose than normal control.

On the other hand, the localization of TGF-β1 mRNA in the segments of the spinal cords of mice was investigated with *in situ* hybridization techniques (Nagata *et al.,* 1999b). The tissues of lower cervical segments of the spinal cords of BALB/c mice, from embryonic days 12, 14, 16, and 19 and postnatal days 1, 3, 7, 14, 21, 28, 42, and 70, were used. For *in situ* hybridization, ³⁵S-labeled oligonucleotide probes for TGF-β1 were used to detect their messenger RNA. Cryosections were incubated under silicon cover slides with 100 μl of preincubation solution plus a final concentration of 2.4×10^6 cpm/ml probes and 100 mM dithiothreitol (DTT) for 16 h. After washing with standard sodium citrate (SSC) and DTT, the slides were dried and processed for radioautography by dipping in Konica NR-M2 emulsion, exposed, and developed. The results showed that GF-β1 mRNA was detectable in the meninges surrounding the spinal cord, but scarcely detected in spinal cord parenchyma. The localization of TGF-β1 mRNA in the spinal cord suggests that

---

epithelium (bottom) of an adult mouse, demonstrating intense silver grains (white dots) by *in situ* hybridization for TGF-β1 mRNA in the three layers. Compare this picture to the next picture ($\times$450; bar = 100 μm). Permission from T. Nagata and Y. Kong (1998, Fig. 1, p. 92). (F) LM photograph of the skleral layer (SL); choroid layer (CL), and pigment epithelium (PE) of an adult mouse, demonstrating immunostaining for TGF-β1. The three layers show intense immunoreactivity ($\times$450; bar = 100 μm). Permission from T. Nagata and Y. Kong (1998, Fig. 1, p. 92). (G) LMRAG of the cornea of a mouse at postnatal day 14, labeled with [³H]thymidine. Note that a nucleus (arrow) in the corneal epithelium is labeled with silver grains, but there are none in the stroma ($\times$900; bar = 50 μm). (H) LMRAG of the skin of a forelimb of a salamander at 6 weeks after hatching, labeled with [³H]thymidine. Three nuclei (arrows) at the basal layer are labeled ($\times$900; bar = 50 μm). Permission from T. Nagata (1999c, Fig. 32, p. 702).
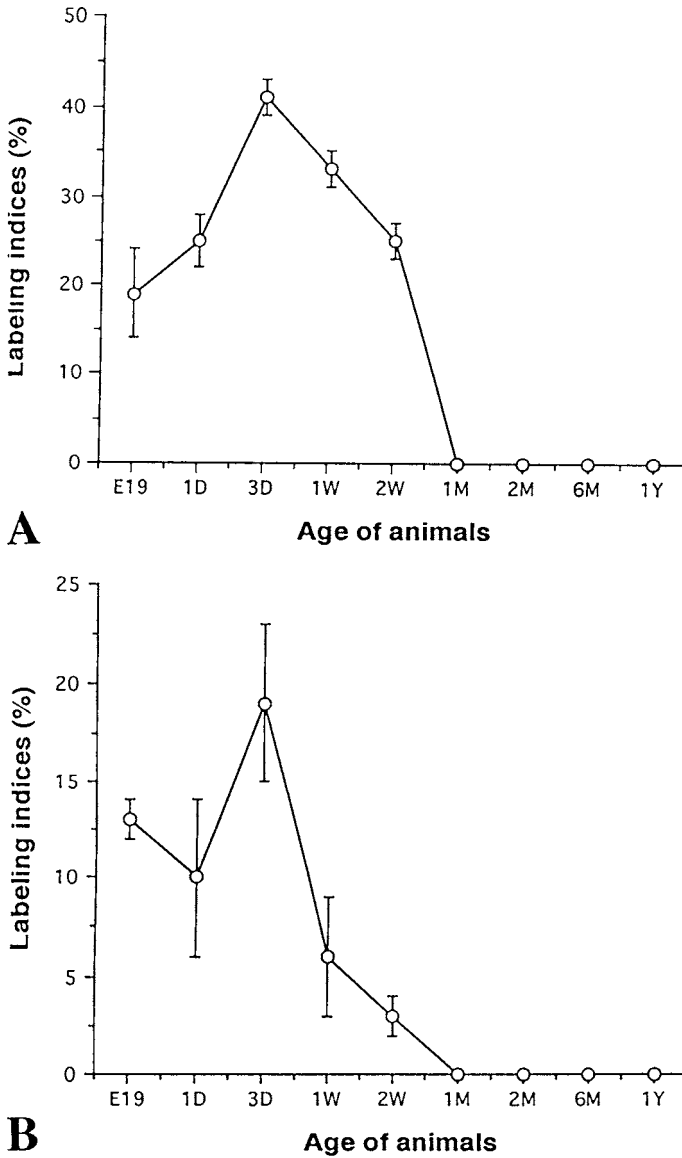
FIG. 26   Transitional curves of the labeling indices in the external granular layer of mouse cerebellum injected with [³H]thymidine, indicating DNA synthesis at various ages. (A) Labeling indices of neuroblasts. (B) Labeling indices of glioblasts (mean ± standard deviation). Permission from T. Nagata (1999c, Fig. 26, p. 700).

TGF-β1 acts through paracrine mechanism in the morphogenesis of the spinal cord in mice (Nagata *et al.,* 1999b).

Protein kinase C activity was examined in rabbit cerebellum (Usuda *et al.,* 1991a). Protein kinase C is generally accepted as playing important roles in cell immunity, mitosis, and cytoskeletal movement (Usuda *et al.,* 1991a). We first purified protein kinase C from rabbit retina and studied immunocytochemical localization of protein kinase C isozymes (types I, II, and III) in the retina and cerebellum using monoclonal antibodies. The cerebella of male rabbits were fixed in 4% paraformaldehyde/0.1 M phosphate buffer at pH 7.4, immersed in graded sucrose solutions, 10, 15, 20%, frozen in a mixture of dry-ice and acetone, cryo-sectioned on a cryostat microtome, picked up on gelatin-coated glass slides, and immunostained for a modified PAP method. The results showed that type I isozymes were localized only in the cytoplasm of Purkinje cells and their processes in the cerebella. The granular layer excluding Purkinje cells was stained with the antibody for type II, while weak staining with type III was observed diffusely in the whole layers of the cerebellar cortex (Usuda *et al.,* 1991a).

The localization of TGF-β1 and its mRNA in the segments of the spinal cords of mice was also investigated with immunocytochemical techniques (Nagata *et al.,* 1999b). The tissues of lower cervical segments of the spinal cords of BALB/c mice, from embryonic days 12, 14, 16, and 19 and postnatal days 1, 3, 7, 14, 21, 28, 42, and 70, the same as in the *in situ* hybridization, were used. For immunocytochemistry, transverse cryosections of the spinal cords were cut and stained with rabbit anti-TGF-β1 polyclonal antibody followed with the ABC method. The results showed that positive immunoreactivities arose in the ventral horn motoneurons from the embryonic stage up to the adult. The extracellular matrix of the white matter showed positive immunocytochemical staining from postnatal day 14 (Fig. 25B), and thereafter, the immunoreactivity remained with aging. However, the whole white matter showed only background level of staining before postnatal day 14. The results led us to propose that TGF-β1 regulates motoneuron growth and differentiation and is probably correlated with formation, differentiation, and regeneration of myelin of nerve tracts. Since TGF-β1 mRNA was detectable in the meninges surrounding the spinal cord by *in situ* hybridization but scarcely detected in spinal cord parenchyma, the disparate localization of TGF-β1 polypeptide and TGF-β1 mRNA in the spinal cord suggest that TGF-β1 acts through paracrine mechanism in the morphogenesis of the spinal cord in mice (Nagata *et al.,* 1999b).

We first studied the degeneration and regeneration of autonomous nerve cells in the plexuses of Auerbach and Meissner of the jejunums of 15 dogs which were operated upon to produce experimental ischemia of the jejunal loops by perfusing with Tyrode's solution via the mesenteric arteries for 1, 2, 3, and 4 h (Nagata, 1965, 1967; Nagata and Steggerda, 1963, 1964). Tissue blocks were obtained from the deganglionated portions and the adjoining normal portions, which were fixed in Carnoy's fluid, embedded in paraffin, sectioned, and stained with

buffered thionine, methyl-green, pyronine, and PAS. Some animals were injected with either [³H]thymidine or [³H]cytidine and the intestinal tissues obtained from ischemic portions and normal portions were processed for light microscopic radioautography. The results revealed that the ganglion cells in Auerbach's plexus showed various degenerative changes in accordance with the duration of ischemia. After 4 h of ischemia, most of the ganglion cells in Auerbach's plexus were completely destroyed. The degenerative changes in Auerbach's plexus after 4 h of ischemia were irreversible after 1 week of recovery. The ganglion cells in the Meissner's plexus, on the other hand, were less sensitive to the ischemia. They recovered completely even after 4 h ischemia. The PAS-positive substances in degenerative ganglion cells in both plexuses decreased immediately after 4 h of ischemia. The DNA contents of ganglion cells in both Auerbach's and Meissner's plexus did not show any change before or after ischemia. The RNA contents decreased immediately after the ischemia (Nagata and Steggerda, 1963). The number of binucleate cells in ganglion cells in both Auerbach's and Meissner's plexuses after 4 h of ischemia increased to 4.6 and 5.7%, respectively. In contrast, in the nonischemic normal control preparations, the binucleate cells occurred only 0.5 and 1.8% in Auerbach's and Meissner's plexuses, respectively. The high frequency of binucleate cells in the ganglion cells persisted for more than 100 days after the ischemia, indicating a possible regeneration of ganglion cells (Nagata, 1965; Nagata and Steggerda, 1964). The radioautographic study revealed that there was no evidence for DNA synthesis in both Auerbach's and Meissner's plexuses from either ischemic or normal loops. The RNA synthesis was observed to be higher in ganglion cells in the normal loop than those in the ischemic loop and higher in Auerbach's than in Meissner's plexus. It was higher in binucleate ganglion cells than in mononucleate cells (Nagata, 1967). As for the autonomic innervation in the cerebral arteries we tried to demonstrate aminergic and cholinergic nerves consecutively on whole mount preparations of rat cerebral arteries (Kobayashi et al., 1981a). For demonstration of aminergic nerves the glyoxilic acid method was used, while for cholinergic nerves the direct coloring thiocholine method for thiocholinesterase by Karnovsky and Roots (1964) was used consecutively. The results revealed that both aminergic and cholinergic nerves were distributed densely in the proximal portions of the major cerebral arteries. Each nerve distributed circularly and longitudinally in the proximal portions of the arteries, while the longitudinal distribution was predominantly observed in the distal portions (Kobayashi et al., 1981a). Utilizing this procedure, postnatal development of autonomic nerves major cerebral arteries of aging mice from postnatal days 1, 4, 7, 14, 21, and 28 to 5 months was observed (Kobayashi et al., 1981b). In 1-day-old mice, a few aminergic nerve fibers can be seen in the major cerebral arteries but cholinergic nerves were scarcely observed. The cholinergic nerves were clearly observed in 1-week-old animals, and then both nerves increased rapidly in the first 2 weeks and completed development between postnatal weeks 3 and 4 (Kobayashi et al., 1981b). Similar results were also obtained in the iris of aging

mice from 1 day to 5 months (Tsukahara *et al.,* 1982). Many aminergic nerve fibers were already found in the iris of 1-day-old animals, while cholinergic nerves were scarcely observable. Both types of nerves increased rapidly in the first 2 weeks and completed development between postnatal weeks 3 and 4, although aminergic nerves developed earlier than cholinergic nerves (Tsukahara *et al.,* 1982).

2. Ocular Cells

Ocular cells are the components of the visual organs, which consist of the cornea, iris, cilliary body, lens, retina, choroid, and sclera. We studied mainly the macro-molecular synthesis in the retina of chickens and mice as well as enzyme immuno-cytochemistry.

The nucleic acid syntheses, both DNA and RNA, were first studied in the ocular tissues of chick embryos from day 1 to day 14 incubation by LM and EMRAG (Gunarso, 1984a,b, Gunarso *et al.,* 1997). It was shown that the labeled cells with [3H]thymidine were most frequently observed in the posterior region of the day 2 chick embryo optic vesicle (Fig. 25C) and the labeled cells moved from anterior to posterior regions, decreasing from day 3 to day 7. On the other hand, the number of silver grains incorporating [3H]uridine increased from day 1 to day 7 and it was more in the anterior region than in the posterior region (Gunarso *et al.,* 1996). Then, DNA and RNA syntheses in the ocular tissues of aging mice were also studied (Gao *et al.,* 1992a,b; Gao *et al.,* 1993; Kong, 1993; Kong *et al.,* 1992a). The ocular tissues obtained from groups of litter ddY mice at ages varying from fetal days 9, 12, 14, 16, and 19 to postnatal days 1, 3, 7, and 14 were labeled with [3H]thymidine *in vitro* and radioautographed (Gao *et al.,* 1992a,b). The labeling indices of retina and pigment epithelium were higher in earlier stages than in later stages, during which they steadily declined (Fig. 27). However, the retina and pigment epithelium followed different courses in their changes of labeling indices during embryonic development. In the retina, the labeling indices in the vitreal portions were more than those in the scleral portions during the earlier stages. However, the indices of scleral portions were more than those in the vitreal portions in the later stages. Comparing the three regions of the retina of mouse, anterior, equatorial, and posterior, the labeling indices of the anterior regions were generally higher than those of the equatorial and posterior regions (Fig. 27A). In the pigment epithelium (Fig. 27B), the labeling indices gradually increased in the anterior region, but decreased in the equatorial and the posterior regions through all developmental stages. These results suggest that the proliferation of both the retina and the pigment epithelium in the central region occurred earlier than those of the peripheral regions (Gao *et al.,* 1992a,b). In the juvenile and adult stages, however, the labeled cells were localized at the middle of the bipolar-photoreceptor layer of the retina, which was supposed to be the undifferentiated zone (Kong, 1993; Kong *et al.,* 1992a). In the corneas of aging mice, the labeled cells with [3H]thymidine were localized in the epithelial cells at prenatal day 19 to postnatal year 1. The
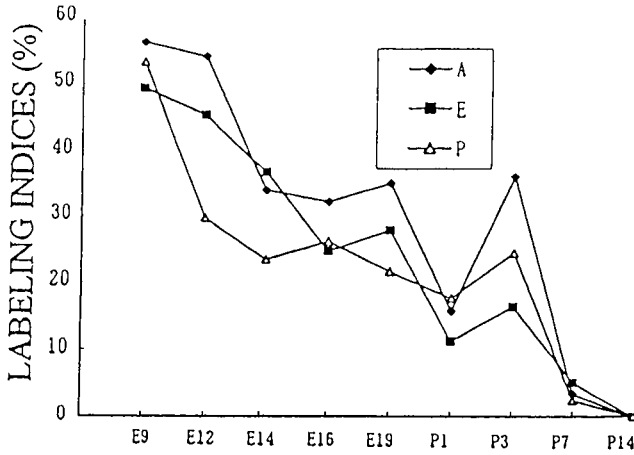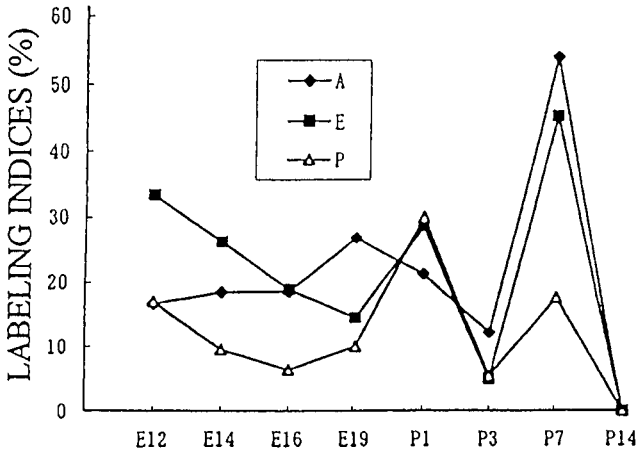
FIG. 27   Transitional curves of the labeling indices in the three regions (A, anterior; E, equator; P, posterior) of the retina and pigment epithelium of mice injected with [³H]thymidine, indicating DNA synthesis at various ages. (A) Labeling indices in the retina. (B) Labeling indices in the pigment epithelium (mean ± standard deviation). Permission from T. Nagata (1999c, Fig. 28, p. 701).

labeling index of the corneal epithelial cells reached a peak at 1 month after birth and decreased to 1 year, while the indices of stromal and endothelial cells reached a peak at 3 days after birth and disappeared completely from postnatal month 1 to year 1 (Gao *et al.,* 1993). In the cilliary body, the labeled cells were located in the cilliary and pigment epithelial cells and stromal cells and smooth muscle cells

from prenatal day 19 to postnatal week 1, but no labeled cells were observed in any cell types from postnatal day 14 to year 1. The labeling indices of all the cell types in the cilliary body were at maximum at prenatal day 19 and decreased gradually after birth, reaching 0 at postnatal day 14 (Nagata *et al.,* 1994). On the other hand, when the ocular tissues were labeled with [³H]uridine (Fig. 23D), silver grains appeared over all cell types at all stages of development and aging (Kong *et al.,* 1992b). The grain counts in the retina and the pigment epithelium increased from prenatal day 9 to postnatal day 1 in the retinal cells, while they increased from prenatal day 12 to postnatal day 7 in the pigment epithelial cells (Kong *et al.,* 1992b; Kong and Nagata, 1994). In the cornea of aging ddY mice, DNA synthesis was observed in all three layers, i.e., epithelial, stromal, and endothelial layers, at perinatal stages (Fig. 23G). The labeling index of the corneal epithelial cells increased from perinatal stages to postnatal month 2 and kept a constant level (10–14%), and the indices of stromal (5–10%) and endothelial cells (15–25%) increased to postnatal day 3, reaching a peak, and decreased to 1 month (a few percent). The labeled cells in the latter two layers were not observed from 1 month to 1 year.

The protein synthesis of the retina in aging mouse as revealed by [³H]leucine incorporation demonstrated that the number of silver grains in bipolar cells and photoreceptor cells was most intense at the embryonic stage and early postnatal days. The peak was 1 day after birth and decreased from 14 days to 1 year after birth. (Toriyama, 1995). The collagen synthesis in the ocular tissues was also demonstrated by the incorporation of [³H]proline in four groups of mice at various ages, from prenatal day 20 and postnatal days 3, 7, and 30 (Nagata, 1997c). Results showed that the sites of [³H]proline incorporation were located in the stromal fibroblasts in both cornea and the trabecular meshwork in the iridocorneal angle in prenatal and postnatal newborn mice. No silver grains were observed in the epithelial and endothelial cells. On EMRAG, silver grains were localized over the endoplasmic reticulum and Golgi apparatus of fibroblasts and over intercellular matrices consisting of collagen fibrils. From the quantitative analysis, the grain densities were higher in the fibroblasts of postnatal day 7 animals than in those of younger animals at fetal day 20 and postnatal days 3, 7, and 30. In the same age groups, the grain densities were more in the cornea than the iridocorneal angle. It was concluded that the collagen synthetic activity was localized in the fibroblasts in the cornea and the trabecular meshwork in the iridocorneal angle and the activity changed with aging, reaching the maximum at postnatal day 7 (Nagata, 1997c).

The distribution and localization of TGF-β1 and βFGF, and their mRNAs in mice were studied by *in situ* hybridization (Nagata and Kong, 1998). The posterior segments of BALB/c mouse eyes, from embryonic days 14, 16, and 19 and postnatal days 1, 3, 5, 7, 14, 28, 42, and 70, were used as materials. For *in situ* hybridization, ³⁵S-labeled oligonucleotide probes for TGF-β1 and βFGF were used to detect their mRNAs. Cryosections were placed on glass slides which were processed for *in situ*

hybridization and radioautographed. As a result, the silver grains, represented the hybridization with ^{35}S-labeled antisense oligonucleotide probe for TGF-β1 and βFGF mRNAs, mainly located in the scleral layers and some in the choroidal and pigment epithelial layers but only background level of silver grains was found in whole retina (Fig. 25E). In the radioautograms from embryonic day 14 (E14) to adult mice (10 weeks), the significant distribution of silver grains represented TGF-β1 mRNA was not detected in whole retina. However, significant silver grains, just fewer numbers, were detected in scleral and choroidal layers and mesenchymal cells at E14 and E16, and then the grains became much more from E19 until adult (Fig. 25E), in particular in sclera. These results suggested that mRNAs for TGF-β1 and βFGF were synthesized in scleral, choroidal, and pigment epithelial layers, but their proteins were transferred to the target cells of the retina and elsewhere. Furthermore, it is suggested that TGF-β1 and βFGF may play important roles on retinal differentiation, development and aging, in particular during the late embryonic and newborn stages (Nagata and Kong, 1998).

On the other hand, protein synthesis of the cornea as revealed by [^{3}H]leucine incorporation (Nagata, 2000c) and glycoprotein synthesis demonstrated by [^{3}H]glucosamine (Nagata *et al.,* 1995) were studied in several groups of aging mice. Silver grains of both [^{3}H]leucine and [^{3}H]glucosamine incorporations were located in the epithelial cells, the stromal fibroblasts, and the endothelial cells from prenatal day 19 to postnatal month 6. No silver grains were observed in the lamina limitans anterior (Bowman's membrane) and the lamina limitans posterior (Descemet's membrane). The grain densities by [^{3}H]leucine incorporation in three layers, i.e., epithelial, stromal, and endothelial layers, increased from embryonic stage to postnatal days 3 and 7, then decreased to 2 weeks and 1 year. The grain densities by [^{3}H]glucosamine were higher in the endothelial cells of prenatal day 19 animals, but higher in the epithelial cells of postnatal day 1, 3, and 7 animals. From the results, it was shown that the glycoprotein synthetic activity in respective cell types in the cornea of mouse changed with age (Nagata *et al.,* 1995).

On the other hand, the distributions of some of the ophthalmological drugs used for the treatment of glucoma patients were examined in the ocular tissues. Bupranolol is a beta-blocking agent widely used for glaucoma as an eye drop in the United States and Japan (Tsukahara *et al.,* 1980). [^{14}C]Bupranolol (Kaken Co., Tokyo, Japan) was experimentally instilled into the eyes of white rabbits and the ocular tissues were enucleated after 15 and 30 min, which were cryo-fixed in liquid nitrogen and the frozen tissues were cryo-sectioned and either freeze–dried or thaw–mounted onto glass slides, followed by either dry-mounting or wet-mounting LMRAG. The results showed that silver grains by dry-mounting RAG appeared intensely in the conjuctival and corneal epithelia at 15 min, and then they decreased there and increased in the cilliary bodies at 30 min. These results demonstrated that this drug penetrated the conjunctiva and cornea and accumulated into the cilliary bodies (Tsukahara *et al.,* 1980). Befunolol is a beta-blocking agent synthesized by Kaken Co. (Tokyo, Japan). Its chemical structure

is 2-acetyl-7(2-hydroxy-3-isopropylamino-propoxy) benzofuran hydrochloride, which was labeled with ^{3}H and used for LM and EMRAG (Yamabayashi *et al.,* 1981; Nagata and Yamabayashi, 1983). The ocular tissues of chickens were taken out, cut into small pieces, and labeled with [3H]befunolol in modified Eagle's medium (MEM) (3.7 MBq/ml) in a CO_2 incubator for 30 to 60 min. The tissues were cryo-fixed in liquid nitrogen and some of them were dry-sectioned, some were freeze–dried or freeze–substituted and embedded in Epon, dry-sectioned, and dry-mounted. Some other tissues were chemically fixed, embedded, and wet-mounted. Dry-mounting EM radioautograms revealed that many silver grains were found over the melanosomes of the pigmented cells demonstrating soluble compounds. On the contrary, only few silver grains were found over the melonosomes of the pigmented cells of the iris and the cilliary bodies by conventional wet-mounting EMRAG. From the results, it was found that soluble [3H]befunolol was accumulated specifically over the melanosomes of the pigmented cells, which correlated well with the clinical findings (Nagata and Yamabayashi, 1983).

We studied protein kinase C activity in normal rabbit retina from an immunocytochemical standpoint (Usuda *et al.,* 1991a). Protein kinase C is a diacylglycerol-phospholipid- and calcium-ion-independent protein kinase and it is generally accepted as playing important roles in cell immunity, mitosis, and cytoskeletal movement (Usuda *et al.,* 1991a). We first purified protein kinase C from rabbit retina and studied immunocytochemical localization of protein kinase C isozymes (types I, II, and III) in the retina using monoclonal antibodies. The retinal tissues of male rabbits were fixed in 4% paraformaldehyde/0.1 M phosphate buffer, pH 7.4, immersed in graded sucrose solutions (10, 15, and 20%), frozen in a mixture of dry-ice and acetone, cryo-sectioned on a cryostat microtome, placed on gelatin-coated glass slides, and immunostained for a modified PAP method. The results showed that the retinal neurons were negative for type I isozymes but positive for types II and III isozymes. Type II was more diffusely distributed through the retinal layer, but was distinctive in ganglion cells, bipolar cells, and the outer segment of the retina. The immunoreactivity was stronger for type III isozymes as well as rod bipolar cells and amacrine cells. Using immuno-electron microscopy, it was seen that the cytoplasm of the cell body, the axon, and the dendrites of rod bipolar cells were strongly reactive for type III isozymes. The rod bipolar cells were observed to form synapses with rod receptor cells. From the results, it was concluded that these differential localizations of respective isozymes in retinal neurons suggested that each isozyme, I, II, and III, had a different site of function in each neuron (Usuda *et al.,* 1991a).

Distribution and localization of TGF-β1 and βFGF were also studied with the immunocytochemical method (Nagata and Kong, 1998). The posterior segments of BALB/c mouse eyes, from embryonic days 14, 16, and 19 and postnatal days 1, 3, 5, 7, 14, 28, 42, and 70, the same materials as in the *in situ* hybridization, were used. For immunocytochemistry, cryo-sections were stained with rabbit anti-TGF-β1 and anti-βFGF polyclonal antibodies followed by the ABC method. The

results showed positive immunoreactivities located in ganglion cell layers and the vessels of retina and choroid. By light microscopic observation, the positive im-munoreactivities were located in ganglion cell layers, inner and outer plexiform layers, cytoplasm of pigment epithelial cells, scleral layers, and the endothelial cells and walls of vessels in retinal and choroidal layers. The inner and outer nuclear layers and segments of photoreceptors showed no immunoreactivity. The intensely positive staining was found in the vessel wall of choroid and scleral layers (Fig. 25F) and ganglion cells but not glial cells of the ganglion cell layer. The neg-ative control abolished virtually all reactivity when using the normal rabbit serum instead of primary antibody or using the avidin–biotin–peroxidase complex so-lution only. The immunostaining with βFGF antibody presented the same basal pattern as shown in TGF 1 immunocytochemistry (Nagata and Kong, 1998). The positive imunoreactivities were detected in the ganglion cell layer, inner and outer plexiform layers, retinal pigment epithelial layer, and choroidal and scleral layers. However, the thin processes of Müller cells oriented vertically showed specific immunoreactivity in inner plexiform layer and their feet-ends positively stained located in the ganglion cell layer. It was noted, as shown in TGF-β1, that the small glial cells located in ganglion cell layers could not be stained. In the immuno-cytochemical study on βFGF, similar age-related changes were detected as those with TGF-β1. Weakly positive immunostaining presented in the cells of retinal vitreal portion at embryonic day 14 and the inner neuroblastic cells (presumptive ganglion cells) at embryonic day 16, and became moderate at day 19, intense immunoreactivity from newborn to adult. However, the changes of immunoreac-tivities with TGF-β1 antibody in the scleral layers were not detected in βFGF immunostaining. It is noted that densely stained thin processes of Müller cells in the inner plexiform layers with βFGF antibody did not appear until postnatal week 2 and were first observed from postnatal week 3. As age-related changes, the cells in the retinal vitreal portion at embryonic day 14 and the inner neuroblastic cells (presumptive ganglion cells) at day 16 showed weakly positive immunostaining, which was likely in the cytoplasm or intracellular matrix. However, the cells in the ganglion cell layers became moderately positive from embryonic day 19 and presented intense immunoreactivity after birth. It was noted that the monolayer of ganglion cells showed almost positive staining except for some small glial cells from postnatal day 5. The scleral layers also presented more intense staining from postnatal day 5 than those in earlier stages.

We also studied the age-related changes of mouse ocular cells by lectin cyto-chemistry (Nagata and Kong, 2000). Six groups of litter ddY strain mice at various ages, fetal day 18, postnatal days 1, 5, and 21, and 1 and 11 months, were used. Ocular tissues were fixed in 4% paraformaldehyde/0.1 M sodium phosphate solu-tion, pH 7.4, for 24 h, immersed in graded sucrose solutions, frozen in a mixture of dry ice and n-hexane, sectioned on a cryostat microtome, and stained with 16 kinds of biotinylated lectins followed by the ABC method. The results showed that the age-related changes in lectin-binding pattern in the retina and pigment

epithelium were found in seven kinds of lectins (ConA, WGA, ABA, LCA, DBA, SBA, and MAM). The ganglion cells in the retina were negative from fetal to post-natal day 3, but became positive from postnatal day 5 to 11 months with ConA, WGA, and ABA. On the contrary, they were positive from fetal day 18 to postnatal day 1 and became negative from day 5 to 11 months with LCA. The nerve fiber layer and inner limiting membrane showed negative staining from fetal day 18 to postnatal day 21 and became positive from postnatal day 1 to 11 months with DBA and SBA. The staining patterns with MAM also presented dense changes in the Bruch's membrane, photoreceptor segments, and nerve fiber layer due to aging. Nine other kinds of lectins (PHA-E4, PNA, RCA120, UEA-I, DSA, Lotus, PHA-L4, RCA60, SSA) did not show any staining change with development and aging of animals. These results suggested that the retina and pigment epithelium of mouse changed their molecular sequences in glycoproteins with development, differentiation, and aging of animals (Nagata and Kong, 2000).

3. Cutaneous Cells

The cutaneous cells are the components of the skin which cover the surface of the animal body. They are divided into epidermal cells, dermal cells, and hypo-dermal cells. We studied only the epidermal cells of salamanders after hatching by radioautography. The forelimbs and hindlimbs of salamanders are composed of skeletons consisting of bones and cartilages which are covered with skeletal muscles, connective tissues, and epidermis consisting of stratified squamous epi-thelial cells in the outermost layer. We observed both the cartilage cells in the bone and the epithelial cells in the epidermis to compare the two cell populations (Nagata, 1998c). The skin of a salamander consisted of epidermis and dermis or corium which were lined with connective tissue layers designated as the subcu-taneous layer. The former consisted of stratified squamous epithelium, while the latter consisted of dense connective tissues. The epithelial cells in the juvenile ani-mals at 4 weeks after hatching were cuboidal and not keratinized. Radioautograms labeled with [^{3}H]thymidine at this stage showed that many cells were labeled demonstrating DNA synthesis at both the superficial and deeper layers (Fig. 25H), resulting very high labeling index. At 6 weeks after hatching, the superficial cells changed their shape from cuboidal to flattened squamous, while the deeper and basal cells remained cuboidal. The numbers of labeled cells were almost the same as the previous stage at 4 weeks, but they were localized at the basal layer. The shape of epithelial cells in juvenile animals at 8, 9, 10, and 11 weeks differentiated, gradually forming the superficial corneum layer, which appeared keratinized, and the deeper basal layer. Radioautograms at these stages showed that the labeled cells remarkably reduced as compared with that seen at 4 and 6 weeks. In the adult salamanders at 8 to 12 months, the dermal and epidermal cells showed complete mature structure and examination of radioautograms revealed that the labeled cells were localized at only the basal cell layer and their number reached a very low

but constant level. No difference was found on the morphology and labeling between the forelimbs and hind-limbs at any stage. Comparing the labeling indices of both epidermal cells and the cartilage cells in the limbs, the labeling index of the epidermal cells was higher than the cartilage cells. The index of the dermal cells in the hind-limbs was at its maximum, about 25%, at 4 weeks and declined markedly with time from 6 to 9 weeks. The labeling index of epidermal cells of the hind-limbs, on the other hand, had its maximum, about 23%, at 6 weeks, increasing from 20% at 4 weeks, and decreasing to about 18% at 8 weeks, and then declined progressively with time, dropping to 5% at 9 weeks. The labeling indices of the epidermal cells of both forelimbs and hindlimbs were almost the same from 9 weeks to 12 months, keeping a low constant level about 4–5%, but never reaching 0. These results indicate that the cutaneous cell belongs to the renewing cell population (Nagata, 1998c).

I. Cancer Cells

There are many cell types of cancer cells available. We studied only several cell types of cancer cells from both human origin and experimental animals. Ultrastructural localization of PA-TCH-SP-positive substances in the human gastric scirrhus in several human patients was studied by electron microscopy (Tei *et al.,* 1978). The gastric scirrhus consist mainly of collagen fibrils and cancer cells. The cancer cells contained moderately developed endoplasmic reticulum, Golgi apparatus, mitochondria, and markedly irregular shaped granules. The PA-TCH-SP-positive deposits were localized on the granules and the Golgi apparatus. From the results, it was suggested that the gastric scirrhus cells could produce neutral glycoproteins by adding the sugar portions in the Golgi apparatus and stored in the granules (Tei *et al.,* 1978).

Several experiments dealing with the nucleic acid synthesis in cancer cells by means of LM and EMRAG were carried out. The DNA and RNA synthesis in mitochondria of cultured HeLa cells, an established cell line obtained from the carcinoma of the human uterus, labeled with [^{3}H]thymidine and [^{3}H]uridine, was demonstrated to localize over the mitochondrial matrix by EMRAG (Nagata, 1972c,d). The DNA synthesis of primary cultured myeloma cells obtained from a human myeloma patient was studied by [^{3}H]thymidine RAG (Fujii *et al.,* 1980). From the results, it was demonstrated that the labeled myeloma cells contained poorly developed endoplasmic reticulum compared with the unlabeled cells, suggesting that immature cells synthesized more DNA than mature cells containing well developed endoplasmic reticulum (Fujii *et al.,* 1980). On the other hand, DNA, RNA, and mucosubstance syntheses of mastocytoma and mast cells from rats (Murata *et al.,* 1977c, 1978b) were studied by [^{3}H]thymidine, [^{3}H]uridine, and $^{35}SO_4$ radioautography, demonstrating that the mastocytoma cells synthesized more DNA, RNA, and mucosubstances than normal mast cells (Murata

*et al.,*1977d). On the other hand, when rat ascites hepatoma cells, YS cells, were treated *in vitro* with several carcinogens such as dimethylamine, dimethylnitrosamine, butylbutanolamine, butylurea, or butylnitrosourea and processed through EMRAG, no significant difference of [^{3}H]thymidine and [^{3}H]uridine incorporation was observed between the treated and untreated groups (Nagata *et al.,* 1977c). Human thyroid cancer tissues obtained from a struma patient by surgery were labeled *in vitro* with ^{203}HgCl$_2$ and ^{205}HgCl$_2$ and processed through both conventional chemically fixed wet-mounting radioautography and freeze–dried dry-mounting radioautography (Nagata *et al.,* 1977b). The results revealed that numerous silver grains showing the soluble component of mercury were found diffusely in thyroid cancer cells but fewer silver grains showing the insoluble component were observed in cancer and normal thyroid cells (Nagata *et al.,* 1977b). The results supported the clinical findings on the high concentration of hot mercury in the thyroid cancers of the struma patients.

Thyroid cancer cells obtained from human patients were stained immunocytochemically for protein kinase C isozymes (Shimizu *et al.,* 1991). The thyroid tissues surgically removed from 49 human patients suffering from the thyroid diseases, consisting of 5 adenomatous goiter, 5 Grave's disease, 17 follicular adenoma, 11 papillary carcinoma, and 11 follicular carcinoma, were examined. Small tissue pieces were fixed in 10% phosphate-buffered formalin solution, dehydrated, embedded in paraffin, cut, and placed on glass slides. The sections were stained with the PAP method according to Sternberger (1979), as described in the section on thyroid glands. As the results, both the normal thyroid cells and cancer cells showed negative reaction for type I, and normal cells were weakly positive while cancer cells were strongly positive for type II, and both normal and cancer cells were weakly positive for type III (Shimizu *et al.,* 1991). The cytoplasm of papillary and follicular carcinoma cells stained more intensely than normal thyroid cells. These results indicated that the type II isozyme was more expressed in thyroid cancer cells than normal thyroid cells. Proliferative activity of human thyroid cancer cells evaluated by proliferating cell nuclear antigen/cyclin (PCNA) was also studied by the immunocytochemical method (Shimizu *et al.,* 1993). The results demonstrated that the proliferative activity as expressed by PCNA activity was much stronger in thyroid cancer cells than in normal thyroid cells (Shimizu *et al.,* 1993).

V. Concluding Remarks

The cytochemical techniques can be divided into three categories: chemical, physical, and biological. These technologies were well developed in the 20th century and should be designated as "general cytochemistry." On the other hand, these techniques have been applied to various cells in various organ systems in men

and animals, such as the skeletal, muscular, digestive, respiratory, urinary, reproductive, endocrine, circulatory, nervous, and sensory systems. We summarized the results of cytochemical studies on various cells composing various organs in various animals including men carried out in our laboratory by many collaborators during the years since 1955. These data include the structures of various kinds of cells based on the chemical components of cells and cell organelles showing the aging changes in morphogenesis, development, and senescence from embryos, neonates, sucklings, weanlings, and mature and senescent adults. The data include not only the three-dimensional structure of cells but also the four-dimensional features taking the time dimension into account using cytochemical methods such as chemical, physical, and biological techniques by labeling specific cells in connection with the time lapse. The application of these cytochemical techniques to special cells in various organ systems should be designated as "special cytochemistry." It is hoped that this novel concept would be accepted and well developed to form a new prospect in biological sciences in the 21st century.

Acknowledgments

References

Adamston, F. B., and Tayler, A. B. (1948). The rapid preparation of frozen tissue sections. *Stain Technol.* **23,** 109–116.

Alanen, K. (1989). Comparison of fresh, ethanol preserved and paraffin-embedded samples in DNA flow cytometry. *Cytometry* **10,** 81–90.

Alfert, M., and Geschwind, I. I. (1953). A selective staining method for the basic proteins of cell nuclei. *Proc. Natl. Acad. Sci. USA* **39,** 991–999.

Altmann, R. (1889). Über die Fettumsetzungen im Organismus. *Arch. Anat. Physiol.* **1889** (Suppl.), 86–104.

Altmann, R. (1894). "Die Elementorganismen und ihre Beziehungen zu den Zellen." Veit und Comp, Leipzig.

Angermüller, S., and Fahimi, H. D. (1981). Selective cytochemical localization of peroxidase, cytochrome oxidase and catalase in rat liver with 3, 3′-diamino-benzidine. *Histochemistry* **71,** 33–44.

Appleton, T. C. (1964). Autoradiography of soluble labeled compounds. *J. R. Microsc. Soc.* **83,** 277–281.

Augusten, K., Hesse, G., and Zschiesche, W. (1969). Quantitative mikrophotometrische Untersuchungen zum Tryptophannachweiss nach Adams. *Histochemie* **19,** 44–57.

Bando, Y. (1995). Microstructure analysis of advanced ceramics by high-resolution analytical transmission electron microscopy. *J. Electron Microsc.* **44,** 115–123.

Bando, Y., Matsui, Y., and Uemura, Y. (1985). The usefulness of a 400 kV high-resolution analytical electron microscope. *Ultramicroscopy* **18,** 117–124.

Barka, T., and Anderson, P. J. (1963). "Histochemistry, Theory, Practice and Bibliography." Hoeber Medical Division, Harper and Row, New York, Evanston, London.

Beaudoin, A. R., Groudin, G., Lord, A., and Pelletier, M. (1985). –NADPH– and TMPase-positive "snake-like tubules" in the exocrine pancreas. *J. Histochem. Cytochem.* **33,** 569–575.

Bendayan, M. (1981). Ultrastructural localization of nucleic acids by the use of enzyme–gold complexes. *J. Histochem. Cytochem.* **29,** 531–541.

Bendayan, M. (1982). Double immunocytochemical labeling applying the protein A–gold technique. *J. Histochem. Cytochem.* **30,** 81–89.

Bensley, R. R., and Gersh, I. (1933). Studies on cell structure by freeze–drying method; nature of mitochondria in hepatic cells of amblyostoma. *Anat. Rec.* **57,** 217–226.

Bradbury, S., and Stoward, P. J. (1967). The specific cytochemical demonstration in the electron microscope of periodate-reactive mucosubstances and polysaccharides containing vic-glycol groups. *Histochemie* **11,** 71–80.

Cafrany, E. J., di Stefano, H. S., and Farah, H. (1955). Cytophotometric determination of protein-bound sulfhydryl groups. *Science* **116,** 323–327.

Caspersson, T. (1936). Über die chemischen Aufbau des Struktur des Zellkernes. *Skandinav. Arch. Physiol.* **73** (Suppl. 8), 1–151.

Caspersson, T. (1950). "Cell Growth and Cell Function." W. W. North, New York.

Chandler, J. A. (1976). X-ray microanalysis in the electron microscope. *In* "Practical Methods in Electron Microscopy" (A. M. Glauert, Ed.), pp. 319–547. North Holland, Amsterdam.

Chen, S., Gao, F., Kotani, A., and Nagata, T. (1995). Age-related changes of male mouse submandibular gland: A morphometric and radioautographic study. *Cell. Mol. Biol.* **41,** 117–124.

Christensen, A. K. (1971). Frozen thin sections of fresh tissue for electron microscopy, with a description of pancreas and liver. *J. Cell Biol.* **51,** 772–804.

Clermont, Y. (1963). Renewal of spermatogonia in man. *Am. J. Anat.* **112,** 35–51.

Coons, A. H., Creech, H. J., and Jones, R. N. (1941). Immunological properties of an antibody containing a fluorescent group. *Proc. Exp. Biol. (NY)* **47,** 200–202.

Cui, H. (1995). Light microscopic radioautographic study on DNA synthesis of nerve cells in the cerebella of aging mice. *Cell. Mol. Biol.* **41,** 1139–1154.

Cui, H., Gao, F., and Nagata, T. (2000). Light microscopic radioautographic study on protein synthesis in perinatal mice corneas. *Acta Histochem. Cytochem.* **33,** 31–37.

Daddi, L. (1896). Nouvelle methode pour colorer la graisse dans les tissue. *Arch. Ital. Biol.* **26,** 143–146.

Danielli, J. F. (1953). "Cytochemistry, A Critical Approach." Wiley, New York, Chapman and Hall, London.

Dean, P. N. (1985). Methods of data analysis in flow cytometry. *In* "Flow Cytometry: Instrumentation and Data Analysis" (M. A. van Dilli, P. N. Dean, O. D. Laerum, and M. R. Melamed, Eds.), pp. 195–223. Academic Press, London.

Deitch, A. D. (1955). Microspectrophotometric study of the binding of the anionic dye, naphthol yellow S by tissue sections and by purified proteins. *Lab. Invest.* **4,** 324–351.

Deitch, A. D. (1961). An improved Sakaguchi reaction for microspectrophotometric use. *J. Histochem. Cytochem.* **9,** 477–483.

Duan, H., Gao, F., Li, S., Hayashi, K., and Nagata, T. (1992). Aging changes and fine structure and DNA synthesis of esophageal epithelium in neonatal, adult and old mice. *J. Clin. Electron Microsc.* **25,** 452–453.

Duan, H., Gao, F., Li, S., and Nagata, T. (1993). Postnatal development of esophageal epithelium in mouse: A light and electron microscopic radioautographic study. *Cell. Mol. Biol.* **39,** 309–316.

Duan, H., Gao, F., Oguchi, K., and Nagata, T. (1994). Light and electron microscopic radioautographic study on the incorporation of 3H-thymidine into the lung by means of a new nebulizer. *Drug Res.* **44,** 880–883.

Duan, H., and Nagata, T. (1993). Glomerular extracellular matrices and anionic sites in aging ddY mice: A morphometric study. *Histochemistry* **99,** 81–91.

Edwards, L. C., and Udupa, K. N. (1957). Autoradiographic determination of S35 in tissues after injection of methionin-S35 and sodium sulfate-S35 *J. Biophys. Biochem. Cytol.* **3,** 757–770.

Enzyme Committee (1979). "Recommendations of the Nomenclature Committee of the International Union of Biochemistry on the Nomenclature and Classification of Enzymes." Academic Press, New York, San Francisco, London.

Eränkö, O. (1955). "Quantitative Methods in Histology and Microscopic Histochemistry." Karger, Basel and New York.

Fand, S. B., and Thorell, B. (1962). Spectrophotometry of periodic acid-Schiff reaction with pituitary hormones in vitro and in histological sections. *J. Cell Biol.* **13,** 239–247.

Fernandez-Moran, H. (1952). Application of ultra-thin freezing sectioning technique to the study of cell structure with electron microscopy. *Arkiv. Phys.* **4,** 471–475.

Feulgen, R., and Rossenbeck, H. (1924). Mikroskopisch-chemischetr Nachweiss einen Nukleinsäure von Typus der Thymonukleinsäure. *Z. Physik. Chem.* **135,** 203–248.

Flax, M. H., and Himes, M. H. (1952). Microspectrophotometric analysis of metachromatic staining of nucleic acids. *Physiol. Zool.* **25,** 297–311.

Fujii, Y., Ohno, S., Yamabayashi, S., Usuda, N., Saito, H., Furuta, S., and Nagata, T. (1980). Electron microscopic radioautography of DNA synthesis in primary cultured cells from an IgG myeolma patient. *J. Clin. Electron Microsc.* **13,** 582–583.

Fujiwara, I., Nagata, T., and Shimamura, K. (1957). On the distribution of calcium in the stratified squamous epithelia. *Acta Anat. Nippon.* **32,** 305–310.

Futaesaku, Y., and Mizuhira, V. (1986). Negative-staining autoradiography: A new technique for ultracryotomy utilizing an interposed film. *J. Histochem. Cytochem.* **34,** 1085–1094.

Gahrton, G. (1966). Normal human neutrophil leukocytes as a reference system for the microspectrophotometrically quantitated periodic acid-Schoff reaction. *J. Histochem. Cytochem.* **14,** 45–48.

Gao, F. (1993). Study on the macromolecular synthesis in aging mouse seminiferous tubules by light and electron microscopic radioautography. *Cell. Mol. Biol.* **39,** 659–672.

Gao, F., Chen, S., Sun, L., Kang, W., Wang, Z., and Nagata, T. (1995a). Radioautographic study of the macromolecular synthesis of Leydig cells in aging mice testis. *Cell. Mol. Biol.* **41,** 145–150.

Gao, F., Jin, C., Ma, H., Sun, L., and Nagata, T. (1995b). Ultrastructural and radioautographic studies on DNA synthesis in Leydig cells of aging mouse testis. *Cell. Mol. Biol.* **41,** 151–160.

Gao, F., Li, S., Duan, H., Ma, H., and Nagata, T. (1992b). Electron microscopic radioautography on the DNA synthesis of prenatal and postnatal mice retina after labeled thymidine injection. *J. Clin. Electron Microsc.* **25,** 721–722.

Gao, F., Ma, H., Sun, L., Jin, C., and Nagata, T. (1994). Electron microscopic radioautographic study on the nucleic acids and protein synthesis in the aging mouse testis. *Med. Electron Microsc.* **27,** 360–362.

Gao, F., Toriyama, K., Ma, H., and Nagata, T. (1993). Light microscopic radioautographic study on DNA synthesis in aging mice corneas. *Cell. Mol. Biol.* **39,** 435–441.

Gao, F., Toriyama, K., and Nagata, T. (1992a). Light microscopic radioautographic study on the DNA synthesis of prenatal and postnatal aging mouse retina after labeled thymidine injection. *Cell. Mol. Biol.* **38,** 661–668.

Gersh, I. (1932). The Altmann technique for fixation by drying while freezing. *Anat. Rec.* **53,** 309–324.

Gersh, I. (1956). The preparation of frozen–dried tissues for electron microscopy. *J. Biophys. Biochem. Cytol.* **2**(Suppl.), 37–43.

Glick, D. (1949). "Technique of Histo- and Cyto-chemistry." Interscience, New York.

Goldstein, I. J., and Hayes, C. E. (1978). The lectins: Carbohydrate-binding proteins of plants and animals. *Adv. Carbohydr. Chem. Biochem.* **35,** 127–340.

Gomori, G. (1939). Microtechnical demonstration of phosphatase in tissue sections. *Proc. Soc. Exp. Biol. Med.* **42,** 23–26.

Gomori, G. (1952). "Microscopic Histochemistry." Chicago Univ. Press, Chicago.

Graumann, W., and Neumann, K. (Eds.) (1958–1974). "Handbuch der Histochemie," Band 1, Erster Teil, Allgemeine Methodik, 697 Seiten. Gustav Fischer Verlag, Stuttgart, 1958. [Band II, III, IV, V, VI, VII, VIII, 1974].

Gunarso, W. (1984a). Radioautographic studies on the nucleic acid synthesis of the retina of chick embryo. I. Light microscopic radioautography. *Shinshu Med. J.* **32,** 231–240.

Gunarso, W. (1984b). Radioautographic studies on the nucleic acid synthesis of the retina of chick embryo. I. Electron microscopic radioautography. *Shinshu Med. J.* **32,** 241–248.

Gunarso, W., Gao, F., Cui, H., Ma, H., and Nagata, T. (1996). A light and electron microscopic radioautographic study on RNA synthesis in the retina of chick embryo. *Acta Histochem.* **98,** 309–322.

Gunarso, W., Gao, F., and Nagata, T. (1997). Development and DNA synthesis in the retina of chick embryo observed by light and electron microscopic radioautography. *Cell. Mol. Biol.* **43,** 189–201.

Hanai, T. (1993). Light microscopic radioautographic study of DNA synthesis in the kidneys of aging mice. *Cell. Mol. Biol.* **39,** 81–91.

Hanai, T., and Nagata, T. (1994a). Study on the nucleic acid synthesis in the aging mouse kidney by light and electron microscopic radioautography. *In* "Radioautography in Medicine" (T. Nagata, Ed.), pp. 209–214. Shinshu University Press, Matsumoto.

Hanai, T., and Nagata, T. (1994b). Electron microscopic study on nucleic acid synthesis in perinatal mouse kidney tissue. *Med. Electron Microsc.* **27,** 355–357.

Hanai, T., Usuda, N., Morita, T., and Nagata, T. (1994a). Light microscopic lectin histochemistry in aging mouse kidney: Study of compositional changes in glycoconjugates. *J. Histochem. Cytochem.* **42,** 897–906.

Hanai, T., Usuda, N., Morita, T., and Nagata, T. (1994b). Correspondence to changes in lectin binding pattern during fetal and postnatal development of renal corpuscles of rat kidney as revealed by light and electron microscopy. *Acta Histochem. Cytochem.* **27,** 185–188.

Hanai, T., Usuda, N., Morita, T., and Nagata, T. (1994c). Light microscopic lectin histochemistry in aging mouse kidney: Study of compositional changes in glycoconjugates. *J. Histochem. Cytochem.* **42,** 897–906.

Hanai, T., Usuda, N., Morita, T., and Nagata, T. (1994d). Changes in lectin binding pattern during fetal and postnatal development of renal corpuscles of the rat kidney as revealed by light and electron microscopy. *Acta Histochem. Cytochem.* **27,** 185–188.

Hanai, T., Usuda, N., Morita, T., Shimizu, T., and Nagata, T. (1993). Proliferative activity in the kidneys of aging mice evaluated by PCNA/cyclin immunohistochemistry. *Cell. Mol. Biol.* **39,** 181–191.

Hayashi, K., Gao, F., and Nagata, T. (1993). Radioautographic study on 3H-thymidine incorporation at different stages of muscle development in aging mice. *Cell. Mol. Biol.* **39,** 553–560.

Hayashi, K., and Nagata, T. (1991). Three-dimensional structure of the sarcoplasmic reticulum of skeletal myofibers in chicken and frog. *J. Submicrosc. Cytol. Pathol.* **23,** 509–517.

Hayat, M. A. (Ed.) (1972–1977). "Electron Microscopy of Enzymes, Principles and Methods," Vols. 1–5. Van Nostrand Reihhold, New York.

Hodges, G. M., and Muir, M. D. (1975). Quantitative evaluation of autoradiographs in X-ray spectroscopy. *J. Microsc.* **104,** 173–178.

Hsu, S. M., Raine, L., and Fanger, H. (1981). Use of avidin-biotin-peroxidase complex (ABC) in immunoperoxidase techniques: A comparison between ABC and unlabeled antibody (PAP) procedures. *J. Histochem. Cytochem.* **29,** 577–580.

Ichikawa, R., Hayashi, K., and Nagata, T. (1994). X-ray microanalysis of the secretory granules in the intestinal goblet cells of aging mice. *Med. Electron Microsc.* **27,** 337–339.

Iida, F., Murata, F., and Nagata, T. (1978). Histochemical studies of mucosubstances in metaplastic epithelium of the stomach, with special reference to the development of intestinal metaplasia. *Histochemistry* **56,** 229–237.

Ito, M. (1996). The radioautographic studies on aging change of DNA synthesis and the ultrastructural development of mouse adrenal gland. *Cell. Mol. Biol.* **42,** 279–292.

Ito, M., and Nagata, T. (1996). Electron microscopic radioautographic studies on DNA synthesis and ultrastructure of aging mouse adrenal gland. *Med. Electron Microsc.* **29,** 145–152.

Izumiyama, K., Kogure, K., Kataoka, S., and Nagata, T. (1987). Quantitative analysis of glucose after transient ischemia in the gerbil hippocampus by light and electron microscope radioautography. *Brain Res.* **416,** 175–179.

Jamieson, J. D., and Palade, G. E. (1967). Intracellular transport of secretory proteins in the pancreatic exocrine cells. *J. Cell Biol.* **34,** 577–615.

Jin, C. (1996). Study on DNA synthesis of aging mouse colon by light and electron microscopic radioautography. *Cell. Mol. Biol.* **42,** 255–268.

Jin, C., and Nagata, T. (1995a). Light microscopic radioautographic study on DNA synthesis in cecal epithelial cells of aging mice. *J. Histochem. Cytochem.* **43,** 1223–1228.

Jin, C., and Nagata, T. (1995b). Electron microscopic radioautographic study on DNA synthesis in cecal epithelial cells of aging mice. *Med. Electron Microsc.* **28,** 71–75.

Jobst, K., and Sandritter, W. (1965). Cytophotometric determinations of basic proteins of cell nuclei with basic dyes. *Nature* **206,** 204–204.

Joukura, K. (1996). The aging changes of glycoconjugate synthesis in mouse kidney studied by 3H-glucosamine radioautography. *Acta Histochem. Cytochem.* **29,** 57–63.

Joukura, K., and Nagata, T. (1995). Aging changes of 3H-glucosamine incorporation into mouse kidney observed by radioautography. *Acta Histochem. Cytochem.* **28,** 494–494.

Joukura, K., Usuda, N., and Nagata, T. (1996). Quantitative study on the aging change of glycoconjugates synthesis in aging mouse kidney. Proc. Xth Internat. Cong. Histochem. Cytochem. *Acta Histochem. Cytochem.* **29** (Suppl.), 507–508.

Kametani, K., Ichikawa, R., and Nagata, T. (1998). X-ray microanalysis of secretory granules in goblet cells of mouse intestinal tracts: Changes with age. *Med. Electron Microsc.* **31,** 107–114.

Karnovsky, M. J., and Roots, L. (1964). A "direct-coloring" thiocholine method for cholinesterase. *J. Histochem. Cytochem.* **12,** 219–221.

Kobayashi, K., and Nagata, T. (1994). Light microscopic radioautographic studies on DNA, RNA and protein syntheses in human synovial membranes of rheumatoid arthritis patients. *J. Histochem. Cytochem.* **42,** 982–982.

Kobayashi, S., Tsukahara, S., Sugita, K., Matuo, K., and Nagata, T. (1981b). Histochemical studies on the postnatal development of autonomic nerves in mice cerebral arteries. *Histochemistry* **73,** 15–20.

Kobayashi, S., Tsukahara, S., Sugita, K., and Nagata, T. (1981a). Adrenergic and cholinergic innervation of rat cerebral arteries, consecutive demonstration on whole mount preparations. *Histochemistry* **70,** 129–138.

Komiyama, K., Iida, F., Furihara, R., Murata, F., and Nagata, T. (1978). Electron microscopic radioautographic study on 125I-albumin in rat gastric mucosal epithelia. *J. Clin. Electron Microsc.* **11,** 428–429.

Kong, Y. (1993). Electron microscopic radioautographic study on DNA synthesis in perinatal mouse retina. *Cell. Mol. Biol.* **39,** 55–64.

Kong, Y., and Nagata, T. (1994). Electron microscopic radioautographic study on nucleic acid synthesis of perinatal mouse retina. *Med. Electron Microsc.* **27,** 366–368.

Kong, Y., Usuda, N., Morita, T., Hanai, T., and Nagata, T. (1992b). Study on RNA synthesis in the retina and retinal pigment epithelium of mice by light microscopic radioautography. *Cell. Mol. Biol.* **38,** 669–678.

Kong, Y., Usuda, N., and Nagata, T. (1992a). Radioautographic study on DNA synthesis of the retina and retinal pigment epithelium of developing mouse embryo. *Cell. Mol. Biol.* **38,** 263–272.

Leblond, C. P. (1981). The life history of cells in renewing systems. *Am. J. Anat.* **160,** 113–158.

Lehmann, C. G. (1842). "Lehrbuch der Physiologischen Chemie." Vogel, Leipzig.

Li, S. (1994). Relationship between cellular DNA synthesis, PCNA expression and sex steroid hormone receptor status in the developing mouse ovary, uterus and oviduct *Histochemistry* **102,** 405–413.

Li, S., Duan, H., and Nagata, T. (1994). Age-related alterations of proteoglycan in mouse tracheal cartilage matrix: An electron histochemical analysis with the cationic dye of polyethylenimine *Cell. Mol. Biol.* **40,** 129–135.

Li, S., Gao, F., Duan, H., and Nagata, T. (1992). Radioautographic study on the uptake of $^{35}SO_4$ in mouse ovary during the estrus cycle *J. Clin. Electron Microsc.* **25,** 709–710.

Li, S., and Nagata, T. (1995). Nucleic acid synthesis in the developing mouse ovary, uterus and oviduct studied by light and electron microscopic radioautography *Cell. Mol. Biol.* **41,** 185–195.

Liang, Y. (1998). Light microscopic radioautographic study on RNA synthesis in the adrenal glands of aging mice *Acta Histochem. Cytochem.* **31,** 203–210.

Liang, Y., Ito, M., and Nagata, T. (1999). Light and electron microscopic radioautographic studies on RNA synthesis in aging mouse adrenal gland. *Acta Anat. Nippon.* **74,** 291–300.

Lillie, R. D. (1944). Various oil soluble dyes as fat stains in supersaturated isopropanol technic. *Stain Technol.* **19,** 55–58.

Lillie, R. D. (1954). "Histopathologic Technique and Practical Histochemistry," 1st ed. Blackistone, New York.

Lillie, R. D., and Fullmer, H. M. (1976). "Histopathologic Technic and Practical Histochemistry," 4th ed. Blackistone, New York, San Francisco, Toronto.

Lison, L. (1936). "Histochimie et Cytochimie Animales, Principles et Methodes." Gauthier-Villars, Paris.

Ma, H. (1988). Light microscopic radioautographic study on DNA synthesis of the livers in aging mice. *Acta Anat. Nippon.* **63,** 137–147.

Ma, H., Gao, F., Olea, M. T., and Nagata, T. (1991). Protein synthesis in the livers of aging mice studied by electron microscopic radioautography. *Cell. Mol. Biol.* **37,** 607–615.

Ma, H., and Nagata, T. (1988a). Electron microscopic radioautographic study on DNA synthesis of the livers in aging mice. *J. Clin. Electron Microsc.* **21,** 335–343.

Ma, H., and Nagata, T. (1988b). Studies on DNA synthesis of aging mice by means of electron microscopic radioautography. *J. Clin. Electron Microsc.* **21,** 715–716.

Ma, H., and Nagata, T. (1990a). Electron microscopic radioautographic studies on DNA synthesis in the hepatocytes of aging mice as observed by image analysis. *Cell. Mol. Biol.* **36,** 73–84.

Ma, H., and Nagata, T. (1990b). Study on RNA synthesis in the livers of aging mice by means of electron microscopic radioautography. *Cell. Mol. Biol.* **36,** 589–600.

Ma, H., and Nagata, T. (2000). Collagen and protein synthesis in the livers of aging mice as studied by electron microscopic radioautography. *Ann. Microsc.* **1,** 13–22.

MacManus, J. F. A. (1948). Histological and histochemical uses of periodic acid. *Stain Technol.* **23,** 99–102.

Maruyama, M., and Nagata, T. (1987). X-ray microanalysis with a high voltage electron microscope quantifying sulfur in colonic goblet cells of aging mice. *J. Clin. Electron Microsc.* **20,** 678–679.

Matsumura, H., Kobayashi, Y., Kobayashi, K., and Nagata, T. (1994). Light microscopic radioautographic study of DNA synthesis in the lung of aging salamander, Hynobius nebulosus. *J. Histochem. Cytochem.* **42,** 1004–1004.

Mayahara, H., and Chang, J. P. (1978). Electron microscopic study of acid phosphatase activity in cultured human cystic fibrosis fibroblasts. *Acta Histochem. Cytochem.* **11,** 449–459.

Mazia, D., Brewer, P. A., and Alfert, M. (1953). Cytochemical staining and measurement of protein with mercuric bromphenol blue. *Biol. Bull.* **104,** 57–64.

Mellors, R. C. (1955). "Analytical Cytology." McGraw Hill, New York.

Miescher, F. (1874). "Ein Beitrag zur Histochemie." Vogel, Leipzig.

Miller, O. L., Jr., Stone, G. E., and Prescott, D. M. (1964). Autoradiography of soluble materials. *J. Cell Biol.* **23,** 654–658.

Mizuhira, V., Shiihashi, M., and Futaesaku, Y. (1981). High-speed electron microscope autoradiographic studies of diffusible compounds. *J. Histochem. Cytochem.* **29,** 143–160.

Mizuhira, V., Uchida, K., Totsu, J., and Shindo, H. (1968). Studies on the absorption of S-benzoyl-thiamine O-monophosphate. *Vitamins (Tokyo)* **38,** 334–346.

Momose, Y., and Nagata, T. (1993). Radioautographic study on the intracellular localization of a hypolipidemic agent, bezafibrate, a peroxisome proliferator, in cultured rat hepatocytes *Cell. Mol. Biol.* **39,** 773–781.

Momose, Y., Naito, J., and Nagata, T. (1989). Radioautographic study on the localization of an antiallergic agent, tranilast, in the rat liver *Cell. Mol. Biol.* **35,** 347–355.

Momose, Y., Naito, J., Suzawa, H., Kanzawa, M., and Nagata, T. (1995). Radioautographic study on the intracellular localization of bezafibrate in cultured rat hepatoctyes. *Acta Histochem. Cytochem.* **28,** 61–66.

Momose, Y., Shibata, N., Kiyosawa, I., Naito, J., Watanabe, T., Horie, S., Yamada, J., Suga, T., and Nagata, T. (1993). Morphometric evaluation of species differences in the effects of bezafibrate, a hypolipidemic agent, on hepatic peroxisomes and mitochondria. *J. Toxicol. Pathol.* **6,** 33–45.

Morita, T. (1993). Radioautographic study on the aging change of 3H-glucosamine uptake in mouse ileum. *Cell. Mol. Biol.* **39,** 875–884.

Morita, T., Hanai, T., Usuda, N., and Nagata, T. (1992). Electron microscopic lectin histochemistry of rat liver. *J. Clin. Electron Microsc.* **25,** 524–525.

Morita, T., Usuda, N., Hanai, T., Kong, Y., and Nagata, T. (1991). Lectin histochemistry of the developing and aging mice colons. *Acta Histochem. Cytochem.* **24,** 527–527.

Morita, T., Usuda, N., Hanai, T., Kong, Y., and Nagata, T. (1994b). Lectin histochemistry of the developing and aging mice colons. *Acta Histochem. Cytochem.* **24,** 527–527.

Morita, T., Usuda, N., Hanai, T., and Nagata, T. (1994a). Changes of colon epithelium proliferation due to individual aging with PCNA/cyclin immunostaining comparing with 3H-thymidine radioautography. *Histochemistry* **101,** 13–20.

Murata, F., Momose, Y., and Nagata, T. (1977b). Demonstration of intracytoplasmic glycogen of megakaryocytes and blood platelets by means of the periodic acid–thiocarbohydrazide–silver proteinate method. *Histochemistry* **52,** 307–316.

Murata, F., Momose, Y., Yoshida, K., and Nagata, T. (1977c). Incorporation of 3H-thymidine into the nucleus of mast cells in adult rat peritoneum *Shinshu Med. J.* **25,** 72–77.

Murata, F., Momose, Y., Yoshida, K., Ohno, S., and Nagata, T. (1977d). Nucleic acid and mucosubstance metabolism of mastocytoma cells by means of electron microscopic radioautography. *Acta Pharmacol. Toxicol.* **41,** 58–59.

Murata, F., and Nagata, T. (1976). Fine structure and acid mucosubstance localization of the human basophilic leukocytes. *J. Clin. Electron Microsc.* **9,** 207–214.

Murata, F., Nagata, T., and Spicer, S. S. (1975). Fine structural localization of arylsulfatase B activity in the rabbit blood platelets. *Histochemistry* **44,** 307–312.

Murata, F., Wholtman, H., Spicer, S. S., and Nagata, T. (1977a). Fine structural and ultracytochemical studies on the lymphocytes in three types of genetic mucopolysaccharidoses. *Virchows Arch. B Cell Pathol.* **25,** 61–73.

Murata, F., Yokota, S., and Nagata, T. (1968). Electron microscopic demonstration of lipase in pancreatic acinar cells of mouse. *Histochemie* **13,** 215–222.

Murata, F., Yoshida, K., Ohno, S., and Nagata, T. (1978a). Ultrastructural localization of glycogen in the granulocytes of normal rabbit bone marrow. *Histochemistry* **58,** 103–111.

Murata, F., Yoshida, K., Ohno, S., and Nagata, T. (1978b). Ultrastructural and electron microscopic radioautographic studies on the mastocytoma cells and mast cells. *J. Clin. Electron Microsc.* **11,** 561–562.

Murata, F., Yoshida, K., Ohno, S., and Nagata, T. (1979). Mucosubstances of rabbit granulocytes studied by means of electron microscopic radioautography and X-ray microanalysis. *Histochemistry* **61,** 139–150.

Murayama, T., Usuda, N., and Nagata, T. (1986). Effects of thyrotropic hormone on the thyroid carcinoma in primary culture. *Tissue Culture (Tokyo)* **12,** 258–263.

Nagata, T. (1956). On the relationship between cell division and cytochrome oxidase in the Yoshida sarcoma cells. *Shinshu Med. J.* **5,** 383–386.

Nagata, T. (1961a). Quantification of DNA contents in rat hepatocytes by means of microspectrophotometry, with special reference to binucleate cells. *Arch. Histol. Jpn.* **22,** 81–82.

Nagata, T. (1961b). A new method for preparing specimens suitable to micropectrophotometry of binucleate cell nuclei stained with the Feulgen reaction. *Med. J. Shinshu Univ.* **6,** 137–141.

Nagata, T. (1961c). A quantitative study of the DNA contents in rat hepatic cell nuclei by means of microspectrophotometry, with special reference to binucleate cells. *Med. J. Shinshu Univ.* **6,** 143–153.

Nagata, T. (1962). A radioautographic study of the DNA synthesis in rat liver, with special reference to binucleate cells. *Med. J. Shinshu Univ.* **7,** 17–25.

Nagata, T. (1965). A quantitative study on the ganglion cells in the small intestine of the dog. *Med. J. Shinshu Univ.* **10,** 1–11.

Nagata, T. (1966a). Theory and application of microspectrophotometry: Introduction to quantitative histochemistry. *Shinshu Med. J.* **15,** 148–157.

Nagata, T. (1966b). A radioautographic study on the RNA synthesis in the hepatic and the intestinal epithelial cells of mice after feeding with special reference to binuclearity. *Med. J. Shinshu Univ.* **11,** 49–61.

Nagata, T. (1967a). On the increase of binucleate cells in the ganglion cells of dog small intestine due to experimental ischemia. *Med. J. Shinshu Univ.* **12,** 93–113.

Nagata, T. (1967b). A radioautographic study on the protein synthesis in the hepatic and the intestinal epithelial cells of mice, with special reference to binucleate cells. *Med. J. Shinshu Univ.* **12,** 247–257.

Nagata, T. (1972a). Application of microspectrophotometry to various substances. *In* "Introduction to Microspectrophotometry" (S. Isaka, T. Nagata, and N. Inui, Eds.), Chap. 3, pp. 49–155. Olympus, Tokyo.

Nagata, T. (1972b). Electron microscopic dry-mounting autoradiography "Proceedings, 4th International Congress of Histochemistry and Cytochemistry" (Kyoto), pp. 43–44.

Nagata, T. (1972c). Electron microscopic radioautography of intramitochondrial RNA synthesis of HeLa cells in culture. *Histochemie* **32,** 163–170.

Nagata, T. (1972d). Quantitative electron microscope radioautogrphy of intramitochondrial nucleic acid synthesis. *Acta Histochem. Cytochem.* **5,** 201–203.

Nagata, T. (1974). Lipase. *In* "Electron Microscopy of Enzymes, Principles and Methods" (M. A. Hayat, Ed.), Vol. 2, Chap. 7, pp.132–148. Van Nostrand Reinhold, New York.

Nagata, T. (1991). Electron microscopic radioautography and analytical electron microscopy *J. Clin. Electron Microsc.* **24,** 441–442.

Nagata, T. (1992). Radiolabeling of soluble and insoluble compounds as demonstrated by light and electron microscopy. *In* "Recent Advances in Cellular and Molecular Biology" (R. J. Wegmann and M. A. Wegmann, Eds.), Vol. 6, pp. 9–21. Peeters, Leuven.

Nagata, T. (1993). Quantitative analysis of histochemical reactions: Image analysis of light and electron microscopic radioautograms. *Acta Histochem. Cytochem.* **26,** 281–291.

Nagata, T. (1994a). Introductory remarks to advances in cytochemistry with physical method *Acta Histochem. Cytochem.* **27,** 465–469.

Nagata, T. (1994b). Electron microscopic radioautography with cryo-fixation and dry-mounting procedure. *Acta Histochem. Cytochem.* **27,** 471–489.

Nagata, T. (1994c). Application of electron microscopic radioautography to clinical electron microscopy. *Med. Electron Microsc.* **27,** 191–212.

Nagata, T. (1994d). "Radioautography in Medicine." Shinshu Univ. Press, Matsumoto.

Nagata, T. (1995a). Light and electron microscopic radioautographic study on macromolecular synthesis in digestive organs of aging mice. *Cell. Mol. Biol.* **41,** 21–38.

Nagata, T. (1995b). Histochemistry of the organs: Application of histochemistry to anatomy. *Acta Anat. Nippon.* **70,** 448–471.

Nagata, T. (1995c). Three-dimensional observation of whole mount cultured cells stained with histochemical reactions by ultrahigh voltage electron microscopy *Cell. Mol. Biol.* **41,** 783–792.

Nagata, T. (1996a). Technique and application of electron microscopic radioautography. *J. Electron Microsc.* **45,** 258–274.

Nagata, T. (1996b). Techniques of light and electron microscopic radioautography. *Acta Histochem. Cytochem.* **29** (Suppl.), 343–344.

Nagata, T. (1997a). Techniques and applications of microscopic radioautography. *Histol. Histopathol.* **12,** 1091–1124.

Nagata, T. (1997b). Three-dimensional observation on whole mount cultured cells and thick sections stained with histochemical reactions by high voltage electron microscopy. *In* "Recent Advances in Microscopy of Cells, Tissues and Organs" (P. Motta, Ed.), pp. 37–44. Antonio Delfino Editore, Roma, Italy.

Nagata, T. (1997c). Radioautographic study on collagen synthesis in the ocular tissues. *J. Kaken Eye Res.* **15,** 1–9.

Nagata, T. (1998a). Techniques of radioautography for medical and biological research. *Braz. J. Biol. Med. Res.* **31,** 185–195.

Nagata, T. (1998b). Radioautographology, the advocacy of a new concept. *Braz. J. Biol. Med. Res.* **31,** 201–241.

Nagata, T. (1998c). Radioautographic studies on DNA synthesis of the bone and skin of aging salamander. *Bull. Nagano Women's Jr. College* **6,** 1–14.

Nagata, T. (1999a). 3D observation of cell organelles by high voltage electron microscopy. *Microsc. Anal. Asia Pacific Ed.* **9,** 29–32.

Nagata, T. (1999b). Application of histochemistry to anatomy: Histochemistry of the organs, a novel concept. Proc. XV Congress of the International Federation of Associations of Anatomists. *Ital. J. Anat. Embryol.* **104** (Suppl. 1), 486–486.

Nagata, T. (1999c). Aging changes of macromolecular synthesis in various organ systems as observed by microscopic radioautography after incorporation of radiolabeled precursors. *Methods Find. Exp. Clin. Pharmacol.* **21,** 683–706.

Nagata, T. (1999d). Radioautographic study on the aging changes of mouse tracheal cartilage. *Acta Histochem. Cytochem.* **32,** 530–530.

Nagata, T. (1999e). Radioautographic Study on protein synthesis in mouse cornea. *J. Kaken Eye Res.* **8,** 8–14.

Nagata, T. (2000a). Three-dimensional observations on thick biological specimens by high voltage electron microscopy. *Image Anal. Stereol.* **19,** 51–56.

Nagata, T. (2000b). Study of the effects of aging on macromolecular synthesis in mouse steroid secreting cells using microscopic radioautography. *Methods Find. Exp. Clin. Pharmacol.* **22,** 5–18.

Nagata, T. (2000c). Special radioautographology: The eye. *J. Kaken Eye Res.* **18,** 1–13.

Nagata, T. (2000d). Biological microanalysis of radiolabeled and unlabeled compounds by radioautography and X-ray microanalysis. *Scanning Microsc. Int.* **14,** on line.

Nagata, T. (2000e). Electron microscopic radioautographic study on protein synthesis in pancreatic cells of perinatal and aging mice. *Bull. Nagano Women's Jr. Coll.* **8,** 1–22.

Nagata, T. (2000f). Light microscopic radioautographic study on radiosulfate incorporation into the tracheal cartilage in aging mice. *Acta Histochem. Cytochem.* **33,** 377–383.

Nagata, T. (2001). Three-dimensional high voltage electron microscopy of thick biological specimens. *Micron* **32,** 387–404.

Nagata, T., Cui, H., and Gao, F. (1995). Radioautographic study on glycoprotein synthesis in the ocular tissues. *J. Kaken Eye Res.* **13,** 11–18.

Nagata, T., Cui, H., and Kong, Y. (1999b). The localization of TGF-1 and its mRNA in the spinal cords of prenatal and postnatal aging mice demonstrated with immunohistochemical and in situ hybridization techniques. *Bull. Nagano Women's Jr. Coll.* **7,** 75–88.

Nagata, T., Fujiwara, I., and Shimamura, K. (1957a). On the argentaffine reaction of melanins and their precursors. *Shinshu Med. J.* **6,** 515–517.

Nagata, T., Fujiwara, I., and Shimamura, K. (1957b). On the distribution of calcium in the stratified squamous epithelia. *Acta Anat. Nippon* **32,** 305–310.

Nagata, T., Hirano, I., Shibata, O., and Nagata, T. (1966). A radioautographic study on the DNA synthesis in the hepatic and the pancreatic acinar cells of mice during the postnatal growth, with special reference to binuclearity. *Med. J. Shinshu Univ.* **11,** 35–42.

Nagata, T., Ito, M., and Chen, S. (2000b). Aging changes of Dna synthesis in the submandibular glands of mice as observed by light and electron microscopic radioautography. *Ann. Microsc.* **1,** 4–12.

Nagata, T., Ito, M., and Liang, Y. (2000a). Study of the effects of aging on macromolecular synthesis in mouse steroid secreting cells using microscopic radioautography. *Methods Find. Exp. Clin. Pharmacol.* **22,** 5–18.

Nagata, T., and Iwadare, N. (1984). Electron microscopic demonstration of phospholipase B activity in the liver and the kidney of the mouse. *Histochemistry* **80,** 149–152.

Nagata, T., Iwadare, I., and Murata, F. (1977c). Electron microscopic radioautography of nucleic acid synthesis in cultured cells treated with several carcinogens. *Acta Pharmacol. Toxicol.* **41,** 64–65.

Nagata, T., Kametani, K., and Maruyama, M. (2000c). X-ray microanalysis of sulfur in cryo-fixed colonic goblet cells by high voltage electron microscopy. *Scanning Microsc. Int.* **14,** on line.

Nagata, T., and Kawahara, I. (1999). Radioautographic study of the synthesis of sulfomucin in digestive organs of mice. *J. Trace Microprobe Anal.* **17,** 339–355.

Nagata, T., Kawahara, I., Usuda, N., Maruyama, M., and Ma, H. (1988a). Radioautographic studies on the glycoconjugate synthesis in the gastrointestinal mucosa of the mouse. *In* "Glycoconjugate in Medicine" (M. Ohyama and T. Muramatsu, Eds.), pp. 251–256. Professional Postgrad. Service, Tokyo.

Nagata, T., and Kong, Y. (1998). Distribution and localization of TGF 1 and FGF, and their mRNAs in aging mice. *Bull. Nagano Women's Jr. Coll.* **6,** 87–105.

Nagata, T., and Kong, Y. (2000). Histochemical studies on the age-related changes in glycoconjugates of mouse ocular tissues as shown by lectin binding patterns. *Bull. Nagano Women's Jr. Coll.* **8,** 109–129.

Nagata, T., Morita, T., and I. Kawahara, I. (1999a). Radioautographic studies on radiosulfate incorporation in the digestive organs of mice. *Histol. Histopathol.* **14,** 1–8.

Nagata, T., and Murata, F. (1972). Supplemental studies on the method for electron microscopic demonstration of lipase in the pancreatic acinar cells of mice and rats. *Histochemie* **29,** 8–15.

Nagata, T., and Murata, F. (1977). Electron microscopic dry-mounting radioautography for diffusible compounds by means of ultracryotomy *Histochemistry* **54,** 75–82.

Nagata, T., and Murata, F. (1980). Esterase. *In* "Enzyme Histochemistry" (T. Takeuchi and K. Ogawa, Eds.), pp. 225–253. Asakura Shoten, Tokyo.

Nagata, T., Murata, F., and Yokota, S. (1968). On the lipase activity in the crystalloids in the pancreatic acinar cells of the mouse. *Med. J. Shinshu Univ.* **13,** 23–33.

Nagata, T., and Nawa, T. (1966a). A modification of dry-mounting technique for radioautography of water-soluble compounds. *Histochemie* **7,** 370–371.

Nagata, T., and Nawa, T. (1966b). A radioautographic study on the nucleic acids synthesis of binucleate cells in cultivated fibroblasts of chick embryos. *Med. J. Shinshu Univ.* **11,** 1–5.

Nagata, T., Nawa, T., and Yokota, S. (1969). A new technique for electron microscopic dry-mounting radioautography of soluble compounds. *Histochemie* **18,** 241–249.

Nagata, T., Nishigaki, T., and Momose, Y. (1986). Localization of anti-allergic agent in rat mast cells demonstrated by light and electron microscopic radioautography. *Acta Histochem. Cytochem.* **19,** 669–683.

Nagata, T., Ohno, S., and Murata, F. (1977a). Electron microscopic dry-mounting radioautography for soluble compounds. *Acta Phamacol. Toxicol.* **41,** 62–63.

Nagata, T., Ohno, S., Yoshida, K., and Murata, F. (1978). A simple picking-up device for cryosections. *Sci. Tools* **25,** 59–60.

Nagata, T., Ohno, S., Yoshida, K., and Murata, F. (1982). Nucleic acid synthesis in proliferating peroxisomes of rat liver as revealed by electron microscopical radioautography. *Histochem. J.* **14,** 197–204.

Nagata, T., and Olea, M. T. (1999). Electron microscopic radioautographic study on the protein synthesis in aging mouse spleen. *Bull. Nagano Women's Jr. Coll.* **7,** 1–9.

Nagata, T., Shibata, O., and Nawa, T. (1967). Incorporation of tritiated thymidine into mitochondrial DNA of the liver and kidney cells of chickens and mice in tissue culture. *Histochemie* **10,** 305–308.

Nagata, T., Shibata, O., and Omochi, S. (1961). A new method for radioautographic observation on isolated cells. *Histochemie* **2,** 255–259.

Nagata, T., and Shimamura, K. (1958). Radioautographic studies on calcium absorption. I. Calcium absorption in the stomach of rat. *Med. J. Shinshu Univ.* **3,** 83–90.

Nagata, T., and Shimamura, K. (1959a). Radioautographic studies on calcium absorption. II. Calcium absorption in the intestines of rat. *Med. J. Shinshu Univ.* **4,** 1–10.

Nagata, T., and Shimamura, K. (1959b). Radioautographic studies on calcium absorption. III. Distribution of radiocalcium in the liver and the kidney of rat after oral administration. *Med. J. Shinshu Univ.* **4,** 11–18.

Nagata, T., and Steggerda, F. R. (1963). Histological study on the deganglionated small intestine of the dog. *Physiologist* **6,** 242–242.

Nagata, T., and Steggerda, F. R. (1964). Observations on the increase of binucleate cells in the ganglion cells of the dog's intestine due to experimental ischemia. *Anat. Rec.* **148,** 315–315.

Nagata, T., Toriyama, K., Kong, Y., Jin, C., and Gao, F. (1994). Radioautographic study on DNA synthesis in the ciliary bodies of aging mice. *J. Kaken Eye Res.* **12,** 1–11.

Nagata, T., and Usuda, N. (1985). Image processing of electron microscopic radioautograms in clinical electron microscopy. *J. Clin. Electron Microsc.* **18,** 451–452.

Nagata, T., and Usuda, N. (1986). Studies on the nucleic acid synthesis in pancreatic acinar cells of aging mice by means of electron microscopic radioautography. *J. Clin. Electron Microsc.* **19,** 486–487.

Nagata, T., and Usuda, N. (1993). Electron microscopic radioautography of protein synthesis in pancreatic acinar cells of aging mice. *Acta Histochem. Cytochem.* **26,** 481–481.

Nagata, T., Usuda, N., and Ma, H. (1984). Electron microscopic radioautography of nucleic acid synthesis in pancreatic acinar cells of prenatal and postnatal aging mice. *Proc. XIth Int. Cong. Electron Microsc.* **3,** 2281–2282.

Nagata, T., Usuda, N., and Ma, H. (1990). Electron microscopic radioautography of lipid synthesis in pancreatic cells of aging mice. *J. Clin. Electr. Microsc.* **23,** 841–842.

Nagata, T., Usuda, N., Maruyama, M., and Ma, H. (1988b). Electron microscopic radioautographic study on lipid synthesis in perinatal mouse pancreas. *J. Clin. Electr. Microsc.* **21,** 756–757.

Nagata, T., Usuda, N., Suzawa, H., and Kanzawa, M. (1992). Incorporation of 3H-glucosamine into the pancreatic cells of aging mice as demonstrated by electron microscopic radioautography. *J. Clin. Electron Microsc.* **25,** 646–647.

Nagata, T., and Yamabayashi, S. (1983). Intracellular localization of 3H-befunolol by means of electron microscopic radioautography of cryo-fixed ultrathin sections. *J. Clin. Electron Microsc.* **16,** 737–738.

Nagata, T., Yoshida, K., and Murata, F. (1977b). Demonstration of hot and cold mercury in the human thyroid tissues by means of radioautography and chemography. *Acta Pharmacol. Toxicol.* **41,** 60–61.

Naora, H. (1951). Microspectrophotometry and cytochemical analysis of nucleic acids. *Science* **114,** 279–280.

Nawa, T., Nagata, T., and Omochi, S. (1965). An apparatus for freeze-drying of tissue. *Med. J. Shinshu Univ.* **10,** 1–11.

Nawa, T., Nagata, T., Yokota, S., Murata, F., and Omochi, S. (1969). Two new models of freeze–drying apparatus for tissues. *Med. J. Shinshu Univ.* **14,** 1–15.

Nishigaki, T., Momose, Y., and Nagata, T. (1987). Light microscopic radioautographic study of the localization of anti-allergic agent, Tranilast, in rat mast cells. *Histochem. J.* **19,** 533–536.

Nishigaki, T., Momose, Y., and Nagata, T. (1990). Localization of the anti-allergic agent tranilast in the urinary bladder of rat as demonstrated by light microscopic radioautography. *Drug Res.* **40,** 272–275.

Novikoff, A. B., and Goldfisher, S. (1961). Nucleoside diphosphatase activity in the Golgi apparatus and its usefulness for cytological studies. *Proc. Nat. Acad. Sci. USA* **47,** 802–810.

Nussdorfer, G. G. (1986). Cytophysiology of the adrenal cortex. *In* "International Review of Cytology" (G. H. Bourne, J. F. Danielli, and K. W. Jeon, Eds.), Vol. 98, pp. 1–405. Academic Press, New York.

Ogawa, K., and Barka, T. (Eds.) (1993). "Electron Microscopic Cytochemistry and Immunocytochemistry in Biomedicine." CRC Press, Boca Raton, Ann Arbor, London, Tokyo.

Oguchi, K., and Nagata, T. (1980). A radioautographic study of activated satellite cells in dystrophic chicken muscle. *In* "Current Research in Muscular Dystrophy Japan. Annual Report on Neurological Diseases 1980," pp. 16–17. Ministry of Welfare of Japan, Tokyo.

Oguchi, K., and Nagata, T. (1981). Electron microscopic radioautographic observation on activated satellite cells in dystrophy chickens. *In* "Clinical Studies on the Etiology of Muscular Dystrophy. Annual Report on Neurological Diseases 1981," pp. 30–33. Ministry of Welfare of Japan, Tokyo.

Ohno, S. (1985). Peroxisomes of the kidney. *In* "International Review of Cytology" (G. H. Bourne, J. F. Danielli, and K. W. Jeon, Eds.), Vol. 95, pp. 131–162. Academic Press, New York.

Ohno, S., Fujii, Y., Usuda, N., Murata, F., and Nagata, T. (1982). Peroxisome proliferation of rat kidney induced with DEHP. I. Numerical changes by light microscopic morphometry. *Acta Histochem. Cytochem.* **15,** 40–57.

Ohno, S., Murata, F., Yoshida, K., Tei, I., and Nagata, T. (1978). Ultrastructural changes of rat kidneys treated with DEHP. *J. Clin. Electron Microsc.* **11,** 841–842.

Ohno, S., Ohtake, N., Fujii, Y., Yamabayashi, S., Usuda, N., and Nagata, T. (1981). Histochemical studies on peroxisomes of rat livers during DEHP administration and after withdrawal of thick sections by means of light microscopic and high voltage electron microscopy. *Acta Histochem. Cytochem.* **14,** 125–142.

Olea, M. T. (1991). An ultrastructural localization of lysosomal acid phosphatase activity in aging mouse spleen: A quantitative X-ray microanalytical study. *Acta Histochem. Cytochem.* **24,** 201–208.

Olea, M. T., Ma, H., and Nagata, T. (1991). Quantitative assessment of lysosomal size, number and enzyme activity in mouse kidney during maturational development. *Cell Mol. Biol.* **37,** 679–685.

Olea, M. T., and Nagata, T. (1991). X-ray microanalysis of cerium in mouse spleen cells demonstrating acid phosphatase activity using high voltage electron microscopy. *Cell. Mol. Biol.* **37,** 155–163.

Olea, M. T., and Nagata, T. (1992a). Simultaneous localization of ^{3}H-thymidine incorporation and acid phosphatase activity in mouse spleen: EM radioautography and cytochemistry. *Cell. Mol. Biol.* **38,** 115–122.

Olea, M. T., and Nagata, T. (1992b). A radioautographic study on RNA synthesis in aging mouse spleen after ^{3}H-uridine labeling in vitro. *Cell. Mol. Biol.* **38,** 399–405.

Oliveira, S. F., Abrahamsohn, P. A., Nagata, T., and Zorn, T. M. T. (1995). Incorporation of ^{3}H-amino acids by endometrial stromal cells during decidualization in the mouse. A radioautographical study. *Cell. Mol. Biol.* **41,** 107–116.

Oliveira, S. F., Nagata, T., Abrahamsohn, P. A., and Zorn, T. M. T. (1991). Electron microscopic radioautographic study on the incorporation of ^{3}H-proline by mouse decidual cells. *Cell. Mol. Biol.* **37,** 315–323.

Ono, S. (1991). Electron microscopy and electron probe X-ray microanalysis of human lumbar yellow ligaments by frozen-dried cyrosections. *J. Clin. Electron Microsc.* **24,** 377–388.

Ono, S., and Nagata, T. (1988). X-ray microanalysis of Ca and S in human lumbar yellow ligaments. *J. Clin. Electron Microsc.* **21,** 644–645.

Ono, S., and Nagata, T. (1989). Electron microscopic observation on the ossification of human lumbar yellow ligaments. *J. Clin. Electron Microsc.* **22,** 723–724.

Ono, S., and Nagata, T. (1992). Electron microscopic study on human lumbar yellow ligaments with aging. *J. Clin. Electron Microsc.* **25,** 493–494.

Ono, S., Otsuka, K., Terayama, K., and Nagata, T. (1994). Quantitative electron probe X-ray microanalysis of calcium and phosphorus inhuman lumbar yellow ligaments. *Med. Electron Microsc.* **27,** 323–325.

Pearse, A. G. E. (1953). "Histochemistry, Theoretical and Applied," 1st ed., pp. 998. Little Brown, Boston.

Pearse, A. G. E. (1980–1991). "Histochemistry, Theoretical and Applied," (P. Stoward, Ed.), 4th ed., Vol. 1, 1980; Vol. 2, 1985; Vol. 3, 1991. Churchill Livingstone, Edinburgh, London, and New York.

Pollister, A. W., and Ris, H. (1947). Nucleoprotein determination in cytological preparations. *Cold Spring Harber Symp. Quant. Biol.* **12,** 147–157.

Rambourg, A. (1967). An improved silver methenamine technique for the detection of periodic acid-reactive complex. *J. Histochem. Cytochem.* **15,** 409–412.

Rasch, E., and Swift, H. (1960). Microphotometric analysis of the cytochemical Millon reaction. *J. Histochem. Cytochem.* **8,** 4–17.

Raspail, F. V. (1825). Development de la fécale dans le organes de la fructification des céréales et analyse microscopique de la fécale, suivie d'expériences propres àen expliquer la conversion en gomme. *Ann. Sci. Nat.* **6,** 224–239.

Raspail, F. V. (1830). "Essai de chimie microscopique appliquée à la physilogie." Paris.

Ritter, C., and Berman, J. (1963). The quantitative photometric analysis of tyrosine by a modified diazotization-coupling method. *J. Histochem. Cytochem.* **11,** 590–602.

Ritter, C., di Stefano, H. S., and Farah, A. (1961). A method for cytophotometric estimation of ribonucleic acid. *J. Histochem. Cytochem.* **9,** 97–102.

Roth, J. (1983). The colloidal gold marker system for light and electron microscopic cytochemistry. *In* "Techniques in Immunocytochemistry" (G. R. Bullock and P. Petrusz, Eds.), Vol. 2, pp. 217–284. Academic Press, London, New York.

Roth, J., Bendayan, M., and Orci, L. (1978). Ultrastructural localization of intracellular antigens by the use of protein A–gold complex. *J. Histochem. Cytochem.* **26,** 1074–1081.

Roth, J., and Binder, M. (1978). Colloidal gold, ferritin and peroxidase for electron microscopic double labeling lectin technique. *J. Histochem. Cytochem.* **26,** 163–169.

Sakai, Y., Ikado, S., and Nagata, T. (1977). Electron microscopic radioautography of satellite cells in regenerating muscles. *J. Clin. Electron Microsc.* **10,** 508–509.

Sato, A. (1978). Quantitative electron microscopic studies on the kinetics of secretory granules in G-cells. *Cell Tissue Res.* **187,** 45–59.

Sato, A., Iida, F., Furihara, R., and Nagata, T. (1977). Electron microscopic raioautography of rat stomach G-cells by means of ^{3}H-amino acids. *J. Clin. Electron Microsc.* **10,** 358–359.

Sauren, Y. M. H. F., Mierement, R. H. P., Groot, C. G., and Scherfft, J. P. (1991). Polyethyleneimine as a contrast agent for ultrastructural localization and characterization of proteoglycans in the matrix of cartilage and bone. *J. Histochem. Cytochem.* **39,** 331–340.

Scott, G. H., and Horning, H. (1953). Microincineration of tissues. *In* "Cytology and Cell Physiology" (G. H. Scott and H. Horning, Eds.), 2nd ed. Oxford.

Scott, J. E. (1972). The histochemistry of alcian blue. Note on the presence and removal of boric acid as the major diluent in alcian blue 8GX. *Histochemie* **29,** 129–133.

Schiff, H. (1865). Reagent for aldehyde. *Compt. Rend. Soc. Chim.* **61,** 45–46.

Schultz-Brauns, O. (1931). Eine neue Methode des Gefreirschneidens für Histologische Schnell-Untersuchungen. *Klin. Wochschrift.* **10,** 113–116.

Seligman, A. M., Karnovsky, M. J., Wasserkrug, H. L., and Hanker, J. S. (1968). Nondroplet ultra-structural demonstration of cytochrome oxidase activity with a polymerizing osmiophilic reagent, diaminobenzidine (DAB). *J. Cell Biol.* **38,** 1–14.

Sharon, N., and Lis, H. (1972). Lectins: Cell agglutinating and sugar specific proteins. *Science* **177,** 949–959.

Sheldon, H., Zetterqvist, H., and Brandis, O. (1955). Histochemical techniques for electron microscopy: Acid phosphatase. *Exp. Cell Res.* **9,** 592–596.

Shimada, M., and Watanabe, M. (1994). Recent progress in whole-body radioautography. *Cell. Mol. Biol.* **41,** 39–48.

Shimizu, T., Usuda, N., Sugenoya, A., Masuda, H., Hagiwara, M., Hidaka, H., Nagata, T., and Iida, F. (1991). Immunohistochemical evidence for the over-expression of protein kinase C in proliferative diseases of human thyroid. *Cell. Mol. Biol.* **37,** 812–821.

Shimizu, T., Usuda, N., Yamanda, T., Sugenoya, A., and Iida, F. (1993). Proliferative activity of human thyroid tumors evaluated by proliferating cell nuclear antigen/cyclin immunohistochemical studies. *Cancer* **71,** 2807–2812.

Singer, S. J. (1959). Preparation of electron dense antibody conjugate. *Nature* **183,** 1523–1524.

Smitherman, T. C., Debons, A. F., Pittman, J. A., and Stephens, V. (1963). Movement of water-soluble material in Mayer's albumin and a simplified dry-mounting method for autoradiography. *Nature* **198,** 499–500.

Sternberger, L. A. (1979). The unlabeled antibody peroxidase-antiperoxidase (PAP) method. *In* "Immunohistochemistry"(L. A. Sternberger, Ed.), pp. 104–164. Wiley, New York.

Stirling, C. E., and Kinter, W. B. (1967). High resolution radioautography of galactose-3H accumulation in rings of hamster intestine. *J. Cell Biol.* **35,** 585–604.

Sun, L. (1995). Age related changes of RNA synthesis in the lungs of aging mice by light and electron microscopic radioautography. *Cell. Mol. Biol.* **41,** 1061–1072.

Sun, L., Gao, F., Duan, H., and Nagata, T. (1994). Light microscopic radioautography of DNA synthesis in pulmonary cells in aging mice. *In* "Radioautography in Medicine"(T. Nagata, Ed.), pp. 201–205. Shinshu Univ. Press, Matsumoto.

Sun, L., Gao, F., Jin, C., and Nagata, T. (1997a). DNA synthesis in the tracheae of aging mice by means of light and electron microscopic radioautography. *Acta Histochem. Cytochem.* **30,** 211–220.

Sun, L., Gao, F., Jin, C., Duan, H., and Nagata, T. (1995b). An electron microscopic radioautographic study on the DNA synthesis of pulmonary tissue cells in aging mice. *Med. Electron Microsc.* **28,** 129–131.

Sun, L., Gao, F., and Nagata, T. (1995a). Study on the DNA synthesis of pulmonary cells in aging mice by light microscopic radioautography. *Cell. Mol. Biol.* **41,** 851–859.

Sun, L., Gao, F., and Nagata, T. (1997b). A light microscopic radioautographic study on protein synthesis in pulmonary cells of aging mice. *Acta Histochem. Cytochem.* **30,** 463–470.

Suzuki, K., Imada, T., Gao, F., Ma, H., and Nagata, T. (1994). Radioautographic study of benidipine hydrochloride: Localization in the mesenteric artery of spontaneously hypertensive rat. *Drug Res.* **44,** 129–133.

Takamatsu, H. (1938). Morphological study on alkaline phosphatase. *Manchurian Med. J.* **29,** 1351–1351. [in Japanese]

Takamatsu, H. (1939). Morphological demonstration of alkaline phosphatase. *Trans. Soc. Pathol. Jpn.* **29,** 492–492. [in Japanese]

Takebe, H. (1992). Morphological changes in the hepatocyte peroxisomes by age in mice administered with an anti-hyperlipidemic agent, clofibrate. *J. Clin. Electron Microsc.* **25,** 95–110.

Takebe, H., and Nagata, T. (1986). Effect of an aantihyperlipidemic (clofibrate) to the morphological changes of peroxisomes in hepatocytes in aging mice. *Proc. XIth Internat. Cong. Electron Microsc.* **3,** 2581–2582.

Tei, I., Murata, F., Yoshida, K., Ohno, S., Iida, F., Furihara, R., Katsuyama, T., and Nagata, T. (1978). Ultrastructural localization of PA-TCH-SP positive substances in the human gastric scirrhus. *J. Clin. Electron Microsc.* **11,** 467–468.

Terauchi, A., Mori, T., Kanda, H., Tsukada, M., and Nagata, T. (1988). Radioautographic study of 3H-taurine uptake in mouse skeletal muscle cells. *J. Clin. Electron Microsc.* **21,** 627–628.

Terauchi, A., and Nagata, T. (1993). Observation on incorporation of 3H-taurine in mouse skeletal muscle cells by light and electron microscopic radioautography. *Cell. Mol. Biol.* **39,** 397–404.

Thiéry, J. P. (1967). Mise en évidence des polysaccharides sur coupes fines en microscopie électronique. *J. Microscopie* **6,** 987–1018.

Tice, L. W., and Barrnett, R. J. (1962). The fine structural localization of glucose-6-phosphatase in rat liver. *J. Histochem. Cytochem.* **10,** 754–762.

Toriyama, K. (1995). Study on the aging changes of DNA and protein synthesis of bipolar and photo-receptor cells of mouse retina by light and electron microscopic radioautography. *Cell. Mol. Biol.* **41,** 593–601.

Tsukahara, S., Yoshida, K., and Nagata, T. (1980). A radioautographic study on the incorporation of ^{14}C-bupranolol (beta-blocking agent) into the rabbit eye. *Histochemistry* **68,** 237–244.

Tsukahara, S., Kobayashi, S., Sugita, K., and Nagata, T. (1982). Histochemical study of the postnatal development of autonomic nerve in the mouse iris, using a whole-mount preparation method. *Histochemistry* **74,** 481–486.

Ullberg, S. (1954). Studies on the distribution and fate of S35-labelled benzylpenicillin in the body. *Acta Radiol.* **118,** 1–110.

Ullberg, S. (1977). The techniques of whole body autoradiography. Cryosectioning of large specimens. *Sci. Tools* (Special Issue) 195–199.

Usuda, N. (1985). Immunohistochemical localization of low molecular weight plasm proteins in the human kidney. *J. Clin. Electron Microsc.* **18,** 389–399.

Usuda, N., Hanai, T., and Nagata, T. (1995). Immunogold studies on peroxisomes: Review of the localization of specific proteins in vertebrate peroxisomes *Microsc. Res. Tech.* **31,** 79–92.

Usuda, N., Hayashi, S., Fujiwara, S., Noguchi, T., Nagata, T., Rao, M. S., Alvares, K., Reddy, J. K., and Yeldandi, A. B. (1994). Uric acid degrading enzymes, urate oxidase and allantoinase, are associated with different subcellular organelles in frog liver and kidney. *J. Cell Sci.* **107,** 1073–1091.

Usuda, N., Kameko, M., Kanai, T., and Nagata, T. (1983). Immunocytochemical demonstration of retinol-binding protein in the lysosomes of the proximal tubules of the human kidney. *Histochemistry* **78,** 487–490.

Usuda, N., Kong, Y., Hagiwara, M., Uchida, C., Terasawa, M., Nagata, T., and Hidaka, H. (1991a). Differential localization of protein kinase C in retinal neurons. *J. Cell Biol.* **112,** 1241–1247.

Usuda, N., Kuwabara, T., Ichikawa, R., Hashimoto, T., and Nagata, T. (1991b). Immunoelectron microscopic evidence for organ difference in the composition of peroxisome-specific membrane polypeptides among three rat organs: Liver, kidney and intestine. *J. Histochem. Cytochem.* **39,** 1357–1366.

Usuda, N., Ma, H., Hanai, T., Yokota, S., Hashimoto, T., and Nagata, T. (1990). Immunoelectron microscopy of tissues processed by rapid freezing and freeze-substitution without chemical fixatives. Application to catalase in rat liver hepatocytes. *J. Histochem. Cytochem.* **38,** 617–623.

Usuda, N., and Nagata, T. (1984). Immunohistochemical characterization of microperoxisomes of small intestinal epithelial cells. *Acta Histochem. Cytochem.* **17,** 726–726.

Usuda, N., and Nagata, T. (1991). Post-embedding immunoelectron microscopy of tissues processed by rapid freezing and freeze-substitution without chemical fixatives. Authors' response. *J. Histochem. Cytochem.* **39,** 546–547.

Usuda, N., Nakazawa, A., Terasawa, M., Reddy, J. K., and Nagata, T. (1996). Immunocytochemical study of the ultrastructure of peroxisomes and the effects of peroxisome proliferators. Peroxisomes, biology and role in toxicology and disease. *Ann. NY Acad. Sci.* **804,** 297–309.

Usuda, N., Yokota, S., Hashimoto, T., and Nagata, T. (1986). Immunohistochemical localization of D-amino acid oxidase in the central clear matrix of rat kidney peroxisomes. *J. Histochem. Cytochem.* **34,** 1709–1718.

Usuda, N., Yokota, S., Ichikawa, R., Hashimoto, T., and Nagata, T. (1991c). Immunoelectron microscopic study of a new D-amino acid oxidase-immunoreactive subcompartment in rat liver peroxisomes. *J. Histochem. Cytochem.* **39,** 95–102.

Venkataraman, K. (1952). "Chemistry of Synthetic Dyes." Academic Press, New York, NY, USA.

Vrensen, G., and de Groot, D. (1974). Osmium zinc iodide staining and the quantitative study of central synapses. *Brain Res.* **74,** 131–142.

Wachstein, M., and Meissel, E. (1956). On the histochemical demonstration of glucose-6-phosphatase. *J. Histochem. Cytochem.* **4,** 592–592.

Widström, G. (1928). Über die Verwendbarkeit der Schiffschen Fuchsinschwefelifsäure-Reaktion zur quantitativen Bestimmung von Thymonuklensäure. *Biochem. Z.* **199,** 298–308.

Wied, G. L. (1966). "Introduction to Quantitative Cytochemistry." Academic Press, New York, NY.

Xiao-Lin, P., Koide, N., Kobayashi, S., Kobayashi, M., Sugenoya, A., Iida, F., Katsuyama, T., Usuda, N., and Nagata, T. (1996). Assessment of proliferative activity of glandular cells in hyperfunctioning parathyroid gland using flow cytometric and immunohistochemical methods. *World J. Surg.* **20,** 361–367.

Yamabayashi, S., Gunarso, W., Tsukahara, S., and Nagata, T. (1981). Incorporation of 3H-befunolol (beta-blocking agent) into melanin granules of ocular tissues in the pigmented rabbits. I. Light microscopic radioautography. *Histochemistry* **73,** 371–375.

Yamada, A. T. (1993). Timely and topologically defined protein synthesis in the periimplanting mouse endometrium revealed by light and electron microscopic radioautography. *Cell. Mol. Biol.* **39,** 1–12.

Yamada, A., and Nagata, T. (1992a). Ribonucleic acid and protein synthesis in the uterus of pregnant mouse during activation of implantation window. *Med. Electron Microsc.* **27,** 363–365.

Yamada, A., and Nagata, T. (1992b). Light and electron microscopic raioautography of DNA synthesis in the endometria of pregnant-ovariectomized mice during activation of implantation window. *Cell. Mol. Biol.* **38,** 763–774.

Yamada, A., and Nagata, T. (1993). Light and electron microscopic raioautography of RNA synthesis of peri-implanting pregnant mouse during activation of receptivity for blastocyst implantation. *Cell. Mol. Biol.* **39,** 211–233.

Yanagiya, N. (1994). Ultrastructural and histochemical changes of mitochondria in global ischemic cardiac muscle of rat. *Cell. Mol. Biol.* **40,** 1151–1164.

Yanagiya, N., Usuda, N., Hayashi, K., and Nagata, T. (1994). Ultrastructural changes in myocardial and endothelial cells of microvasculature of rat heart after global ischemia. *Med. Electron Microsc.* **27,** 73–79.

Yokota, S., and Nagata, T. (1968). Electron microscopic study of mouse liver after administration of sodium dehydrocholate. *Med. J. Shinshu Univ.* **13,** 207–239.

Yokota, S., and Nagata, T. (1973). Study on mouse liver urate oxidase. III. Fine localization of urate oxidase in liver cells revealed by means of ultracryotomy-immunoferritin method. *Histochemistry* **39,** 243–250.

Yokota, S., and Nagata, T. (1974). Ultrastructural localization of catalase on ultracryotomic sections of mouse liver by ferritin-conjugated antibody technique. *Histochemistry* **40,** 165–174.

Yokota, S., and Nagata, T. (1977). Urate oxidase. *In* "Electron Microscopy of Enzymes, Principles and Methods" (M. A. Hayat, Ed.), Vol. 5, pp. 72–97. Van Nostrand Reinhold, New York.

Yoshinaga, K. (1988). Uterine receptivity for blastocyst implantation. *Ann. NY Acad. Sci.* **541,** 424–431.

Yoshizawa, S., Nagata, A., Honma, T., Oda, M., Murata, F., and Nagata, T. (1974). Study of ethionine pancreatitis by means of electron microscopic radioautography. *J. Clin. Electron Microsc.* **7,** 349–350.

Yoshizawa, S., Nagata, A., Honma, T., Oda, M., Murata, F., and Nagata, T. (1977). Radioautographic study of protein synthesis in pancreatic exocrine cells of alcoholic rats. *J. Clin. Electron Microsc.* **10,** 372–373.

This Page Intentionally Left Blank

Plasticity and Stabilization of Neuromuscular and CNS Synapses: Interactions between Thrombin Protease Signaling Pathways and Tissue Transglutaminase

Barry W. Festoff,[1] Zhiming Suo,[1] and Bruce A. Citron[1]

[1]Neurobiology Research Laboratory, University of Kansas Medical Center, Kansas City Veterans Affairs Medical Center, Kansas City, Missouri 64128

The first association of the synapse as a potential site of neurodegenerative disease burden was suggested for Alzheimer's disease (AD) almost 30 years ago. Since then protease:protease inhibitor (P:PI) systems were first linked to functional regulation of synaptogenesis and synapse withdrawal at the neuromuscular junction (NMJ) more than 20 years ago. Confirmatory evidence for the involvement of the synapse, the rate-limiting or key unit in neural function, in AD did not become clear until the beginning of the 1990s. However, over the past 15 years evidence for participation of thrombin, related serine proteases and neural PIs, homologous and even identical to those of the plasma clot cascade, has been mounting. Throughout development a balance between stabilization forces, on the one hand, and breakdown influences, on the other, becomes established at synaptic junctions, just as it does in plasma clot proteins. The formation of protease-resistant cross-links by the transglutaminase (TGase) family of enzymes may add to the stability for this balance. The TGase family includes coagulation factor XIIIA and 8 other different genes, some of which may also influence the persistence of neural connections. Synaptic location of protease-activated, G-protein-coupled receptors (PARs) for thrombin and related proteases, their serpin and Kunitz-type PIs such as protease nexin I (PNI), α_1-antichymotrypsin (α-ACT), and the Kunitz protease inhibitor (KPI)-containing

secreted forms of β-amyloid protein precursor (β-APP), along with the TGases and their putative substrates, have all been amply documented. These findings strongly add to the conclusion that these molecules participate in the eventual structural stability of synaptic connections, as they do in coagulation cascades, and focus trophic activity on surviving terminals during periods of selective contact elimination. In disease states, this imbalance is likely to be shifted in favor of destabilizing forces: increased and/or altered protease activity, enhanced PAR influence, decreased and/or altered protease inhibitor function, reduction and/or alteration in tTG expression and activity, and alteration in its substrate profile. This imbalance further initiates a cascade of events leading to inappropriate programmed cell death and may well be considered evidence of *synaptic apoptosis.*

KEY WORDS: Synapse elimination, Proteases, Serpin inhibitors, Thrombin, Signal transduction, G-protein, Transglutaminase, Plasticity. © 2001 Academic Press.

I. Introduction

Early synaptic remodeling in the nervous system occurs as a consequence of the need to ensure that appropriate functional connections result from the growth of axons to their targets in development. The collateral sprouting and withdrawal of axon terminals that occurs in synaptic remodeling has been studied in detail in invertebrate nervous systems (Schuster *et al.,* 1996a; Sun and Schacher, 1996), the vertebrate visual (Missler *et al.,* 1993; Schoop *et al.,* 1997) and olivo-cerebellar (Kano *et al.,* 1995; Lohof *et al.,* 1996) systems, and the hippocampus (Woolley *et al.,* 1996). However, the *sine qua non* for synaptic remodeling has been, and continues to be, the developing vertebrate neuromuscular junction (NMJ). The NMJ has become the model from which most theories explaining this process have emerged (Colman and Lichtman, 1993; Sanes and Lichtman, 1999).

In the mammalian neuromuscular system, skeletal muscle fibers are each innervated by three or more motoneurons at birth and during the next several weeks this is reduced to mononeuronal innervation of each fiber. This polyneuronal innervation followed by synapse elimination is repeated in the event of regeneration of peripheral neuromuscular damage (Brown and Ironton, 1978). It is consistent with an evolved system to provide insurance that sufficient connections are made during wiring, when either the ultimate connections cannot yet be determined or, perhaps, the added complexity of precise modeling would be less efficient. In any case, cellular biochemical mechanisms are in place to stabilize the

necessary synapses after confirming their actual use while eliminating the less active synapses.

Neurotransmission of electrical activity plays a central role in the restructuring of synaptic inputs. Although under some experimental conditions, inactivation of motor axons favors retention of polyneuronal innervation at the motor endplate (Colman *et al.,* 1997), persistence and withdrawal of single axon collaterals terminating at the same synaptic site is primarily determined by Hebbian principles; surviving synapses being characterized by superior strength (greater synaptic length and quantal content of transmitter release) (Balice-Gordon and Lichtman, 1994; Nelson *et al.,* 1995). In essence, those terminals that "fire together, stay together." Moreover, focal blockade of transmission accelerates the competitive elimination of smaller and less active terminals by more active ones (Zhu *et al.,* 1995). Even in regenerating NMJs, in the rat, synapse elimination is prevented by lidocaine administration (Benoit and Changeux, 1978), supporting the idea that the remodeling requires sensing of relative activity between terminals. Presynaptic Ca^{2+} influx (Carlson, 1992; Sun and Schacher, 1996) and increased cyclic AMP (cAMP) levels (Balice-Gordon and Lichtman, 1993) may contribute to the changing patterns of spontaneous transmitter release which characterize the surviving contacts. Persistence of postsynaptic transmitter receptor patches (Scheetz and Constantine-Paton, 1994) and changes in their ionophore subunit composition (Liu and Westerfield, 1990) also may contribute to the strengthening of the neurotransmitter signaling pathway during the period when surviving synapses are undergoing permanent stabilization.

Retention of terminals through the supply of survival (neurotrophic) factors (Zhu *et al.,* 1995) may be linked to activity-dependent processes. In contrast, evidence that the junctional distributions of activity-independent molecular "organizers" such as the neuronal cell adhesion molecule (N-CAM) (Schuster *et al.,* 1996a), the agrin transduction system (Schuster *et al.,* 1996b), and laminin-b (Nguyen and Lichtman, 1996) are temporally linked to periods of synaptic elimination is weak. It seems that these molecules are more likely to be important in initial contact formation than in synaptic competition.

The pre-, post-, and perisynaptic cells (Culican *et al.,* 1998) are all involved in "matching" successful motor terminals to their target muscle cells. This has been demonstrated most convincingly in lower vertebrates and invertebrates, where developmental competition of incoming axon sprouts is less important than in mammals (Connold *et al.,* 1986; Vrbová and Fisher, 1989). These studies have shown that activity-independent molecular organizers can work together with neurotransmission to ensure the maturation of the newly formed synapse (Balice-Gordon and Lichtman, 1993; Connold and Vrbova, 1994; Hantaï *et al.,* 1989). No theory for synaptic selection has yet gained universal approval, but the most plausible are those supported by evidence that explains the persistence of surviving terminals not only in their own right, but in a transitional competition between coinnervating

neurites. The central feature of these theories is a role for presynaptic activity with a postsynaptic mechanism for selection (Chang and Balicegordon, 1997; Liu *et al.,* 1994).

II. Proteolysis, Basal Lamina Degradation, and Contact Elimination

Vrbová and her colleagues (Connold *et al.,* 1986; O'Brien *et al.,* 1978) first demonstrated that the cysteine protease inhibitor, leupeptin, could reverse the activity-dependent elimination of polyneuronal innervation at the mammalian NMJ. At about the same time, an hypothesis was presented by one of us that was based on preexisting concepts of "dying-back" as applied to the fatal neurodegenerative disease amyotrophic lateral sclerosis (ALS, or Lou Gehrig's disease). Also known as motor neuron disease (MND) and *maladie de Charcot,* the novel hypothesis presented for ALS at that time was that one or more endogenous PIs must be localized at an NMJ to prevent proteolytic detachment at normal adult synapses (Festoff, 1980, 1982). This hypothesis was based on evidence accrued in studies of the asymmetric (A_{12}), collagen-tailed molecular form of acetylcholinesterase (AChE) (Bon *et al.,* 1979; Fernandez, 1981). Loss of synaptic AChE localization occurring with experimental denervation was found to be due to excessive secreted neutral protease activity that led to degradation of basement membrane (BM) components to which A_{12} was attached at the NMJ (Fernandez and Duell, 1980; Fernandez *et al.,* 1979; Festoff, 1987). The most critical protease was later found to be a plasminogen-dependent enzyme subsequently identified as urokinase plasminogen activator (uPA) (Beach *et al.,* 1982; Festoff et al., 1982). uPA was present at low levels in adult muscle but was rapidly activated upon denervation (Festoff *et al.,* 1986) and is the principal secreted neutral protease from muscle (Romstedt *et al.,* 1983).

   Since then, evidence has accumulated for a role of extracellular (secreted) proteolytic activity in contact elimination. The theory has grown in popularity primarily since it embodies the competition of terminals for available target space or for trophic factors ("colonization or consumption"). Moreover, if a mechanism for targeting resistance to proteolysis is added, such as the localization of an inhibitor (Festoff, 1980), it can model a selective process explaining removal by action of successful neurites and surrender on the part of others. Early candidates such as calpain-1 (Connold *et al.,* 1986) fell out of favor since very high concentrations of added cysteine protease inhibitors (and the enzyme itself) were required to modulate synapse elimination from developing motor endplates. In addition, no evidence for secretion or extracellular action of calpains had been presented. Other early candidates were secreted plasminogen-dependent proteases, uPA, and its close cousin, tissue PA (tPA). Both were increased on denervation of adult muscle

(Festoff *et al.,* 1986). However, despite an early increase, neither seemed likely as developmental agents since activity levels actually diminished during the period of maximal postnatal polyneuronal synapse elimination (Hantaï *et al.,* 1989). *In vitro* inhibitor studies subsequently ruled out a major role at the myoneural synapse for several members of the serine protease family, such as trypsin, plasmin, and t-chymotrypsin (Liu *et al.,* 1994), despite the fact that several were involved in injury-induced synaptic remodeling (Hantaï *et al.,* 1990) and elsewhere in the nervous system (Abraham *et al.,* 1990), along with their PIs (Akaaboune *et al.,* 1994).

The most compelling evidence for an enzyme-mediated theory of programmed, developmental motor terminal withdrawal favors the serine protease, thrombin (activated prothrombin; coagulation Factor II), whose central classical role in plasma coagulation is the specific cleavage of fibrinogen (Fenton, 1986) and its activation of Factor XIII (Lorand and Conrad, 1984). A role for thrombin in synapse elimination is best supported by experiments reporting the reversal of motor synapse elimination in developing muscles using picomolar to nanomolar amounts of the specific exogenous thrombin inhibitor from the medicinal leech, hirudin, and of the endogenous thrombin-inhibiting serpin, protease nexin I (PNI). PNI has a spectrum of inhibitor activity, but unlike PA inhibitors (PAIs), when bound to the extracellular matrix (ECM) potently inhibits thrombin (Chang and Balicegordon, 1997; Donovan *et al.,* 1994; Zoubine *et al.,* 1996). Further supporting thrombin's physiological role are studies showing its induction by acetylcholine (ACh) and activity-dependence both *in vivo* (Yang *et al.,* 1997) and *in vitro* (Chang and Balice-Gordon, 1997; Glazner *et al.,* 1997).

The prominent place thrombin has now taken is also based on evidence which links the mechanism of structural synaptic plasticity with the functionally related processes of histiotypic cell death (Donovan *et al.,* 1997; Festoff *et al.,* 1996b; Smirnova *et al.,* 1996; Smirnova *et al.,* 1998b; Smith-Swintosky *et al.,* 1995; Vaughan *et al.,* 1995) and axon regeneration (Nishibori *et al.,* 1995; Suidan *et al.,* 1992). However, although clear evidence of thrombin-induced apoptosis has been found in several neuronal culture models, evidence for neuronal death accompanying synapse elimination during the neonatal period is lacking (Oppenheim, 1986). This is in contrast to the synapse loss detected robustly in brains of AD patients (DeKosky and Scheff, 1990; Masliah *et al.,* 1990; Terry *et al.,* 1991) and spinal cords of ALS patients (Sasaki and Maruyama, 1994). While PAs activate extracellular proteolysis cascades mediated through peripheral membrane receptors that allow localized proteolysis (Conese and Blasi, 1995), thrombin, with its unique tethered-ligand transmembrane receptor-mediated activation (Suidan *et al.,* 1996; Vu *et al.,* 1991), acts through a specific cytoplasmic signal pathway for contact withdrawal and neuronal apoptosis in which several key elements (Donovan and Cunningham, 1998; Jalink and Moolenaar, 1992; Smirnova *et al.,* 1998a,b; Suidan *et al.,* 1992) have been identified.

III. Protease-Activated Signaling Mechanisms and Plasticity

Initial concepts related to proteolytic synaptic plasticity implicated the progressive degradation of basement membrane (BM) components. Although it may also be true that certain BM components are degraded during plasticity events, the current mechanism is thought to relate to activation of G-protein-coupled, seven-transmembrane-domain receptors now known as protease-activated receptors (PARs). PAR1 was the first of a family of PARs cloned (Vu *et al.,* 1991) and is amply expressed in the nervous system (Niclou *et al.,* 1994; Suidan *et al.,* 1996; Weinstein *et al.,* 1995). The novel tethered-ligand hypothesis allowed for synthesis of synthetic peptides that mimic the new amino terminus in PAR1's extracellular domain after thrombin-specific cleavage at R41–S42 (in human PAR1) (Vu *et al.,* 1991). These thrombin receptor agonist peptides (TRAPs) qualitatively mimic thrombin's action without PAR1 cleavage but with similar desensitization (Beecher *et al.,* 1994; Smirnova *et al.,* 1998a,b), further demonstrating action at a common receptor site. The next two PARs to be cloned, along with PAR1, form a gene cluster at human chromosome 5*q*13–*q*15 (Schmidt *et al.,* 1998). Of interest for human hematologic diseases, the thrombin receptor PAR1 has been implicated in the 5*q* syndrome and its potential role in megakaryocytopoiesis (Bahou and Demetrick, 1997).

Of potential relevance to signal transduction mechanisms, located between PAR1 and PAR3 on chromosome 5, a Rho GAP (no hydrolytic activity), IQGAP2, was recently detected (Bahou, 2000), suggesting the presence of a functional genomic unit. This IQGAP2 is expressed in platelets, is complexed with GTP-Rac1 (minimally with GTP-CDC42), and interacts with calmodulin as well as these GTPases (Brill *et al.,* 1996). It appears to be recruited to the actin cytoskeleton with platelet activation. Definitive function of IGQAP2 in activation-dependent platelet cytoskeletal reorganization is currently under investigation (W. F. Bahou, pers. commun.). Studies of its localization to the synapse have been initiated. This may relate to recent evidence that PAR1 is dramatically upregulated in an autosomal recessive murine condition that serves as a model for ALS and other motor neuron degenerations. The *wobbler* mouse loses cervical > lumbar motor neurons beginning in the first postnatal week (Pioro and Mitsumoto, 1996). We have found that *wr/wr* homozygotes overexpress PAR1 in postnatal cervical cords as high as fivefold (Salcedo *et al.,* 1998). This appears to be limited to motor neurons and, using genotyping to detect homozygous animals, occurs prior to phenotypic changes, as high as eightfold in the first week, and is greater than in +/+ littermates as early as E12 (Festoff *et al.,* 2000). Suggesting a possible role in human motor neuron diseases, the PAR gene cluster is located to the same locus on chromosome 5*q* as the neuronal inhibitor of apoptosis (*naip*) gene and the survival motor neuron (*smn*) gene, and the same locus for all forms of spinal muscular atrophy (SMA) mutations (Brahe and Bertini, 1996).

IV. Protease Inhibition and Resistance: Mechanisms for Competitive Survival?

A. Serpins

For a theory of synaptic remodeling to be taken seriously it needs to explain the permanent diversion of unsuccessful axon collaterals away from the occupied target area, and their apparent inability to innervate, or reinnervate, that area as long as an existing synapse is already functioning (Balice-Gordon and Lichtman, 1994; Chang and Balicegordon, 1997; Connold and Vrbova, 1994). It must also explain the tenacity of the enduring contacts at the same synaptic locations where, over a period that may last several weeks (Gramsbergen *et al.,* 1997; Hassan *et al.,* 1994), their competitors are being displaced. The proteolysis model for contact elimination necessitates a role both for the post- and the presynaptic cell (Colman and Lichtman, 1993). It also suggests a role for perisynaptic cells, such as teloglial Schwann cells (Hirata *et al.,* 1997; Love and Thompson, 1998; Lubischer and Thompson, 1999; Trachtenberg and Thompson, 1996). However, it is not yet clear why some nerve terminals are able to resist the actions of thrombin (and, perhaps other serine proteases) while others are not. This was actually hypothesized earlier by Vrbová (Vrbová *et al.,* 1978). Classical mechanisms in the control of fibrinolysis and the stabilization of fibrin networks in plasma have since aided the quest for an extended protease model explaining synaptic selection.

Key processes in the plasma coagulation cascade are the activation of prothrombin by the prothrombinase complex (F.V, F.X, Ca^{2+}, and phospholipids), and dual Ca^{2+}-dependent functions of thrombin. The first is the proteolytic cleavage of fibrinogen (to form the fibrin matrix) and proteolytic activation of F.XIII to F.XIIIa (fibrin-stabilizing factor), which rapidly cross-links the matrix into a stable polymer resistant to the fibrinolytic actions of plasmin (Fenton, 1988; Lorand and Conrad, 1984). Both the actions of thrombin and the formation of plasmin are negatively regulated by members of a large family of serpins. Chief among these are the PAIs 1 and 2 (Canfield *et al.,* 1989; Wagner *et al.,* 1991) and PNI (Carter *et al.,* 1995; Stone *et al.,* 1994). However, PNI is not present to any appreciable degree in plasma, although it is concentrated in the cerebrospinal fluid (CSF) (Festoff *et al.,* 1992). Although PNI inhibits PAs with less potency than PAIs it is the most potent tissue-based inhibitor of thrombin (Stone and Hermans, 1995). A number of serpins, both classical and novel (Hastings *et al.,* 1997; Luthi *et al.,* 1997; Murphy *et al.,* 1993; Nakaya *et al.,* 1996; Nishibori *et al.,* 1995; Osterwalder *et al.,* 1998; Rao *et al.,* 1990, 1993), have been characterized within neurons and glia. Despite this characterization, the possible effects of most of them in synaptic remodeling and neural plasticity have yet to be explored. Among these, PNI was the first to be shown concentrated at NMJ

synapses (Festoff *et al.,* 1991). On the other hand, only neuroserpin, which does not inhibit thrombin, has been shown to be released presynaptically (Osterwalder *et al.,* 1998). PNI, in contrast, can form complexes at the surface with thrombin (Verdiere-Sahuqué *et al.,* 1996) and also at the NMJ (Festoff *et al.,* 1991). Although it is clearly associated with the NMJ and its expression is either unchanged or downregulated during the period of synaptic elimination in development (Akaaboune *et al.,* 1998), gene expression of PNI, unlike thrombin, does not appear to be regulated by neurotransmission (Glazner *et al.,* 1997). In contrast, secretion of PNI active protein is increased by neuropeptides such as VIP in spinal cord neuron:astrocyte (Festoff *et al.,* 1996a) and Schwann cell cultures (Bleuel and Monard, 1995). Evidence has been presented that protease inhibition can be a means of activity-dependent selection of neuronal survival (Festoff *et al.,* 1996a) and that PNI can protect against programmed embryonic and neonatal axotomy-induced motor neuronal death (Houenou *et al.,* 1995). These and other results support the assertion that the thrombin:PNI axis participates in synapse elimination and neuronal cell death, so-called synaptic apoptosis (Mattson *et al.,* 1998), or *synapoptosis*.

B. F.XIII and Type 2 TGase, the Tissue Transglutaminase (tTG)

The inactive protease precursors, prothrombin and plasminogen, along with its converting enzymes, the PAs, are classically synthesized in the liver, bone marrow, and blood platelets. However, they are also found in other peripheral tissues in the same, or tissue-specific, forms. F.XIII, the ultimate enzyme in the coagulation cascade, and the only nonprotease, forms protease-resistant complexes of the fibrin α and γ chains (Aeschlimann and Paulsson, 1994). It is interesting that F.XIII is the only two-chain member of TGase family, which now numbers some nine members, and is one of two members to be proteolytically-activated by thrombin. Thus, the TGases are associated both with plasma coagulation and with the formation of stable extracellular protein complexes in tissues (Greenberg *et al.,* 1991). Table I shows the current known members of the TGase family with their common and specific characteristics.

Like thrombin, all mammalian TGases are Ca^{2+}-dependent enzymes. It may be significant that the catalytic mechanism of TGases is analogous to that of cysteine proteases such as papain and caspases, except they culminate with exclusion of NH_3 and not H_2O (Folk, 1969, 1983; Folk and Chung, 1985). It entails the cross-linking of a primary or peptide-bound amine (peptidyl-ε-lysine) to an acyl amine acceptor (peptidyl-γ-glutamine:γ-carboxylic acid), to form the $N\varepsilon$ (γ-glutamyl)lysine isodipeptide bond, uniquely characteristic of TGase reactions (Lorand and Conrad, 1984). Essentially indestructible, although isopeptidases have been found in invertebrates (Baskova *et al.,* 1995; Parameswaran *et al.,* 1997), isodipeptide bonds

TABLE I

Transglutaminases and Related Genes

Protein	Gene	Activity	Location	Size	Refs.
Tissue transglutaminase (TG$_C$)/G$_h$ TGase-H	TGM2 20q11.2–q12	Retinoic acid induced, Ca^{2+} stimulated, crosslinks laminin/nidogen, βAPP, osteonectin, midkine, galectin-3, latent transforming growth factor-β (TGF-β) binding protein-1, serpin PNI; also functions as a G protein	Epidermis and many tissues; brain, spinal cord	687 aa 77/74–80 kDa + shorter isoforms	Aeschlimann et al., 1998; Muszbek et al., 1996; Nakaoka et al., 1994a
Keratinocyte TGase (TG$_K$)	TGM1 14q11.2	Crosslinks epidermal protines producing cornified cell envelop, crosslinks serpin elafin	Epidermis, keratinocytes, membrane bound; brain	817 aa 90 kDa	Kim et al., 1991; Nemes et al., 1999; Phillips et al., 1990
Epidermal TGase (TG$_E$)	TGM3 20q12	Protease activated, Ca^{2+} dependent crosslinking of epidermal proteins	Epidermis, hair follicles and differentiated epidermal cells; brain	693 aa 77 kDa	Dubbink et al., 1996; Grant et al., 1994; Kim et al., 1994
Prostate TGase (TG$_P$)	TGM4 3p22–p21.33	Ca^{2+} dependent crosslinking of polyamines and seminal tract proteins	Prostate	679 aa 77 kDa + shorter isoform	Gentile et al., 1995
TGase X	TGM5 15q15	Ca^{2+} dependent crosslinking of envelope proteins	Keratinocytes	720 aa 81 kDa + shorter isoform	Aeschlimann et al., 1998
TGase 3 like	TGM6 20q12	Similar to epidermal TGase?	Lung small cell carcinoma?		Sanger Center
TGase 7	TGM7 15q15	Similar to epidermal TGase?	Keratinocytes, Prostate carcinoma		
Coagulation factor XIII	F13A 6p25–p24	Cleavage to FXIIIA (by thrombin in plasma) and Ca^{2+} dependent crosslinking of fibrin chains, fibronectin, vitronectin, and serpins (including α2-macroglobulin and α2-antiplasmin)	Circulatory system, cytoplasmic and secreted (in plasma)	731 aa 84 kDa	Takahashi et al., 1986
Band 4.2 protein Pallidin	EPB42 15q15	Regulates erythrocyte structure, no TGase activity, regulates ankyrin association	Erythrocyte membrane skeleton	720 aa 76.8 + shorter isoform	Korsgren et al., 1990

formed in this way between polypeptide chains create persistent protein complexes that are highly resistant to physical and biochemical conditions that otherwise separate proteins in molecular complexes united by noncovalent or other forms of covalent bonding. This property of TGase-mediated protein polymers now forms the basis of a hypothesis for the neuropathological role of TGases in neuronal inclusion body formation.

When TGase activity undergoes sustained elevation, such as in response to high $[Ca^{2+}]_i$ during neurodegeneration or by induction with retinoic acid (RA) in cultured cells, increased transglutamination reactions occur in which glutamine-rich natural neuronal proteins (Jensen *et al.,* 1995) or abnormal proteins containing polyglutamine (Qn; CAG)-repeat sequences (Appelt and Balin, 1997; Cooper *et al.,* 1997; Kahlem *et al.,* 1996) become substrates that are then cross-linked into insoluble neurofibrillary structures. However, these conditions are distinct from those of normal physiological regulation, when TGases may form complexes limited to two or three molecules from preferred substrates. A number of extracellular proteins have been found both to be good substrates for TGases *in vitro* and to undergo cross-linking *in vivo* in a spatially and developmentally regulated manner into complexes of established stoichiometry and structure. The most important of these are listed in Table I.

Plasma proTGase F.XIII is activated by thrombin. However, in contrast, cellular F.XIII, comprising only the catalytic A subunit (Aeschlimann and Paulsson, 1994), assumes an active configuration following elevation of $[Ca^{2+}]_i$. Since thrombin activation of its receptors, PAR1, PAR3, and PAR4, results in mobilization of $[Ca^{2+}]_i$ (Hou *et al.,* 1998), this may also represent an indirect form of thrombin activation for these intracellular TGases. A similar process results in the activation of tTG, and both enzymes are externalized by cells in a fully active form. Solidifying the adhesive interactions at cell surfaces by TGases involves binding at specific integrins and cytoskeletal reorganization through as yet unidentified tyrosine kinase (TK) signal pathways (Akimov *et al.,* 2000; Ueki *et al.,* 1996). Extracellular matrix fibronectin is bound by tTG via its 42-kDa gelatin-binding domain and in a number of tissues, tTG translocates to the ECM, where it interacts with various substrates at the onset of the period of tissue maturation (Schittny *et al.,* 1997). How this is accomplished, since tTG does not possess a signal peptide, is currently under study. One possibility is that this adhesive function of tTG which does not require its cross-linking activity, depends on its stable noncovalent association with integrins (Akimov *et al.,* 2000).

This function is also separate from the GTP-binding domain of tTG, (Im *et al.,* 1997), as discussed below. More recent evidence identifies this as being specific for tTG, as it does not occur with a catalytic subunit of Factor XIII (Akimov *et al.,* 2000). The timing of this activity suggests that tTG's main physiological role is one of regulating morphogenesis by stabilizing cell–cell interactions. It may also be one of signal transduction, through its role as a GTP-binding protein. In nonneural

tissues, adhesive glycoproteins of the ECM are among the most important substrates of both Factor XIIIA and tTG (Aeschlimann and Paulsson, 1991; Hand *et al.,* 1993b). At the mammalian NMJ, tTG is concentrated (Citron *et al.,* 2000a; Hand *et al.,* 1993a) along with a number of substrates and isodipeptide bonds that are classical postsynaptic proteins: collagen-tailed (A_{12}) acetylcholinesterase (AChE) (Fernandez *et al.,* 1979; Hand *et al.,* 2000; Hand and Haynes, 1992) and unidentified nicotinic acetylcholine receptor (AChR)-associated proteins (Hucho and Bandini, 1986), were found to be among its substrates. Additionally, we found that the thrombin inhibiting serpin PNI, also concentrated at adult NMJs (Festoff *et al.,* 1991), is progressively localized there during early postnatal development (Akaaboune *et al.,* 1998). During this period, when thrombin-induced elimination of polyneuronal synapse elimination peaks (Zoubine *et al.,* 1996), there is transient dimerization of PNI antigen extracted from neonatal muscle (Akaaboune *et al.,* 1998). From *in vitro* experiments, we recently found that guinea pig tTG is able to cross-link recombinant PNI, and that the amount of oligimerization increases with increasing pH (Festoff *et al.,* 2001b), and this cross-linked PNI remains active as a thrombin inhibitor.

There is evidence that TGase-mediated protein complex formation may be regulated both by synaptic activity (Friedrich *et al.,* 1991) and by ACh or neuronal depolarization (Ando *et al.,* 1993). Since tTG is localized postsynaptically at NMJs, there is evidence for it occurring in an isoform having a lower K_m for Ca^{2+} activation than in extrajunctional parts of the muscle (Hand *et al.,* 1993a). This property of the enzyme could form the basis of its selective activation opposite neurites with only the highest quantal content. While tTG has been found to have a postjunctional distribution, our evidence as well as those of others, indicates that it is also a component of neurites and has a growth cone localization in cultured neurons (Heywood *et al.,* 1999; Lesort *et al.,* 2000), indicating that it is also presynaptic. Figure 1 (see color insert) shows preliminary studies, in collaboration with L. Haynes (University of Bristol, UK), using monoclonal antibodies (mAbs) to long (L) and short (S) tTG proteins in immunopurified E13.5 rat motor neurons (Heywood *et al.,* 1999) in which apoptosis is induced by α-thrombin. The L-form (Figs. 1A and 1B) was localized to the cytoplasm and cell membranes in untreated motor neurons. Four hours after treatment with 10 U/ml thrombin, the L isoform was reduced in intensity and moved from its peripheral distribution. The S form was localized exclusively in the neuronal soma but was undetectable in the axon in untreated motor neurons. After thrombin exposure, intense labeling for the S isoform was then seen in the axon. In dying motor neurons the S-tTG was prominently localized to extranuclear organelles or cytoplasmic inclusions. In addition, a recent report indicates that a F. XIII complex similar to that of plasma F. XIII is present in and can be released from peripheral nerves (Monsonego *et al.,* 1998). If its release proves in part to be synaptic, the activation of neural F.XIII may also be under the control of thrombin.

One other mechanism may operate to activate TGase in the absence of extremely high $[Ca^{2+}]_i$ and that relates to the dual enzymatic function of tTG/Gαh found in a number of cells. First found in hepatocytes, but also present in brain astrocytes in culture (Monsonego *et al.,* 1997), as mentioned above, tTG is also a GTPase belonging to a small family of G-proteins and classed as Gαh (Im *et al.,* 1997; Nakaoka *et al.,* 1994b). GTP negatively regulates cross-linking activity and increases the Ca^{2+} required by a factor of 1000. When brain astrocytes were incubated with injury-related cytokines, a switch in expression to a shorter (S) mRNA isoform lacking one of the putative GTP binding domains occurred and this was sufficient to activate TGase at lower Ca^{2+} (Monsonego *et al.,* 1997). We since have found the first indication of this switch in adult tissue in studies of rat spinal cord injury (SCI), where expression of a truncated S-isoform (also detected in embryonic spinal cord) is upregulated 4–8 h after injury (Festoff *et al.,* 2001a), in advance of peak apoptosis (Yong *et al.,* 1998). We have also recently found in hippocampi of Alzheimer's disease (AD) patients' brains, but not aged control brains, alternative transcription with appearance of a similar S isoform (Citron *et al.,* 2000b).

V. Potential Mechanisms of Contact Stabilization/Reinforcement by Cross-Linking Reactions

The molecular messengers of cross-link stabilization are likely to be numerous and complex, since several classes of potential TGase substrates may be implicated. We consider at least three different processes that may underlie TGase-mediated persistence of newly formed contacts.

A. Structural Stabilization of Neurites and Synapses

In neuroblastoma cells, TGase cross-linking is associated with neurite extension and stabilization (Maccioni and Seeds, 1986), while serine protease activity initiates neurite retraction (Friedman and Seeds, 1995). In the developing cerebellar cortex, the serine protease uPA is expressed at the time of granule cell migration (Friedman and Seeds, 1995) and extracellular proteolysis may play an important part in this process. The concentration of isodipeptide reported in the NMJ region of skeletal muscle (Hand *et al.,* 1993a; Hand and Haynes, 1992) suggests that presynaptic terminal fortification occurs at the synapse by tTG. The potential tTG substrates mediating this process have not been identified but may include the laminin–nidogen complex (Aeschlimann and Paulsson, 1991), β-APP (PNII)

(Akaaboune *et al.,* 1993, 1994, 2000), and PNI (Festoff *et al.,* 2001b), all major constituents of neural ECMs, including the synaptic basal lamina of the NMJ. Stable complexes of laminin could retard its proteolysis by plasmin, a process that is implicated in neuronal plasticity in the brain (Chen and Strickland, 1997), and was previously found in skeletal muscle (Hantaï and Festoff, 1987). The supply of exogenous neurotrophic substances during early postnatal development retards the process of NMJ synapse elimination in rats (English and Schwartz, 1995; Zhu *et al.,* 1995). There is no definite evidence that the local delivery of neurotrophic factors to selected presynaptic terminals, or their local sequestration in the synaptic ECM, causes these terminals to be retained for the formation of permanent synapses. Similarly, no evidence currently exists that neurotrophic factors (CNTF, LIF, neurotrophins, FGFs), to which motor neurons respond, are tTG substrates. However, tTG has been shown to participate directly in the activation of two pleiotrophic growth factors, both of which promote neurite outgrowth and are localized at the NMJ. In fact, tTG is required for the formation of active TGF-β through the formation of latent TGF-β binding protein complexes in the ECM (Nunes *et al.,* 1997). The creation of highly localized concentrations of the complex may be needed for the proteolytic activation of TGF-β. This "focal activation" phenomenon may be well suited to the unusual mode of action of TGF-β as a potentiator rather than an initiator of neurotrophic responses in motor neurons (Gouin *et al.,* 1996). TGase also forms stable dimers of the cytokine midkine, whose neurite-promoting activity after covalent cross-linking becomes 10-fold more potent (Mahoney *et al.,* 1996). In the developing cerebellar cortex, where tTG activity is highest in the nervous system and concentrated in developing granule neurons (Hand *et al.,* 1993b), a number of prominent protein substrates are associated with the neuronal membrane and surface. Like other TK receptor factors, midkine requires dimerization for its activity (Iwasaki *et al.,* 1997). Unlike most other TK factors, covalent midkine dimers are formed by tTG catalysis. These dimers are metabolically stable and can be immobilized within the ECM when dimerization occurs. Midkine is synthesized presynaptically at the NMJ and on its release becomes localized to the synaptic ECM (Zhou *et al.,* 1997). In this regard, the cross-linking of midkine by tTG following its release at the NMJ may serve to potentiate an autocrine neurite-promoting action in persisting terminals.

B. Local Sequestration of Serpins

Two of the major substrates for plasma F.XIIIA are serpin PIs. The immobilization of serpins by TGase cross-linking within either clot or tissue ECMs may serve to concentrate their activity. New minimal requirements for modification of a particular glutamine residue in a polypeptide chain to produce preferred TGase

substrate sites have recently been described (Pastor *et al.,* 1999). A subfamily of serpins containing similar sequence motifs includes the uPA-preferring serpin, PAI-2 (Jensen *et al.,* 1993), but not PAI-1. Our recent data showing that PNI is crosslinked by tTG *in vitro* supports this, since both have the sequence motif (Fig. 2). As with PAI-2, PI (thrombin-inhibiting) activity of PNI dimers is preserved (Festoff *et al.,* 2001b). This finding may correlate with the observation that PNI dimers occur in muscle extracts only during the time of developmental elimination of polyneuronal synapses in the mouse (Zoubine *et al.,* 1996), just prior to PNI localization to synaptic sites (Akaaboune *et al.,* 1998). Although PAI-2 is a prominent tTG substrate *in vivo,* it is not present in measurable concentrations in neurons or muscle, and it is unlikely that covalent cross-linking, where it occurs, influences the serpin activity of the protein. In contrast, β-APP, the secreted form of which contains a PNII (Kunitz protease inhibitor) motif, is also subject to regulation by TGase-catalyzed polymer-formation (Ho *et al.,* 1994). β-APP is both concentrated at the NMJ (Akaaboune *et al.,* 1994), regulated in concert with the timing of
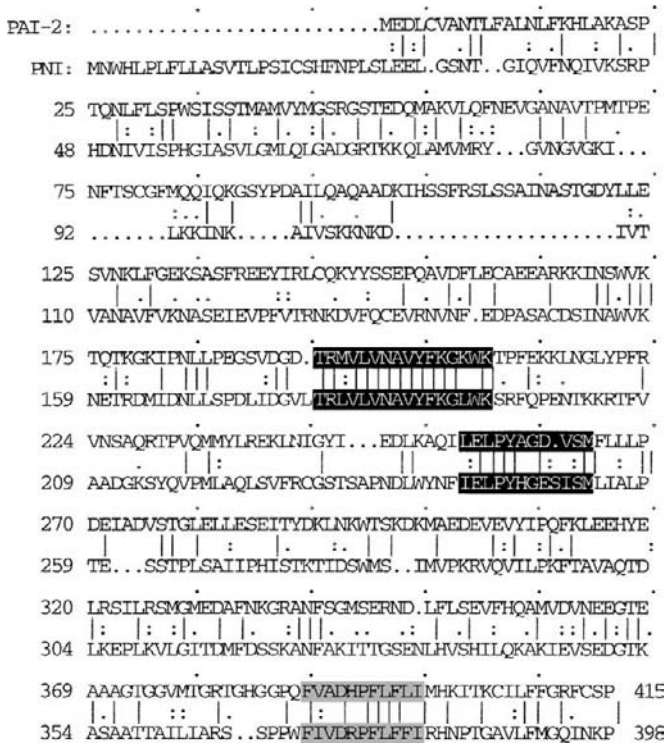
FIG. 2 Sequence similarities between PAI-2 and PNI. In addition to the serine protease bait sites at 388–398 (PNI) and 373–383 (PAI-2), there are additional regions with greater similarity.

synaptogenesis (Akaaboune *et al.,* 1995), and implicated in regulating functional innervation (Akaaboune *et al.,* 2000; Schubert *et al.,* 1991). As mentioned above, our data further indicate that serpin (PNI) cross-linking by tTG occurs with increasing pH (Festoff *et al.,* 2001b). Increasing alkalinity of synaptic contacts with development, both in the periphery and in the CNS, has been described (Hopkins *et al.,* 1985; Stella *et al.,* 1995). Thus, there is a precedent for the local deployment of PIs by TGase cross-linking within the synapse as well as in plasma and that this may be developmentally regulated along with progressive alkalinization of maturing contacts.

VI. Concluding Remarks

Neurotransmission and increased $[Ca^{2+}]_i$ release at postsynaptic sites, are envisioned to activate serine proteases in the proteolysis model of contact-elimination and remodeling. Conventional wisdom held that their targets were typical synaptic receptors or ECM glycoprotein substrates at the nerve terminal. Our model (as shown in Fig. 3) predicts that diminishing contact areas due to withdrawal of these synaptic contacts results from thrombin's activation of PAR1, its protease-activated receptor that is concentrated on presynaptic terminals. Reduced focal neurotransmission results in release of thrombin with access to PAR1 on the presynaptic terminals. This culminates in local absence of restraints over the cycle of protease release and signaling. This model allows for the fact that reinnervation in uninjured systems is inhibited, since the fully activated cycle actually blocks attempted reinnervation by protease-sensitive axon collaterals, which also express concentrated PAR1 on their surfaces.

On the other hand, the progressive increased stability of the surviving contacts may be due to the highly localized action of serpins and other PIs, such as PNI and β-APP, along with tTG and its substrates. This cross-linking enzyme may focus and solidify the surviving contacts by increasing the stability of presynaptic terminals focally. In this way, tTG cross-linking can be seen to balance the effects of protease signaling. The latter may occur both through the formation of covalently bonded ECM protein complexes with reduced metabolic turnover, and an increase in the neurotrophic potency of certain cytokines and serpins immobilized within the synaptic ECM.

Even in a simple synapse such as the NMJ, the targeting of both protease inhibition and cross-linking must be sufficiently accurate to discriminate between fine terminal axon branches occupying subregions of a single motor endplate. This can be explained if the proteins concerned are produced postsynaptically and their activity is controlled by local depolarization within synaptic subdomains. Since the NMJ is a model for central synapses, in this regard, even more accuracy in discrimination must be envisioned. A full and detailed model of this phenomenon
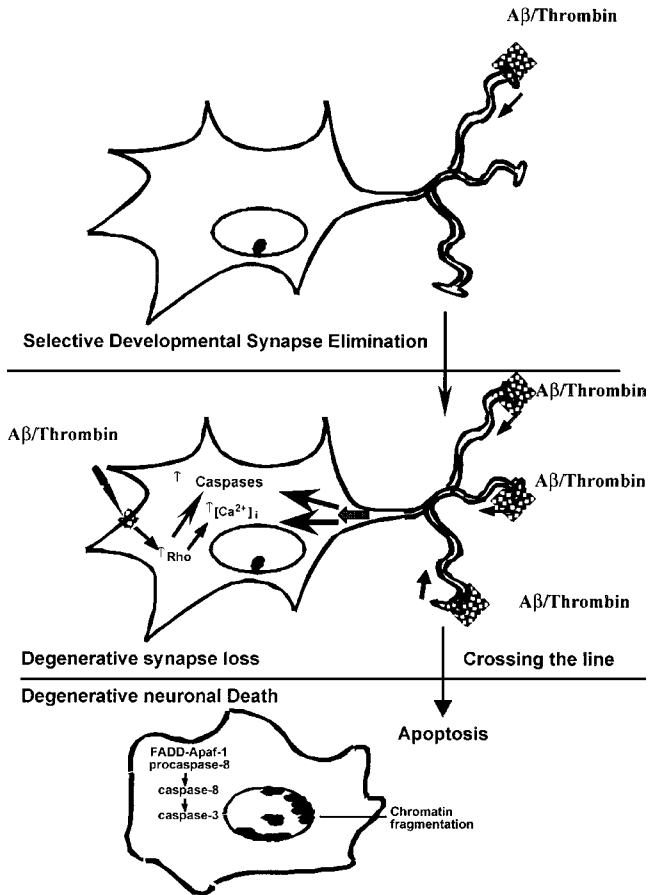
FIG. 3 Neuronal plasticity. During development, less active processes are retracted from polyneuronal innervated endplates with the participation of thrombin (Top). During degenerative processes, inappropriate thrombin action signals loss of functional processes (middle) and apoptotic neuronal death (bottom).

will come into place only when the precise mode of activation and identities of the target proteins, synapse-specific serpins, and tTG have become clear.

Acknowledgments

References

Abraham, C. R., Shirahama, T., and Potter, H. (1990). Alpha 1-antichymotrypsin is associated solely with amyloid deposits containing the beta-protein. Amyloid and cell localization of alpha 1-antichymotrypsin. *Neurobiol. Aging* **11,** 123–129.

Aeschlimann, D., Koeller, M. K., Allen-Hoffmann, B. L., and Mosher, D. F. (1998). Isolation of a cDNA encoding a novel member of the transglutaminase gene family from human keratinocytes. Detection and identification of transglutaminase gene products based on reverse transcription–polymerase chain reaction with degenerate primers. *J. Biol. Chem.* **273,** 3452–3460.

Aeschlimann, D., and Paulsson, M. (1991). Cross-linking of laminin-nidogen complexes by tissue transglutaminase. A novel mechanism for basement membrane stabilization. *J. Biol. Chem.* **266,** 15,308–15,317.

Aeschlimann, D., and Paulsson, M. (1994). Transglutaminases: Protein cross-linking enzymes in tissues and body fluids. *Thromb. Haemostasis* **71,** 402–415.

Akaaboune, M., Allinquant, B., Farza, H., Roy, K., Magoul, R., Fiszman, M., Festoff, B. W., and Hantai, D. (2000). Developmental regulation of amyloid precursor protein at the neuromuscular junction in mouse skeletal muscle. *Mol. Cell. Neurosci.* **15,** 355–367.

Akaaboune, M., Hantaï, D., Kapsimal, M., Smirnova, I. V., Verdière-Sahuqué, M., and Festoff, B. W. (1998). Topographic and molecular size changes in protease nexin I during activity-dependent polyneuronal synapse elimination in mouse skeletal muscle. *J. Comp. Neurol.* **397,** 572–579.

Akaaboune, M., Ma, J., Festoff, B. W., Greenberg, B. D., and Hantai, D. (1993). The influence of denervation on beta-amyloid protein precursor and alpha 1-antichymotrypsin in mouse skeletal muscle. *Neuromuscular Disord.* **3,** 477–481.

Akaaboune, M., Ma, J., Festoff, B. W., Greenberg, B. D., and Hantai, D. (1994). Neurotrophic regulation of mouse muscle beta-amyloid protein precursor and alpha 1-antichymotrypsin as revealed by axotomy. *J. Neurobiol.* **25,** 503–514.

Akaaboune, M., Verdiere-Sahuque, M., Lachkar, S., Festoff, B. W., and Hantai, D. (1995). Serine proteinase inhibitors in human skeletal muscle: Expression of beta-amyloid protein precursor and alpha 1-antichymotrypsin in vivo and during myogenesis in vitro. *J. Cell. Physiol.* **165,** 503–511.

Akimov, S. S., Krylov, D., Fleischman, L. F., and Belkin, A. M. (2000). Tissue transglutaminase is an integrin-binding adhesion coreceptor for fibronectin. *J. Cell Biol.* **148,** 825–838.

Ando, M., Kunii, S., Tatematsu, T., and Nagata, Y. (1993). Selective alterations in transglutaminase activity of rat superior cervical ganglia in response to neurotransmitters, high potassium and sialic acid-containing compounds. *Brain Res.* **604,** 64–68.

Appelt, D. M., and Balin, B. J. (1997). The association of tissue transglutaminase with human recombinant tau results in the formation of insoluble filamentous structures. *Brain Res.* **745,** 21–31.

Bahou, W. F. (2000). Molecular genetics of protease activated receptors. NY Acad. Sci. Biochem. Pharm. Disc. Group: Recent Advances in Understanding the Biological and Pathological Functions of Protease Activated G-Protein Receptors.

Bahou, W. F., and Demetrick, D. J. (1997). The human thrombin receptor gene and the 5q-syndrome. *Leuk. Lymphoma* **27,** 1–10.

Balice-Gordon, R. J., and Lichtman, J. W. (1993). In vivo observations of pre- and postsynaptic changes during the transition from multiple to single innervation at developing neuromuscular junctions. *J. Neurosci.* **13,** 834–855.

Balice-Gordon, R. J., and Lichtman, J. W. (1994). Long-term synapse loss induced by focal blockade of postsynaptic receptors. *Nature* **372,** 519–524.

Baskova, I. P., Aguejouf, O. M., Azougagh-Oualane, F., Zavalova, L. L., Basanova, A. V., and Doutremepuich, C. (1995). Arterial antithrombotic effect of piyavit, the novel pharmacological preparation from the medicinal leech, and of its components, prostanoids and enzyme destabilase. *Thromb. Res.* **77,** 483–492.

Beach, R. L., Burton, W. V., Hendricks, W. J., and Festoff, B. W. (1982). Extracellular matrix synthesis by skeletal muscle in culture. Proteins and effect of enzyme degradation. *J. Biol. Chem.* **257,** 11,437–11,442.

Beecher, K. L., Andersen, T. T., Fenton, J. W., and Festoff, B. W. (1994). Thrombin receptor peptides induce shape change in neonatal murine astrocytes in culture. *J. Neurosci. Res.* **37,** 108–115.

Benoit, P., and Changeux, J. P. (1978). Consequences of blocking the nerve with a local anaesthetic on the evolution of multiinnervation at the regenerating neuromuscular junction of the rat. *Brain Res.* **149,** 89–96.

Bleuel, A., and Monard, D. (1995). Regulation of protease nexin-1 and angiotensin II receptor subtype 1 expression: Inverse relationship in experimental models of nerve injury. *J. Neurosci. Res.* **42,** 562–570.

Bon, S., Vigny, M., and Massoulie, J. (1979). Asymmetric and globular forms of acetylcholinesterase in mammals and birds. *Proc. Natl. Acad. Sci. USA* **76,** 2546–2550.

Brahe, C., and Bertini, E. (1996). Spinal muscular atrophies: recent insights and impact on molecular diagnosis. *J. Mol. Med.* **74,** 555–562.

Brill, S., Li, S., Lyman, C. W., Church, D. M., Wasmuth, J. J., Weissbach, L., Bernards, A., and Snijders, A. J. (1996). The Ras GTPase-activating-protein-related human protein IQGAP2 harbors a potential actin binding domain and interacts with calmodulin and Rho family GTPases. *Mol. Cell. Biol.* **16,** 4869–4878.

Brown, M. C., and Ironton, R. (1978). Sprouting and regression of neuromuscular synapses in partially denervated mammalian muscle. *J. Physiol.* **278,** 325–348.

Canfield, A. E., Schor, A. M., Loskutoff, D. J., Schor, S. L., and Grant, M. E. (1989). Plasminogen activator inhibitor-type I is a major biosynthetic product of retinal microvascular endothelial cells and pericytes in culture. *Biochem. J.* **259,** 529–535.

Carlson, C. G. (1992). Early postnatal changes in presynaptic potassium sensitivity. *Brain Res. Dev. Brain Res.* **68,** 183–191. [**LHM:** Dykes Library currently receives this title]

Carter, R. E., Cerosaletti, K. M., Burkin, D. J., Fournier, R. E., Jones, C., Greenberg, B. D., Citron, B. A., and Festoff, B. W. (1995). The gene for the serpin thrombin inhibitor (P17), protease nexin I, is located on human chromosome 2q33–q35 and on syntenic regions in the mouse and sheep genomes. *Genomics* **27,** 196–199.

Chang, Q., and Balicegordon, R. J. (1997). Nip and tuck at the neuromuscular junction: A role for proteases in developmental synapse elimination. *BioEssays* **19,** 271–275.

Chen, Z. L., and Strickland, S. (1997). Neuronal death in the hippocampus is promoted by plasmin-catalyzed degradation of laminin. *Cell* **91,** 917–925.

Citron, B. A., Gregory, E. J., Steigerwalt, D. S., Qin, F., and Festoff, B. W. (2000a). Regulation of the dual function tissue transglutaminase/Ga$_h$ during murine neuromuscular development: Gene and enzyme isoform expression. *Neurochem. Int.* **37,** 337–349.

Citron, B. A., SantaCruz, K. S., Davies, P. J., and Festoff, B. W. (2001b). Intron–exon swapping of transglutaminase mRNA and neuronal tau aggregation in Alzheimer's disease. *J. Biol. Chem.* **276,** 3295–3301.

Colman, H., and Lichtman, J. W. (1993). Interactions between nerve and muscle: Synapse elimination at the developing neuromuscular junction. *Dev. Biol.* **156,** 1–10.

Colman, H., Nabekura, J., and Lichtman, J. W. (1997). Alterations in synaptic strength preceding axon withdrawal. *Science* **275,** 356–361.

Conese, M., and Blasi, F. (1995). Urokinase/urokinase receptor system: Internalization/degradation of urokinase-serpin complexes: Mechanism and regulation. *Biol. Chem. Hoppe Seyler* **376,** 143–155.

Connold, A. L., Evers, J. V., and Vrbova, G. (1986). Effect of low calcium and protease inhibitors on synapse elimination during postnatal development in the rat soleus muscle. *Brain Res.* **393,** 99–107.

Connold, A. L., and Vrbova, G. (1994). Neuromuscular contacts of expanded motor units in rat soleus muscles are rescued by leupeptin. *Neuroscience* **63,** 327–338.

Cooper, A. J. L., Sheu, K. R., Burke, J. R., Onodera, O., Strittmatter, W. J., Roses, A. D., and Blass,

J. P. (1997). Transglutaminase-catalyzed inactivation of glyceraldehyde 3-phosphate dehydrogenase and alpha-ketoglutarate dehydrogenase complex by polyglutamine domains of pathological length. *Proc. Natl. Acad. Sci. USA* **94,** 12,604–12,609.

Culican, S. M., Nelson, C. C., and Lichtman, J. W. (1998). Axon withdrawal during synapse elimination at the neuromuscular junction is accompanied by disassembly of the postsynaptic specialization and withdrawal of Schwann cell processes. *J. Neurosci.* **18,** 4953–4965.

DeKosky, S. T., and Scheff, S. W. (1990). Synapse loss in frontal cortex biopsies in Alzheimer's disease: Correlation with cognitive severity. *Ann. Neurol.* **27,** 457–464.

Donovan, F. M., and Cunningham, D. D. (1998). Signaling pathways involved in thrombin-induced cell protection. *J. Biol. Chem.* **273,** 12,746–12,752.

Donovan, F. M., Pike, C. J., Cotman, C. W., and Cunningham, D. D. (1997). Thrombin induces apoptosis in cultured neurons and astrocytes via a pathway requiring tyrosine kinase and RhoA activities. *J. Neurosci.* **17,** 5316–5326.

Donovan, F. M., Vaughan, P. J., and Cunningham, D. D. (1994). Regulation of protease nexin-1 target protease specificity by collagen type IV. *J. Biol. Chem.* **269,** 17,199–17,205.

Dubbink, H. J., Verkaik, N. S., Faber, P. W., Trapman, J., Schroder, F. H., and Romijn, J. C. (1996). Tissue specific and androgen-regulated expression of human prostate-specific transglutaminase. *Biochem. J.* **315,** 901–908.

English, A. W., and Schwartz, G. (1995). Both basic fibroblast growth factor and ciliary neurotrophic factor promote the retention of polyneuronal innervation of developing skeletal muscle fibers. *Dev. Biol.* **169,** 57–64.

Fenton, J. W. (1986). Thrombin. *Ann. NY Acad. Sci.* **485,** 5–15.

Fenton, J. W. (1988). Regulation of thrombin generation and functions. *Semin. Thromb. Hemost.* **14,** 234–240.

Fernandez, H. L. (1981). Properties of 16S acetylcholinesterase from rat motor nerve skeletal muscle. *Neurochem. Res.* **6,** 1005–1017.

Fernandez, H. L., and Duell, M. J. (1980). Protease inhibitors reduce effects of denervation on muscle end-plate acetylcholinesterase. *J. Neurochem.* **35,** 1166–1171.

Fernandez, H. L., Duell, M. J., and Festoff, B. W. (1979). Neurotrophic control of 16S acetyl-cholinesterase at the vertebrate neuromuscular junction. *J. Neurobiol.* **10,** 441–454.

Festoff, B. W. (1980). Neuromuscular junction macromolecules in the pathogenesis of amyotrophic leteral sclerosis. *Med. Hypotheses* **6,** 121–131.

Festoff, B. W. (1982). Release of acetylcholinesterase in amyotrophic lateral sclerosis. *Adv. Neurol.* **36,** 503–517.

Festoff, B. W. (1987). Proteases, their inhibitors and the extracellular matrix: Factors in nerve-muscle development and maintenance. *Adv. Exp. Med. Biol.* **209,** 25–39.

Festoff, B. W., D'Andrea, M. R., Citron, B. A., Salcedo, R. M., Smirnova, I. V., and Andrade-Gordon, P. (2000). Motor neuron cell death in wobbler mutant mice follows overexpression of the G-protein-coupled, protease-activated receptor for thrombin. *Mol. Med.* **6,** 410–429.

Festoff, B. W., Hantai, D., Soria, J., Thomaidis, A., and Soria, C. (1986). Plasminogen activator in mammalian skeletal muscle: Characteristics of effect of denervation on urokinase-like and tissue activator. *J. Cell Biol.* **103,** 1415–1421.

Festoff, B. W., Nelson, P. G., and Brenneman, D. E. (1996a). Prevention of activity-dependent neuronal death: Vasoactive intestinal polypeptide stimulates astrocytes to secrete the thrombin-inhibiting, neurotrophic serpin, protease nexin I. *J. Neurobiol.* **30,** 255–266.

Festoff, B. W., Patterson, M. R., and Romstedt, K. (1982). Plasminogen activator: The major secreted neutral protease of cultured skeletal muscle cells. *J. Cell. Physiol.* **110,** 190–195.

Festoff, B. W., Rao, J. S., and Chen, M. (1992). Protease nexin I, thrombin- and urokinase-inhibiting serpin, concentrated in normal human cerebrospinal fluid. *Neurology* **42,** 1361–1366.

Festoff, B. W., Rao, J. S., and Hantaï, D. (1991). Plasminogen activators and inhibitors in the neuromuscular system. III. The serpin protease nexin I is synthesized by muscle and localized at neuromuscular synapses. *J. Cell. Physiol.* **147,** 76–86.

Festoff, B. W., SantaCruz, K., Arnold, P. M., Sebastian, C. T., Davies, P. J. A., and Citron, B. A. (2001a). Spinal cord injury induces a GTP-independent alternative transcript of retinoic acid-inducible transglutaminase and reverses changes in development. Submitted for publication.

Festoff, B. W., Smirnova, I. V., Ma, J. X., and Citron, B. A. (1996b). Thrombin, its receptor and protease nexin I, its potent serpin, in the nervous system. *Semin. Thrombos. Hemostas.* **22,** 267–271.

Festoff, B. W., Zoubine, M. N., Suo, Z., and Citron, B. A. (2001b). Tissue transglutaminase catalyzes the pH-dependent cross-linking of the synaptic serpin, protease nexin I. (In press).

Folk, J. E. (1969). Mechanism of action of guinea pig liver transglutaminase. VI. Order of substrate addition. *J. Biol. Chem.* **244,** 3707–3713.

Folk, J. E. (1983). Mechanism and basis for specificity of transglutaminase-catalyzed epsilon-(gamma-glutamyl) lysine bond formation. *Adv. Enzymol. Relat. Areas Mol. Biol.* **54,** 1–56.

Folk, J. E., and Chung, S. I. (1985). Transglutaminases. *Methods Enzymol.* **113,** 358–375.

Friedman, G. C., and Seeds, N. W. (1995). Tissue plasminogen activator mRNA expression in granule neurons coincides with their migration in the developing cerebellum. *J. Comp. Neurol.* **360,** 658–670.

Friedrich, P., Fesus, L., Tarcsa, E., and Czeh, G. (1991). Protein cross-linking by transglutaminase induced in long-term potentiation in the Ca1 region of hippocampal slices. *Neuroscience* **43,** 331–334.

Gentile, V., Grant, F. J., Porta, R., and Baldini, A. (1995). Localization of the human prostate transglutaminase (type IV) gene (TGM4) to chromosome 3p21.33–p22 by fluorescence in situ hybridization. *Genomics* **27,** 219–220.

Glazner, G. W., Yadav, K., Fitzgerald, S., Coven, E., Brenneman, D. E., and Nelson, P. G. (1997). Cholinergic stimulation increases thrombin activity and gene expression in cultured mouse muscle. *Dev. Brain Res.* **99,** 148–154.

Gouin, A., Bloch-Gallego, E., Tanaka, H., Rosenthal, A., and Henderson, C. E. (1996). Transforming growth factor-beta 3, glial cell line-derived neurotrophic factor, and fibroblast growth factor-2, act in different manners to promote motoneuron survival in vitro. *J. Neurosci. Res.* **43,** 454–464.

Gramsbergen, A., J. I. J.-P., Nikkels, P. G., and Hadders-Algra, M. (1997). Regression of polyneural innervation in the human psoas muscle. *Early Hum. Dev.* **49,** 49–61.

Grant, F. J., Taylor, D. A., Sheppard, P. O., Mathewes, S. L., Lint, W., Vanaja, E., Bishop, P. D., and O'Hara, P. J. (1994). Molecular cloning and characterization of a novel transglutaminase cDNA from a human prostate cDNA library. *Biochem. Biophys. Res. Commun.* **203,** 1117–1123.

Greenberg, C. S., Birckbichler, P. J., and Rice, R. H. (1991). Transglutaminases: Multifunctional cross-linking enzymes that stabilize tissues. *FASEB J.* **5,** 3071–3077.

Hand, D., Campoy, F. J., Clark, S., Fisher, A., and Haynes, L. W. (1993a). Activity and distribution of tissue transglutaminase in association with nerve-muscle synapses. *J. Neurochem.* **61,** 1064–1072.

Hand, D., Dias, D., and Haynes, L. W. (2000). Stabilization of collagen-tailed acetylcholinesterase in muscle cells through extracellular anchorage by transglutaminase-catalyzed cross-linking. *Mol. Cell. Biochem.* **204,** 65–76.

Hand, D., and Haynes, L. W. (1992). Anchorage of asymmetric acetylcholinesterase by isodipeptide crosslinking in muscle cells. *Biochem. Soc. Trans.* **20,** 158S.

Hand, D., Perry, M. J., and Haynes, L. W. (1993b). Cellular transglutaminases in neural development. *Int. J. Dev. Neurosci.* **11,** 709–720.

Hantaï, D., and Festoff, B. W. (1987). Degradation of muscle basement membrane zone by locally generated plasmin. *Exp. Neurol.* **95,** 44–55.

Hantaï, D., Rao, J. S., and Festoff, B. W. (1990). Rapid neural regulation of muscle urokinase-like plasminogen activator as defined by nerve crush. *Proc. Natl. Acad. Sci. USA* **87,** 2926–2930.

Hantaï, D., Rao, J. S., Kahler, C., and Festoff, B. W. (1989). Decrease in plasminogen activator correlates with synapse elimination during neonatal development of mouse skeletal muscle. *Proc. Natl. Acad. Sci. USA* **86,** 362–366.

Hassan, S. M., Jennekens, F. G., Wieneke, G., and Veldman, H. (1994). Elimination of superfluous neuromuscular junctions in rat calf muscles recovering from botulinum toxin-induced paralysis. *Muscle-Nerve* **17,** 623–631. [LHM: Dykes Library currently receives this title]

Hastings, G. A., Coleman, T. A., Haudenschild, C. C., Stefansson, S., Smith, E. P., Barthlow, R., Cherry, S., Sandkvist, M., and Lawrence, D. A. (1997). Neuroserpin, a brain-associated inhibitor of tissue plasminogen activator is localized primarily in neurons. Implications for the regulation of motor learning and neuronal survival. *J. Biol. Chem.* **272,** 33,062–33,067.

Heywood, D., Rawle, H., Desoutter, A., Citron, B. A., Festoff, B. W., and Haynes, L. W. (1999). Thrombin induces apoptosis in primary motoneurons in vitro: Localization of PAR-1, Rho-A and MAP kinase activation. *Br. Neurosci. Assoc. Abstr.* S197.

Hirata, K., Zhou, C., Nakamura, K., and Kawabuchi, M. (1997). Postnatal development of Schwann cells at neuromuscular junctions, with special reference to synapse elimination. *J. Neurocytol.* **26,** 799–809.

Ho, G. J., Gregory, E. J., Smirnova, I. V., Zoubine, M. N., and Festoff, B. W. (1994). Cross-linking of beta-amyloid protein precursor catalyzed by tissue transglutaminase. *FEBS Lett.* **349,** 151–154.

Hopkins, W. G., Brown, M. C., and Keynes, R. J. (1985). Postnatal growth of motor nerve terminals in muscles of the mouse. *J. Neurocytol.* **14,** 525–540.

Hou, L., Howells, G. L., Kapas, S., and Macey, M. G. (1998). The protease-activated receptors and their cellular expression and function in blood-related cells. *Br. J. Haematol.* **101,** 1–9.

Houenou, L. J., Turner, P. L., Li, L., Oppenheim, R. W., and Festoff, B. W. (1995). A serine protease inhibitor, protease nexin I, rescues motoneurons from naturally occurring and axotomy-induced cell death. *Proc. Natl. Acad. Sci. USA* **92,** 895–899.

Hucho, F., and Bandini, G. (1986). Ca2+-dependent inactivation of acetylcholine receptors by an endogenous transglutaminase. *FEBS Lett.* **200,** 279–282.

Im, M. J., Russell, M. A., and Feng, J. F. (1997). Transglutaminase II: A new class of GTP-binding protein with new biological functions. *Cell. Signal.* **9,** 477–482.

Iwasaki, W., Nagata, K., Hatanaka, H., Inui, T., Kimura, T., Muramatsu, T., Yoshida, K., Tasumi, M., and Inagaki, F. (1997). Solution structure of midkine, a new heparin-binding growth factor. *EMBO J.* **16,** 6936–6946.

Jalink, K., and Moolenaar, W. H. (1992). Thrombin receptor activation causes rapid neural cell rounding and neurite retraction independent of classic second messengers. *J. Cell Biol.* **118,** 411–419.

Jensen, P. H., Lorand, L., Ebbesen, P., and Gliemann, J. (1993). Type-2 plasminogen-activator inhibitor is a substrate for trophoblast transglutaminase and factor **XIIIa**. Transglutaminase-catalyzed cross-linking to cellular and extracellular structures. *Eur. J. Biochem.* **214,** 141–146.

Jensen, P. H., Sorensen, E. S., Petersen, T. E., Gliemann, J., and Rasmussen, L. K. (1995). Residues in the synuclein consensus motif of the alpha-synuclein fragment, NAC, participate in transglutaminase-catalysed cross-linking to Alzheimer-disease amyloid beta A4 peptide. *Biochem. J.* **310,** 91–94.

Kahlem, P., Terre, C., Green, H., and Djian, P. (1996). Peptides containing glutamine repeats as substrates for transglutaminase-catalyzed cross-linking: Relevance to diseases of the nervous system. *Proc. Natl. Acad. Sci. USA* **93,** 14,580–14,585.

Kano, M., Hashimoto, K., Chen, C., Abeliovich, A., Aiba, A., Kurihara, H., Watanabe, M., Inoue, Y., and Tonegawa, S. (1995). Impaired synapse elimination during cerebellar development in PKC gamma mutant mice. *Cell* **83,** 1223–1231.

Kim, H. C., Idler, W. W., Kim, I. G., Han, J. H., Chung, S. I., and Steinert, P. M. (1991). The complete amino acid sequence of the human transglutaminase K enzyme deduced from the nucleic acid sequences of cDNA clones. *J. Biol. Chem.* **266,** 536–539.

Kim, I. G., Lee, S. C., Lee, J. H., Yang, J. M., Chung, S. I., and Steinert, P. M. (1994). Structure and organization of the human transglutaminase 3 gene: Evolutionary relationship to the transglutaminase family. *J. Invest. Dermatol.* **103,** 137–142.

Korsgren, C., Lawler, J., Lambert, S., Speicher, D., and Cohen, C. M. (1990). Complete amino acid sequence and homologies of human erythrocyte membrane protein band 4.2. *Proc. Natl. Acad. Sci. USA* **87,** 613–617.

Lesort, M., Tucholski, J., Miller, M. L., and Johnson, G. V. (2000). Tissue transglutaminase: A possible role in neurodegenerative diseases. *Prog. Neurobiol.* **61,** 439–463.

Liu, D. W., and Westerfield, M. (1990). The formation of terminal fields in the absence of competitive interactions among primary motoneurons in the zebrafish. *J. Neurosci.* **10,** 3947–3959. [LHM: Dykes Library currently receives this title]

Liu, Y., Fields, R. D., Festoff, B. W., and Nelson, P. G. (1994). Proteolytic action of thrombin is required for electrical activity-dependent synapse reduction. *Proc. Natl. Acad. Sci. USA* **91,** 10,300–10,304.

Lohof, A. M., Delhaye-Bouchaud, N., and Mariani, J. (1996). Synapse elimination in the central nervous system: Functional significance and cellular mechanisms. *Rev. Neurosci.* **7,** 85–101.

Lorand, L., and Conrad, S. M. (1984). Transglutaminases. *Mol. Cell. Biochem.* **58,** 9–35.

Love, F. M., and Thompson, W. J. (1998). Schwann cells proliferate at rat neuromuscular junctions during development and regeneration. *J. Neurosci.* **18,** 9376–9385.

Lubischer, J. L., and Thompson, W. J. (1999). Neonatal partial denervation results in nodal but not terminal sprouting and a decrease in efficacy of remaining neuromuscular junctions in rat soleus muscle. *J. Neurosci.* **19,** 8931–8944.

Luthi, A., Putten, H., Botteri, F. M., Mansuy, I. M., Meins, M., Frey, U., Sansig, G., Portet, C., Schmutz, M., Schroder, M., Nitsch, C., Laurent, J. P., and Monard, D. (1997). Endogenous serine protease inhibitor modulates epileptic activity and hippocampal long-term potentiation. *J. Neurosci.* **17,** 4688–4699.

Maccioni, R. B., and Seeds, N. W. (1986). Transglutaminase and neuronal differentiation. *Mol. Cell. Biochem.* **69,** 161–168.

Mahoney, S. A., Perry, M., Seddon, A., Bohlen, P., and Haynes, L. (1996). Transglutaminase forms midkine homodimers in cerebellar neurons and modulates the neurite-outgrowth response. *Biochem. Biophys. Res. Commun.* **224,** 147–152.

Masliah, E., Iimoto, D. S., Saitoh, T., Hansen, L. A., and Terry, R. D. (1990). Increased immunoreactivity of brain spectrin in Alzheimer's disease a marker for synapse loss? *Brain Res.* **531,** 36–44.

Mattson, M. P., Keller, J. N., and Begley, J. G. (1998). Evidence for synaptic apoptosis. *Exp. Neurol.* **153,** 35–48.

Missler, M., Wolff, A., Merker, H. J., and Wolff, J. R. (1993). Pre- and postnatal development of the primary visual cortex of the common marmoset. II. Formation, remodelling, and elimination of synapses as overlapping processes. *J. Comp. Neurol.* **333,** 53–67. [LHM: Dykes Library currently receives this title]

Monsonego, A., Mizrahi, T., Eitan, S., Moalem, G., Bardos, H., Adany, R., and Schwartz, M. (1998). Factor XIIIa as a nerve-associated transglutaminase. *FASEB J.* **12,** 1163–1171.

Monsonego, A., Shani, Y., Friedmann, I., Paas, Y., Eizenberg, O., and Schwartz, M. (1997). Expression of GTP-dependent and GTP-independent tissue-type transglutaminase in cytokine-treated rat brain astrocytes. *J. Biol. Chem.* **272,** 3724–3732.

Murphy, P. G., Lenz, S. P., Dobson, M., Arndt, A. D., and Hart, D. A. (1993). Purification and characterization of the plasminogen activator inhibitors PAI-1, PAI-2, and PN-1 from the human glioblastoma U138. *Biochem. Cell Biol.* **71,** 248–254.

Muszbek, L., Adany, R., and Mikkola, H. (1996). Novel aspects of blood coagulation factor XIII. I. Structure, distribution, activation, and function. *Crit. Rev. Clin. Lab. Sci.* **33,** 357–421.

Nakaoka, H., Perez, D. M., Baek, K. J., Das, T., Husain, A., Misono, K., Im, M. J., and Graham, R. M. (1994a). Gh: A GTP-binding protein with transglutaminase activity and receptor signaling function. *Science* **264,** 1593–1596.

Nakaoka, H., Perez, D. M., Baek, K. J., Das, T., Husain, A., Misono, K., Im, M. J., and Graham, R. M. (1994b). Gh: A GTP-binding protein with transglutaminase activity and receptor signaling function. *Science* **264,** 1593–1596.

Nakaya, N., Nishibori, M., Kawabata, M., and Saeki, K. (1996). Cloning of a serine proteinase inhibitor from bovine brain: Expression in the brain and characterization of its target proteinases. *Mol. Brain Res.* **42,** 293–300.

Nelson, P. G., Fields, R. D., and Liu, Y. (1995). Neural activity, neuron-glia relationships, and synapse development. *Perspect. Dev. Neurobiol.* **2,** 399–407.

Nemes, Z., Marekov, L. N., Fesus, L., and Steinert, P. M. (1999). A novel function for transglutaminase 1: Attachment of long-chain omega-hydroxyceramides to involucrin by ester bond formation. *Proc. Natl. Acad. Sci. USA* **96,** 8402–8407.

Nguyen, Q. T., and Lichtman, J. W. (1996). Mechanism of synapse disassembly at the developing neuromuscular junction. *Curr. Opin. Neurobiol.* **6,** 104–112.

Niclou, S., Suidan, H. S., Brown-Luedi, M., and Monard, D. (1994). Expression of the thrombin receptor mRNA in rat brain. *Cell. Mol. Biol.* **40,** 421–428.

Nishibori, M., Chikai, T., Kawabata, M., Ohta, J., Ubuka, T., and Saeki, K. (1995). Purification of a novel serpin-like protein from bovine brain. *Neurosci. Res.* **24,** 47–52.

Nunes, I., Gleizes, P. E., Metz, C. N., and Rifkin, D. B. (1997). Latent transforming growth factor-beta binding protein domains involved in activation and transglutaminase-dependent cross-linking of latent transforming growth factor-beta. *J. Cell Biol.* **136,** 1151–1163.

O'Brien, R. A., Ostberg, A. J., and Vrbova, G. (1978). Observations on the elimination of polyneuronal innervation in developing mammalian skeletal muscle. *J. Physiol. (London)* **282,** 571–582.

Oppenheim, R. W. (1986). The absence of significant postnatal motoneuron death in the brachial and lumbar spinal cord of the rat. *J. Comp. Neurol.* **246,** 281–286.

Osterwalder, T., Cinelli, P., Baici, A., Pennella, A., Krueger, S. R., Schrimpf, S. P., Meins, M., and Sonderegger, P. (1998). The axonally secreted serine proteinase inhibitor, neuroserpin, inhibits plasminogen activators and plasmin but not thrombin. *J. Biol. Chem.* **273,** 2312–2321.

Parameswaran, K. N., Cheng, X. F., Chen, E. C., Velasco, P. T., Wilson, J. H., and Lorand, L. (1997). Hydrolysis of gamma: Epsilon isopeptides by cytosolic transglutaminases and by coagulation factor XIIIa. *J. Biol. Chem.* **272,** 10,311–10,317.

Pastor, M. T., Diez, A., Perez-Paya, E., and Abad, C. (1999). Addressing substrate glutamine requirements for tissue transglutaminase using substance P analogues. *FEBS Lett.* **451,** 231–234.

Phillips, M. A., Stewart, B. E., Qin, Q., Chakravarty, R., Floyd, E. E., Jetten, A. M., and Rice, R. H. (1990). Primary structure of keratinocyte transglutaminase. *Proc. Natl. Acad. Sci. USA* **87,** 9333–9337.

Pioro, E. P., and Mitsumoto, H. (1996). Animal models of ALS. *Clin. Neurosci.* **3,** 375–385.

Rao, J. S., Baker, J. B., Morantz, R. A., Kimler, B., Evans, R., and Festoff, B. W. (1990). Serpin inhibitors of urokinase and thrombin in normal rat brain and the 9L brain tumor: Evidence for elevated expression of protease nexin I-like inhibitor and a novel sodium dodecyl sulfate-activated tumor antithrombin. *Cancer Res.* **50,** 5039–5044.

Rao, J. S., Rayford, A., Morantz, R. A., Festoff, B. W., and Sawaya, R. (1993). Increased levels of plasminogen activator inhibitor-1 (PAI-1) in human brain tumors. *J. Neurooncol.* **17,** 215–221.

Romstedt, K., Beach, R. L., and Festoff, B. W. (1983). Acetylcholine receptor turnover in clonal muscle cells: Role of plasmin and effects of protease inhibitors. *Muscle Nerve* **6,** 283–290.

Salcedo, R. M., Festoff, B. W., and Citron, B. A. (1998). Quantitative reverse transcriptase PCR to gauge increased protease-activated receptor 1 (PAR-1) mRNA copy numbers in the Wobbler mutant mouse. *J. Mol. Neurosci.* **10,** 113–119.

Sanes, J. R., and Lichtman, J. W. (1999). Development of the vertebrate neuromuscular junction. *Annu. Rev. Neurosci.* **22,** 389–442.

Sasaki, S., and Maruyama, S. (1994). Synapse loss in anterior horn neurons in amyotrophic lateral sclerosis. *Acta Neuropathol.* **88,** 222–227.

Scheetz, A. J., and Constantine-Paton, M. (1994). Modulation of NMDA receptor function: implications for vertebrate neural development. *FASEB J.* **8,** 745–752.

Schittny, J. C., Paulsson, M., Vallan, C., Burri, P. H., Kedei, N., and Aeschlimann, D. (1997). Protein cross-linking mediated by tissue transglutaminase correlates with the maturation of extracellular matrices during lung development. *Am. J. Respir. Cell Mol. Biol.* **17,** 334–343.

Schmidt, V. A., Nierman, W. C., Maglott, D. R., Cupit, L. D., Moskowitz, K. A., Wainer, J. A., and Bahou, W. F. (1998). The human proteinase-activated receptor-3 (PAR-3) gene. Identification within a Par gene cluster and characterization in vascular endothelial cells and platelets. *J. Biol. Chem.* **273,** 15,061–15,068.

Schoop, V. M., Gardziella, S., and Muller, C. M. (1997). Critical period-dependent reduction of the permissiveness of cat visual cortex tissue for neuronal adhesion and neurite growth. *Eur. J. Neurosci.* **9,** 1911–1922.

Schubert, W., Prior, R., Weidemann, A., Dircksen, H., Multhaup, G., Masters, C. L., and Beyreuther, K. (1991). Localization of Alzheimer beta A4 amyloid precursor protein at central and peripheral synaptic sites. *Brain Res.* **563,** 184–194.

Schuster, C. M., Davis, G. W., Fetter, R. D., and Goodman, C. S. (1996a). Genetic dissection of structural and functional components of synaptic plasticity. I. Fasciclin II controls synaptic stabilization and growth. *Neuron* **17,** 641–654.

Schuster, C. M., Davis, G. W., Fetter, R. D., and Goodman, C. S. (1996b). Genetic dissection of structural and functional components of synaptic plasticity. II. Fasciclin II controls presynaptic structural plasticity. *Neuron* **17,** 655–667.

Smirnova, I. V., Citron, B. A., Arnold, P. M., and Festoff, B. W. (1996). Thrombin mimics serum withdrawal causing apoptosis in model motor neurons. *Am. Soc. Cell Biol. Abs.* **7,** 1115.

Smirnova, I. V., Vamos, S., Wiegmann, T., Citron, B. A., Arnold, P. M., and Festoff, B. W. (1998a). Calcium mobilization and protease-activated receptor cleavage after thrombin stimulation in motor neurons. *J. Mol. Neurosci.* **10,** 31–44.

Smirnova, I. V., Zhang, S. X., Citron, B. A., Arnold, P. M., and Festoff, B. W. (1998b). Thrombin is an extracellular signal that activates intracellular death protease pathways inducing apoptosis in model motor neurons. *J. Neurobiol.* **36,** 64–80.

Smith-Swintosky, V. L., Zimmer, S., Fenton, J. W., II, and Mattson, M. P. (1995). Protease nexin-1 and thrombin modulate neuronal Ca2+ homeostasis and sensitivity to glucose deprivation-induced injury. *J. Neurosci.* **15,** 5840–5850.

Stella, N., Pellerin, L., and Magistretti, P. J. (1995). Modulation of the glutamate-evoked release of arachidonic acid from mouse cortical neurons: Involvement of a pH-sensitive membrane phospholipase A2. *J. Neurosci.* **15,** 3307–3317.

Stone, S. R., Brown-Luedi, M. L., Rovelli, G., Guidolin, A., McGlynn, E., and Monard, D. (1994). Localization of the heparin-binding site of glia-derived nexin/protease nexin-1 by site-directed mutagenesis. *Biochemistry* **33,** 7731–7735.

Stone, S. R., and Hermans, J. M. (1995). Inhibitory mechanism of serpins. Interaction of thrombin with antithrombin and protease nexin 1. *Biochemistry* **34,** 5164–5172.

Suidan, H. S., Niclou, S. P., and Monard, D. (1996). The thrombin receptor in the nervous system. *Semin. Thromb. Hemostasis* **22,** 125–133.

Suidan, H. S., Stone, S. R., Hemmings, B. A., and Monard, D. (1992). Thrombin causes neurite retraction in neuronal cells through activation of cell surface receptors. *Neuron* **8,** 363–375.

Sun, Z. Y., and Schacher, S. (1996). Tetanic stimulation and cyclic adenosine monophosphate regulate segregation of presynaptic inputs on a common postsynaptic target neuron in vitro. *J. Neurobiol.* **29,** 183–201.

Takahashi, N., Takahashi, Y., and Putnam, F. W. (1986). Primary structure of blood coagulation factor XIIIa (fibrinoligase, transglutaminase) from human placenta. *Proc. Natl. Acad. Sci. USA* **83,** 8019–8023.

Terry, R. D., Masliah, E., Salmon, D. P., Butters, N., DeTeresa, R., Hill, R., Hansen, L. A., and Katzman, R. (1991). Physical basis of cognitive alterations in Alzheimer's disease: Synapse loss is the major correlate of cognitive impairment. *Ann. Neurol.* **30,** 572–580.

Trachtenberg, J. T., and Thompson, W. J. (1996). Schwann cell apoptosis at developing neuromuscular junctions is regulated by glial growth factor. *Nature* **379,** 174–177.

Ueki, S., Takagi, J., and Saito, Y. (1996). Dual functions of transglutaminase in novel cell adhesion. *J. Cell Sci.* **109,** 2727–2735.

Vaughan, P. J., Pike, C. J., Cotman, C. W., and Cunningham, D. D. (1995). Thrombin receptor activation protects neurons and astrocytes from cell death produced by environmental insults. *J. Neurosci.* **15,** 5389–5401.

Verdiere-Sahuqué, M., Akaaboune, M., Lachkar, S., Festoff, B. W., Jandrot-Perrus, M., Garcia, L., Barlovatz-Meimon, G., and Hantaï, D. (1996). Myoblast fusion promotes the appearance of active protease nexin I on human muscle cell surfaces. *Exp. Cell Res.* **222,** 70–76.

Vrbová, G., and Fisher, T. J. (1989). The effect of inhibiting the calcium activated neutral protease, on the motor unit size after partial denervation of the rat soleus muscle. *Eur. J. Neurosci.* **1,** 616–625.

Vrbová, G., Gordon, T., and Jones, R. (1978). "Nerve–Muscle Interaction." Chapman and Hall, London.

Vu, T. K., Hung, D. T., Wheaton, V. I., and Coughlin, S. R. (1991). Molecular cloning of a functional thrombin receptor reveals a novel proteolytic mechanism of receptor activation. *Cell* **64,** 1057–1068.

Wagner, S. L., Lau, A. L., Nguyen, A., Mimuro, J., Loskutoff, D. J., and Isackson, P. J. (1991). Inhibitors of urokinase and thrombin in cultured neural cells. *J. Neurochem.* **56,** 234–242.

Weinstein, J. R., Gold, S. J., Cunningham, D. D., and Gall, C. M. (1995). Cellular localization of thrombin receptor mRNA in rat brain: Expression by mesencephalic dopaminergic neurons and codistribution with prothrombin mRNA. *J. Neurosci.* **15,** 2906–2919.

Woolley, C. S., Wenzel, H. J., and Schwartzkroin, P. A. (1996). Estradiol increases the frequency of multiple synapse boutons in the hippocampal CA1 region of the adult female rat. *J. Comp. Neurol.* **373,** 108–117.

Yang, Y. X., Akiyama, H., Fenton, J. W., and Brewer, G. J. (1997). Thrombin receptor on rat primary hippocampal neurons: Coupled calcium and camp responses. *Brain Res.* **761,** 11–18.

Yong, C., Arnold, P. M., Zoubine, M. N., Citron, B. A., Watanabe, I., Berman, N. E., and Festoff, B. W. (1998). Apoptosis in cellular compartments of rat spinal cord after severe contusion injury. *J. Neurotrauma* **15,** 459–472.

Zhou, H., Muramatsu, T., Halfter, W., Tsim, K. W., and Peng, H. B. (1997). A role of midkine in the development of the neuromuscular junction. *Mol. Cell. Neurosci.* **10,** 56–70.

Zhu, H., Wu, F., and Schacher, S. (1995). Changes in expression and distribution of Aplysia cell adhesion molecules can influence synapse formation and elimination in vitro. *J. Neurosci.* **15,** 4173–4183.

Zoubine, M. N., Ma, J. Y., Smirnova, I. V., Citron, B. A., and Festoff, B. W. (1996). A molecular mechanism for synapse elimination: Novel inhibition of locally generated thrombin delays synapse loss in neonatal mouse muscle. *Dev. Biol.* **179,** 447–457.

This Page Intentionally Left Blank

Adipokinetic Hormones of Insect: Release, Signal Transduction, and Responses

Dick J. Van der Horst, Wil J. A. Van Marrewijk,
and Jacques H. B. Diederen

Department of Biochemical Physiology, Faculty of Biology and Institute of
Biomembranes, Utrecht University, 3584 CH Utrecht, The Netherlands

Flight activity of insects provides an attractive yet relatively simple model system for regulation of processes involved in energy metabolism. This is particularly highlighted during long-distance flight, for which the locust constitutes a well-accepted model insect. Peptide adipokinetic hormones (AKHs) are synthesized and stored by neurosecretory cells of the corpus cardiacum, a neuroendocrine gland connected with the insect brain. The actions of these hormones on their fat body target cells trigger a number of coordinated signal transduction processes which culminate in the mobilization of both carbohydrate (trehalose) and lipid (diacylglycerol). These substrates fulfill differential roles in energy metabolism of the contracting flight muscles. The molecular mechanism of diacylglycerol transport in insect blood involving a reversible conversion of lipoproteins (lipophorins) has revealed a novel concept for lipid transport in the circulatory system. In an integrative approach, recent advances are reviewed on the consecutive topics of biosynthesis, storage, and release of insect AKHs, AKH signal transduction mechanisms and metabolic responses in fat body cells, and the dynamics of reversible lipophorin conversions in the insect blood.
KEY WORDS: Neurohormones, Adipokinetic hormones, Insect flight, Signal transduction, Fat body lipase, Lipid transport, Lipophorin, Apolipophorin III.

I. Introduction

Insects that engage in long-distance flights provide a fascinating model system for studying metabolic key processes and their regulation during sustained physical exercise. Active insect flight muscles are among the most energy-demanding tissues known, which is reflected in the extremely high metabolic rates sustained during long-distance flight. On the other hand, the relative simplicity of the insect system offers possibilities to penetrate the molecular mechanisms of energy metabolism-related processes such as mobilization of endogenous energy reserves and substrate transport, as well as the regulation of these processes by metabolic neurohormones, while the insight obtained may be pertinent also to more complex vertebrate systems. In the past decade, considerable progress has been made in the areas of biosynthesis, storage, and release of neurohormones involved in insect flight (adipokinetic hormones, AKHs), their signal transduction in target cells, and the metabolic responses of energy substrate mobilization and transport. This review is not intended to be comprehensive but rather is confined to recent advances and will mainly focus on an internationally recognized model insect, the migratory locust, *Locusta migratoria,* in which these consecutive areas are particularly integrated. A survey of this integrative model is presented in Fig. 1. Flight activity of the locust triggers the release of AKHs. These peptides are synthesized and stored by neuroendocrine adipokinetic cells in the corpus cardiacum; the complex
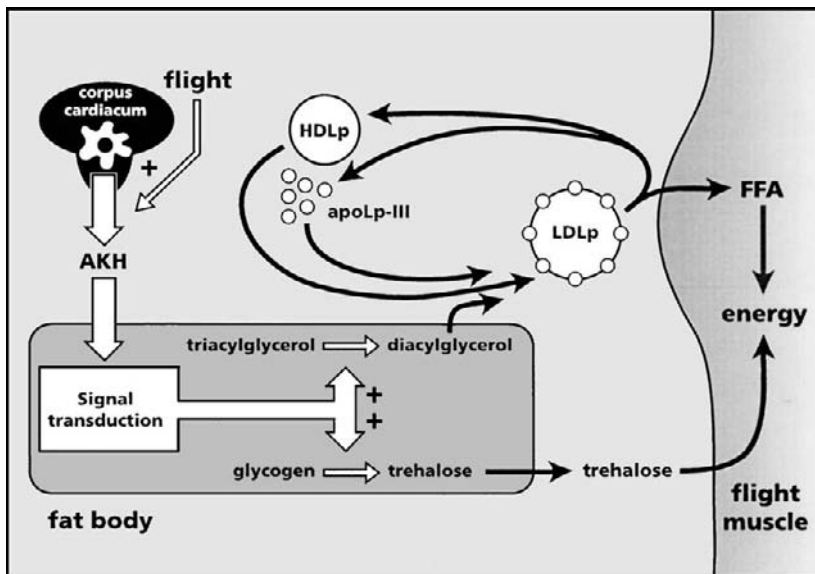
FIG. 1   Schematic overview of AKH-controlled substrate mobilization from insect fat body during flight activity. AKH, adipokinetic hormones; HDLp, high-density lipophorin; LDLp, low-density lipophorin; apoLp-III, apolipophorin III; FFA, free fatty acids.

multifactorial control mechanism for AKH release assessed *in vitro* includes both stimulatory and inhibitory factors. The AKHs are synthesized continuously, resulting in the accumulation of large amounts of AKH-containing secretory granules, while progressively, intracisternal granules are produced that seem to represent additional stores of secretory material. This strategy allows the adipokinetic cells to comply with large variations in secretory demands; recent data show that changes in secretory activity do not affect the rate of biosynthetic activity.

AKH signal transduction at the fat body target cells involves stimulation of cAMP production dependent on the presence of extracellular Ca^{2+}. Additionally, the AKHs enhance the production of inositol phosphates ($InsP_n$) including $Ins(1,4,5)P_3$, which may mediate the mobilization of Ca^{2+} from intracellular stores. This depletion of Ca^{2+} from intracellular stores stimulates the influx of extracellular Ca^{2+}, indicative for the operation of a capacitative (store-operated) calcium entry mechanism. The interactions between the AKH signaling pathways ultimately result in the mobilization of stored reserves as fuels for flight. While the carbohydrate (mainly trehalose) in the insect blood (hemolymph) provides the energy for the initial period of flight, additional trehalose is mobilized from glycogen reserves. At the same time, lipid (diacylglycerol, DAG) concentration in the hemolymph is progressively increased by mobilization of stored triacylglycerol (TAG) and constitutes the principal fuel for long-term flight. The mechanism for hormonal activation of fat body glycogen phosphorylase, the key enzyme in trehalose formation, has been well established. The mechanism by which the pivotal enzyme TAG lipase catalyzes AKH-controlled production of the DAG on which long-distance flight is dependent is, however, poorly understood.

The action of AKH on lipid release has revealed a novel concept for lipid transport in the circulation of animal organisms. DAG loading onto the multifunctional lipoprotein in insect hemolymph, high-density lipophorin (HDLp), is accompanied by association of multiple copies of the exchangeable apolipoprotein, apolipophorin III (apoLp-III), with the expanding particle. At the flight muscles, the DAG is hydrolyzed and the resulting fatty acids (FAs) are oxidized for energy generation. HDLp and apoLp-III are, however, recovered and reutilized for lipid uptake at the fat body, thus acting as an efficient lipid shuttle mechanism. Although recent advances on the structural properties of HDLp and apoLp-III demonstrate a remarkable similarity to their counterparts in the mammalian system, the functioning of the insect lipoprotein in this shuttle mechanism is intriguingly different.

II. Insect Adipokinetic Hormones

A. Adipokinetic Hormone-Producing Cells

The locust corpus cardiacum is located caudal to the brain and consists of a storage lobe fused to the ventral wall of the aorta and of two glandular lobes which enclose

the aorta (Figs. 2a and 2b). The storage lobe consists of two compartments: a neural part on the hemocoelic side containing neuronal cell bodies that are protected by a blood–brain barrier, and a neurohemal part adjacent to the aorta, which releases into the hemolymph neurohormones produced by neurosecretory brain cells, the axons of which end in this neurohemal part (Vullings *et al.,* 1995). The two glandular lobes constitute the glandular part of the corpus cardiacum; this part contains the AKH-producing neurosecretory cells, also called adipokinetic cells. It is only in locusts that the adipokinetic cells form a distinct glandular part, whereas the neurohormones produced by neurosecretory brain cells are confined to the storage lobe. In the immediate vicinity of the caudolateral side of the corpus cardiacum, the corpus allatum is situated, which forms together with the corpus cardiacum the retrocerebral complex.

The adipokinetic cells are neuron-like unipolar cells, the cell bodies and short (20 to 200 μm) cell processes of which are intermingled within the glandular part of the corpus cardiacum (Fig. 3a) (Orchard and Shivers, 1986). Therefore, the hormones which are produced by the adipokinetic cells are released within the
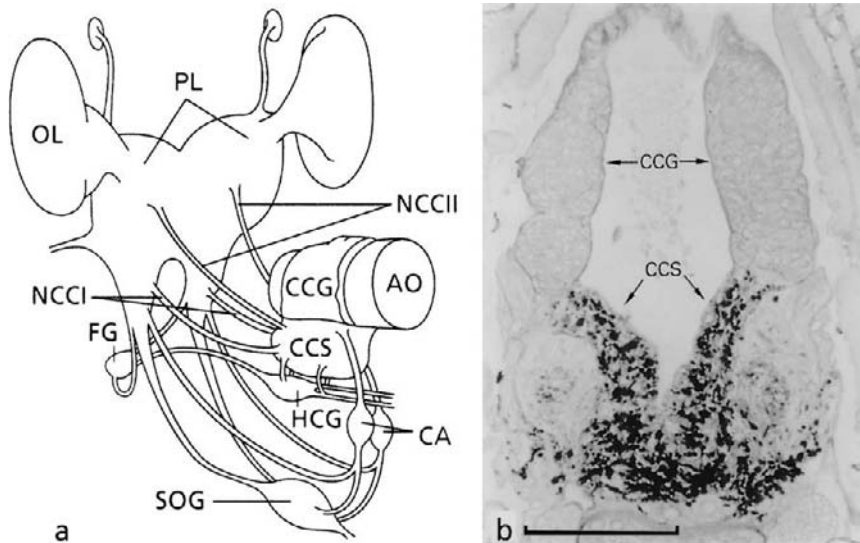
FIG. 2   (a) Schematic representation of the retrocerebral complex and the nerves connecting it to the central nervous system. The corpus cardiacum has been drawn out of proportion; it is too large compared to the brain. (b) Five-micrometer frontal section of the corpus cardiacum of *L. migratoria,* stained by a histochemical method for peptidergic neurosecretory material rich in sulfur-containing amino acids (Diederen *et al.,* 1988), which stains only the neurosecretory material in the storage part, not in the glandular part. AO, aorta; CA, corpora allata; CCG, corpus cardiacum, glandular part; CCS, corpus cardiacum, neurohemal storage part; FG, frontal ganglion; HCG, hypocerebral ganglion; NCCI, II, nervi corporis cardiaci I and II; OL, optic lobe; PL, protocerebrum, pars lateralis; SOG, suboesophageal ganglion. Bar = 100 μm.
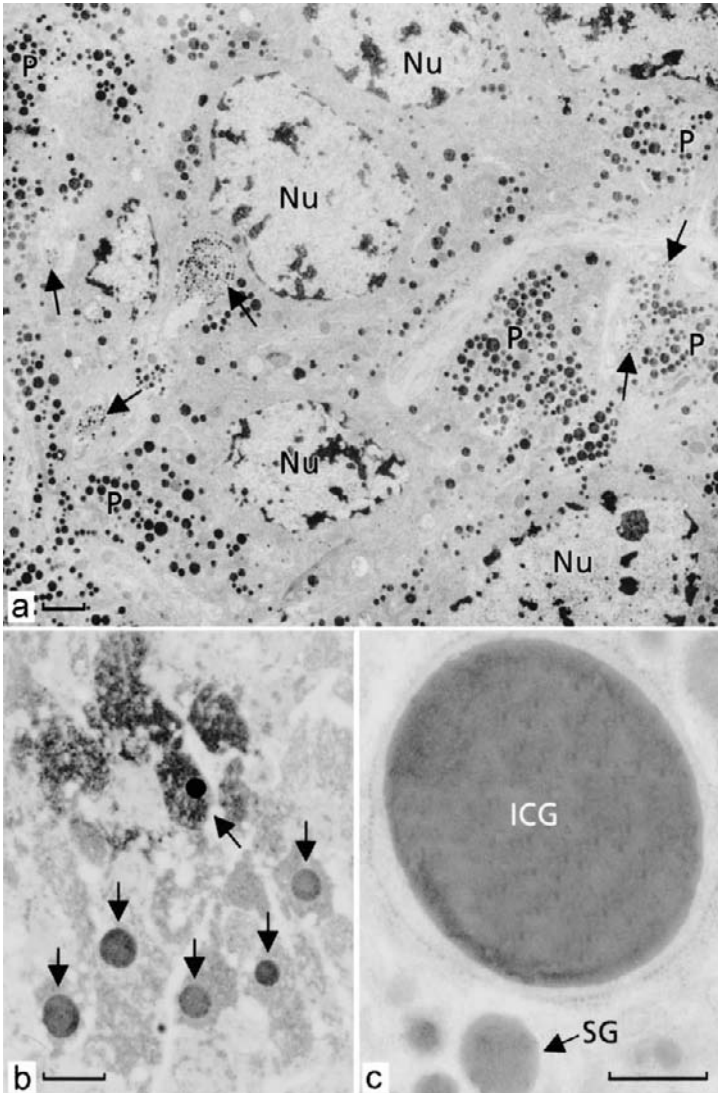
FIG. 3   (a) Ultrathin section of the glandular part of the corpus cardiacum of an adult locust (*L. migratoria,* 12 days after the final ecdysis). Cell bodies with nuclei and cell processes of the adipokinetic cells are intermingled. Secretory granules are accumulated in the processes. Between the adipokinetic cells axons from cerebral origin (arrows) can be seen. Locusts of this age hardly contain any intracisternal granules. (b) Semithin section of the glandular part of the corpus cardiacum of an adult locust (*L. migratoria,* 43 days after the final ecdysis) containing several intracisternal granules (arrows). (c) Ultrathin section showing an intracisternal granule enveloped by a ribosome-studded membrane. ICG, intracisternal granule; Nu, nucleus; P, process; SG, secretory granule. Bar (a) 1 μm, (b) 10 μm, (c) 0.5 μm.

glandular part of the corpus cardiacum; there is no separate neurohemal area for these hormones elsewhere. Despite the fact that in the glandular part of the corpus cardiacum of *L. migratoria* three AKHs have been identified, as will be discussed below, morphologically only one type of adipokinetic cell has been shown to be present in the corpus cardiacum (Diederen *et al.,* 1987).

B. Flight Activity and Adipokinetic Hormones

Flight activity is the only known natural stimulus triggering the release of AKHs from the locust corpus cardiacum (Orchard and Lange, 1983). Release of AKH during flight has been demonstrated in only a few other insects, such as the hawk-moth *Manduca sexta* (Ziegler and Schulz, 1986) and blowflies (Wilps and Gäde, 1990).

In the glandular part of the corpus cardiacum of *L. migratoria,* three AKHs have been identified, the decapeptide AKH-I, and the octapeptides AKH-II and AKH-III (Oudejans *et al.,* 1991). Interestingly, only two AKHs (-I and -II) have been detected in the closely related locust *Schistocerca gregaria.* Recently, another AKH-III has been reported to be present in two other grasshopper species (Siegert *et al.,* 2000), which is the second AKH-III identified so far.

At present, over 30 different AKHs have been identified from representative species of most insect orders (Gäde, 1996, 1997a,b; Köllisch *et al.,* 2000; Siegert *et al.,* 2000). Their structure is clearly related to that of the red pigment-concentrating hormone (RPCH) from crustaceans, for which reason this group of peptides became known as the AKH/RPCH family of peptides. Most insect species investigated so far have only one of these peptides, some have two, and only three species (all grasshoppers) have three AKH/RPCH peptides.

All members but one of the AKH/RPCH family of peptides consist of 8 to 10 amino acids, N-terminally blocked by a pyroglutamic acid residue and C-terminally blocked by an amide group, with an aromatic amino acid residue at position 8 (always tryptophan) and at position 4 (mostly phenylalanine). In contrast to this general rule, Köllisch *et al.* (2000) recently discovered in the painted lady butterfly, *Vanessa cardui,* the presence of an AKH that consists of 11 amino acid residues and is not amidated.

The insect AKH/RPCH peptides can exert a wide range of effects after their release from the corpus cardiacum. Clearly, a major function is mobilization of lipid (diacylglycerol) and/or carbohydrate (trehalose) in many insect species, and proline in some dipterans and beetles. The target tissue for the mobilization of these energy substrates is the fat body. Although all three AKHs of *L. migratoria* are involved in the regulation of the mobilization of lipids and carbohydrates, their action is differential (Vroemen *et al.,* 1998a). Several additional physiological actions of AKH/RPCH peptides have been reported, including inhibition of biosynthesis of proteins, RNA, and lipids in locust fat body. In cockroach fat

body, however, these peptides stimulate juvenile hormone-dependent protein synthesis, as well as the synthesis of heme and the expression of a cytochrome gene (Gäde, 1996). AKH/RPCH peptides also stimulate heartbeat in cockroaches (Baumann *et al.,* 1990). The physiological significance of the influences of the AKH/RPCH peptides on energy substrate mobilization is obvious, but the significance of the additional actions remains to be determined.

Socha *et al.* (1999) reported that AKH injected into the thorax of the flightless bug, *Pyrrhocoris apterus,* stimulates general locomotor activity. Milde *et al.* (1995), however, did not find any effect on the locomotor activity of AKH injected into the circulatory system of *M. sexta,* whereas injection of AKH directly into the mesothoracic ganglion evoked strong muscle responses. Apparently, hormonal AKH from the general circulation cannot penetrate into the central nervous system, due to some kind of "blood–brain barrier." It is not clear from the data of Socha *et al.* (1999) what tissues were reached by the injections of AKH. The presence of AKH-like immunoreactivity in the central nervous system (Schooneveld *et al.,* 1985) suggests that AKH or AKH-like substances produced within the central nervous system might function as neurotransmitter or neuromodulator, which is beyond the scope of the present chapter.

Recently, Siegert (1999) identified an AKH-type peptide from the storage part of the corpus cardiacum of *L. migratoria.* This peptide is, therefore, probably synthesized in neurosecretory cells in the brain that send their axons into the storage lobe, from where it may be released into the hemolymph. In locusts, this peptide has no biological activity usually associated with AKHs.

C. Biosynthesis of Adipokinetic Hormones

The AKH prohormones are synthesized in the cell bodies of the adipokinetic cells at the rough endoplasmic reticulum, transported to the Golgi complex, and packaged into secretory granules at the *trans*-Golgi network (Jansen *et al.,* 1989). Proteolytic processing of the prohormones to bioactive AKHs is considered to take place in a post-*trans*-Golgi compartment, presumably the secretory granules (O'Shea and Rayne, 1992). The secretory granules, which have a mean diameter of about 300 nm, are transported into the cell processes, where they are either stored, or released by exocytosis into the hemolymph (Diederen *et al.,* 1987, 1993). Especially in the adipokinetic cells of older adult locusts, also intracisternal granules may be present, which are dense accumulations of peptidergic biosynthetic products within dilated cisternae of the rough endoplasmic reticulum (Figs. 3b and 3c). These granules, which originally were called ergastoplasmic granules and may attain diameters of up to 5 μm and even more, function as stores of AKH prohormones (Diederen *et al.,* 1999; Harthoorn *et al.,* 2000), as will be discussed below.

In the adipokinetic cells of *L. migratoria,* all three locust AKHs are translated from separate mRNAs, each encoded on a separate gene. *In situ* hybridization

demonstrated that the sites for expression of the three AKH mRNAs are colo-
calized in the cell bodies. The resulting preprohormones have a simple structure,
consisting of a signal peptide, one single copy of AKH, and a peptide portion termed
AKH-associated peptide (Fig. 4). Surprisingly large differences in the number and
sequence of amino acid residues exist between the preprohormone of Lom-AKH-
III on the one hand and those of Lom-AKH-I and -II on the other, whereas minor
differences exist between the latter two preprohormones (Bogerd *et al.,* 1995).
Sequences have been established also for the preprohormones of AKH/RPCHs of
some other insect and crustacean species, which all show a structure similar to that
of the AKH precursors in *L. migratoria* (Klein *et al.,* 1995; Lewis *et al.,* 1997; for
more references see Bogerd *et al.,* 1995).

The processing of the preprohormones has been elucidated in detail for AKH-
I and -II of *S. gregaria* (O'Shea and Rayne, 1992; Rayne and O'Shea 1993,
1994). After cotranslational cleavage of the signal peptide (Fig. 4), the resulting
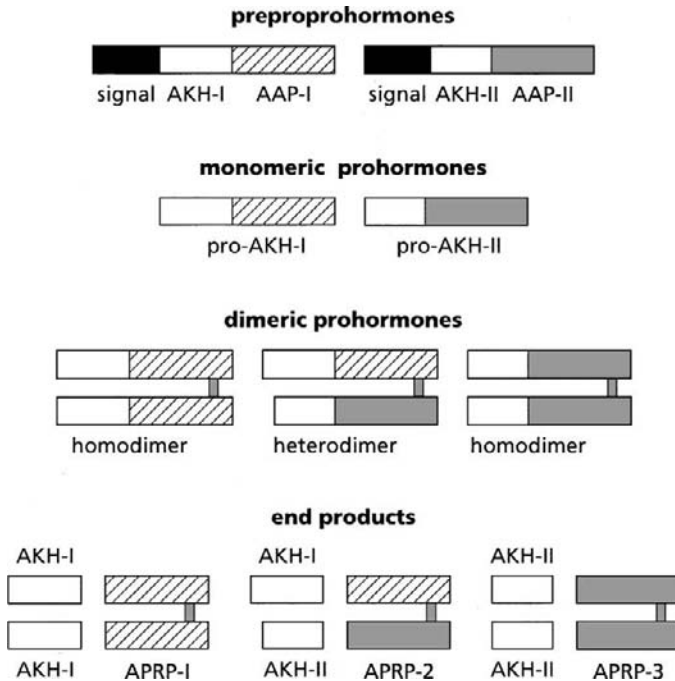
FIG. 4   The biosynthesis of the locust adipokinetic hormones AKH-I and -II and the adipokinetic
precursor-related peptides APRP-1, -2 and -3. After cleavage of the signal peptide from the prepro-
hormones, the resulting monomeric prohormones, which consist of the AKH-sequence and the AKH-
associated peptide (AAP), form three dimeric prohormones, which are then processed to the AKHs
and the APRPs. After O'Shea and Rayne (1992).

prohormones of AKH-I and -II dimerize at random by oxidation of their cysteine residues and give rise to a mixture of one heterodimeric (AKH-I/II) and two homodimeric (AKH-I/I and AKH-II/II) prohormones. Further proteolytic processing of the dimeric prohormones in the secretory pathway results in the (monomeric) bioactive hormones, as well as one hetero- and two homodimeric AKH precursor-related peptides (APRPs, the dimeric AKH-associated peptides). Until now, all data obtained suggest that the processing of the preprohormones of AKH-I and -II in *L. migratoria* is similar to that in *S. gregaria.* The details of the processing of the preprohormone of AKH-III have not yet been elucidated. In *L. migratoria,* the synthesis of the prohormones of the AKHs, their packaging into secretory granules, and their processing to the bioactive hormones is completed in less than 75 min (Oudejans *et al.,* 1990, 1991).

D. Intracellular Location of Adipokinetic (Pro)hormones

AKH-I and -II have been established to be colocalized within the secretory granules by means of immunocytochemistry using polyclonal antisera raised against these two hormones (Diederen *et al.,* 1987). In addition, the intracisternal granules showed clear immunopositivity with these antisera. When a few years later the existence of AKH-III in the corpora cardiaca of *L. migratoria* was disclosed (Oudejans *et al.,* 1991), it appeared not possible to produce antibodies discriminating between AKH-I and -III, which is most likely due to the close resemblance of the amino acid sequences of these two hormones. The intracellular location of the AKHs in *L. migratoria,* therefore, was investigated indirectly, by using antibodies against the corresponding AKH-associated peptides, the amino acid sequences of which differ to a larger degree from each other than those of the AKHs (Harthoorn *et al.,* 1999). Since the proteolytic processing of AKH-prohormones presumably occurs in the secretory granules (O'Shea and Rayne, 1992), AKH-I, -II, and -III will be localized in the same granules as their corresponding APRPs, whereas in the intracisternal granules, which are pre-Golgi structures, the AKHs and their associated peptides still are parts of the unprocessed prohormones.

Immunocytochemically, all three AKH-associated peptides were shown to be colocalized in the secretory granules (Fig. 5). This implies that also all three AKHs are colocalized in these granules. The immunoreactivity of the intracisternal granules, however, was restricted to the antisera specific for AKH-I- and AKH-II-associated peptides; with the antiserum specific for AKH-III-associated peptide, the intracisternal granules did not show any specific reaction. The presence of AKH-I- and AKH-II-associated peptides in the intracisternal granules indicates that these granules function as stores of AKH-I and -II prohormones and not, however, of AKH-III prohormone. This points to differences in physiological function between AKH-III and the other two hormones in *L. migratoria.*
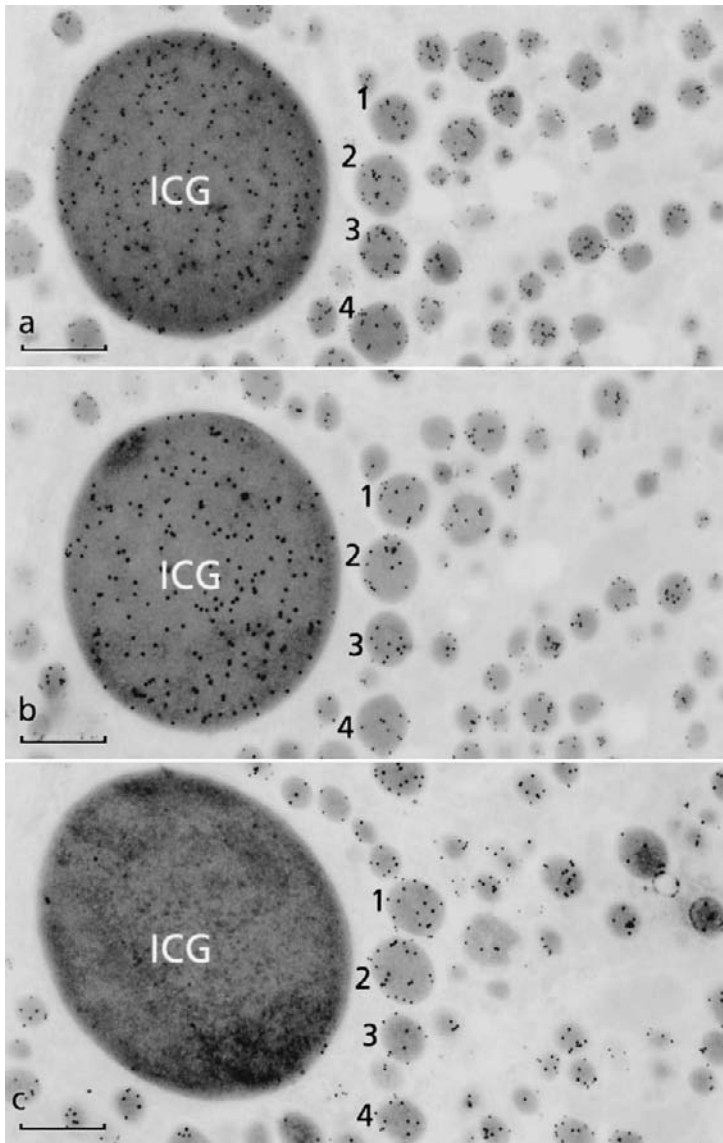
FIG. 5 Three consecutive ultrathin sections of part of an adipokinetic cell of *L. migratoria*. The secretory granules show immunogold labeling with antisera specific for AAP-I (a), AAP-II (b), and AAP-III (c), respectively, whereas the intracisternal granule shows immunoreactivity only with the antisera specific for AAP-I and AAP-II and not with the antiserum specific for AAP-III. The same secretory granules have the same *number* in the three electron micrographs. AAP-(I, -II, -III) = AKH-(I, -II, -III)-associated peptide; ICG, intracisternal granule. Bars = 0.5 μm.

Studies on the total content of the three AKHs in the corpus cardiacum of larval stages and adults of *L. migratoria* show a continuous increase in the amounts of these hormones (Oudejans *et al.,* 1993), which is reflected by an increase in the number of secretory granules, at least in aging adults (Diederen *et al.,* 1992). In corpora cardiaca from adult animals, the molar ratio between AKH-I, -II, and -III is approximately 14:2:1. The ratio between AKH-I and -II remains constant throughout the life cycle, whereas the amount of AKH-III is relatively lower during larval development than in the adult stage (Oudejans *et al.,* 1993). Also in the corpus cardiacum of *S. gregaria* the amounts of AKH-I and -II continuously increase during the life cycle. Interestingly, the ratio between AKH-I and -II in *S. gregaria* does not remain constant (Hekimi *et al.,* 1991), but changes from 1:1 in the first larval stage to 5:1 in the adult stage.

E. Innervation of the Adipokinetic Cells and Regulation of Cellular Activity

The adipokinetic cells appear to be subjected to quite a number of regulatory stimulating, inhibiting, and modulating substances, which exert their influences either via nerve fibers innervating these cells or via the hemolymph.

1. Neural Regulation

The retrocerebral complex, which contains the glandular part of the corpus cardiacum, is connected to the central nervous system by several paired nerves, such as the nervi corporis cardiaci (NCC)-I and -II (Fig. 2a). Neuroanatomical tracing experiments showed that nerve fibers from the brain reach the glandular part of the corpus cardiacum only via the NCC-II. Electrical stimulation of the NCC-II induces release of AKHs from corpora cardiaca *in vitro.* Stimulation of the NCC-I alone does not cause release, but it potentiates NCC-II-stimulated AKH release. This suggests that axons of the NCC-I play no part in the initiation of hormone release, but could have a neuromodulatory role. When release of AKH activity was assessed *in vivo,* however, severance of both the NCC-I and NCC-II was required to prevent lipid mobilization during flight. The fibers of a group of about 15 secretomotor neurons situated laterally in the protocerebrum are the only fibers known to enter the glandular part of the corpus cardiacum, via the NCC-II, and to make direct synaptic contact with ipsilateral adipokinetic cells (Fig. 6a) (Konings *et al.,* 1989). Orchard and Shivers (1986) presented evidence for the existence of electrical coupling between adipokinetic cells via gap junctions, which might favor the synchronization of the secretory activity of the individual adipokinetic cells.

The origin of the stimuli that act on the protocerebral secretomotor neurons, which in turn are supposed to regulate the release of AKH during flight, is unknown.
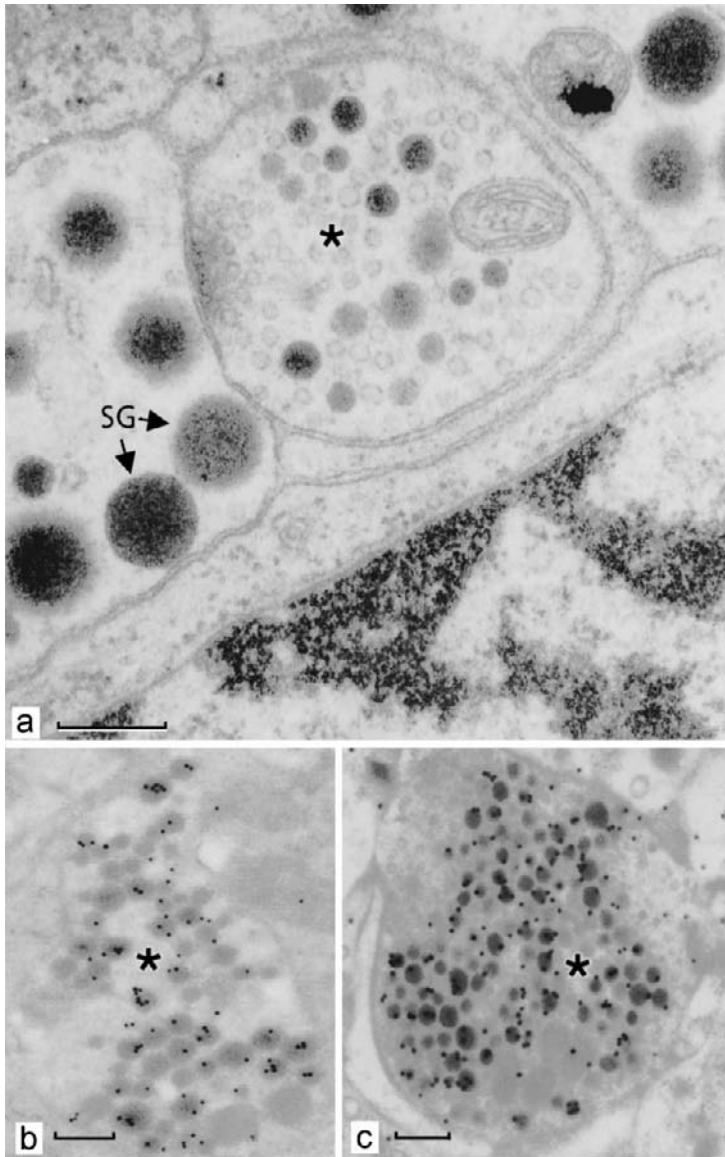
FIG. 6   Synaptic axon endings (asterisks) in the glandular part of the corpus cardiacum of *L. migratoria*. The endings contain both electron-lucent and electron-dense vesicles (a). The electron-dense vesicles in some endings show immunoreactivity (immunogold labeling) with an antiserum specific for Lom-TK (b), whereas in other endings these vesicles are SchistoFLRFamide-immunopositive (c). SG, secretory granules in adipokinetic cell. Bars = 0.5 μm.

Since these stimuli must be associated with flight, sensory organs involved in flight movement might be concerned. Deprivation of antennae and/or immobilization of sensory hairs on the head, and cauterization of the wing tegulae, however, did not prevent the flight-induced release of AKH. This indicates that activation of the secretomotor neurons does not depend on direct information from these organs. It is conceivable that the secretomotor neurons are controlled by the flight-generating neural circuitry in the central nervous system (Bloemen and Beenakkers, 1985).

Retrograde tracing of the NCC-II *in vitro* with Lucifer yellow in combination with immunocytochemistry using antisera specific for locustatachykinins (Lom-TKs) revealed that four or five of the secretomotor neurons in the lateral part of the protocerebrum that project into the glandular part of the corpus cardiacum are Lom-TK-immunopositive. Also axonal endings in the glandular part appeared to be Lom-TK-immunopositive (Fig. 6b). The role of two of the Lom-TKs (I and II) in the regulation of the release of AKH-I was investigated *in vitro;* these two peptides induced release of AKH-I. They also rapidly and transiently elevated the cAMP level in the glandular part of the corpus cardiacum. These results strongly suggest that Lom-TKs released from axon terminals in the glandular part are involved as neuroactive compounds in the initiation of the release of AKH by elevating the cAMP level in the adipokinetic cells (Nässel *et al.,* 1999). Veelaert *et al.* (1999), however, failed to detect any immunopositive staining in the glandular part of the corpus cardiacum with antisera used to immunolocate tachykinin receptor-like proteins, which casts some doubt on the role of Lom-TKs in the neural regulation of AKH release.

Antisera raised against the tetrapeptide FMRFamide and the decapeptide SchistoFLRFamide, which belong to the large superfamily of FMRFamide-related peptides (FaRPs), also labeled neuronal processes that impinge on adipokinetic cells (Fig. 6c). Retrograde tracing of the axons in the NCC-II with Lucifer yellow revealed that about five of the secretomotor neurons in the lateral part of the protocerebrum that project into the glandular part of the corpus cardiacum reacted with the SchistoFLRFamide antiserum. Double-labeling immunocytochemistry showed that the FaRP-containing axonal processes in the glandular part are distinct from neuronal processes reacting with an antiserum specific for Lom-TKs. The effect of SchistoFLRFamide and FMRFamide on the release of AKH-I was studied *in vitro.* These peptides did not influence the spontaneous release of AKH-I. Release of AKH-I induced by the phosphodiesterase inhibitor 3-isobutyl-1-methylxanthine (IBMX), however, was reduced significantly by both peptides. IBMX raises the intracellular cAMP level, which in turn induces the release of AKHs. These results point to an involvement of FaRPs as inhibitory modulators in the regulation of the release of AKHs (Vullings *et al.,* 1998).

The Locustamyoinhibiting peptide (Lom-MIP), which suppresses the spontaneous contractions of the hindgut and oviduct of *L. migratoria,* also inhibited the release of AKHs induced by IBMX *in vitro* (Harthoorn *et al.,* 2001). Immunocytochemistry revealed a small number of Lom-MIP-positive neurons in the brain

of locusts, and immunopositive fibers were found to be present in the NCC-II with arborizations in the glandular part of the corpus cardiacum (Schoofs *et al.,* 1996). These results suggest an inhibitory modulatory role of Lom-MIP in the regulation of the release of AKHs.

2. Humoral Regulation

In addition to neural regulation, humoral regulation of the adipokinetic cells by substances that reach these cells via the hemolymph may be involved as well. Crustacean cardioactive peptide (CCAP) initiated the release of AKH-I in a dose-dependent manner when tested *in vitro* in concentrations ranging between 10^{-5} and 10^{-9} M (Veelaert *et al.,* 1997). Such low concentrations imply that CCAP meets the requirements for a neurohormonal status. Axons from CCAP-immunoreactive neurons situated in the suboesophageal ganglion project to the storage part of the corpus cardiacum, but do not clearly extend into the glandular part of the corpus cardiacum, where the adipokinetic cells are located (Dircksen and Homberg, 1995). Thus, it is likely that humoral CCAP, which has its origin either in the storage part of the corpus cardiacum or in varicose fibers that run at the surface of the NCC-II and its branches, exerts the AKH-releasing effect. Most of the humoral effects that were reported for CCAP appear to be related to a physiological situation that corresponds with periods of increased activity and higher energy metabolism.

Octopamine also is involved in the regulation of the adipokinetic cells. When tested *in vitro,* it potentiates the effect of stimulation of the adipokinetic cells by several release-initiating substances, but cannot induce AKH release on its own. Octopamine could not be found to be present in the glandular part (nor in the storage part) of the corpus cardiacum, neither immunocytochemically with an antiserum against octopamine, nor by means of an electrochemical detection method. The hemolymph titer of octopamine is known to increase threefold at the onset of flight, which suggests a humoral role for octopamine in the regulation of AKH release, reaching the adipokinetic cells from the hemolymph which bathes the corpus cardiacum (Passier *et al.,* 1995).

Like octopamine, also the amines dopamine, serotonin, and tyramine only potentiate the AKH release induced by release-initiating agents and cannot induce AKH release on their own. Dopamine and serotonin could be found to be present only in the storage part of the corpus cardiacum, not in the glandular part. Tyramine, which is known to be present in the locust central nervous system, could not at all be detected in the corpus cardiacum. The natural role of these substances, if any, in the regulation of AKH release is unclear. Since dopamine and serotonin have been shown immunocytochemically to be present in NCC-I axons, these substances might be involved in the supposed neuromodulatory role of the NCC-I in AKH release (Passier *et al.,* 1995).

The transport form of carbohydrate in insects, the disaccharide trehalose, was shown to inhibit the spontaneous release of AKH-I from the locust corpus

cardiacum *in vitro* in a dose-dependent manner. At a concentration of 80 mM, which is the concentration found in the hemolymph at rest, trehalose significantly decreased the amount of released AKH-I, whereas at 40 mM trehalose, which is the concentration during prolonged flight, no inhibitory effect could be observed. A concentration of 80 mM trehalose also significantly decreased the release of AKH-I induced by AKH release-inducing agents such as Lom-TK-I or IBMX. These data support the hypothesis that *in vivo* the relatively high concentration of trehalose (80 mM) at rest strongly inhibits the release of AKHs. At the onset of flight, the demand for energy substrates results in a decrease of the trehalose concentration in the hemolymph. This relieves the inhibitory effect of trehalose on the release of AKHs, which in turn start to mobilize lipids (and glycogen) from the fat body (Passier *et al.,* 1997). A more extensive review on the control of the release of AKHs has recently been published by Vullings *et al.* (1999).

F. Release of Adipokinetic Hormones

All substances discussed above may act in concert in the regulation of the release of AKHs, activating intracellular signal transduction pathways, which ultimately induce the release process. The first pathway known to be involved is the adenylyl cyclase pathway, which uses cAMP to activate protein kinase A (Nässel *et al.,* 1999). Recently, it was demonstrated that also activation of protein kinase C by the specific activator phorbol-12-myristate-13-acetate stimulates the release of AKHs (Harthoorn *et al.,* 2001). This points to the possible involvement of a transduction pathway starting with the activation of membrane-bound phospholipase C, which generates two signal molecules. Additionally to Ins(1,4,5)P$_3$, DAG is generated, which eventually mediates the activation of protein kinase C.

The presence of all three AKH-associated peptides and thus likely of all three AKHs in the secretory granules of almost all adipokinetic cells in *L. migratoria,* as shown immunocytochemically by Harthoorn *et al.* (1999) (Fig. 5), allows for the supposition that all three AKHs will be released after secretory stimulation of these cells, together with their APRPs. The release of between 2 and 6% of the AKHs present in the corpora cardiaca has been reported to occur after *in vitro* IBMX stimulation for 30 min (Sharp-Baker *et al.,* 1996). Application of dibutyryl cAMP to corpora cardiaca *in vitro* also significantly increased the release of all three AKHs in comparison with the spontaneous release occurring from nonstimulated corpora cardiaca *in vitro* (Harthoorn *et al.,* 1999). The stimulation:control ratio between the amounts released during 2 h was approximately 2.0 for all three AKHs. This points to parallel secretion of the three hormones by the glandular part of the corpus cardiacum.

A different pattern of release of AKH-III is conceivable, since also differences between AKH-III or its prohormone on the one hand and AKH-I and -II or their

prohormones on the other were found as to the level of biosynthesis, storage, and degradation. As discussed above, the content of AKH-III in the corpora cardiaca increases exponentially with age in contrast to those of AKH-I and -II, which increase linearly (Oudejans *et al.,* 1993). The intracisternal granules show no immunoreactivity with an anti-AKH-III-associated peptide antiserum and in some adipokinetic cells also the secretory granules show no or very low immunoreactivity with this antiserum (Harthoorn *et al.,* 1999). AKH-III has the shortest half-life time of all three AKHs in the hemolymph, both under rest conditions and during flight activity (Oudejans *et al.,* 1996). Apart from regulated parallel secretion of AKH-III together with the other two AKHs in response to physiological stimulation as described above, a pattern of constitutive release or of regulated preferential release (nonparallel secretion) of AKH-III might be envisaged. The necessary transport vesicles for constitutive release and secretory granules for regulated release, both containing only or mainly AKH-III (pro) hormones, however, are not known to be present in the adipokinetic cells.

The APRPs will most likely be released into the hemolymph together with the release of the AKHs. Hekimi and O'Shea (1989) reported a potassium-stimulated release of two APRPs in *S. gregaria.* Using very sensitive mass spectrometric techniques, Clynen *et al.* (2001) could, however, not always detect APRPs in the incubation media of potassium-treated corpora cardiaca from *L. migratoria.* Whether this is indicative of an absence of APRP release or due to sample pretreatment and/or imperfections in the detection method remains elusive. It is unclear whether the APRPs have any physiological function outside the adipokinetic cells (Hatle and Spring, 1999).

1. Preferential Release of Newly Synthesized AKHs

Whereas all three AKHs accumulate within the adipokinetic cells with age (and the number of AKH-containing secretory granules increases continuously), during flight only a relatively small fraction of the total store of AKHs is released (Cheeseman and Goldsworthy, 1979). Consequently, the store of hormones in the adipokinetic cells consists of a mixture of young and old secretory granules. This raises the question: is there a relationship between the age of a secretory granule and its chance of being released during flight? To answer this question, Sharp-Baker *et al.* (1995, 1996) investigated the influence of secretory stimulation on the release of newly synthesized AKHs, both at the level of secretory granules (*in vivo*) and at the level of hormone molecules (*in vitro*).

Two labeling methods were applied to distinguish young, newly formed secretory granules from older, preexisting ones (Sharp-Baker *et al.,* 1995). One method was based on the endocytic incorporation of the enzyme horseradish peroxidase conjugated with the lectin wheat-germ agglutinin (WGA-HRP). This lectin binds to the plasma membrane due to its high affinity for specific sugar residues. Endocytosed fragments of plasma membrane with bound label are transported to the

trans-Golgi network and used for the production of new secretory granules, which thus become labeled with peroxidase (Fig. 7a) (Diederen and Vullings, 1995). During a 31.5-h period several WGA-HRP injections and several periods of secretory stimulation by flight were applied. At the end of this period, the corpora cardiaca were dissected and fixed, and the HRP was visualized enzyme-cytochemically by electron microscopy.

The other method for labeling young, newly formed secretory granules was based on the biosynthetic incorporation of [^{3}H]amino acids into newly synthesized peptides/proteins at the rough endoplasmic reticulum. These substances are then packaged into new secretory granules at the *trans*-Golgi network, which results in radiolabeled new secretory granules. Five hours after the injection of the radioactive amino acids, during which period the locusts had flown twice, the corpora cardiaca were dissected and fixed, and the incorporated radioactive amino acids were visualized autoradiographically by electron microscopy (Fig. 7b).

Both methods used to label young secretory granules revealed that flight-stimulated adipokinetic cells contained significantly less labeled secretory granules than unstimulated cells. At the same time, the total number of secretory granules
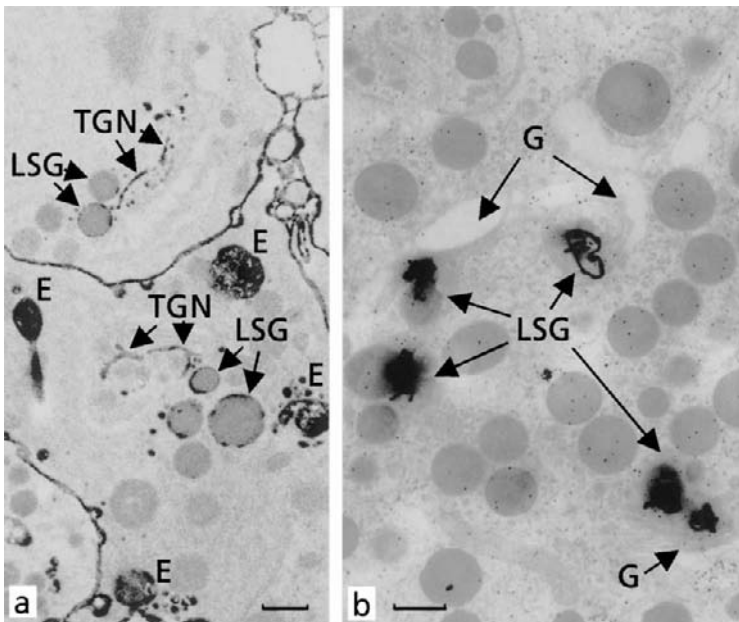
FIG. 7 The ultrastructural appearance of newly formed secretory granules in adipokinetic cells after labeling with horseradish peroxidase conjugated with wheat-germ agglutinin (a) and after labeling with radioactive (tritiated) amino acids (b). E, endosomal/lysosomal structure; G, Golgi complex; LSG, labeled secretory granule; TGN, *trans*-Golgi network. Bars = 0.25 μm.

was nearly unaffected. Consequently, the percentage of labeled secretory granules was significantly lower in flight-stimulated than in unstimulated cells. This means that during secretory stimulation, young secretory granules are preferentially released over older ones.

The influence of secretory stimulation on the release of newly synthesized AKHs at the level of molecules was studied by *in vitro* incubation of corpora cardiaca supplied with tritiated amino acids (Sharp-Baker *et al.,* 1996). Since all three AKHs contain one phenylalanine residue, incorporation of radiolabeled phenylalanine into the AKHs was used to distinguish newly synthesized (radioactive) AKHs from older, preexisting (nonradioactive) AKHs. In pulse-chase labeling experiments of varying duration, with the pulse period being maximally 3.5 h, AKH secretion was stimulated for 30 min by IBMX. The total incubation time varied from 2.5 to 16.5 h. Both released (medium) and nonreleased (tissue) AKHs were then screened by reversed-phase high-performance liquid chromatography and scintillation spectrometry, and the specific radioactivity of each of the AKHs in both fractions was determined.

The ratio of specific radioactivities of the released and the nonreleased AKHs was always greater than 1.0, which indicates that the newly synthesized hormones are released preferentially over older (nonradioactive) ones, which corresponds with the observed preferential release of newly formed secretory granules. The percentages of newly synthesized AKH-I that were released, increased during the first ~8.5 h of incubation but decreased thereafter. The synthesis, packaging into secretory granules and processing of the AKH prohormones to bioactive AKHs takes less than 75 min, while the transport of secretory granules along the 20- to 200-μm-long axonal processes by means of fast axonal transport presumably takes only a few minutes. Thus, the observed pattern of increase and decrease in the percentage of newly synthesized AKH-I released with time suggests that, in addition to the time required for synthesis, packaging and processing of the AKH-I prohormones and for the transportation of the secretory granules to the cellular processes for release, some further maturation of the secretory granules occurs before they are able to release their content. Moreover, the decrease in the percentage of radioactive (newly synthesized) AKH-I that was released after 8.5 h suggests that after this time secretory granules containing radioactive AKH-I enter a non-releasable pool of older secretory granules. This topic clearly needs more detailed investigation.

Since in *L. migratoria* all three AKHs are colocalized in the secretory granules (Diederen *et al.,* 1987; Harthoorn *et al.,* 1999), the findings for AKH-I, in all likelihood, also hold for AKH-II and -III. This supposition is strengthened by the observations that the percentages of released radioactive (newly formed) AKH-II followed a pattern roughly similar to that of AKH-I and that the percentages of released newly synthesized AKH-III peaked at about 8 h (Sharp-Baker *et al.,* 1996). As an important conclusion of the above data, it may be inferred that the existence of a probably large nonreleasable pool of AKH-containing secretory granules stresses

the fact that determination of the total hormone content of a neuroendocrine gland has only limited physiological value; only the releasable amount of hormone is relevant.

G. Function of Intracisternal Granules

Harthoorn *et al.* (2000) assessed the rate of formation of intracisternal granules in locusts by studying autoradiographically the biosynthetic incorporation of radioactive amino acids by corpora cardiaca in an *in vitro* system. Heavily labeled granules were found already 1.5 h after administration of the radioactive amino acids, which indicates that these granules were formed largely or even completely within this 1.5-h period.

Locusts exhibit density-dependent phase polymorphism; crowding induces the gregarious phase, whereas isolation leads to the solitary phase (Pener *et al.,* 1997). The number and size of intracisternal granules in the adipokinetic cells is much larger in older solitary than in older gregarious locusts (Diederen *et al.,* 1999). Moreover, the compartment of intracisternal granules increases with age (Diederen *et al.,* 1992; Michel and Lafon-Cazal, 1978). This raises the question of what the function of these granules might be.

1. Intracisternal Granules Are Not Degraded

The intracisternal granules may be supposed to contain improperly folded or non-correctly assembled or in some other way defective, transport-incompetent secretory proteins, as is assumed for intracisternal granules in other cell types, and may thus be destined for degradation (Hurtley and Helenius, 1989). Harthoorn *et al.* (2000) investigated the possibility of degradation of the intracisternal granules in adipokinetic cells. After administration of the endocytic tracers HRP and WGA-HRP to the adipokinetic cells, these tracers can be visualized cytochemically in endosomal, autophagic and lysosomal organelles (Diederen and Vullings, 1995; Jansen *et al.,* 1989). If intracisternal granules were to be degraded by autophagy, they would have to be taken up in autophagic vacuoles, which would also have received (WGA-)HRP by fusing with endosomes or lysosomes that contained these tracers. However, no intracisternal granules could be found in any (WGA-)HRP containing lysosomal or autophagic structure. Apparently, these granules in locust adipokinetic cells are not degraded by means of autophagy.

If (WGA-)HRP-labeled lysosomal structures were to fuse with intracisternal granules directly, as has to be expected if these granules were to be degraded by a crinophagy-like process, then intracisternal granules should be found which contained (WGA-)HRP. However, no such granules were found. Apparently, intracisternal granules in locust adipokinetic cells are also not degraded by crinophagy.

The absence of autophagic and crinophagic degradation of intracisternal granules was confirmed by enzyme-cytochemical demonstration of the lysosomal

enzyme acid phosphatase. Acid phosphatase was found in all categories of organelles belonging to the lysosomal and autophagic systems (see also Jansen *et al.,* 1989), but was never seen within intracisternal granules, nor could these granules be found to be present within any acid phosphatase-positive organelle. In conclusion, the intracisternal granules in the adipokinetic cells are not degraded.

2. Intracisternal Granules Are Stores of Hormonal Substances

Although intracisternal granules have never been reported to release their content directly to the cell exterior like secretory granules do, they decrease in number during a short flight (2 h) and even completely disappear during sustained flight (20 h) (Michel and Lafon-Cazal, 1978). This strongly suggests that flight activity can stimulate the transport of intracisternal granule prohormonal content for further processing to the Golgi system and secretory granules, which may ultimately result in release of bioactive hormones. On the other hand, solitary *L. migratoria* contain more and larger intracisternal granules in their adipokinetic cells than gregarious locusts, which is most probably related to phase-dependent differences in energy metabolism (Diederen *et al.,* 1999). The amount of lipid reserves, resting levels of hemolymph lipids, and hyperlipemic responses to flight and AKHs are lower in solitary than in gregarious locusts, which correlates well with the general locomotor activity also being lower in solitary than in gregarious locusts (Pener *et al.,* 1997). This might imply that less fuel has to be mobilized from the fat body and, consequently, assuming that also in nonflying locusts some AKH has to be released to provide the insect with sufficient fuel, less AKHs have to be released from the adipokinetic cells in solitary than in gregarious locusts. This could lead to accumulation of AKH prohormones in solitary locusts, because earlier studies indicate that AKHs are synthesized continuously (Diederen *et al.,* 1992; Diederen and Vullings, 1995; Oudejans *et al.,* 1993). Although release of AKHs in nonflying, resting locusts is uncertain, it may occur, as judged from the presence of exocytic profiles in the adipokinetic cells seen by electron microscopy (Rademakers and Beenakkers, 1977), as well as a small amount of AKH activity in the hemolymph of resting locusts (Cheeseman and Goldsworthy, 1979). Harthoorn *et al.* (1999) report the spontaneous release of small amounts of all three AKHs under *in vitro* conditions from dissected corpora cardiaca, which, consequently, are no longer under any neural or humoral (stimulatory or inhibitory) regulatory influence.

Pener *et al.* (1997) explain the higher content of hormonal substances in the adipokinetic cells of solitary locusts by assuming that these locusts need more AKHs for mobilization of sufficient lipids for longer flights than gregarious locusts, because the solitary locusts have lower adipokinetic responses to AKHs than the gregarious locusts. This explanation implies the unlikely supposition that solitary locusts synthesize more adipokinetic hormones than gregarious locusts in anticipation of flight. In conclusion, AKH prohormones, presumably in their unprocessed form, accumulate in intracisternal granules when the rate of synthesis

of these prohormones is too high for storage in and release from ordinary secretory granules. The intracisternal granules thus may be considered to represent a spatially economic way for the cell to store extra AKH prohormones.

Ayali *et al.* (1996a) reported that the corpora cardiaca contain more APRPs in solitary locusts than in gregarious ones. The content of AKHs (I and II) of the corpus cardiacum also was higher in solitary than in gregarious locusts, at least in adults between 12 and 19 days old (Ayali *et al.,* 1996b). No such difference was found in older adults between 25 and 30 days old. This may be explained by the assumption that the AKH prohormones in the intracisternal granules have not been processed into APRPs and AKHs, as the intracisternal granules are part of the rough endoplasmic reticulum, whereas proteolytic processing of the prohormones is considered to occur in a post-*trans*-Golgi-compartment (O'Shea and Rayne, 1992). Therefore, the observation that the compartment of intracisternal granules is much larger in older solitary than in older gregarious locusts (Diederen *et al.,* 1999) does not necessarily implicate a similar difference in the amounts of free bioactive AKHs. In this context, however, the observation of Ayali *et al.* (1996a) that older adult solitary locusts (25–30 days old) contain more APRPs than gregarious locusts of the same age is difficult to explain. Moreover, Harthoorn *et al.* (2000) found significant amounts of AKH-I, -II, -III also to be present in the intracisternal granules, the origin of which also is difficult to explain from a cell-biological point of view. Obviously, more detailed investigation into this matter is needed.

Harthoorn *et al.* (2000) performed a biochemical analysis also of the AKH-I prohormones in the intracisternal and secretory granules using reversed-phase HPLC. This method allowed for the identification of the prohormone of AKH-I, which is present in a relatively high amount. The prohormone was found to be present in the HPLC-profiles in the form of two peaks with a very small difference between their retention times, one in the intracisternal granules and the other in the secretory granules. They suggested that the prohormone is present in the intracisternal granules in a nondimerized form and in the secretory granules in a dimerized form as far as it has not been processed.

H. Coupling between Release and Biosynthesis of Adipokinetic Hormones

Bogerd *et al.* (1995) reported an increase in the steady-state levels of the mRNAs of all three AKH preprohormones in the locust corpus cardiacum after 1 h of flight. This increase appeared to be differential, since the levels of AKH-I and -II mRNAs were about two times higher and that of AKH-III mRNA even over four times higher compared to the resting levels. This observation was rather unexpected because only a very small fraction (1–2% per h) of the total store of AKHs is released during flight (Cheeseman and Goldsworthy, 1979). The observed increase in mRNAs during flight might be related to the relatively small pools of

AKHs available for direct use, as discussed above, rendering up-regulation vital. On the other hand, it should be stressed that elevations in mRNA content may not always reflect a direct increase in protein synthesis (Bean *et al.,* 1994).

The results of ample experimentation with a more sophisticated technique involving an RNase protection assay instead of Northern blotting, however, did not confirm the earlier findings on flight-induced AKH-gene expression (Harthoorn *et al.,* 2001). Until now, no clear upregulation of any of the AKH-specific mRNAs could be found, neither after inducing AKH release by flight activity during 0.5–2 h, nor after treatment of corpora cardiaca, *in vitro* with AKH release-inducing substances during 2 h. In addition, no influence of secretory stimulation on the levels of the AKH prohormones and on the rate of biosynthesis of (pro-)AKHs could be detected.

Sharp-Baker *et al.* (1995) observed that the total number of secretory granules did not clearly diminish in flight-stimulated ($\geq$1.5 h) adipokinetic cells, which points to an increase in the formation of new secretory granules in these cells, to compensate for the flight-induced exocytosis of secretory granules. This supposition is strengthened by the tendency of the flight-stimulated cells to display more WGA-HRP-labeled *trans*-Golgi networks than unstimulated cells, which suggests that flight activity stimulates the process of membrane recycling concomitant with the flight-induced exocytosis and production of secretory granules. This is in agreement with findings of Diederen and Vullings (1995), which also point to a flight-induced (1 h) enhancement, albeit slight, of secretory granule production by the *trans*-Golgi network. Therefore, the continuous production of AKH-containing secretory granules may not be entirely adequate to provide the adipokinetic cells with sufficient young granules needed for exocytosis upon secretory stimulation by flight. The slight enhancement in the production of secretory granules that might be induced by flight activity apparently does not need to be accompanied by a clear increase in the biosynthesis of the AKHs. In conclusion, a coupling between release and biosynthesis of AKHs in the adipokinetic cells is very loose or does not even exist. The strategy of these cells to cope with variations in secretory demands rather seems to be a continuous biosynthetic activity, thereby producing an apparently sufficient pool of secretory material. This suggests that the large stores of hormonal substances in the adipokinetic cells are the result of its biosynthesis not being tuned to the release of the AKHs, rather than being the reason for the absence of a coupling between release and biosynthesis.

I. Degradation of Adipokinetic Hormones

Although knowledge on the amounts of hormones that are released by neuroendocrine cells after secretory stimulation is important to interpret experimental effects in the *in vivo* situation, the balance between hormone release and the rate

of degradation of released hormones in the hemolymph (or blood) will ultimately determine their availability for action on their target cells. Particularly when a mixture of released hormones will be degraded differentially, the changing ratio between the hormones may dramatically alter their joint regulatory effects. The degradation of the AKHs was studied *in vivo* using radiolabeled AKHs with very high specific radioactivities at physiological doses as low as 1.0 pmol per locust (Oudejans *et al.,* 1996).

All three AKHs are inactivated by endoproteolytic cleavage of the N-terminal tripeptide pGlu-Leu-Asn; the resulting peptides have no adipokinetic activity. The degradation of the AKHs appeared to be differential; half-lives obtained for AKH-I, -II, and -III were 51, 40, and 5 min, respectively, in animals at rest, and 35, 37, and 3 min, respectively, in animals during flight. The initial ratio of the hormones in the corpus cardiacum will therefore change rather drastically upon release. As will be elaborated below, the disparity in half-lives of the AKHs, combined with the variance in their initial amounts, suggests that AKH-I is the most important hormone for prolonged flight activity, when lipid is the predominantly mobilized fuel. AKH-II, which is less abundant and degraded more rapidly than AKH-I at rest, may be more important in the early period of flight, when carbohydrate mobilization is the main source of energy. AKH-III, in view of its low abundance and rapid degradation, may be presumed to play a more modulatory role at rest (Oudejans *et al.,* 1996; Van der Horst *et al.,* 1999).

III. Adipokinetic Hormone Signaling

A. Regulation of Flight-Directed Substrate Mobilization

The action of the AKHs on the insect fat body ultimately results in the mobilization of stored reserves as fuels for flight (Fig. 8). Carbohydrate, released from the fat body in the form of the disaccharide trehalose, is mobilized from glycogen reserves. This implies hormonal activation, by phosphorylation, of the key enzyme, glycogen phosphorylase, which initiates the conversion of glycogen into trehalose. Similarly, lipid is mobilized from stored TAG as 1,2-DAG, which implies hormonal activation of the fat body triacylglycerol lipase. Unlike TAG, DAG is efficiently transferred across the fat body cell membranes, where it binds extracellularly to its hemolymph transport vehicle, lipophorin. The carbohydrate and lipid substrates are transported in the hemolymph to the working flight muscles. Carbohydrate provides most of the energy for the initial period of flight; thereafter, in long-term flying insects like locusts, the concentration of lipid substrate in the blood increases and gradually takes over, so the principal substrate for long-term flight is lipid. The involvement of AKHs or other peptides of the AKH/RPCH family in the regulation of carbohydrate and lipid mobilization in insects was demonstrated *in vivo* by the activation of fat
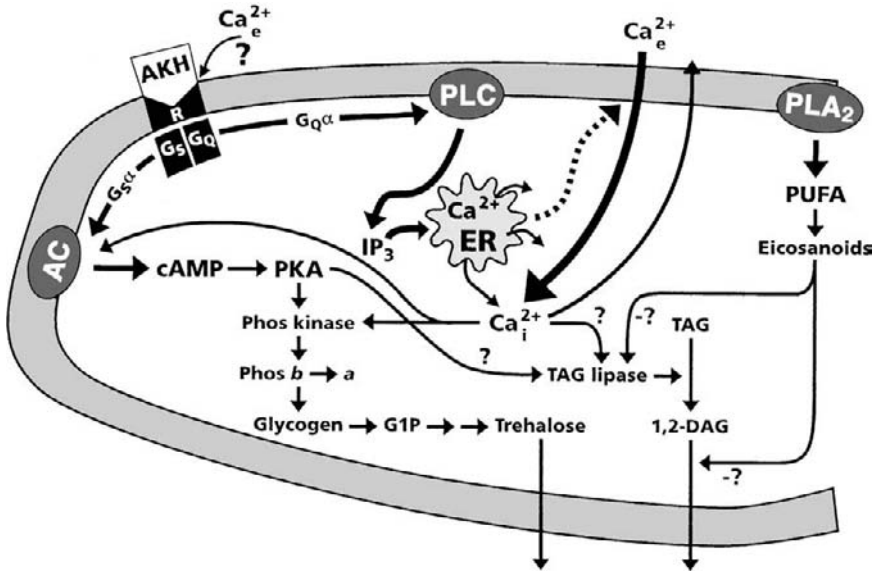
FIG. 8   Tentative model for the coupling of AKH signaling pathways mediating the mobilization of carbohydrates and lipids in the locust fat body cell. The broken line suggests that depletion of ER Ca^{2+} stores somehow leads to increased permeability of the plasma membrane for Ca_e^{2+}. AKH, adipokinetic hormones; R, receptor; G_s, G_s protein; G_q, G_q protein; $G_s\alpha$ and $G_q\alpha$, α-subunit of G_s and G_q, respectively; ER, endoplasmic reticulum; AC, adenylyl cyclase; PLC, phospholipase C; PLA$_2$, phospholipase A$_2$; cAMP, cyclic AMP; IP$_3$, inositol-1,4,5-trisphosphate; PUFA, polyunsaturated fatty acids; Ca_e^{2+}, extracellular Ca^{2+}; Ca_i^{2+}, intracellular Ca^{2+}; PKA, protein kinase A; Phos, phosphorylase; GIP, glucose-1-phosphate; TAG, triacylglycerol; DAG, diacylglycerol.

body glycogen phosphorylase or the increase in trehalose or DAG levels in insect hemolymph after hormone injection. Additionally, this involvement was evidenced in fat body *in vitro* by activation of phosphorylase, increase of trehalose release into the medium, and accumulation of DAG in isolated fat body tissue incubated in the presence of hormone (reviewed in Van der Horst *et al.,* 1999).

Although in a bioassay all three locust AKHs are able to activate both glycogen phosphorylase and triacylglycerol lipase, differences in potency were noticed. Results obtained with combinations of two or three AKHs, which are likely to occur together in locust hemolymph under physiological conditions *in vivo,* revealed that the maximal responses for both the carbohydrate- and the lipid-mobilizing effects were much lower than the theoretically calculated responses that were based on dose–response curves for the individual hormones. In the lower (probably physiological) range, however, combinations of the AKHs were more effective or at least as effective as the theoretical values calculated from the responses to the individual hormones (Oudejans *et al.,* 1992). In addition to their different potencies in eliciting substrate mobilization, all three AKHs inhibit RNA synthesis in the

locust fat body *in vitro* (Kodrík and Goldsworthy, 1995). In males, the responses were dose-dependent with their potencies decreasing in the order AKH-III > AKH-II > AKH-I. All three AKHs were equally efficacious. These data may point to the occurrence of different receptors for the AKHs or, alternatively, the observed differences in effectiveness of the three AKHs may be due to differences in the mechanism of hormonal signal transduction. However, a decisive factor for the ability to elicit physiological responses is the relative abundance of each of the hormones, which is determined by their rates of synthesis and release, but also depends on the rate of inactivation of the hormones, as has been discussed above.

B. Activation of Glycogen Phosphorylase in Insect Fat Body

Hormonal stimulation of glycogenolysis in the insect fat body leading to an increased biosynthesis and release of trehalose has been investigated extensively in cockroaches, which mainly rely on carbohydrate as a fuel for flight activity. Hypertrehalosemic hormones (HTHs), members of the AKH/RPCH family, were shown to activate fat body glycogen phosphorylase and stimulate trehalose synthesis in the cockroaches *Periplaneta americana* (Steele, 1985) and *Blaberus discoidalis* (Park and Keeley, 1995; Keeley *et al.,* 1995). Activation of fat body phosphorylase by AKH peptides has been demonstrated, in addition to locusts, in larvae of *M. sexta* (Ziegler *et al.,* 1990), and in the cetoniid beetle *P. sinuata* (Auerswald and Gäde, 2000).

Although in the locust fat body, glycogen phosphorylase is converted into its phosphorylated active form within a few minutes of flight activity, it takes almost half an hour before newly synthesized trehalose is released. A possible explanation for this lag period may be that the allosteric enzyme is kept in its inactive T (tense) state as long as the concentration of trehalose is high and will switch to its active R (relaxed) state only after a substantial reduction of trehalose levels in the fat body, as may occur during flight activity. A similar mechanism has been described for the inhibition of phosphorylase *a* by glucose in vertebrate liver (Johnson, 1992). Alternatively, there may be another regulatory step in trehalose biosynthesis, in additon to glycogen phosphorylase, as has been suggested by Steele *et al.* (1988) and Keeley *et al.* (1996). The latter authors have shown that treatment of isolated fat body of *B. discoidalis* with Bld-HTH doubled the activity of trehalose-6-P synthase activity, and they speculate that hormonal regulation of trehalose synthesis occurs at two levels. The first level is activation of glycogen phosphorylase, the rate-limiting step in trehalose biosynthesis producing the hexose precursors (glucose-1-P and glucose-6-P) that can be used for either trehalose biosynthesis or by several competing pathways. The second site of regulation would be at the level of trehalose-6-P synthase to increase the activity of this enzyme and thus direct the conversion of the glycolytic products to trehalose biosynthesis.

Moreover, it has been demonstrated that during trehalogenesis in cockroach fat body, glycolysis is inhibited, possibly by an HTH-induced decrease of fructose 2,6-bisphosphate, which is a potent activator of the key glycolytic enzyme phosphofructokinase (Becker *et al.,* 1996; Becker and Wegener, 1998). In this way, HTH would alter the balance of glucose metabolism in favor of trehalose synthesis. If these regulatory processes are also involved in AKH-controlled carbohydrate mobilization in locusts, this could explain the observed delay in the release of newly synthesized trehalose after the rapid hormonal activation of glycogen phosphorylase.

C. Triacylglycerol Mobilization in Insects versus Vertebrates

In both vertebrates and invertebrates sustained physical exercise is fueled largely by the oxidation of long-chain FAs, which are derived from stored TAG reserves. In vertebrates, FAs, are mobilized from TAG stores in adipose tissue, and a crucial role in this process is played by hormone-sensitive lipase (HSL). This enzyme controls the rate of lipolysis, catalyzing the first and rate-limiting step in the hydrolysis of the stored TAG, and also the subsequent hydrolysis of DAG and monoacylglycerols (MAGs) (reviewed in Holm *et al.,* 1997; Gibbons *et al.,* 2000). The FAs liberated in adipose tissue are released into the blood and transported bound to serum albumin for uptake and oxidation in muscle.

Unlike FA in vertebrates, lipid in insects is released as DAG and transported to the flight muscles by lipophorin, the major lipoprotein present in the hemolymph. At the flight muscles, DAG is hydrolyzed and the liberated FAs are taken up and oxidized to provide energy.

There is a clear functional similarity between vertebrate adipose tissue HSL and insect fat body TAG lipase, as both enzymes catalyze the hydrolysis of TAG stores to meet energy demands. However, there is an essential difference in the mode of action of both lipolytic enzymes. The vertebrate HSL catalyzes hydrolysis of TAG as well as of DAG and MAG, resulting in the release of FA, whereas the action of the insect TAG lipase eventually causes the formation and release of DAG (Fig. 8). How these differences in the modes of action of vertebrate HSL and insect TAG lipase are brought about is physiologically relevant question that remains elusive. Because insight in the mode of action and the regulation of vertebrate HSL may contribute to our understanding of the mechanism of lipolysis in insects, both the vertebrate HSL and the insect TAG lipase are discussed below.

1. Regulation of Hormone-Sensitive Lipase in Vertebrate Adipocytes

In vertebrate HSL, specific sites have been identified as regulatory and basal sites. The regulatory site is phosphorylated *in vitro* by cAMP-dependent protein

kinase (PKA), resulting in activation of HSL. AMP-activated protein kinase (AMP-PK) is the most likely kinase responsible for phosphorylation of the basal site in unstimulated adipocytes *in vivo*. Phosphorylation of the two sites seems to be mutually exclusive, suggesting that phosphorylation of the basal site has an antilipolytic role *in vivo,* and that phosphorylation of the regulatory site by PKA is preceded by dephosphorylation of the basal site (Holm *et al.,* 1997). Recently, two other PKA phosphorylation sites have been identified which were shown to be critical activity-controlling sites in rat HSL *in vitro* (Anthonsen *et al.,* 1998).

The mechanism behind lipolytic activation upon HSL phosphorylation by PKA is poorly understood, but seems to involve translocation of HSL from the cytosol to the lipid droplet (Egan *et al.,* 1992) as well as conformational changes in the HSL molecule. Different phosphorylation sites in HSL may play different roles in the process of translocation and increase of specific activity of the enzyme. In this connection, it is worth noting that perilipins have been suggested to be involved in lipolysis (Greenberg *et al.,* 1991, 1993). Perilipins are a family of unique proteins intimately associated with the limiting surface of neutral lipid storage droplets. These proteins are acutely polyphosphorylated by PKA on lipolytic stimulation, hinting at a role for perilipins in this process. Phosphorylated perilipin may serve as a docking protein for HSL, allowing lipase association only when cells are hormonally stimulated. Alternatively, conformational changes of phosphorylated perilipins may expose the neutral lipid cores of the lipid droplets, facilitating the ensuing hydrolysis. Results of a recent study provide evidence in favor of latter possibility, demonstrating that in stimulated adipocytes, translocation of perilipin away from the lipid droplet occurs in concert with movement of HSL toward the droplet (Clifford *et al.,* 1997). Thus, perilipin might act as a barrier to deny access of HSL to its lipid substrate in unstimulated adipocytes. Further evidence for a barrier function of perilipins has been presented by Brasaemle *et al.* (2000). When perilipin A, the predominant isoform, was expressed in fibroblastic 3T3-L1 preadipocytes that normally lack the perilipins, the lipolysis of stored TAG was five times slower than in control cells. This stabilization of TAG, resulting in increases of the TAG content in perilipin expressing cells, was not due to the suppression of TAG lipase activity by perilipin A, but was caused by a reduced accessibility of soluble lipases to stored lipids. Whether the phosphorylation of perilipin A by PKA upon lipolytic stimulation of adipocytes plays a role in attenuating the barrier to lipolysis remains to be established. Recently Syu and Saltiel (1999) have described the existence of a fat-associated docking protein, lipotransin, which would facilitate the movement of HSL to the lipid droplet. Upon phosphorylation, HSL could interact directly with lipotransin, which would serve to dock the protein at the outer surface of the lipid droplet. The authors propose that once bound, lipotransin can then undergo a cycle of ATP hydrolysis due to the intrinsic ATPase activity of lipotransin, permitting the dissociation of HSL and its direct association with the lipid droplet.

In addition to droplet-associated proteins involved in the direct interaction of HSL with the lipid droplet (perilipins, lipotransin), HSL might be tethered in the cytoplasm in the basal state by the interaction with other cellular proteins, while after phosphorylation HSL could be released. Shen *et al.* (1999) have identified one such protein as the major intracellular adipocyte lipid-binding protein (ALBP). They suggest that fatty acid trafficking during lipolysis is mediated by ALBP and that the ALBP-HSL complex is the first step in an organized lipid transfer process. Whether the interaction of HSL with ALBP influences the function of perilipins or other proteins potentially involved in lipolysis presently remains unclear.

The importance of HSL translocation in hormone-sensitive lipolysis is further emphasized by the studies of Morimoto *et al.* (1999, 2001). These authors have demonstrated that in rat fat cells neither norepinephrine and ACTH-induced lipolysis, nor the antilipolytic actions of propranolol and insulin, involve fluctuations in HSL activity. They concluded that lipolytic agents do not increase the catalytic activity of HSL when lipolytic activation in fat cells occurs. The induced increase in lipolysis would rather be due to HSL translocation from the cytosol to the lipid droplets and changes in the physicochemical character of the endogenous lipid droplet surfaces.

2. Regulation of Lipolysis in Insects

In spite of the importance of lipid mobilization for sustained insect flight, the regulation of lipolysis in insect fat body is poorly understood, mainly due to technical problems in isolating or activating the key enzyme of lipolysis, TAG lipase. The involvement of AKHs in lipolysis was demonstrated *in vivo* from enhanced levels of DAG in hemolymph of insects injected with the hormones (reviewed in Beenakkers *et al.,* 1985) and *in vitro* by the accumulation of DAG in isolated *L. migratoria* fat body tissue that was incubated in the presence of AKH (Lum and Chino, 1990; Wang *et al.,* 1990). In latter *in vitro* experiments, both cAMP and Ca^{2+} were shown to play an important role in the effect of AKH on lipolysis. The involvement of cAMP suggests a role for PKA in the phosphorylation and activation of fat body TAG lipase, which is in line with a previous study of Pines *et al.* (1981) demonstrating a ca. 60% increase of locust fat body TAG lipase *in vitro* upon incubation with cAMP. A recent study reported also a ca. 60% increase of fat body TAG lipase activity in locusts *in vivo* when gregarious *S. gregaria* were injected with 10 pmol AKH-I (Ogoyi *et al.,* 1998). AKH-I administration had no significant effect on lipase activity in solitary locusts. The reason why in these and other similar studies the measured increases of lipase activity after stimulation with lipolytic agents are relatively small may reside in the applied experimental procedure, in which the enzyme is assayed in extracts of fat body or adipose tissue in the presence of optimally accessible TAG substrate. In this way, only the effects of (de)phosphorylation or other conformational changes of the enzyme on

its lipolytic activity will be measured, while other potential effects like enzyme translocation and the involvement of lipid droplet-associated proteins, factors that may be highly important for lipase activity as discussed above for vertebrate HSL, remain out of consideration. This may also explain why phosphorylation by PKA did not change the activity of TAG lipase that had been purified from fat body of adult *M.* sexta (Arrese and Wells, 1994).

In two insect species that rely on lipid mobilization during flight activity, *L. migratoria* and *M. sexta,* it has been shown that the DAG, which is released from the fat body by the action of AKH, is stereospecific and has the *sn*-1,2-configuration (reviewed in Ryan and Van der Horst, 2000). The pathway for the stereospecific synthesis of this *sn*-1,2-DAG is largely unknown. Pathways that have been proposed involve stereospecific hydrolysis of TAG into *sn*-1,2-DAG by a stereospecific lipase acting at the *sn*-3 position of the TAG, and hydrolysis of TAG into *sn*-2-MAG, followed by stereospecific reacylation of *sn*-2-MAG (reviewed in Van der Horst, 1990). As a third possibility, *de novo* synthesis of *sn*-1,2-DAG from *sn*-glycerol-3-phosphate via phosphatidic acid using FA produced by TAG hydrolysis has been suggested (Arrese and Wells, 1994).

Results from experiments on the synthesis of *sn*-1,2-DAG in *M. sexta* conducted with purified TAG lipase (Arrese and Wells, 1994) or a MAG acyltransferase assay (Arrese *et al.,* 1996a), as well as lipolysis in decapitated insects (Arrese *et al.,* 1996b; Arrese and Wells, 1997) led the latter authors to conclude that the pathway for AKH-stimulated synthesis of *sn*-1,2-DAG is stereospecific hydrolysis of TAG. However, some of the data obtained are conflicting (reviewed in Ryan and Van der Horst, 2000). Moreover, stereospecific hydrolysis of TAG into *sn*-1,2-DAG involves hydrolysis of the ester bond of the *sn*-3 fatty acid. The fate of this *sn*-3 fatty acid, which was accumulated neither in the fat body nor in the hemolymph, presently remains unclear (Arrese *et al.,* 2001). It thus appears that although circumstantial evidence may point to a stereospecific hydrolysis of TAG into *sn*-1,2-DAG, conclusive data demonstrating unambiguously the occurrence of this mode of TAG lipase action is still lacking.

In conclusion, unlike the functional similarity between HSL in vertebrate adipose tissue and TAG lipase in insect fat body, there is a discrepancy in the mode of action of both lipolytic enzymes. The vertebrate HSL catalyzes nonstereospecific hydrolysis of TAG as well as of DAG and MAG, resulting in the release of FAs, whereas the, most likely stereospecific, action of the insect TAG lipase causes the formation and release of *sn*-1,2-DAG. So far, the reason for this discrepancy is unknown, but both structural and regulatory aspects may be involved. Elucidation of the mechanism of TAG lipase action and the regulation of its activity is essential for a better insight in the as yet poorly understood mechanism of flight-directed lipolysis in insects. In addition, data obtained may provide clues for a better understanding of the basic processes involved in activation and inactivation of HSL in vertebrates.

D. Hormonal Signal Transduction in Insect Fat Body

Binding of the peptide hormones to their plasma membrane receptor(s) results in the induction of a variety of signal transduction events that ultimately lead to the activation of target enzymes. Throughout our investigations on AKH signal transduction, we have used the activation of glycogen phosphorylase, which initiates the conversion of glycogen to trehalose, as a measure to study the effects of the AKHs on the fat body, since (in contrast to TAG lipase) its activity and hormonal activation can be measured rapidly and accurately in an *in vitro* assay system (Vroemen *et al.,* 1998a). Over the past few years, the signal transduction of the three AKHs has been extensively studied, focusing on GTP-binding (G) proteins, cyclic AMP (cAMP), Ca^{2+}, inositol phosphates ($InsP_n$), signaling crosstalk, and AKH receptor(s). These studies were performed not only to get more insight into AKH signaling in general, but also to answer the physiologically relevant question as to why in locusts (and animals in general) several structurally and functionally related hormones coexist (instead of just one hormone). It has been suggested that the multiplicity in neuropeptides observed in invertebrates imparts complex chemical signaling properties to simple nervous systems and therefore increases their information handling capacity (Geraerts and Smit, 1991; Nässel, 1996). The experimental results presented here will be discussed in view of this intriguing possibility.

1. Cyclic AMP and G Proteins

In the fat body of *L. migratoria,* an accumulation of the second messenger cAMP brought about by AKH-I has been demonstrated earlier both *in vivo* and *in vitro* (review by Beenakkers *et al.,* 1985; Goldsworthy *et al.,* 1986; Wang *et al.,* 1990). Moreover, this accumulation of cAMP has been shown to enhance the activity of glycogen phosphorylase (Van Marrewijk *et al.,* 1993), an observation in favor of a role of cAMP in AKH signal transduction (Fig. 8). It was demonstrated that each of the AKHs dose-dependently stimulates cAMP production in the fat body within 1 min (Vroemen *et al.,* 1995a). At a rather physiological dose of 4 nM, AKH-III is the most potent and AKH-I the least potent peptide hormone in stimulating cAMP production, and the same order of potency holds for the activation of glycogen phosphorylase by this hormonal dose. The observation that AKH-II is somewhat stronger than AKH-I in activating glycogen phosphorylase is in line with previous suggestions that the second AKH would be the major trigger for carbohydrate mobilization from the fat body and that the action of cAMP is more directed toward carbohydrate mobilization than lipid mobilization (Orchard and Lange, 1983; Oudejans *et al.,* 1992). The involvement of cAMP in the stimulation of glycogen mobilization is not a general feature of insects, since the hypertrehalosemic hormones (HTHs) of the cockroaches *P. americana* (Orr *et al.,* 1985; Steele *et al.,* 1988), *B. discoidalis* (Keeley *et al.,* 1996), and

Blaptica dubia (Becker *et al.*, 1998) do not utilize this second messenger for their activating effects on trehalose synthesis in the fat body.

Recently cAMP was demonstrated to be involved in the AKH-induced lipolysis of TAG in *M. sexta* fat body (Arrese *et al.*, 1999). After AKH treatment, cAMP-dependent protein kinase activity in the fat body rapidly increased, while forskolin, an adenylyl cyclase activator, and 8Br-cAMP, a membrane-permeable analog of cAMP, induced a substantial increase in the secretion of DAG from the fat body.

In beetles, the amino acid proline may play an important role in flight metabolism. Auerswald and Gäde (2000) have shown that flight of *Pachnoda sinuata* and injection of the endogenous AKH peptide, which cause a hyperprolinemic and a hypertrehalosemic response in the beetle, induce an increase in the cAMP levels in the fat body. Injection of the phosphodiesterase inhibitor IBMX or of cpt-cAMP, a cell-permeable cAMP analog, caused a stimulation of proline synthesis but no mobilization of carbohydrate reserves. The combined data suggested that cAMP is involved in hormonal control of proline levels but not in regulation of carbohydrates.

Although no G protein-coupled receptors had been demonstrated in insects so far, experiments on locust fat body using cholera toxin (CTX) and pertussis toxin (PTX) suggested that the AKH receptor(s) are coupled to the G_s protein (and not to G_i) (Vroemen *et al.*, 1995a) (Fig. 8). The demonstration that AKH-I-, -II-, and -III-stimulated phosphorylase activation is ablated by the universal G protein inhibitor guanosine-5′-*O*-(2-thiodiphosphate) (GDPβS) strongly substantiates this suggestion.

2. Calcium

The relative importance of Ca^{2+} in signal transduction in the fat body is not equal in several closely related insect species. For example, the influx of extracellular Ca^{2+} into the fat body of *L. migratoria* has a much stronger stimulating effect on glycogen phosphorylase activity than the release of calcium ions from intracellular stores (Van Marrewijk *et al.*, 1993), while in *B. discoidalis* the opposite has been observed (Keeley *et al.*, 1996). The presence of extracellular Ca^{2+} ions has been shown to be indispensable for the induction of fat body phosphorylase by AKH-I in *L. migratoria* (Van Marrewijk *et al.*, 1991) and by HTH in *P. americana* (Steele and Paul, 1985). In the absence of Ca^{2+} in the medium, none of the three locust AKHs is capable of enhancing cAMP production and inducing glycogen phosphorylase activation in the fat body, while 1.5 mM Ca^{2+} (which is the concentration of Ca^{2+} in the insect blood) is sufficient for complete activation (Vroemen *et al.*, 1995b). Since the induction of phosphorylase by cAMP in fat body was shown to be independent of extracellular Ca^{2+}, data suggest that at least part of the action of extracellular Ca^{2+} is at a site proximal to cAMP, e.g., the binding of the hormones to their receptor(s) or a Ca^{2+}-sensitive adenylyl cyclase (Fig. 8). Ziegler *et al.* (1995) have demonstrated that binding of *M. sexta* AKH to its receptor is dependent on the presence of divalent cations like Ca^{2+}.

As the Ca^{2+} ionophore A23187 has been demonstrated to mimic (in part) the activating effect of AKH on glycogen phosphorylase, AKH was shown to activate Ca^{2+} uptake by the fat body cells. This hormone-induced Ca^{2+} influx appeared to be mediated through depletion of intracellular Ca^{2+} stores (Fig. 8), suggesting the functioning of a store-operated or capacitative Ca^{2+} entry mechanism (Van Marrewijk *et al.,* 1991, 1993). All three AKHs appeared to be capable of stimulating the Ca^{2+} inflow into the locust fat body within 30 s with equal potency (Vroemen *et al.,* 1995b). However, the AKHs also enhanced the efflux of Ca^{2+} from the fat body within the same time. At a physiological dose, AKH-III caused the strongest efflux and AKH-I the weakest, while their efficacy at a massive dose was equal. As the influx of Ca^{2+} exceeded the efflux, it is feasible that the intracellular Ca^{2+} concentration rises as a result of incubation of fat body with AKH. The fact that AKH-II induced a slightly higher Ca^{2+} efflux than AKH-I suggests that the rise in intracellular Ca^{2+} induced by AKH-I is higher. This might make AKH-I a better candidate for lipid mobilization than AKH-II, since activation of TAG lipase may require a translocation of this enzyme from the cytosol to the lipid droplets in a similar manner as discussed above for the activation of vertebrate HSL, and analogous to cytosolic phospholipase A_2, which upon cell activation translocates to the perinuclear region in a highly Ca^{2+}-dependent fashion (Hirabayashi and Shimizu, 2000).

In addition to their critical role in the AKH second-messenger cascade toward carbohydrate mobilization, Ca^{2+} ions are indispensable for the activating effect of AKH on the lipolysis of TAG in the locust fat body (Lum and Chino, 1990; Wang *et al.,* 1990). Also in *M. sexta,* AKH was shown to increase the influx of Ca^{2+} into the fat body, and chelation of extracellular Ca^{2+} strongly inhibited AKH-dependent mobilization of lipids (Arrese *et al.,* 1999). Ca^{2+} mobilizing agents greatly stimulated the mobilization of DAG from the fat body.

3. Inositol Phosphates

For a maximal effect of AKH on glycogen phosphorylase activity in locust fat body, release of Ca^{2+} from intracellular stores is required in addition to the availability of extracellular calcium (Van Marrewijk *et al.,* 1993). The same holds for the activation of glycogen phosphorylase and the stimulation of trehalose synthesis by HTH in *B. discoidalis* fat body (Keeley and Hesson, 1995; Keeley *et al.,* 1996). In the regulation of Ca^{2+} mobilization from intracellular stores, $InsP_n$ plays a pivotal role, and formation of these putative second messengers has been shown to be induced by AKH-I and -II in *S. gregaria* (Pancholi *et al.,* 1991; Stagg and Candy, 1996), and by AKH-I, -II, and -III in *L. migratoria* (Van Marrewijk *et al.,* 1996; Vroemen *et al.,* 1997). Each of the *Locusta* AKHs stimulates the synthesis of total $InsP_n$ within 1 min with different potency: AKH-II hardly induces any $InsP_n$ and AKH-III is more potent than AKH-I. The observation that the activation of glycogen phosphorylase by each of the AKHs is dampened by the phospholipase

C (PLC) inhibitor U73122 (Tatrai *et al.,* 1994) suggests the involvement of $InsP_n$ (and/or DAG) in AKH-signaling in locust fat body.

All individual forms of $InsP_n$ ($InsP_{1-6}$) are elevated by the AKHs, $InsP_3$ and $InsP_4$ being the most interesting because of their presumed Ca^{2+} mobilizing actions (Van Marrewijk *et al.,* 1996; Vroemen *et al.,* 1997). With respect to $InsP_3$, AKH-III is again more potent than AKH-I, and the AKH-II-enhanced $InsP_3$ formation is quite small and detectable only using a highly specific radioreceptor assay for $Ins(1,4,5)P_3$ instead of a protocol using radiolabeled $InsP_n$ (as in the experiments described above). The most prolonged effect on $InsP_3$ is caused by AKH-III. The high potency and prolonged effects of AKH-III with respect to the induction of various second messenger systems apparently compensate (in part) for its low abundance relative to the other AKHs (Oudejans *et al.,* 1991), and therefore the effects of this hormone may be stronger than estimated from its relative amount in the circulation. The fact that AKH-I gives rise to higher $InsP_3$ levels than AKH-II points again toward a stronger effect of AKH-I on intracellular Ca^{2+} concentrations and is therefore in line with the previous suggestion that the first hormone might serve predominantly as a lipid mobilizing hormone, while AKH-II may be the main trigger for carbohydrate mobilization. The role of $InsP_3$ in mediating intracellular signaling of locust AKH is shown in Fig. 8.

Stagg and Candy (1998) have tested analogs of *S. gregaria* AKH-II for their ability to stimulate the turnover of inositol trisphosphates and the accumulation of cAMP in the fat body *in vitro.* The results from the $InsP_3$ experiments led them to suggest that in AKH-II [2]Leu, [3]Asn, and [5]Ser may be important for the initial recognition of the peptide by the AKH receptor, and that [1]pGlu and [7]Gly may be involved in conveying the message to the interior of the cell.

$Ins(1,4,5)P_3$ levels were greatly increased by HTH in the fat body of *B. discoidalis* in a time- and dose-dependent manner, which, along with the strong evidence for Ca^{2+} as component in the HTH second-messenger cascade, argues strongly for IP_3 as a primary second messenger in response to HTH followed by the mobilization of intracellular Ca^{2+} (Park and Keeley, 1996; Keeley *et al.,* 1996).

4. Eicosanoids

Eicosanoids are biologically active metabolites of C20 polyunsaturated fatty acids (PUFAs). Usually, their synthesis is thought to begin with hydrolysis of arachidonic acid from the *sn*-2 position of membrane phospholipids by phospholipase A_2 (PLA_2). There are three major pathways of eicosanoid biosynthesis. The cyclooxygenase pathways convert arachidonic acid into prostaglandins and thromboxanes. The lipoxygenase pathways yield various hydroxyeicosatetraenoic acids and leukotrienes. The epoxygenases are cytochromes P_{450}, which convert arachidonic acid into various epoxyeicosatrienoic acids. Eicosanoids act as local hormones with widely divergent regulatory functions in, among others, ion transport,

reproduction and immunity. They are widely appreciated with respect to their actions in mammals and other vertebrates, while there is increasing recognition of their significance in invertebrates. The biological significance of eicosanoids in insects and other invertebrates, including their contribution in signal transduction systems, has been reviewed comprehensively by Stanley-Samuelson (1994) and Stanley (2000). Here, a short survey is given of our present understanding of the role eicosanoids may play in the regulation of energy substrate mobilization, with special emphasis on the participation of eicosanoids in insect peptide hormone signal transduction.

In mammalian adipose tissue, prostaglandin E_2 (PGE_2) inhibits basal lipolysis (Fain *et al.,* 2000). Moreover, PGE_2 reduces the amount of lipid that is mobilized in response to epinephrine, presumably by lowering cAMP levels (Mead *et al.,* 1986). Also in insects, evidence has been provided that eicosanoids may modulate hormone-controlled mobilization of energy reserves. Already two decades ago, Yamaja Setty and Ramaiah (1982) concluded that PGE_1 downregulates lipid mobilization in pupal fat bodies of the silkworm, *Bombyx mori.* Wagemans, Van der Horst, and Stanley-Samuelson (preliminary data reported in Stanley, 2000) have shown that AKH-induced lipid release from locust fat body *in vitro* declines when PGE_2 is included in the incubation medium, which suggests that prostaglandins may modulate the action of AKH (Fig. 8).

To evaluate the potential for eicosanoids to mediate the action of HTH in *B discoidalis,* Keeley *et al.* (1996) have measured the effects of inhibitors of arachidonic acid metabolism on trehalose biosynthesis in isolated fat body. Treatment with the general inhibitor of eicosanoid biosynthesis, eicosatetraenoic acid, strongly enhanced the intermediate hypertrehalosemic effect produced by a low dose of HTH. The authors also applied the cyclooxygenase inhibitor indomethacin and the lipoxygenase inhibitor BW4AC. Both compounds were highly synergistic with HTH, resulting in a full hypertrehalosemic response by a low dose of hormone. These results, though not conclusive, do suggest that HTH may stimulate production of arachidonic acid, which in turn enhances trehalose synthesis. Alternatively, trehalose biosynthesis might be suppressed by eicosanoid derivatives of arachidonic acid, and therefore suppression of eicosanoid formation would enhance the hypertrehalosemic action of HTH.

In dispersed fat body trophocytes of another cockroach, *P. americana,* addition of HTH increased the concentration of free fatty acids including linoleic acid, which may serve as precursor of arachidonic acid (Ali and Steele, 1997a). Activation of PLA_2 with melittin mimicked this HTH action, while inhibition of PLA_2 with bromophenacyl bromide (BPB) eliminated the increase in linoleic and other fatty acids evoked by HTH (Ali and Steele, 1997b). Moreover, PLA_2-inhibitors BPB and mepacrine were also effective in decreasing the efflux of trehalose from HTH-challenged fat body (Ali *et al.,* 1998). These data indicate that PUFAs are necessary for a full stimulatory effect of HTH on trehalose synthesis and/or release in *P. americana* fat body. This proposal has been substantiated by the observation that

trehalose synthesis in trophocytes is stimulated when cells are incubated with fatty acids. Arachidonic acid was as effective as linoleic acid in stimulating efflux of trehalose (Ali and Steele, 1997c). Activation of trehalose efflux from the fat body by HTH was completely blocked by the cyclooxygenase inhibitors indomethacin and diclofenac, and by nordihydroguaiaretic acid, an inhibitor of lipoxygenase (Ali *et al.,* 1998). These data led Steele (1999) to suggest that either a prostaglandin or a leukotriene may exert a permissive effect on the release of trehalose from the fat body of *P. americana.*

   In conclusion, data obtained so far suggest that eicosanoids reduce hormone-stimulated lipid mobilization; however, there appears to be a discrepancy in the way eicosanoids are thought to modulate the HTH-induced hypertrehalosemic effect in different cockroach species. In both *B. discoidalis* and *P. americana* HTH has been suggested to increase the production of arachidonic acid by activating PLA_2 activity, resulting in an increased hypertrehalosemic response. However, in *B. discoidalis* inhibition of the formation of eicosanoids from arachidonic acid increased the hypertrehalosemic effect of HTH, while the same action in *P. americana* completely blocked HTH-induced trehalose efflux from the fat body. The reason for this discrepancy is as yet unclear, but data presented here justify the conclusion that further research will be required for a better understanding of the role of PUFA and eicosanoids in insect hormone peptide signal transduction.

5. Signaling Cross-talk

Cross-talk between signal transduction cascades provides the cell with a complex intracellular system for fine-tuning of hormone-induced signals. In locust fat body an elevation of cAMP levels does not influence the intracellular $InsP_n$ content, implying that the basal PLC activity is not regulated by this cyclic nucleotide (Vroemen *et al.,* 1998b). Moreover, none of the signal transducing elements between the AKH receptor and PLC is affected by cAMP, since pre-incubation of fat body tissue with forskolin or dibutyryl-cAMP does not impact on AKH-induced $InsP_n$ production (W. J. A. Van Marrewijk *et al.,* unpublished observations). Proof of a direct linkage between the AKH receptor(s) and PLC (instead of a route via cAMP) came from the substantiation that the G protein activator, aluminum fluoride (AIF_4^-) increases $InsP_n$ levels. Experiments using CTX, PTX, and GPAntagonist-2A, a specific inhibitor of G_q, preclude the involvement of G_i and a $G_s\beta\gamma$-sensitive isoform of PLC and evidence the involvement of G_q in the transduction of AKH signals towards fat body PLC (Fig. 8).

   As plasma membrane Ca^{2+} channels may constitute another possible target site for cAMP-mediated modulation (Kass *et al.,* 1994; Kitamura and Miller, 1994), the type of Ca^{2+} channels involved in AKH signaling was assessed using a variety of inhibitors of L-, T-, and N-type voltage-dependent Ca^{2+} channels. In contrast to the universal Ca^{2+} channel blocker La^{3+}, none of these inhibitors blocks glycogen phosphorylase activation by the AKHs, which suggests (together with previous

data) that the Ca^{2+} channels involved in AKH signaling are voltage-independent, calcium-release activated channels (Vroemen *et al.,* 1998b).

Another interesting example of signaling cross-talk has been proposed by Steele (1999). According to his tentative model for HTH signaling in *P. americana* fat body, HTH triggers the activation of both PLC and PLA_2. Activation of PLC generates IP_3, which mobilizes Ca^{2+} from the ER, leading to an increased influx of extracellular Ca^{2+} either through a Ca^{2+}-dependent protein kinase or via a store-operated Ca^{2+}-entry mechanism. The increase in intracellular Ca^{2+} then activates glycogen phosphorylase, which yields the glucosyl residues required for the synthesis of trehalose. The activation of PLA_2 leads to an enhanced production of arachidonic acid and, via the cyclooxygenase or lipoxygenase pathways, its eicosanoid metabolites. These products appear to regulate the trehalose biosynthetic rate (from the glucosyl residues yielded through the PLC pathway) and the trehalose efflux from the trophocyte, possibly by regulating trehalose 6-phosphatase or the transport of trehalose across the plasma membrane.

IV. Adipokinetic Hormone-Induced Effects on the Lipophorin System

A. Insect Lipophorins and Lipid Transport

1. Structure of Lipophorins

In the circulatory system of animals, transport of lipids is generally associated with lipoprotein complexes, the apolipoprotein components of which serve to stabilize the lipids and modulate metabolism of the lipoprotein particle. Insect hemolymph generally contains abundant amounts of a single multifunctional lipoprotein particle, high-density lipophorin (HDLp), the main function of which is to transport lipids throughout the insect body during all developmental stages. A characteristic feature of HDLp is its ability to function as a reusable shuttle for a variety of lipids by the selective loading and unloading of lipid components at target tissues (reviewed in Ryan, 1990; Van der Horst, 1990; Law *et al.,* 1992; Ryan and Van der Horst, 2000). For insect species that recruit fat body TAG depots to power their flight muscles during the vast distances covered nonstop by migratory flight, an efficient mechanism for lipid transfer is a premier issue. Also in this adult-specific mechanism, lipophorin particles play a central role. The DAG mobilized from fat body cells in response to the action of flight-induced release of AKH is loaded onto preexisting HDLp particles in the circulatory system. Concomitant with this lipid loading process, multiple copies of an exchangeable apolipoprotein, apolipophorin III (apoLp-III) associate with the particle. As a result, the

particle changes in size and density and is converted to low-density lipophorin (LDLp), a lipophorin subspecies with a considerably higher capacity to transport fuel molecules between fat body and flight muslce (see Fig. 1). Lipophorin structures and that of flight-induced subspecies have been the subject of several recent reviews (Van der Horst *et al.,* 1993; Blacklock and Ryan, 1994; Soulages and Wells, 1994; Ryan, 1994, 1996; Ryan and Van der Horst, 2000). Briefly, HDLp is a spherical particle of 450–600 kDa with a density of ∼1.12 g/ml. It generally contains two non-exchangeable apolipoproteins, apolipophorin I (apoLp-I) and apolipophorin II (apoLp-II), with molecular weights of ∼240 and ∼80 kDa, respectively. In addition to phospholipids, sterols and hydrocarbons, DAG is usually the prevalent lipid component.

However, in a few insect species, the structure of their HDLp differs from that of the other lipophorins studied so far. For instance, in the mosquito, *Aedes aegypti,* HDLp lipid composition is different since TAG constitutes the most abundant neutral lipid (47%), whereas the DAG content is only 7% (Ford and Van Heusden, 1994; Pennington *et al.,* 1996). At variance with the general rule on apolipophorin composition, the HDLp from the cochineal insect (*Dactylopius confusus*) appeared to contain apolipophorins of ∼25 and ∼22 kDa although its molecular weight and lipid composition are similar to those of other lipophorins (Ziegler *et al.,* 1999).

2. Lipophorin Biosynthesis

In insects, the primary site for synthesis of proteins, including lipophorin, is the fat body. Studies on apolipophorin biosynthesis revealed that apoLp-I and -II are synthesized from a common precursor. Immunoprecipitation using antibodies specific for apoLp-I or apoLp-II resulted in the isolation of a proapolipophorin from locust fat body homogenates, while subsequent pulse-chase experiments demonstrated the conversion of this apolipophorin precursor to apoLp-I and apoLp-II through posttranslational cleavage (Weers *et al.,* 1993).

Molecular characterization of the apolipophorin precursor has recently been disclosed for a few insect species. The protein sequence of the apolipophorin precursor of *L. migratoria* deduced from the cloned cDNA revealed that a 3380-amino-acid long precursor protein is produced, the first 21 amino acids of which constitute a signal peptide (Bogerd *et al.,* 2000). The presence of a signal peptide is in accordance with the extracellular nature of the proteins derived from this precursor. Analysis of the deduced amino acid sequence of the *L. migratoria* precursor revealed significant sequence homology with other apolipophorin precursor proteins, viz. the apolipoprotein precursor of larval *M. sexta* (Sundermeyer *et al.,* 1996) (27% identical, 45% similar), the putative apolipophorin precursor (retinoid- and fatty acid-binding glycoprotein, RFABG) of *D. melanogaster* (Kutty *et al.,* 1996) (25% identical, 43% similar), and the partial apoLp-II sequence of *A. aegypti* (Van Heusden *et al.,* 1998) (35% identical, 52% similar) (Bogerd *et al.,* 2000). In addition, the N-terminal ∼900 amino acid residues of the apolipophorin

precursors showed significant homology with the same part of invertebrate and vertebrate vitellogenins, human apolipoprotein B (apoB), and the large subunit of mammalian microsomal triglyceride transfer protein (MTP) (Babin *et al.,* 1999; Mann *et al.,* 1999). These homologies indicate that the apolipophorin precursors are members of a large lipid transfer protein (LLTP) superfamily that emerged from an ancestral molecule designed to ensure a pivotal event in the intra- and extracellular transfer of lipids and liposoluble substances (Babin *et al.,* 1999). Based on the X-ray crystal structure of lamprey lipovitellin, the mature from of vitellogenin (Anderson *et al.,* 1998) and the sequence homologies, three-dimensional models of the 600-amino-acid-long N-terminal fragments of most of the family members, including the apolipophorins, can be constructed (Mann *et al.,* 1999). These models give important insight into the structural organization of the different protein parts and show how the major structural differences between these proteins relate specifically to their different lipid binding and lipid transfer properties. Importantly, these models may also explain why the N-terminal part of the apolipophorins contain relatively few cysteine residues involved in disulfide bond formation, as compared to that in their mammalian homolog, apoB.

The apolipophorin precursor protein of the three insect species known so far (*D. melanogaster, M. sexta,* and *L. migratoria*) is arranged with apoLp-II at the N-terminal end and apoLp-I at the C-terminal end (hence also termed apoLp-II/I). In the locust apolipophorin precursor, the N-terminus of apoLp-I is preceded by the amino acid sequence RQKR in the precursor protein, which is reminiscent of the consensus cleavage sequence R*X*(K/R)R for dibasic processing endoproteases of the subtilisin family. Therefore, in the generation of apoLp-II and apoLp-I by proteolytical processing of the precursor protein at this position, such a protease is likely involved. Sundermeyer *et al.* (1996) did not identify the position where the *Manduca* precursor protein was cleaved, since they were unable to determine the amino-terminal sequence of the >200-kDa polypeptide moiety of *Manduca* apoLp-I. However, based on alignment studies with *Locusta* apoLp-II/I, a similar proteolytic processing site (RGRR) was inferred to be present in *Manduca* apoLp-II/I (Bogerd *et al.,* 2000). In *Drosophila* RFABG, Kutty *et al.* (1996) identified an RARR cleavage site after comparison with the N-terminal sequence of blowfly apoLp-I (Trowell *et al.,* 1994). Interestingly, whereas apoB and MTP interact in human lipoprotein assembly (reviewed in Wetterau *et al.,* 1997; Gordon and Jamil, 2000) and the N-terminal region of apoB is necessary for enabling MTP responsiveness (Gretch *et al.,* 1996; Mann *et al.,* 1999), the cleavage of the insect apoLp-II/I precursor protein occurs within the MTP homologous domain. The two apolipophorins are thought to interact with lipid to form the HDLp particle; however, the mechanism of assembly and secretion of lipophorin has not been elucidated and constitutes one of the major issues in insect lipoprotein metabolism. In this respect, it should be noted that in the two insect species that are widely used as a model system for AKH-induced lipophorin conversions, *L. migratoria* and *M. sexta,* lipophorin biosynthesis appears to proceed differentially. Whereas

lipophorin in *L. migratoria* is secreted into the hemolymph as a mature particle, lipophorin in *M. sexta* is released as a nascent particle that loads specific lipids from other sites (reviewed in Van der Horst *et al.,* 1993; Ryan and Van der Horst, 2000). In this respect it should be noted that insect *Sf*-21 cells (derived from ovarian tissue from the fall army worm, *Spodoptera frugiperda*) transfected with apoB and MTP gene constructs, secrete lipid-rich apolipoprotein B-containing lipoproteins (Gretch *et al.,* 1996). This indicates that the components required for the basal lipidation and secretion of lipoproteins are present in both vertebrate and insect cells.

The presence of several putative glycosylation consensus sites in the *L. migratoria* apoLp-II/I precursor protein in consistent with the finding that apoLp-I and apoLp-II have an N-linked carbohydrate content of approximately 1–2% and 5%, respectively (Weers *et al.,* 1993). Only two of these sites, one in apoLp-II and the other in apoLp-I, seem to have their homolog in the *Manduca* and *Drosophila* precursor proteins (Bogerd *et al.,* 2000).

An interesting recent finding shows that, in addition to its expression in locust fat body, *apoLp-II/I* is strongly expressed in the insect brain. *In situ* hybridization on locust brain sections showed *apoLp-II/I* expression in the optic lobe; specific hybridization of the antisense apoLp-II/I cRNA probe was confined to the pigmented glial cells of the lamina underlying the retinal layer and in cells or cellular processes interspersed in the basement membrane. Concomitantly, by immunofluorescence labeling with a specific anti-apoLp-I, synthesis of the corresponding protein was detected in these cells (Bogerd *et al.,* 2000). In view of the blood–brain barrier, apoLp-II/I synthesis, and the putative synthesis of lipophorin particles, the pigmented glial cells of locust eyes may be of fundamental importance for the redistribution of lipids and liposoluble molecules within the lamina-retina compartment and particularly function to transport retinoids and/or fatty acids to the insect retina (Bogerd *et al.,* 2000).

3. Lipophorin as a Lipid Shuttle

As indicated above, a unique feature of lipophorin as a lipid delivery vehicle is its ability to function as a reusable lipid shuttle operating between the sites of storage (fat body) and utilization (flight muscles) in insects capable of migratory flights (see Fig. 1). This lipid loading and unloading of lipophorin particles during sustained flight activity does not require their internalization by either lipid donor or recipient cells and consequently, the increased capacity for lipid transport is achieved without additional lipophorin biosynthesis (reviewed in Van der Horst, 1990, Ryan, 1990, 1996; Van der Horst *et al.,* 1993; Soulages and Wells, 1994; Ryan and Van der Horst, 2000). Pertinent to his novel concept for lipid transport during exercise is that, in response to the AKH-stimulated mobilization of fat body TAG stores resulting from flight activity, DAG is loaded onto circulating HDLp particles, ultimately transforming them into LDLp. In the course of this loading process, which is facilitated by lipid transfer particles (LTP; see below), several copies of the amphipathic

exchangeable apolipoprotein, apoLp-III ($\sim$18–20 kDa), associate with the particle. Whereas HDLp is abundantly present in *L. migratoria* during all developmental stages, apoLp-III expression is developmentally regulated and its hemolymph level is high only in adults (De Winther *et al.,* 1996). At the flight muscles, the DAG is depleted from the lipoprotein through the action of a membrane-bound lipophorin lipase in the extracellular space (Wheeler *et al.,* 1984; Van Heusden *et al.,* 1986; Van Antwerpen *et al.,* 1988; Van Heusden, 1993) and the resulting FAs are taken up and oxidized to provide energy. The diminution of the lipid content of the particle induces dissociation of apoLp-III and finally, both protein constituents (HDLp and apoLp-III) are recovered in the hemolymph and may return to the fat body for another cycle of DAG uptake and transport. Consequently, apoLp-III in the hemolymph alternates between a lipid-free and a lipophorin-bound state.

An intriguing phenomenon pertinent to this shuttle mechanism is the association of the exchangeable apoLp-III with the expanding surface of the lipophorin particle during AKH-induced lipid loading. ApoLp-III circulates in the hemolymph as a stable, water-soluble protein; however, in response to DAG loading onto lipophorin, it binds to the surface area and provides a hydrophilic coating of the expanding particle. Enzymatic studies have shown that apoLp-III is exclusively associated with the DAG moiety (Kawooya *et al.,* 1991). Injection of *L. migratoria* apoLp-III underneath lipid monolayers also demonstrated high affinity interaction with DAG (Demel *et al.,* 1992), which is consistent with the function of the apoLp-III in the LDLp particle. In the course of LDLp formation, particles of intermediate size and density are recovered, resulting from the progressive loading of HDLp with DAG and an increase in apoLp-III content (Soulages *et al.,* 1996). The structure and lipid binding properties of apoLp-III are outlined below.

B. Apolipophorin III

1. Structure of Apolipophorin III

Insect apoLp-III is one of the best examples of the reversible existence of exchangeable apolipoproteins in lipid-free and lipoprotein-associated states and serves as a model for studies of apolipoproteins with lipoprotein surfaces (recently reviewed in Soulages and Wells, 1994; Ryan, 1996; Ryan and Van der Horst, 2000). Characterization of apoLp-III has revealed that it is rich in α-helices, which are amphipathic in nature (Cole *et al.,* 1987; Kanost *et al.,* 1988; Narayanaswami *et al.,* 1995). Such helices are characterized by well-defined polar and nonpolar faces, which are proposed to interact with the aqueous milieu (blood or hemolymph) and hydrophobic lipids, respectively, at the lipoprotein surface (reviewed in Narayanaswami and Ryan, 2000). Importantly, there is considerable similarity between the structural organization of apoLp-III and the N-terminal domain of human apolipoprotein E

(apoE), as is apparent from comparison of apoLp-III from *L. migratoria,* which represents the only full-length apolipoprotein of which the three-dimensional structure has been determined by X-ray crystallographic studies (Breiter *et al.,* 1991), and the 22-kDa N-terminal domain of human apoE, the X-ray structure of which has also been elucidated (Wilson *et al.,* 1991). This similarity suggests that elucidation of the mechanism of interaction of apoLp-III with lipids would be directly applicable to vertebrate apolipoproteins. The three-dimensional structures, which were determined for the proteins in the lipid-free state, reveal that both proteins consist of elongated amphipathic α-helices, which are organized as an antiparallel α-helix bundle. ApoLp-III is a five-helix bundle while the N-terminal domain of human apoE is a four-helix bundle. These helices are organized such that their hydrophobic faces are oriented toward the center of the bundle while their hydrophilic faces are exposed to the aqueous environment. This molecular architecture explains the water solubility of these proteins in the absence of lipid and additionally allows for postulating that conformational changes of the protein may accompany its association with lipid. Toward this end it has been proposed that both apoLp-III and the N-terminal domain of human apoE undergo a dramatic opening of the helix bundle at putative hinge regions, resulting in exposure of its hydrophobic interior upon lipid binding (Kawooya *et al.,* 1986; Wells *et al.,* 1987; Breiter *et al.,* 1991; Weisgraber, 1994). The global fold and secondary structure organization of *M. sexta* apoLp-III was recently elucidated using three-dimensional heteronuclear NMR spectroscopy, showing that the arrangement of amphipathic helices in *M. sexta* apoLp-III is (very) similar to that in *L. migratoria* apoLp-III (Wang *et al.,* 1997).

2. Interaction of Apolipophorin III with Lipophorin

The association of insect apoLp-III with lipophorin represents a unique model for studying lipid–protein interactions, which may have general and wider implications for our understanding of this process. Within the scope of this chapter, we will consider a few important aspects of this mechanism. Although high-resolution structural data of apoLp-III in the lipid-bound conformation is not available to date, experimental evidence supports the conformational opening hypothesis mentioned above. For studies of interaction of apolipophorins with lipids and lipoprotein surfaces, particularly apoLp-III from *L. migratoria* and *M. sexta* were used as model apolipophorins. Interestingly, despite considerable differences in primary structure (only 20% sequence identity is shared) while additionally, *L. migratoria* apoLp-III is a glycoprotein containing complex carbohydrate structures (Hård *et al.,* 1993), whereas *M. sexta* apoLp-III is not glycosylated, both apolipophorins are functionally indistinguishable (Van der Horst *et al.,* 1988). Studies of the properties of apoLp-III in association with model phospholipids support a major conformational change of the apolipophorin. In the lipid-bound state of apoLp-III it is assumed that the protein spreads on the lipid surface by the movement of helices 1, 2, and 5

in one direction and helices 3 and 4 in the other (180°) around "hinges" located in the loops between helices 2 and 3 and between helices 4 and 5 (Breiter *et al.*, 1991) (Fig. 9). Addition of apoLp-III to sonicated vesicles of dimyristoylphosphatidyl-choline (DMPC) resulted in the formation of disc-like complexes (Wientzek *et al.*, 1994; Weers *et al.*, 1994). Spectroscopic and structural evidence indicated that apoLp-III had adopted an open conformation and was aligned around the perimeter of these discs with its α-helices perpendicular to the fatty acyl chains of the phospholipids ("belt" arrangement). In an alternate approach to investigate conformational changes associated with lipid interaction, by site-directed mutagenesis two cysteine residues were introduced into apoLp-III, which spontaneously formed a disulfide bond tethering the hinge regions proposed to be implicated in the conformational opening hypothesis (Narayanaswami *et al.*, 1996). Formation of this disulfide bond appeared to abolish the ability of the mutant protein to interact with lipoprotein surfaces whereas upon reduction of the disulfide bond, binding
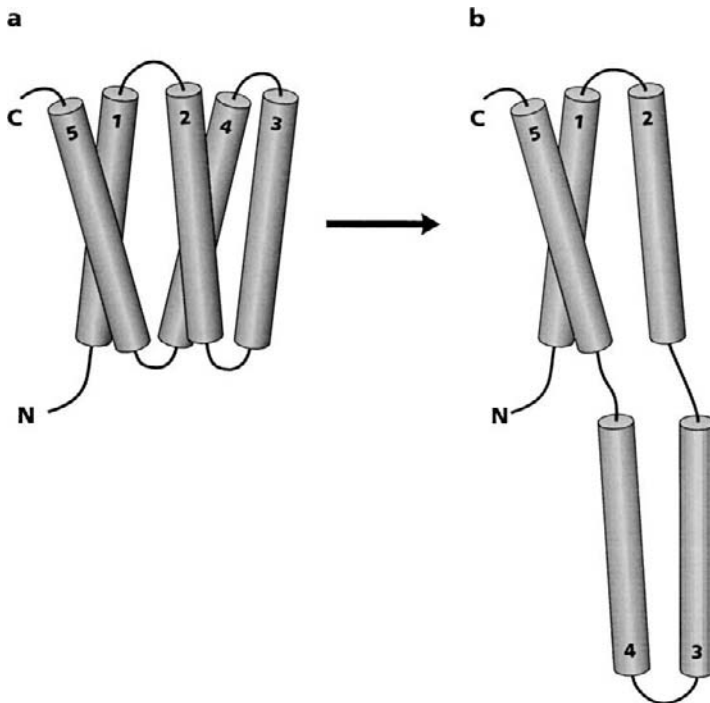
FIG. 9   Model of the conformational change of apolipophorin III upon binding to a lipophorin particle. (a) Schematic representation of the overall molecular architecture of apoLp-III in the lipid-free state. The apolipophorin consists of a bundle of five amphipathic α-helices connected by short loops; the hydrophobic faces of the helices are oriented inward. (b) The putative unfolded form of apoLp-III in the lipophorin-bound state, resulting from lipid-triggered helix-bundle opening allowing lipid–protein interaction. After Breiter *et al.* (1991).

activity was restored. From these data it was concluded that the disulfide bond prevented exposure of its hydrophobic interior through conformational opening and the creation of an elongated amphipathic structure that represents the lipid binding conformation of the protein.

The presence of carbohydrate in apoLp-III of several insects and its role in apoLp-III structure and function has been a subject of much speculation. Recombinant *L. migratoria* apoLp-III lacking carbohydrate showed enhanced activity in association of the protein with lipid when compared to that of the native apoLp-III (Soulages *et al.,* 1998), indicating that relatively small changes in structural properties of the protein have a considerable impact on its functional properties. Also the kinetics of binding of deglycosylated apoLp-III from *L. migratoria* to model phospholipids appeared to be faster than that of the native apoLp-III. However, in binding assays with the surface of lipoproteins only minor differences were noted (Weers *et al.,* 2000). These findings support the view that interaction of apoLp-III with phospholipid vesicles and lipoprotein surfaces are two fundamentally different processes (Weers *et al.,* 1999). The interaction of apoLp-III with lipid bilayers requires that, prior to conformational opening of the helix bundle, the protein penetrates the bilayer and disrupts it, inducing transformation into much smaller disc-like structures. ApoLp-III oligosaccharide chains impede the latter process. On the other hand, the glycosyl moieties do not affect lipoprotein-binding interaction, as it does not involve deep protein penetration into the lipid milieu. Rather, lipoprotein binding is based on oriented protein contact with the lipid surface followed by conformational opening of the helix bundle, covering surface-exposed hydrophobic sites (Weers *et al.,* 2000).

An important question pertains to the structural features of exchangeable apolipoproteins, which are responsible for initiation of lipoprotein binding. In the insect system there is now convincing evidence that a perturbation of the phospholipid monolayer of the lipophorin surface caused by the appearance of DAG patches at the lipoprotein particle surface ("hydrophobic defect") is a key event in exchangeable apolipoprotein recruitment. The physicochemical properties of DAG allow for the destabilization of ordered phospholipid layer structures (recently reviewed in Goñi and Alonso, 1999). An intriguing hypothesis proposes that apolipoprotein binding to these hydrophobic defects is regulated by a small region of hydrophobic amino acids, a "hydrophobic sensor," located at one end of the apolipoprotein (Soulages *et al.,* 1995). ApoLp-III molecules from several insect species were noted to contain a region of hydrophobic amino acids including two conserved leucines located at or near positions 32 and 93 in the loops between helices 1 and 2 and between 3 and 4 (Smith *et al.,* 1994). These amino acids are thought to play a critical role in initiation of binding, associating with the lipoprotein with the long axis of the protein perpendicular to the particle surface. Important initial evidence in favor of the hydrophobic sensor mechanism has been obtained through experiments employing surface plasmon resonance spectroscopy, in which binding of *M. sexta* apoLp-III to a phospholipid bilayer as a

function of the concentration of DAG in the bilayer was studied (Soulages *et al.,* 1995). This hypothesis has been studied further in both *L. migratoria* and *M. sexta* apoLp-III. Using site-directed mutagenesis to substitute leucine residues in the loops that connect helices 1 and 2 (leucine 32 and leucine 34) and helices 3 and 4 (leucine 95) in *L. migratoria* apoLp-III, evidence was presented that these loops are involved in the recognition of hydrophobic defects on lipoprotein surfaces by apoLp-III and that its leucine residues function in initiating lipoprotein binding (Weers *et al.,* 1999). In *M. sexta* apoLp-III, helices 3 and 4 are connected by a short, six-residue (95PDVEKE100) linker helix, termed helix 3′, which resides outside the helix bundle (Wang *et al.,* 1997). Using site-directed mutagenesis in conjunction with lipoprotein binding assays, Narayanaswami *et al.* (1999) showed that recognition of lipoprotein surface hydrophobic defects by valine 97 triggers opening of the helix bundle, whereas as aspartic acid 96 and glutamic acid 98 appeared to be irrelevant for initiating binding to lipoproteins. In the presence of sufficient surface-exposed hydrophobic material, the protein opens to form a stable binding interaction.

Recently, an alternative model for the conformational change that is expected to occur upon binding of apoLp-III to lipid was proposed (Soulages and Arrese, 2000a). The dynamics and properties of the five amphipathic helices of *L. migratoria* apoLp-III were studied in the lipid-free state using five single-tryptophan mutants (one tryptophan "reporter" residue in each of the five helices). The properties of the helices and the inferred interhelical interactions suggest that, in the presence of an appropriate lipid surface, the exposure of the hydrophobic domains of the helices may take place through the disruption of the weak interhelical contacts between helices 1 and 5. The weakness of the interaction between helices 1 and 5 was suggested to result from the parallel arrangement of these helices in the bundle. This model is significantly different from the currently accepted model discussed above and speculates that the most mobile helices in apoLp-III, helices 1 and 5, constitute a gate to the hydrophobic core of the apolipoprotein molecule. Subsequent studies on the interaction of the single-tryptophan mutants with phospholipid (DMPC) suggest that only helices 1, 4, and 5 are interacting with the lipid surface (Soulages and Arrese, 2000b), whereas the accepted model for the lipid-bound state of apoLp-III assumes that all helices interact with the lipid surface. Clearly, additional studies will be required to address the precise mechanism of the major conformational change of apoLp-III as well as the roles of its amphipathic helices in the interaction of this exchangeable apolipoprotein with a lipoprotein surface.

C. Interactions of Lipophorin with Fat Body Cells

1. Lipid Transfer Particles

In the mammalian system, distinct lipid transfer proteins function in the redistribution of lipid molecules. In the operating of the lipophorin shuttle in insects, with

repeated cycles of lipid loading and depletion, analogous transfer catalysts may facilitate these interconversions. From the hemolymph of *M. sexta,* Ryan *et al.* (1986a,b) isolated a lipid transfer particle (LTP) that facilitated vectorial redistribution of lipids among plasma lipophorin subspecies. This LTP was strongly implicated to function *in vivo* in the conversion of HDLp to LDLp in response to AKH (Van Heusden and Law, 1989). The concept that LTP functions in flight-related lipophorin conversions is congruent with an increased hemolymph concentration of LTP in adults compared with other developmental stages (Van Heusden *et al.,* 1996; Tsuchida *et al.,* 1998). Within the scope of this chapter, the structure and action of LTP, which were recently reviewed in Ryan and Van der Horst (2000), will be discussed briefly. Compared to the lipid transfer protein involved in mammalian processes, the insect transfer catalyst appeared to exhibit novel structural characteristics. *M. sexta* LTP is a high-molecular-weight complex of three apoproteins (apoLTP-I, Mw ∼320 kDa; apoLTP-II, Mw ∼85 kDa; and apoLTP-III, Mw ∼55 kDa) and 14% lipid. Catalysts with similar structural properties have been isolated from other insects including *L. migratoria* (Hirayama and Chino, 1990). Sequence information on the apoprotein components of insect LTP is not available, implying that the structural and evolutionary relationships to the lipid transfer catalysts from vertebrates remains to be elucidated. The lipid component of LTP resembles that of lipophorin in that it contains predominantly phospholipid and DAG. Although its precise function is not known, studies on the dynamics of the lipid moiety of LTP revealed that this component is not merely a static structural entity of the particle but, instead, may play a key role in the facilitation of lipid transfer (Ryan, 1990). Although LTP may facilitate transfer of other lipids like hydrocarbons or carotenoids among lipophorin particles (Takeuchi and Chino, 1993; Tsuchida *et al.,* 1997, 1998), DAG was transferred preferentially. Alternatively, the observed preference for DAG may be related to the accessibility of this substrate within the donor lipophorin.

An interesting hypothesis on the function of LTP put forward by Gretch *et al.* (1996) suggests that, in view of the contrasting mechanisms of DAG mobilization in insects and TAG mobilization in mammals, the extracellular insect LTP may function similar to the intracellular mammalian MTP in lipoprotein assembly. However, this suggested role of LTP does not necessarily have to take over completely the function of an MTP in insects. The latter is supported by the presence of an insect MTP gene in the recently disclosed *Drosophila* genome sequence (K. W. Rodenburg, unpublished observation).

2. Lipophorin Receptors

A major difference between insect lipophorins and vertebrate lipoproteins is the selective mechanism by which the insect lipoproteins transport their hydrophobic cargo. Thus, for instance at the insect fat body cell, circulating HDLp particles may serve as DAG donor or acceptor, dependent on the physiological situation. During dietary lipid storage in the fat body, which is a prominent process in larval

and younger adult insects, lipid is extracted from HDLp, whereas during flight activity at the adult stage, fat body lipid is exported and loaded onto HDLp. For lipid transfer in both directions, the interaction between lipophorins and fat body cells is likely to be mediated by specific binding sites. High-affinity HDLp binding sites have been characterized in intact fat body tissue and fat body membranes of larval and adult *L. migratoria* (Van Antwerpen *et al.,* 1989; Schulz *et al.,* 1991; Dantuma *et al.,* 1996) as well as in the fat body of larval *M. sexta* (Tsuchida and Wells, 1990). The number of HDLp binding sites at the locust fat body cell surface increased between day 7 and day 11 after imaginal ecdysis (Dantuma *et al.,* 1996), suggesting a role in an adult-specific process such as flight activity. Both HDLp binding at the fat body and LDLp formation are inhibited by monoclonal antibodies specific for apoLp-II and not by those directed against apoLp-I (Hiraoka and Hayakawa, 1990; Schulz *et al.,* 1991). As yet, however, no conclusive evidence has been presented for the involvement of HDLp binding sites in LDLp formation.

In apparent contrast to the concept of the functioning of HDLp as a reusable lipid shuttle as discussed above, the HDLp binding site in larval and young adult locusts was identified as an endocytic receptor involved in receptor-mediated uptake of HDLp (Dantuma *et al.,* 1997). Endocytic internalization of HDLp appeared to be developmentally downregulated in the adult stage. Also in larvae of the dragonfly, *Aeshna cyanea,* HDLp can be internalized by the fat body (Bauerfeind and Komnick, 1992a). This process was not observed in the midgut epithelium (Bauerfeind and Komnick, 1992b), implying that endocytosis of HDLp does not occur in all target tissues. The specific HDLp binding sites identified in fat body and gut of larval *M. sexta* appear to be not involved in endocytic uptake of the ligand (Tsuchida and Wells, 1988, 1990; Gondim and Wells, 2000).

An endocytic uptake of HDLp seems to conflict with the selective process of lipid transport between HDLp and fat body cells without degradation of the lipophorin matrix. However, the pathway followed by the internalized HDLp may be different from the classical endosomal/lysosomal pathway. In experiments in which HDLp containing ^{3}H-labeled DAG and apolipoproteins was incubated with fat body tissue from young adult locusts, [^{3}H]DAG appeared to be taken up selectively without substantial concomitant accumulation of the radiolabeled apolipoproteins (Dantuma *et al.,* 1997). This suggests the existence of a retroendocytic pathway as had also been postulated for larval dragonfly fat body by Bauerfeind and Komnick (1992a). By contrast, studies at the electron-microscopic level using either gold-labeled HDLp or fluorescent dye (DiI)-labeled HDLp revealed recovery of internalized labeled HDLp in the endosomal/lysosomal compartment of fat body cells of both young and older adults, although labeling in older adults was much less abundant (Dantuma *et al.,* 1998a,b). Therefore, in view of the accumulation of HDLp in lysosomes it needs to be evaluated whether a substantial part of the internalized HDLp is resecreted after intracellular trafficking. In addition, the function

of receptor-mediated endocytosis remains unclear since inhibition of endocytosis did not affect the exchange of DAG or cholesterol between HDLp and the fat body cell (Dantuma *et al.,* 1997).

Recently, the putative receptor involved in endocytic uptake of HDLp in the locust fat body was cloned and sequenced and identified as a novel member of the low-density lipoprotein (LDL) receptor family that may be implicated in receptor-mediated uptake of HDLp during larval development (Dantuma *et al.,* 1999). The members of this family share structural and functional features and appear to originate from an ancient receptor in view of the identification of a similarly composed cell surface molecule in *Caenorhabditis elegans* (Yochem and Greenwald, 1993) and two insect vitellogenin receptors belonging to this gene superfamily (Schonbaum *et al.,* 1995; Sappington *et al.,* 1996). The insect lipophorin receptor, which in addition to the fat body was also expressed in oocytes, brain, and midgut, appeared to be a homolog of the mammalian very low-density lipoprotein (VLDL) receptor as it contains eight cysteine-rich repeats in its putative ligand-binding domain (Dantuma *et al.,* 1999). It represents the first identification of an invertebrate LDL receptor family member with an extracellular domain composed of a single ligand-binding domain and EGF-precursor homology domain, a type of lipoprotein receptors that has been found in many vertebrates. Recent preliminary data indicate the presence of a specific lipophorin receptor in mosquito oocytes, which is homologous to the *Locusta* fat body lipophorin receptor and to the vertebrate VLDL receptor (Sun *et al.,* 2000). African green monkey COS-7 kidney cells that were transiently transfected with the locust lipophorin receptor and incubated with HDLp that was labeled in the lipid moiety with DiI revealed a punctate fluorescent staining which was absent from mock-transfected cells. Clones of an LDL receptor-deficient Chinese hamster ovary (CHO) cell line stably transfected with this receptor revealed a similar punctate staining upon incubation with lipid (DiI)-labeled HDLp. These data suggest that the insect lipophorin receptor may function as an endocytic lipophorin receptor *in vivo* (Dantuma *et al.,* 1999). When HDLp, covalently labeled in the protein moiety with Oregon Green 488, was used in incubations with clones of the latter CHO cell line, a clear punctate fluoescent staining was also observed which was not detected in wild-type CHO cells (containing the LDL receptor), substantiating that internalization of HDLp is specifically mediated by the insect lipophorin receptor (Fig. 10) (D. Van Hoof, K. W. Rodenburg, and D. J. Van der Horst, unpublished observations).

Expression of the receptor mRNA in fat body cells is downregulated during adult development, which is consistent with the previously reported downregulation of receptor-mediated endocytosis of lipophorins in fat body tissue (Dantuma *et al.,* 1997). An important question that remains to be answered, however, is whether this novel insect lipophorin receptor, in contrast to the other members of the LDL receptor family, is able to recycle its ligand after intracellular trafficking. Recent observations on the uptake and trafficking of protein-labeled HDLp in CHO cells,
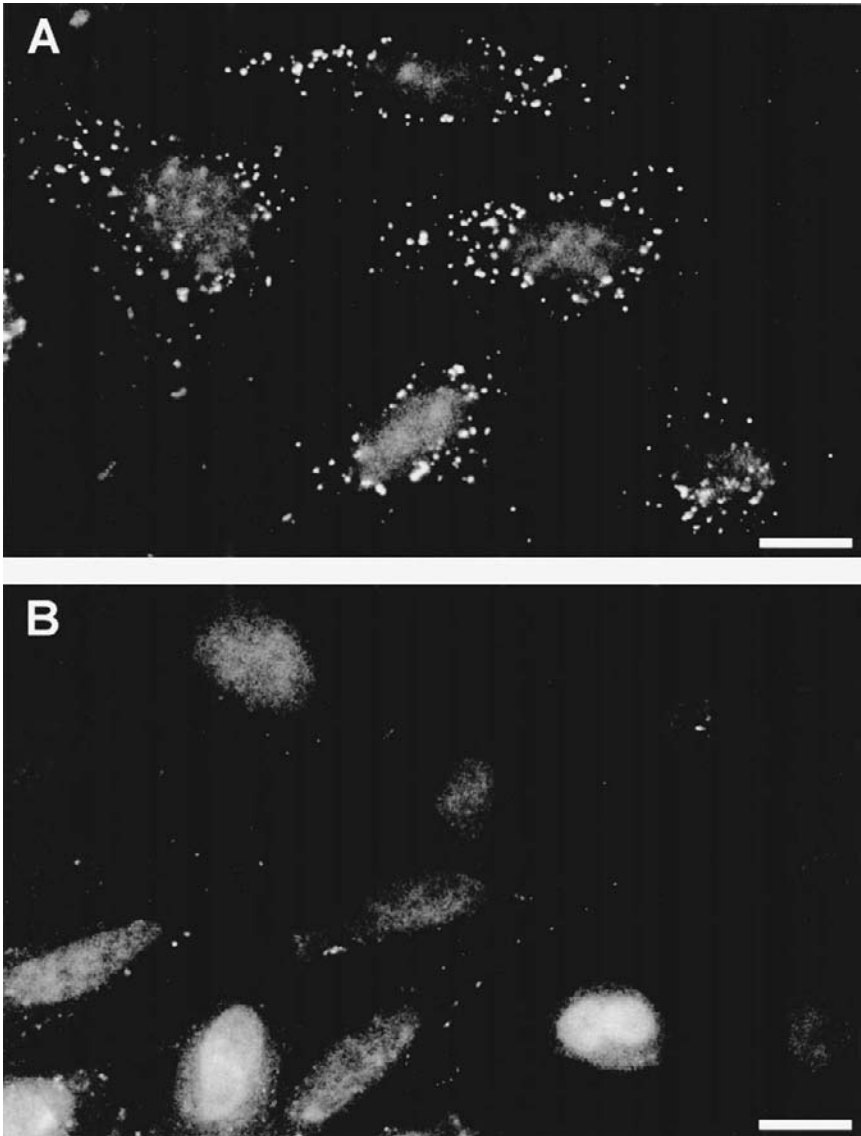
FIG. 10   Functional expression of the insect lipophorin receptor in Chinese hamster ovary (CHO) cells. LDL receptor-deficient CHO cells stably transfected with the insect lipophorin receptor demonstrate a fluorescent punctate staining after incubation with protein-labeled HDLp (A), whereas uptake of labeled HDLp is absent in wild-type CHO cells (B), indicating that the insect lipophorin receptor mediates internalization of HDLp. Light spots (diameter $\sim$10 μm) in both panels show the cell nuclei; cell size can be estimated from the particle distribution in A. Bars $=$ 10 μm (D. Van Hoof, K. W. Rodenburg, and D. J. Van der Horst, unpublished observations).

mediated by the insect lipophorin receptor, indicate that the HDLp indeed escapes from the classical receptor-mediated lysosomal pathway typical for LDL receptor-internalized ligands (D. Van Hoof, K. W. Rodenburg, and D. J. Van der Horst, unpublished observations).

V. Concluding Remarks and Perspectives

While a number of basic processes operative in the regulation of metabolic processes in insects are similar to those in vertebrates, insects have evolved to have different hormonal mechanisms for regulation of substrate mobilization and make use of other carrier molecules for substrate transport, offering adaptations to their specific requirements. The research field covering the release of insect AKHs from the corpus cardiacum and the effects of these peptide hormones on the regulation of carbohydrate and lipid mobilization and transport during flight activity has led to a valuable research model. Knowledge on the key events of this model has provided a coherent understanding as well as an integrated view. Several questions, however, remain elusive.

The release of AKHs involves a complex of regulatory factors acting on the adipokinetic cells; the exact role of each of these factors in the mechanism of AKH release during flight activity remains to be established. Recent research on hormone release on the one hand and biosynthetic activity on the other has significantly advanced our understanding of the strategy these neuroendocrine cells apply to cope with variations in secretory demands. Obviously, an important question relates to the roles of the different storage forms of AKH, particularly the contribution of the older secretory granules and the intracisternal granules to the releasable amount of hormone molecules remains to be resolved.

The AKHs released into the hemolymph bind to receptors at the fat body cell membrane. The structures of these receptors are as yet unidentified and provide an important research goal. At their target cells, the neuropeptides regulate and modulate a sequence of metabolic processes including the mobilization of trehalose and DAG.

The data presented above have allowed us to propose a tentative model for the AKH signal transduction mechanism in the locust fat body. Although this model seems to apply to each of the three AKHs, the research on cell signaling described in this chapter has established a number of interesting dissimilarities between the AKHs, which may support a physiological role for the presence of three structurally and functionally related hormones in *Locusta*. AKH-I, which is by far the most abundant AKH and degrades relatively slowly, will still be present in reasonable amounts after prolonged flight activity (when lipid is the major fuel), even in case it would be released only at the onset of flight. Moreover, since AKH-I induces a stronger InsP$_3$ effect and less Ca^{2+} efflux than AKH-II, the effect of AKH-I results

in a higher intracellular Ca^{2+} level, which is likely to be crucial for activation of the TAG lipase, implying AKH-I likely to be the major lipid-mobilizing hormone. Because AKH-II is less abundant and it breaks down in the hemolymph more rapidly than AKH-I, it will only play a major role in the first period of flight, when carbohydrate is the major energy source utilized. The observation that AKH-II is more powerful in generating cAMP and activating glycogen phosphorylase (whose activation depends on cAMP) *in vitro* also designates this hormone as the major trigger for carbohydrate mobilization. AKH-III, considering its low abundance and rapid degradation, plays only a minor role during flight, but as it is the only AKH that may be released constitutively, it may provide the animal with energy when it is not flying. Its strong effect on cAMP, $InsP_3$, and glycogen phosphorylase then compensates in part for its low amount.

Although studies on the involvement of eicosanoids in hormone-controlled mobilization of energy substrates in insects are scarce, results obtained so far are promising and do suggest a modulatory role for representatives of this group of compounds on the action of AKH and HTH. For acquisition of more conclusive data on the role of eicosanoids in the regulation of carbohydrate and lipid mobilization, however, further research is required.

Increased knowledge on the structure and mechanism of action of the TAG lipase is another important future research goal, which is essential for a better insight in the as yet poorly understood mechanism of hormonal control of flight-induced lipolysis in insects.

The transport of the released DAG in the hemolymph requires the AKH-stimulated transformation of lipophorins, which are capable of alternating between relatively lipid-poor (HDLp) and lipid-enriched (LDLp) forms. In these reversible conversions the exchangeable apolipoprotein, apoLp-III, which exists in a lipid-free and a lipid-bound form, plays an essential role. In the past decade, considerable information has been gained on many aspects of lipophorin such as interconversion of lipophorin subspecies, primary sequence of their apolipophorins, and evolutionary relationships, but much additional data is required for a complete understanding of this unique system and to apply the insight obtained into corresponding processes in higher organisms. An important unresolved issue concerns lipophorin biosynthesis and relates to the question how, upon synthesis of the apolipophorin precursor, the lipophorin particle is assembled and secreted. Additional information on the functioning of the mechanism of apoLp-III binding to the lipophorin lipid surface represents an important ongoing research effort, which will continue to provide essential insight into lipid–protein interaction.

For a fuller understanding of the structure of LTP and its activity and specificity in lipid mobilization, sequence information on its apoprotein components is required. Additional structural information on LTP may provide the basis for further deepening of our insight into the molecular mechanism of the lipophorin shuttle system.

Significant progress in the area of insect lipoprotein receptors has been made by the identification of the fat body HDLp receptor as a novel member of the LDL receptor family implicated in receptor-mediated uptake of HDLp during larval development. As the generally accepted functioning of HDLp as a reusable shuttle involves a selective lipid transport between HDLp particles and fat body cells without degradation of the lipophorin matrix, pivotal questions to be resolved are whether this receptor, in contrast to the other LDL receptor family members, is able to recycle its ligand after intracellular trafficking and, if so, which cellular and molecular mechanisms may be involved. Current studies using mammalian cell lines transfected with the insect lipophorin receptor constitute crucial tools for providing answers to these important aspects.

It may be concluded that through persistent research efforts on the many intriguing issues concerning AKH-related aspects of flight metabolism, this model system will continue to provide fundamental discoveries of profound biological significance.

References

Ali, I., Finley, C., and Steele, J. E. (1998). Evidence for the participation of arachidonic acid metabolites in trehalose efflux from the hormone activated fat body of the cockroach (*Periplaneta americana*). *J. Insect Physiol.* **44,** 1119–1126.

Ali, I., and Steele, J. E. (1997a). Hypertrehalosemic hormones increase the concentration of free fatty acids in trophocytes of the cockroach (*Periplaneta americana*) fat body. *Comp. Biochem. Physiol.* **118**A, 1225–1231.

Ali, I., and Steele, J. E. (1997b). Evidence that free fatty acids in trophocytes of *Periplaneta americana* fat body may be regulated by the activity of phospholipase A_2 and cyclooxygenase. *Insect Biochem. Mol. Biol.* **27,** 681–692.

Ali, I., and Steele, J. E. (1997c). Fatty acids stimulate trehalose synthesis in trophocytes of the cockroach (*Periplaneta americana*) fat body. *Gen. Comp. Endocrinol.* **108,** 290–297.

Anderson, T. A., Levitt, D. G., and Banaszak, L. J. (1998). Crystal structure of lamprey lipovitellin, a member of a novel class of lipid-carrying proteins. *Structure* **6,** 895–909.

Anthonsen, M. W., Rönnstrand, L., Wernstedt, C., Degerman, E., and Holm, C. (1998). Identification of novel phosphorylation sites in hormone-sensitive lipase that are phosphorylated in response to isoproterenol and govern activation properties *in vitro*. *J. Biol. Chem.* **273,** 215–221.

Arrese, E. L., Canavoso, L. E., Jouni, Z. E., Pennington, J. E., Tsuchida, K., and Wells, M. A. (2001). Lipid storage and mobilization in insects: Current status and future directions. *Insect Biochem. Mol. Biol.* **31,** 7–17.

Arrese, E. L., Flowers, M. T., Gazard, J. L., and Wells, M. A. (1999). Calcium and cAMP are second messengers in the adipokinetic hormone-induced lipolysis of triacylglycerols in *Manduca sexta* fat body. *J. Lipid Res.* **40,** 556–564.

Arrese, E. L., Rojas-Rivas, B. I., and Wells, M. A. (1996a). Synthesis of *sn*-1,2-diacylglycerol by monoacylglycerol-acyltransferase from *Manduca sexta* fat body. *Arch. Insect Biochem. Physiol.* **31,** 325–335.

Arrese, E. L., Rojas-Rivas, B. I., and Wells, M. A. (1996b). The use of decapitated insects to study lipid mobilization in adult *Manduca sexta*: Effects of adipokinetic hormone and trehalose on fat body lipase activity. *Insect Biochem. Mol. Biol.* **26,** 775–782.

Arrese, E. L., and Wells, M. A. (1994). Purification and properties of a phosphorylatable triacylglycerol lipase from the fat body of an insect, *Manduca sexta*. *J. Lipid Res.* **35,** 1652–1660.

Arrese, E. L., and Wells, M. A. (1997). Adipokinetic hormone-induced lipolysis in the fat body of an insect, *Manduca sexta*: Synthesis of *sn*-1,2-diacylglycerols. *J. Lipid Res.* **38,** 68–76.

Auerswald, L., and Gäde, G. (2000). Cyclic AMP mediates the elevation of proline by AKH peptides in the cetoniid beetle, *Pachnoda sinuata*. *Biochim. Biophys. Acta* **1495,** 78–89.

Ayali, A., Pener, M. P., and Girardie, J. (1996a). Comparative study of neuropeptides from the corpora cardiaca of solitary and gregarious *Locusta*. *Arch. Insect Biochem. Physiol.* **31,** 439–450.

Ayali, A., Pener, M. P., Sowa, S. M., and Keeley, L. L. (1996b). Adipokinetic hormone content of the corpora cardiaca in gregarious and solitary migratory locusts. *Physiol. Entomol.* **21,** 167–172.

Babin, P. J., Bogerd, J., Kooiman, F. P., Van Marrewijk, W. J. A., and Van der Horst, D. J. (1999). Apolipophorin II/I, apolipoprotein B, vitellogenin, and microsoma triglyceride transfer protein genes are derived from a common ancestor. *J. Mol. Evol.* **49,** 150–160.

Bauerfeind, R., and Komnick, H. (1992a). Immunocytochemical localization of lipophorin in the fat body of dragonfly larvae (*Aeshna cyanea*). *J. Insect Physiol.* **38,** 185–198.

Bauerfeind, R., and Komnick, H. (1992b). Lipid loading and unloading of lipophorin in the midgut epithelium of dragonfly larvae (*Aeshna cyanea*). A biochemical and immunocytochemical study. *J. Insect Physiol.* **38,** 147–160.

Baumann, E., Gäde, G., and Penzlin, H. (1990). Structure-function studies on neurohormone D: Activity of naturally occurring hormone analogues. *J. Comp. Physiol.* **160**B, 423–429.

Bean, A. J., Zhang, X., and Hökfelt, T. (1994). Peptide secretion: What do we know? *FASEB J.* **8,** 630–638.

Becker, A., Liewald, J. F., and Wegener, G. (1998). Signal transduction in isolated fat body from the cockroach *Blaptica dubia* exposed to hypertrehalosaemic neuropeptide. *J. Comp. Physiol.* **168**B, 159–167.

Becker, A., Schlöder, P., Steele, J. E., and Wegener, G. (1996). The regulation of trehalose metabolism in insects. *Experientia* **52,** 433–439.

Becker, A., and Wegener, G. (1998). Hypertrehalosaemic neuropeptides decrease levels of the glycolytic signal fructose-2,6-bisphosphate in cockroach fat body. *J. Exp. Biol.* **201,** 1939–1946.

Beenakkers, A. M. T., Van der Horst, D. J., and Van Marrewijk, W. J. A. (1985). Biochemical processes directed to flight muscle metabolism. *In* "Comprehensive Insect Physiology, Biochemistry and Pharmacology" (G. A. Kerkut and L. I. Gilbert, Eds.), Vol. 10, pp. 451–486. Pergamon Press, Oxford.

Blacklock, B. J., and Ryan, R. O. (1994). Hemolymph lipid transport. *Insect Biochem. Mol. Biol.* **24,** 855–873.

Bloemen, R. E. B., and Beenakkers, A. M. T. (1985). The effect of sense organ deprivation on the release of adipokinetic hormone in *Locusta migratoria*. *Comp. Biochem. Physiol.* **81**A, 915–919.

Bogerd, J., Babin, P. J., Kooiman, F. P., André, M., Ballagny, C., Van Marrewijk, W. J. A., and Van der Horst, D. J. (2000). Molecular characterization and gene expression in the eye of the apolipophorin II/I precursor from *Locusta migratoria*. *J. Comp. Neurol.* **427,** 546–558.

Bogerd, J., Kooiman, F. P., Pijnenburg, M. A. P., Hekking, L. H. P., Oudejans, R. C. H. M., and Van der Horst, D. J. (1995). Molecular cloning of three distinct cDNAs, each encoding a different adipokinetic hormone precursor, of the migratory locust, *Locusta migratoria*. Differential expression of the distinct adipokinetic hormone precursor genes during flight activity. *J. Biol. Chem.* **270,** 23038–23043.

Brasaemle, D. L., Rubin, B., Harten, I. A., Gruia-Gray, J., Kimmel, A. R., and Londos, C. (2000). Perilipin A increases triacylglycerol storage by decreasing the rate of triacylglycerol hydrolysis. *J. Biol. Chem.* **275,** 38486–38493.

Breiter, D. B., Kanost, M. R., Benning, M. M., Wesenberg, G., Law, J. H., Wells, M. A., Rayment, I., and Holden, H. M. (1991). Molecular structure of an apolipoprotein determined at 2.5-Å resolution. *Biochemistry* **30,** 603–608.

Cheeseman, P., and Goldsworthy, G. J. (1979). The release of adipokinetic hormone during flight and starvation in *Locusta*. *Gen. Comp. Endocrinol.* **37,** 35–43.

Clifford, G. M., McCormick, D. K. T., Vernon, R. G., and Yeaman, S. J. (1997). Translocation of perilipin and hormone-sensitive lipase in response to lipolytic hormones. *Biochem. Soc. Trans.* **25,** S672.

Clynn, E., Baggerman, G., Veelaert, D., Cristiaens, A., Van der Horst, D. J., Harthoorn, L. F., Derua, R., Waelkens, E., De Loof, A., and Schoofs, L. (2001). Peptidomics of the pars intercerebralis-corpus cardiacum complex of the mogratory locust, *Locusta migratoria. Eur. J. Biochem.,* 1929–1939.

Cole, K. D., Fernando-Warnakulasuriya, G. J. P., Boguski, M. S., Freeman, M., Gordon, J. I., Clark, W. A., Law, J. H., and Wells, M. A. (1987). Primary structure and comparative equence analysis of an insect apolipoprotein: Apolipophorin III from *Manduca sexta. J. Biol. Chem.* **262,** 11794–11800.

Dantuma, N. P., Pijnenburg, M. A. P., Diederen, J. H. B., and Van der Horst, D. J. (1997). Developmental down-regulation of receptor-mediated endocytosis of an insect lipoprotein. *J. Lipid Res.* **38,** 254–265.

Dantuma, N. P., Pijnenburg, M. A. P., Diederen, J. H. B., and Van der Horst, D. J. (1998a). Multiple interactions between insect lipoproteins and fat body cells: Extracellular trapping and endocytic trafficking. *J. Lipid Res.* **39,** 1877–1888.

Dantuma, N. P., Pijnenburg, M. A. P., Diederen, J. H. B., and Van der Horst, D. J. (1998b). Electron microscopic visualization of receptor-mediated endocytosis of Dil-labeled lipoproteins by diaminobenzidine photoconversion. *J. Histochem. Cytochem.* **46,** 1085–1089.

Dantuma, N. P., Potters, M., De Winther, M. P. J., Tensen, C. P., Kooiman, F. P., Bogerd, J., and Van der Horst, D. J. (1999). An insect homolog of the vertebrate low density lipoprotein receptor mediates endocytosis of lipophorins. *J. Lipid Res.* **40,** 973–978.

Dantuma, N. P., Van Marrewijk, W. J. A., Wynne, H. J., and Van der Horst, D. J. (1996). Interaction of an insect lipoprotein with its binding site at the fat body. *J. Lipid Res.* **37,** 1345–1355.

Demel, R. A., Van Doorn, J. M., and Van der Horst, D. J. (1992). Insect apolipophorin III: Interaction of locust apolipophorin III with diacylglycerol. *Biochim. Biophys. Acta* **1124,** 151–158.

De Winther, M. P. J., Weers, P. M. M., Bogerd., J., and Van der Horst, D. J. (1996). Apolipophorin III levels in *Locusta migratoria*. Developmental regulation of gene expression and homolymph protein concentration. *J. Insect Physiol.* **42,** 1047–1052.

Diederen, J. H. B., Maas, H. A., Pel, H. J., Schooneveld, H., Janssen, W. F., and Vullings, H. G. B. (1987). Co-localization of the adipokinetic hormones I and II in the same glandular cells and in the same secretory granules of the corpus cardiacum of *Locusta migratoria* and *Schistocerca gregaria. Cell Tissue Res.* **249,** 379–389.

Diederen, J. H. B., Peppelenbosch, M. P., and Vullings, H. G. B. (1992). Ageing adipokinetic cells in *Locusta migratoria:* An ultrastructural morphometric study. *Cell Tissue Res.* **268,** 117–121.

Diederen, J. H. B., Van Etten, E. W. M., Biegstraaten, A. I. M., Terlou, M., Vullings, H. G. B., and Jansen, W. F. (1988). Flight-induced inhibition of the cerebral median peptidergic neurosecretory system in *Locusta migratoria. Gen. Comp. Endocrinol.* **71,** 257–264.

Diederen, J. H. B., Verkade, P., Jansen, W. F., and Vullings, H. G. B., (1993). Endocytosis in flight-stimulated adipokinetic cells of *Locusta migratoria. Cell Tissue Res.* **271,** 485–489.

Diederen, J. H. B., Verstegen, M. M. A., Oudejans, R. C. H. M., Vullings, H. G. B., and Van der Horst, D. J. (1999). Number and size of intracisternal granules in the adipokinetic hormone-secreting cells of locusts: A phase-dependent characteristic. *Physiol. Entomol.* **24,** 51–55.

Diederen, J. H. B., and Vullings, H. G. B. (1995). Secretory granule formation and membrane recycling by the trans-Golgi network in adipokinetic cells of *Locusta migratoria* in relation to flight and rest. *Cell Tissue Res.* **279,** 585–590.

Dircksen, H., and Homberg, U. (1995). Crustacean cardioactive peptide-immunoreactive neurons innervating brain neuropils, retrocerebral complex and stomatogastric nervous system of the locust, *Locusta migratoria. Cell Tissue Res.* **279,** 495–515.

Egan, J. J., Greenberg, A. S., Chang, M.-K., Wek, S. A., Moos, M. C., Jr., and Londos, C. (1992). Mechanism of hormone-stimulated lipolysis in adipocytes: Translocation of hormone-sensitive lipase to the lipid storage droplet. *Proc. Natl. Acad. Sci. USA* **89,** 8537–8541.

Fain, J. N., Leffler, C. W., and Bahouth, S. W. (2000). Eicosanoids as endogenous regulators of leptin release and lipolysis by mouse adipose tissue in primary culture. *J. Lipid Res.* **41,** 1689–1694.

Ford, P. S., and Van Heusden, M. C. (1994). Triglyceride-rich lipophorin in *Aedes aegypti* (Diptera: Culicudae). *J. Med. Entomol.* **31,** 435–441.

Gäde, G. (1996). The revolution in insect neuropeptides illustrated by the adipokinetic hormone/red pigment-concentrating hormone family of peptides. *Z. Naturforsch.* **51**C, 607–617.

Gäde, G. (1997a). Distinct sequences of AKH/RPCH family members in beetle (*Scarabaeus*-species) corpus cardiacum contain three aromatic amino acid residues. *Biochem. Biophys. Res. Commun.* **230,** 16–21.

Gäde, G. (1997b). Hyperprolinaemia caused by novel members of the adipokinetic hormone/red pigment-concentrating hormone family of peptides isolated from corpora cardiaca of onitine beetles. *Biochem. J.* **321,** 201–206.

Geraerts, W. P. M., and Smit, A. B. (1991). The role of peptide diversity in the molluscan CNS. *In* "Molluscan Neurobiology" (K. S. Kits, H. H. Boer, and J. Joosse, Eds.), pp. 300–308. North Holland, Amsterdam.

Gibbons, G. F., Islam, K., and Pease, R. J. (2000). Mobilisation of triacylglycerol stores. *Biochim. Biophys. Acta* **1483,** 37–57.

Goldsworthy, G. J., Mallison, K., and Wheeler, C. H. (1986). The relative potencies of two known locust adipokinetic hormones. *J. Insect Physiol.* **32,** 95–101.

Gondim, K. C., and Wells, M. A. (2000). Characterization of lipophorin binding to the midgut of larval *Manduca sexta*. *Insect Biochem. Mol. Biol.* **30,** 405–413.

Goñi, F. M., and Alonso, A. (1999). Structure and functional properties of diacylglycerol in membranes. *Prog. Lipid Res.* **38,** 1–48.

Gordon, D. A., and Jamil, H. (2000). Progress towards understanding the role of microsomal triglyceride transfer protein in apolipoprotein-B lipoprotein assembly. *Biochim. Biophys. Acta* **1486,** 72–83.

Greenberg, A. S., Egan, J. J., Wek, S. A., Garty, N. B., Blanchette-Mackie, E. J., and Londos, C. (1991). Perilipin, a major hormonally regulated adipocyte-specific phosphoprotein associated with the periphery of lipid storage droplets. *J. Biol. Chem.* **266,** 11341–11346.

Greenberg, A. S., Egan, J. J., Wek Moos, M. C. Jr., Londos, C., and Kimmel, A. R. (1993). Isolation of cDNAs for perilipins A and B: sequence and expression of lipid droplet-associated proteins of adipocytes. *Proc. Natl. Acad. Sci. USA* **90,** 12035–12039.

Gretch, D. G., Sturley, S. L., Wang, L., Lipton, B. A., Dunning, A., Grunwald, K. A. A., Wetterau, J. R., Yao, Z., Talmundi, P., and Attie, A. D. (1996). The amino terminus of apolipoprotein B is necessary but not sufficient for microsomal triglyceride transfer protein responsiveness. *J. Biol. Chem.* **271,** 8682–8691.

Hård, K., Van Doorn, J. M., Thomas-Oates, J. E., Kamerling, J. P., and Van der Horst, D. J. (1993). Structure of the Asn-linked oligosaccharides of apolipophorin III from the insect *Locusta migratoria*. Carbohydrate-linked 2-aminoethylphosphonate as a constituent of a glycoprotein. *Biochemistry* **32,** 766–775.

Harthoorn, L. F., Diederen, J. H. B., Oudejans, R. C. H. M., and Van der Horst, D. J. (1999). Differential location of peptide hormones in the secretory pathway of insect adipokinetic cells. *Cell Tissue Res.* **298,** 361–369.

Harthoorn, L. F., Diederen, J. H. B., Oudejans, R. C. H. M., Verstegen, M. M. A., Vullings, H. G. B., and Van der Horst, D. J. (2000). Intracisternal granules in the adipokinetic cells of locusts are not degraded and apparently function as supplementary stores of secretory material. *Eur. J. Cell Biol.* **79,** 27–34.

Harthoorn, L. F., Oudejans, R. C. H. M., Diederen, J. H. B., Van de Wijngaart, D. J., and Van der Horst, D. J. (2001). Absence of coupling between release and biosynthesis of peptide hormones in insect neuroendocrine cells. *Eur. J. Cell Biol.* **80,** 451–457.

Hatle, J. D., and Spring, J. H. (1999). Tests of potential adipokinetic hormone precursor-related peptide (APRP) functions: lack of responses. *Arch. Insect Biochem. Physiol.* **42,** 163–166.

Hekimi, S., Fischer-Lougheed, J., and O'Shea, M. (1991). Regulation of neuropeptide stoichiometry in neurosecretory cells. *J. Neurosci.* **11,** 3246–3256.

Hekimi, S., and O'Shea, M. (1989). Biosynthesis of adipokinetic hormones (AKHs): Further characterization of precursors and identification of novel products of processing. *J. Neurosci.* **9,** 996–1003.

Hirabayashi, T., and Shimizu, T. (2000). Localization and regulation of cytosolic phospholipase A$_2$. *Biochim. Biophys. Acta* **1488,** 124–138.

Hiraoka, T., and Hayakawa, Y. (1990). Inhibition of diacylglycerol uptake from the fat body by a monoclonal antibody against apolipophorin II in *Locusta migratoria*. *Insect Biochem.* **20,** 793–799.

Hirayama, Y., and Chino, H. (1990). Lipid transfer particle in locust hemolymph: purification and characterization. *J. Lipid Res.* **31,** 793–799.

Holm, C., Langin, D., Manganiello, V., Belfrage, P., and Degerman, E. (1997). Regulation of hormone-sensitive lipase activity in adipose tissue. *Methods Enzymol.* **286,** 45–67.

Hurtley, S. M., and Helenius, A. (1989). Protein oligomerization in the endoplasmic reticulum. *Annu. Rev. Cell Biol.* **5,** 277–307.

Jansen, W. F., Diederen, J. H. B., Dorland, M., Langermans, J., Meessen, B. P. M., Mink, K., and Vullings, H. G. B. (1989). Ultrastructural enzyme-cytochemical study of the intrinsic glandular cells in the corpus cardiacum of *Locusta migratoria:* Relation to the secretory and endocytotic pathways, and to the lysosomal system. *Cell Tissue Res.* **255,** 167–178.

Johnson, L. N. (1992). Glycogen phosphorylase: control by phosphorylation and allosteric effectors. *FASEB J.* **6,** 2274–2282.

Kanost, M. R., Boguski, M. S., Freeman, M., Gordon, J. I., Wyatt, G. R., and Wells, M. A. (1988). Primary structure of apolipophorin III from the migratory locust, *Locusta migratoria*. Potential amphipathic structures and molecular evolution of an insect apolipoprotein. *J. Biol. Chem.* **263,** 10568–10573.

Kass, G. E. N., Gahm, A., and Llopis, J. (1994). Cyclic AMP stimulates Ca^{2+} entry in rat hepatocytes by interacting with the plasma membrane carriers involved in receptor-mediated Ca^{2+} influx. *Cell. Signal.* **6,** 493–501.

Kawooya, J. K., Meredith, S. C., Wells, M. A., Kézdy, F. J., and Law, J. H. (1986). Physical and surface properties of insect apolipophorin III. *J. Biol. Chem.* **261,** 13,588–13,591.

Kawooya, J. K., Van der Horst, D. J., Van Heusden, M. C., Brigot, B. L. J., Van Antwerpen, R., and Law, J. H. (1991). Lipophorin structure analyzed by *in vitro* treatment with lipases. *J. Lipid Res.* **32,** 1781–1788.

Keeley, L. L., and Hesson, A. S. (1995). Calcium-dependent signal transduction by the hepertrehalosemic hormone in the cockroach fat body. *Gen. Comp. Endocrinol.* **99,** 373–381.

Keeley, L. L., Park, J. H., Lu, K.-H., and Bradfield, J. Y. (1996). Neurohormone signal transduction for dual regulation of metabolism and gene expression in insects: Hypertrehalosemic hormone as a model. *Arch. Insect Biochem. Physiol.* **33,** 283–301.

Keeley, L. L., Sowa, S. M., and Hesson, A. S. (1995). *In vitro* bioassay for hypertrehalosemic hormone-dependent trehalose biosynthesis by fat body from *Blaberus discoidalis* cockroaches. *Arch. Insect Biochem. Physiol.* **28,** 313–324.

Kitamura, K., and Miller, R. T. (1994). Regulation of hormone-sensitive calcium influx by the adenylyl cyclase system in renal epithelial cells. *J. Clin. Invest.* **94,** 328–336.

Klein, J. M., Mohrherr, C. J., Sleutels, F., Jaenecke, N., Riehm, J. P., and Rao, K. R. (1995). A highly conserved red pigment-concentrating hormone precursor in the blue crab *Callinectes sapidus*. *Biochem. Biophys. Res. Commun.* **212,** 151–158.

Kodrík, D., and Goldsworthy, G. J. (1995). Inhibition of RNA synthesis by adipokinetic hormones and brain factor(s) in adult fat body of *Locusta migratoria*. *J. Insect Physiol.* **41,** 127–133.

Köllisch, G. V., Lorenz, M. W., Kellner, R., Verhaert, P. D., and Hoffmann, K. H. (2000). Structure elucidation and biological activity of an unusual adipokinetic hormone from corpora cardiaca of the butterfly, *Vanessa cardui*. *Eur. J. Biochem.* **267,** 5502–5508.

Konings, P. N. M., Vullings, H. G. B., Kok, O. J. M., Diederen, J. H. B., and Jansen, W. F. (1989). The innervation of the corpus cardiacum of *Locusta migratoria:* A neuroanatomical study with the use of Lucifer yellow. *Cell Tissue Res.* **258,** 301–308.

Kutty, R. K., Kutty, G., Kambadur, R., Duncan, T., Koonin, E. V., Rodriguez, I. R., Odewald, W. F., and Wiggert, B. (1996). Molecular characterization and developmental expression of a retinoid- and fatty acid-binding glycoprotein from *Drosophila.* A putative lipophorin. *J. Biol. Chem.* **272,** 20,641–20,649.

Law, J. H., Ribeiro, J. M. C., and Wells, M. A. (1992). Biochemical insights derived from insect diversity. *Annu. Rev. Biochem.* **61,** 87–111.

Lee, Y.-H., and Keeley, L. L. (1994). Intracellular transduction of trehalose synthesis by hypertrehalosemic hormone in the fat body of the tropical cockroach, *Blaberus discoidalis. Insect Biochem. Mol. Biol.* **24,** 473–480.

Lewis, D. K., Jezierski, M. K., Keeley, L. L., and Bradfield, J. Y. (1997). Hypertrehalosemic hormone in a cockroach: Molecular cloning and expression. *Mol. Cell. Endocrinol.* **130,** 101–108.

Lum, P. Y., and Chino, H. (1990). Primary role of adipokinetic hormone in the formation of low density lipophorin in locusts. *J. Lipid Res.* **31,** 2039–2044.

Mann, C. J., Anderson, T. A., Read, J., Chester, S. A., Harrison, G. B., Köchl, S., Ritchie, P. J., Bradbury, P., Hussain, F. S., Almey, J., Vanloo, B., Rosseneu, M., Infante, R., Hancock, J. M., Levitt, D. G., Banaszak, L. J., Scott, J., and Shoulders, C. (1999). The structure of vitellogenin provides a molecular model for the assembly and secretion of atherogenic lipoproteins. *J. Mol. Biol.* **285,** 391–408.

Mead, J. F., Alfin-Slater, R. B., Howton, D. R., and Popjak, G. (1986). "Lipids: Chemistry, Biochemistry and Nutrition." Plenum Press, New York.

Michel, R., and Lafon-Cazal, M. (1978). Ergastoplasmic granules, cytophysiological adaptation of the locusts corpora cardiaca to migratory flights? *Experientia* **34,** 812–813.

Milde, J. J., Ziegler, R., and Wallstein, M. (1995). Adipokinetic hormone stimulates neurones in the insect central nervous system. *J. Exp. Biol.* **198,** 1307–1311.

Morimoto, C., Sumiyoshi, M., Kameda, K., Tsujita, T., and Okuda, H. (1999). Relationship between hormone-sensitive lipolysis and lipase activity in rat fat cells. *J. Biochem.* **125,** 976–981.

Morimoto, C., Kameda, K., Tsujita, T., and Okuda, H. (2001). Relationships between lipolysis induced by various lipolytic agents and hormone-sensitive lipase in rat fat cells. *J. Lipid Res.* **42,** 120–127.

Narayanaswami, V., and Ryan, R. O. (2000). Molecular basis of exchangeable apolipoprotein function. *Biochim. Biophys. Acta* **1483,** 15–36.

Narayanaswami, V., Wang, J., Kay, C. M., Scraba, D. G., and Ryan, R. O. (1996). Disulfide bond engineering to monitor conformational opening of apolipophorin III during lipid binding. *J. Biol. Chem.* **271,** 26855–26862.

Narayanaswami, V., Wang, J., Schieve, D., Kay, C. M., and Ryan, R. O. (1999). A molecular trigger of lipid-binding induced opening of a helix bundle exchangeable apolipoprotein. *Proc. Natl. Acad. Sci. USA* **96,** 4366–4371.

Narayanaswami, V., Weers, P. M. M., Bogerd, J., Kooiman, F. P., Kay, C. M., Scraba, D. G., Van der Horst, D. J., and Ryan, R. O. (1995). Spectroscopic and lipid binding studies on the amino and carboxyl terminal fragments of *Locusta migratoria* apolipophorin III. *Biochemistry* **34,** 11822–11830.

Nässel, D. R. (1996). Peptidergic neurohormonal control systems in invertebrates. *Curr. Opin. Neurobiol.* **6,** 842–850.

Nässel, D. R., Vullings, H. G. B., Passier, P. C. C. M., Lundquist, C. T., Schoofs, L., Diederen, J. H. B., and Van der Horst, D. J. (1999). Several isoforms of Locustatachykinins may be involved in cyclic AMP-mediated release of adipokinetic hormones from the locust corpora cardiaca. *Gen. Comp. Endocrinol.* **113,** 401–412.

Ogoyi, D. O., Osir, E. O., and Olembo, N. K. (1998). Fat body triacylglycerol lipase in solitary and gregarious phases of *Schistocerca gregaria* (Forskal) (Orthoptera: Acrididae). *Comp. Biochem. Physiol.* **119**B, 163–167.

Orchard, I., and Lange, A. B. (1983). Release of identified adipokinetic hormones during flight and following neural stimulation in *Locusta migratoria*. *J. Insect Physiol.* **29,** 425–429.

Orchard, I., and Shivers, R. (1986). Electrical coupling and gap junctions between neurosecretory cells in an insect. *Brain Res.* **397,** 359–364.

Orr, G. L., Gole, J. W. D., Jahagirdar, A. P., Downer, R. G. H., and Steele, J. E. (1985). Cyclic AMP does not mediate the action of synthetic hypertrehalosemic peptides from the corpus cardiacum of *Periplaneta americana*. *Insect Biochem.* **15,** 703–709.

O'Shea, M., and Rayne, R. C. (1992). Adipokinetic hormones: Cell and molecular biology. *Experientia* **48,** 430–438.

Oudejans, R. C. H. M., Dijkhuizen, R. M., Kooiman, F. P., and Beenakkers, A. M. T. (1992). Dose–response relationships of adipokinetic hormones (Lom-AKH-I, II and III) from the migratory locust, *Locusta migratoria*. *Proc. Section Exp. Appl. Entomol. Neth. Entomol. Soc.* **3,** 165–166.

Oudejans, R. C. H. M., Kooiman, F. P., Schulz, T. K. F., and Beenakkers, A. M. T. (1990). *In vitro* biosynthesis of locust adipokinetic hormones: Isolation and identification of the bioactive peptides and their prohormones. *In* "Chromatography and Isolation of Insect Hormones and Pheromones" (A. R. McCaffery and I. D. Wilson, Eds.), pp. 183–194. Plenum Press, New York.

Oudejans, R. C. H. M., Kooiman, F. P., Heerma, W., Versluis, C., Slotboom, A. J., and Beenakkers, A. M. T. (1991). Isolation and structure elucidation of a novel adipokinetic hormone (Lom-AKH-III) from the glandular lobes of the corpus cardiacum of the migratory locust, *Locusta migratoria*. *Eur. J. Biochem.* **195,** 351–359.

Oudejans, R. C. H. M., Mes, T. H. M., Kooiman, F. P., and Van der Horst, D. J. (1993). Adipokinetic peptide hormone content and biosynthesis during locust development. *Peptides* **14,** 877–881.

Oudejans, R. C. H. M., Vroemen, S. F., Jansen, R. F. R., and Van der Horst, D. J. (1996). Locust adipokinetic hormones: Carrier-independent transport and differential inactivation at physiological concentrations during rest and flight. *Proc. Natl. Acad. Sci. USA* **93,** 8654–8659.

Pancholi, S., Barker, C. J., Candy, D. J., Gokuldas, M., and Kirk, C. J. (1991). Effects of adipokinetic hormones on inositol phosphate metabolism in locust fat body. *Biochem. Soc. Trans.* **19,** 104S.

Park, J. E., and Keeley, L. L. (1995). *in vitro* hormonal regulation of glycogen phosphorylase activity in fat body of the tropical cockroach, *Blaberus discoidalis*. *Gen. Comp. Endocrinol.* **98,** 234–243.

Park, J. E., and Keeley, L. L. (1996). Calcium-dependent action of hypertrehalosemic hormone on activation of glycogen phosphorylase in cockroach fat body. *Mol. Cell. Endocrinol.* **116,** 199–205.

Passier, P. C. C. M., Vullings, H. G. B., Diederen, J. H. B., and Van der Horst, D. J. (1995). Modulatory effects of biogenic amines on adipokinetic hormone secretion from locust corpora cardiaca *in vitro*. *Gen. Comp. Endocrinol.* **97,** 231–238.

Passier, P. C. C. M., Vullings, H. G. B., Diederen, J. H. B., and Van der Horst, D. J. (1997). Trehalose inhibits the release of adipokinetic hormones from the corpus cardiacum in the African migratory locust, *Locusta migratoria,* at the level of the adipokinetic cells. *J. Endocrinol.* **153,** 299–305.

Pener, M. P., Ayali, A., and Golenser, E. (1997). Adipokinetic hormone and flight fuel related characteristics of density-dependent locust phase polymorphism: A review. *Comp. Biochem. Physiol.* **117**B, 513–524.

Pennington, J. E., Nussenzveig, R. H., and Van Heusden, M. C. (1996). Lipid transfer from insect fat body to lipophorin: Comparison between a mosquito triacylglycerol-rich lipophorin and a sphinx moth diacylglycerol-rich lipophorin. *J. Lipid Res.* **37,** 1144–1152.

Pines, M., Tietz, A., Weitraub, H., Applebaum, S. W., and Josefsson, L. (1981). Hormonal activation of protein kinase and lipid mobilization in the locust fat body *in vitro*. *Gen. Comp. Endocrinol.* **43,** 427–431.

Rademakers, L. H. P. M., and Beenakkers, A. M. T. (1977). Changes in the secretory activity of the glandular lobe of the corpus cardiacum of *Locusta migratoria* induced by flight. *Cell Tissue Res.* **180,** 155–171.

Rayne, R. C., and O'Shea, M. (1993). Structural requirements for processing of proadipokinetic hormone I. *Eur. J. Biochem.* **217,** 905–911.

Rayne, R. C., and O'Shea, M. (1994). Reconstitution of adipokinetic hormone biosynthesis *in vitro* indicates steps in prohormone processing. *Eur. J. Biochem.* **219,** 781–789.

Ryan, R. O. (1990). Dynamics in insect lipophorin metabolism. *J. Lipid Res.* **31,** 1725–1739.

Ryan, R. O. (1994). The structures of insect lipoproteins. *Curr. Opin. Struct. Biol.* **4,** 499–506.

Ryan, R. O. (1996). Structural studies of lipoproteins and their apolipoprotein components. *Biochem. Cell Biol.* **74,** 155–174.

Ryan, R. O., Prasad, S. V., Henriksen, E. J., Wells, M. A., and Law, J. H. (1986a). Lipoprotein interconversions in an insect, *Manduca sexta*. Evidence for a lipid transfer factor in the hemolymph. *J. Biol. Chem.* **261,** 563–568.

Ryan, R. O., and Van der Horst, D. J. (2000). Lipid transport biochemistry and its role in energy production. *Annu. Rev. Entomol.* **45,** 233–260.

Ryan, R. O., Wells, M. A., and Law, J. H. (1986b). Lipid transfer protein from *Manduca sexta* hemolymph. *Biochem. Biophys. Res. Commun.* **136,** 260–265.

Sappington, T. W., Kokoza, V. A., Cho, W. L., and Raikhel, A. S. (1996). Molecular characterization of the mosquito vitellogenin receptor reveals unexpected high homology to the *Drosophila* yolk protein receptor. *Proc. Natl. Acad. Sci. USA* **93,** 8934–8939.

Schonbaum, C. P., Lee, S., and Mahowald, A. P. (1995). The *Drosophila* yolkless gene encodes a vitellogenin receptor belonging to the low density lipoprotein superfamily. *Proc. Natl. Acad. Sci. USA* **92,** 1485–1489.

Schoofs, L., Veelaert, D., Vanden Broeck, J., and De Loof, A. (1996). Immunocytochemical distribution of Locustamyoinhibiting peptide (Lom-MIP) in the nervous system of *Locusta migratoria*. *Regul. Pept.* **63,** 171–179.

Schooneveld, H., Romberg-Privee, H. M., and Veenstra, J. A. (1985). Adipokinetic hormone-immunoreactive peptide in the endocrine and central nervous system of several insect species: A comparative inmmunocytochemical approach. *Gen. Comp. Endocrinol.* **57,** 184–194.

Schulz, T. K. F., Van der Horst, D. J., and Beenakkers, A. M. T. (1991). Binding of locust high-density lipophorin to fat body proteins monitored by an enzyme-linked immunosorbant assay. *Biol. Chem. Hoppe-Seyler* **372,** 5–12.

Sharp-Baker, H. E., Diederen, J. H. B., Mäkel, K. M., Peute, J., and Van der Horst, D. J. (1995). The adipokinetic cells in the corpus cardiacum of *Locusta migratoria* preferentially release young secretory granules. *Eur. J. Cell Biol.* **68,** 268–274.

Sharp-Baker, H. E., Oudejans, R. C. H. M., Kooiman, F. P., Diederen, J. H. B., Peute, J., and Van der Horst, D. J. (1996). Preferential release of newly synthesized, exportable neuropeptides by insect neuroendocrine cells and the effect of ageing of secretory granules. *Eur. J. Cell Biol.* **71,** 72–78.

Shen, W.-J., Sridhar, K., Bernlohr, D. A., and Kraemer, F. B. (1999). Interaction of rat hormone-sensitive lipase with adipocyte lipid-binding protein. *Proc. Natl. Acad. Sci. USA* **96,** 5528–5532.

Siegert, K. J. (1999). Locust corpora cardiaca contain an inactive adipokinetic hormone. *FEBS Lett.* **447,** 237–240.

Siegert, K. J., Kellner, R., and Gäde, G. (2000). A third active AKH is present in the pyrgomorphid grasshoppers *Phymateus morbillosus* and *Dictyophorus spumans*. *Insect Biochem. Mol. Biol.* **30,** 1061–1067.

Smith, A. F., Owen, L. M., Strobel, L. M., Chen, H., Kanost, M. R., Hanneman, E., and Wells, M. A. (1994). Exchangeable apoliporoteins of insects share a common structural motif. *J. Lipid Res.* **35,** 1976–1984.

Socha, R., Kodrík, D., and Zemek, R. (1999). Adipokinetic hormone stimulates insect locomotor activity. *Naturwissenschaften* **88,** 85–86.

Soulages, J. L., and Arrese, E. L. (2000a). Dynamics and hydration of the α-helices of apolipophorin III. *J. Biol. Chem.* **275,** 17,501–17,509.

Soulages, J. L., and Arrese, E. L. (2000b). Fluorescence spectroscopy of single tryptophan mutants of apolipophorin-III in discoidal lipoproteins of dimyristoylphosphatidylcholine. *Biochemistry* **39,** 10,574–10,580.

Soulages, J. L., Pennington, J., Bendavid, O., and Wells, M. A. (1998). Role of glycosylation in the lipid-binding activity of the exchangeable apolipoprotein, apolipophorin-III. *Biochem. Biophys. Res. Commun.* **243,** 372–376.

Soulages, J. L., Salamon, Z., Wells, M. A., and Tollin, G. (1995). Low concentrations of diacylglycerol promote the binding of apolipophorin III to a phospholipid bilayer: A surface plasmon resonance spectroscopy study. *Proc. Natl. Acad. Sci. USA* **92,** 5650–5654.

Soulages, J. L., Van Antwerpen, R., and Wells, M. A. (1996). Role of diacylglycerol and apolipophorin-III in regulation of the physicochemical properties of the lipophorin surface: Metabolic implications. *Biochemistry* **35,** 5191–5198.

Soulages, J. L., and Wells, M. A. (1994). Lipophorin: The structure of an insect lipoprotein and its role in lipid transport in insects. *Adv. Prot. Chem.* **45,** 371–415.

Stagg, L. E., and Candy, D. J. (1996). The effect of adipokinetic hormones on the levels of inositol phosphates and cyclic AMP in the fat body of the desert locust *Schistocerca gregaria. Insect Biochem. Mol. Biol.* **26,** 537–544.

Stagg, L. E., and Candy, D. J. (1998). The effect of analogues of adipokinetic hormone II on second messenger systems in the fat body of *Schistocerca gregaria. Insect Biochem. Mol. Biol.* **28,** 59–68.

Stanley, D. W. (2000). "Eicosanoids in Invertebrate Signal Transduction Systems." Princeton University Press, Princeton.

Stanley-Samuelson, D. W. (1994). Prostaglandins and related eicosanoids in insects. *Adv. Insect Physiol.* **24,** 115–212.

Steele, J. E. (1985). Control of metabolic processes. *In* "Comprehensive Insect Physiology, Biochemistry and Pharmacology" (G. A. Kerkut and L. I. Gilbert, Eds.), Vol. 8, pp. 99–145. Pergamon Press, Oxford.

Steele, J. E. (1999). Activation of fat body in *Periplaneta americana* (Blattoptera: Blattidae) by hypertrehalosemic hormones (HTH): New insights into the mechanism of cell signalling. *Eur. J. Entomol.* **96,** 317–322.

Steele, J. E., McDougall, G. E., and Shadwick, R. (1988). Trehalose efflux from cockroach fat body *in vitro:* Paradoxical effects of the corpus cardiacum and methylxanthines. *Insect Biochem.* **18,** 585–590.

Steele, J. E., and Paul, T. (1985). Corpus cardiacum stimulated trehalose efflux from cockroach (*Periplaneta americana*) fat body: Control by calcium. *Can. J. Zool.* **63,** 63–66.

Sun, J., Hiraoka, T., Dittmer, N. T., Cho, K.-H., and Raikhel, A. S. (2000). Lipophorin as a yolk protein in the mosquito, *Aedes aegypti. Insect Biochem. Mol. Biol.* **30,** 1161–1171.

Sundermeyer, K., Hendricks, J. K., Prasad, S. V., and Wells, M. A. (1996). The precursor protein of the structural apolipoproteins of lipophorin: cDNA and deduced amino acid sequence. *Insect Biochem. Mol. Biol.* **26,** 735–738.

Syu, L.-J., and Saltiel, A. R. (1999). Lipotransin: A novel docking protein for hormone-sensitive lipase. *Mol. Cell* **4,** 109–115.

Takeuchi, N., and Chino, H. (1993). Lipid transfer particle in the hemolymph of the American cockroach: Evidence for its capacity to transfer hydrocarbons between lipophorin particles. *J. Lipid Res.* **34,** 543–551.

Tatrai, A., Lee, S. K., and Stern, P. H. (1994). U-73122, a phospholipase C antagonist, inhibits effects of endothelin-1 and parathyroid hormone on signal transduction in UMR-106 osteoblastic cells. *Biochim. Biophys. Acta* **1224,** 575–582.

Trowell, S. C., Hines, E. R., Herlt, A. J., and Rickards, R. W. (1994). Characterization of a juvenile hormone binding lipophorin from the blowfly *Lucilia cuprina. Comp. Biochem. Physiol.* **109**B, 339–357.

Tsuchida, K., Arai, M., Tanaka, Y., Ishihara, R., Ryan, R. O., and Maekawa, H. (1998). Lipid transfer particle catalyzes transfer of carotenoids between lipophorins of *Bombyx mori*. *Insect Biochem. Mol. Biol.* **28,** 927–934.

Tsuchida, K., Soulages, J. L., Moribayashi, A., Suxuki, K., Maekawa, H., and Wells, M. A. (1997). Purification and properties of a lipid transfer particle from *Bombyx mori:* Comparison to the lipid transfer particle from *Manduca sexta*. *Biochim. Biophys. Acta* **1337,** 57–65.

Tsuchida, K., and Wells, M. A. (1988). Digestion, absorption, transport and storage of fat during the last larval stadium of *Manduca sexta*. Changes in the role of lipophorin in the delivery of dietary lipid to the fat body. *Insect Biochem.* **18,** 263–268.

Tsuchida, K., and Wells, M. A. (1990). Isolation and characterization of a lipoprotein receptor from the fat body of an insect, *Manduca sexta*. *J. Biol. Chem.* **265,** 5761–5167.

Van Antwerpen, R., Linnemans, W. A. M., Van der Horst, D. J., and Beenakkers, A. M. T. (1988). Immunocytochemical localization of lipophorins in the flight muscle of the migratory locust (*Locusta migratoria*) at rest and during flight. *Cell Tissue Res.* **252,** 661–668.

Van Antwerpen, R., Wynne, H. J. A., Van der Horst, D. J., and Beenakkers, A. M. T. (1989). Binding of lipophorin to the fat body of the migratory locust. *Insect Biochem.* **19,** 809–814.

Van der Horst, D. J. (1990). Lipid transport function of lipoproteins in flying insects. *Biochim. Biophys. Acta* **1047,** 195–211.

Van der Horst, D. J., Ryan, R. O., Van Heusden, M. C., Schulz, T. K. F., Van Doorn, J. M., Law, J. H., and Beenakkers, A. M. T. (1988). An insect lipoprotein hybrid helps to define the role of apolipophorin III. *J. Biol. Chem.* **263,** 2027–2033.

Van der Horst, D. J., Van Marrewijk, W. J. A., Vullings, H. G. B., and Diederen, J. H. B. (1999). Metabolic neurohormones: Release, signal transduction and physiological responses of adipokinetic hormones in insects. *Eur. J. Entomol.* **96,** 299–308.

Van der Horst, D. J., Weers, P. M. M., and Van Marrewijk, W. J. A. (1993). Lipoproteins and lipid transport. *In* "Insect Lipids: Chemistry, Biochemistry and Biology." (D. W. Stanley-Samuelson and D. R. Nelson, Eds.), pp. 1–24. University of Nebraska Press, Lincoln, NE.

Van Heusden, M. C. (1993). Characterization and identification of a lipoprotein lipase from *Manduca sexta* flight muscle. *Insect Biochem. Mol. Biol.* **23,** 785–792.

Van Heusden, M. C., and Law, J. H. (1989). An insect lipid transfer particle promotes lipid loading from fat body to lipoprotein. *J. Biol. Chem.* **264,** 17287–17292.

Van Heusden, M. C., Thompson, F., and Dennis, J. (1998). Biosynthesis of *Aedes aegypti* lipophorin and gene expression of its apolipoproteins. *Insect Biochem. Mol. Biol.* **28,** 733–738.

Van Heusden, M. C., Van der Horst, D. J., Van Doorn, J. M., Wes, J., and Beenakkers, A. M. T. (1986). Lipoprotein lipase activity in the flight muscle of *Locusta migratoria* and its specificity for hemolymph lipoproteins. *Insect Biochem.* **16,** 517–523.

Van Heusden, M. C., Yepis-Placencia, G. M., Walker, A. M., and Law, J. H. (1996). *Manduca sexta* lipid transfer particle, synthesis by fat body and occurrence in hemolymph. *Arch. Insect Biochem. Physiol.* **31,** 39–51.

Van Marrewijk, W. J. A., Van den Broek, A. T. M., and Beenakkers, A. M. T. (1991). Adipokinetic hormone is dependent on extracellular Ca^{2+} for its stimulatory action on the glycogenolytic pathway in locust fat body *in vitro*. *Insect Biochem.* **21,** 375–380.

Van Marrewijk, W. J. A., Van den Broek, A. T. M., and Beenakkers, A. M. T. (1993). Adipokinetic hormone-induced influx of extracellular calcium into insect fat body cells is mediated through depletion of intracellular calcium stores. *Cell. Signal.* **5,** 753–761.

Van Marrewijk, W. J. A., Van den Broek, A. T. M., Gielbert, M.-L., and Van der Horst, D. J. (1996). Insect adipokinetic hormone stimulates inositol phosphate metabolism: Roles for both $Ins(1,4,5)P_3$ and $Ins(1,3,4,5)P_4$ in signal transduction? *Mol. Cell. Endocrinol.* **122,** 141–150.

Van Marrewijk, W. J. A., and Van der Horst, D. J. (1998). Signal transduction of adipokinetic hormone. *In* "Recent Advances in Arthropod Endocrinology" (G. M. Coast and S. G. Webster, Eds), pp. 172–188. Cambridge University Press, Cambridge.

Veelaert, D., Oonk, H. B., Vanden Eynde, G., Torfs, H., Meloen, R. H., Schoofs, L., Parmentier, M., De Loof, A., and Vanden Broeck, J. (1999). Immunolocalization of a tachykinin-receptor-like protein in the central nervous system *of Locusta migratoria migratorioides* and *Neobellieria bullata*. *J. Comp. Neurol.* **407,** 415–426.

Veelaert, D., Passier, P., Devreese, B., Vanden Broeck, J., Van Beeumen, J., Vullings, H. G. B., Diederen, J. H. B., Schoofs, L., and De Loof, A. (1997). Isolation and characterization of an adipokinetic hormone release-inducing factor in locusts: the crustacean cardioactive peptide. *Endocrinology* **138,** 138–142.

Vroemen, S. F., De Jonge, H., Van Marrewijk, W. J. A., and Van der Horst, D. J. (1998b). The phospholipase C signaling pathway in locust fat body is activated via G_q and not affected by cAMP. *Insect Biochem. Mol. Biol.* **28,** 483–490.

Vroemen, S. F., Van der Horst, D. J., and Van Marrewijk, W. J. A. (1998a). New insights into adipokinetic hormone signaling. *Mol. Cell. Endocrinol.* **141,** 7–12.

Vroemen, S. F., Van Marrewijk, W. J. A., De Meijer, J., Van den Broek, A. T. M., and Van der Horst, D. J. (1997). Differential induction of inositol phosphate metabolism by three adipokinetic hormones. *Mol. Cell. Endocrinol.* **130,** 131–139.

Vroemen, S. F., Van Marrewijk, W. J. A., Schepers, C. C. J., and Van der Horst, D. J. (1995b). Signal transduction of adipokinetic hormones involves Ca^{2+} fluxes and depends on extracellular Ca^{2+} to potentiate cAMP-induced activation of glycogen phosphorylase. *Cell Calcium* **17,** 459–467.

Vroemen, S. F., Van Marrewijk, W. J. A., and Van der Horst, D. J. (1995a). Stimulation of glycogenolysis by three locust adipokinetic hormones involves G_s and cAMP. *Mol. Cell. Endocrinol.* **107,** 165–171.

Vullings, H. G. B., Diederen, J. H. B., Veelaert, D., and Van der Horst, D. J. (1999). Multifactorial control of the release of hormones from the locust retrocerebral complex. *Microsc. Res. Techn.* **45,** 142–153.

Vullings, H. G. B., Passier, P. C. C. M., Van der Jagt, E. M., and Diederen, J. H. B. (1995). Morphology of neurones in the storage part of the corpus cardiacum of *Locusta migratoria:* No evidence for their involvement in the regulation of adipokinetic cell activity. *Cell Tissue Res.* **282,** 321–329.

Vullings, H. G. B., Ten Voorde, S. E. C. G., Passier, P. C. C. M., Diederen, J. H. B., Van der Horst, D. J., and Nässel, D. R. (1998). A possible role of Schisto FLRFamide in inhibition of adipokinetic hormone release from locust corpora cardiaca. *J.Neurocytol.* **27,** 901–913.

Wang, J., Gagné, S. M., Sykes, B. D., and Ryan, R. O. (1997). Insight into lipid surface recognition and reversible conformational adaptations of an exchangeable apolipoprotein by multidimensional heteronuclear NMR techniques. *J. Biol. Chem.* **272,** 17,912–17,920.

Wang, Z., Hayakawa, Y., and Downer, R. G. H. (1990). Factors influencing cyclic AMP and diacyl-glycerol levels in fat body of *Locusta migratoria*. *Insect Biochem.* **20,** 325–330.

Weers, P. M. M., Kay, C. M., Oikawa, O., Wientzek, M., Van der Horst, D. J., and Ryan, R. O. (1994). Factors affecting the stability and conformation of *Locusta migratoria* apolipophorin III. *Biochemistry* **33,** 3617–3624.

Weers, P. M. M., Narayanaswami, V., Kay, C. M., and Ryan, R. O. (1999). Interaction of an exchangeable apolipoprotein with phospholipid vescicles and lipoprotein particles. Role of leucines 32, 34, and 95 in *Locusta migratoria* apolipophorin III. *J. Biol. Chem.* **274,** 21,804–21,810.

Weers, P. M. M., Van der Horst, D. J., and Ryan, R. O. (2000). Interaction of apolipophorin III with lipoproteins and phospholipid vescicles: Effect of glycosylation. *J. Lipid Res.* **41,** 416–423.

Weers, P. M. M., Van Marrewijk, W. J. A., Beenakkers, A. M. T., and Van der Horst, D. J. (1993). Biosynthesis of locust lipophorin: Apolipophorin I and II originate from a common precursor. *J. Biol. Chem.* **268,** 4300–4303.

Weers, P. M. M., Wang, J., Van der Horst, D. J., Kay, C. M., Sykes, B. D., and Ryan, R. O. (1998). Recombinant locust apolipophorin III: Characterization and NMR spectroscopy. *Biochim. Biophys. Acta* **1393,** 99–107.

Weisgraber, K. H. (1994). Apolipoprotein E: Structure–function relationships. *Adv. Protein Chem.* **45,** 249–302.

Wells, M. A., Ryan, R. O., Kawooya, J. K., and Law, J. H. (1987). The role of apolipophorin III in *in vivo* lipoprotein interconversions in adult *Manduca sexta*. *J. Biol. Chem.* **262,** 4172–4176.

Wetterau, J. R., Lin, M. C. M., and Jamil, H. (1997). Microsomal triglyceride transfer protein. *Biochim. Biophys. Acta* **1345,** 136–150.

Wheeler, C. H., Van der Horst, D. J., and Beenakkers, A. M. T. (1984). Lipolytic activity in the flight muscles of *Locusta migratoria* measured with haemolymph lipoproteins as substrates. *Insect Biochem.* **14,** 261–266.

Wientzek, M., Kay, C. M., Oikawa, K., and Ryan, R. O. (1994). Binding of insect apolipophorin III to dimyristoylphosphatidylcholine vesicles: Evidence for a conformational change. *J. Biol. Chem.* **269,** 4605–4612.

Wilps, H., and Gäde, G. (1990). Hormonal regulation of carbohydrate metabolism in the blowfly *Phormia terraenovae*. *J. Insect Physiol.* **36,** 41–449.

Wilson, C., Wardell, M. R., Weisgraber, K. H., Mahley, R. W., and Agard, D. A. (1991). Three dimensional structure of the LDL-receptor binding domain of human apolipoprotein E. *Science* **252,** 1817–1822.

Yamaja Setty, B. N., and Ramaia, T. R. (1982). Effect of PGE_1 on lipid mobilization from pupal fat bodies of the silkworm, *Bombyx mori*. *Indian J. Exp. Biol.* **19,** 115–118.

Yochem, J., and Greenwald, I. (1993). A gene for a low density receptor-related protein in the nematode *Caenorhabditis elegans*. *Proc. Natl. Acad. Sci. USA* **90,** 4572–4576.

Ziegler, R., Eckart, K., and Law, J. H. (1990). Adipokinetic hormone controls lipid metabolism in adults and carbohydrate metabolism in larvae of *Manduca sexta*. *Peptides* **11,** 1037–1040.

Ziegler, R., Jasensky, R. D., and Morimoto, H. (1995). Characterization of the adipokinetic hormone receptor from the fat body of *Manduca sexta*. *Regul. Pept.* **57,** 329–338.

Ziegler, R., and Schulz, M. (1986). Regulation of lipid metabolism during flight *in Manduca sexta*. *J. Insect Physiol.* **32,** 903–908.

Ziegler, R., Willingham, L. A., Engler, D. L., Toleman, K. J., Bellows, D., Van der Horst, D. J., Yepiz Plascencia, G. M., and Law, J. H. (1999). A novel lipoprotein from the hemolymph of the cochineal insect, *Dactylopius confusus*. *Eur. J. Biochem.* **261,** 285–290.

Iron Metabolism in Mammalian Cells

Brandie L. Walker, Jacqueline W. C. Tiong, and Wilfred A. Jefferies
Biotechnology Laboratory and Biomedical Research Centre, and Departments of Medical
Genetics, Microbiology and Immunology, and Zoology, University of British Columbia,
Vancouver, BC, Canada V6T 1Z3

Most living things require iron to exist. Iron has many functions within cells but
is rarely found unbound because of its propensity to catalyze the formation of toxic
free radicals. Thus the regulation of iron requirements by cells and the acquisition
and uptake of iron into tissues in multicellular organisms is tightly regulated. In
humans, understanding iron transport and utility has recently been advanced by a
"great conjunction" of molecular genetics in simple organisms, identifying genes
involved in genetic diseases of metal metabolism and by the application of
traditional cell physiology approaches. We are now able to approach a rudimentary
understanding of the "iron cycle" within mammals. In the future, this information
will be applied toward modulating the outcome of therapies designed to overcome
diseases involving metals.
KEY WORDS: Iron metabolism, Iron absorption, DMT-1, IREG, Transferrin,
Transferrin receptor, Melanotransferrin, Ferritin.   © 2001 Academic Press.

I. Introduction

Other than certain strains of *Lactobacillus,* there are no known organisms that can
exist without iron (Archibald, 1983). Iron has a range of critical roles in cells. These
include acting as cofactors to proteins involved in DNA synthesis (such as ribonu-
cleotide reductase) and energy generation (such as iron–sulfur cluster proteins in
the electron transport chain). Other iron–containing enzymes such as peroxidases
and superoxide dismutases play crucial roles in detoxification of free radicals.

Iron metabolism is extensively studied in many different organisms from yeast
through mammals. The information gained from the study of each individual sys-
tem has both directly and indirectly increased our understanding of iron metabolism

in humans. The role of iron in physiological processes has gained greater interest because of the increasing number of human diseases that are associated with iron imbalances. Examination of these diseases has shed light on the close nature of the relationship between iron metabolism and the immune and nervous systems. Cloning of the gene for HFE, a nonclassical major histocompatibility complex molecule, has advanced our understanding of hereditary hemochromatosis (HH), a recessive genetic disease that is carried by 10% of the male caucasian population (Feder *et al.,* 1996). The disease genes involved in X-linked sideroplastic anemia with ataxia and Friedreich ataxia play a crucial role in iron homeostasis, the dysregulation of which results in severe spinocerebellar ataxia (Campuzano *et al.,* 1996; Pagon *et al.,* 1985; Raskind *et al.,* 1991). The discoveries of the multicopper protein, hephaestin, and the iron exporter IREG1 have revealed the intricate connections between copper and iron metabolism.

We now have some detailed insight into the regulation of iron absorption from our diets through recent discoveries of several proteins involved in this process. Absorption of iron in the intestine is closely regulated since there is no known pathway for iron excretion. Overabsorption of iron has been shown to result in many deleterious effects, often related to iron's capacity to generate reactive oxygen species via the Fenton reaction (McCord, 1998). Excess iron can also react directly with unsaturated fatty acids to form alkoxyl radicals (Schaich, 1992). Therefore, in order to maintain the balanced pool of iron required for erythropoiesis and many other crucial cellular functions such as those summarized in Fig. 1 (see color insert), cells have many checkpoints to control both iron absorption in the intestine and iron uptake in other cells. We will not attempt to cover all of the known roles of iron in cellular functions. Instead, we will illustrate what is currently known regarding iron absorption in intestinal cells, the transfer of iron to blood transporters, and the association of these blood transporters with cells in different tissues. Finally we will outline the current models of iron transport across the biological membranes of target tissues.

II. Understanding Homeostatic Regulation of Iron

A sensitive and elegant system of control has evolved which modulates the production of many proteins that are involved in iron utilization, uptake, and storage. This regulation involves iron responsive elements (IREs) (found in the mRNA of iron regulated proteins) and the iron regulatory proteins (IRPs) (which bind to the IREs) (Fig. 2; see color insert). In general, IREs located at the 5′ end of mRNA allow the IRP to bind in low iron conditions and thus result in decreased translation of the iron storage protein. For example, the first protein in the pathway of heme biosynthesis, the erythroid isoform of delta-aminolevulinate synthase (eALAS) has one IRE in the 5′ untranslated region (UTR) of the mRNA, as does ferritin (Aziz and Munro, 1987; Dandekar *et al.,* 1991). In both cases, low levels of iron

cause IRPs to bind to the IREs, thus blocking translation of the mRNA and preventing the protein from being made. If intracellular levels of iron are high, the IRP changes conformation and cannot bind to the IRE. In this case ferritin and eALAS synthesis will proceed, resulting in a greater capacity for storing pools of iron intracellularly. Conversely, if IREs are found within the 3′ end of mRNAs, IRP will bind to the nascent mRNA molecule under low cellular iron conditions and stabilize it, thus allowing more protein to be translated. The IREs within the transferrin receptor (TfR) are located in the 3′UTR of the mRNA. When iron concentrations are low and the IRPs are able to bind, the TfR transcript is stabilized and increased amounts of the TfR are made (Mullner and Kuhn, 1988). If iron concentrations are high (and therefore no need exists for increased levels of the TfR on the cell surface), the IRP cannot bind to the 3′ IREs and the TfR transcript becomes targeted for rapid degradation. To further complicate the story, early indications are that while iron-regulated transporter-1 (IREG1) has an IRE in the 5′ UTR, like ferritin, the response to cell conditions that promote IRP binding seems to be an increase in IREG1 mRNA and protein levels. This upregulation effect is similar to that observed for TfR, a protein with a 3′ IRE that leads to stabilization of the transcript upon IRP binding and an increase in protein synthesis rather than a blockage of translation (McKie *et al.,* 2000).

The IREs of the mRNAs which respond to iron regulation are not identical, but do contain a 28-nucleotide consensus sequence which seems to be necessary for proper function. The IRE is a hairpin-shaped stem–loop structure found in the UTR of the mRNA of various proteins (Laing and Hall, 1996). The loop seems to be of particular importance, with the sequence CAGUGN being present in all sequences examined to date, as well as an unpaired cytosine found five bases upstream of the loop, or an internal loop bulge as is the case with ferritin (Laing and Hall, 1996; Ke *et al.,* 1998). IRE sequences are highly specific to the individual mRNA species (>95% sequence conservation of the same gene's mRNA in different animals) and can differ from 36 to 85% between various mRNAs of a single organism (Theil, 1998). As already mentioned, the IRE can be found in the 3′ UTR, as with divalent metal transporter 1 (DMT1), or in the 5′ UTR, as with ferritin. Further, the IRE can be in a single copy, such as observed with eALAS, or multiple copies, like TfR.

There are two known IRPs, termed IRP1 and IRP2. The human IRP1 shows 61% sequence identity to IRP2 and 79% similarity to IRP2. IRP2 is 73 amino acids longer than IRP1 due to the inclusion of a protein segment that makes IRP2 vulnerable to proteolytic cleavage in cells with high levels of iron (Thomson *et al.,* 1999). The amounts of IRPs 1 and 2 in different cell types varies and possibly accounts for the precise regulation of protein levels by iron in various systems, together with differential binding of IRPs 1 and 2 to various IREs. For example, IREs with a cytosine bulge in the stem bind IRP2 less strongly (Ke *et al.,* 2000).

IRP1 was originally shown to have a high degree of homology (30%) (Hentze and Argos, 1991) to rabbit and other mitochondrial aconitases, and in fact IRP1 was later confirmed to be the cytosolic form of the previously identified mitochondrial

aconitase. The aconitase enzyme catalyzes the formation of isocitrate from citrate in the citric acid cycle. It is a protein that, given iron replete conditions within the cell, contains an iron–sulfur cubane structure (4Fe–4S) bound by three cysteine residues in the cleft of the protein. The binding of iron to form the 4Fe–4S cluster occludes the mRNA binding site, preventing the IRP from binding to the IRE, but leaving aconitase activity unaffected. Low iron conditions, on the other hand, lead to a shift in conformation of the protein whereby the RNA binding site is accessible. IRP1 can then bind to mRNA, but forfeits its aconitase activity. Experimental evidence has shown that if IRP1 is unable to form the iron–sulfur cluster, constitutive IRE binding results, leading to an increase in TfR synthesis and decrease in ferritin synthesis (DeRusso *et al.,* 1995). The cysteine residues C437, C503, and C506 have all been shown to reside in the IRP1 cleft and are necessary for both formation of the iron–sulfur cluster and RNA binding (Hirling *et al.,* 1994).

A number of factors besides iron levels have been shown to affect IRP1 binding to IRE. An increase in IRP1 binding to IRE is observed if cellular protein kinase Cs (PKC) are activated with phorbol-12,13-myristate acetate, which leads to phosphorylation of IRP1 (Schalinske and Eisenstein, 1996). This could be a result of the phosphorylation of IRP1 by the PKC, preventing the iron–sulfur cluster from assembling. As well, erythropoietin, a glycoprotein that stimulates proliferation and differentiation of red blood cell progenitors has been shown to increase binding of IRP1 to the IRE of TfR in erythroid cells (Weiss *et al.,* 1997). Similarly, nitric oxide (NO) causes a slow (>12 h) increase in IRP1 binding to IRE, leading eventually to an increase in TfR expression and decrease in ferritin expression in all cell types and tissues studied thus far (Domachowske, 1997). This activation is posttranslational, and the precise mechanism is unclear (Pantopoulos *et al.,* 1996). Through cell lysate experiments with iron-replete or chelated conditions, Wardrop and associates determined that the NO may activate the IRP1 RNA binding through both a direct effect on the [4Fe–4S] cluster and by mobilizing iron from intracellular iron stores. This results in iron depletion, which indirectly leads to increased IRP1 binding (Wardrop *et al.,* 2000). Recently Oliveira and Drapier (2000) showed that the expression of IRP1 is also affected by NO. In fact IRP1 expression was decreased by approximately 40% 16 h after activation by interferon (IFN)-γ and lipopolysaccharide, which also induce the IRP1 mRNA binding activity through nitric oxide. The decrease in IRP1 protein levels directly correlates to the amount of NO produced. It is interesting that the gain of mRNA binding activity of IRP1 and the decrease in IRP1 protein expression both occur after NO exposure. A resolution to this apparent dichotomy is that a controlled decrease in IRP1 synthesis (about 60% reduction) should occur to compensate for the broad effects of a general increase in IRP1 mRNA binding that is triggered by NO (Oliveira and Drapier, 2000). Finally, oxidative stress in the form of H_2O_2 leads to a very rapid (<60 min) increase in IRP1 binding activity (Pantopoulos and Hentze, 1998).

Similar to IRP1, IRP2 is also found in many species from insects to mammals. (Guo *et al.,* 1994; Henderson *et al.,* 1993). The ratios of IRP1:IRP2 in cells seems

to be tissue specific with levels of IRP1 > IRP2 in liver, kidney, intestine, and brain, while IRP2 > IRP1 in pituitary and the Ba/F3 pro-B lymphocyte cell line (Schalinske *et al.,* 1997). This suggests that both IRPs play an important role in the regulation of iron proteins. No experimental evidence yet supports the existence of an iron–sulfur cluster in IRP2, and the protein also lacks aconitase activity (Phillips *et al.,* 1996). Also unlike IRP1, increases in IRP2 binding activity and IRP2 protein level in response to low iron levels requires protein synthesis (Henderson and Kuhn, 1995). High iron levels lead to increased degradation of the IRP2 protein, although no change is observed in the levels of IRP2 mRNA or protein biosynthesis. This degradation effect is also dependent on *de novo* protein synthesis, indicating that a specific protein is probably involved in the proteolysis of IRP2 in response to increased iron levels (Guo *et al.,* 1995).

IRP2 seems to be upregulated by PKC-activated phosphorylation in a manner similar to that described for IRP1, although the putative phosphorylation sites for the two proteins are not identical (Schalinske and Eisenstein, 1996; Schalinske *et al.,* 1997). There may be cell-specific increases in binding activity due to NO for IRP2; however, this effect is controversial (Pantopoulos *et al.,* 1996; Phillips *et al.,* 1996). Kim and Ponka describe a rapid decrease in IRP2 binding to mRNA and an associated decrease in TfR mRNA levels after treatment of a murine macrophage cell line with NO^+, a nitrosonium ion that causes *S*-nitrosylation of thiol groups (1999). As well, these authors demonstrated that treatment with lipopolysaccharide (LPS) and IFN-γ leads to decreases in both mRNA binding by IRP2 and protein levels of IRP2, and this effect was not observed if an inhibitor of nitric oxide synthase was utilized (Kim and Ponka, 2000). This decrease in IRP2 activity leads both to a decrease in TfR mRNA levels and to an increase in ferritin synthesis. Finally, unlike IRP1, H_2O_2 does not seem to have any affect on binding affinity of IRP2 (Hentze and Kuhn, 1996; Kuhn, 1998).

In a study by Smith and associates of the IRP distribution in the brains of Alzheimer's disease (AD) patients, it was demonstrated that IRP2 shows a markedly different distribution than seen in normal brains, while IRP1 distribution is unaffected (1998). IRP2 is present in senile plaques and neurofibrillary tangles of AD brains. This suggests that IRP2 may be somehow involved in the impaired brain iron homeostasis observed in AD or is affected by the pathology of AD (Smith *et al.,* 1998).

III. Duodenal Iron Absorption

The recent cloning of an iron exporter protein (iron-regulated transporter-1 (IREG1), also known as ferroportin and MTP1) and a ferric reductase from the duodenum membrane has increased our understanding of iron egress from intestinal villus cells (McKie *et al.,* 2000; Donovan *et al.,* 2000; Abboud and Haile,

2000; Lee *et al.,* 2000). Absorbing iron from dietary sources is the responsibility of duodenal villus cells. However, the ability of the villus cells to absorb dietary iron seems to be predetermined at the time they are developing crypt cells (Conrad and Crosby, 1963). The present theory is that the transferrin (Tf)/TfR/HFE complex senses the iron content of blood plasma and conveys the information to the intestinal crypt cell. In turn the level of iron inside the crypt cell dictates the expression level of divalent metal transporter-1 (DMT-1) and IREG1 as the crypt cell matures into an absorptive villus cell. Dietary iron in the form of Fe^{3+} is believed to be first reduced to Fe^{2+} by the NADH-ferric reductase on the plasma membrane before being transported across the membrane by DMT-1. Once inside the villus cell, the iron can either be sequestered by ferritin or exported into the blood plasma.

The transfer of Fe^{2+} into the plasma is thought to be mediated by IREG1 and hephaestin at the basal lateral side of the villus cell. It has been shown that IREG1 is able to facilitate the egress of ferrous iron in the presence of soluble ceruloplasmin (Cp), which requires ferroxidase activity (McKie *et al.,* 2000). The current understanding is that Fe^{2+} is exported by IREG1 to the plasma and hephaestin oxidizes Fe^{2+} to Fe^{3+}, which is then incorporated into Tf in plasma. In the absence of hephaestin, iron egress is impaired, as seen in the sex-linked anemic (*sla*) mouse (Vulpe *et al.,* 1999). However, there is still a gap in our understanding of iron egress. For example, it seems implausible that iron can exist freely inside the cell. Is there a chaperone molecule involved in shuttling iron to the iron exporter or ferritin once it is transported across the apical surface? Recent studies with the Caco-2 cell line (an intestinal model) suggest that apo-Tf may play a role in iron export (Alvarez-Hernandez *et al.,* 2000). Using confocal laser microscopy, the authors were able to show that apo-Tf and holo-Tf are transported to different compartments within the cell. Apo-Tf is endocytosed and then sorted to the apical face of the cell, which allows it to interact with the newly absorbed iron and exocytose at the basal lateral surface. Other proteins such as paraferritin, which is a proposed 520-kDa complex containing integrin, mobilferrin, and flavin monooxygenase, has also been implicated as the missing chaperone (Umbreit *et al.,* 1996). The major proteins involved in iron transport into and out of the intestinal cells are discussed in detail in this section, and listed in Table I.

A. Divalent Metal Transporter 1

Using two different cloning approaches, a gene related to the natural resistance-associated macrophage protein (Nramp1) was identified in microcytic anemia (*mk*) mice and *Belgrade* (*b*) rats (Gunshin *et al.,* 1997; Fleming *et al.,* 1997, 1998). The gene identified was *DMT-1*, also known as *Nramp2* and *DCT-1*. It consists of 561 amino acids with 12 membrane-spanning domains. Voltage-clamp analysis showed that DMT-1 is a membrane potential-dependent metal ion transporter with a broad

TABLE I

Proteins Involved in Iron Metabolism

Protein	Function
IRP1, IRP2	Regulates the expression level of various proteins containing iron-responsive elements.
DMT-1	Takes up ferrous iron and other metals in the duodenum and facilitates iron exit from endosomes.
IREG1	Responsible for iron egress from the intestinal villus cell to the plasma.
Hephaestin	Ferroxidase required for oxidizing ferrous iron to ferric iron during iron egress from cells.
Transferrin	Binds iron and transports it through blood until binding transferrin receptor and delivering iron to cell.
Ceruloplasmin	Ferroxidase which converts ferrous to ferric iron.
Transferrin receptor	Plasma membrane receptor for transferrin, responsible for the uptake of holo-transferrin into the cell.
HFE	Moderates iron uptake by transferrin receptor.
Transferrin receptor 2	Uncertain, may be involved in binding of holo-transferrin and uptake of iron.
SFT	May be involved in regulation of iron uptake by transferrin and nontransferrin pathways.
Frataxin	May be involved in regulation of iron homeostasis in the mitochondria.
ABC7	Involved in iron homeostasis in mitochondria.
Ferritin	Cellular iron storage protein.

substrate range. Transported ions include not only Fe^{2+} but also Zn^{2+}, Mn^{2+}, Co^{2+}, Cd^{2+}, Cu^{2+}, Ni^{2+}, and Pb^{2+}. DMT-1 has a relatively ubiquitous expression pattern with high levels of expression in the intestine, brain, thymus, proximal kidney, and bone marrow (Gunshin *et al.,* 1997; Gruenheid *et al.,* 1995). In addition to the plasma membrane expression, DMT-1 has also been shown to localize to recycling endosomes (Gruenheid *et al.,* 1999), late endosomes, and lysosomes by immunofluorescence microscopy (Tabuchi *et al.,* 2000). It is therefore possible that DMT-1 plays an important role in the export from endosomes of iron acquired through the Tf and TfR pathway.

There are at least two different splice forms of DMT-1 in mouse, rat, and human that may be the result of alternative use of polyadenylation signal exons (Gruenheid *et al.,* 1995; Gunshin *et al.,* 1997; Kishi and Tabuchi, 1997; Lee *et al.,* 1998). One form contains an IRE in the 3′ UTR region (DMT-1 (IRE)) and the other form lacks an IRE (DMT-1 (non-IRE)). The presence of the IRE indicates that the expression level of DMT-1 in the duodenal cells is regulated posttranscriptionally by the

level of iron in the cells (reflecting the amounts in the bloodstream). Rats fed an iron-deficient diet show a marked increase in the level of DMT-1 transcripts by Northern blot analysis (Gunshin *et al.,* 1997). It is likely that the IRE in the 3′ UTR of DMT-1 functions just like the one in TfR, through stabilizing the transcript with the binding of IRP and thereby increasing protein expression levels. Another regulation mechanism could be transcriptional in response to metal levels as there are several metal response elements in the putative promoter of human DMT-1. This form of transcriptional regulation remains to be demonstrated experimentally (Lee *et al.,* 1998).

Since DMT-1 seems to be the major gateway for intestinal iron absorption, one might predict that in the case of HH additional mutations that result in a nonfunctional DMT-1 gene would reduce the iron overload phenotype. Indeed, Fleming and associates (1999) were able to show that in HFE knock-out mice carrying a mutation in DMT-1, hepatic iron accumulation is much reduced. In light of this, it may be possible to devise a treatment to downregulate the expression level of DMT-1 and thus modulate the level of iron absorption in patients with HH. The role of DMT-1 in iron acquisition in the brain has recently been investigated. This is of interest because oxidative stress due to abnormally high levels of iron and other metals has been demonstrated in neurodegenerative disorders such as Parkinson's disease, Alzheimer's disease, and multiple sclerosis (Huang *et al.,* 2000; Yantiri and Andersen, 1999; Rocha *et al.,* 2000; Kienzl *et al.,* 1999). In the developing rat brain, DMT-1 mRNA was found in the striatum, cortex, hippocampus, and cerebellum. The cell types that express DMT-1 in the brain include Purkinjc and granule cells in the cerebellum. In cultured astrocytes, Northern blot analysis was able to detect the presence of DMT-1 mRNA (Williams *et al.,* 2000). Whether DMT-1 plays a role in the pathogenesis of these neurodegenerative diseases remains to be investigated.

The homolog of DMT-1, Nramp1, which was the first to be identified by positional cloning from the *Bcg/Ity/Lsh* (*mycobacteria-*, *salmonella-*, and *leishmania-*) is thought to regulate macrophage activation for antimicrobial activity against intracellular pathogens (Vidal *et al.,* 1993). Unlike DMT-1, the expression of Nramp1 is limited to the endosomal and phagosomal compartments of cell lineages of macrophage/monocyte and B- and T-lymphocytes (Vidal *et al.,* 1993; Kishi *et al.,* 1996). A single mutation of G169D in Nramp1 has been known to confer susceptibility in mice to infection by *Mycobacterium avium* (Govoni *et al.,* 1996; Hackam *et al.,* 1998). It is suggested that the mechanism of conferring resistance to microbial infection by Nramp1 is to import iron into the endosome/phagosome compartments of the cell and to stimulate the formation of reactive oxygen species (Pierre and Fontecave, 1999). Barton and associates have been able to show that Nramp1 expression supports increased acute cytoplasmic influx of iron, detected using the fluorescent iron sensor dye calcein (Barton *et al.,* 1999). Recently, Lafuse *et al.* have shown that RAW 264.7 macrophage transfected with Nramp1 was able to import more than twice the amount of iron into phagosomes compared to the RAW 264.7 transfected with mutated Nramp1 (2000). It is interesting to note that

despite the 64% amino acid sequence identity of Nramp1 and DMT-1, Nramp1 functions to import iron into vesicles such as endosomes and lysosomes where as DMT-1 facilitates the export of iron from endocytic vesicles.

B. IREG1/Ferroportin

The quest for an iron exporter on the basal lateral surface of the intestine and placenta has been troublesome. Various proteins such as paraferritin (Umbreit *et al.,* 1998), SFT (Gutierrez *et al.,* 1997) and apo-Tf (Alvarez-Hernandez *et al.,* 2000; Alvarez-Hernandez *et al.,* 1998) were thought to be likely candidates. Recently, a protein thought to be involved in this process was identified. Using positional cloning, Donovan and associates were able to isolate a gene responsible for the hypochromic anemia of zebrafish mutant "*weissherrbst*" (2000). This gene, named ferroportin-1 (*fpn1*), encodes a 10-transmembrane-domain protein. In zebrafish, fpn1 mRNA is detected at the yolk syncytial layer 18 to 48 h postfertilization. The fact that this expression is on the basal lateral side over which the blood flows suggests that ferroportin is likely to provide the iron from the yolk to the embryonic circulation for blood cell formation. Northern blot analysis has shown that fpn1 is expressed in human placenta, liver, spleen, kidney as well as mouse duodenum and large intestine. In human placenta, the expression of ferroportin on the basal side of the syncytiotrophoblasts suggests a role in iron transport from mother to embryo. McKie and associates (2000) were able to isolate the same gene from human and mouse duodenal cDNAs using subtractive cloning on homozygous hypotransferrinemic mice (*hpx/hpx*).

The protein, which was termed IREG1 is able to stimulate iron efflux in the presence of soluble Cp following expression of both proteins in *Xenopus* oocytes. The authors were also able to show an increase in duodenal IREG1 mRNA in mice fed an iron-deficient diet for 4 weeks compared to mice fed an iron-replete diet. Regulation of IREG1 expression by the IRE/IRP complex is not completely understood yet. There is an IRE in the 5′ UTR region of the IREG1 mRNA, as is also the case with ferritin, aconitase, and eALAS (Aziz and Munro, 1987; Dandekar *et al.,* 1991; Zheng *et al.,* 1992). In the condition of iron deficiency, the increased binding of IRP to the 5′ IRE blocks translation of these mRNAs. In contrast, IREG1 mRNA and protein levels seem to increase under these conditions, a response similar to the regulation of TfR through the 3′ IREs. The precise mechanism of 5′ IRE regulation of IREG1 mRNA by IRP needs to be examined further.

C. Hephaestin

Hephaestin represents a bridge that links iron metabolism with copper metabolism. It has been known for some time that the *sla* mouse has a block in intestinal

iron transport that results in moderate to severe microcytic hypochromic anemia (Grewal, 1962). Recently the gene responsible for this disorder, hephaestin, was identified (Vulpe *et al.,* 1999). Mouse hephaestin has a 50% protein identity to mouse Cp at the amino-acid level. All three different types of copper-binding sites in Cp are conserved in hephaestin, as are the cysteine residues which form the disulfide bridges. In contrast to Cp, which has both a glycosylphosphatidylinositol (GPI)-anchored form and a soluble form, hephaestin is only present as a trans-membrane type I protein (Vulpe *et al.,* 1999). Northern blot analysis demonstrates that hephaestin is expressed in the intestine, colon, lung, and kidney. Little or no transcript was detected in the liver, where Cp is highly expressed (Klomp and Gitlin, 1996). *In situ* hybridization of cross sections of the proximal small intestine show that hephaestin is expressed mainly in the villi, consistent with the location of iron absorption.

The high level of homology between Cp and hephaestin indicates that hephaestin likely plays a significant role in iron release from the cell. Examination of *sla* mice crossed with *hfe*−/− mice (which usually suffer from HH) provides evidence for this contention. In *hfe*−/− *sla* mice, there is a significant decrease in hepatic iron overload (Levy *et al.,* 2000). This effect could be due to a decrease in the transfer of iron from villi cells to plasma. Two groups proposed that hephaestin is required to facilitate the binding of iron to serum apo-Tf by oxidizing ferrous iron to ferric iron once IREG1 transports the iron across the basal lateral surface of the intestinal villi cell (McKie *et al.,* 2000; Donovan *et al.,* 2000). Interestingly, there is a similar iron uptake system in yeast involving Fet3 and Ftr1 (Askwith *et al.,* 1994; Stearman *et al.,* 1996). Fet3 is a plasma membrane multicopper oxidase with homology to Cp and extracellular ferroxidase activity. Ftr1 is a ferric (Fe^{3+}) iron transporter. Fet3 functions to convert ferrous (Fe^{2+}) iron to ferric iron, which is then transported into the cell through Ftr1 (De Silva *et al.,* 1995). However, unlike with hephaestin and IREG1, the Fet3/Ftr1 system in yeast actually functions to import iron rather than export it from the cell. Although hepaestin and Cp have high sequence homology and similar functional activity, the difference in tissue expression suggests that they perform distinct functions. The iron transporter associated with hephaestin, IREG1, has been identified, while the iron transporter associated with Cp has yet to be discovered. Figure 3 (see color insert) outines the proposed model for intestinal iron absorption.

D. Heme Absorption

Heme is an important source of dietary iron. Hemoglobin and myoglobin-derived iron are known to be absorbed more efficiently by the intestine than inorganic iron as the presence of amino acids from proteolytic digestion helps to prevent polymerization and precipitation of heme (Raffin *et al.,* 1974; (Turnbull *et al.,* 1989; Majuri and Grasbeck, 1987). There is evidence to suggest the presence of a

heme receptor on the luminal side of villus cells that brings iron into the intestinal cell, largely in the metalloporphyrin form (Grasbeck *et al.,* 1982). Once heme is inside the cell, iron is released via heme oxygenase 1 (HO1), which cleaves the heme ring to generate bilirubin, carbon monoxide, and ferrous iron (Maines, 1997). In mice deficient in HO1, tissue iron stores are high while serum iron is low, suggesting that the enzyme is involved in discharge of iron from certain cells (Poss and Tonegawa, 1997a, b). The method by which the iron liberated from heme is subsequently routed for use systemically is not fully understood.

Recently, a mammalian iron ATPase associated with the microsomal membrane and codistributed in tissues with HO1 was identified (Baranano *et al.,* 2000). There is some evidence to suggest that HO1 is functionally coupled to the Fe-ATPase (Poss and Tonegawa, 1997a; Ferris *et al.,* 1999). This novel Fe-ATPase is enriched in spleen, and the iron transport it mediates is dependent upon hydrolyzable nucleotide triphosphate, magnesium, time, and temperature. Barañano and associates suggest a model in which Fe-ATPase and HO1 colocalize to the endoplasmic reticulum (ER) where heme is first degraded by HO1 and the freed iron is transported by the Fe-ATPase to the luminal side of the ER (2000). They propose that the iron in the ER can then bind to Tf and subsequently be recycled back to the cell surface for exocytosis.

IV. Iron Proteins in Circulation

Iron is not found circulating freely in the serum because it has the potential to catalyze the formation of free radicals (McCord, 1998). Therefore iron is sequestered by amino acids, small chelators such as citrate, and other plasma proteins such as Tf and albumin. In iron-overload conditions such as HH and transfusion siderosis, the toxicity of excess iron present in the serum results in serious damage to most organs of the body. A number of different proteins play key roles in circulating iron in plasma for efficient delivery to those cells where it is required.

A. Transferrin

Human serum Tf was first identified by Schade and Caroline (1946) from the non-hemoglobin fraction of blood plasma. The primary structure of the protein revealed two highly homologous halves with 40% sequence homology, which are bridged by a connecting peptide. There are two N-linked sites of glycosylation through two asparagine residues in the C-terminal lobe. The crystal structure of rabbit serum Tf shows that the protein has 13 disulfide bridges, six of which are conserved in homologous positions in each lobe (Bailey *et al.,* 1988). The presence of six bilobally conserved disulfide bridges led to the proposal that the present day transferrins

arose from an ancient gene duplication event. The presence of greater homology between the two lobes of the same protein then between various orthologs of Tf suggests that the gene duplication event happened before species divergence.

Crystallographic studies of rabbit serum Tf have revealed that the ferric ion is coordinated by the carboxylate oxygen of D63, two phenolate oxygens from Y95 and Y188 and the imidazole nitrogen of H249. T120, R124, and S125 provide the hydrogen bonding network to the synergistic carbonate anion (Bailey *et al.,* 1988). A "Venus flytrap" mechanism of iron binding was proposed by Anderson *et al.* (1990) whereby the open lobe structure of Tf closes tightly when the ferric ion and its synergistic anion bind to the binding site. Kinetic studies show that anion binding as the first step in this process is most favorable for the purposes of neutralizing charges around the binding site and completing the octahedral coordination required for iron binding. After the anion is bound, Fe^{3+}, along with its chelator, binds to the anion, as well as Y95 and Y188. The chelator is then displaced and D63 and H249 complete the coordination.

The mechanism of iron release from holo-Tf has triggered a great deal of curiosity because of its extremely high-affinity iron binding. In order to be an effective iron delivery vehicle for cellular metabolism, there has to be a mechanism that allows for rapid release of the iron from the Tf/TfR complex within the cell. Iron release *in vitro* from diferric Tf appears to be a complex mechanism. This may be due to the active role that the TfR plays in aiding iron release *in vivo* (Bali and Aisen, 1992). To date, studies in this area have used either single-lobe Tf or monoferric Tf. In general, iron release is thought to be more facile from the N-lobe. A dilysine "trigger" mechanism was proposed for iron release in the N-lobe, whereby the protonation of Lys 206 and Lys 296 results in electrostatic repulsion in the two domains that make up the iron binding pocket and hence cause release of the iron ligand (Dewan *et al.,* 1993). However, the dilysine motif is missing from lactoferrin (Lf) and the C-lobe of Tf. Hence the mechanism of release from Tf is still a puzzle. In addition, mutation of the iron ligand His 249 to Glu in the N-lobe of human Tf abolishes the dilysine trigger but does not significantly affect iron release (MacGillivray *et al.,* 2000). Comparison of the two different conformations of the recombinant N-Lobe of the human Tf crystal structure revealed that the protonation of the carbonate anion and the resulting partial removal of the anion from Arg 124 may be the initial step in pH-induced release of iron from Tf (MacGillivray *et al.,* 1998). Our understanding of release of iron from Tf will not be complete until iron release from the Tf/TfR complex is directly examined.

The Tf gene is on the long arm of chromosome 3, at $3q21–q25$, very near the gene for the TfR (Rabin *et al.,* 1985). Transferrin synthesis occurs primarily in the liver and the protein is secreted into plasma for delivery to other tissues. In the kidney, spleen, lung, heart, and muscle of mice, mRNA levels of Tf increase until just before birth, and then drop to a very low level that is maintained as an adult (Kahn *et al.,* 1987). In brain and testis, levels of Tf mRNA are low throughout fetal development and increase after birth, finally remaining steady at

a level about 10% of that seen in the adult liver (Kahn *et al.,* 1987). Transferrin is found mainly in oligodendrocytes in the brain (Connor and Benkovic, 1992; Bloch *et al.,* 1985). It is also found in myelinating Schwann cells in the peripheral nervous system (Connor and Benkovic, 1992). Transferrin expression is controlled by both positive and negative regulatory elements found 5′ of the transcription start site, although no IRE exists in the mRNA of this molecule.

Transcriptional regulation involves four elements: a tissue-specific promoter, a distal promoter, a negative acting region and an enhancer element (Schaeffer *et al.,* 1989). The tissue-specific promoter, located at −125 to −45 includes two regions, termed proximal regions I and II (PRI and PRII). Transcriptional activators bind to these elements, specifically HNF-4 to PRI (Sladek *et al.,* 1990) and C/EBPα to PRII (Petropoulos *et al.,* 1991). For full activity of the promoter, both PRI and PRII must be intact (Schaeffer *et al.,* 1989). The enhancer element of the Tf gene contains two domains, termed A and B. Transcriptional activators bind to A, while B blocks the activity of the negative element downstream. Domain B has four protein-binding sites, which at least three liver proteins interact with, including the NF1 factor (which binds to two sites) (Jones *et al.,* 1987), AP4 (Hu *et al.,* 1990), and a third as yet unidentified factor. Rolfs and associates have shown that the Tf enhancer contains two HIF-1 binding sites, which allow Tf expression to be regulated by oxygen (1997). In Sertoli cells, which show lower Tf expression than the liver, the enhancer is not active and the transcriptional factors that interact with the promoter are different than in liver cells (Zakin, 1992; Guillou *et al.,* 1991). Fischbach and associates demonstrated through deletion studies that the region >0.6 kb upstream of the transcription start site of the Tf gene also contains negative elements that are active in cells that do not produce Tf (1990). In the central nervous system, production and secretion of Tf seems to be regulated by hormones and neurotransmitters such as serotonin (Tsutsumi *et al.,* 1989).

Disruption of the Tf gene results in a rare form of iron deficiency anemia called atransferrinemia. Only 8 cases of hereditary atransferrinemia have been reported (Beutler *et al.,* 2000). In one case, the disease was a result of two separate mutations in the Tf gene (Beutler *et al.,* 2000). It is an autosomal recessive disorder in which the patient has an almost total lack of serum Tf and it is manifested by a maldistribution of iron in the liver, heart, pancreas, thyroid, and kidney (Hayashi *et al.,* 1993; Hamill *et al.,* 1991). Presumably, dietary iron is able to enter these parenchymal tissues through a Tf-independent pathway (de Silva *et al.,* 1996). The Tf independent pathway is, however, unable to provide the necessary iron for erythropoiesis and hence the deficiency is fatal if transfusions of Tf are not provided. An important characteristic of this anemia is that the patients do not respond to oral iron therapy but instead to Tf infusion. A mouse model of atransferrinemia has been studied extensively. The mice show very low (less then 1%) plasma levels of transferrin, have iron deposits in the liver and other organs, and can be treated with injections of Tf (Bernstein, 1987). In the mouse the disease is a result of a defect in Tf mRNA processing that causes the majority of the transcript to remain

in the 5-kb precursor form, rather than maturing to the 2.5-kb functional form seen in normal mice (Huggenvik *et al.,* 1989).

B. Melanotransferrin

Melanotransferrin (MTf) is a 97-kDa protein which shares a 40% sequence identity with human Lf (Rose *et al.,* 1986). It was first identified as a cell surface marker for human skin cancer (Woodbury *et al.,* 1980, 1981; Brown *et al.,* 1981). However, the protein was subsequently found expressed at various levels on other tissues such as the liver, intestine, umbilical cord, placenta, sweat gland, and more recently on human brain endothelium (Sciot *et al.,* 1989; Rothenberger *et al.,* 1996; Barresi and Tuccari, 1994). Unlike the other members of the transferrin family, MTf has two different forms. It can be found as a membrane protein attached to the cell surface via a GPI anchor or as a soluble form in serum and cerebrospinal fluid (Alemany *et al.,* 1993; Food *et al.,* 1994; Brown *et al.,* 1981; Kennard *et al.,* 1996). Metal binding studies on a cell line transfected with human MTf show the iron uptake process is both temperature-dependent and saturable (Kennard *et al.,* 1995).

Like other members of the transferrin family, MTf is a bilobed metal-binding protein. Sequence alignment of MTf and members of the transferrin family shows that the amino acids involved in coordinating the iron atom of the N-terminal lobe are totally conserved (Rose *et al.,* 1986). However, there is a D395S change in the C-terminal lobe which could affect iron binding. In the crystal structure of bovine Lf that has a D60S change in the N-terminal lobe, a water molecule was able to fill the iron coordination site and participate in interdomain hydrogen bonding. The binding of iron to the modified pocket in this situation may have been weakened (Faber *et al.,* 1996). Baker and associates have shown that MTf has only one functional iron binding site, but recent data suggest that under certain conditions, both lobes can bind iron (1992; Tiong and Jefferies, 2001). Similar to Tf, MTf is able to bind to other metals in addition to iron. Using a competitive metal binding assay, it has been demonstrated that metals such as aluminum, copper, and zinc are able to compete for the iron-binding site in MTf (Tiong and Jefferies, 2001).

In contrast to the TfR and ferritin, where the level of protein expression is regulated by the level of iron through the IRE/IRP system, there is no identifiable IRE motif in MTf and level of expression is not regulated by iron (Richardson, 2000). However, a regulatory element is located 2 kb upstream from the promoter region of the gene. Deletion of this element severely impairs the expression of MTf (Duchange *et al.,* 1992). This regulatory element was shown to be part of an enhancer composed of two binding sites for AP-1 transcription factor. AP-1 is a transcription factor that is upregulated after ultraviolet irradiation, a suspected risk factor in melanoma (Devary *et al.,* 1991), (Derijard *et al.,* 1994). AP-1 is formed by the dimerization of the Jun and Fos proteins through their leucine-zipper domains. The transcription factor recognizes the phorbol 12-myristate 13-acetate-responsive element (Angel and Karin, 1991; Sassone-Corsi, 1994). Gel retardation

assay shows that the expression of MTf correlates with increased AP-1-binding activity (Roze-Heusse *et al.,* 1996). A secondary unidentified nuclear factor is involved with AP-1 to form a ternary complex at the two AP-1 sites in the MTf enhancer region (Roze-Heusse *et al.,* 1996). This may explain how MTf is upregulated in melanoma cells.

Many pieces of evidence point to a role for MTf in iron transport to the brain. It has long been believed that the Tf/TfR system is exclusively responsible for iron delivery to the brain, but recent studies suggest this may not be the case. For example, hypotransferrinemic mice, deficient in Tf, have normal brain iron levels (Dickinson and Connor, 1995). Examination of the distribution of MTf and TfR through immunohistochemistry shows protein expression limited to the capillary endothelium in the human brain, whereas Tf itself is mainly localized to glial cells (Rothenberger *et al.,* 1996). Some evidence suggests that soluble MTf can bind to the TfR; thus the colocalization on capillary endothelium may indicate a system of iron uptake via the TfR and MTf. Expression of MTf has been examined in brains from AD patients as well as brains from patients suffering from other neurological diseases. While immunohistochemical staining of MTf in normal brains shows distribution limited to the blood–brain barrier, MTf in AD is also found to be highly expressed in a subset of reactive microglia cells associated with β-amyloid-positive senile plaques, but not other microglia distal from plaques (Jefferies *et al.,* 1996). This was further confirmed by *in situ* hybridization of MTf mRNA, which shows that MTf is expressed in the reactive microglia cells in the AD brain but not in normal brain or nonreactive microglia in AD brains (Yamada *et al.,* 1999). Soluble MTf was also found to be elevated in the CSF and serum of patients with AD compared with healthy controls (Kennard *et al.,* 1996; Moroo, 1999; Kim, 2001). Metals such as iron and zinc which bind to MTf have been shown to be able to nucleate the formation of insoluble β-amyloid from soluble amyloid (Bush *et al.,* 1994). The soluble form of MTf can cross the blood–brain barrier (BBB) and deliver iron across the BBB more efficiently than Tf, if both are injected into the tail vein of the mouse (Moroo *et al.,* 2001). These results may be an indication that MTf functions in shuttling iron across the BBB from the blood to the neutropil, transporting the iron needed for normal brain function. How MTf is regulated in reactive microglia and how its function in metal transcytosis interplays with its elevation in bodily fluids of AD patients is of current interest.

C. Ceruloplasmin

Ceruloplasmin (Cp) is a copper-containing ferroxidase that is found in plasma and is secreted by hepatocytes. The multicopper oxidase can hold up to six atoms of copper, and it binds nearly all the copper present in plasma. It appears to play an important role in iron transport as well as copper transport (Gitlin, 1998). The exact role of Cp is still not understood, although studies in yeast have identified a species ortholog multicopper oxidase protein in the yeast system that is required for

high-affinity iron uptake (de Silva *et al.,* 1997). In mammals there is evidence that Cp has a role as a serum ferroxidase that is required to oxidize iron for subsequent incorporation into Tf and to transport iron out of tissues (Osaki and Johnson, 1969; Roeser *et al.,* 1970).

In one study Cp increased the rate of non-Tf bound iron uptake two- to three-fold in iron-deficient K562 cells, and this effect requires transcription (Attieh *et al.,* 1999). This induction of non-Tf bound iron uptake could be completely inhibited by the addition of excess trivalent cations, indicating a trivalent cation-specific transporter is involved in this phenomenon (Attieh *et al.,* 1999). The model proposed by Attieh and associates suggests that iron reduction by a surface ferrireductase followed by reoxidation carried out by Cp is important for this iron uptake pathway. Another interesting finding that may help shed light on the induction of Cp by iron deficiency is that the $5'$ UTR of the Cp gene has three pairs of consensus hypoxia-responsive elements (HRE) and the hypoxic-inducible factor-1 (HIF-1) element has been implicated in binding to these HREs (Mukhopadhyay *et al.,* 2000). The existence of HREs in Cp is consistent with the finding that iron deficiency leads to an increase in plasma levels of Cp.

The importance of Cp in human iron metabolism is illustrated in the iron over-load disease known as aceruloplasminanemia. This disease results from various mutations in the Cp gene. It manifests itself in middle age as diabetes mellitus and progressive neurodegeneration of retina and basal ganglia and subsequent de-mentia. An excess of tissue iron is found in the liver, pancreas, and brain (Morita *et al.,* 1995). *In situ* hybridization has demonstrated the presence of Cp in glial cells associated with brain microvasculature (specifically surrounding dopamin-ergic neurons in the substantia nigra and in the inner nuclear layer of the retina) (Klomp and Gitlin, 1996). This indicates that Cp may have a specialized role in iron metabolism and homeostasis within the central nervous system (Sheth and Brittenham, 2000). Very recently, the form of Cp in glia was shown to be an al-ternate splice form of Cp RNA in which 5 C-terminal amino acids of the secreted form are spliced out to be replaced by an additional 30 amino acids. This splicing leads to the generation of a GPI-linked form of Cp (Patel *et al.,* 2000). In brain, almost all the Cp transcript is in the GPI-linked form, and the soluble form of Cp does not appear to cross the BBB.

V. Proteins of Cellular Iron Uptake and Storage

A. Proteins of Iron Uptake into the Cell

Much is known about the major pathways of iron uptake into cells and iron storage within cells. The Tf/TfR mediated pathway of iron uptake is one of the most studied examples of receptor mediated endocytosis. Even so, new and vital players in this

pathway have recently been discovered, such as TfR 2 and HFE. Through the study of hemochromatosis patients it was recognized that these two proteins are very important for maintenance of proper iron levels in the body. Researchers have also long been aware of the existence of Tf-independent mechanisms of iron uptake. The fact that in cell lines in which the Tf/TfR uptake system is nonfunctional, iron uptake can still occur efficiently enough to allow normal cell growth points to the presence of an alternate iron uptake system in cells. SFT (stimulator of iron transport) is implicated as one participant in this pathway.

1. Transferrin Receptor

The TfR is a key gatekeeper that regulates iron uptake into cells. The TfR gene is found on chromosome $3q26.2–q$ter and consists of 19 exons (Evans and Kemp, 1997). The TfR is highly expressed on rapidly dividing cells including immature erythroid cells and placental tissue. Many nonproliferating cell types also express TfR, including hepatocytes, endothelial cells of the BBB, reticulocytes, and Sertoli cells (Kuhn *et al.,* 1990; Jefferies *et al.,* 1984).

The TfR is a type II membrane protein with a 61-residue N-terminal cytoplasmic domain, a 28-residue domain that crosses the membrane once, and a 671-amino-acid extracellular C-terminal domain. The TfR has three major domains called the apical domain, protease-like domain, and helical domain (Lawrence *et al.,* 1999) (Fig. 4). Electron cryomicroscopy studies have shown that the binding domain is separated from the membrane by a stalk of about 2.9 nm while the dimensions of the globular binding domains are approximately 6.4 nm high, 10.5 nm across the homodimer, and 7.5 nm deep (Fig. 4) (Fuchs *et al.,* 1998). The receptor undergoes both N- and O-linked glycosylation as well as phosphorylation. Recombinant receptors lacking glycosylation sites have a decreased Tf binding, while mutations that eliminate phosphorylation of the cytoplasmic serine residue do not seem to have any effect on receptor internalization efficiency (Williams and Enns, 1991; Rothenberger *et al.,* 1987). A tyrosine based internalization motif (20YTRF23) is present in the cytoplasmic portion of the protein, and through mutational studies has been demonstrated necessary for endocytosis of the receptor (Collawn *et al.,* 1993).

The TfR functions as a homodimer. Two disulfide bonds form between the cysteines at positions 89 and 98 (Fig. 4) (Jing and Trowbridge, 1987). Each of the two C-terminal lobes of one TfR homodimer can bind one Tf protein in a pH-dependent manner. The binding affinity of the TfR for Tf is dependent on the amount of iron bound to Tf: the highest affinity at physiological pH is seen with diferric Tf binding to the TfR and the lowest for apo-Tf (Young *et al.,* 1984). The residues involved in Tf binding to the TfR are not yet fully known, although Lawrence and associates (1999) have produced a model based on crystal structure analysis that proposes that Tf would interact with all three domains of the TfR (apical, protease-like, and helical) (Fig. 4). Mutational studies have shown that

pH-dependent binding is a key component in the Tf/TfR recycling pathway, as the TfR strongly binds Tf saturated with iron at the pH of serum ($K_d \sim 10^{-7}$ to 10^{-9} mol/liter). The complex is then internalized via receptor-mediated endocytosis in a clathrin coated pit and routed to the endosome, where the low pH allows Tf to release iron. In fact, iron is released from Tf at low pH faster and more efficiently when the Tf is complexed with the TfR then if Tf is unbound, demonstrating that interaction with the TfR enhances iron release (Bali *et al.,* 1991; Sipe and Murphy, 1991). The complex is then recycled back to the cell surface, where the apo-Tf is released and replaced once more by holo-Tf.

In order to study the physiological role of the TfR, Levy and associates have created a knock-out mouse lacking the TfR (1999). In this model, TfR$-/-$ mutants die by embryonic day 12.5, and from day E8.5 to E12.5 the embryos demonstrate growth retardation, pericardial effusions, and severe pallor, while histological analysis shows edema and diffuse necrosis throughout the tissues (Levy *et al.,* 1999). As late as E10.5, however, some TfR$-/-$ animals are indistinguishable from wild-type mice and do not show visible signs of anemia although they do not survive past day E12.5. Both the anemic and nonanemic TfR$-/-$ animals have defective erythropoiesis and abnormal development of the nervous system, with kinking of neural tubes. Levy and associates speculate that the reason the observed phenotype for the TfR knockout mice is more severe then that of the hypotransferrinemic mice (mice with little or no Tf) is that if Tf is missing from serum then unchelated iron is present in serum and available for use in cells via an alternate iron uptake system. In the TfR knockout mice, in contrast, the vast majority of iron is bound to serum Tf and therefore is not available because the receptor is not present to bring the Tf into cells. There is also evidence that the TfR may be involved in iron transport involving iron binding proteins other then Tf, such as MTf, especially within specialized barrier systems such as the BBB and Sertoli cells (Moroo *et al.,* 2001).

Regulation of TfR expression is complicated and occurs at both the transcriptional level and the posttranscriptional level. A region of 100 bp upstream of the transcriptional start site has been demonstrated to be involved in driving basal and serum/mitogenic stimulation of TfR promoter activity via an AP-1 like site (Owen and Kuhn, 1987; Miskimins *et al.,* 1986; Casey *et al.,* 1988). AP-1/CREB-like factors have been shown to bind to the AP-1-like site of the TfR (Beard *et al.,* 1991; Lok *et al.,* 1996). TRAC, which is a nuclear protein that copurifies with the Ku autoantigen, binds specifically to the transcriptional control element TRA of the *TfR* gene (located at nucleotides -77 to -70 and necessary for increased expression in proliferation) (Roberts *et al.,* 1994). Differentiating erythroid cells exhibit specific upregulation of *TfR* transcription linked to both the Ets-binding site and the AP-1 binding site in the 5′ flanking region of the transcription start site (Sieweke *et al.,* 1996). Very recently, Lok and Ponka have shown that a region (-118 to $+14$) of the *TfR* promoter is necessary for erythroid differentiation induced promoter activity, and that mutation of EBS or the AP-1/CRE-like motif inhibit this inducible

promoter activity (2000). Further, they found that CREB/ATF-like factors and Ets-like factors bind to the identified element. Lok and Ponka also describe an element in the promoter region of the *TfR* that is responsive to hypoxia. This region contains a binding site for hypoxia inducible factor 1 (HIF-1) and the motif organization is similar to that of many hypoxia-inducible genes such as erythropoietin and Cp (Lok and Ponka, 1999).

Posttranscriptional regulation of the *TfR* is mediated by the binding of IRPs to 5 IREs in the 3′ untranslated region of the TfR mRNA. When cellular iron levels are low, the IRPs can bind to the IREs, thus stabilizing the transcript and allowing more TfR to be translated (Mullner and Kuhn, 1988). This elegant system regulates many proteins involved in iron metabolism, allowing coordinated expression of proteins involved. Transferrin receptor is also detectable as a soluble protein in serum, and is measured clinically to help differentiate iron deficiency anemia and chronic disease anemia. Anemia of chronic disease is common in patients presenting with chronic inflammation and neoplasia, and is associated with normal iron stores but decreased serum iron. If a patient has iron-deficiency anemia, serum TfR levels are high, while levels are normal for patients with anemia of chronic disease. Serum TfR levels reflect the iron status of cells—thus levels are high in cases of iron deficiency or if there is a mass of immature erythroid cells.

2. HFE

HFE is a protein that seems to be important for regulation of iron absorption and uptake into cells. It was identified by Feder and associates in 1996 and maps approximately 4 megabases telomeric to HLA-A on chromosome 6 (Feder *et al.,* 1996). HFE is a major histocompatibility complex class I-like protein, and through analysis of the knock-out mouse phenotype has since been shown to be the gene responsible for the most common type of HH (Zhou *et al.,* 1998). Hereditary Hemochromatosis is a disease of iron overload, and is the most common auto-somal recessive disorder in persons of European descent. In screening studies, the prevalence of HH has been estimated at 1 in 200 to 1 in 400, with a carrier rate of 1 in 7 to 1 in 10 in Caucasian populations (Burke *et al.,* 1998; Goldwurm and Powell, 1997; Bulaj *et al.,* 1996; George *et al.,* 1998; Ramm *et al.,* 1997; Jazwinska and Powell, 1997; Crawford *et al.,* 1998). The disease is characterized by two- to threefold increase in dietary iron absorption that leads to iron deposi-tion in parenchymal cells of the liver, joints, pancreas, heart, skin, and pituitary gland. Prolonged iron deposition may lead to fibrosis and organ failure, frequently including hepatic cirrhosis, diabetes mellitus, cardiac dysfunction, arthritis, and hypogonadism (Adams and Chakrabarti, 1998; Burke *et al.,* 1998; Cullen *et al.,* 1997; Bacon *et al.,* 1999; Niederau *et al.,* 1985, 1996).

HFE was originally found expressed in the gastrointestinal tract and placenta (Parkkila *et al.,* 1997a,b). More recently it has been found in tissue macrophages and circulating monocytes and granulocytes (Parkkila *et al.,* 2000). In duodenum,

HFE is expressed primarily in crypt cells, and remarkably there is very little HFE expressed in villus enterocytes (Parkkila *et al.,* 1997b).

The HFE protein forms a heterodimer with beta 2 microglobulin (β_2m) and the two proteins form a cell surface complex with the TfR (Fig. 4). (Feder *et al.,* 1997; Waheed *et al.,* 1997; Parkkila *et al.,* 1997a; Lebron *et al.,* 1998). The wild-type HFE protein seems to have a significant effect on the uptake of Tf and Fe by the TfR endocytosis pathway. In experiments in which HFE is transfected into cells (thus overexpressed), HFE seems to decrease receptor-mediated Tf-bound iron uptake by about 50% (Ikuta *et al.,* 2000; Roy *et al.,* 1999). An increase in the dissociation constant from 1.9 to 4.3 nM is also observed, which indicates a decrease in the affinity of TfR for Tf (Ikuta *et al.,* 2000). It is not clear what the physiological significance of this decrease in affinity would be as the concentration of diferric Tf in blood is high enough to saturate all TfRs, even with HFE present (Ikuta *et al.,* 2000). The overexpression of HFE also seems to slow the rate at which the TfR complex recycles to the cell surface (in hepatoma cells), and this may lead to a decrease in iron uptake by the cell (Ikuta *et al.,* 2000). HuTu-80 cells (a polarized duodenal epithelial cell line) transfected with wild-type HFE show a markedly reduced level of ferritin compared to those transfected with the HH C282Y mutant (Ramalingam *et al.,* 2000). Further, Ramalingam and associates show that this reduction in ferritin levels requires HFE binding with high affinity to the TfR.

The majority of patients with HH are homozygous for a C282Y mutation in HFE (Feder *et al.,* 1996). This mutation has been shown to prevent β_2m from associating with the HFE protein, thus HFE is not expressed at the cell surface or associated with the TfR. The mutant form of the protein is localized intracellularly, and colocalizes with calnexin, indicating that the protein may be retained in the endoplasmic reticulum/Golgi due to improper folding (Ramalingam *et al.,* 2000). The mechanism by which this *HFE* mutation leads to deregulation of controls on iron absorption and thus a huge increase in dietary iron uptake is under debate. Presumably, HFE must play a significant role in the iron absorption pathway, possibly in the "programming" of crypt cells. *HFE*−/− mice show increased expression of duodenal DMT1. This observation lends support to the idea that *HFE* mutations in HH somehow lead to a decreased level of crypt cell iron. The crypt cell senses a decreased level of body iron and this prompts the cell, once it matures into a villus cell, to express increased levels of DMT1 leading to increased dietary iron absorption (Fleming *et al.,* 1999). If the crypt cell originally senses abundant iron then the level of DMT1 expressed by the mature villus cell will be low.

Levy and associates have recently completed a study of *HFE* mutant mice crossed with various mouse strains with mutations of iron uptake or metabolism (2000). One interesting mouse cross was between *HFE*−/−and β_2m−/−. As expected, the absence of β_2m leads to a more severe iron overload phenotype in the *HFE* knockout mice. This suggests that an unknown molecule may also interact with and be involved in the iron uptake pathway. Another possible explanation is that the compromising of the immune system that results from a β_2m−/−

itself leads to a more severe iron overload phenotype. The plethora of papers in which β_2m-deficient mice have been used to describe the tenants of T lymphocyte development and function have completely disregarded the possibility that β_2m is involved in mediating other functions besides those of the immune system. One wonders whether some of these studies require reinterpretation in light of the role of β_2m in HFE function.

HFE knockout mice bred to *mk* mice, which are characterized by a loss of function in DMT1, maintained the *mk* phenotype, resulting in extremely low iron stores. This indicates that iron uptake in HH is probably mediated through a pathway involving DMT1. Mice bred to possess a loss of function mutation in both *HFE* and hephaestin (a protein necessary for basolateral iron transport out of intestinal microvilli cells) also have decreased iron loading in the liver. However, this did not lead to a complete block in iron transfer from enterocytes. This work shows that the iron overload observed in HH due to an *HFE* mutation is mediated through the DMT1/Heph pathway. When *HFE* knockout mice are bred to *TfR+/−* mice, the animals have a more severe iron loading phenotype in hepatocytes than the *Hfe* mutants alone. Levy and associates have hypothesized that this apparent contradiction occurs because the *TfR+/−* mice have small erythrocytes with less hemoglobin than normal due to the decreased level of TfRs. This leads to an even greater increase in dietary iron absorption, possibly due to an erythroid signal to increase dietary iron absorption and compensate for the erythroid iron deficiency. Much work has yet to be done to discover what role HFE plays in iron absorption regulation, and to further illuminate the effect HFE has on the Tf/TfR pathway.

Some forms of hemochromatosis are not linked to mutations in HFE. One recently discovered mutation in TfR2 is present in a group of Italian patients who present with HH and is discussed below. Juvenile hemochromatosis, which manifests as severe iron loading in the first three decades of a patient's life has been mapped to chromosome lq, although not as yet to a specific gene (Roetto *et al.,* 1999). Another form of iron overload is seen in neonates and has yet to be mapped to any specific locus. This disease is characterized by liver failure due to excessive iron loading in hepatocytes, but it is not known whether this iron loading is the result of some underlying problem with the hepatocytes (Blisard and Bartow, 1986; Witzleben and Uri, 1989).

3. Transferrin Receptor 2

One recently discovered molecule has been termed transferrin receptor 2 (TfR2). The extracellular portion of this type II membrane protein shares 45% identity and 66% similarity with the TfR (Kawabata *et al.,* 1999). Two splice forms have been discovered: the α form has a transcript of approximately 2.9 kb, and a shorter (2.5 kb) β form lacks the amino terminal portion of the protein. This shorter transcript probably encodes an intracellular protein as both the transmembrane and signal sequences are missing. Transferrin receptor 2 has a putative

tyrosine-based internalization motif (YQRV) similar, although not identical, to that of the classical TfR (YTRF) (Kawabata *et al.,* 1999). As well, two cysteine residues are present (109 and 112) in approximately the same location as those of the TfR (89 and 98), which may allow the formation of disulfide bridges. This remains to be demonstrated experimentally.

The TfR2 α mRNA has been observed by northern analysis to be mainly expressed in the liver (Kawabata *et al.,* 1999) (author's observations); however, by RT-PCR small amounts of transcript can also be detected in spleen, muscle, prostate, human peripheral blood mononuclear cells, and a number of human cell lines. The β transcript appears to be much more widespread, with expression detected by RT-PCR in many different tissues and most cell lines tested. West and associates have shown that a recombinant TfR2 binds iron-loaded Tf with a 25-fold lower affinity than classical TfR and that HFE cannot be coimmunoprecipitated with TfR2 as it can with the TfR(2000).

Transferrin receptor 2 has been cloned in mice and shows 39% identity (53% similarity) to the classical mouse TfR (mTfR) (Fleming *et al.,* 2000). Murine TfR2 (mTfR2) shares 84% identity with its human ortholog. Fleming and associates also demonstrated that the 3' untranslated region of murine TfR2 is significantly shorter than that of TfR, and does not contain any regions similar to the consensus sequences of IREs. An examination of the hepatic expression of mTfR and mTfR2 supports this lack of iron regulation. A mouse model of HH shows downregulation of mTfR mRNA in HH mice, while no such downregulation occurs with mTfR2 (Fleming *et al.,* 2000). It was recently demonstrated that CHO cells transfected with TfR2 are resistant to the iron deprivation effects of desferroxamine (an iron chelator), which suggests that TfR2 has the ability to increase the cellular iron pool and support cell growth, much as TfR does (Kawabata *et al.,* 2000). It was speculated that perhaps TfR2 is a lower affinity form of the TfR and could in fact be a more primitive form, as TfR2 seems to be more closely related to the prostate-specific membrane antigen than TfR.

A form of HH has been linked to the TfR2 gene. Camaschella and associates (2000) found a C-to-G transversion in exon 6 of TfR2 (position 750 of the cDNA), which causes a truncation of the extracellular portion of the protein (a stop codon replaces a tyrosine at residue 250). It is unclear why this particular truncation, in which the Tf binding portion of the TfR2 protein is removed, should lead to an iron overload phenotype. African iron overload, an iron overload disorder that is similar to HH but does not map to HFE or any MHC locus will be interesting to reexamine in the light of the new TfR2 data. It has slightly different symptoms than HH, in that the pattern of iron deposition differs between the two diseases. Iron loading of Kupffer's cells and hepatocytes is observed in African iron overload, which mimics the phenotype of patients with transfusional siderosis and may indicate a defect in erythroid iron recycling (Andrews, 1999). Further characterization of the role of TfR2 in iron metabolism is needed. Perhaps a knockout of TfR2 will help to uncover why a seemingly nonfunctional truncation of the receptor should lead to such a severe iron overload phenotype.

4. SFT

Using functional expression cloning in *Xenopus* oocytes, another Tf-independent iron transporter called SFT (stimulator of Fe transport) was identified (Gutierrez *et al.,* 1997). SFT is an integral membrane protein of 338 amino acids. Fluorescence microscopy revealed that the protein is localized to the plasma membrane and endosomal domains. The expression of SFT in HeLa cells stimulates both Tf-dependent and Tf-independent Fe uptake (Gutierrez *et al.,* 1997). Sequence analysis shows that it contains the REXXE motif which is the same motif involved in Fe binding in ferritin (Gutierrez *et al.,* 1997). Kyte–Doolittle analysis revealed that SFT has at least six membrane spanning regions and the ability to form a dimer, suggesting a 12-membrane-spanning complex similar to DMT-1. However, unlike DMT-1 that transports iron along with other metals, SFT seems to transport Fe alone. The only exception is cadmium, which can inhibit Fe uptake by SFT. In addition, DMT-1 transports iron only in the Fe^{2+} form under conditions of acidic pH (pH < 6) (Gunshin *et al.,* 1997), whereas SFT stimulates either Fe^{2+} or Fe^{3+} uptake at physiological pH (Yu and Wessling-Resnick, 1998). Another interesting characteristic of this transport system is that ATP is required for Fe transport. Hence, it is possible that SFT belongs to the ATP-binding cassette (ABC) family, although it is missing the Walker motifs, which define this group of proteins (Gutierrez *et al.,* 1997). Iron uptake by SFT is also copper- and ferrireductase-dependent (Yu and Wessling-Resnick, 1998).

Despite all that is known about SFT, the exact mechanism of iron transport remains unknown. Interestingly, the expression of SFT seems to respond to cellular iron levels. When HeLa cells are depleted of iron by desferroxamine, the level of SFT transcript increases (Yu *et al.,* 1998). However, no IRE has been identified in the transcripts of SFT and therefore the modulation of SFT expression is likely to be independent of the IRP/IRE system. The level of expression of SFT in patients suffering from HH has been examined and the level of SFT was found to be elevated in the liver of these patients, perhaps contributing to the pathophysiology of the disease (Yu *et al.,* 1998).

B. Iron Metabolism in Mitochondria

Mitochondria, being the site of heme and iron–sulfur cluster synthesis is one of the organelles in the cell that requires tightly regulated iron transport. Recent discoveries in several diseases with mitochondrial pathology have allowed researchers to identify genes involved in iron homeostasis in the mitochondria. One of the genes involved in regulation of iron efflux in the mitochondria is frataxin (Campuzano *et al.,* 1996, 1997; Radisky *et al.,* 1999). In patients with an autosomal recessive neurodegenerative disorder called Friedreich's ataxia there is an intronic expansion of the GAA trinucleotides in the first intron of the frataxin gene and hence no functional protein is made (Gacy *et al.,* 1998). Studies on the yeast homolog of

frataxin (YFH) have provided great insight into the probable function of the protein. Deletion of *Yfh1* results in severe defects in mitochondrial respiration and loss of mitochondrial DNA. This may be a result of toxic oxidative stress associated with increased accumulation of iron in the mitochondria (Babcock *et al.,* 1997; Koutnikova *et al.,* 1997; Wilson and Roof, 1997; Delatycki *et al.,* 1999). Friedreich ataxia patients also suffer from severe cardiomyopathy in addition to symptoms of ataxia such as loss of muscular control and speech. This could be due to the fact that mitochondria are essential for ATP generation and when ATP production is disrupted by an imbalance of iron homeostasis, tissues such as skeletal and cardiac muscle which require high levels of ATP are severely affected (Lodi *et al.,* 1999).

Another gene associated with human mitochondrial iron homeostasis is the ABC7 gene which encodes an ABC transporter (Leighton and Schatz, 1995; Senbongi *et al.,* 1999; Kispal *et al.,* 1997). A mutation in the human *ABC7* gene has been shown to be responsible for X-linked sideroblastic anemia and ataxia (Allikmets *et al.,* 1999). This gene has a homolog in yeast called *ATM1* (Csere *et al.,* 1998). Previous studies have shown that Atm1p transports the precursor of the mitochondrial Fe/S cluster into the cytosol (Kispal *et al.,* 1999). Mutation in the yeast *ATM1* gene would therefore result in free iron accumulation in the mitochondria, which may result in oxidative damage (Senbongi *et al.,* 1999).

A human mitochondrial ABC protein designated MTABC3, which maps to chromosome 2*q*36, has recently been identified. It has 31% identity to Atm1p and was also shown to play an important role in mitochondrial iron homeostasis (Mitsuhashi *et al.,* 2000). In yeast with a mutation in the Atm1p protein, there is an increased accumulation of free iron in the mitochondria, mitochondria DNA damage, and respiratory dysfunction (Senbongi *et al.,* 1999). However, when the *ATM1* mutant was transformed with human *MTABC3,* iron accumulation was partially suppressed and mitochondrial DNA damage was completely reversed (Mitsuhashi *et al.,* 2000). Interestingly, a lethal neonatal metabolic disorder associated with iron metabolism has been mapped to the same region as *MTABC3* (between D2S164 and D2S163) (Fellman *et al.,* 1998; Visapaa *et al.,* 1998). It remains to be seen whether mutations in *MTABC3* are indeed the cause of this disorder.

C. Iron Storage in Ferritin

Iron storage and detoxification within cells are mediated through ferritin. Ferritin is a protein shell that can hold up to 4500 atoms of Fe^{3+} within its internal cavity (Ford *et al.,* 1984). It consists of two types of subunits: light (L) at 19 kDa and heavy (H) at 21 kDa (Drysdale, 1977). The ferritin structure has an internal diameter of 7–8 nm and an external diameter of 12–13 nm (Ford *et al.,* 1984). It is possible that the entry and exit of iron from the structure is accomplished through pores in the ferritin complex. Iron is stored within the protein shell in the ferric state

as ferric hydroxyphosphate (Harrison and Arosio, 1996). Each complete protein shell is composed of 24 subunits made of various proportions of L-type and H-type subunits. The specific ratio of H:L subunits allows ferritin the potential to store iron differentially in different tissues (Connor *et al.,* 1994). In recombinant ferritin studies, H-ferritin incorporates iron much more quickly then L-ferritin, perhaps due to the ferroxidase center that is associated with the H subunit (Santambrogio *et al.,* 1996). Further, the L subunit, but not the H, promotes iron core formation. If more H subunits are present in ferritin, the complex is more active in iron metabolism, whereas if more L subunits are present the ferritin is used for long-term iron storage (Harrison and Arosio, 1996). Recent studies on H ferritin knockout mice have shown that although the heterozygotes are healthy and phenotypically normal, the homozygotic knockout is lethal between embryo days 3.5 and 9.5 (Ferreira *et al.,* 2000). Studies of the overexpression of H-ferritin have demonstrated that H-homopolymers are functional, but the ferritin iron storage activity is greatly enhanced by the presence of the L subunit (Cozzi *et al.,* 2000).

Ferritin's presence in plasma as a soluble protein has been recognized for some time. The physiological role of the soluble form of this protein, however, is still unknown. Serum ferritin, in contrast to cellular ferritin, is glycosylated and therefore may be synthesized on the rough endoplasmic reticulum. An increase in the level of serum ferritin can be observed during changes in body iron stores, inflammatory responses, and cancer (Lipschitz *et al.,* 1974; Aungst, 1968). A receptor for serum ferritin has also been proposed, and a 1999 study of mouse brains indicated the existance of specific, saturable, and reversible binding in mouse brains that is characteristic of receptor binding (Hulet *et al.,* 1999). Further, a study of oligodendrocyte progenitor cells shows that ferritin binding is saturable and competitive, with a K_d of 5 nM. As well, uptake of ferritin can be inhibited by treatment with agents that block receptor-mediated endocytosis (Hulet *et al.,* 2000). The intracellular level of ferritin is regulated through a posttranscriptional mechanism involving IREs in the 5′ untranslated region of the mRNA. When cellular iron concentrations are low, IRP binds to the IRE and translation of the protein is inhibited. If iron levels are high, IRP does not bind to the IRE and translation of the protein can proceed.

Hyperferritinemia is a disease associated with multiple point mutations in the IRE of L-ferritin mRNA that changes the IRE consensus loop required for binding of IRP (Beaumont *et al.,* 1995; Girelli *et al.,* 1995). It is an autosomal dominant disorder of iron metabolism that leads to bilateral nuclear cataracts and somewhat raised levels of serum ferritin (Bonneau *et al.,* 1995). In a study of cultured lymphoblastoid cells from patients with hyperferritinemia, the mutation led to eradication of IRP binding and L-ferritin synthesis which was no longer downregulated by lack of iron (Bonneau *et al.,* 1995). The disease has an early onset and is characterized by ferritin that consists mostly of the L-type subunit with undetectable levels of the H subunit (Beaumont *et al.,* 1995). Certain neurodegenerative disorders have been linked to changes in iron levels in the brain. Elevated iron levels

are present in the parkinsonian nigra and lateral portion of globus pallidus in the brains of Parkinson's disease (PD) patients (Griffiths *et al.,* 1999). In these regions, the only iron binding protein present is ferritin. Thus, as the ferritin is more highly loaded with iron in the PD brains than in age-matched controls it is possible that the increased iron load of the ferritin leads to an increased role of free radical damage by iron. This in turn can lead to the selective death of dopaminergic cells and thus significantly contribute to the pathology of PD. Much work remains to uncover the true nature of this neurodegenerative disorder and the role iron and ferritin play in it (Youdim *et al.,* 1993; Youdim and Riederer, 1993).

VI. Concluding Remarks

The field of iron metabolism is rapidly expanding. Each new experiment increases our current knowledge of many aspects of this intricate system. Iron is an important micronutrient required for normal cellular processes. Dysregulation of iron homeostasis can result in a severe imbalance in cellular functions, which can in turn lead to diseases such as iron deficiency anemia or iron overload. Recent identification of genes involved in iron absorption and other regulatory pathways in mice and humans provides new insight into the mechanisms involved in iron transport and its regulation. A large number of coregulated proteins and receptors interplay to maintain intra- and extracellular iron levels. Furthermore, accessory proteins such as HFE or SFT can influence the function of proteins such as the TfR. The expression of these various proteins is also modulated by IRP activity. These multilevel checkpoints in the iron metabolic pathway function to provide specific and controlled uptake of iron by various cell types in the body. The mechanisms responsible for intracellular iron transport, egress of iron, and the means by which accessory proteins such as SFT and HFE affect transmembrane transport of iron will need to be clarified for full understanding of how iron metabolism is managed. Future studies may involve the characterization of the role of iron and other factors such as nitric oxide, erythropoietin, and hypoxia in regulating the expression of proteins that affect iron metabolism at the transcriptional and posttranscriptional levels. The functions of newly discovered proteins such as TfR2 and IREG1 will also need to be investigated in more detail. With an increased comprehension of the absorption and regulation of various iron metabolic pathways one can begin the process of designing novel treatments to various iron-homeostasis-related diseases.

Acknowledgment

References

Abboud, S., and Haile, D. J. (2000). A novel mammalian iron-regulated protein involved in intracellular iron metabolism. *J. Biol. Chem.* **275,** 19,906–19,912.

Adams, P. C., and Chakrabarti, S. (1998). Genotypic/phenotypic correlations in genetic hemochromatosis: Evolution of diagnostic criteria. *Gastroenterology* **114,** 319–323.

Alemany, R., Vila, M. R., Franci, C., Egea, G., Real, F. X., and Thomson, T. M. (1993). Glycosyl phosphatidylinositol membrane anchoring of melanotransferrin (p97): Apical compartmentalization in intestinal epithelial cells. *J. Cell Sci.* **104,** 1155–1162.

Allikmets, R., Raskind, W. H., Hutchinson, A., Schueck, N. D., Dean, M., and Koeller, D. M. (1999). Mutation of a putative mitochondrial iron transporter gene (ABC7) in X-linked sideroblastic anemia and ataxia (XLSA/A). *Hum. Mol. Genet.* **8,** 743–749.

Alvarez-Hernandez, X., Smith, M., and Glass, J. (1998). The effect of apotransferrin on iron release from Caco-2 cells, an intestinal epithelial cell line. *Blood* **91,** 3974–3979.

Alvarez-Hernandez, X., Smith, M., and Glass, J. (2000). Apo-transferrin is internalized and routed differently from Fe-transferrin by caco-2 cells: A confocal microscopy study of vesicular transport in intestinal cells. *Blood* **95,** 721–723.

Anderson, B. F., Baker, H. M., Norris, G. E., Rumball, S. V., and Baker, E. N. (1990). Apolactoferrin structure demonstrates ligand-induced conformational change in transferrins. *Nature* **344,** 784–787.

Andrews, N. C. (1999). Disorders of iron metabolism [published erratum appears in *N. Engl. J. Med.* (2000) **342**(5), 364]. *N. Engl. J. Med.* **341,** 1986–1995.

Angel, P., and Karin, M. (1991). The role of Jun, Fos and the AP-1 complex in cell-proliferation and transformation. *Biochim. Biophys. Acta* **1072,** 129–157.

Archibald, F. (1983). Lactobacillus plantarum, an organism not requiring iron. *FEMS Microbiol. Lett.* **19,** 29–32.

Askwith, C., Eide, D., Van Ho, A., Bernard, P. S., Li, L., Davis-Kaplan, S., Sipe, D. M., and Kaplan, J. (1994). The FET3 gene of *S. cerevisiae* encodes a multicopper oxidase required for ferrous iron uptake. *Cell* **76,** 403–410.

Attieh, Z. K., Mukhopadhyay, C. K., Seshadri, V., Tripoulas, N. A., and Fox, P. L. (1999). Ceruloplasmin ferroxidase activity stimulates cellular iron uptake by a trivalent cation-specific transport mechanism. *J. Biol. Chem.* **274,** 1116–1123.

Aungst, C. W. (1968). Ferritin in body fluids. *J. Lab. Clin. Med.* **71,** 517–522.

Aziz, N., and Munro, H. N. (1987). Iron regulates ferritin mRNA translation through a segment of its 5′ untranslated region. *Proc. Natl. Acad. Sci. USA* **84,** 8478–8482.

Babcock, M., de Silva, D., Oaks, R., Davis-Kaplan, S., Jiralerspong, S., Montermini, L., Pandolfo, M., and Kaplan, J. (1997). Regulation of mitochondrial iron accumulation by YfhCH. lp, a putative homolog of frataxin. *Science* **276,** 1709–1712.

Bacon, B. R., Powell, L. W., Adams, P. C., Kresina, T. F., and Hoofnagle, J. H. (1999). Molecular medicine and hemochromatosis: At the crossroads. *Gastroenterology,* **116,** 193–207.

Bailey, S., Evans, R. W., Garratt, R. C., Gorinsky, B., Hasnain, S., Horsburgh, C., Jhoti, H., Lindley, P. F., Mydin, A., and Sarra, R., *et al.* (1988). Molecular structure of serum transferrin at 3.3-A resolution. *Biochemistry* **27,** 5804–5812.

Baker, E. N., Baker, H. M., Smith, C. A., Stebbins, M. R., Kahn, M., Hellstrom, K. E., and Hellstrom, I. (1992). Human melanotransferrin (p97) has only one functional iron-binding site. *FEBS Lett.* **298,** 215–218.

Bali, P. K., and Aisen, P. (1992). Receptor-induced switch in site-site cooperativity during iron release by transferrin. *Biochemistry* **31,** 3963–3967.

Bali, P. K., Zak, O., and Aisen, P. (1991). A new role for the transferrin receptor in the release of iron from transferrin. *Biochemistry* **30,** 324–328.

Baranano, D. E., Wolosker, H., Bae, B. I., Barrow, R. K., Snyder, S. H., and Ferris, C. D. (2000). A mammalian iron ATPase induced by iron. *J. Biol. Chem.* **275,** 15,166–15,173.

Barresi, G., and Tuccari, G. (1994). Immunocytochemical demonstration of melanotransferrin (p97) in thyroid tumors of follicular cell origin. *Pathology* **26,** 127–129.

Barton, C. H., Biggs, T. E., Baker, S. T., Bowen, H., and Atkinson, P. G. (1999). Nrampl: A link between intracellular iron transport and innate resistance to intracellular pathogens. *J. Leukocite Biol.* **66,** 757–762.

Beard, P., Offord, E., Paduwat, N., and Bruggmann, H. (1991). SV40 activates transcription from the transferrin receptor promoter by inducing a factor which binds to the CRE/AP-1 recognition sequence. *Nucleic Acids Res.* **19,** 7117–7123.

Beaumont, C., Leneuve, P., Devaux, I., Scoazec, J. Y., Berthier, M., Loiseau, M. N., Grandchamp, B., and Bonneau, D. (1995). Mutation in the iron responsive element of the L ferritin mRNA in a family with dominant hyperferritinaemia and cataract. *Nat. Genet.* **11,** 444–446.

Bernstein, S. E. (1987). Hereditary hypotransferrinemia with hemosiderosis, a murine disorder resembling human atransferrinemia. *J. Lab. Clin. Med.* **110,** 690–705.

Beutler, E., Gelbart, T., Lee, P., Trevino, R., Fernandez, M. A., and Fairbanks, V. F. (2000). Molecular characterization of a case of atransferrinemia. *Blood* **96,** 4071–4074.

Blisard, K. S., and Bartow, S. A. (1986). Neonatal hemochromatosis. *Hum. Pathol.* **17,** 376–383.

Bloch, B., Popovici, T., Levin, M. J., Tuil, D., and Kahn, A. (1985). Transferrin gene expression visualized in oligodendrocytes of the rat brain by using in situ hybridization and immunohistochemistry. *Proc. Natl. Acad. Sci. USA* **82,** 6706–6710.

Bonneau, D., Winter-Fuseau, I., Loiseau, M. N., Amati, P., Berthier, M., Oriot, D., and Beaumont, C. (1995). Bilateral cataract and high serum ferritin: A new dominant genetic disorder? *J. Med. Genet.* **32,** 778–779.

Brown, J. P., Woodbury, R. G., Hart, C. E., Hellstrom, I., and Hellstrom, K. E. (1981). Quantitative analysis of melanoma-associated antigen p97 in normal and neoplastic tissues. *Proc. Natl. Acad. Sci. USA* **78,** 539–543.

Bulaj, Z. J., Griffen, L. M., Jorde, L. B., Edwards, C. Q., and Kushner, J. P. (1996). Clinical and biochemical abnormalities in people heterozygous for hemochromatosis. *N. Engl. J. Med.* **335,** 1799–1805.

Burke, W., Thomson, E., Khoury, M. J., McDonnell, S. M., Press, N., Adams, P. C., Barton, J. C., Beutler, E., Brittenham, G., Buchanan, A., Clayton, E. W., Cogswell, M. E., Meslin, E. M., Motulsky, A. G., Powell, L. W., Sigal, E., Wilfond, B. S., and Collins, F. S. (1998). Hereditary hemochromatosis: Gene discovery and its implications for population-based screening. *JAMA* **280,** 172–178.

Bush, A. I., Pettingell, W. H., Multhaup, G., d Paradis, M., Vonsattel, J. P., Gusella, J. F., Beyreuther, K., Masters, C. L., and Tanzi, R. E. (1994). Rapid induction of Alzheimer A beta amyloid formation by zinc. *Science* **265,** 1464–1467.

Camaschella, C., Roetto, A., Cali, A., De Gobbi, M., Garozzo, G., Carella, M., Majorano, N., Totaro, A., and Gasparini, P. (2000). The gene TFR2 is mutated in a new type of haemochromatosis mapping to 7q22. *Nat. Genet.* **25,** 14–15.

Campuzano, V., Montermini, L., Lutz, Y., Cova, L., Hindelang, C., Jiralerspong, S., Trottier, Y., Kish, S. J., Faucheux, B., Trouillas, P., Authier, F. J., Durr, A., Mandel, J. L., Vescovi, A., Pandolfo, M., and Koenig, M. (1997). Frataxin is reduced in Friedreich ataxia patients and is associated with mitochondrial membranes. *Hum. Mol. Genet.* **6,** 1771–1780.

Campuzano, V., Montermini, L., Molto, M. D., Pianese, L., Cossee, M., Cavalcanti, F., Monros, E., Rodius, F., Duclos, F., and Monticelli, A., and *et al.* (1996). Friedreich's ataxia: Autosomal recessive disease caused by an intronic GAA triplet repeat expansion. *Science* **271,** 1423–1427.

Casey, J. L., Di Jeso, B., Rao, K. K., Rouault, T. A., Klausner, R. D., and Harford, J. B. (1988). Deletional analysis of the promoter region of the human transferrin receptor gene. *Nucleic Acids Res.* **16,** 629–646.

Collawn, J. F., Lai, A., Domingo, D., Fitch, M., Hatton, S., and Trowbridge, I. S. (1993). YTRF is the conserved internalization signal of the transferrin receptor, and a second YTRF signal at position 31–34 enhances endocytosis. *J. Biol. Chem.* **268,** 21,686–21,692.

Connor, J. R., and Benkovic, S. A. (1992). Iron regulation in the brain: Histochemical, biochemical, and molecular considerations. *Ann. Neurol.* **32,** S51–S61.

Connor, J. R., Boeshore, K. L., Benkovic, S. A., and Menzies, S. L. (1994). Isoforms of ferritin have a specific cellular distribution in the brain. *J. Neurosci. Res.* **37,** 461–465.

Conrad, M. E., and Crosby, W. H. (1963). Intestinal mucosal mechanisms controlling iron absorption. *Blood* **22,** 406–415.

Cozzi, A., Corsi, B., Levi, S., Santambrogio, P., Albertini, A., and Arosio, P. (2000). Overexpression of wild type and mutated human ferritin H-chain in HeLa cells: In vivo role of ferritin ferroxidase activity. *J. Biol. Chem.* **275,** 25122–25129.

Crawford, D. H., Jazwinska, E. C., Cullen, L. M., and Powell, L. W. (1998). Expression of HLA-linked hemochromatosis in subjects homozygous or heterozygous for the C282Y mutation. *Gastroenterology* **114,** 1003–1008.

Csere, P., Lill, R., and Kispal, G. (1998). Identification of a human mitochondrial ABC transporter, the functional orthologue of yeast Atm1p. *FEBS Lett.* **441,** 266–270.

Cullen, L. M., Summerville, L., Glassick, T. V., Crawford, D. H., Powell, L. W., and Jazwinska, E. C. (1997). Neonatal screening for the hemochromatosis defect [letter]. *Blood* **90,** 4236–4237.

Dandekar, T., Stripecke, R., Gray, N. K., Goossen, B., Constable, A., Johansson, H. E., and Hentze, M. W. (1991). Identification of a novel iron-responsive element in murine and human erythroid delta-aminolevulinic acid synthase mRNA. *EMBO J.* **10,** 1903–1909.

de Silva, D., Davis-Kaplan, S., Fergestad, J., and Kaplan, J. (1997). Purification and characterization of Fet3 protein, a yeast homologue of ceruloplasmin. *J. Biol. Chem.* **272,** 14,208–14,213.

De Silva, D. M., Askwith, C. C., Eide, D., and Kaplan, J. (1995). The FET3 gene product required for high affinity iron transport in yeast is a cell surface ferroxidase. *J. Biol. Chem.* **270,** 1098–1101.

de Silva, D. M., Askwith, C. C., and Kaplan, J. (1996). Molecular mechanisms of iron uptake in eukaryotes. *Physiol. Rev.* **76,** 31–47.

Delatycki, M. B., Camakaris, J., Brooks, H., Evans-Whipp, T., Thorburn, D. R., Williamson, R., and Forrest, S. M. (1999). Direct evidence that mitochondrial iron accumulation occurs in Friedreich ataxia. *Ann. Neurol.* **45,** 673–675.

Derijard, B., Hibi, M., Wu, I. H., Barrett, T., Su, B., Deng, T., Karin, M., and Davis, R. J. (1994). JNK1: A protein kinase stimulated by UV light and Ha-Ras that binds and phosphorylates the c-Jun activation domain. *Cell* **76,** 1025–1037.

DeRusso, P. A., Philpott, C. C., Iwai, K., Mostowski, H. S., Klausner, R. D., and Rouault, T. A. (1995). Expression of a constitutive mutant of iron regulatory protein 1 abolishes iron homeostasis in mammalian cells. *J. Biol. Chem.* **270,** 15,451–15,454.

Devary, Y., Gottlieb, R. A., Lau, L. F., and Karin, M. (1991). Rapid and preferential activation of the c-jun gene during the mammalian UV response. *Mol. Cell Biol.* **11,** 2804–2811.

Dewan, J. C., Mikami, B., Hirose, M., and Sacchettini, J. C. (1993). Structural evidence for a pH-sensitive dilysine trigger in the hen ovotransferrin N-lobe: Implications for transferrin iron release. *Biochemistry* **32,** 11,963–11,968.

Dickinson, T. K., and Connor, J. R. (1995). Cellular distribution of iron, transferrin, and ferritin in the hypotransferrinemic (Hp) mouse brain. *J. Comp. Neurol.* **355,** 67–80.

Domachowske, J. B. (1997). The role of nitric oxide in the regulation of cellular iron metabolism. *Biochem. Mol. Med.* **60,** 1–7.

Donovan, A., Brownlie, A., Zhou, Y., Shepard, J., Pratt, S. J., Moynihan, J., Paw, B. H., Drejer, A., Barut, B., Zapata, A., Law, T. C., Brugnara, C., Lux, S. E., Pinkus, G. S., Pinkus, J. L., Kingsley, P. D., Palis, J., Fleming, M. D., Andrews, N. C., and Zon, L. I. (2000). Positional cloning of zebrafish ferroportin1 identifies a conserved vertebrate iron exporter. *Nature* **403,** 776–781.

Drysdale, J. J. (1977). Ferritin phenotypes: Structure and metabolism. "Ciba Foundation Symposium 51 Iron Metabolism," pp. 41–67. Elsevier-North Holland, Amsterdam.

Duchange, N., Ochoa, A., Plowman, G. D., Roze, A., Amdjadi, M., and Zakin, M. M. (1992). Identification of an enhancer involved in the melanoma-specific expression of the tumor antigen melanotransferrin gene. *Nucleic Acids Res.* **20,** 2853–2859.

Evans, P., and Kemp, J. (1997). Exon/intron structure of the human transferrin receptor gene. *Gene* **199,** 123–131.

Faber, H. R., Bland, T., Day, C. L., Norris, G. E., Tweedie, J. W., and Baker, E. N. (1996). Altered domain closure and iron binding in transferrins: The crystal structure of the Asp60Ser mutant of the amino-terminal half-molecule of human lactoferrin. *J. Mol. Biol.* **256,** 352–363.

Feder, J. N., Gnirke, A., Thomas, W., Tsuchihashi, Z., Ruddy, D. A., Basava, A., Dormishian, F., Domingo, R. Jr., Ellis, M. C., Fullan, A., Hinton, L. M., Jones, N. L., Kimmel, B. E., Kronmal, G. S., Lauer, P., Lee, V. K., Loeb, D. B., Mapa, F. A., McClelland, E., Meyer, N. C., Mintier, G. A., Moeller, N., Moore, T., Morikang, E., and Wolff, R. K., *et al.* (1996). A novel MHC class I-like gene is mutated in patients with hereditary haemochromatosis. *Nat. Genet.* **13,** 399–408.

Feder, J. N., Tsuchihashi, Z., Irrinki, A., Lee, V. K., Mapa, F. A., Morikang, E., Prass, C. E., Starnes, S. M., Wolff, R. K., Parkkila, S., Sly, W. S., and Schatzman, R. C. (1997). The hemochromatosis founder mutation in HLA-H disrupts beta2-microglobulin interaction and cell surface expression. *J. Biol. Chem.* **272,** 14,025–14,028.

Fellman, V., Rapola, J., Pihko, H., Varilo, T., and Raivio, K. O. (1998). Iron-overload disease in infants involving fetal growth retardation, lactic acidosis, liver haemosiderosis, and aminoaciduria. *Lancet* **351,** 490–493.

Ferreira, C., Bucchini, D., Martin, M. E., Levi, S., Arosio, P., Grandchamp, B., and Beaumont, C. (2000). Early embryonic lethality of H ferritin gene deletion in mice. *J. Biol. Chem.* **275,** 3021–3024.

Ferris, C. D., Jaffrey, S. R., Sawa, A., Takahashi, M., Brady, S. D., Barrow, R. K., Tysoe, S. A., Wolosker, H., Baranano, D. E., Dore, S., Poss, K. D., and Snyder, S. H. (1999). Haem oxygenase-1 prevents cell death by regulating cellular iron. *Nat. Cell Biol.* **1,** 152–157.

Fischbach, K., Lu, Y., Tiffany-Castiglioni, E., Minter, A., Bowman, B. H., and Adrian, G. S. (1990). Expression of chimeric human transferrin genes in vitro. *J. Neurosci. Res.* **27,** 633–641.

Fleming, M. D., Romano, M. A., Su, M. A., Garrick, L. M., Garrick, M. D., and Andrews, N. C. (1998). Nramp2 is mutated in the anemic Belgrade (b) rat: Evidence of a role for Nramp2 in endosomal iron transport. *Proc. Natl. Acad. Sci. USA* **95,** 1148–1153.

Fleming, M. D., Trenor, C. C., 3rd, Su, M. A., Foernzler, D., Beier, D. R., Dietrich, W. F., and Andrews, N. C. (1997). Microcytic anaemia mice have a mutation in Nramp2, a candidate iron transporter gene. *Nat. Genet.* **16,** 383–386.

Fleming, R. E., Migas, M. C., Holden, C. C., Waheed, A., Britton, R. S., Tomatsu, S., Bacon, B. R., and Sly, W. S. (2000). Transferrin receptor 2: Continued expression in mouse liver in the face of iron overload and in hereditary hemochromatosis. *Proc. Natl. Acad. Sci. USA* **97,** 2214–2219.

Fleming, R. E., Migas, M. C., Zhou, X., Jiang, J., Britton, R. S., Brunt, E. M., Tomatsu, S., Waheed, A., Bacon, B. R., and Sly, W. S. (1999). Mechanism of increased iron absorption in murine model of hereditary hemochromatosis: Increased duodenal expression of the iron transporter DMT1. *Proc. Natl. Acad. Sci. USA* **96,** 3143–3148.

Food, M. R., Rothenberger, S., Gabathuler, R., Haidl, I. D., Reid, G., and Jefferies, W. A. (1994). Transport and expression in human melanomas of a transferrin-like glycosylphosphatidylinositol-anchored protein. *J. Biol. Chem.* **269,** 3034–3040.

Ford, G. C., Harrison, P. M., Rice, D. W., Smith, J. M., Treffry, A., White, J. L., and Yariv, J. (1984). Ferritin: Design and formation of an iron-storage molecule. *Philos. Trans. R. Soc. London B* **304,** 551–565.

Fuchs, H., Lucken, U., Tauber, R., Engel, A., and Gessner, R. (1998). Structural model of phospholipid-reconstituted human transferrin receptor derived by electron microscopy. *Structure* **6,** 1235–1243.

Gacy, A. M., Goellner, G. M., Spiro, C., Chen, X., Gupta, G., Bradbury, E. M., Dyer, R. B., Mikesell, M. J., Yao, J. Z., Johnson, A. J., Richter, A., Melancon, S. B., and McMurray, C. T. (1998). GAA instability in Friedreich's Ataxia shares a common, DNA-directed and intraallelic mechanism with other trinucleotide diseases. *Mol. Cell* **1,** 583–593.

George, D. K., Ramm, G. A., Powell, L. W., Fletcher, L. M., Walker, N. I., Cowley, L. L., and Crawford, D. H. (1998). Evidence for altered hepatic matrix degradation in genetic haemochromatosis. *Gut* **42,** 715–720.

Girelli, D., Corrocher, R., Bisceglia, L., Olivieri, O., De Franceschi, L., Zelante, L., and Gasparini, P. (1995). Molecular basis for the recently described hereditary hyperferritinemia-cataract syndrome: A mutation in the iron-responsive element of ferritin L-subunit gene (the "Verona mutation") [see comments]. *Blood* **86,** 4050–4053.

Gitlin, J. D. (1998). Aceruloplasminemia. *Pediatr. Res.* **44,** 271–276.

Goldwurm, S., and Powell, L. W. (1997). Haemochromatosis after the discovery of HFE ("HLA-H"). *Gut* **41,** 855–856.

Govoni, G., Vidal, S., Gauthier, S., Skamene, E., Malo, D., and Gros, P. (1996). The Bcg/Ity/Lsh locus: Genetic transfer of resistance to infections in C57BL/6J mice transgenic for the Nramp1 Gly169 allele. *Infect. Immunol.* **64,** 2923–2929.

Grasbeck, R., Majuri, R., Kouvonen, I., and Tenhunen, R. (1982). Spectral and other studies on the intestinal haem receptor of the pig. *Biochim. Biophys. Acta* **700,** 137–142.

Grewal, M. S. (1962). A sex-linked anemia in the mouse. *Genet. Res.* **3,** 238–247.

Griffiths, P. D., Dobson, B. R., Jones, G. R., and Clarke, D. T. (1999). Iron in the basal ganglia in Parkinson's disease. An in vitro study using extended X-ray absorption fine structure and cryo-electron microscopy. *Brain* **122,** 667–673.

Gruenheid, S., Canonne-Hergaux, F., Gauthier, S., Hackam, D. J., Grinstein, S., and Gros, P. (1999). The iron transport protein NRAMP2 is an integral membrane glycoprotein that colocalizes with transferrin in recycling endosomes. *J. Exp. Med.* **189,** 831–841.

Gruenheid, S., Cellier, M., Vidal, S., and Gros, P. (1995). Identification and characterization of a second mouse Nramp gene. *Genomics* **25,** 514–525.

Guillou, F., Zakin, M. M., Part, D., Boissier, F., and Schaeffer, E. (1991). Sertoli cell-specific expression of the human transferrin gene. Comparison with the liver-specific expression. *J. Biol. Chem.* **266,** 9876–9884.

Gunshin, H., Mackenzie, B., Berger, U. V., Gunshin, Y., Romero, M. F., Boron, W. F., Nussberger, S., Gollan, J. L., and Hediger, M. A. (1997). Cloning and characterization of a mammalian proton-coupled metal-iron transporter. *Nature* **388,** 482–488.

Guo, B., Phillips, J. D., Yu, Y., and Leibold, E. A. (1995). Iron regulates the intracellular degradation of iron regulatory protein 2 by the proteasome. *J. Biol. Chem.* **270,** 21,645–21,651.

Guo, B., Yu, Y., and Leibold, E. A. (1994). Iron regulates cytoplasmic levels of a novel iron-responsive element-binding protein without aconitase activity. *J. Biol. Chem.* **269,** 24,252–24,260.

Gutierrez, J. A., Yu, J., Rivera, S., and Wessling-Resnick, M. (1997). Functional expression cloning and characterization of SFT, a stimulator of Fe transport [published erratum appears in *J. Cell. Biol.* (1999) **147**(1), following 204]. *J. Cell Biol.* **139,** 895–905.

Hackam, D. J., Rotstein, O. D., Zhang, W., Gruenheid, S., Gros, P., and Grinstein, S. (1998). Host resistance to intracellular infection: mutation of natural resistance-associated macrophage protein 1 (Nramp1) impairs phagosomal acidification. *J. Exp. Med.* **188,** 351–364.

Hamill, R. L., Woods, J. C., and Cook, B. A. (1991). Congenital atransferrinemia. A case report and review of the literature. *Am. J. Clin. Pathol.* **96,** 215–218.

Harrison, P. M., and Arosio, P. (1996). The ferritins: Molecular properties, iron storage function and cellular regulation. *Biochim. Biophys. Acta* **1275,** 161–203.

Hayashi, A., Wada, Y., Suzuki, T., and Shimizu, A. (1993). Studies on familial hypotransferrinemia: Unique clinical course and molecular pathology. *Am. J. Hum. Genet.* **53,** 201–213.

Henderson, B. R., and Kuhn, L. C. (1995). Differential modulation of the RNA-binding proteins IRP-1 and IRP-2 in response to iron. IRP-2 inactivation requires translation of another protein. *J. Biol. Chem.* **270,** 20,509–20,515.

Henderson, B. R., Seiser, C., and Kuhn, L. C. (1993). Characterization of a second RNA-binding protein in rodents with specificity for iron-responsive elements. *J. Biol. Chem.* **268,** 27,327–27,334.

Hentze, M. W., and Argos, P. (1991). Homology between IRE-BP, a regulatory RNA-binding protein, aconitase, and isopropylmalate isomerase. *Nucleic Acids Res.* **19,** 1739–1740.

Hentze, M. W., and Kuhn, L. C. (1996). Molecular control of vertebrate iron metabolism: mRNA-based regulatory circuits operated by iron, nitric oxide, and oxidative stress. *Proc. Natl. Acad. Sci. USA* **93,** 8175–8182.

Hirling, H., Henderson, B. R., and Kuhn, L. C. (1994). Mutational analysis of the [4Fe–4S]-cluster converting iron regulatory factor from its RNA-binding form to cytoplasmic aconitase. *EMBO J.* **13,** 453–461.

Hu, Y. F., Luscher, B., Admon, A., Mermod, N., and Tjian, R. (1990). Transcription factor AP-4 contains multiple dimerization domains that regulate dimer specificity. *Genes Dev.* **4,** 1741–1752.

Huang, X., Cuajungco, M. P., Atwood, C. S., Moir, R. D., Tanzi, R. E., and Bush, A. I. (2000). Alzheimer's disease, beta-amyloid protein and zinc. *J. Nutr.* **130,** 1488S–1492S.

Huggenvik, J. I., Craven, C. M., Idzerda, R. L., Bernstein, S., Kaplan, J., and McKnight, G. S. (1989). A splicing defect in the mouse transferrin gene leads to congenital atransferrinemia. *Blood* **74,** 482–486.

Hulet, S. W., Hess, E. J., Debinski, W., Arosio, P., Bruce, K., Powers, S., and Connor, J. R. (1999). Characterization and distribution of ferritin binding sites in the adult mouse brain. *J. Neurochem.* **72,** 868–874.

Hulet, S. W., Heyliger, S. O., Powers, S., and Connor, J. R. (2000). Oligodendrocyte progenitor cells internalize ferritin via clathrin-dependent receptor mediated endocytosis. *J. Neurosci. Res.* **61,** 52–60.

Ikuta, K., Fujimoto, Y., Suzuki, Y., Tanaka, K., Saito, H., Ohhira, M., Sasaki, K., and Kohgo, Y. (2000). Overexpression of hemochromatosis protein, HFE, alters transferrin recycling process in human hepatoma cells [In Process Citation]. *Biochim. Biophys. Acta* **1496,** 221–231.

Jazwinska, E. C., and Powell, L. W. (1997). Hemochromatosis and "HLA-H": Definite! *Hepatology* **25,** 495–496.

Jefferies, W. A., Brandon, M. R., Hunt, S. V., Williams, A. F., Gatter, K. C., and Mason, D. Y. (1984). Transferrin receptor on endothelium of brain capillaries. *Nature* **312,** 162–163.

Jefferies, W. A., Food, M. R., Gabathuler, R., Rothenberger, S., Yamada, T., Yasuhara, O., and McGeer, P. L. (1996). Reactive microglia specifically associated with amyloid plaques in Alzheimer's disease brain tissue express melanotransferrin. *Brain Res.* **712,** 122–126.

Jing, S. Q., and Trowbridge, I. S. (1987). Identification of the intermolecular disulfide bonds of the human transferrin receptor and its lipid-attachment site. *EMBO J.* **6,** 327–331.

Jones, K. A., Kadonaga, J. T., Rosenfeld, P. J., Kelly, T. J., and Tjian, R. (1987). A cellular DNA-binding protein that activates eukaryotic transcription and DNA replication. *Cell* **48,** 79–89.

Kahn, A., Levin, M. J., Zakin, M. M., and Bloch, B. (1987). The transferrin gene. *In* "Oncogenes, Genes, and Growth Factors" (G. Guroff, Eds.), pp. 277–309. Wiley-Interscience, New York.

Kawabata, H., Germain, R. S., Vuong, P. T., Nakamaki, T., Said, J. W., and Koeffler, H. P. (2000). Transferrin receptor 2-alpha supports cell growth both in iron-chelated cultured cells and *in vivo*. *J. Biol. Chem.* **275,** 16,618–16,625.

Kawabata, H., Yang, R., Hirama, T., Vuong, P. T., Kawano, S., Gombart, A. F., and Koeffler, H. P. (1999). Molecular cloning of transferrin receptor 2. A new member of the transferrin receptor-like family. *J. Biol. Chem.* **274,** 20,826–20,832.

Ke, Y., Sierzputowska-Gracz, H., Gdaniec, Z., and Theil, E. C. (2000). Internal loop/bulge and hairpin loop of the iron-responsive element of ferritin mRNA contribute to maximal iron regulatory protein 2 binding and translational regulation in the iso-iron-responsive element/iso-iron regulatory protein family. *Biochemistry* **39,** 6235–6242.

Ke, Y., Wu, J., Leibold, E. A., Walden, W. E., and Theil, E. C. (1998). Loops and bulge/loops in iron-responsive element isoforms influence iron regulatory protein binding. Fine-tuning of mRNA regulation? *J. Biol. Chem.* **273,** 23,637–23,640.

Kennard, M. L., Feldman, H., Yamada, T., and Jefferies, W. A. (1996). Serum levels of the iron binding protein p97 are elevated in Alzheimer's disease. *Nat. Med.* **2,** 1230–1235.

Kennard, M. L., Richardson, D. R., Gabathuler, R., Ponka, P., and Jefferies, W. A. (1995). A novel iron uptake mechanism mediated by GPI-anchored human p97. *EMBO J.* **14,** 4178–4186.

Kienzl, E., Jellinger, K., Stachelberger, H., and Linert, W. (1999). Iron as catalyst for oxidative stress in the pathogenesis of Parkinson's disease? *Life Sci.* **65,** 1973–1976.

Kim, D. K., Seo, M. Y., Lim, S. W., Kim, S., Kim, J. W., Carroll, B. J., Kwon, D. Y., Kwon, T., and Kang, S. S. (2001). Serum melanotransferrin, p97 as biochemical marker of Alzheimer's disease. *Neuropsychopharmacology* **25**(1), 84–90.

Kim, S., and Ponka, P. (1999). Control of transferrin receptor expression via nitric oxide-mediated modulation of iron-regulatory protein 2. *J. Biol. Chem.* **274,** 33,035–33,042.

Kim, S., and Ponka, P. (2000). Effects of interferon-gamma and lipopolysaccharide on macrophage iron metabolism are mediated by nitric oxide-induced degradation of iron regulatory protein 2. *J. Biol. Chem.* **275,** 6220–6226.

Kishi, F., and Tabuchi, M. (1997). Complete nucleotide sequence of human NRAMP2 cDNA. *Mol. Immunol.* **34,** 839–842.

Kishi, F., Yoshida, T., and Aiso, S. (1996). Location of NRAMP1 molecule on the plasma membrane and its association with microtubules. *Mol. Immunol.* **33,** 1241–1246.

Kispal, G., Csere, P., Guiard, B., and Lill, R. (1997). The ABC transporter Atm1p is required for mitochondrial iron homeostasis. *FEBS Lett* **418,** 346–350.

Kispal, G., Csere, P., Prohl, C., and Lill, R. (1999). The mitochondrial proteins Atm1p and Nfs1p are essential for biogenesis of cytosolic Fe/S proteins. *EMBO J.* **18,** 3981–3989.

Klomp, L. W., and Gitlin, J. D. (1996). Expression of the ceruloplasmin gene in the human retina and brain: Implications for a pathogenic model in aceruloplasminemia. *Hum. Mol. Genet.* **5,** 1989–1996.

Koutnikova, H., Campuzano, V., Foury, F., Dolle, P., Cazzalini, O., and Koenig, M. (1997). Studies of human, mouse and yeast homologues indicate a mitochondrial function for frataxin. *Nat. Genet.* **16,** 345–351.

Kuhn, L. C. (1998). Iron and gene expression: Molecular mechanisms regulating cellular iron homeostasis. *Nutr. Rev.* **56,** s11–s19; discussion s54–s75.

Kuhn, L. C., Schulman, H. M., and Ponka, P. (1990). Iron-transferrin requirements and transferrin receptor expression in proliferating cells. *In* "Iron Transport and Storage" (P. Ponka, R. C. Schulman, and R. C. Woodworth, Eds.), pp.149–191. CRC, Boca Raton, FL.

Lafuse, W. P., Alvarez, G. R., and Zwilling, B. S. (2000). Regulation of nramp1 mRNA stability by oxidants and protein kinase C in RAW264.7 macrophages expressing Nramp1Gly169 [In Process Citation]. *Biochem. J.* **351**(3), 687–696.

Laing, L. G., and Hall, K. B. (1996). A model of the iron responsive element RNA hairpin loop structure determined from NMR and thermodynamic data. *Biochemistry* **35,** 13,586–13,596.

Lawrence, C. M., Ray, S., Babyonyshev, M., Galluser, R., Borhani, D. W., and Harrison, S. C. (1999). Crystal structure of the ectodomain of human transferrin receptor. *Science* **286,** 779–782.

Lebron, J. A., Bennett, M. J., Vaughn, D. E., Chirino, A. J., Snow, P. M., Mintier, G. A., Feder, J. N., and Bjorkman, P. J. (1998). Crystal structure of the hemochromatosis protein HFE and characterization of its interaction with transferrin receptor. *Cell* **93,** 111–123.

Lee, P. L., Gelbart, T., West, C., Halloran, C., and Beutler, E. (1998). The human Nramp2 gene: Characterization of the gene structure, alternative splicing, promoter region and polymorphisms. *Blood Cells Mol. Dis.* **24,** 199–215.

Lee, P. L., Halloran, C., Cross, A. R., and Beutler, E. (2000). NADH-ferric reductase activity associated with dihydropteridine reductase. *Biochem. Biophys. Res. Commun.* **271,** 788–795.

Leighton, J., and Schatz, G. (1995). An ABC transporter in the mitochondrial inner membrane is required for normal growth of yeast. *EMBO J.* **14,** 188–195.

Levy, J. E., Jin, O., Fujiwara, Y., Kuo, F., and Andrews, N. C. (1999). Transferrin receptor is necessary for development of erythrocytes and the nervous system. *Nat. Genet.* **21,** 396–399.

Levy, J. E., Montross, L. K., and Andrews, N. C. (2000). Genes that modify the hemochromatosis phenotype in mice [see comments]. *J. Clin. Invest.* **105,** 1209–1216.

Lipschitz, D. A., Cook, J. D., and Finch, C. A. (1974). A clinical evaluation of serum ferritin as an index of iron stores. *N. Engl. J. Med.* **290,** 1213–1216.

Lodi, R., Cooper, J. M., Bradley, J. L., Manners, D., Styles, P., Taylor, D. J., and Schapira, A. H. (1999). Deficit of in vivo mitochondrial ATP production in patients with Friedreich ataxia. *Proc. Natl. Acad. Sci. USA* **96,** 11,492–11,495.

Lok, C. N., Chan, K. F., and Loh, T. T. (1996). Transcriptional regulation of transferrin receptor expression during phorbol-ester-induced HL-60 cell differentiation. Evidence for a negative regulatory role of the phorbol-ester-responsive element-like sequence. *Eur. J. Biochem.* **236,** 614–619.

Lok, C. N., and Ponka, P. (1999). Identification of a hypoxia response element in the transferrin receptor gene. *J. Biol. Chem.* **274,** 24,147–24,152.

Lok, C. N., and Ponka, P. (2000). Identification of an erythroid active element in the transferrin receptor gene. *J. Biol. Chem.* **275,** 24185–24190.

MacGillivray, R. T., Bewley, M. C., Smith, C. A., He, Q. Y., Mason, A. B., Woodworth, R. C., and Baker, E. N. (2000). Mutation of the iron ligand His 249 to Glu in the N-lobe of human transferrin abolishes the dilysine "trigger" but does not significantly affect iron release. *Biochemistry* **39,** 1211–1216.

MacGillivray, R. T., Moore, S. A., Chen, J., Anderson, B. F., Baker, H., Luo, Y., Bewley, M., Smith, C. A., Murphy, M. E., Wang, Y., Mason, A. B., Woodworth, R. C., Brayer, G. D., and Baker, E. N. (1998). Two high-resolution crystal structures of the recombinant N-lobe of human transferrin reveal a structural change implicated in iron release. *Biochemistry* **37,** 7919–7928.

Maines, M. D. (1997). The heme oxygenase system: A regulator of second messenger gases. *Annu. Rev. Pharmacol. Toxicol.* **37,** 517–554.

Majuri, R., and Grasbeck, R. (1987). A rosette receptor assay with haem-microbeads. Demonstration of a haem receptor on K562 cells. *Eur. J. Haematol.* **38,** 21–25.

McCord, J. M. (1998). Iron, free radicals, and oxidative injury. *Semin. Hematol.* **35,** 5–12.

McKie, A. T., Marciani, P., Rolfs, A., Brennan, K., Wehr, K., Barrow, D., Miret, S., Bomford, A., Peters, T. J., Farzaneh, F., Hediger, M. A., Hentze, M. W., and Simpson., R. J. (2000). A novel duodenal iron-regulated transporter, IREG1, implicated in the basolateral transfer of iron to the circulation. *Mol. Cell* **5,** 299–309.

Miskimins, W. K., McClelland, A., Roberts, M. P., and Ruddle, F. H. (1986). Cell proliferation and expression of the transferrin receptor gene: Promoter sequence homologies and protein interactions. *J. Cell Biol.* **103,** 1781–1788.

Mitsuhashi, N., Miki, T., Senbongi, H., Yokoi, N., Yano, H., Miyazaki, M., Nakajima, N., Iwanaga, T., Yokoyama, Y., Shibata, T., and Seino, S. (2000). MTABC3, a novel mitochondrial ATP-binding cassette protein involved in iron homeostasis. *J. Biol. Chem.* **275,** 17,536–17,540.

Morita, H., Ikeda, S., Yamamoto, K., Morita, S., Yoshida, K., Nomoto, S., Kato, M., and Yanagisawa, N. (1995). Hereditary ceruloplasmin deficiency with hemosiderosis: A clinicopathological study of a Japanese family. *Ann. Neurol.* **37,** 646–656.

Moroo, I., Yamada, T., Gabathuler, R., Kennard, M. L., Nurminen, J., and Jefferies, W. A. (1999). Use of p97 in the diagnosis of Alzheimer's disease. *Alzheimer's Rep.* **2,** 353–358.

Moroo, I., Ujiie, M., Tiong, J. W. C., Walker, B. L., and Jefferies, W. A. (2001). The role of p97 in iron transport across the blood-brain barrier. In preperation.

Mukhopadhyay, C. K., Mazumder, B., and Fox, P. L. (2000). Role of hypoxia-inducible factor-1 in transcriptional activation of ceruloplasmin by iron deficiency. *J. Biol. Chem.* **275,** 21,048–21,054.

Mullner, E. W., and Kuhn, L. C. (1988). A stem–loop in the 3′ untranslated region mediates iron-dependent regulation of transferrin receptor mRNA stability in the cytoplasm. *Cell* **53,** 815–825.

Niederau, C., Fischer, R., Purschel, A., Stremmel, W., Haussinger, D., and Strohmeyer, G. (1996). Long-term survival in patients with hereditary hemochromatosis. *Gastroenterology* **110,** 1107–1119.

Niederau, C., Fischer, R., Sonnenberg, A., Stremmel, W., Trampisch, H. J., and Strohmeyer, G. (1985). Survival and causes of death in cirrhotic and in noncirrhotic patients with primary hemochromatosis. *N. Engl. J. Med.* **313,** 1256–1262.

Oliveria, L., and Drapier, J. C. (2000). Down-regulation of iron regulatory protein 1 gene expression by nitric oxide [In Process Citation]. *Proc. Natl. Acad. Sci. USA* **97,** 6550–6555.

Osaki, S., and Johnson, D. A. (1969). Mobilization of liver iron by ferroxidase (ceruloplasmin). *J. Biol. Chem.* **244,** 5757–5758.

Owen, D., and Kuhn, L. C. (1987). Noncoding $3'$ sequences of the transferrin receptor gene are required for mRNA regulation by iron. *EMBO J.* **6,** 1287–1293.

Pagon, R. A., Bird, T. D., Detter, J. C., and Pierce, I. (1985). Hereditary sideroblastic anaemia and ataxia: An X linked recessive disorder. *J. Med. Genet.* **22,** 267–273.

Pantopoulos, K., and Hentze, M. W. (1998). Activation of iron regulatory protein-1 by oxidative stress in vitro. *Proc. Natl. Acad. Sci. USA* **95,** 10,559–10,563.

Pantopoulos, K., Weiss, G., and Hentze, M. W. (1996). Nitric oxide and oxidative stress (H2O2) control mammalian iron metabolism by different pathways. *Mol. Cell Biol.* **16,** 3781–3788.

Parkkila, S., Parkkila, A. K., Waheed, A., Britton, R. S., Zhou, X. Y., Fleming, R. E., Tomatsu, S., Bacon, B. R., and Sly, W. S. (2000). Cell surface expression of HFE protein in epithelial cells, macrophages, and monocytes. *Haematologica* **85,** 340–345.

Parkkila, S., Waheed, A., Britton, R. S., Bacon, B. R., Zhou, X. Y., Tomatsu, S., Fleming, R. E., and Sly, W. S. (1997a). Association of the transferrin receptor in human placenta with HFE, the protein defective in hereditary hemochromatosis. *Proc. Natl. Acad. Sci. USA* **94,** 13,198–13,202.

Parkkila, S., Waheed, A., Britton, R. S., Feder, J. N., Tsuchihashi, Z., Schatzman, R. C., Bacon, B. R., and Sly, W. S. (1997b). Immunohistochemistry of HLA-H, the protein defective in patients with hereditary hemochromatosis, reveals unique pattern of expression in gastrointestinal tract. *Proc. Natl. Acad. Sci. USA* **94,** 2534–2539.

Patel, B. N., Dunn, R. J., and David, S. (2000). Alternative RNA splicing generates a glycosylphosphatidylinositol-anchored form of ceruloplasmin in mammalian brain. *J. Biol. Chem.* **275,** 4305–4310.

Petropoulos, I., Auge-Gouillou, C., and Zakin, M. M. (1991). Characterization of the active part of the human transferrin gene enhancer and purification of two liver nuclear factors interacting with the TGTTTGC motif present in this region. *J. Biol. Chem.* **266,** 24,220–24,225.

Phillips, J. D., Guo, B., Yu, Y., Brown, F. M., and Leibold, E. A. (1996). Expression and biochemical characterization of iron regulatory proteins 1 and 2 in Saccharomyces cerevisiae. *Biochemistry* **35,** 15,704–15,714.

Phillips, J. D., Kinikini, D. V., Yu, Y., Guo, B., and Leibold, E. A. (1996). Differential regulation of IRP1 and IRP2 by nitric oxide in rat hepatoma cells. *Blood* **87,** 2983–2992.

Pierre, J. L., and Fontecave, M. (1999). Iron and activated oxygen species in biology: The basic chemistry. *Biometals* **12,** 195–199.

Poss, K. D., and Tonegawa, S. (1997a). Heme oxygenase 1 is required for mammalian iron reutilization. *Proc. Natl. Acad. Sci. USA* **94,** 10,919–10,924.

Poss, K. D., and Tonegawa, S. (1997b). Reduced stress defense in heme oxygenase 1-deficient cells. *Proc. Natl. Acad. Sci. USA* **94,** 10,925–10,930.

Rabin, M., McClelland, A., Kuhn, L., and Ruddle, F. H. (1985). Regional localization of the human transferrin receptor gene to 3q26.2–*q*ter. *Am. J. Hum. Genet.* **37,** 1112–1116.

Radisky, D. C., Babcock, M. C., and Kaplan, J. (1999). The yeast frataxin homologue mediates mito-chondrial iron efflux. Evidence for a mitochondrial iron cycle. *J. Biol. Chem.* **274,** 4497–4499.

Raffin, S. B., Woo, C. H., Roost, K. T., Price, D. C., and Schmid, R. (1974). Intestinal absorption of hemoglobin iron-heme cleavage by mucosal heme oxygenase. *J. Clin. Invest.* **54,** 1344–1352.

Ramalingam, T. S., West, A. P., Lebron, J. A., Nangiana, J. S., Hogan, T. H., Enns, C. A., and Bjorkman, P. J. (2000). Binding to the transferrin receptor is required for endocytosis of HFE and regulation of iron homeostasis. *Nat. Cell Biol.* **2,** 953–957.

Ramm, G. A., Crawford, D. H., Powell, L. W., Walker, N. I., Fletcher, L. M., and Halliday, J. W. (1997). Hepatic stellate cell activation in genetic haemochromatosis. Lobular distribution, effect of increasing hepatic iron and response to phlebotomy. *J. Hepatol.* **26,** 584–592.

Raskind, W. H., Wijsman, E., Pagon, R. A., Cox, T. C., Bawden, M. J., May, B. K., and Bird, T. D. (1991). X-linked sideroblastic anemia and ataxia: Linkage to phosphoglycerate kinase at Xq13. *Am. J. Hum. Genet.* **48,** 335–341.

Richardson, D. R. (2000). The role of the membrane-bound tumour antigen, melanotransferrin (p97), in iron uptake by the human malignant melanoma cell. *Eur. J. Biochem.* **267,** 1290–1298.

Roberts, M. R., Han, Y., Fienberg, A., Hunihan, L., and Ruddle, F. H. (1994). A DNA-binding activity, TRAC, specific for the TRA element of the transferrin receptor gene copurifies with the Ku autoantigen. *Proc. Natl. Acad. Sci. USA* **91,** 6354–6358.

Rocha, M. E., Bandy, B., Costa, C. A., de Barros, M. P., Pinto, A. M., and Bechara, E. J. (2000). Iron mobilization by succinylacetone methyl ester in rats. A model study for hereditary tyrosinemia and porphyrias characterized by 5-aminolevulinic acid overload. *Free Radical Res.* **32,** 343–353.

Roeser, H. P., Lee, G. R., Nacht, S., and Cartwright, G. E. (1970). The role of ceruloplasmin in iron metabolism. *J. Clin. Invest.* **49,** 2408–2417.

Roetto, A., Totaro, A., Cazzola, M., Cicilano, M., Bosio, S., D'Ascola, G., Carella, M., Zelante, L., Kelly, A. L., Cox, T. M., Gasparini, P., and Camaschella, C. (1999). Juvenile hemochromatosis locus maps to chromosome 1q. *Am. J. Hum. Genet.* **64,** 1388–1393.

Rolfs, A., Kvietikova, I., Gassmann, M., and Wenger, R. H. (1997). Oxygen-regulated transferrin expression is mediated by hypoxia-inducible factor-1. *J. Biol. Chem.* **272,** 20,055–20,062.

Rose, T. M., Plowman, G. D., Teplow, D. B., Dreyer, W. J., Hellstrom, K. E., and Brown, J. P. (1986). Primary structure of the human melanoma-associated antigen p97 (melanotransferrin) deduced from the mRNA sequence. *Proc. Natl. Acad. Sci. USA* **83,** 1261–1265.

Rothenberger, S., Food, M. R., Gabathuler, R., Kennard, M. L., Yamada, T., Yasuhara, O., McGeer, P. L., and Jefferies, W. A. (1996). Coincident expression and distribution of melanotransferrin and transferrin receptor in human brain capillary endothelium. *Brain Res.* **712,** 117–121.

Rothenberger, S., Iacopetta, B. J., and Kuhn, L. C. (1987). Endocytosis of the transferrin receptor requires the cytoplasmic domain but not its phosphorylation site. *Cell* **49,** 423–431.

Roy, C. N., Penny, D. M., Feder, J. N., and Enns, C. A. (1999). The hereditary hemochromatosis protein, HFE, specifically regulates transferrin-mediated iron uptake in HeLa cells. *J. Biol. Chem.* **274,** 9022–9028.

Roze-Heusse, A., Houbiguian, M. L., Debacker, C., Zakin, M. M., and Duchange, N. (1996). Melanotransferrin gene expression in melanoma cells is correlated with high levels of Jun/Fos family transcripts and with the presence of a specific AP1-dependent ternary complex. *Biochem. J.* **318,** 883–888.

Santambrogio, P., Levi, S., Cozzi, A., Corsi, B., and Arosio, P. (1996). Evidence that the specificity of iron incorporation into homopolymers of human ferritin L- and H-chains is conferred by the nucleation and ferroxidase centres. *Biochem. J.* **314,** 139–144.

Sassone-Corsi, P. (1994). Goals for signal transduction pathways: Linking up with transcriptional regulation. *EMBO J.* **13,** 4717–4728.

Schade, A. L., and Caroline, L. (1946). An iron-binding component in human blood plasma. *Science* **104,** 340.

Schaeffer, E., Boissier, F., Py, M. C., Cohen, G. N., and Zakin, M. M. (1989). Cell type-specific expression of the human transferrin gene. Role of promoter, negative, and enhancer elements. *J. Biol. Chem.* **264,** 7153–7160.

Schaich, K. M. (1992). Metals and lipid oxidation. Contemporary issues. *Lipids* **27,** 209–218.

Schalinske, K. L., Anderson, S. A., Tuazon, P. T., Chen, O. S., Kennedy, M. C., and Eisenstein, R. S. (1997). The iron-sulfur cluster of iron regulatory protein 1 modulates the accessibility of RNA binding and phosphorylation sites. *Biochemistry* **36,** 3950–3958.

Schalinske, K. L., Blemings, K. P., Steffen, D. W., Chen, O. S., and Eisenstein, R. S. (1997). Iron regulatory protein 1 is not required for the modulation of ferritin and transferrin receptor expression by iron in a murine pro-B lymphocyte cell line. *Proc. Natl. Acad. Sci. USA* **94,** 10,681–10,686.

Schalinske, K. L., and Eisenstein, R. S. (1996). Phosphorylation and activation of both iron regulatory proteins 1 and 2 in HL-60 cells. *J. Biol. Chem.* **271,** 7168–7176.

Sciot, R., de Vos, R., van Eyken, P., van der Steen, K., Moerman, P., and Desmet, V. J. (1989). In situ localization of melanotransferrin (melanoma-associated antigen P97) in human liver. A light- and electronmicroscopic immunohistochemical study. *Liver* **9,** 110–119.

Senbongi, H., Ling, F., and Shibata, T. (1999). A mutation in a mitochondrial ABC transporter results in mitochondrial dysfunction through oxidative damage of mitochondrial DNA. *Mol. Gen. Genet.* **262,** 426–436.

Sheth, S., and Brittenham, G. M. (2000). Genetic disorders affecting proteins of iron metabolism: Clinical implications. *Annu. Rev. Med.* **51,** 443–464.

Sieweke, M. H., Tekotte, H., Frampton, J., and Graf, T. (1996). MafB is an interaction partner and repressor of Ets-1 that inhibits erythroid differentiation. *Cell* **85,** 49–60.

Sipe, D. M., and Murphy, R. F. (1991). Binding to cellular receptors results in increased iron release from transferrin at mildly acidic pH. *J. Biol. Chem.* **266,** 8002–8007.

Sladek, F. M., Zhong, W. M., Lai, E., and Darnell, J. E. (1990). Liver-enriched transcription factor HNF-4 is a novel member of the steroid hormone receptor superfamily. *Genes Dev.* **4,** 2353–2365.

Smith, M. A., Wehr, K., Harris, P. L. R., Siedlak, S. L., Connor, J. R., and Perry, G. (1998). Abnormal localization of iron regulatory protein in Alzheimer's disease. *Brain Res.* **788,** 232–236.

Stearman, R., Yuan, D. S., Yamaguchi-Iwai, Y., Klausner, R. D., and Dancis, A. (1996). A permease-oxidase complex involved in high-affinity iron uptake in yeast. *Science* **271,** 1552–1557.

Tabuchi, M., Yoshimori, T., Yamaguchi, K., Yoshida, T., and Kishi, F. (2000). Human NRAMP2/DMT1, which mediates iron transport across endosomal membranes, is localized to late endosomes and lysosomes in HEp-2 cells. *J. Biol. Chem.* **275,** 22,220–22,228.

Theil, E. C. (1998). The iron responsive element (IRE) family of mRNA regulators. Regulation of iron transport and uptake compared in animals, plants, and microorganisms. *Met. Ions Biol. Syst.* **35,** 403–434.

Thomson, A. M., Rogers, J. T., and Leedman, P. J. (1999). Iron-regulatory proteins, iron-responsive elements and ferritin mRNA translation. *Int. J. Biochem. Cell Biol.* **31,** 1139–1152.

Tiong, J. W. C., and Jefferies, W. A. (2001). Metal binding properties of melanotransferrin. Manuscript in preperation.

Tsutsumi, M., Skinner, M. K., and Sanders-Bush, E. (1989). Transferrin gene expression and synthesis by cultured choroid plexus epithelial cells. Regulation by serotonin and cyclic adenosine 3′, 5′-monophosphate. *J. Biol. Chem.* **264,** 9626–9631.

Turnbull, A., Cleton, F., and Finch, C. A. (1989). The Journal of clinical Investigation, Volume 41, 1962: Iron absorption. IV. The absorption of hemoglobin iron [classical article]. *Nutr. Rev.* **47,** 51–53.

Umbreit, J. N., Conrad, M. E., Moore, E. G., Desai, M. P., and Turrens, J. (1996). Paraferritin: A protein complex with ferrireductase activity is associated with iron absorption in rats. *Biochemistry* **35,** 6460–6469.

Umbreit, J. N., Conrad, M. E., Moore, E. G., and Latour, L. F. (1998). Iron absorption and cellular transport: the mobilferrin/paraferritin paradigm. *Semin. Hematol.* **35,** 13–26.

Vidal, S. M., Malo, D., Vogan, K., Skamene, E., and Gros, P. (1993). Natural resistance to infection with intracellular parasites: isolation of a candidate for Bcg. *Cell* **73,** 469–485.

Visapaa, I., Fellman, V., Varilo, T., Palotie, A., Raivio, K. O., and Peltonen, L. (1998). Assignment of the locus for a new lethal neonatal metabolic syndrome to 2q33–37. *Am. J. Hum. Genet.* **63,** 1396–1403.

Vulpe, C. D., Kuo, Y. M., Murphy, T. L., Cowley, L., Askwith, C., Libina, N., Gitschier, J., and Anderson, G. J. (1999). Hephaestin, a ceruloplasmin homologue implicated in intestinal iron transport, is defective in the sla mouse. *Nat. Genet.* **21,** 195–199.

Waheed, A., Parkkila, S., Zhou, X. Y., Tomatsu, S., Tsuchihashi, Z., Feder, J. N., Schatzman, R. C., Britton, R. S., Bacon, B. R., and Sly, W. S. (1997). Hereditary hemochromatosis: Effects of C282Y and H63D mutations on association with beta2-microglobulin, intracellular processing, and cell surface expression of the HFE protein in COS-7 cells. *Proc. Natl. Acad. Sci. USA* **94,** 12,384–12,389.

Wardrop, S. L., Watts, R. N., and Richardson, D. R. (2000). Nitrogen monoxide activates iron regulatory protein 1 RNA-binding activity by two possible mechanisms: Effect on the [4Fe–4S] cluster and iron mobilization from cells. *Biochemistry* **39,** 2748–2758.

Weiss, G., Houston, T., Kastner, S., Johrer, K., Grunewald, K., and Brock, J. H. (1997). Regulation of cellular iron metabolism by erythropoietin: Activation of iron-regulatory protein and upregulation of transferrin receptor expression in erythroid cells. *Blood* **89,** 680–687.

West, A. P., Bennet, M. J., Sellers, V. M., Andrews, N. C., Enns, C. A., and Bjorkman, P. J. (2000). Comparison of the interactions of transferrin receptor and transferrin receptor 2 with transferrin and the hereditary hemochromatosis protein HFE. *J. Biol. Chem.* **275,** 38135–38138.

Williams, A. M., and Enns, C. A. (1991). A mutated transferrin receptor lacking asparagine-linked glycosylation sites shows reduced functionality and an association with binding immunoglobulin protein. *J. Biol. Chem.* **266,** 17,648–17,654.

Williams, K., Wilson, M. A., and Bressler, J. (2000). Regulation and developmental expression of the divalent metal-ion transporter in the rat brain. *Cell Mol. Biol. (Noisy-Le-Grand)* **46,** 563–571.

Wilson, R. B., and Roof, D. M. (1997). Respiratory deficiency due to loss of mitochondrial DNA in yeast lacking the frataxin homologue. *Nat. Genet.* **16,** 352–357.

Witzleben, C. L., and Uri, A. (1989). Perinatal hemochromatosis: Entity or end result? *Hum. Pathol.* **20,** 335–340.

Woodbury, R. G., Brown, J. P., Loop, S. M., Hellstrom, K. E., and Hellstrom, I. (1981). Analysis of normal neoplastic human tissues for the tumor-associated protein p97. *Int. J. Cancer* **27,** 145–149.

Woodbury, R. G., Brown, J. P., Yeh, M. Y., Hellstrom, I., and Hellstrom, K. E. (1980). Identification of a cell surface protein, p97, in human melanomas and certain other neoplasms. *Proc. Natl. Acad. Sci. USA* **77,** 2183–2187.

Yamada, T., Tsujioka, Y., Taguchi, J., Takahashi, M., Tsuboi, Y., Moroo, I., Yang, J., and Jefferies, W. A. (1999). Melanotransferrin is produced by senile plaque-associated reactive microglia in Alzheimer's disease. *Brain Res.* **845,** 1–5.

Yantiri, F., and Andersen, J. K. (1999). The role of iron in Parkinson disease and 1-methyl-4-phenyl-1,2,3,6-tetrahydropyridine toxicity. *IUBMB Life* **48,** 139–141.

Youdim, M. B., Ben-Shachar, D., and Riederer, P. (1993). The possible role of iron in the etiopathology of Parkinson's disease. *Mov. Disord.* **8,** 1–12.

Youdim, M. B., and Riederer, P. (1993). The role of iron in senescence of dopaminergic neurons in Parkinson's disease. *J. Neural Transm. Suppl.* **40,** 57–67.

Young, S. P., Bomford, A., and Williams, R. (1984). The effect of the iron saturation of transferrin on its binding and uptake by rabbit reticulocytes. *Biochem J,* **219,** 505–510.

Yu, J., and Wessling-Resnick, M. (1998). Structural and functional analysis of SFT, a stimulator of Fe Transport. *J. Biol. Chem.* **273,** 21,380–21,385.

Yu, J., Yu, Z. K., and Wessling-Resnick, M. (1998). Expression of SFT (stimulator of Fe transport) is enhanced by iron chelation in HeLa cells and by hemochromatosis in liver. *J. Biol. Chem.* **273,** 34,675–34,678.

Zakin, M. M. (1992). Regulation of transferrin gene expression. *FASEB J.* **6,** 3253–3258.

Zheng, L., Kennedy, M. C., Blondin, G. A., Beinert, H., and Zalkin, H. (1992). Binding of cytosolic aconitase to the iron responsive element of porcine mitochondrial aconitase mRNA. *Arch. Biochem. Biophys.* **299,** 356–360.

Zhou, X. Y., Tomatsu, S., Fleming, R. E., Parkkila, S., Waheed, A., Jiang, J., Fei, Y., Brunt, E. M., Ruddy, D. A., Prass, C. E., Schatzman, R. C., O'Neill, R., Britton, R. S., Bacon, B. R., and Sly, W. S. (1998). HFE gene knockout produces mouse model of hereditary hemochromatosis [see comments]. *Proc. Natl. Acad. Sci. USA* **95,** 2492–2497.

INDEX

L

M